

LEVEL

AGARD-CP-298

AGARD-CP-298

AD A100109

AGARD

ADVISORY GROUP FOR AEROSPACE RESEARCH & DEVELOPMENT

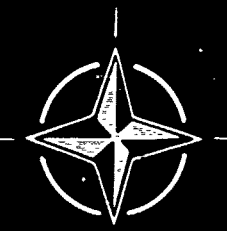
7 RUE ANCELLE 92200 NEUILLY SUR SEINE FRANCE

AGARD CONFERENCE PROCEEDINGS No. 298

Precision Positioning and Inertial Guidance Sensors Technology and Operational Aspects

DTIC
ELECTED
JUN 12 1981

NORTH ATLANTIC TREATY ORGANIZATION



DISTRIBUTION AND AVAILABILITY
DISTRIBUTION STATEMENT ON BACK COVER

Approved for public release;
Distribution Unlimited

81 6 12 002

FILE COPY

NORTH ATLANTIC TREATY ORGANIZATION
ADVISORY GROUP FOR AEROSPACE RESEARCH AND DEVELOPMENT
(ORGANISATION DU TRAITE DE L'ATLANTIQUE NORD)

(11) Mar 82

(12) 378



AGARD Conference Proceedings No. 298

6) PRECISION POSITIONING AND INERTIAL GUIDANCE SENSORS
TECHNOLOGY AND OPERATIONAL ASPECTS.

DISTRIBUTION STATEMENT A

Approved for public release;
Distribution Unlimited

Papers presented at the Guidance and Control Panel Symposium held at Church House, Westminster, London, United Kingdom - 14-17 October 1980.

400043

THE MISSION OF AGARD

The mission of AGARD is to bring together the leading personalities of the NATO nations in the fields of science and technology relating to aerospace for the following purposes:

- Exchanging of scientific and technical information;
- Continuously stimulating advances in the aerospace sciences relevant to strengthening the common defence posture;
- Improving the co-operation among member nations in aerospace research and development;
- Providing scientific and technical advice and assistance to the North Atlantic Military Committee in the field of aerospace research and development;
- Rendering scientific and technical assistance, as requested, to other NATO bodies and to member nations in connection with research and development problems in the aerospace field;
- Providing assistance to member nations for the purpose of increasing their scientific and technical potential;
- Recommending effective ways for the member nations to use their research and development capabilities for the common benefit of the NATO community.

The highest authority within AGARD is the National Delegates Board consisting of officially appointed senior representatives from each member nation. The mission of AGARD is carried out through the Panels which are composed of experts appointed by the National Delegates, the Consultant and Exchange Programme and the Aerospace Applications Studies Programme. The results of AGARD work are reported to the member nations and the NATO Authorities through the AGARD series of publications of which this is one.

Participation in AGARD activities is by invitation only and is normally limited to citizens of the NATO nations

The content of this publication has been reproduced
directly from material supplied by AGARD or the authors.

Published March 1981

Copyright © AGARD 1981
All Rights Reserved

ISBN 92-835-0287-6



Printed by Technical Editing and Reproduction Ltd
Harford House, 7-9 Charlotte St, London, W1P 1HD

THEME

A new class of precision positioning systems, including GPS (Global positioning systems), and MIDS (Multiple information distribution system) hold enormous significance to NATO systems effectiveness. This symposium addressed the status of such programs and the strap-down inertial technology which emerged as the core element in guidance and control.

This meeting further addressed advanced filtering concepts for hybrid navigation systems, redundancy management, and operational requirements and concepts.

Accession For	
NTIS GRA&I	<input checked="" type="checkbox"/>
DTIC TAB	<input type="checkbox"/>
Unannounced	<input type="checkbox"/>
Justification	
Distribution/	
Availability Codes	
Dist	Air Mail and/or Special
P	

AGARD GUIDANCE AND CONTROL PANEL OFFICERS

Panel Chairman: Mr G.C.Howell, UK
Panel Deputy Chairman: Mr R.S.Vaughn, US
Panel Executive: Colonel J.C. de Chassey, FAF

PROGRAMME COMMITTEE FOR THE 31st GCP SYMPOSIUM

Chairman: Mr R.S.Vaughn, US
Members: IPA J.M.Deveaux, Fr
IPA C.Moreau,* Fr
ICA D.Pichoud, Fr
Dr R.C.Onken, Ge
Dr Th Spathopoulos, Gr
Mr J.L.Hollington, UK
Mr R.W.Wedan, US

HOST COORDINATOR

Group Captain R.D.Hillary, RAF (retired)

* AVP member

CONTENTS

	Page
THEME	iii
PANEL AND PROGRAMME OFFICERS	iv
TECHNICAL EVALUATION REPORT by J.H.Briggs	vii
KEYNOTE ADDRESS by J.H.Ahmann	x-i
Reference	
<hr/> SESSION I -- INERTIAL SENSORS AND SYSTEMS TECHNOLOGY <hr/>	
INVESTIGATION OF A STRAPDOWN ATTITUDE AND HEADING REFERENCE SYSTEM UTILIZING RING LASER GYROS by G.M.Siouris	1
SMART INERTIAL MEASUREMENT UNITS AND THE COMPENSATION OF DYNAMICALLY TUNED GYROS FOR STRAPDOWN INERTIAL SYSTEMS by C.S.Edwards and R.J.Chaplin	2
ESG INERTIAL TECHNOLOGY: AN APPROACH TO SELF-CONTAINED PRECISION NAVIGATION AND POSITIONING ON AND OVER THE BATTLEFIELD by M.J.Hadfield	3
<hr/> SESSION II -- POSITIONING SYSTEMS. DEVELOPMENT AND STATUS <hr/>	
THE POTENTIAL OF A MULTIFUNCTION INFORMATION DISTRIBUTION SYSTEM (MIDS) FOR POSITION LOCATION by G.Hoefgen	4
JTIDS DISTRIBUTED TDMA (DTDMA) TERMINAL DEVELOPMENT RESULTS WITH EMPHASIS ON RELATIVE NAVIGATION PERFORMANCE by J.Rubin and S.Welt	5
JTIDS DUAL GRID NAVIGATION USING TIME SYNCHRONIZED DATA LINKS by R.C.Stow and I.D.Reiss	6
LE SINTAC ET SES PERFORMANCES EN LOCALISATION SINTAC AND ITS POSITIONING PERFORMANCE by Lj.Milosevic, J.C.Charavit and M.Ronsin	7
NAVSTAR GPS PROGRAMME REVIEW by H.Coriat	8
<hr/> SESSION III -- EVALUATION METHODS AND RESULTS <hr/>	
NAVSTAR FIELD TEST RESULTS by R.L.Peterson	9
ESTIMATION OF STRAPDOWN SENSOR PARAMETERS FOR INERTIAL SYSTEM ERROR-COMPENSATION by D.K.Joos and U.K.Krogmann	10
EVALUATION D'UN SYSTEME DE NAVIGATION HYBRIDE A GYROLASERS "SEXTAN" par D.Regnault, J.Leclerc, B. de Salaberry et J.P.Prado	11
FLIGHT TEST RESULTS OF AN ADVANCED DEVELOPMENT MODEL RING LASER GYRO NAVIGATOR (RLGN) by K.L.Bachman	12

Reference

- JTIDS RELATIVE NAVIGATION TEST AND EVALUATION
by L.Newman and P.J.Finnegan

13

SESSION IV - FILTERING AND ESTIMATE

- INTEGRATED NAVIGATION SYSTEMS BASED ON MULTIPLE DME
by U.Brokof and K.Hurrass 14
- DYNAMIC PERFORMANCE ANALYSIS OF NAVSTAR/GPS NAVIGATION FILTERS
by M.J.Dymant and D.F.Liang 15
- RAPID ALIGNMENT OF AIRCRAFT STRAPDOWN INERTIAL NAVIGATION SYSTEMS
USING NAVSTAR GLOBAL POSITIONING SYSTEM (GPS)
by R.W.Tafel, Jr and D.Krasnjanski 16
- TERPROM - A TERRAIN PROFILE MATCHING SYSTEM FOR MISSILE GUIDANCE†
by R.S.Dale 17

SESSION V - FAULT TOLERANCE DESIGN AND REDUNDANCY TECHNIQUES

- NEW NAVY PROGRAMS FOR DEVELOPMENT OF INTEGRATED INERTIAL SENSORS
by C.R.Abrams and R.J.Skoyles 18
- F-8 DIGITAL FLY-BY-WIRE AIRCRAFT ANALYTIC REDUNDANCY MANAGEMENT
FLIGHT TEST EXPERIENCE
by J.C.Deckert 19
- PRECISION POSITIONING FOR REMOTELY PILOTED VEHICLES‡
by Y.K.Ameen 20
- ENHANCING POSITION RELIABILITY BY FULLY INTEGRATING JTIDS AND GPS
by H.J.Rome, R.A.Reilly and C.R.Ward 21

SESSION VI - SYSTEMS REQUIREMENTS AND APPLICATIONS

- NAVSTAR GPS RECEIVER FOR SATELLITE APPLICATIONS
by R.Thorensen, K.M.Joseph, J.J.Winterhalter and J.R.Champion 22
- THE INERTIAL ELEMENT IN INTEGRATED AVIONICS SYSTEMS FOR HIGH
PERFORMANCE COMBAT AIRCRAFT†
by W.H.McKinlay 23
- FUTURE TACTICAL GUIDANCE AND POSITIONING SYSTEMS†
by P.A.Bross 24
- JTIDS STRAPDOWN INERTIAL MIDCOURSE GUIDANCE PERFORMANCE ANALYSIS
by S.C.Bose 25
- INTEGRATION OF POSITIONING AND NAVIGATION INTO THE C³I STRUCTURE
by R.Denaro, F.Karkalik and S.W.Gilbert 26

TECHNICAL EVALUATION REPORT

by
J H Briggs
Woodlea, Priorswood, Compton
Guildford GU3 1DR
UK

1. INTRODUCTION

The 31st GCP Symposium was held in London, England 14-17 October 1980. The detailed programme presented is given in Appendix 1. The full text of papers is published in Conference Proceedings CP 298.

This Technical Evaluation was prepared by an independent observer, amended and edited by the symposium chairman. It includes material drawn from comments provided in answer to the questionnaire circulated (Appendix 2). 34 written responses (from over 250 registered) were received along with verbal comments.

2. THEME AND OBJECTIVES

The symposium was intended to cover the technological progress made in precision positioning and navigation systems (PP/NS) since the issue of AG 245 (Principles and Operational Aspects of Precision Position Determining Systems by Icordes) and in inertial sensors. In addition, it was intended to examine the problems of integrating inertial sensors with a PP/NS, integrating such combined systems with other vehicular systems and assessing the benefits to be gained therefrom. The PP/N Systems to be covered included NAVSTAR/GPS, the use of JTIDS or MIDS for precise relative positioning and navigation and those using terrain matching techniques.

If successful the symposium would assist in achieving the following objectives:-

- (i) to provide information (cost of ownership, lethality, availability, safety, etc.) on which the cost/effectiveness of systems employing these techniques can be established
- (ii) to enhance, through exchange of ideas and mutual criticism, the capability of individual participating nations.

and secondarily:-

- (iii) to enable military planners to assess the relative contribution of individual techniques to meeting overall system requirements.

To achieve this the symposium was organised in six sessions

- I INERTIAL SENSORS AND SYSTEMS TECHNOLOGY
- II POSITIONING SYSTEMS - DEVELOPMENT AND STATUS
- III EVALUATION METHODS AND RESULTS
- IV FILTERING AND ESTIMATE
- V FAULT TOLERANT DESIGN AND REDUNDANCY TECHNIQUES
- VI SYSTEM REQUIREMENTS AND APPLICATIONS

There was inevitably appreciable overlap between the sessions as many of the papers covered more than one of the topics. The technical evaluation that follows does not, therefore, depend solely on the activity in the individual session discussed.

3. TECHNICAL EVALUATION

3.1 KEYNOTE ADDRESS

Major General J AHMANN, USAF, Assistant Chief of Staff for Operations, SHAPE gave the symposium a stimulating start with an address having considerable relevance to its objectives. His main thesis was that the principal avenue open to NATO to counter the quantity of men and weapons available to the potential enemy was through quality. Depressing conclusions as to the capability of the Western world would be inevitable without avoiding the twin dangers of assuming an unrealistic perfection in the enemy and of failing to continue to provide NATO with superior technology and the capability to apply it. He cited instances where an increase in the precision of weapons could bring

about an equivalent reduction in the numbers needed to ensure mission success. In addition to quality of individual armaments, there was a need to be able to create, through mobility and rapid use of more comprehensive information, local numerical superiority as and when required. Offensive air requirements, therefore, demanded improvements in:-

- (i) Air/Ground Weapons
- (ii) Information/Intelligence collection and sorting
- (iii) Survivable information distribution systems

He gave some details of the requirements in these areas and the status of some R&D that would contribute to their attainment. The impact that the capability of PP/NS would have in, at least three of the major activities, was stressed.

He concluded with an appeal for improved exchanges between the military and technical communities within NATO and expressed the hope that AGARD symposia would help. He also pointed out the need for operational trade-off analyses arising from the severe funding restrictions.

3.2 SESSION I - INERTIAL SENSORS AND SYSTEM TECHNOLOGY

The three papers presented covered three significantly different application areas

For very low dynamic applications, where frequent zero velocity updates could be performed, sub-metre positioning accuracy was claimed using Electrostatically Supported Gyroscopes of 0.1 nm/hr quality. Field tests had shown better than 100cm accuracy with updates every 4 minutes and better than 15cm with 1 minute update in both land vehicles and helicopters.

For missiles the advantages of strapdown techniques have already been demonstrated in many applications. Surprisingly, in spite of the ring-laser performance established elsewhere, the statement was made and not challenged that for missiles "the rate sensor requirements for the immediate future will continue to be met by the well proven conventional spinning mass gyroscopes". The Dynamically Tuned Gyro was given preference over others such as the Rate Integrating Gyro.

For high dynamic applications of strapdown inertial systems it seems clear that ring laser gyros have little competition since they (a) are not g-sensitive (b) provide relatively noise-free body rates and (c) are cheaper than conventional gyros of equivalent measurement accuracy.

This session provoked little discussion - maybe the symposium had not yet warmed up. It was one which could have benefited from a 'round table' of the authors, with discussion initiated by some prepared questions. This would have clarified the relative merits of strapdown and gimbaled systems and of laser and mechanical gyros.

3.3 SESSION II - POSITIONING SYSTEMS - DEVELOPMENT AND STATUS

A most unfortunate absence in this Session was that of two promised papers, one on JTIDS and the other on MIDS, which might have given those not fully familiar with them a better insight into the techniques involved, their potential application and their current status. NAVSTAR/GPS (a system dedicated to global positioning and navigation) and the added capabilities that could be provided for relative positioning inherent in the Multifunction Information Distribution System (MIDS), the Joint Tactical Information Distribution System (JTIDS) and the French SINTAC were covered. The absence of programme review papers on MIDS and JTIDS made time for showing an explanatory film on NAVSTAR/GPS.

The rivalry, never fully debated, was between the ability of the Information Distribution Systems, through their accurate measurement of elapsed time, to provide precise (but unreported) relative positioning restricted to the area covered by the participating community and the global coverage of NAVSTAR giving very high accuracy (test results fully supporting the claims) in a world-wide grid translatable without significant degradation to a local geodetic grid.

For all the systems, the continuous availability of precise information in highly manoeuvring vehicles and in the presence of enemy countermeasures requires integration with an INS of good quality (1 - 10 nm/hr).

3.4 SESSION III - EVALUATION METHODS AND RESULTS

With one glaring exception this was a very good session. Evidence of the increasingly effective role of simulators in evaluation was apparent. With care in establishing adequately realistic test conditions, results are being obtained which are fully confirmed in trials under operational conditions. This could be significant in reducing the length and cost of the evaluation process - a concern of many present.

The following points from the presentations were especially noteworthy:-

- (i) The very impressive test results of NAVSTAR/GPS fully confirm the claims for precision and availability (in ECM-free environment) made for it.
- (ii) The results of two independent sets of tests of different Inertial Measurement Units, both using laser gyros in a strapdown format, were convincing as to their superior cost/effectiveness for many applications. More important than accuracy in this assessment was the remarkable reliability of early development models (no failures or even maintenance actions over extensive trial periods) and their probable cost.
- (iii) The absence of results in the JTIDS presentation on grounds of security (in a NATO Confidential symposium!) made the time spent hard to justify. Many present deeply resented this seemingly cavalier treatment.

3.5 SESSION IV - FILTERING AND ESTIMATE

Although this was concerned with the highly theoretical field of Kalman Filters et al, it provided the sole opportunity for more general information to be presented on two systems of navigation not covered elsewhere in the symposium. These were the multiple DME system proposed as a more accurate replacement for the VOR/DME system currently in such universal civil use and a terrain profile matching system for missile guidance.

The DME presentation gave flight test results in a typical West European environment where, using a Kalman filter of 2 seconds time constant and 4/5 DME stations, accuracies better than 200 m were obtained as low as 4500ft. It was suggested in discussion that elsewhere, even in North America, densities of DME were unlikely to be sufficient except at much higher altitudes. It was contended that integration with INS would enable figures little worse to be obtained with only 2 DMEs in line of sight. It was also pointed out that if and when MLS is installed its integral precision DME would alleviate the situation.

More evidence of the mutual assistance provided by INS and PP/NS in the filtering problems involved in aligning aircraft INS with only coarse information available on parent vessels and in improving the performance of 2 channel NAVSTAR/GPS receivers in manoeuvring vehicles was given.

The use of fixes obtained from terrain profile matching to update an INS showed signs of being remarkably promising, as judged from raw data obtained from the aircraft flights so far undertaken. Since the filtering has not been done in real time the true potential has not yet been demonstrated. The adequacy of terrain mapping in potential operational areas was questioned.

3.6 SESSION V - FAULT TOLERANCE AND REDUNDANCY TECHNIQUES

An objective of this session was highlighted by the chairman who pointed out that in deciding what redundancy techniques to employ and how much fault tolerance to build into a design, various trade-off studies had to be undertaken. Two critical assessments were those between safety and availability and between accuracy and cost. This aspect, however, could only receive effective consideration in a system context much wider than PP/NS. This and the subsequent session went some way to airing the point but a thorough examination must await a more suitable opportunity. This might be provided at the 33rd G&C Symposium in Athens in October 1981.

Several useful techniques were analysed in papers in this session. The ability to be more selective in the application of redundancy by attacking lower design levels rather than multiplexing systems was exemplified in two ways. One paper showed that similar levels of fault tolerance could be obtained from inertial sensors disposed in 6 different slewed axes to that provided by three independent 3 axis IMUs. In the final session it was shown that the large number of inertial sensors required to meet Flight Control Systems fault tolerance requirements were more than adequate to provide reliable sensor inputs to the navigation system, which could thereby be reduced in complexity.

Another technique to achieve equivalent reliability at greater availability and lower cost was 'analytic redundancy'. The example presented showed that the use of triple redundancy or self-monitoring could be avoided by using data derived from entirely different and independent sensors to determine which of two redundant devices is in error. With the advent of digital data buses the wider use of this principle becomes possible but at the cost of heavy responsibility being thrown on to the software.

A proposal for full integration of JTIDS and NAVSTAR (and, of course, INS) would provide the last word in graceful degradation. Whilst the claim that all the hardware and software techniques needed were available was accepted, many were sceptical as to the feasibility of designing, developing and proving a system with such complexity, particularly of software, in view of the limited number of applications that might justify its cost. A lower level of integration, while not so effective, might well prove more acceptable. Nevertheless, this was a refreshing presentation by an author clearly well versed in his subject.

Additionally, two examples of the design of remotely piloted vehicle navigation

systems were given. One was for use in a helicopter type RPV and the other underwater. In both, low cost inertial systems were used with different forms of position updating. As would be expected in such different applications the nature of the positioning/navigation systems were radically different but the overall concepts were similar.

3.7 SESSION VI - SYSTEMS REQUIREMENTS AND APPLICATIONS

For the many that stayed to the end this was a most rewarding session, which went a long way to ensuring that symposium objectives were largely met. Applications made possible by the accuracy of PP/NS now achievable, in both the short and long term, were considered as were some of the critical operational analyses that will be required before informed decisions can be taken on the details of integrating these systems into the command, control, communications and intelligence (C³I) structure needed for the type of operations foreseen by NATO.

The papers ranged from a description of a nearly completed development of a NAVSTAR/GPS receiver for satellite applications through (a) a discussion of the dominant role of inertial sensors (even when PP/NS was present) in high performance combat aircraft, (b) a futuristic look at ways of meeting the stringent guidance and positioning needs of the more severe tactical missions foreseen, using highly integrated, multifunction, multiredundant systems and (c) a description of a more immediately available JTIDS/Strapdown Laser IN system for missile mid-course guidance, to the final all embracing operationally oriented paper. This last brought out the all-pervasive role of PP/NS in the C³I structure and set out the extensive programme of analysis needed to quantify the benefits to be obtained and relate them to mission effectiveness.

While all of the papers addressed effectively the interaction between specific missions and the PP/NS design requirements it was the final one which went some way to satisfying the cri-du-coeur in the keynote address.

The abbreviated and sole round table discussion which took place during this session concentrated on the redundancy/fault tolerance topic of the previous session. During this, total integration of airborne equipment was opposed in view of the more stringent requirements of Flight Control as compared with other avionics. However, integration of other avionics through the data bus, using an autonomous flight control system as an input (eg for inertial sensor information), emerged with considerable support. At the same time, a warning was issued doubting the availability and capability of software designers to meet this challenge. The problems involved are not only those of providing the integration of complex and redundant systems but of designing and proving adequate redundancy in the software itself, maybe incorporating dissimilar formulations of certain algorithms, in order to avoid common software faults which could take a very long time to detect.

This session brought out one heartfelt (and apparently well-supported) plea to "KEEP IT SIMPLE". This poses one of the major problems for the future - the quality demanded to offset lack of quantity may require more and more integration of many sensors, sub-systems, etc.; if so, doubts about the achievability of the complex designs involved is likely, at some stage, to call a halt to this expanding integration process. With the apparent excess of technological capability one of the most important of future decisions will be what to leave out.

4. CONCLUSIONS AND RECOMMENDATIONS

4.1 GENERAL

The overall impression given was that of a successful, timely and relevant symposium. The replies to the questionnaire were helpful not only in reaching this conclusion but in formulating the more detailed conclusions and the recommendations that follow.

4.2 TECHNICAL CONTENT

There were a number of areas in which there appeared to be a concensus view. These included:-

- (i) The outstanding problem to be faced was that of 'integration'. This covers not only integration of INS with each of the proposed PP/NS and of one with another but also integration with the other systems within a vehicle. As well as determining how this can be achieved, the questions of how much should be attempted and the quantification of the benefits must not be overlooked.
- (ii) For all applications involving high manoeuvrability, high precision of PP/NS will only be maintained, particularly in the presence of enemy countermeasures, if a reasonable quality ($\pm 10 \text{ nm/hr}$) INS is integrated with it, whether the PP/NS is NAVSTAR/GPS with its global absolute accuracy or one of the Information Distribution Systems and their more local relative positioning and navigation capability.
- (iii) It would appear that the most promising Inertial Measuring Unit for use in (ii) and many other applications will be one using laser ring gyroscopes in a strapdown format.

- (iv) The most challenging part of (ii) will be the production of reliable software and its proving, which will in its own right set a limit to the complexity of integration that can be achieved.
- (v) The realism of simulators has been sufficiently adequate in the measurement of performance of many types of navigation system to ensure confirmation of results obtained thereby in subsequent flight tests. Simulators can in consequence be expected, in future, to carry more of the burden of proof.

If this concensus was present it was unfortunate that challenging statements along these lines were not made at the end of the symposium and openly considered in a structured discussion in order to reach more authoritative conclusions.

Only two of the replies gave a serious and considered verdict of 'failed to live up to expectations'. The views of the others, while suggesting various means of improvement (sometimes conflicting), encourage the belief that the symposium successfully covered, with one or two notable exceptions, the theme and adequately met most of its objectives.

The exceptions were:-

- (i) the absence of overviews of JTIDS and MIDS
- (ii) the shortage of operational analyses of the benefits of PP/NS both in specific missions and in meeting broader operational objectives
- (iii) insufficient recognition of the 'NATO Confidential' security arrangements which should have enabled the presentation of classified material essential to fuller achievement of the objectives
- (iv) on the one hand there was some complaint that papers included too much already published material; on the other hand the omission of introductory descriptions of the subject to help the non-expert was noted as marring others
- (v) there was criticism of the lack of objectivity in some of the papers from commercial sources
- (vi) the brevity of discussions - in particular the absence of comment from military staff and defence analysts.

The enthusiasm generated by the keynote address and the pleas contained therein could with advantage be pursued further. To this end any future coverage of the topic should include contributions on systems analysis, more evidence of the cost/effectiveness in various types of operations of the systems concerned, and discussion of the modifications to operational practices that might follow their adoption.

In summary, although the symposium, as was to be expected, did not completely meet all its objectives (eg information for cost/effectiveness) it went a long way to satisfying most of them. In particular, the healthy informal discussion outside the formal sessions, but stimulated by them, did much to provide the interchange of ideas called for.

4.3 PRESENTATIONAL AND ADMINISTRATIVE

With the exception of a few points (mostly hardy annuals) the arrangements met with approval. There was plenty of room for everyone to attend the formal sessions in comfort (apart from headsets) and the space and opportunity for informal discussion outside the symposium hall was appreciated and well used.

The complaints received include:-

- (i) The late availability (sometimes absence) of papers and their somewhat disorganised distribution.
- (ii) The illegibility of visual aids. In addition to usual complaints of 'overbusyness' (one case may have been deliberate) the unnecessary use of colour - an increasing habit - was a major factor in reducing contrast.
- (iii) Ideal correlation of symposium activity and the availability of refreshments was not realised.
- (iv) Reading of lengthy extracts from papers (particularly when already distributed) deadens interest in their content and detracts from the authority awarded to the presenter. (There was one excellent example of the reverse.)
- (v) Varied criticisms of chairmen (by no means universal) included excessive intervention and, possibly contradictorily, failure to set the technical scene and link papers to the theme of the session.

4.4 RECOMMENDATIONS

- (i) The problems of the integration of complex systems, involving precision position determination and navigation, with particular reference to redundancy and fault tolerance aspects should be further pursued - possibly at the 33rd G&C symposium in October 1981.
- (ii) In future symposia of this nature more participation by military staff and defence system analysts should be sought. There are known difficulties in arranging this and an alternative might be to set aside special sessions or even symposia devoted more exclusively to their interests.
- (iii) Some of the sessions could, with advantage, be more structured especially with respect to discussion. More co-operation between presenters could ensure the existence of introductions to the techniques or systems involved for the benefit of the non-expert. The relation of one paper to another and to the topic could be clarified and unnecessary repetition avoided. An independent critical review of the papers at the end of the session should initiate a more useful discussion between authors and other participants.
- (iv) A final round table session would increase the usefulness of symposia of this type if, by selecting highlights for a structured discussion, added force could be given to any conclusions emerging.
- (v) Earlier availability and better distribution of papers should be attempted.

APPENDIX 1
FINAL PROGRAMME

OPENING CEREMONY

KEYNOTE ADDRESS by Major General J AHMANN, USAF
Assistant Chief of Staff for Operations, SHAPE

TUESDAY 14 OCTOBER

SESSION I - INERTIAL SENSORS AND SYSTEMS TECHNOLOGY
Chairman: ICA D Fichoud, FR

INVESTIGATION OF A STRAPDOWN ATTITUDE AND HEADING REFERENCE
SYSTEM (AHRS) UTILISING RING LASER GYROS
by G M Siouris, AF Systems Command, Wright-Patterson AFB, OH, USA

SMART INERTIAL MEASUREMENT UNITS AND THE COMPENSATION OF DYNAMICALLY
TUNED GYROS FOR STRAPDOWN INERTIAL SYSTEMS
by C S Edwards, R J Chaplin, British Aerospace Dynamics Group,
Stevenage, UK

ESG INERTIAL TECHNOLOGY: AN APPROACH TO SELF-CONTAINED PRECISION
NAVIGATION AND POSITIONING ON AND OVER THE BATTLEFIELD
by M J Hadfield, Honeywell Inc Avionics Division, St Petersburg,
FL, USA

SESSION II - POSITIONING SYSTEMS - DEVELOPMENT AND STATUS
Chairman: Dr C T Leondes, USA

THE POTENTIAL OF A MULTIFUNCTION INFORMATION DISTRIBUTION SYSTEM (MIDS)
FOR POSITION LOCATION
by G Hoefgen, Standard Elektrik Lorenz AG, Stuttgart, GE

JTIDS DISTRIBUTED TDMA (DTDMA) TERMINAL DEVELOPMENT RESULTS WITH
EMPHASIS ON RELATIVE NAVIGATION PERFORMANCE
by J Rubin, S Welt, ITT Avionics Division, Nutley, NJ, USA

JTIDS DUAL GRID NAVIGATION UTILIZING TIME SYNCHRONIZED DATA LINKS
by R C Stow, J D Reiss, Singer Kearfott Division, Wayne, NJ, USA

WEDNESDAY 15 OCTOBER

LE SINTA : ET SES PERFORMANCES EN LOCALISATION
by Ij Milosevic, Thomson-CSF, Bagneux, FR
and M Ronsin, Thomson-CSF, Gennevilliers, FR

NAVSTAR GPS PROGRAMME OVERVIEW
by H Coriat, Wing Commander, RAF, HQ Space Division (AFSC),
Los Angeles Air Force Station, Ca, USA

SESSION III - EVALUATION METHODS AND RESULTS
Chairman: Dr A Benoit, BE

NAVSTAR GPS TEST RESULTS
by R L Peterson, Colonel, US Marine Corps, HQ Space Division (AFSC),
Los Angeles Air Force Station, Ca, USA

ESTIMATION OF STRAPDOWN SENSOR PARAMETERS FOR INERTIAL SYSTEMS
ERROR-COMPENSATION
by D K Joos, U K Krogmann, Bodenseewerk Geraetetechnik,
Ueberlingen, GE

EVALUATION D'UN SYSTEME EUROPEEN DE NAVIGATION HYBRIDE A
GYROLASER POUR HELICOPTERE: "SEXTAN"
by D Regnault, Centre d'Essais en Vol de Bretigny, FR
and J P Pradoux, SV2 Crouzet-SFENA, Boulogne-Billancourt, FR

THURSDAY 16 OCTOBER

FLIGHT TEST RESULTS OF AN ADVANCED DEVELOPMENT MODEL RING LASER
GYRO NAVIGATOR (RLGN)
by K L Bachman, Naval Air Development Center, Warminster, PA, USA

SESSION III - EVALUATION METHODS AND RESULTS (Continued)

JTIDS RELATIVE NAVIGATION TEST AND EVALUATION
by P J Finnegan, L Newman, Naval Air Development Center,
Warminster, PA, USA

SESSION IV - FILTERING AND ESTIMATE
Chairman: Prof J T Shepherd, UK

INTEGRATED NAVIGATION SYSTEMS BASED ON MULTIPLE DME
by K Hurrass, U Brokof, DFVLR, Braunschweig, GE

DYNAMIC PERFORMANCE ANALYSIS OF NAVSTAR/GPS NAVIGATION FILTERS
by J M Dymant, Canadian Marconi Company, Montreal, Quebec, CA
and D F Liang, Defence Research Establishment, Ottawa, Ontario, CA

RAPID ALIGNMENT OF AIRCRAFT STRAPDOWN INERTIAL NAVIGATION SYSTEMS
USING NAVSTAR/GPS
by R W Tafel, Jr, D Krasnjanski, Naval Air Development Center,
Warminster, PA, USA

TERPROM - A TERRAIN PROFILE MATCHING SYSTEM FOR MISSILE GUIDANCE
by R S Dale, British Aerospace Dynamics Group, Filton, Bristol, UK

SESSION V - FAULT TOLERANCE DESIGN & REDUNDANCY TECHNIQUES
Chairman: Dr R C Onken, GE

NEW NAVY PROGRAMS FOR DEVELOPMENT OF INTEGRATED INERTIAL SENSORS
by C R Abrams, R J Skoyle, Naval Air Development Center,
Warminster, PA, USA

F-8 DIGITAL FLY-BY-WIRE AIRCRAFT ANALYTIC REDUNDANCY MANAGEMENT
FLIGHT TEST EXPERIENCE
by J C Deckert, J J Deyst, The Charles Stark Draper Laboratory,
Inc, Cambridge, MA, USA
and K J Szalai, NASA Dryden Flight Research Center, Edwards, Ca, USA

PRECISION POSITIONING FOR REMOTELY PILOTED VEHICLES
by Y K Ameen, Marconi Avionics Limited, Rochester, Kent, UK

ENHANCING POSITIONAL RELIABILITY BY FULLY INTEGRATING JTIDS and GPS
by H J Rome, University of Lowell, MA, USA
and R A Reilly, C R Ward, ITT Avionics Division, Nutley, NJ, USA

FRIDAY 17 OCTOBER

SESSION VI - SYSTEMS REQUIREMENTS AND APPLICATIONS
Chairman: Mr Lou Urban, USA

NAVSTAR GLOBAL POSITIONING SYSTEM RECEIVER FOR SATELLITE APPLICATIONS
by R Thorensen, K M Joseph, J J Winterhalter, J R Champion,
Magnavox Government and Industrial Co, Torrance, Ca, USA

THE INERTIAL ELEMENT IN INTEGRATED AVIONICS SYSTEMS FOR HIGH
PERFORMANCE COMBAT AIRCRAFT
by W H McKinlay, Ferranti Limited, Edinburgh, Scotland, UK

FUTURE TACTICAL GUIDANCE AND POSITIONING SYSTEMS
by P A Bross, Electronik System GmbH, Muenchen, GE

JTIDS STRAPDOWN INERTIAL MIDCOURSE, GUIDANCE PERFORMANCE ANALYSIS
by S C Bose, Litton Guidance and Control Systems Division,
Woodland Hills, Ca, USA

INTEGRATION OF POSITIONING AND NAVIGATION INTO THE COMMAND, CONTROL,
COMMUNICATIONS AND INTELLIGENCE STRUCTURE
by D Denaro, F Karkalik, Systems Control Inc, Palo Alto, Ca, USA
and S W Gilbert, Colonel, USAF, Office of the Assistant Secretary
of Defense, C3I, USA

APPENDIX 2

QUESTIONNAIRE CALLING FOR COMMENTS ON AGARD 31st GCP SYMPOSIUM

TO ALL ATTENDEES

Considerable time and effort was expended by a number of countries in the organisation and hosting of this symposium. As a result, the Program Committee Chairman is obligated to prepare an evaluation report. To aid him in preparing a timely, meaningful report, and since we have assembled here leading technical experts in the field, we solicit any feedback or comments you may desire to submit. These may be handwritten notes, and anonymous. If you have any questions, please contact the AGARD staff, the Program or Panel Chairman.

The following are typical examples of areas in which observations, comments and assessments are desired:

(a) General Observations

- 1 Quality, and relevance of papers, sessions and questions
- 2 Did papers support the theme ?
- 3 Did symposium live up to your expectations ?

(b) Technical Observations

- 1 Views on operational issues and requirements
- 2 Assessment of technology (state-of-the-art)
- 3 Views on pacing technology or critical need for R&D
- 4 What do you see as major challenges and trends ?
- 5 Views on systems integration aspects
- 6 What area or problem(s) are unresolved ?
- 7 What future or further action should NATO and AGARD undertake in this area ?

(c) Suggested improvements for symposium (new or special topics, procedures for enrolment, authors' instructions, logistics, etc.).

KEYNOTE ADDRESS

by

Major General James H. Ahmann, USAF
Assistant Chief of Staff for Operations
SHAPE, Brussels, Belgium

First let me thank you for the opportunity of opening this, your thirty-first symposium. It is always an honor to be invited to address such a prestigious group, but in this instance it is both an honor and a pleasure, as I happen to feel that your areas of concern, precision positioning and inertial guidance, are an integral part of the most significant opportunities that we have to apply technology to the problems of combat operations in the 1980s.

However, I would like to be very straight forward with you at the outset and tell you that I have no intention of trying to dazzle you — to impress you — with my detailed technical knowledge in the areas of precision positioning and inertial guidance. Despite having picked up a masters degree in Electrical Engineering during my wanderings through the American military scene, I'm sure that if we had a technical aptitude test in these areas in this hall this morning I'd be graded dead last.

I am basically a military commander with present responsibilities as the Assistant Chief of Staff for Operations at SHAPE, for assisting SACEUR in insuring that all of the forces of the Alliance are at their maximum readiness to fight — so that we have the greatest possible deterrent to war . . . and so that should deterrence fail, we shall be able to successfully defend Western Europe. In discharging these responsibilities, I see our primary job to be one of increasing the capabilities of our ground, sea and air forces to fight because whatever the contribution to deterrence that is made by political actions and economic policies, the greatest military contribution to deterrence of a third world war is made by having ships and Brigades and Air Wings with the greatest possible fighting capability — with the greatest possible capability to destroy the ships, Brigades and aircraft of potential enemies.

That said, I would like to tell you that despite being a fearless fighter pilot — today's world and tomorrow's world — the decade of the 1980s — scares me to death. In both the strategic and tactical nuclear areas we have reached a state of rough equivalence — of balance. Arms control can, and I predict will, change the level at which the achieved balance is maintained but is unlikely to tilt the East-West equivalence at whatever level is attained through such arms control.

There are arguments that such a situation is one to be desired — that *major* conflict at least can be avoided by the omnipresent threat of nuclear escalation. I agree that this threat of nuclear escalation and the close coupling of the US and UK strategic capabilities with the in-place tactical nuclear forces provide two key legs of the NATO synergistic TRIAD of forces which in sum provide deterrence, but I am also convinced that maintaining a real — a ready and effective conventional force as the third leg of that TRIAD of forces is an absolutely essential element of the West's deterrent strategy in the 1980s.

I argue that such significant NATO conventional capability may be even more important in the 1980s — in the era of precarious nuclear balance. Without it, the East could seriously miscalculate the West's definition of what constitutes a major conflict — of what will be met by nuclear response. The potential enemy could be encouraged by a conventional imbalance to take chances — to trust that a quick slice of the Western salami by conventional forces could be accomplished.

- The Soviet's move into Afghanistan -- the first use of Soviet troops outside their perceived sphere of influence in Eastern Europe — should give us pause in this regard.
- The present and potential problems within the Eastern Bloc — the discontent evident among Eastern European people, the continued failure of agricultural programs in the East, the probability that the USSR in the next few years may become a net importer of oil, are all additionally worrisome when one meditates on what global strategy the USSR will adapt for the 1980s.
- The oil situation in itself, and its potential effect on the economies of Western nations is not a happy one. Two major oil producers are locked in combat, bombing each other's major refineries today. A spread of that conflict into other regions of the Gulf could imperil the oil supplies to the West and thus the health of the West's oil gulping economies.

All of these thoughts are gloomy but they are thoughts that we in the West can ignore only at our great peril. If they are ignored we in the West could find ourselves in the same position as the naive young girl during her first sea voyage. Her diary entries were as follows:

On Monday she wrote: "I received the great honor of being asked to dine at the Captain's table."

On Tuesday: "The Captain was kind enough to allow me to spend most of my day on the bridge and took me on a tour of the ship."

On Wednesday: "Today the Captain made a number of rude, abhorrent and unacceptable proposals -- I found them very demeaning."

On Thursday: "The Captain threatened to sink the ship unless I acquiesce to his demands."

And finally on Friday, "This evening, I saved 700 lives."

I do not believe we of the Western Alliance are prepared to put ourselves in such a position -- I further believe that our nations have accepted the challenge of improving our conventional capability -- in fact have accepted as an absolute requirement that we must do so . . . and many positive actions are being taken. Nations have committed themselves to increased expenditures for defense; we are working on a Long Term Defense Program which entails improvements across the spectrum of conventional defense in Readiness; in Reserve Mobilization; in Air Defense; in Command, Control and Communications; in Maritime Operations; in Electronic Warfare.

But real progress will not be easy. There is a limit on the funds that can be made available for conventional defense improvements in the West. There are those who argue that, even with maximum national support and the funding contributions that such support entails, the best we can hope for is to minimize a continued unfavorable divergence between the relative conventional power of the Soviet Bloc and NATO. These arguments are reasonably persuasive . . . after all, they say, in the decade of the 1970s the Soviet Union spent almost 250 billion dollars more than the US on military equipment . . . The future holds more of the same divergent spending, therefore, there is no hope. I am unprepared to accept such arguments and I hope you are also.

Part of my reason for not accepting the inevitability of Warsaw Pact conventional superiority are somewhat personal and subjective. Our troops, our airmen, our sailors, from observations, are better trained, are more adaptable and will give a better account of themselves than we may think and the results of conflict even today may be different than some of our computer analyses have indicated. We tend *not* to measure work-arounds, leadership, bravery, or initiative on the battlefield. From my study of History I reckon that if the *winners* of many historical battles had been prebriefed on relative firepower indices, they might have surrendered in lieu of fighting and *winning*.

A second reason for not accepting the inevitability of our conventional inferiority is the fact that we do tend to paint our potential enemy as ten feet tall. He doesn't seem to be susceptible to Murphy's first law of "whatever can go wrong will go wrong"; we tend to give him perfect command and control capabilities with which to execute his centrally prepared and complex offensive plans; we tend to discount any problems he may have in getting the forces of the other Pact countries to fight as vigorously as he might like.

But the third reason -- perhaps the key reason that we will not be inferior is that people like you, backed by the superior technology of the west, will provide our military forces with the tie-breakers which I adjudge to be, very simply, technologically superior weapons and technologically superior ability to use those weapons to effectively put steel on a numerically superior enemy force. It is this third area that I would like to discuss with you today.

Undoubtedly -- we have a challenge.

How are we -- Western military and industry -- to meet this challenge? Well, we have long accepted the fact that we cannot match the Soviet Bloc in numbers. Even if we wanted to, we probably could not. And if we did match them on the equipment level, we couldn't afford the associated manpower and other support costs.

Further complicating this issue is the fact that their force size advantage, coupled with the proximity of a large part of this force to the most probable combat zones, places the Warsaw Pact in a position to initiate a short-notice offensive which could conceivably achieve its ends before the nations of NATO would be able to fully mobilize and reinforce.

Thus, we find ourselves in a position where we could face a war outnumbered, and with little time to prepare.

I would submit to you that the only solution open to us in NATO is to have war fighting systems adapted to the kind of war WE intend to fight, to develop the capability to use what we have better than the other side can, and to make the enemy fight our kind of war. I'd like to cover with you some ideas of how we can apply this direction of thinking . . . specifically to our ability to use our offensive air to best advantage. Such improved use would be a considerable step toward achieving the improved conventional capabilities that we need.

During World War One, Lancaster evolved a set of relationships describing the engagement of two opposing air forces. His conclusion was that the attrition experienced by each would be a linear function of their respective quality, but vary with the square of their quantity.

I believe Lancaster was close to right and if we consider his theory in the context of an air war in Europe, it means we must not only be equal or better in quality, but develop some means of assuring local QUANTITATIVE superiority in spite of size differences in the total force. And we must be able to rapidly shift our forces to achieve local quantitative superiority as the combat situation demands.

I submit that a considerable portion of the answer to doing this lies first in improved air-ground weapons; second in sophisticated and highly automated intelligence and surveillance fusion; and lastly in a survivable information distribution system that will permit us to fully exploit the first two.

NATO forces are slowly building an inventory of precision guided munitions, or, as they are more commonly referred to, PGMs.

At present for air forces, this inventory consists of television-guided missiles and laser-guided bombs.

Operationally, however, these first-generation weapons have serious limitations. To partially correct these, they will be followed shortly by advanced laser-guided missiles.

But even with these weapons we will have major deficiencies. They are weather limited and require a target designator either on the ground or in the air. The operators of these designator systems are highly vulnerable. And the weapons themselves are susceptible to countermeasures.

As these newer weapons are being introduced, another family of still more capable weapons is being developed. These will have a "launch and leave" capability, greatly increasing the user's chances of surviving. And, they will have an all-weather capability. The technology employed here, as you are aware, will be focal plane arrays, different types of imaging infra-red systems, and millimeter wave radars, active and passive.

Of equal importance, these weapons will be equipped with microprocessors able to discriminate between targets and nontargets, then guiding attacks on the targets they identify.

While these weapons are still in the developmental stages, within the next few years they will transition from experimental to operational status. When they do, we will for the first time have a true all-weather, day-night tactical air force.

However, PGMs are not the entire answer. Depending on how well we do in attaining precision navigation equipment we may well be able to make very effective use of non PGM weapons particularly to hit static targets such as groups of airfield shelters with hard target munitions and to hit groups of vehicles with wide area anti-armored munitions.

To apply these new weapons effectively we must provide commanders with surveillance and intelligence information, making it possible for them to get weapons on any target offered by the enemy, no matter how fleeting.

Twenty-six years ago when I entered the Air Force and began flying fighters, surveillance was by eyeball, cameras, rather basic radars, and the monitoring of radio transmissions.

We have come a long way since then. It could be said that the technology is largely available to solve most of the larger problems of surveillance systems. The first of these problems, area coverage, has largely been overcome by placing our systems in airplanes and satellites.

The second major problem, the screening of targets from sensors by both natural and man-made phenomena is also yielding to the application of new technologies. Such breakthroughs as imaging infra-red systems, infra-red scanners, imaging radars, and other sophisticated signal surveillance systems are well advanced in their development.

These things will at last provide the information needed to locate and track enemy targets in the detail necessary to take full advantage of the new families of weapons.

But the finest weapons and surveillance cannot, by themselves, do the job. One thing still needed is a method of correlating and sorting this information rapidly and for the right user. The information must be broken down to meet the needs of battle managers at all levels, from Major NATO Commanders down to Fire Support Coordinators at Division and Brigade level and the pilot in the cockpit. The great mass of surveillance data must be fused, divided to meet the requirements of each element of the combat team, and only those bits needed by each made available to them.

And, all of this processing must be fast. Reducing the time from detection to decision to attack from hours to minutes, or even seconds, is the key to real-time targeting. And in my opinion real-time targeting is a primary key to offsetting the numerical disadvantage at which NATO would find itself.

The OASIS, or Operational Application of Special Intelligence Systems, now operational in the AFCENT War Headquarters, is an early attempt to achieve the type of fusion needed. We have more advanced systems under development, but in my opinion we need to devote a lot more resources to these programs to get them the priority they deserve, and to get them into the field.

The other element, of course, necessary in a complete surveillance and fusion system is locating friendly forces. Those making attack decisions must be able to do so without fear of endangering friendly forces and with the knowledge necessary to select the most appropriate attacker. Further development of the Global Positioning System or MIDS offers one way of making it possible to know where our forces are within a few meters – even to the point as I said earlier where non-PGM can become very effective at night or in all-weather conditions.

Knowing exactly where both the enemy is and friendly units are represents a revolution in battlefield management. Commanders will be able to do their jobs with a confidence never before possible.

Having briefly discussed with you the first two of the elements I told you I felt were absolutely necessary to meet the threat posed by Warsaw Pact forces, improved weapons and intelligence surveillance and fusion, I will now turn to my final requirement, an information distribution system, making it possible to fully exploit the other two.

A system is needed to get target information to targeteers and weapon system operators quickly enough to allow ordnance to be delivered before the enemy can conceal or protect his resources. And this same system must be able to pass target information directly to the pilot in the cockpit.

At least three nations have been working to develop such systems. I am speaking of the French SINTAC, the German MACS and the US JTIDS. While they differ in detail and comprehensiveness, all are intended to do essentially the same job.

Later in this symposium you will be briefed on the MIDS or Multifunctional Information Distribution System, NATO's general approach to information system distribution.

Development of the MIDS was begun simultaneously by two groups, one, a MIDS team of national experts, worked with the SHAPE Technical Center in examining technical aspects of the system. The second group, at SHAPE, undertook development of a comprehensive operational requirement.

The final report of the Technical MIDS team will hopefully be distributed within the next few weeks; the operational requirement has been coordinated within SHAPE and is with the Nations and NATO military commanders for comment. It is our intention to have it completed by year's end, and work on the type A cost estimate will begin shortly thereafter.

Those of us working on MIDS are excited about its possibilities and are pressing for its realization at the earliest possible time. In my opinion MIDS will be a most significant system development in NATO.

Given the right weapons, surveillance and intelligence fusion systems, and a compatible system for distributing the information and directing attacks, the commander of the future will have the tools to identify areas where establishing local air superiority would be most advantageous, and be capable of employing his forces to achieve maximum damage on enemy ground and air resources in the shortest possible period. He will be able to win within Lancaster's equations.

Although I have talked about the applications of these exciting developments to the air battle merely to be somewhat specific, these same three developmental areas also have great applicability to naval and ground forces – and must be developed to improve our capability in all three forces.

Thus far I have presented, after a rather *pessimistic* beginning, what could probably be considered a somewhat *optimistic* view of our ability to meet the future challenge we will face. I would be remiss were I not to mention some of the practical problems entailed in introducing and employing these systems.

The overriding problem in developing these type capabilities will be money. With an unlimited budget I am 100% confident that Western Technology can build a near perfect system of weapons/intelligence and surveillance fusion/and information distribution that would provide us a tie breaker in conventional capability.

Unfortunately, we will not have an unlimited budget. . . .

We never do.

One solution is to convince the nations that the application of these technical possibilities are indeed worth additional cost. In this regard, I'm reminded of a golf game I had with one of my bosses a few months ago.

We had come to the fifth hole, where you have to carry your drive across a small lake. I hit mine over and the boss put his right in the middle.

He said, "I'm out of balls; how about letting me have one". So I gave him one of my new Titleists. Which he also hit into the lake.

Well, after doing this three more times I'm not only running out of balls, but I'm beginning to worry at a dollar and a half a ball. So I suggested he might want to just drop on the other side and play from there since it was getting a little expensive.

He sort of turned around, looked me right in the eye, and said, "Jim, if you can't afford the game, you ought to give it up".

Unfortunately, the Alliance, like me, has trouble affording the game but surely cannot give it up.

One answer then is for us to do a better job of selling the need — the pay off — from such systems. It is a job we must do. And I contend that it is a job that can only be done by the technologists and the military working closely together.

But I would counsel that our selling effort won't be completely successful if we ask for *everything* — as we too often do from both the Military and Technological side of the house. There are dozens of trade off studies and operational analyses that I think need doing before we really know how much we *have* to sell.

A few examples:

- What is the benefit of offensive attack of the enemy's airfields? Has the right measure of merit for this type study been determined? Is it e., change ratio between attacking and attacked aircraft or is a more sophisticated M.O.M. required — one that relates the decreased number of sorties that an enemy can launch tomorrow and the more macro payoffs from this relative to potential decrease in the "enemy's" ability to destroy our ground forces and targets in our area. We need answers to these type questions to "sell" new hard target munitions and to establish how much surveillance needs to be directed against the enemy air order of battle.
- Further, in the area of INTEL/Surveillance fusion we need answers as to what information is required at what command level. How many INTEL/Surveillance systems do we build -- a central system for a region or a number of systems for each region?
- A MIDS can theoretically be built that can do not only information distribution but the precision navigation task and the identification task as well. But will it fit in our aircraft? Can we afford its cost? Would we better off doing the Identification job off line from the MIDS? Would we be better off doing the Navigation job off line and, if so, how? Should we spend our money on central navigation systems like NAV IAR with receivers on aircraft or put our effort into possible improvements in inertial navigation systems — self contained on the aircraft.

We badly need answers to these and many other operational pay-off questions and I don't believe we have them all yet.

To sum up —

- Our challenge is to find ways to make NATO equal or better than the Warsaw Pact in conventional capabilities.
- From the technology point of view
 - Better munitions
 - An effective intelligence/surveillance fusion system
 - And an effective information distribution systemcan all contribute to solving this challenge.
- From the implementation point of view it's going to be difficult because it's going to cost a lot of money.
- From the common sense point of view, we military and technologists together need to find the answers to a great number of critical questions — in order to determine what systems or system elements we *have* to sell to get the greatest incremental increases in combat capability in the shortest possible time.

I'm convinced that we can do it — we must do it. The answer lies in large part with persons such as yourself — in your ability and willingness to press us dumb military for answers -- for answers that will allow you to design and "sell" the *right* systems, the effective systems.

Gentlemen, Winston Churchill once said "Do not ask us to take sides against arithmetic". However, we have no choice. We must take sides and we must figure out a way to beat the odds.

**INVESTIGATION OF A STRAPDOWN ATTITUDE
AND HEADING REFERENCE SYSTEM
UTILIZING RING LASER GYROS**

DR. GEORGE M. SIOURIS
AIR FORCE SYSTEMS COMMAND
AERONAUTICAL SYSTEMS DIVISION (ASD/ENACA)
WRIGHT-PATTERSON AFB, OHIO 45433

SUMMARY

There exists a requirement for a low-cost, lightweight strapdown attitude and heading reference system, that will satisfy the needs for navigation, fire control, flight control, and weapon delivery in the 1980s and beyond. Above all, the system must be highly reliable, be easy to maintain and repair, be medium to high accuracy, have rapid reaction time capability, and perform satisfactorily under extreme dynamic environments. This paper assesses the potential benefits of utilizing ring laser gyro technology in a strapdown attitude and heading reference system configuration for rotary- and fixed-wing aircraft. The ring laser gyro has demonstrated highly acceptable performance with the promise of even better results and greater design margins to enhance the low cost goals. System performance is evaluated using a strapdown covariance error analysis simulation. The covariance matrix represents the standard deviations of the errors in the system at any point in time of the trajectory or mission. Coupled with a transition matrix that propagates the covariance matrix forward along the route, the errors along the entire route can be computed.

Analysis and tradeoff studies of various configurations of conventional gyros indicate that an attitude and heading reference system using ring laser gyros, has indeed the best potential for achieving cost-effectiveness, reliability, and performance.

1. INTRODUCTION

During the past decade, gimbaled Inertial Navigation Systems (INS) have provided precise autonomous navigation and position information for both military and commercial aircraft. The mechanical complexity and penalties such as reliability, maintainability, and Life-Cycle-Cost (LCC) limit their application. These systems cannot realize the low-cost and reliability of future inertial systems. Furthermore, the INS of the 1980s must significantly reduce its LCC without sacrificing performance and accuracy. To this end, the INS function is most economically achieved by a strapdown mechanization, and the availability of small, high-speed digital minicomputers now permits a truly effective INS design. Strapdown INS systems, although presently do not have the accuracy of gimbaled systems, it is believed that in a few years they will be competitive with present systems.

This paper investigates another area equally important to that of an INS, namely, Attitude and Heading Reference Systems (AHRS). Conventional spinning mass gyroscopes presently used in INS and AHRS systems employing ball bearings, electrostatic, gas or other suspension principle have performed very well over the years. However, these inertial sensors have relatively high failure rates, are expensive to maintain and repair, and somewhat difficult to calibrate. For these reasons, attention has now turned to unconventional inertial rotation sensors such as the sonic gyro, the vibrating wire rate sensor, the "superjet" solid state gyro, the nuclear magnetic resonance gyro, and the ring laser gyro. Among these unconventional angular rate sensors, the ring laser gyroscope remains the most promising. Judging from recent impressive flight test results by the U.S. Navy and the U.S. Air Force, it appears that the credibility of the laser gyro as a viable angular rate sensor is now fairly well established. Consequently, the latest advances in Ring Laser Gyro (RLG) make it a strong contender for a broad spectrum of applications such as inertial navigation and guidance for aircraft and missiles, flight control, fire control, and the AHRS which this paper explores.

The AHRS described in this paper has a specific application, which is used to improve the navigation performance of a Doppler navigator and provide high quality attitude, angular rates, and accelerations as airframe referenced outputs. This particular application of AHRS, consisting of a simple, low-cost inertial sensor package configuration, will provide body angle increments measured by three ring laser gyros and body velocity increments by three linear accelerometers. The information from the inertial sensors will be fed into a digital computer (or microprocessor), which will process the inertially derived information and combine it with other sensor information such as Doppler radar velocity to yield high accuracy aircraft attitude and heading data. Inertially derived information will be processed by means of standard strapdown computational algorithms and then combined with the reference data in a Kalman filter to generate optimal estimates of aircraft attitude and heading. For the system under consideration, it will be assumed that magnetic heading from a Magnetic Azimuth Detector (MAD) or flux valve will be available for heading reference. It is anticipated that the system would be operated with and significantly improve the performance of Doppler navigation and global positioning systems. The Doppler radar navigation system performance (if this is the only means of navigation) would improve through the use of the high accuracy heading data of the RLG AHRS. The

Global Positioning System (GPS) performance would benefit through the use of velocity data from the RLG AHRS which would substantially reduce the GPS tracking loop bandwidths and thereby improve satellite signal acquisition time as well as signal-to-noise and signal-to-jamming ratios.

Communication between the AHRS and the aircraft avionics will be accomplished via a dually redundant MIL-STD-1553 multiplex data bus under the control of a master bus controller. Typically, the program memory cards will provide 20,480 16-bit words. In addition, 3072 words of Random Access Memory (RAM) and 1024 electrically alterable non-volatile RAM for constants and status storage will be available. If desired, an additional space of 4096 words for future growth may be provided. The system will contain a separate resident bus control software module and a Control and Display Unit (CDU) data module unit, which will operate in conjunction with the different aircraft transfer control protocol and control and display equipment.

2. RING LASER GYRO THEORY OF OPERATION

For completeness, this section presents an overview of the theory of operation of the Ring Laser Gyro (RLG) as a foundation for better understanding the discussion of error sources given later in this section, and the problems encountered in rotation rate measurements with laser gyros. For a complete description of the laser gyro operating principles, mathematical modeling, and optical characteristics the reader is referred to [1], [5], and [10].

The ring laser gyro combines the properties of an optical oscillator and general relativity to produce the function of mechanical gyroscopes presently used for inertial navigation and guidance systems. It has the notable advantages of no rotating mechanical parts, simple construction, inherent digital output, and the capability of precision high and low angular rate measurement. This latter property makes it well suited for strapdown inertial systems, which offer low-cost features as opposed to gimbaled systems. A ring laser gyro is an optical cavity that contains two oppositely traveling light beams generated by stimulated emission of radiation. Thus, light is the inertial rate sensing element. When the gyro is at rest, the light beams have the same optical frequency and form a standing wave pattern. That is, the two beams oscillate at identical frequencies. Rotation of the ring in a clockwise direction, causes the clockwise traveling beam to travel a longer path length than the anticlockwise one. In other words, the frequency of the clockwise directed beam decreases while the frequency of the oppositely traveling beam increases. The frequency difference is proportional to the sensed rotational rate and is detected by heterodyning the two beams on a photosensitive device. In order to sustain oscillation and thus maintain lasing, two basic conditions must be met: 1) the path length must be an exact number of wavelengths, that is, the phase shift around the cavity must be zero, and 2) the gain must be unity at some power level set by the lasing medium. The frequency difference between the counter-rotating beams is given by

$$\Delta f = f_1 - f_2 = \left(\frac{4A}{\lambda L}\right) \Omega_{in} \quad (1a)$$

where Ω_{in} is the input rotation rate, A is the area enclosed by the ring, λ is the laser wavelength, and L is the total length of the cavity. Eq. (1a) is the ideal ring laser gyro equation. This equation can be further written as

$$\Delta f = \left(\frac{4A}{\lambda L}\right) \Omega_{in} + \Omega_B \quad (1b)$$

which includes the biasing frequency Ω_B . Again, for an ideal ring laser gyro, the ideal scale factor is given by

$$K = \frac{\Delta f}{\Omega_{in}} = \frac{4A}{\lambda L}$$

measured in units of counts/radian or arcsec/pulse. From this relationship, it can be seen that the scale factor sensitivity will increase by increasing the enclosed ring area while at the same time decreasing the optical path length L (or the wavelength λ). As a result, any variation in these parameters will appear as an output error. Scale factor is measured in the laboratory on a rate table. If an ideal gyro is rotated about its input axis through an angle equal to the pulse weight, an output of one pulse occurs. Before a measurement can be made, the rate table must be indexed at 0° in position. Output measurements can then be made at different values of input rotation. For example, for a given temperature and sample time, the rate table can be rotated clockwise and anti-clockwise from 0.5 deg/sec to 720 deg/sec in increments of 25 deg/sec. Scale factor can be determined in the laboratory from the equation [2]

$$K = \frac{\phi}{N \pm N_B \left(\frac{\Delta T}{\Delta T_B} \right)}$$

where ϕ = angle through which the table moved during the sampling interval (arcsec).

N = number of gyro output pulses during ΔT (pulses).

N_B = total number of output pulses obtained during gyro bias determination (pulses).

ΔT = sample interval (sec).

ΔT_B = sampling interval during gyro bias determination (sec).

Scale factor deviations with temperature changes and internal thermal gradients is common to laser gyros. It must be pointed out, however, that scale factor is not constant, but a function of input rotation rate and temperature.

Commonly, the laser gyro block is made of a glass-ceramic material (CERVIT) or Zerodur, that has a small bore along each side of a triangular shape. The bore serves as the cavity for the plasma section. This is called an active He-Ne gas laser gyro, as opposed to those called "Sagnac Interferometer" where the plasma is external to the cavity. Three mirrors are mounted on each corner to form a closed optical path. One of the mirrors allows sufficient transmission (about 0.1%) of the laser beams for signal detection. As mentioned above, the laser gyro is inherently a digital output instrument. That is, the instrument has a digital output quantized in incremental input axis rotation. Therefore, when the input rotational angle of an ideal instrument equals the quantized data size, an output pulse occurs. For example, if an ideal laser gyro is rotated about its input axis through an angle equal to the pulse weight, an output of one pulse occurs. The rate at which the output pulses appear is directly proportional to the input rate, thus the total angle of rotation is determined by counting the incremental pulses. Depending on the size and type of laser gyro, each pulse represents approximately 2^{-16} radians of rotation in inertial space about the laser gyro input axis. A ring laser gyro inertial navigation system mechanized as a strapdown, Schuler-tuned system, will provide such output information as position, inertial acceleration and velocity, true heading, synchro attitude and heading, inertial altitude, and Built-In-Test (BIT) [3].

One of the main error sources in laser gyros is the so-called "lock-in" phenomenon. The lock-in occurs for any resonant system with frequencies close in magnitude, and is characteristic of laser gyros. Lock-in is caused by imperfections in any reflecting surface around the perimeter of the laser path and polarization anisotropies. These imperfect mirrors will cause some backscatter of the laser light, which in turn causes the clockwise and anticlockwise beams to couple together; this results in a zero beatnote for nonzero rotation. The magnitude of lock-in is defined as one-half the deadband around zero rate. Typical values may range from 0.1deg/hr to 15deg/hr. In order to avoid this deadband and nonlinear performance region, Sperry uses the optical bias mirror principle, while Honeywell uses a mechanical dithering in the order of 250-500Hz depending on the type of gyro. Another promising principle of avoiding this deadband is Raytheon's four-frequency or multioscillator ring laser gyro. Unlike the Sperry or Honeywell laser gyros, this laser gyro uses four beams in the same triangular cavity. The artificial bias is removed through a logic algorithm which may be either implemented in the software or hardware. Another error source or problem encountered in laser gyros is scale factor changes due to mode pulling and pushing effects. It might be pointed out that the two key parameters that describe the laser gyro's performance are drift and scale factor.

Laser gyros exhibit random noise caused primarily by laser noise, and is present in the gyro data as a random white noise frequency modulation of the gyro pulse train output. The noise will be reduced in amplitude dependent upon the integration time used for data averaging, and is proportional to $1/\sqrt{\Delta T}$ where ΔT is the period of the sample in hours. Therefore, random noise is constant, but its effect on the data varies according to the sample period. Data shows that the noise level increases with more rapid sampling. Another type of noise that can limit the laser gyro performance is the so-called quantization error caused by the use of readout schemes that count only integral output pulses. However, this error source is not a fundamental error, since it can be circumvented by the use of more sophisticated readout schemes. The following Companies are engaged in laser gyro development: Autonetics, Honeywell, Litton, Singer-Kearfott, and Sperry Gyroscope. As of this writing, Honeywell and Sperry have laser gyro production capability. In summary, the ring laser gyro is an ideal inertial rotation sensor for strapdown INS applications for the following reasons: 1) it has no moving parts and it is simple in construction, therefore the life expectancy is significantly longer than conventional gyros yielding a much higher reliability, 2) it is insensitive to accelerations, 3) it is a rugged instrument, 4) it has a wide dynamic range, 5) it has excellent parameter stability, 6) its output is in digital form, resulting in much simpler interface with microprocessors and airborne computers, 7) it is insensitive to thermal gradients, and 8) it is cost-effective.

3. SYSTEM DESCRIPTION

This section describes an Attitude and Heading Reference System (AHRS) which is typical of many systems found in military aircraft. External Doppler radar velocity will be compared to the AHRS calculated values in order to provide damping for leveling loop transients. The function of an AHRS is to determine the orientation of the carrying vehicle relative to a given or known coordinate frame. In particular, the strapdown AHRS considered here measures directly body angular rates and accelerations by means of three ring laser gyros and three single-axis linear accelerometers. These measurements are used to computationally maintain a knowledge of vehicle attitude. Attitude is derived computationally by integrating body rates.

Using a moderately high speed processor, body measurements and attitude can be obtained in any coordinate frame, which may be advantageous in certain applications. In the past, platform AHRS attitude information was derived from gimbal angles. However, body angular rates and accelerations established by this type of system, requires resolvers

and/or computational transformations. Furthermore, these systems have not proved to be cost-effective and reliable. The strapdown approach on the other hand, provides direct measurements of the desired outputs, which are suitable for use in the inner loops of the aircraft flight control system or for use in fire control system, thereby eliminating the requirement for the additional sensors presently in use. Thus, in a strapdown mechanization, the mechanical gimbels are replaced by a computer. Strapdown technology has become possible mainly due to Large Scale Integration (LSI) microelectronics. The advent of microprocessors with their enhanced computational capability, storage, and low cost has made today these systems a reality. Typical AHRS systems presently in use and/or in development using conventional spinning mass gyros are the following: 1) Lear Siegler Inc. Model 6000 Series, 2) Litton LR-80, and 3) Sperry SRS-1000. On January 28, 1980, Sperry Flight Systems started flight testing the SRS-1000 using a SLIC-7 (Sperry Laser Integrated Cluster) in a King-Air aircraft. The results showed that the AHRS system performed well.

The present AHRS is designed as an all-attitude reference system providing roll, pitch, and heading outputs which may be used for display and control inputs to other aircraft systems. Moreover, the AHRS will be MIL-STD-1553 multiplex data bus compatible, which is the data exchange between the AHRS and other avionic subsystems. In other words, the AHRS provides digital outputs via the multiplex data bus, discretes, and analog outputs. Inputs are received as messages via the multiplex data bus and as discretes. The information flow on the data bus comprises messages that are formed by three types of words: command, data, and status. MIL-STD-1553 multiplex data bus is widely accepted and used because: 1) it eases the system design task, 2) defines protocol and format, and 3) facilitates system growth and flexibility without compromising system design. System accuracy requirements are 0.25° rms for true heading and 0.15° rms in pitch and roll. The system is assumed to consist basically of the following Line Replaceable Units (LRU): an Inertial Sensor Assembly (ISA), a microprocessor, a CDU, an Electronics Control Amplifier (ECA), Input/Output electronics, and a Power Supply Unit (PSU). Heading and velocity reference information will be provided by a magnetic azimuth detector and a Doppler radar navigation set respectively. This design concept enhances operational performance, reliability, maintainability, and minimizes the LCC. The ISA will measure incremental changes of attitude ($\Delta\theta$'s) and linear velocity (ΔV 's) relative to three mutually orthogonal body-fixed axes. In the magnetic mode the input to the computer is local magnetic heading [8]. This value is corrected by computed magnetic variation from a stored table to determine local variation. Therefore, in this mode the correction applied to the input value is the current estimate of the compass reference axis orientation with respect to true north. True heading ψ_{TRUE} can be derived by standard techniques, that is, from magnetic heading ψ_{MAG} as measured by the system plus a knowledge of magnetic variation ψ_{MV} for the current location. In addition, true heading can be inputted from the Doppler radar as digital sin/cos data, transformed into a whole angle by the system and outputted as digital or synchro information. Mathematically, the equation for true heading is given by $\psi_{TRUE} = \psi_{MAG} + \psi_{MV}$. True heading is required for navigation. The heading inputs are used as a reference for air alignment and for heading in the Doppler mode. Also, aircraft roll and pitch are supplied for reference purposes and to the Doppler radar as backup antenna stabilization in the absence of inertial measurement pitch and roll outputs. A vertical attitude validity signal is also provided for the pitch and roll output of the AHRS.

The use of Doppler radar navigators in rotary- and fixed-wing aircraft have transitioned from simple dead-reckoning navigation to highly accurate hybrid systems. In its simplest form, a typical Doppler radar navigation system will consist of a Doppler radar set, a heading reference, a navigation computer, and a CDU. Since the navigation accuracy of a Doppler system is dependent on the heading reference, it is important to select a heading reference system that would contribute as small an error as possible. In other words, the heading reference is the major error contributor in such systems. Presently, two types of heading reference systems are available. These are: 1) the magnetic, north-referenced heading system based on a magnetic azimuth detector, and 2) the true north-referenced heading systems based on inertial alignment or gyrocompassing. The advantages or disadvantages of each would depend primarily on mission requirements, performance, reaction time, cost, size, and weight. As was mentioned earlier, a MAD or flux valve will be assumed, since, in addition for the reasons just stated, high accuracy gyrocompassing requires an extremely good knowledge of gyro bias during the period when the earth's measurements are being made. A fifteen-state Kalman filter is included in the software mechanization, which reduces the heading error. The Kalman filter processing will also be used for ground and in-air alignment [6]. The system will be so designed as to transmit a word mode to the CDU and central computer, which identifies the status and availability of specific parameters (e.g., attitude), digital attitude invalid, NAV READY, and control vector acknowledge. A functional block diagram of the proposed system is shown in Fig. 1. The goal of the system's architecture, mechanical, and electrical design will be to provide for an easily assembled and tested low LCC production unit. Ease of maintenance is of paramount importance, therefore the system must be so designed allowing for quick flight line replacement of failed Shop Replaceable Unit (SRU) cards [9]. Moreover, the SRU's will contain individual test connectors for use in isolation to the component level at depot maintenance. The SRU's will interface with the data bus. An AHRS, as part of an INS, provides a backup mode of operation. For example, the C-5A aircraft is equipped with two AHRS systems. In case the INS fails temporarily, the INS automatically switches to this mode. However, it must be point out that the quality of data obtained in this mode would not be as good as the INS itself.

3.1 System Performance

The overall system performance of the proposed system is summarized below:

- Heading accuracy	0.25° (rms)
- Roll and pitch accuracy	0.15° (rms)
- Body rate error	0.02 deg/sec (rms)
- Rate capability	> 75 deg/sec
- Linear acceleration error	0.05 m/sec ² (rms)
- Linear G-capability	> 20 G's
- Reaction time	≤ 2 min.

3.2 Inertial Sensor Description

An assumed set of system error parameters and a set of expected 1-sigma values for these parameters are implicit in the design and system accuracy predictions. These values determine the initial values of the inertial instrument error parameter variance in the operational Kalman filter covariance matrix, and, in part, which parameters should be included in the Kalman filter state vector. The assumed inertial sensors will be compatible with design accuracy goals.

3.2.1 Ring Laser Gyros

The nominal design parameter characteristics of the laser gyros are listed below:

- Bias stability (day-to-day)	0.015 deg/hr
- Bias stability (long term)	0.01 deg/hr/√hr
- Random walk	0.002 deg/√hr
- Scale factor stability	5 ppm (1-sigma)
- Scale factor linearity	5 ppm (1-sigma)
- Scale factor asymmetry	1 ppm (1-sigma)
- Rate	500 deg/sec.

3.2.2 Accelerometers

Linear motion along the three orthogonal axes will be sensed by the accelerometer's seismic mass, which will be converted to an electrical analog signal by the integral rebalance electronics. Therefore, this analog of motion is the useful output of the accelerometer. Temperature compensation of bias and scale factor will be accomplished by an integral thermal sensor, which will be used in the system computer. The performance characteristics of this accelerometer are:

- Bias repeatability	50 μG (1-sigma)
- Random bias	10 μG (1-sigma)
- Scale factor repeatability	0.05% (1-sigma)
- Scale factor	100 ppm (1-sigma)
- Input-Axis alignment	0.1 mrad
- Threshold	1 X 10 ⁻⁵ G

Strapdown accelerometers have a considerable effect on the overall system performance. In particular, accelerometer bias and alignment errors affect the system velocity accuracy. Since in effect, accelerometers measure inertial acceleration minus local gravity field, ring laser inertial navigators must model the local gravitational field and add model gravity values to the accelerometer signals in order to obtain inertial acceleration in the navigation mode. inaccuracies in the modeled value will cause navigation errors.

For a moderate accuracy (1-2 nm/hr) navigation system, gravity can be modeled using earth spheroid model coefficients, which are best suited for the latitude/longitude of operation. Residual uncompensated gravity deflections in the order of 10-20 arcsec will cause significant errors in position and velocity. It might be pointed out that rotary wing aircraft flying Nap-of-the-Earth (NOE) and short ranges, gravity modeling will play no significant role. The gravity model used in most operational systems is based on a gravity model used in most operational systems is based on a gravity field perpendicular to a reference ellipsoid, which approximates the mean sea-level equipotential surface

known as the geoid. However, since the surface of the geoid deviates from the reference ellipsoid, the gravity vector also deviates from the reference ellipsoid. Moderate accuracy navigation systems do not require modeling of the vertical deflection, since this is not a dominant error source, therefore it will not be considered here. A typical gravity model based on the Clarke reference ellipsoid model is given by

$$g = g_0 [1 - \frac{2h}{R_E} + 0.0052884 \sin^2 \lambda]$$

where $g_0 = 32.088222$ (ft/sec²)

h = altitude above the reference ellipsoid

R_E = mean equatorial radius of the earth (=20,926,062 ft)

λ = geographic latitude.

Other more complex gravity error models have been developed, but these are not relevant in this work. Normally, accelerometer pulses are scaled every 5ms and corrected for bias and misalignment every 20 ms.

3.3 Kalman Filter Mechanization

The theory of the Kalman filter has been treated extensively in the literature and will not be repeated here. For the purpose of clarity, only the necessary mechanization equations will be given. For a detailed account of the Kalman filter the reader is referred to [7].

The Kalman filter contains an error model which relates observed errors to each significant error source as a function of time and vehicle dynamics. A fifteen-state filter error model is included in the software mechanization. The state vector consists of the following error states: north velocity, east velocity, vertical velocity, north tilt, east tilt, heading (azimuth), x-gyro drift, y-gyro drift, x-gyro scale factor, y-gyro scale factor, z-gyro scale factor, x-accelerometer bias, y-accelerometer bias, Doppler scale factor, and magnetic heading reference. There are other types of errors that contribute to the overall system accuracy, but these are the major ones. Including more states would only add to the system memory and timing requirements without appreciably increasing the accuracy of the system.

The Kalman filter will be implemented with floating-point arithmetic. The floating-point arithmetic uses 32-bit floating point words consisting of a 24-bit mantissa and an 8-bit signed exponent. The computer program will perform the required error analysis by propagating the covariance matrix of the system state. At any instant of time, the state of the aircraft will be represented by the vector $x(t)$, the components of which represent the aircraft orientation, velocity, etc. The error covariance propagation equations are general matrix equations involving system and filter error model description matrices, noise distribution matrices, output matrices, and system and filter control matrices. These Kalman recursive equations are initialized by specifying the initial filter covariance matrix P_0 . The covariance matrix is a diagonal matrix having elements $P_{0(1,1)}$ through $P_{0(15,15)}$. Since the filter model is completely observable and controllable, the initial value of the covariance matrix P_0 is irrelevant to the steady-state results. However, it may have a minor effect on the filter's transient performance, therefore it has been specified in the simulation. Solution of the state transition, covariance, and gain matrices will be processed at the rate of every 60 seconds. The AHRS Kalman filter used in this study is suboptimal, therefore it is necessary to maintain a real world set of errors with which to compare the Kalman filter covariance matrix in order to ensure filter stability and measure its performance. An important output of the simulation needed for filter design is 1) the real world error standard deviations after being operated on by the filter, and 2) the standard deviations of the Kalman filter covariance matrix. For a proper design, the ratio of the real world filter to the suboptimal filter standard deviations should be near one. The sequence of the covariance matrix computations are summarized below:

1. Propagate the covariance matrix P_i (n:n) according to

$$P_i = \Phi(i,i-1)P_{i-1}\Phi^T(i,i-1) + Q_i \quad (2)$$

2. Calculate the Kalman gain matrix K_i (nxm) according to

$$K_i = P_{i-1}^T(H_i P_i H_i^T + R_i)^{-1} \quad (3)$$

3. Update the covariance matrix according to

$$P_{i+1} = P_i - K_i H_i P_i ; \quad (4)$$

Where $\Phi(i,i-1)$ = state transition matrix for the time period i-1 to i. (nxn)

H_i = measurement matrix (mxn)

R_i = measurement noise covariance matrix (mm)

Q_i = process (or system) noise covariance matrix (nn).

The superscript T denotes matrix transposition. Figure 3 is a flow chart depicting the simulation process.

The process noise covariance matrix Q_i is used to account for unmodeled errors. By proper design of this matrix, the system covariance matrix is made to fit the true prediction of the navigation accuracy. If external observations are made to update the system, the covariance matrix will change accordingly as a result of these updates. Accelerometer error is modeled as a Markovian random process characterized by an autocorrelation function of the form

$$\phi_{x,x}(t, \tau) = \sigma_x^2 e^{-\beta|\tau|}$$

The baseline model for the accelerometers has been chosen to be represented by the first-order stochastic differential equation

$$\dot{d}(t) = -\beta d(t) + \sqrt{2\beta} u(t)$$

where $u(t)$ is a vector of white noise driving functions and the correlation time is $1/\beta$. The solution of this equation is given by the initial conditions and the convolution integral

$$d(t) = d(0)e^{-\beta t} + \sqrt{2\beta} \int_0^t e^{-\beta(t-\tau)} u(\tau) d\tau.$$

The autocorrelation function of $d(t)$ is

$$\phi_{d,d}(t, \tau) = d^2(0)e^{-\beta(2t+\tau)} + 2\sigma_u^2 \int_0^t \int_0^{t+\tau} e^{-\beta(t-x)} e^{-\beta(t+\tau-y)} dx dy$$

$$= d^2(0)e^{-2\beta t} e^{-\beta\tau} + 2\sigma_u^2 \int_0^t e^{-\beta(t-x)} e^{-\beta(t+\tau-x)} dx$$

$$= d^2(0)e^{-2\beta t} e^{-\beta\tau} + \sigma_u^2 [e^{-\beta\tau} - e^{-\beta(2t+\tau)}].$$

For $\sigma_u^2 = \sigma_d^2$ and $d(0) = \sigma_d$,

$$\phi_{d,d}(t, \tau) = \sigma_d^2 e^{-\beta\tau} \quad \text{for } \tau \geq 0.$$

Since the autocorrelation function is an even function, then

$$\phi_{d,d}(t, \tau) = \sigma_d^2 e^{-\beta|\tau|}.$$

The associated power spectral density (PSD) is

$$S(\omega) = \frac{2\tau_c \sigma}{1 + (\tau_c \omega)^2}.$$

Hence, it is seen that an error state described by the above stochastic differential equation, initialized at $d(0) = \sigma_d$ and driven by the white noise $u(t)$ having variance σ_u^2 does indeed generate a Markovian random process having variance σ_d^2 and a correlation time constant equal to $1/\beta$. Therefore, the accelerometer error will be modeled as an exponentially time-correlated noise of the form

$$E[A(t)\Lambda(t+\tau)] = \sigma_A^2 \exp(-|\tau|/T_A) \quad (5)$$

where $E[\cdot]$ is the expected value operator, σ_A is the accelerometer standard deviation, and T_A is the accelerometer time constant. In section 2, it was mentioned that the ring laser gyro error model is considered to be wideband noise with $1/\sqrt{\Delta T}$ behavior where ΔT is the sample time. Wideband noise can be attributed to the frequency fluctuations arising from residual effects preventing complete correlation in the fluctuations of the counter-directed modes. Let $\omega(t)$ represent a white, zero-mean, independent random process. Then, the corresponding autocorrelation is expressed as

$$E[\omega(t_1) \omega(t_2)] = R \delta(t_1 - t_2) \quad (6)$$

$$R = \Delta T \sigma_\omega^2$$

where σ_ω^2 is the variance in the indicated drift rate, $\delta(t_1 - t_2)$ is the Dirac delta function, and ΔT is the time during which the ω 's are computed from the accumulated angle data. This model is mechanized in the covariance analysis program.

The magnetic heading reference error $\Delta\psi_M$ is similarly modeled as a random process [8]. Mathematically, the state equation for this error is of the form

$$\frac{d}{dt} (\Delta\psi_M) = -\frac{1}{\tau_M} \Delta\psi_M + n_M \quad (7)$$

where τ_M is the correlation time constant and n_M is a white noise driver term.

4. STRAPDOWN ALGORITHMS

This section addresses the basic system strapdown algorithms, used during the normal navigate mode, and the compensation terms for the gyros and accelerometers. Since in a strapdown mechanization the accelerometers are not stabilized by a gimbal system, their outputs must undergo a computer coordinate transformation from body (aircraft) coordinates to the earth-referenced (navigation) coordinate frame. Thus, strapdown computation algorithms transform the sensed acceleration from body coordinates into earth-referenced coordinates. One can immediately notice the added computational load imposed on the navigation computer as compared to a conventional gimballed system. Therefore, the designer of the strapdown algorithms must ascertain that any computational errors introduced are within allowable bounds, while at the same time minimizing the time and memory burden on the navigation computer. An efficient solution of strapdown algorithms will consist of: 1) four-parameter (quaternion) attitude representation, 2) a simplified third-order Taylor series attitude integration, 3) orthonormalization of the attitude matrix, 4) Coriolis rotational corrections to body velocity increments, and 5) double precision arithmetic. The outputs from the inertial sensors must be pre-processed in order to be in acceptable format for the computer. The basic algorithm may be expressed as follows:

$$\int_t^{t+\Delta t} A_N d\tau = \int_t^{t+\Delta t} C \cdot A_B d\tau \quad (8)$$

where A_N is a 3×1 vector of accelerations in the navigation frame, A_B is a 3×1 vector of accelerations in the body frame, and C is a 3×3 transformation matrix from body to the earth-referenced frame. The transformation from body axes to the earth-referenced or navigation frame is accomplished by successive rotations and is given by the equation

$$\underline{x}_N = \begin{bmatrix} C(1,1) & C(1,2) & C(1,3) \\ C(2,1) & C(2,2) & C(2,3) \\ C(3,1) & C(3,2) & C(3,3) \end{bmatrix} \underline{x}_B = [C]_B^N \underline{x}_B \quad (9)$$

where the elements of the transformation matrix C are as follows:

$$\begin{aligned} C(1,1) &= \cos\psi\cos\theta \\ C(1,2) &= -\sin\psi\cos\phi + \cos\psi\sin\theta\sin\phi \\ C(1,3) &= \sin\psi\sin\phi + \cos\psi\sin\theta\cos\phi \\ C(2,1) &= \sin\psi\cos\theta \\ C(2,2) &= \cos\psi\cos\phi + \sin\psi\sin\theta\sin\phi \\ C(2,3) &= -\cos\psi\sin\phi + \sin\psi\sin\theta\cos\phi \\ C(3,1) &= -\sin\theta \\ C(3,2) &= \cos\theta\sin\phi \\ C(3,3) &= \cos\theta\cos\phi \end{aligned}$$

Corrections required to maintain alignment between the body and earth-referenced frames are inputs to the gyro drift estimator. The heading ψ is defined as the angle of the aircraft velocity vector measured relative to north (i.e., clockwise from north). A positive heading will correspond to a positive rotation about the z-axis. From the above relationships, aircraft attitude is given by

$$\begin{aligned} \theta &= -\arcsin C(3,1) \\ \psi &= \arctan(C(2,2)/C(1,1)) \\ \phi &= \arctan(C(3,2)/C(3,3)). \end{aligned}$$

Figure 2 shows the aircraft (body) axes orientation. These are the axes which the gyro input axes point. Next, consider the Euler (quaternion) parameter conversion to direction cosines. This operation converts the accurately determined aircraft attitude from the Euler parameter form to the direction cosine matrix form, and subsequently use this result to correct the attitude direction cosine matrix. However, before this operation is performed, an approximate incremental direction cosine integration operation of 100 times per second must be carried out. The accuracy of the direction cosine matrix will be maintained by a periodic update rate of 25 times per second by a direction cosine matrix formed from an accurate quaternion integration of the gyro input angle increments. In other words, gyro sensed angular rates when integrated over a short period of time, provide angular increments ($\Delta\theta$'s) in the body's coordinate system. Therefore, the calculations to be performed are:

$$\begin{bmatrix} b_{i1} \\ b_{i2} \\ b_{i3} \end{bmatrix}_{n+1} = \begin{bmatrix} 1 & \Delta\theta_3 & -\Delta\theta_2 \\ -\Delta\theta_3 & 1 & \Delta\theta_1 \\ \Delta\theta_2 & -\Delta\theta_1 & 1 \end{bmatrix} + \begin{bmatrix} b_{i1} \\ b_{i2} \\ b_{i3} \end{bmatrix}_n \quad (10)$$

where $\Delta\theta_i$ ($i=1,2,3$) are the gyro angular increments and b_{ij} ($i,j=1,2,3$) is the direction cosine matrix obtained from the Euler parameters to direction cosines operation every iteration. The next step required in this procedure is the Euler parameter integration operation. Specifically, the purpose of this operation is to integrate the measured aircraft angular motion, which has been corrected for gyro bias and transformed into the body axes (i.e., roll, pitch, and yaw) coordinate system, to produce an accurate current attitude of the aircraft. From the above discussion, the body attitude information is stored in the direction cosine matrix [B], which obeys the familiar differential equation

$$\dot{B} = [B]\Omega \quad (11a)$$

where Ω is a skew-symmetric matrix formed from the body angular rates. The direction cosine attitude matrix [B], is expressed in terms of the Euler parameters and is given by the well-known equation [4], [11]

$$[B] = \begin{bmatrix} A^2-B^2-C^2+D^2 & 2(AB-CD) & 2(AC+BD) \\ 2(AB+CD) & -A^2+B^2-C^2+D^2 & 2(BC-AD) \\ 2(AC-BD) & 2(BC+AD) & -A^2-B^2+C^2+D^2 \end{bmatrix} \quad (11b)$$

where $A^2+B^2+C^2+D^2 = 1$ satisfies an exact set of Euler parameters of an orthogonal matrix. The A, B, C, and D parameters are updated using the incremental angles as measured by the laser gyros at an update rate of 100 per second. The primary purpose of computing this direction cosine attitude matrix is to transform the velocity increments along the earth-referenced coordinate frame. Thus, the transformation of velocity increments from body coordinates to the earth-referenced coordinate frame is obtained from

$$\begin{bmatrix} \Delta V_N \\ \Delta V_E \\ \Delta V_D \end{bmatrix} = [B] \begin{bmatrix} \Delta V_{Xc} \\ \Delta V_{Yc} \\ \Delta V_{Zc} \end{bmatrix} \quad (11c)$$

Finally, an expression is needed for the selected earth-referenced coordinate frame (i.e., horizontal north, horizontal east, and vertical down) angular rates with respect to inertial space. Since the laser gyros measure angular increments of the aircraft body with respect to inertial space, this expression takes the form

$$\begin{bmatrix} \Delta\theta_{b1} \\ \Delta\theta_{b2} \\ \Delta\theta_{b3} \end{bmatrix} = [B]^{-1} \cdot \frac{\Delta T}{2} \begin{bmatrix} \omega_N \\ \omega_E \\ \omega_D \end{bmatrix} \quad (12)$$

The angular rates of this coordinate frame are given by

$$\begin{aligned} \omega_N &= \Omega_E \cos L + \frac{V_E}{R_p + h} \\ \omega_E &= -\frac{V_N}{R_m + h} \\ \omega_D &= -\frac{V_E}{R_p + h} \tan L - \Omega_E \sin L \end{aligned} \quad (13)$$

where Ω_E = earth rate ($= 7.291151 \times 10^{-5}$ rad/sec)

V_N, V_E = north and east velocity components

R_m = earth's radius in the meridian plan

R_p = earth's radius in the parallel plan

h = aircraft altitude

L = latitude

Δt = computation cycle time ($= 1/20$ sec).

For small increments of time, one can write the velocity algorithm as follows:

$$\Delta V_N(t + \Delta t) = C(t + \Delta t) \Delta V_B(t + \Delta t). \quad (14)$$

The ΔV 's are then accumulated to update the navigation frame velocities

$$V_N(t + \Delta t) = V_N(t) + \Delta V_N(t + \Delta t). \quad (15)$$

The digitized gyro data serves as a reference for the accelerometers for providing angle rate information. Consequently, this angular rate information is used to build a coordinate transformation matrix or direction cosine matrix. Continued updating of this direction cosine matrix enables the acceleration pulses, that is, increments of velocity (ΔV 's), to be resolved into the navigation computational frame. These velocity increments are then accumulated in the standard navigation frame as north, east, and vertical down velocities. Since in the present study latitude and longitude are not required outputs, they can be easily generated and allow for continuous updating of magnetic variation from a stored table. Navigation is accomplished in this standard, north-slaved, velocity-damped mechanization, with the direction cosine matrix being periodically orthonormalized.

Inertial sensor compensation is provided as follows: 1) the gyro data must be corrected for bias (or fixed drift) and scale factor, and 2) the accelerometer information must be corrected for bias, scale factor, misalignments, and nonorthogonalities. The quantization requirement for the gyro output pulses has been determined to be 0.5 sec/pulse. In the simplest form, the system computations that includes the Doppler radar velocity components and compensates for Coriolis effects and accelerometer bias are given below:

$$V_N = V_N + A_{Bx} \Delta t - 2 \Omega_E V_E \sin L \Delta t - K(V_N - V_{DN}) \Delta t \quad (16)$$

$$V_E = V_E + A_{By} \Delta t - 2 \Omega_E V_N \sin L \Delta t - K(V_E - V_{DE}) \Delta t \quad (17)$$

where V_N, V_E = north and east velocities

A_{Bx}, A_{By} = x- and y-accelerometer bias in body frame

K = damping gain.

These computations are corrected at each Kalman filter cycle.

Strapdown inertial navigation systems exhibit what is known as "coning" motion errors. Coning is a simultaneous sinusoidal motion in two axes and 90° out of phase with each other. Specifically, coning errors exist only when the frequency of coning motion falls into the range that is outside the computational bandwidth and inside a gyro's servo bandwidth. In the latter case, the gyro is insensitive to the coning inputs, therefore no errors are present. Coning errors affect the gyro scale factor and linearity. In strapdown systems using mechanically dithered ring laser gyros, this effect is more pronounced, in that errors from one gyro couple into the other.

5 SOFTWARE

The software design is general and performs the tasks necessary to provide outputs of aircraft attitude and other navigation information as required. These tasks are performed by:

- Providing multi-task real-time control, program initialization, interrupt handling, and task scheduling.
- Performing status monitoring and mode sequencing.
- Providing rapid reaction alignment.
- Performing navigation operations and calibration.
- Performing software control and providing the necessary addressing, formatting, and memory access demanded by the 1553 multiplex data bus.
- Processing steering data relative to controlling output aircraft indicators, and providing steering data for display.
- Performing self-test operations.

During program initialization, the operating system performs power-on bit and initializes the operating system routines. Preliminary results indicate that input/output information can be handled by the system at the following rates: a) angular rate and acceleration-10ms, d) Doppler velocity-7.5Hz, c) magnetic heading compensation-20ms, and d) aircraft pitch, roll, and yaw - 20ms. Final values will be established in the overall software package.

6. CONCLUSIONS

It is well known that strapdown mechanizations replace substantial portions of the high cost, low reliability, electromechanical components or conventional gimbaled navigation systems with low cost, high reliability electronics. Also, strapdown systems provide significant improvement in maintainability, flexibility, and reduction in life-cycle-cost. The objectives of the system design were to:

- Minimize hardware complexity, thus enhancing the reliability and reducing maintenance actions.
- Low cost (in the order of \$40K - \$45K).
- Hardware commonality.
- Simplicity of design and mechanization by using modular hardware.

A strapdown AHRS utilizing ring laser gyro will meet the stated objectives. Moreover, the successful realization of such a system is based on optimal filtering and estimation theory.

REFERENCES

- [1] Aronowitz, F., "The Laser Gyro," in *Laser Applications*, Vol. 1, Academic Press, N.Y., 1971, pp. 133-199.
- [2] Coccoli, J.D., and Helfant, S.B., "The Intrinsic Stability of Laser Gyro Scale Factor," *NAECON '78*, Dayton, Ohio, 16-18 May 1978, pp. 574-582.
- [3] Kubbat, W.J., "Application of Strapdown Inertial Navigation to High Performance Aircraft," *NATO AGARD Lecture Series No. 95, "Strap-Down Inertial Systems,"* June 1978, pp. 7-1 to 7-16.
- [4] Levinson, E., "Laser-Gyro Strapdown Inertial System Applications," *NATO AGARD Lecture Series No. 95, "Strap-Down Inertial Systems,"* June 1978, pp. 6-1 to 6-48.
- [5] Morrison, R.F., Levinson, E., and McAdory, R. "The SLIC-15 Laser Gyro IMU for Mid-Course Missile Guidance," *Proceedings of the National Aerospace Symposium of the Institute of Navigation*, April 1976.
- [6] Reddy, P.B., "Laser Gyro Strapdown System Alignment/Calibration and Land Navigation Using Kalman Filters," *NAECON '80*, Dayton, Ohio, 20-22 May 1980, pp. 92-99.
- [7] Sage, A.P., and White, C.C., "Optimum Systems Control," 2nd Edition, Prentice-Hall Inc., N.J., 1977, pp. 230-247.
- [8] San Giovanni, C. Jr., "Performance of a Ring Laser Strapdown Attitude and Heading Reference for Aircraft," *AIAA Guidance and Control Conference*, Palo Alto, California, 7-9 August 1978, pp. 12-19.
- [9] Savage, P.G., "Laser Gyros in Strapdown Inertial Navigation Systems," *IEEE Position Location and Navigation Symposium*, San Diego, California, November 1976, pp. 1-30.
- [10] Siouris, G.M., "The Ring Laser Gyroscope: A State-of-the-Art Inertia Sensor," *Proceedings of the DGON Symposium on Gyro Technology*, Stuttgart, Germany, 28-29 September 1977, pp. 6.0-6.26.
- [11] VanBronkhorst, A., "Strapdown System Algorithms," *NATO AGARD Lecture Series No. 95, "Strap-Down Inertial Systems,"* June 1978, pp. 3-1 to 3-22.

ACKNOWLEDGMENT

The author wishes to thank Mr. H. Dale Little, Common Avionics Division Chief, and Mr. Robert Spaulding, Acting Branch Chief, for their keen interest and constructive criticism of this work. Also, he wishes to thank Dr. R. John Niemela and Mr. Stanley Sokolowski of the U.S. Army Avionics R&D Activity, Ft. Monmouth, New Jersey, for the many invaluable discussions on strapdown AHRS systems. Finally, he would like to thank Ms. Judy Elliott for the skillful typing of this paper.

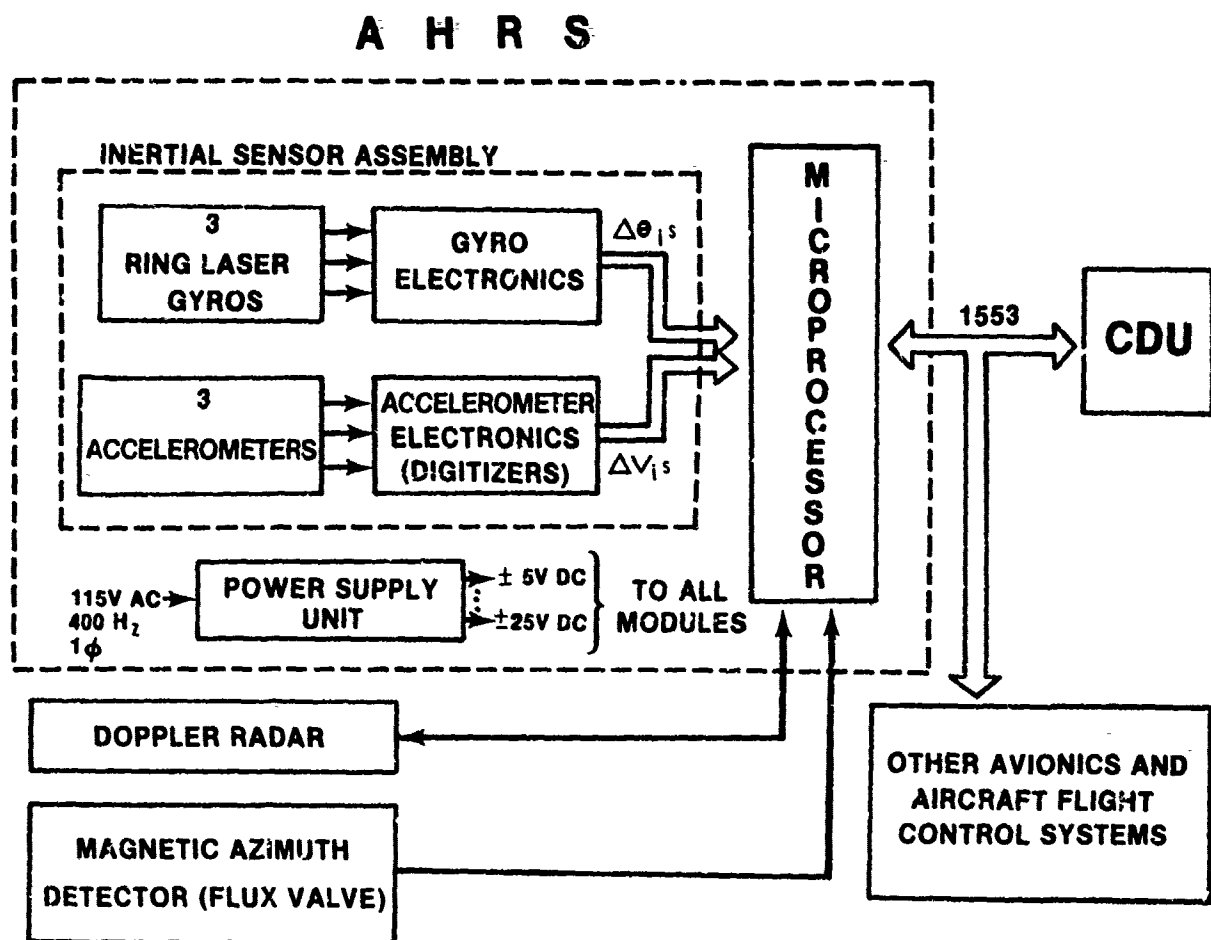
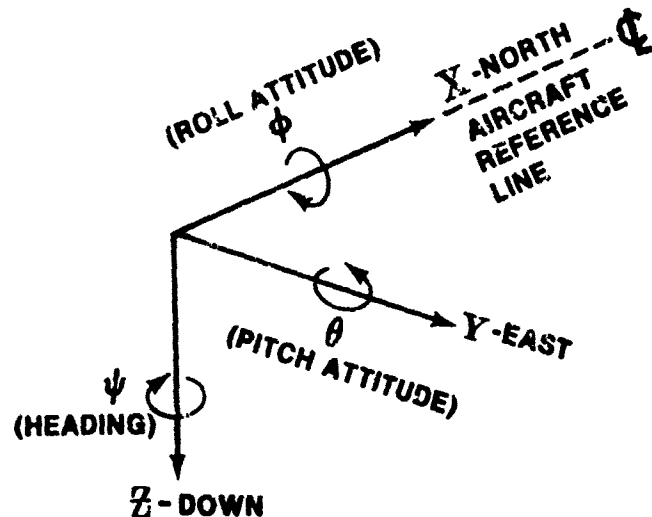


Figure 1. Proposed RLG AHRS Configuration



AIRCRAFT ATTITUDE:

$$\theta = \arcsin C(3,1)$$

$$\psi = \arctan (C(2,2)/C(1,1))$$

$$\phi = \arctan (C(3,2)/C(3,3))$$

Figure 2. Aircraft Axes Orientation

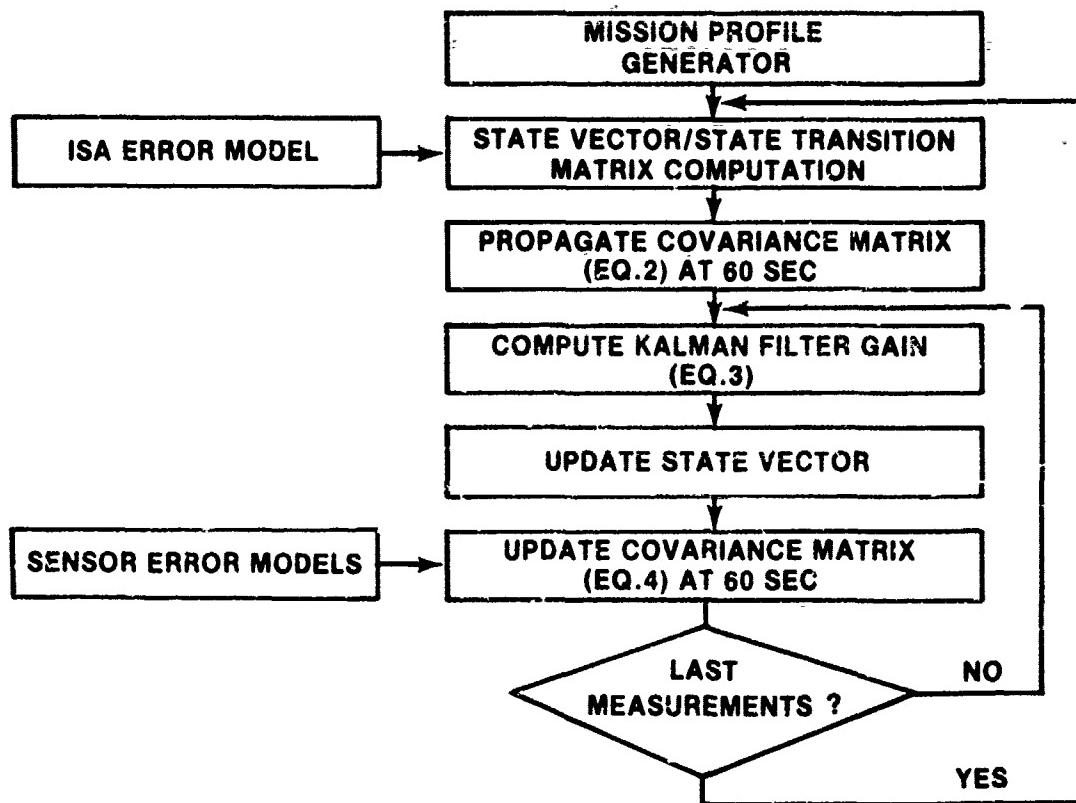


Figure 3. Strapdown Covariance Analysis Simulation Flow Diagram

SMART INERTIAL MEASUREMENT UNITS AND THE COMPENSATION OF DYNAMICALLY TUNED GYROS
FOR STRAIDOWN INERTIAL SYSTEMS

by

C. S. EDWARDS AND R. J. CHAPLIN
BRITISH AEROSPACE
Precision Products Group
Six Hills Way
Stevenage
Herts SG1 2DA
U.K.

SUMMARY

This Paper considers the growth of low cost Strapdown Inertial Guidance Systems that has occurred in recent years. For the majority of current applications the only gyroscopes that are sufficiently mature for such systems are the Rate Integrating Gyro and the Dynamically Tuned Gyro. It is often thought that the error models of these two gyroscopes are very different and that it is more difficult to use the Dynamically Tuned Gyroscope. The Paper shows that such impressions are misconceived and that both types of gyroscope are being offered in packages complete with digital compensation of the error terms.

1. INTRODUCTION

Until about five years ago there was little demand for a rate gyroscope with a performance in the range 0.5 to 10 degrees per hour. When many new applications started to appear requiring instruments of this performance new gyroscopes had to be developed.

There were three possible approaches:-

- 1) Improve the conventional rate gyro designs.
- 2) Adapt Inertial Navigation Sensors - especially those of the Strapdown variety.
- 3) Use a new technology.

In 1980 it is the sensors derived from Inertial Navigation that are most in demand though this will possibly change in 5 - 10 years when new technologies such as the Fibre Optic Gyro become sufficiently well proven to be accepted as a sensor in a particular mission.

The two most common sensors are the Strapdown Rate Integrating Gyro and the various two degree of freedom dry gyros, typified by the Strapdown Dynamically Tuned Gyro.

The purpose of this Paper is three fold. Firstly to compare in a unified manner the two main gyroscope types and to show how similar their error models are.

Secondly to demonstrate how the unwary can be deceived when evaluating these gyros on the assumption that they are 'just better rate gyros'.

Thirdly the Paper describes the developments that are taking place in which the system user is offered a complete package with all the necessary electronics and with sufficient computing ability to compensate for the inevitable sensor errors in a gyro of this performance.

The Paper concludes with a brief description of the hardware being developed by British Aerospace at their Precision Products Group in Stevenage. This includes two types of Dynamically Tuned Gyroscopes and a complete package - The Smart Inertial Measurement Unit or SIMU.

2. NEW REQUIREMENTS FOR LOW GRADE INERTIAL NAVIGATION

Third generation short range tactical missiles, point defence missiles and air to air missiles are demanding an overall increase in the accuracy of their guidance systems. The missiles have to be more autonomous, have an increased stand off range, require improved homing head pointing accuracies and have to arrive at the target with improved CEP's (Circle Error Probabilities). A logical solution to this requirement is to use a strapdown mid-course navigation system which has the ability to provide angular rate and acceleration data for autopilot stabilisation, attitude data for homing head pointing, as well as distance gone and velocity data. As will be seen such solutions imply a rate gyroscope with a performance of typically $5^\circ/\text{hr}$. This should be compared with conventional Inertial Navigation Systems which require rate sensors with a bias stability, in most cases better than $0.01^\circ/\text{hour}$, with $0.1^\circ/\text{hour}$ acceptable in some aided systems. Other applications requiring rate gyroscopes such as line of sight stabilisation, both for optical sights and homing heads, used gyros with much lower performance. Thus only a short time ago the development of rate sensors had tended to

be concentrated into two classes. The first being 0.1°/hour or better for use in inertial navigation and the second, 100°/hr to 1000°/hr for use in autopilot stabilisation. Any application in the middle of these two, i.e. with bias of 1 to 10°/hour had generally been designed using two degree of freedom position gyros.

The constraints imposed by the size, weight, reliability and overall performance make the strapdown mechanisation an obvious choice. It does however put considerable demands on the inertial sensors, particularly the gyro. A typical environment for a rate gyro is shown in Table 1. The gyro has to measure these very high rates and at the same time have a bias stability and scale factor accuracy to meet the mid course guidance specification.

PHASE	TYPICAL RATE Rad/sec.
Launch	4
Mid Course	1
Terminal	10

TABLE 1. TYPICAL RATE PROFILE FOR AN AIR LAUNCHED MISSILE

Demands on the accelerometer are not so stringent and existing force feedback accelerometers can meet the required specification. Development is in progress to provide accelerometers with the required performance at a lower price to give sensible overall life cycle costs.

In order to quantify the sensor requirements that have been introduced, typical specifications have been produced (Table 2). The first specification relates to a hypothetical short range, short time of flight missile at the lower performance end of the applications considered. The second is for a long range medium flight time missile of moderate performance.

PARAMETER	TYPICAL SPECIFICATIONS	
	1.RANGE 30 KM	2.RANGE 500 KM
<u>RATE SENSORS PLUS READ OUT</u>		
Full Scale Range °/Sec		
Continuous	+200	+120
Short Term	±500	±250
Zero Stability °/hr 1 sigma (over temperature range)	70	2 - 10
Mass Unbalance °/hr/g 1 sigma	36	2 - 5
g^2 Sensitivity °/hr/ g^2 1 sigma	0.5	0.2
Scale Factor Accuracy (% of specified value)	0.5	0.1
Scale Factor Linearity(% of applied rate)	0.3	0.01
Cross Coupling (% of applied rate)	0.3	0.05
Minimum Loop Bandwidth Hz	100	50
<u>ACCELEROMETER PLUS READ OUT</u>		
Full Scale Range g	±60	±30
Zero Stability mg (over temperature range)	25	1
Scale Factor Accuracy(% of specified value)	0.5	0.1
Scale Factor Linearity(% of applied acceleration)	0.5	0.3
Minimum Bandwidth Hz	80	30 - 100
<u>GENERAL REQUIREMENTS</u>		
Orthogonality of Instruments (mR)	2	1
Readiness Time (Secs)	2	10
Environmental Temperature °C	-40 to +80	-40 to +80

TABLE 2. TYPICAL INERTIAL SENSOR SPECIFICATIONS

3. POSSIBLE INERTIAL SENSORS

The development of inertial sensors for strapdown applications (reference 1) has progressed considerably in the last decade. The gyros, listed in Table 3, have been developed to provide instruments which have the required bias stability and scale factor accuracy for use in the wide dynamic range environment encountered in the strapdown system. Some of the gyro designs have been based on conventional platform sensors. Others have used new techniques more applicable to the strapdown mechanisation.

It is clear that the rate integrating gyro, the dynamically tuned gyro and the ring laser gyro will be the rate sensors considered for use in strapdown mid course guidance systems at the present time and for the immediate future. Although it is likely a laser gyro will eventually replace the conventional spinning mass gyro in the majority of these applications, the exact time frame is not clear. For the immediate future therefore, only the rate integrating gyro and the dynamically tuned gyro are available. These gyros have their relative advantages and disadvantages and a review of their operating principles and error models is useful in establishing the choice of rate sensor.

SENSOR TYPE	FEATURES
RATE INTEGRATING GYRO (RIG)	<ul style="list-style-type: none"> - Single axis gyro, used as a rate gyro - Uses proven techniques - In quantity production
THE DYNAMICALLY TUNED GYRO (DTG)	<ul style="list-style-type: none"> - Two axis free gyro, used as a rate gyro - Uses proven techniques - Demonstrated performance suitable for strapdown applications
THE RING LASER GYRO (RLG)	<ul style="list-style-type: none"> - Single axis rate gyro - Designed for strapdown applications - Quantity production just beginning
THE ELECTROSTATIC SUSPENDED GYRO (ESG)	<ul style="list-style-type: none"> - Two axis attitude gyro available in both platform and strapdown versions - Angular rate data not available directly
OTHER SOLID STATE RATE SENSORS i.e. THE FIBRE OPTIC LASER RATE	<ul style="list-style-type: none"> - Single axis rate sensor - In early development - Potentially a small solid state sensor suitable for missile applications

TABLE 3. STRAPDOWN GYROS

4. COMPARISON OF THE RATE INTEGRATING GYRO AND THE DYNAMICALLY TUNED GYRO

4.1 The Rate Integrating Gyro (RIG)

The rate integrating gyro was developed for platform use where it was used as a position gyro as its output is the integral of the input angular rate. For strapdown use it is used in a rate mode, but the name "rate integrating" is retained.

The gyro has a long production history and numerous types have been manufactured spanning an accuracy range of better than 0.001°/hour to that of typically 1°/hour currently available from the miniature versions. An example is shown in Figure 1 and it can be seen that the instrument consists of three main assemblies; a cylinder containing the gyro rotor and spin motor (usually called the float), an angle pick-off, and an electrical torque motor. The float is supported in a precision suspension system and the small gap between the cylinder and case is filled with a high viscosity fluid. This provides a means of supporting the float at neutral buoyancy and provides viscous damping to resist the relative motion between the float and the gyro case. It is this viscous damping which provides the integration function. The angle pick-off measures the relative float to case position and the electrical torque motor allows precise torques to be applied to the float assembly. A bellows assembly is included to allow for fluid expansion with changes in temperature. Power to the gyro spin motor is via miniature flex leads.

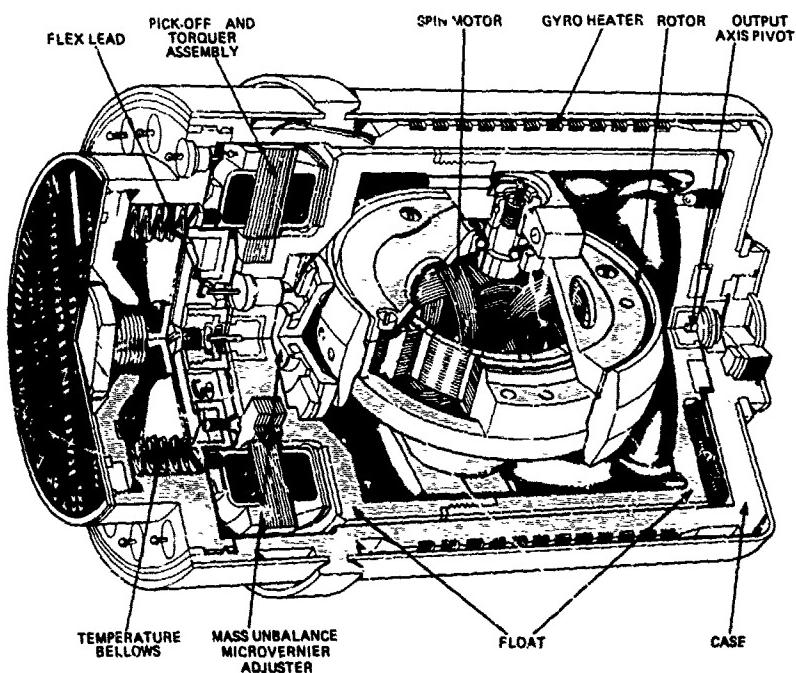


FIGURE 1. THE RATE INTEGRATING GYRO

It is well known that the rate integrating gyro has demonstrated its capabilities as a reliable gyro for all platform applications. The many years of production have provided a technology which is well understood but is rather complex and certain processes require extremely delicate and careful quality control if the performance requirements are to be achieved. For example, the quality of the spin motor bearings and the degree of lubrication have to be tightly controlled if the mass centre stability requirements are to be met. Additionally the construction of the gyro means that it has to be completely assembled and sealed before any actual gyro testing can be carried out. This makes production re-work expensive.

When used in the strapdown configuration, the float is maintained at the null position by an external servo loop between the pick-off and torque motor. The current flowing in the torquer is a measure of the angular rate applied to the gyro.

To cope with the considerably higher body rates encountered in the strapdown mode and at the same time maintain the bias errors associated with navigation applications, the original platform gyros have had to be modified. Firstly far stronger torque motors have been fitted to enable the float to be precessed at the maximum input rate. Secondly, as we shall see, strapdown usage requires considerably better definition of the float axis and this gives rise to considerable design constraints if the friction levels are not to become unacceptably high.

When used as a rate integrating gyro it has to be maintained at an accurate temperature if the correct gyro characteristics are to be achieved. For a strapdown rate gyro various techniques have been adopted to provide mechanical compensation and it is only for the higher performance applications that the gyro has to be maintained at an accurate temperature.

The single axis strapdown rate integrating gyro has to cope with a completely different and far more demanding environment from that encountered in the low rate platform application. For example, the gyro must have the ability to accurately measure small rates about the input axis in the presence of extremely high rates being applied about the output axis. The gyro however has been developed to cope with the strapdown environment and instruments are available from established production lines to meet existing and future requirements.

4.2 The Dynamically Tuned Gyro (DTG)

Although the principle of dynamic tuning was demonstrated some 30 years ago, it is only in recent years that the dynamically tuned gyro (reference 1) has been fully developed. The dynamically tuned gyro, Figure 2, can be considered simply as an electric motor driving a sensitive element, with provision for rotor-to-case angle measurement and torque application to the rotor. In the most common mechanisation the rotor is driven through a Hooke's joint type of suspension. The axis elements of this joint are torsion springs or flexures. The torques applied to the rotor by these elements are reduced by a "negative spring torque" generated as a result of the dynamic effect of the intermediate member of the Hooke's joint, called the gimbal. The dynamic spring effect varies as the square of rotor speed, and the

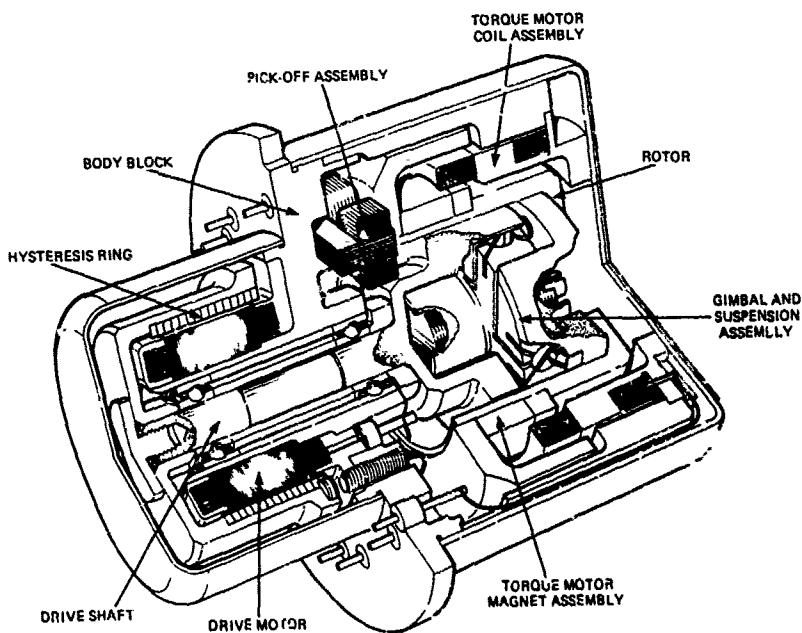


FIGURE 2 THE DYNAMICALLY TUNED GYROSCOPE

unique speed at which the positive spring torques are cancelled by the dynamic effect is called the tuned speed. At this tuned speed the rotor is angularly decoupled from the shaft, and so the instrument acts as a free gyro. Due to damping torques associated with the suspension and rotor drag the angular decoupling is not perfect and a residual elastic restraint is present. The magnitude of this elastic restraint restricts the useful angular range and it is necessary to use the gyros in a feedback loop.

The dynamically tuned gyro is now fully developed and has been in production for many years for use in platform systems. Considerable development has been undertaken to produce a sensor which is comparable in size to the miniature rate integrating gyro, if not smaller, and which has a performance suitable for the new mid-course guidance requirement.

The basic construction of the dynamically tuned gyro is very simple. The instrument consists of three major assemblies; the body block containing the spin motor windings and the pick-off coil assembly, the rotor and torque motor magnet together with the suspension, and finally the case and torque motor coil assembly. The absence of flotation fluids means that the gyro can be easily built and the basic performance quickly established.

In common with the rate integrating gyro the strapdown dynamically tuned gyro has been developed from techniques used in the low rate platform gyro. The major change is the introduction of a far more powerful torque motor in order to precess the rotor at the maximum input rate. Torque motor designs are somewhat more difficult than for a rate integrating gyro since one component has to be mounted on the rotor (rather than a static gimbal). High power magnet materials such as Samarium Cobalt have generally been used to provide an efficient motor but unfortunately they have a poor temperature coefficient.

There are significant advantages for the dynamically tuned gyro when compared with its rate integrating equivalent. There are fewer parts, it has a fluid free suspension, no flex lead torques, simplified spin motor bearing design and a faster warm up characteristic. The gyro is also truly two axis and has demonstrated its ability to measure small body rates around one input axis in the presence of high rates around the second axis. These advantages are to some extent offset by some of the dynamic errors associated with the suspension and by the fact that the torque magnet is on the rotating element.

In summary there is considerable potential for the dynamically tuned gyro and it provides an alternative to the miniature rate integrating gyro in future medium performance missile strapdown navigation systems.

4.3 Comparison of Error Models

Both the rate integrating gyro and the dynamically tuned gyro are used in the torque rebalance mode as rate sensors when used in strapdown systems. In this configuration the torque motor currents are a measure of the angular rates applied to the gyro body. The total current flowing is proportional to the applied rate but is affected by several errors.

To be able to classify these errors and therefore be able to establish the amount of real time error compensation required for each gyro or application, it is necessary to study their error models.

The analytical analysis of the rate integrating gyro and the dynamically tuned gyro has been covered in considerable detail many times. For the purposes of this comparison the input/output equations developed by Savage (reference 1) are used with a modified notation for the rate integrating gyro to present each error model in similar terms.

The actual notation used is given in Table 4 and the axis definitions used are as follows:-

RATE INTEGRATING GYRO

x = input axis (IA)
y = output axis (OA)
z = spin axis (SA)

DYNAMICALLY TUNED GYRO

x = input axis 1
y = input axis 2
z = spin axis

For both gyros xyz form a right handed set. It is therefore to be expected that the x axis of both gyro error models will be somewhat similar while that of the y input axis of the dynamically tuned gyro will differ in some terms since the axes set yxz form a left handed set. Therefore in this comparison, the following discussion concentrates on the x axis.

Using this notation, the torquer demand rate ω_{Tx} for the rate integrating gyro is:-

$$\begin{aligned}\omega_{Tx} = & (1 + \epsilon_x) \left\{ \left(1 + \frac{\delta_{wr}}{\omega_{ro}} \right) \omega_x + \gamma_z \omega_y - (\gamma_y + \theta_y) \omega_z \right. \\ & + \frac{J-I}{H_0} \omega_x \omega_z - \frac{I_y}{H_0} (\dot{\omega}_y + \ddot{\theta}_y) \\ & \left. - C_{H_0}^{\dot{\theta}_y} \right\} + \omega_{Bx}\end{aligned}$$

There are two coupled equations for the dynamically tuned gyro and they can be written so that the major terms occur in the same order as the above equation.

$$\begin{aligned}\omega_{Tx} = & (1 + \epsilon_x) \left\{ \left(1 + \frac{\delta_{wr}}{\omega_{ro}} \right) (\omega_x + \dot{\theta}_x) + \gamma_z \omega_y - (\gamma_y + \theta_y) \omega_z + \beta_{xy} \omega_{Ty} \right. \\ & + \frac{J-I}{H_0} (\omega_x + \dot{\theta}_x) \omega_z - \frac{I_y}{H_0} (\dot{\omega}_y + \ddot{\theta}_y) \\ & \left. - \frac{\theta_y}{H_0} (\Delta K_x - 2 I_G \omega_{ro} \delta_{wr}) + \frac{\theta_x}{\tau} \right\} + \omega_{Bx}\end{aligned}$$

$$\text{and } \omega_{Ty} = (1 + \epsilon_y) \left\{ \left(1 + \frac{\delta_{wr}}{\omega_{ro}} \right) (\omega_y + \dot{\theta}_y) + \gamma_z \omega_x - (\gamma_x + \theta_x) \omega_z + \beta_{yx} \omega_{Tx} \right. \\ \left. + \frac{J-I}{H_0} (\omega_y + \dot{\theta}_y) \omega_z + \frac{I_x}{H_0} (\dot{\omega}_x + \ddot{\theta}_x) \right. \\ \left. - \frac{\theta_x}{H_0} (\Delta K_y - 2 I_G \omega_{ro} \delta_{wr}) + \frac{\theta_y}{\tau} \right\} + \omega_{By}$$

The right hand sides of these 3 equations are the torques experienced by the sensitive element of the gyro, expressed as equivalent precession rates and allowing for the torque motor errors ϵ . Thus ω_{Tx} and ω_{Ty} are the signals that need to be applied via the torque motor to null these torques. In practice of course the controlling currents are generated via servo or rebalance loops which null the pickoff signals θ_x and θ_y . This particular method of analysis omits an important class of errors, the so called coning errors. In the rate integrating gyro these always occur when the input axis of the gyro sweeps out a solid angle. This effect occurs at all frequencies of the coning motion. For the dynamically tuned gyro similar effects only occur when the gyro is used in a rebalance mode, and then only if the coning motion occurs at a frequency within the bandwidth of the loops.

To continue the comparison, inspection of these equations shows they consist of the same error coefficients for anisoinertia, y axis ("output axis") inertia, rotor speed error and axis misalignment terms. However it should be pointed out that for the rate integrating gyro the spin axis inertia J is not a constant but varies as the frequency of the spin axis inertial rate ω_z due to the finite bandwidth of the hysteresis motor used to drive the rotor.

The notable omissions in these common error terms, in the case of the rate integrating gyro, is ϵ_x . This is because in the derivation of the error model it assumes there can be no motion or the float relative to the case about the input axis Ox. In designing a strapdown rate integrating gyro it is essential to ensure that this is achieved in practice. As mentioned earlier this puts severe design restraints on the output axis pivots if large friction and stiction in these pivots is not to occur. If in practice there is a small residual movement of the float about Ox an error will exist similar to the dynamically tuned gyro θ_x/τ term, but cannot be directly compensated as there is no pick-off to measure θ_x .

The detuning error in the dynamically tuned gyro due to the actual rotor speed not at the tuned speed gives an error proportional to θ_y and can be compared directly with the elastic restraint error due to flexlead torques in the rate integrating gyro. Again in the derivation of the error model the elastic restraint was ignored and so the term does not appear in the equation.

Scale Factor Errors

For most strapdown applications both gyros use permanent magnet torque motors. The model of the scale factor error (ϵ) for a permanent magnet torque is usually assumed to be of the form:-

$$\epsilon_x = \epsilon_0 + \epsilon_1 (\text{sign} \omega_x) + \epsilon_2 \omega_x + \epsilon_3 \omega_x^2$$

where ϵ_0 = Basic scale factor calibration error of the torquer

ϵ_1 = Scale factor asymmetry error (positive scale factor different from the negative causing residual biases due to rectification effects).

$\epsilon_2 \ \epsilon_3$ = Linearity errors which modify the scale factor at high rates.

These coefficients are obviously of considerable importance in missile strapdown gyros and real time error compensation is required as described in later sections.

USUAL RIG NOTATION	NOTATION USED FOR COMPARISON WITH DTG	DTG NOTATION
Pick-off angle θ	θ_y (measures about Oy)	$\theta_x \ \theta_y$ (measures about Ox, Oy resp)
Float axes: IA, OA, SA	x y z	Nominal Gyro Axes x, y, z
Float to case axis misalignment angles YIA YOA YSA	$\gamma_x \ \gamma_y \ \gamma_z$	Rotor to case axis misalignment angles $\gamma_x \ \gamma_y \ \gamma_z$
Float moment of inertias J_x, J_y, J_z	I I_y J	Combined moment of inertias of the rotor and gimbal about the x, y and z axes I, I_y , J, where $I = I_y$
Inertial angular rates of rotation of the gyro about the gyro axes $\omega_{IA} \ \omega_{OA} \ \omega_{SA}$	$\omega_x \ \omega_y \ \omega_z$	Inertial angular rates about the nominal gyro axes
Gyro angular momentum at ideal rotor speed ω_{ro}	H_o	H_o
Rotor speed error from ideal $\delta\omega_r$	$\delta\omega_r$	Rotor speed error from ideal $\delta\omega_r$
Bias errors ω_B	ω_{Bx}	$\omega_{Bx} \ \omega_{By}$
Scale factor errors ϵ	ϵ_x	$\epsilon_x \ \epsilon_y$
Additional terms applicable to individual sensors	Viscous torque coefficient C	Gimbal delta moment of inertia L_G Flexure errors $\Delta K_x, \Delta K_y$ Gyro time constant τ Torquer cross coupling $\beta_{xy} \ \beta_{yx}$

TABLE 4. NOTATION USED IN GYRO COMPARISON

Bias Errors

It is usual to assume that the bias errors of the gyroscopes are functions of the acceleration a_x, a_y, a_z applied along each axis of the gyro. Typically the model might be of the following form.

$$\begin{aligned} \omega_{Bx} = & B_F + B_{xax} + B_{yay} + B_{zaz} + B_{xx}a_x^2 + B_{yy}a_y^2 \\ & + B_{zz}a_z^2 + B_{xy}a_xa_y + B_{yz}a_ya_z + B_{zx}a_xa_z \end{aligned}$$

The equation applies to both the RIG and to both axes of the DTG. The B coefficients are assumed to be constants, or well defined functions of temperature for any particular gyro. In fact gyro performance is usually expressed in how stable these coefficients are under various conditions - eg. from day to day or within a run.

From a user point of view all that is required is to know the magnitude of the B coefficients - and then only if they are significantly different from zero! However, for the gyro designer, and for the purposes of this comparison of the RIG and DTG, it is instructive to consider the various gyro effects that give rise to these B error coefficients. Table 5. attempts to do this, it is by no means complete, but does indicate yet again that these two gyros are quite similar. Notice that some terms do not have any known mechanisation and in some specifications are ignored. This can greatly simplify the tests used to verify the gyro, and so reduce the cost of the instrument.

Finally it should be noted that while this model is by far the most commonly used, there are some errors for both gyros that do not fit this model. For example it is well known that for some RIG designs the bias terms change with the sign of the acceleration a_y (along the output axis) but is not proportional to its magnitude. For the DTG an exactly similar effect occurs with the spin axis acceleration a_z .

COEFFICIENT	COMMON NAMES	CAUSE OF ERROR RIG	CAUSE OF ERROR DTG
B_F	'fixed torques' 'fixed restraints' 'g insensitive' 'rectification errors'	1) flex lead torques 2) stray magnetic/eddy current torques 3) output axis pivot friction/stiction 1) Acceleration inputs along spin axis at spin frequency rectifying dynamic rotor unbalance	1) windage torques 2) stray magnetic torques 1) Same as RIG 2) Acceleration inputs at twice spin speed normal to the spin axis rectifying gimbal unbalance 3) Angular inputs at twice spin speed rectifying errors within suspension
B_x	'mass unbalance' 'mass unbalance' 'MUS'	1) c of m of float not on Oy as defined by pivots	1) c of m of rotor not at centre of suspension
B_y	'rope effect' 'screw effect' 'cross mass unbalance'	1) Convection in fluid	1) Errors in flexures
B_z	'mass unbalance' 'MUI'	1) c of m of float not on Oy as defined by pivots	
B_{xz}	'Anisoelasticity'	1) float not equally compliant along Ox and Oz	1) rotor/suspension not equally compliant along Ox and Oz
B_{yz}	'Anisoelasticity'	1) non zero rotor attitude angle	1) rotor/suspension not equally compliant along Oy and Oz
B_{xy}		Effects usually small	Effects usually small
P_{xx} B_{yy} B_{zz} ' g squared'		Effects usually small	Effects usually small

In this table only the x axis of the DTG is considered. For the y axis a very similar table can be produced by interchanging the B_x and B_y terms and similarly B_{xz} and B_{yz} .

TABLE 5. SOURCES OF BIAS ERRORS

4.4 SUMMARY

From this discussion it is clear that there is no significant difference in the complexity of the error models of these two popular gyroscopes. For those accustomed to the conventional autopilot rate gyro, the fact that there are a large number of errors when one requires a gyro of performance better than $1^{\circ}/hr$ may be off-putting. In addition the fact that it is usually impractical to be able to build the sensor to the desired performance without compensation may seem an undesirable complication. However, the experience of high performance Inertial Navigation Systems, where such techniques are common-place, is very encouraging.

In addition there are developments such as LCIGS and SIMU, that we shall discuss later, which make the use of these sensors considerably easier.

Scale factor errors are much more significant in a strapdown gyro than in a platform gyro and the next section outlines some problems that may be encountered when tests are undertaken to evaluate the scale factor error terms.

5. GYRO SCALE FACTOR EVALUATION

5.1 Permanent Magnet Torque Motors

As discussed earlier the Rate Integrating and Dynamically Tuned Gyroscopes have been developed sufficiently to provide a rate sensor of the required accuracy for the new applications. However they both can exhibit an effect which was rarely observed on the conventional rate gyro.

The gyroscopes may have a scale factor (sensitivity) which varies with temperature. This phenomenon is compounded because of the considerable heat dissipated in the torquer when the gyro is subjected to high angular rates. The source of the problem is the permanent magnets used in many torque motor designs. In order to precess the gyro at the maximum rate with reasonable torque currents it is necessary to maximise the energy product of the magnet. With current technology this is achieved with Samarium Cobalt materials and unfortunately the best of these also have the highest temperature sensitivity. However, although the sensitivity is large, roughly -400 parts per million per degree Celsius, the value is very stable and well defined over the whole of the MIL-Spec. temperature range.

One partial solution to this particular problem is to operate a constant power pulse torquing scheme in the gyro rebalance loops, and so minimise the temperature variations during operation. Unfortunately to do this means that the dynamic range of the instrument must be reduced or overheating will result. For those missions where high rates are observed for only a small fraction of the time then a two (or more) level torquing scheme has been used to maintain the dynamic range.

However for the applications considered here these constant power schemes are not quite so relevant. Firstly the mission is often so short that the temperature has not even had sufficient time to stabilise after the initial power up sequencing. Secondly for these applications the period of very high rates tends to last for a much higher percentage of the mission.

An alternative approach to the problem is to employ some form of magnetic shunt to cancel out the temperature effect. This too has its problems, firstly in achieving a practical design for the rotor of a dynamically tuned gyro and secondly it is difficult to maintain a good, and perhaps more important, a well defined temperature sensitivity over the whole working temperature range.

In spite of all this the temperature sensitivity of the gyro is not a critical problem for most applications of the type considered in this Paper. The gyro scale factor can easily be estimated from the time history of the power consumed by the gyro. Even for conventional analogue torquing all the necessary data is contained within the indicated output of the gyro - the torquer currents.

In fact it is more than likely that this temperature sensitivity will be considered a problem when such a gyro is evaluated by a potential customer. In these circumstances it is also probable that a complete time history of the test is not available and so it is difficult to make a retrospective analysis of the gyro scale factor sensitivity.

We have experienced this so often that it is useful to consider the standard test procedure and to perform an approximate analysis of the test for a typical gyro.

5.2 The Conventional Scale Factor Linearity Test

This test has been used for many years and can be used to quantify many gyroscope errors such as non linearities, bias offsets and hysteresis as well as measuring the basic gyro scale factor. The precise details vary from test laboratory to laboratory, but in essence the gyro is mounted on a single axis rate table and a series of constant angular rates applied. Often a gyro measurement is made at each of the 41 angular rates in the following sequence:-

Zero, 0.1R, 0.2R 0.9R, R, C.9R 0.1R, Zero,
-0.1R, -0.2R -R -0.1R, Zero

where R is the maximum rate specified for the mission.

Some test laboratories apply each rate for a fixed period of time and take a gyro measurement for a fraction of this time. Others tend to make a gyro measurement while the rate table turns through a fixed angle (perhaps one revolution) others may use a combination of fixed times at low rates and fixed angles at high rates.

Figure 3. shows the result of a typical test carried out on a gyro with a Samarium Cobalt torquer. The figure shows a graph of the gyro errors from the ideal linear scale factor, plotted against the input rate. Apparently the gyro has very bad hysteresis when rate is applied.

The following section shows with a very simple analysis how the overall shape of this test result may be explained.

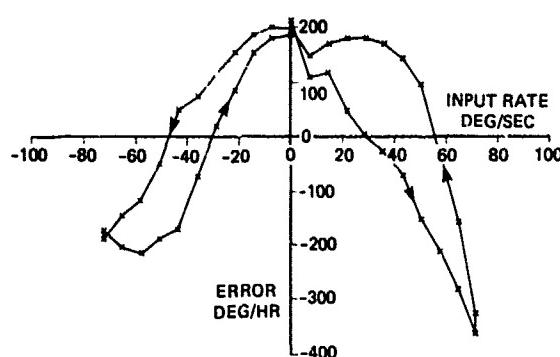


FIGURE 3 SCALE FACTOR LINEARITY TEST

This assumption of course does imply that a constant power pulse torquing scheme is not used. The analysis is thus confined to either analogue or 'pulse on demand' rebalance loops.

Neglecting other heat sources within the gyro the power consumed by the gyro torquer is proportional to

$$Y^2 = Y_0^2 \sin(nt) = Y_0^2(1 - \cos 2nt)/2$$

If the test were to continue (ie repeated) indefinitely then the gyro temperature would rise to a final mean value with a superimposed sinusoidal variation whose magnitude would be proportional to

$$\cos(2nt - \phi)$$

where ϕ is a phase lag and represents the composite thermal lag of the gyro in its test fixture.

In practice however the test is so short that these steady state conditions are not achieved and a much better approximation is to assume that the above sinusoidal variation is superimposed on a linear increase in temperature.

Thus $T_t - T_0 = \beta t + \delta \cos(2nt - \phi)$ for $0 < t < t_f$

where T_t is the temperature at time t

T_0 is the temperature at time $t = 0$

β and δ are constants

It is convenient to define the mean temperature during the test as T_m and the rise in temperature during the test as ΔT

$$T_m - T_0 = \Delta T/2 = \{\int T_t dt\}/t_f = \beta t_f/2$$

$$So T_t - T_m = \Delta T(t/t_f - 1/2) + \delta \cos(2nt - \phi)$$

The scale factor K expected from a permanent magnet is

$$K_T = K_m \{1 + \alpha(T - T_m)\}$$

K_T is the scale factor at temperature T

K_m is the scale factor at temperature T_m

(Units of scale factor are radian/second/ampere)

and α is a constant depending upon the materials but typically -0.0004 per degree Celsius.

5.3 Approximate Analysis of the Scale Factor Linearity Test

Since the standard test for scale factor is so common and can be carried out automatically in most test laboratories, it is useful to have a method of analysis that does not require any further measurements and can therefore be carried out retrospectively using only the final error plot if necessary.

In spite of the gross assumptions that are made in the following derivation it does give reasonable first approximations to the temperature sensitivity magnitude.

The first and major assumption is that the current flowing through the gyro torquer is sinusoidal and of the form:-

$$Y = Y_0 \sin(nt)$$

where Y is the current at time t seconds

Y_0 is the maximum current

and $t_f = 2\pi/n$ = total duration of test.

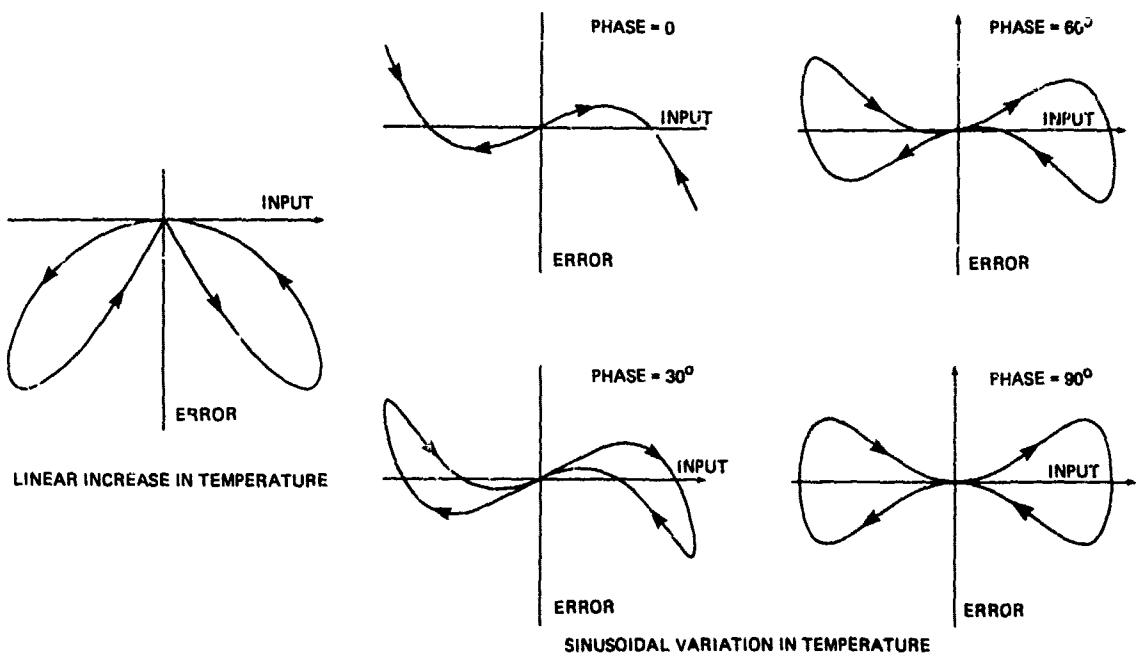


FIGURE 4 ERROR DIAGRAMS FOR GYROS WITH TEMPFRAUTURE SENSITIVE SCALE FACTORS

thus the scale factor at any instant of the test is

$$K = K_m \{1 + \alpha \Delta T(t/t_f - 1/2) + \alpha \delta \cos(2nt - \phi)\}$$

Therefore since the current in the gyro torquer is $Y_o \sin(nt)$, the observed output of the gyro (assuming no other errors) is

$$\begin{aligned} & K_t Y_o \sin(nt) \\ &= K_m Y_o \sin(nt) \{1 + \alpha \Delta T(t/t_f - 1/2) + \alpha \delta \cos(2nt - \phi)\} \end{aligned}$$

Conventional analysis assuming a fixed scale factor would expect an output $K_m Y_o \sin(nt)$ and so the apparent gyro error is

$$= K_m Y_o \sin(nt) \{\alpha \Delta T(t/t_f - 1/2) + \alpha \delta \cos(2nt - \phi)\}$$

$K_m Y_o$ is of course the maximum rate applied during the test and so if the errors are expressed as a fraction of the maximum input then

$$\text{fractional errors} = \alpha \{\Delta T(t/t_f - 1/2) \sin(nt) + \delta \sin(nt) \cos(2nt - \phi)\}$$

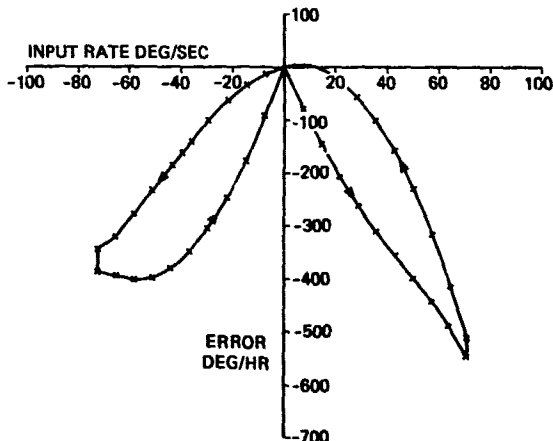


FIGURE 5 PREDICTED ERROR PLOT OF TEST IN FIG.3

The first term is due to the difference in temperature between the the start and finish of the test. With the assumptions made here, the shape of the resulting error plot when plotted against the input rate is fixed and only its amplitude varies from design to design. The second term in the error equation has an extra parameter - the phase lag, which depends on the detail design of the gyro and the test fixture.

Figure 4. shows the shape of the error curves for both the linear and sinusoidal variations. Such diagrams may be used to obtain initial estimates of the temperature effects. More refined values can be calculated by incorporating the error equation in a Linear Least Squares technique when estimating the gyro scale factor from the original test data. This has been completed for the test of Fig 3. The resulting parameters give the theoretical error plot shown in Fig 5. which should be compared with Fig 3.

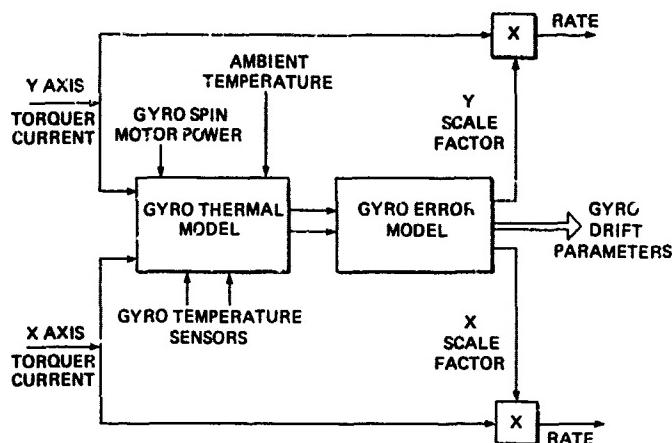


FIGURE 6 D.T.G. THERMAL MODEL

5.4 Temperature Compensation

It is clear from the earlier discussion that in many practical Strapdown Systems some form of temperature compensation for scale factor will be necessary. It is for this reason that most strapdown sensors are designed complete with temperature sensors. For scale factor compensation it is necessary to know the Samarium Cobalt magnet temperature and for DTGs at least this does raise some problems as the magnet is part of the rotor and so is in a most inaccessible location as far as electrical connections are concerned.

The BAe solution is to use two temperature sensors one which is near the torquer coils and the other in the main body block of the gyro. The output of these sensors together with information on the power consumed at any instant is supplied in real time to a thermal model of the gyro. The output of this model is the scale factor of the gyro at that time. This general technique is shown in Figure 6.

Temperature modelling in inertial systems is not new and has been used with considerable success in correcting gyro drift and accelerometer bias changes during the initial warm up phase of conventional platform systems.

6. THE USE OF DYNAMICALLY TUNED AND RATE INTEGRATING GYROSCOPES IN STRAPDOWN SYSTEMS

In order to use either type of Strapdown gyro the following items are required in addition to the basic mechanical sensor itself.

- Spin Motor Supply
- Pickoff Supply
- Inertial Sensor Block (ISB) to maintain the gyroscopes and accelerometers in a rigid relative spatial orientation
- Servo, rebalance or capture loop to ensure the gyro remains at the pickoff null
- Sensor error model coefficients
- Sensor error thermal model

Of course with the exception of the rebalance loops each of these had to be provided in a conventional IN platform or rate gyro autopilot system. What is new in the strapdown field are the strong interactions between the items. For example it is obvious from the previous discussion on scale factor that the detailed design of the Inertial Sensor Block will contribute to the time constants in the thermal model.

As a result of these interactions there have been several systems which have provided the eventual user with a complete package which has sufficient intelligence that the outputs of the package are the best estimates of rate and acceleration with all significant errors having been allowed for.

One example of this approach is the American Low Cost Inertial Guidance System (LCIGS) which uses rate integrating gyroscopes. Another example is the Smart Inertial Measurement Unit (SIMU) which BAe Precision Products are developing at Stevenage using their own dynamically tuned gyroscopes.

When such systems are considered in more detail it is clear that there are many other advantages and it can change the whole philosophy of using inertial sensors.

7. THE PHILOSOPHY OF SMART INERTIAL MEASUREMENT UNITS

In this section we use the term SIMU as a generic name for any Strapdown gyro system that contains its own error models and whose outputs are the best estimates of the quantities to be measured by the inertial sensors. In today's technology the compensation will almost certainly be performed by a microprocessor based system.

The need for a SIMU was indicated by the strong interactions that occur between the various components of the gyro sub-system. In fact there are many other factors that are making the SIMU a logical solution.

One such consideration is the nature of the new applications. Often there is a requirement that the vehicle be stored for several years and then must be relied upon to work for a few minutes as a one shot device. This implies that the conventional manned aircraft requirements of reversionary modes have no meaning. Thus there is great pressure for cost reasons to use only one set of inertial sensors in the vehicle and these sensors will be shared by all sub-systems. The SIMU concept makes it unnecessary for each sub-system (often from different contractors or vendors) to carry out independent sensor compensation. The latter approach would make maintenance - such as sensor replacement - difficult as each sub-system would have to be updated with the new sensor data. The alternative approach of delegating one of the sub-systems responsible for the compensation and then passing data to the other sub-systems also has its problems not the least of which is the resulting vendor to vendor interface requirements.

The same sort of arguments can be used when the other possibilities opened up by the SIMU concept are explored. Firstly the SIMU can be made responsible for the whole power up, power down and BITE of the inertial sensors. Thus it is only necessary for the vehicle main computer to issue a Power-Up command to the SIMU and inspect a status register to verify compliance and correct operation of the SIMU during the mission.

The SIMU approach is particularly suitable for Strapdown Systems as there is rarely any sort of hardware mode control compared with the platform IN systems which had to be switched through a sequence of configurations to cope with platform capture, alignment and gyrocompassing.

Within the SIMU concept there are still plenty of design options which enable the system to be optimised for various classes of mission. For example there is the whole philosophy of maintenance. For LCGS the basic replaceable unit is a single gyro module (but an accelerometer triad) whereas in the BAe SIMU the complete sensor block with gyros and accelerometers is removed for subsequent repair.

The first approach makes it easier to interchange sensors from different vendors but at the expense of an extra defined interface between the gyro module and the ISB. In the BAe approach the gyro and ISB alignment errors are tested together and a composite figure placed in the read only memory of the SIMU.

A further advantage of the concept is that it uses a basic building block approach and so the SIMU with only minor modifications - iteration rates etc. - can be used in a wide variety of applications. This obviously will reflect the Life Cycle Cost of the projects.

In order to elaborate the philosophy outlined in this section the Paper will conclude with consideration of the BAe Precision Products SIMU. Since this system uses strapdown DTGs, the development of these at Precision Products will be outlined before proceeding to the SIMU itself.

8. THE BAe STRAPDOWN DYNAMICALLY TUNED GYROS

The basic principles and the relative advantages of the dynamically tuned gyro have been discussed earlier in this Paper. Precision Products have been developing dynamically tuned gyros both for platform and strapdown use for a number of years. Early work concentrated on a platform gyro suitable for use in gyro compasses and conventional platform Heading and Attitude Reference Units. This development programme provided invaluable knowledge on the design principles and manufacturing techniques required for dynamically tuned gyros.

To overcome some of the difficulties encountered when converting a conventional platform gyro into a strapdown sensor, a range of sensors specifically for strapdown use has been developed, Fig. 7. For the high performance market the FG 312 dynamically tuned gyro, which incorporates many novel features was designed. As high performance implies an expensive instrument, a second strapdown sensor known as FG 313 has been developed. It uses many common features of the FG 312 but was designed with the objective of medium performance at low cost. The main features of these instruments are shown in Table 6.

These two strapdown sensors are part of a family of dynamically tuned gyros manufactured by BAe Precision Products. The others are, the FG 320 which is a very high performance gyro for marine platform applications and the FG 310 which is a platform sensor suitable for gyrocompasses and other avionic systems.

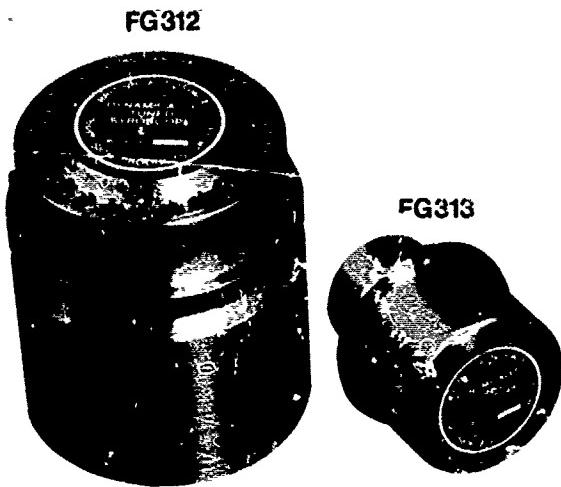


FIGURE 7. BAe DYNAMICALLY TUNED GYROS



FIGURE 8. INERTIAL SENSOR BLOCK

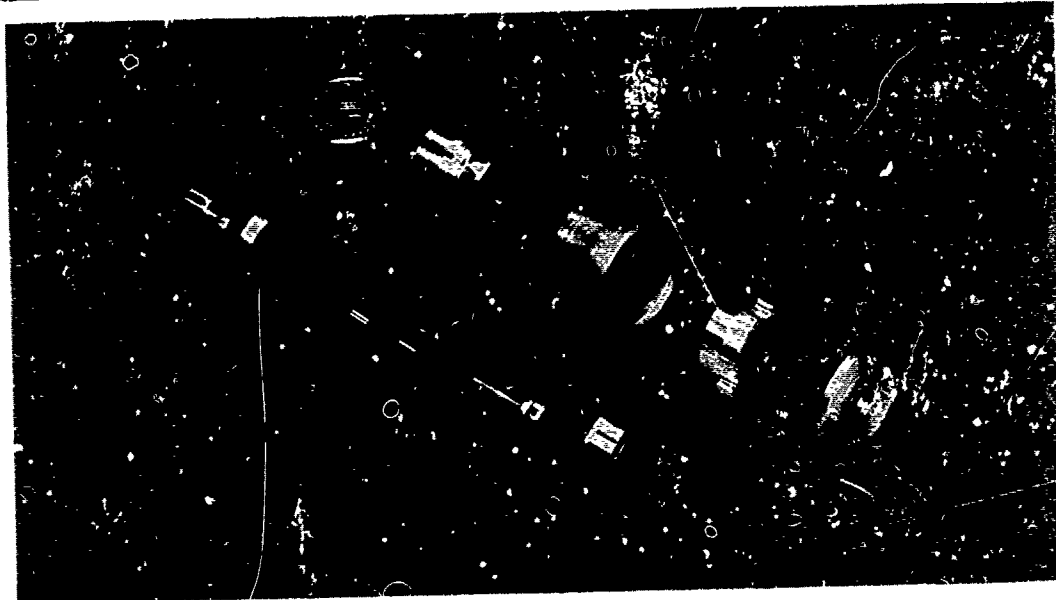


FIGURE 9. FG312 DYNAMICALLY TUNED GYRO

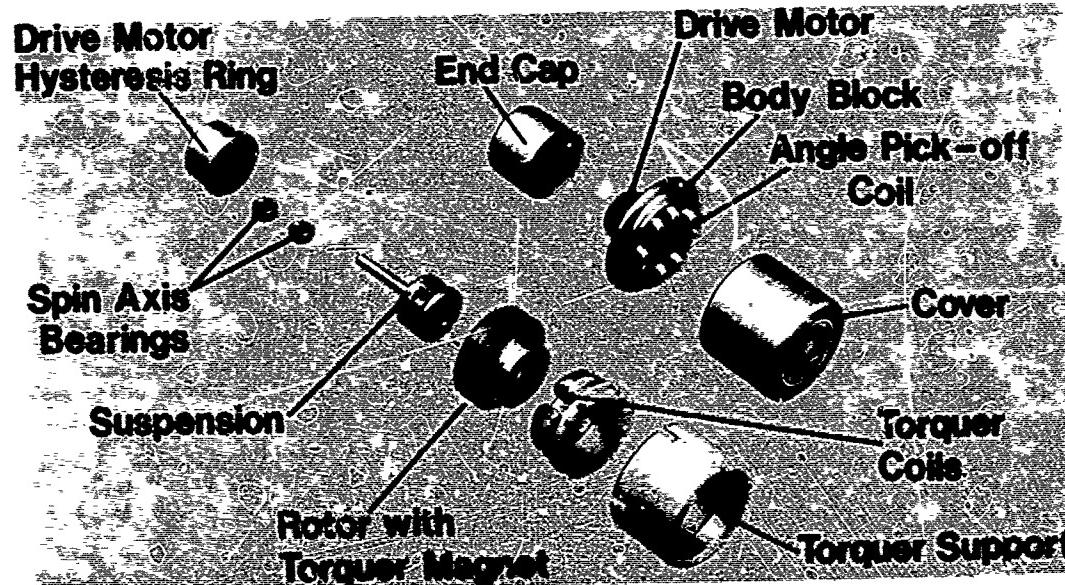


FIGURE 10. FG313 DYNAMICALLY TUNED GYRO

	UNITS	FG312	FG313
Diameter	mm	50	30
Length	mm	55	39
Day to Day Repeatability In Run Repeatability	degree/hour degree/hour	0.07 0.01	3.0 1.0
Maximum Torquing Rates: continuous 1 sec. on 9 sec. off	degree/sec degree/sec	250 400	250 400
Angular Momentum	Nms	.006	0.0012
Torquer: type scale factor power dissipation Linearity	degree/hr/mA watts/(°/sec) ² %	450 0.0003 0.005	700 0.0004 .01
Pickoff: type excitation freq.	kHz	18	Inductive 18
Spin Motor: type excitation rotor speed run up time	Hz Hz sec	400 133.3 6	Hysteresis 256.6 133.3 1 to 6
Temperature Sensors		2	1
Rotor Speed Monitor		Yes	Yes

TABLE 6. CHARACTERISTICS OF BAe STRAPDOWN GYROS

8.1 The FG 312 Dynamically Tuned Gyro

The FG 312 gyro shown in Figure 9 was designed as a strapdown rate sensor which would have the performance suitable for a 3 to 5 nautical mile per hour strapdown inertial navigation system. This performance was to be achieved with body rates of up to 400°/sec.

It is clear from earlier sections of this Paper that the thermal design of the sensor is important and although thermal dissipation can be minimised by careful design, high torquer temperatures are inevitable. These effects have been minimised by separating the torquer from other critical areas such as the angle pick-off and drive motor. This has the additional advantage in that flexibility in torquer and pick-off design is possible as they are independent units. In this way larger power dissipations are accommodated.

Referring to Figure 9, it can be seen that the gyro consists of a central body block on which are mounted the drive motor windings, the spin axis bearings and the pick-off coil assembly. It also provides the mounting flange of the gyro. A central shaft has the rotor and its suspension at one end and the drive motor hysteresis ring at the other. This shaft is carried in a pair of angular contact ball bearings which are lubricated by oil retained in porous cages. Preloading is applied via solid clamped up spacers. The suspension is a single gimbal Hooke's joint. The design is novel and is very easy to manufacture. The gimbal is machined from a single block of material and the flexure leaves are etched in large quantities from selected grain-oriented spring material. As a protection against shock stresses being transmitted to the flexure due to accidental overslew, mechanical stops are incorporated to limit gimbal motion.

As already indicated the design of the torquer is critical. The approach adopted is to use a moving magnet fixed coil assembly. The coils are wound on a special former which has been carefully designed to give maximum flux utilisation and good thermal conduction to the end cap of the gyro. The rotating element of the torquer consists of two radially magnetised samarium cobalt magnets.

The inductive pick-off coils are mounted on the body block with the magnetic circuit completed by a flat lapped surface on the rotor. This attention to geometry ensures low distortion and minimises noise in the pick-off output. To reduce the effects of external magnetic fields the complete gyro is enclosed in a radiometal sleeve.

As the gyro is not temperature controlled, temperature monitoring is provided by sensors in the body block close to the spin axis bearings and another sensor in the torquer body. A rotor speed pick-off is also provided at the torque motor end.

Gyro tuning is achieved by trimming the gimbal transverse inertia. Two eccentrically mounted screws are provided on the spin axis of the gimbal and by moving these in various combinations the pendulosity and transverse inertia of the gimbal can be varied. After tuning, the gyro is filled with helium and sealed.

8.2 The FG313 Dynamically Tuned Gyro

The FG 313 was specifically designed for the new applications discussed in this Paper. Other applications for this gyro include the stabilisation of line-of-sight systems, where high accuracy and slew rates are demanded. The construction methods adopted for the FG 312 were sufficiently flexible to allow a smaller unit to be designed using the same techniques.

As can be seen from Figure 10, certain features of the FG 313 are similar to those used in the FG 312. This is particularly so in the case of the body block, pick-off and suspension. The drive motor is a complete unit from another gyro which is currently in production at BAE Precision Products. The major difference is in the construction of the torquer. This has been considerably simplified to reduce size and cost. The gyro incorporates only 1 temperature sensor but retains the rotor speed pick-off to provide data for use in compensation circuits. Gyro tuning is achieved in the same manner as the FG 312.

8.3 Demonstration of Strapdown Capability

A good demonstration of the strapdown capability of any gyro is to use it to measure a small known input while the other axes are subjected to very high, strapdown, rates. BAE Precision Products call this sort of test the 'Dynamic Range Test'.

The test is carried out using the same test equipment as used to measure scale factor. The gyro is mounted upon a rate table with the X Axis parallel to the vertical rate table axis. The object of the test is to measure on gyro Y Axis a small varying input while X Axis is subjected to a typical strapdown angular rate. (As indicated earlier this type of test causes significant problems for a strapdown rate integrating gyro because of the large angular rate about the output axis).

Axis Y is nominally horizontal and as the table rotates it should indicate an output which is the combination of:-

- (a) a (fixed) component of the table rate due to gyro mounting errors.
- (b) a fixed term due to gyro bias.
- (c) a component of Earth's Rotation which varies sinusoidally as the table rotates.

At Stevenage the horizontal component of Earth Rate is about $9.28^\circ/\text{hr}$ and the aim of the Dynamic Range Test is to measure this cyclic variation. Figure 11. is a typical result. In this case an FG312 was used and the output of Axis Y while Axis X was subjected to an input of $120^\circ/\text{sec}$ ($432,000^\circ/\text{hr}$) is shown. This was applied for a period of about 6 seconds during which time the rate table rotated through two revolutions. The expected sinusoidal variation due to Earth Rate can be easily seen. Other parameters of interest in this test are that the integration interval from the torquer current converters was 0.3 seconds and that one pulse from the converter over this integration interval is equivalent was $0.4^\circ/\text{hr}$. The data shown has not been compensated in any way and shows some drift due to changes in temperature. The misalignment of Axis Y as measured by this test was 1.48 milliradians. The test demonstrates quite clearly that there are no stiction or resolution problems with the gyro and that the noise level of the gyro and its digital converter is at an acceptable level.

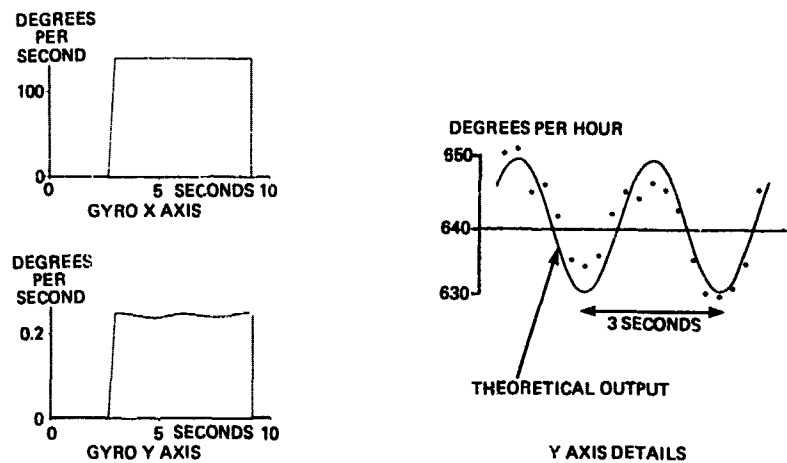


FIGURE 11. DYNAMIC RANGE TEST

The test has also been carried out at higher rates up to the 270°/sec maximum that the particular rebalance loops in the test equipment can capture. These and other tests have demonstrated that the gyro can withstand these rates continuously for several minutes at a time.

9. DESCRIPTION OF THE BAe SMART INERTIAL MEASUREMENT UNIT

The BAe Precision Products concept of a Smart Inertial Measurement Unit (SIMU) shown in Figure 12. is to mount two DTGs and 3 force feedback single axis accelerometers into a single Inertial Sensor Block (ISB). This ISI is then supplied complete with all necessary electronics so that the user has only to supply a DC voltage in order to obtain compensated digital data from the gyroscopes and accelerometer.

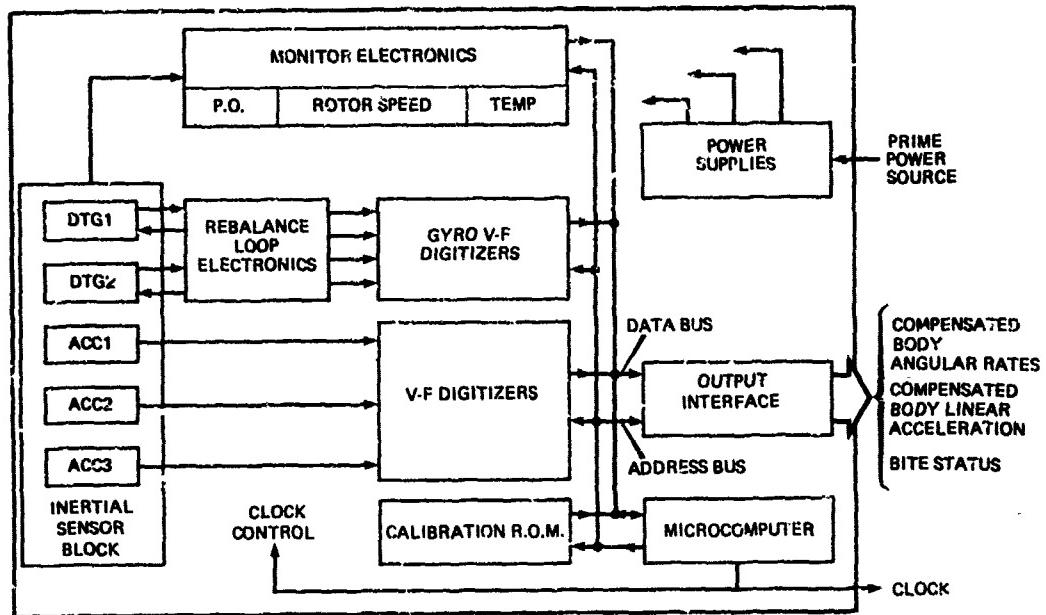


FIGURE 12 THE SMART INERTIAL MEASUREMENT UNIT

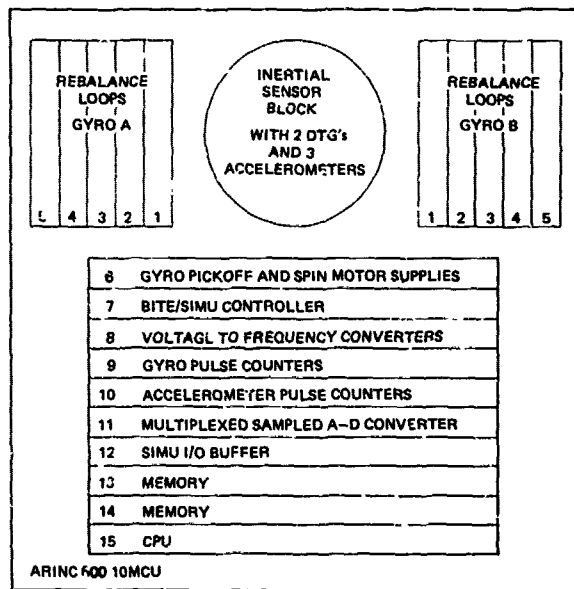


FIGURE 13 LAYOUT OF PROTOTYPE SIMU

In order that potential customers can evaluate the technique, a Prototype SIMU has been designed. It is packaged in a case that conforms physically to the ARINC 704 Specification. The only part of the SIMU which approximates to the Production unit is the ISB itself. This approach allows an accurate assessment of the system performance to be made early in the development cycle of a Project before detailed Specifications for electronic packaging, interfaces and form factors are available. This approach also allows BAE Precision Products to satisfy the particular customers interface requirements by changing a standard Eurocard board. Similarly different power supplies can be catered for by changing another Eurocard. For convenience we have also designed the unit to accept either DTG. This is achieved by exchanging the ISB.

The function of the SIMU will be described in terms of the internal organisation of this prototype SIMU - Figure 13.

Inertial Sensor Block

A typical Inertial Sensor Block is shown in Figure 8. In this case two of the larger, more accurate FG312 DTGs are used in conjunction with three Sundstrand QA2000 accelerometers. The overall size of this package together with 7 sensing resistors is a cylinder 100mm in diameter and 160mm long. For applications where this accuracy is not required a rather smaller ISB is used containing two FG313s and 3 Precision Products A702 accelerometers.

Rebalance Loops

Both accelerometer types are force-rebalance designs and contain hybrid rebalance loops within the packaging of the sensor itself. Unfortunately power considerations do not allow the same technique to be used for the gyroscope rebalance loops and these are mounted externally - on either side of the ISB in the prototype SIMU.

The design of a strapdown rebalance loop for a DTG is rather more complicated than that for a rate Integrating Gyro of an equivalent bandwidth. The reasons for this are summarised in Table 7. It is at the design stage that the task is more difficult for the DTG user. Satisfactory performance can be achieved by careful design and the cost of the eventual hardware is basically not much more than that for the RIG and is much more a function of the need to provide for 4 torquer drivers per SIMU (as opposed to 3 in the case of the RIG) rather than any increase in servo complexity. In the current SIMU the rebalance loops are analogue throughout.

	DTG	RIG
Pickoff Output	Inevitably contains noise at rotor spin frequency and its harmonics	Equivalent noise only if rotor is dynamically unbalanced
Angular Momentum	Appears directly as part of loop gain. So loop may be unstable when rotor stationary	Is outside loop. So loop always stable with stationary rotor
Pickoff and Torquer Misalignments	Affect loop stability	No first order effects on loop stability
Back emf in torquer	Appears as noise at rotor speed and its harmonics	None

TABLE 7. Rebalance Loop Design Comparison

Sensor Support Electronics

The layout of the electronics within the prototype SIMU is a logical progression as one proceeds away from the ISB. Thus the first double Eurocard Electronics board is the A-C supplies board which derives power for the gyroscope pickoffs and spinmotor supplies from an on-board crystal oscillator. (Which optionally may be locked to an external source). Thus this board together with the rebalance loops and the ISB provide a DC In - Analogue Data Out capability.

The next Eurocard is the BITE/Controller board. The purpose of this card is to verify the correct operation of the whole SIMU by monitoring several critical parameters. This board also controls the power up sequence during which the gyroscopes are run up to speed, the rebalance loops closed and the analogue to digital convertors are given a bias calibration. On successful completion of this task, assuming that the BITE checks are also satisfactory, the controller sends a signal to the SIMU processor to start the sensor data compensation. Depending upon the application, this power up sequence takes from 1 to 6 seconds.

Sensor - Microprocessor Interface

The next cards are associated with the precision analogue to digital convertors for both gyros and accelerometers. These convertors use voltage to frequency convertors whose outputs are summed into counters which are then loaded into registers which map into the microprocessor memory space. These convertors are of course crucial to the operation of the SIMU. The design features of the convertors used in this SIMU include:-

- a) Output is true integral of input
- b) In-built bias measurement and compensation
- c) No data lost on reading.

The last card in this group contains a 16 channel multiplexed analogue to digital convertor. This convertor is used to measure the outputs of the various temperature monitors in the ISB and the gyroscopes and accelerometers themselves. The same A-D is also used to monitor the gyro pick-off outputs. This card contains all the necessary signal conditioning for each input and the memory mapped registers.

Microprocessor

The next group of cards consist of the microcomputer used to compensate the sensor errors. It is based on the 16 bit Texas Instruments SBP9900. The compensated data is then passed, via memory mapped registers to the output interface board.

The SIMU is controlled by a single clock frequency which determines the output data rate from the SIMU. This clock causes an interrupt to the 9900 which then carries out the routines listed in Figure 14. After completing these routines the processor returns to the background task of updating the sensor error models. All software is written in the high level language CORAL 66.

The output interface between SIMU and the outside world depends on the exact user requirements. In general a very simple interface is recommended with little hand shaking except for a 'Data Ready' signal from the SIMU. A SIMU status word is also available which the user may interrogate to verify SIMU operation. Alternatively this status register may be used to generate an interrupt to the user computer.

Sensor Compensations

The errors that are corrected by the SIMU are (not in order of compensation):-

- a) Analogue to Digital Convertor Bias and Scale Factor
- b) Gyro Torquer Scale Factor error and non linearity
- c) Gyro Drift - fixed restraints
- d) Gyro Drift - mass unbalances
- e) Gyro Drift - errors due to pickoff outputs
- f) Gyro Axis errors - mounting and pickoff
- g) Accelerometer scale factor errors
- h) Accelerometer biases
- i) Accelerometer Cross Axis sensitivity errors
- j) Accelerometer Axis alignment errors

10. CONCLUSIONS

The advantages of the strapdown approach to missile guidance systems has been adequately demonstrated in many applications. The aim of this Paper has been to examine some of the practical problems the system designer can encounter when selecting the inertial rate sensors and to give an example how these can be simplified.

The missile specifications for strapdown inertial systems will continue to demand improved performance from the inertial sensors. This will have to be provided against a background of increasing emphasis on overall cost of ownership, improved reliability and maintaining acceptable physical sizes.

The rate sensor requirements for the immediate future will continue to be met by the well proven conventional spinning mass gyroscopes. The dynamically tuned gyro can be considered as a rate sensor with considerable design growth available to meet this exacting requirement.

It is accepted that, in common with existing practice, real time error compensation will be required. This will have to include compensation for scale factor errors over the wide dynamic range of the modern missile, together with the more traditional error terms such as warm up characteristic and g sensitivity.

The Smart Inertial Measurement Unit approach incorporating the dynamically tuned gyro, adopted by Bae Precision Products, provides a self contained inertial sensor package which offers significant advantages to the "System" designer. This technique makes the best use of this gyro's potential as a strapdown rate sensor and provides an integrated unit which can be readily incorporated into existing and future missile guidance systems.

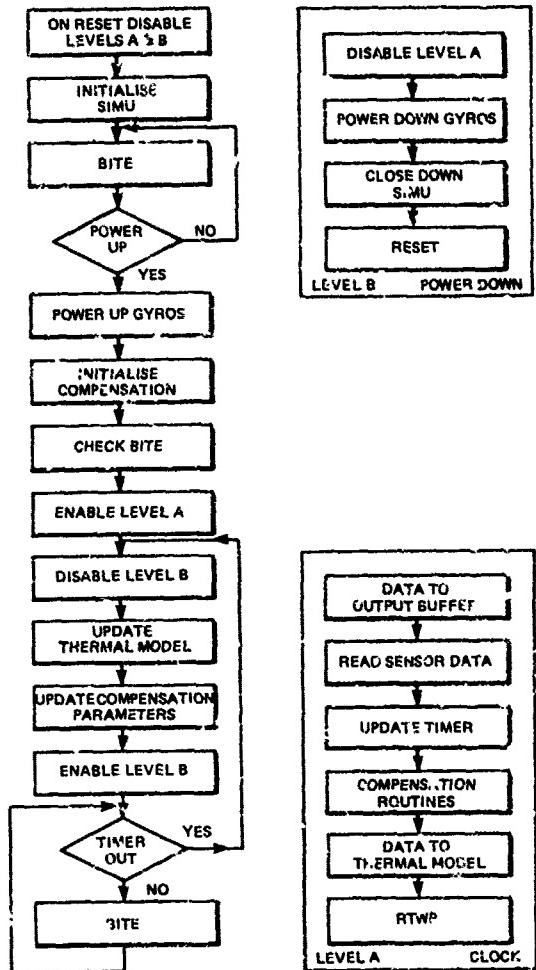


FIGURE 14 SIMU SOFTWARE FLOW

REFERENCE

1. Savage, Paul G., "Strapdown Sensors" AGARD Lecture Series No.95 on Strapdown Inertial Systems June 1978.

**ESG INERTIAL TECHNOLOGY: AN APPROACH TO SELF-CONTAINED
PRECISION NAVIGATION AND POSITIONING ON AND OVER THE BATTLEFIELD**

By: Michael J. Hadfield
 Senior Staff Engineer
 Honeywell Inc. - Avionics Division
 St. Petersburg, Florida, USA

ABSTRACT

As the needs for more accurate, rapid battlefield reconnaissance and deployment develop, so does the need for more secure operation, including a minimum of electromagnetic radiation. These requirements often conflict with each other in the selection of navigation and positioning systems. One result is increased interest in self-contained systems such as high accuracy inertial technologies can provide. An inertial technology which has recently emerged and reached full maturity is that of Electrically Suspended Gyroscopes (ESGs).

First to benefit from ESG inertial system precision were aircraft having long range, high accuracy position, velocity and attitude requirements. Systems such as the U.S. Air Force's 0.1 nmph SPN/GEANS, which are entering the strategic air fleet, have provided an order of magnitude improvement in self-contained aircraft navigation. More recently, the short term accuracy benefits of ESG inertial systems are also being explored. The newest activity, reported in this paper, is that of high accuracy positioning on and over land masses, using helicopters and a variety of land vehicles. This accuracy has also been extended to shipboard use, the subject of another paper. (Reference 6).

For the tactical battlefield situation, recent testing has demonstrated the high precision which is available for both open-loop and closed-loop positioning on the battlefield surface. Open-loop accuracies of ten meters, rms, or less are achievable. Closed-loop accuracies in the submeter range have also been demonstrated. Weapon systems initialization (pointing and positioning) can be easily accomplished with high accuracy, self-contained ESG inertial systems. Linearity and repeatability of inertial system errors are important factors and are explored in this paper. Supporting laboratory and field test data are presented from representative ESG equipments. These data are then related to typical battlefield situations in which they would apply.

Special topics such as the hybrid operation of high precision ESG systems are described and discussed. The relatively low reliance of ESG inertial systems on other navigation aids is considered. The importance of this feature in the adverse electromagnetic radiation environment of the battlefield is evaluated. The importance of effective Kalman filtering to hybrid system operation is reviewed. Specific examples are given for operational filters that have been used with ESG inertial systems.

The hardware developments which led to the emergence of ESG inertial technology are summarized and interrelated with software developments. Critical parameters such as accelerometer and gyro stability in the battlefield environment are addressed and supporting test data provided for the error budget values. Other hardware features, such as the fault tolerant benefits of design-centering as well as built-in fault detection and isolation are described in terms of the SPN/GEANS and GEO-SPIN™ equipments.

In the closing sections of the paper, the potential benefits of ESG inertial systems are summarized for several operational applications of navigation and positioning both on and above the battlefield in modern-day tactical situations.

INTRODUCTION AND DEFINITION OF NEED

Whether operating at 10 km or 100 meters above or down on the surface of the modern day battlefield, the need to know where you are, where you're going, and how to get there quickly is more important than ever before. We face potential enemies who are more mobile and possess more firepower than in previous battles and in addition may be numerically superior to our forces. A key element of our strategy must be to focus our limited resources more effectively in order to neutralize and defeat a larger, fast moving enemy.

Accurate, real time navigation and positioning are necessary prerequisites to success on the battlefield. Many types of systems are becoming available to assist us in meeting these needs. They include the electromagnetic systems such as DME, Radars, Lasers, JTIDS, MACS, PLRS, SiNTAC, GPS*, etc., and self-contained systems such as INSS (for aircraft and helicopters), FADS, IPS, and Land Navigators. A common characteristic shared by the self-contained systems is that they all use inertial technology to some degree. Ranges of accuracy or precision stretch from kilometers per hour (conventional local vertical aircraft INS) down to fractions of a meter (Inertial Positioning System). Objectives of this paper are to discuss the high precision end of this spectrum, from 0.1 nmph or 0.19 kmph (for aircraft) down to submeter positioning and show how a new technology using Electrical Suspended Gyros (ESGs) can satisfy these battlefield needs.

*See Glossary at the end of this paper for definition of acronyms.

Advantages of using self-contained systems are several-fold

1. They do not radiate and hence do not disclose your location to enemy observers.
2. They cannot be jammed by enemy action; the only way to reduce their effectiveness is to destroy them.
3. They can be capable of surviving nuclear attack and still provide nearly continuous navigation and positioning information.
4. They are generally insensitive to weather conditions as long as they have been environmentally designed and qualified to meet the range of expected environmental extremes.
5. Their effectiveness and accuracy during night operations are the same as during daytime.
6. Their performance is not limited by topography, obstacles to line-of-sight operations, etc.
7. They offer continuous navigation and positioning data, including velocity, heading (or bearing) and attitude (leveling) information.

These advantages provide the battlefield commanders with very valuable information, which can easily be tied into a common relative or absolute grid system, to control the movement of their forces, weapon delivery etc. and allow these actions to be coordinated accurately with those of other operating units.

Since these data can be obtained in real time, whether on the move or stationary, the commanders are provided with an additional element of flexibility. Depending upon the level of accuracy required, self-contained ESG inertial systems place very few maneuver restraints on tactical operations. Times between stopping points can be varied from a few to 10-15 minutes or more for positioning systems, depending upon the desired accuracy. Typical battlefield situations will be addressed later in this paper but first we shall proceed with descriptions of ESG navigation and positioning systems.

ESG INERTIAL SYSTEM DESCRIPTIONS

High precision ESG inertial systems are identified as the AN/ASN-136 SPN/GEANS (military aircraft INS) and GEO-SPIN™ (precision positioning and survey system derived from SPN/GEANS) both of which are produced by Honeywell Inc. Before proceeding with a description of ESG system features, a description of the ESG (Electrically Suspended Gyro) will be helpful since this is the truly unique element of the system. The key feature is that the spinning gyro rotor is suspended in an electrical force field which is energized by multiple-axis electrodes whose voltages are controlled by servo electronic circuits. The electrode voltages establish a gradient across an evacuated gap between the electrodes and the rotor. The three axis electrostatic force field then centers the rotor within the electrode cavity, resulting in a w^r with few restraining torques to contribute to its drift characteristics. In the Honeywell ESG a hollow beryllium sphere is used for the gyro rotor. The ESG has the unique characteristics of a highly dimensional stable gyro rotor suspended in a well controlled electrical force field and has the potential for high accuracy when properly mechanized in an inertial system configuration. Day-to-day stability better than 0.001 degree per hour (one sigma) and random drifts even smaller are typical.

The term SPN/GEANS is a U.S. Air Force acronym for Standard Precision Navigator/Gimbaled Electrically Suspended Gyro Aircraft Navigation System. The SPN/GEANS, now type designated as the AN/ASN-136, was developed primarily under sponsorship of the Air Force Avionics Laboratory at Wright-Patterson Air Force Base, Ohio (Reference 7). It was selected by the Air Force for upgrading the navigation capability of the entire B-52 bomber fleet. It is now in production at Honeywell, St. Petersburg, Florida, for that and other programs. During the past several years the high precision of SPN/GEANS has been evaluated and adapted to other applications, including airborne motion compensation/sensor stabilization.

A SPN/GEANS derivative, now known as the GEO-SPN™, performs as a high precision positioning and land survey system. It can perform both position measurements and interpolation of Earth's gravity field changes between locations of known gravity potential and direction, as determined by other means. The term GEO-SPIN™ basically stands for Earth Resource Related-Standard Precision Inertial Navigation/Survey System.

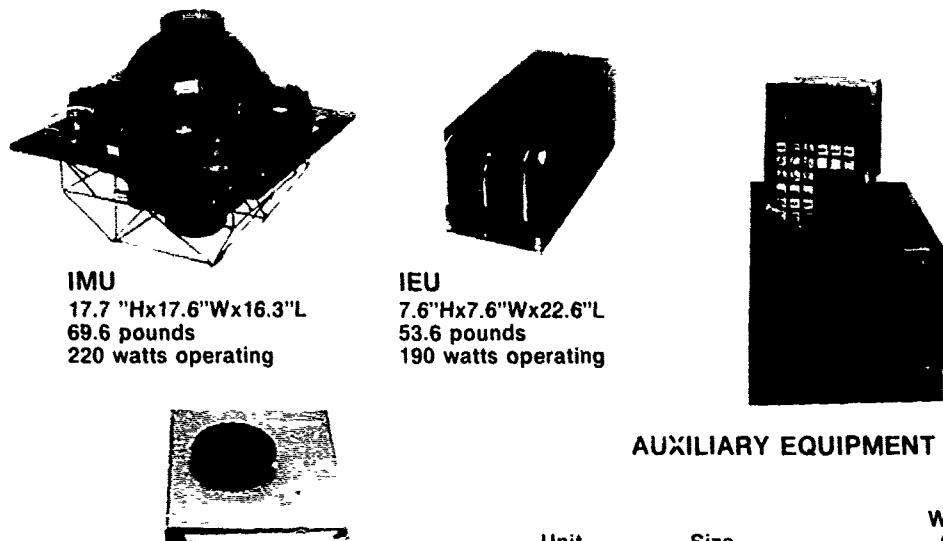
SPN/GEANS and GEO-SPIN™ are products of over 24 years of U.S. Government directed development. Over this period ESGs progressed from being a laboratory curiosity to fully mature, highly producible, operationally proven and mature inertial navigation devices and systems. During this period, it was realized that inertial systems were becoming expensive items to procure, operate, maintain and repair over operational life periods of 5-10 years and more. Hence, in addition to high performance requirements, the Air Force defined specific parameters in the areas of reliability, maintainability, and

productibility (i.e., acquisition cost). Through application of its then newly developed Balanced Design Concept, the Air Force monitored Honeywell progress in each of these areas. In all cases, by keeping aware of the specific requirements, Honeywell was able to apply careful design practices and meet or better all specification parameters. Application of a balanced design approach in this manner has proven out, in the case of SPN/GEANS, to have a major benefit to the user in that he now has a system which delivers high accuracy, provides a high degree of operational availability (predicted IMU/IEU MTBF of more than 1750 hours), is easy to repair when a malfunction does occur (MTTR of 0.3 hour, operational level, and 1.15 hours, intermediate level), and has reasonable acquisition, operation and maintenance costs.

Both SPN/GEANS and GEO-SPIN[™] are highly accurate, reliable, easily maintained inertial systems which use the ESG to maintain their inertial reference. As described above, the ESG has only one moving part, a suspended hollow beryllium ball, which is combined with two optical pickoffs to give gimbal tracking error signals. These are used to drive the Inertial Measurement Unit (IMU) platform gimbals to maintain a stable reference base for the accelerometers. Three highly accurate, single axis accelerometers (contrasted with the two-degree-of-freedom ESGs) are used within the Velocity Measuring Unit (VMU), which is mounted on the stable platform inner element. These accelerometers, oriented in an orthogonal triad configuration, measure accelerations directly and provide the incremental velocity pulses (delta Vs) to the computer, which it uses in its software algorithms to calculate velocity and position parameters.

These data, along with initialization parameters, geodetic reference values, platform gimbal angle measurements (from IMU gimbal angle encoders), and time are used to accomplish the self-contained alignment, navigation and related measurement functions on a worldwide basis with little or no reliance on other navigation aids.

The basic SPN/GEAN system consists of an IMU, an Interface Electronics Unit (IEU), and a complete software library. These hardware units are shown in the left side of Figure 1.



AUXILIARY EQUIPMENT AVAILABLE

	Unit	Size	Weight (Lbs)	Operating Power (Watts)
SOFTWARE	CDU	7.9'Hx5.8'Wx7.6'L	7.6	50
Fully documented and programmed on	DCU	7.6'Hx10.1'Wx19.0'L	63	210
<ul style="list-style-type: none"> • Honeywell Level 6/43 • ROLM 1602 • ROLM 1602/B • ROLM 1650 • ROLM 1664/1666 • IBM A/P101 	TB	4.2'Hx8.5'Wx12.5'L	32	0
	RDU	7.9'Hx5.8'Wx7.6'L	7.6	50

FIGURE 1. STANDARD PRECISION NAVIGATOR (SPN/GEANS)

For a stand-alone system capability, these two units are supplemented with a Digital Computer Unit (DCU) and a Control Display Unit (CDU). Typical units are shown in the right side of Figure 1. Also in that figure is a summary of key physical characteristics, including size, weight, and power.

The IMU contains, in addition to the VMU and two ESGs, temperature control electronics, accelerometer pulse rebalance and delta V readout electronics, gimbal control electronics and built-in test functions (BITE), as well as data bus communication electronics. The IEU provides power conversion, control and sequencing electronics, additional BITE circuits, and a common serial data bus interface with other units of the inertial system and other subsystems.

Operator control of the system can be provided through a CDU or a teletype unit. A typical CDU uses a modified calculator-type keyboard to provide a verbalized form of communication with the DCU. A variety of displays are available from a simple register pair to a 256 character display which allows more complete, simultaneous display of mission data.

The Digital Computer Unit (DCU) performs all computations needed to solve system equations, format and output system data, and generate system control functions. The computer software package includes both operational and diagnostic programs. Operational programs include: (1) on-line navigation and positioning control, including Kalman filter aided mechanizations when required; and (2) off-line or post-process data reduction and analysis functions.

For some applications, like positioning and topographic or artillery survey, on-line data recording may be desired. Therefore, several data recording options are also available for both SPN/GEANS and GEO-SPIN™ systems. These include large (10-inch reel) and small reel type magnetic tape recorders, as well as several types of cassette recorders. One of these, a Quantex Unit, provides an especially reliable method of in-the-field data recording with direct read-after-write data verification. Auxiliary optical equipment options, such as a K&E Electronic Distance Measuring Equipment, are also available for use in surveying and positioning applications.

The major differences between SPN/GEANS and GEO-SPIN™ systems are in the computer software packages and the auxiliary equipment options. Other differences exist in the type and frequency of gyro and accelerometer calibrations and Kalman filter mechanizations. These will be discussed later in this paper under the specific topics.

OVER THE BATTLEFIELD - SPN/GEANS AIRCRAFT INS PERFORMANCE

For several decades inertial navigation systems have been used extensively for self-contained navigation of subsonic and supersonic aircraft and unmanned air vehicles. For many years the standard level of high performance systems was 1.0 nmph (1.9 kmph) or 6080 fph (1854 m/hr) CEP, of position error drift. Accompanying this was velocity measurement error of 5-6 fps (1.5-1.8 m/s) (one sigma) and attitude measurement error on the order of 2-4 milliradians or 6-12 arc-minutes, one sigma. These parameters all applied for pure inertial or unaided performance. Improvements to values 2-3 times better could be achieved with such systems when used in Kalman filter mechanizations aided by doppler radar velocity measurement and position fixes from a variety of sources such as LORAN, OMEGA, Doppler Navigation Satellite (NAVSAT), etc.

The maturing of ESG technology has permitted major breakthroughs in performance for pure inertial and aided inertial operation. For example, SPN/GEANS performance specifications are: 0.12 nmph (0.22 kmph), CEP, for position; 2 fps (0.6 m/s) (one sigma) for velocity; and 3 arc-minutes (one sigma) for attitude (roll, pitch and heading). Against these specifications, SEN/GEANS has demonstrated 0.06 to 0.08 nmph (0.11 to 0.15 kmph), long term, 4 hours or greater, and 0.1 nmph (0.19 kmph) short term 1-3 hours, 1.0-1.2 fps (0.3-0.4 m/s) and 1-2 arc-minutes of position, velocity and attitude error respectively (References 1, 2 and 3).

Typical performance from this level of ESG system performance has required little or no reliance on other navigation aids for most aircraft applications, thus giving a truly self-contained navigation capability. This greatly enhances mission success for long duration flights, particularly where aircraft are "on station." For reconnaissance type missions much closer pattern holding and/or lane control is possible, again with little or no reliance on external aids. For weapon delivery missions, much smaller bomb delivery CEPs and missile system initialization errors are achievable using an ESG system for carrier aircraft navigation and missile system master reference. Cargo and transport aircraft benefit from ESG performance by reducing terminal area errors and allowing enroute adherence to narrower flight corridors with fewer checkpoints.

Antisubmarine warfare and long overwater aircraft patrols can also benefit from the lower error growth rates of an ESG inertial system. Added benefits are reduced heading sensitivity due to improved thermal and magnetic control of the IMU and insensitivity to aircraft and mission flight dynamics. Heading sensitivity of SPN/GEANS, for example, is 5-10 times smaller than other aircraft inertial systems. Higher order g-sensitive terms such as gyro anisoelasticity and accelerometer vibropendulosity are up to 50-400 times smaller in the ESG system when compared to other INSs. These have a direct bearing on flight dynamic sensitivity and are among the reasons why GEANS has been used on the U.S. Navy's Project Magnet P3D aircraft for the last six years and is being considered for current and new generation maritime patrol aircraft. Whereas the existing conventional INS degrades under severe buffeting that's encountered during extended flight at very low altitude on the Magnet aircraft, the GEAN system continues its fully-rated performance level during all parts of the mission. Attempts to excite SPN/GEANS flight dynamic sensitivity were undertaken at Holloman AFB in a high performance F4 aircraft. A full range of aerobatic and tactical maneuvers was used with the result that 0.1 nmph (0.19 kmph) performance was maintained throughout the test. In other words, no degradation in flight performance was observed, compared to quiescent straight and level flight.

Benefits of ESG system performance to a wide variety of aircraft applications will be fully realized during the 1980's as SPN/GEANS deployment continues throughout the entire U.S. strategic aircraft fleet. Widespread use is also expected for long term reconnaissance and patrol missions, as well as specialized cargo and transport usage in both military and civil applications and in tactical military aircraft.

Ultimate airborne performance of ESG systems is limited by the imperfections in the model of the Earth's gravity field. These limitations would be existent for any high accuracy inertial system. The errors between the gravity reference model and the actual values of local gravity deflections from vertical excite Schuler loop oscillations within an inertial system, resulting in 84 minute periodic functions which build errors in velocity and position that grow as a function of the square root of time. As altitude and speed increase, the vertical deflection variations tend to smooth out and cause less pronounced errors. Knowledge of gravity field deflections is improving and expanded modeling of their characteristics is being considered. As the use of gravity modeling increases during the 1980's, it is expected that corresponding improvements in ESG operational accuracies will result. Using today's ESG hardware technology, combined with calibration, alignment, and modeling software improvements, it is conceivable that airborne ESG system performance in the 0.01-0.05 nmph (0.02-0.09 kmph) range with velocity errors less than 0.1 fps (0.03 m/s) and attitude better than 1.0 arc-minute will be available to operational users in the 1980's. The forecast that software and procedural improvements alone will reap these benefits makes the ESG system hardware procured today even more cost effective as it is used during the next 10-15 years.

The above performance levels all apply for pure inertial system performance, that is, without the use of any navigation aids such as doppler radar, LORAN, radar position fixing, DME, etc. For operation over the tactical battlefield, one or more of these aids may be available. Also, there may be tighter requirements for airborne position measurement, on the order of 25-50 meters, CEP, or less. In that case, ESG system precision still offers important advantages. For example, with short term position growth rates of 10-20 meters per minute (pure inertial) down to 2 meters per minute (doppler-inertial), the SPN/GEANS combined with high accuracy position fixes (visual low level radar or DME) could readily satisfy these requirements. Carried to the extreme, well integrated ESG/DME systems could deliver on-line, real-time position accuracies during helicopter flight down to the levels of 1-2 meters, rms. Programs to demonstrate that capability are under discussion in the U.S.

ANOTHER AIRCRAFT APPLICATION - SENSOR STABILIZATION OF MOTION COMPENSATION

In addition to the traditional function of position determination, the higher accuracy outputs of velocity and attitude data from ESG systems have opened up new possibilities for stabilization and/or motion compensation of other (noninertial) sensors. These include high precision radars, sonars, lasers, optical and electro-optical devices. As the technologies associated with these devices have progressed, new requirements for accurately pointing them, either in real-time or through post-processing, have also evolved. Early uses of inertial systems to stabilize these sensors, or the data obtained from them, were generally limited to attitude accuracies of 2-4 milliradians (6 to 12 arc-minutes) or more and velocity measurements good to 5-6 fps (1.5-1.8 m/s) one sigma.

However, with the advances in active and passive sensors, their pointing requirements have now tightened to values on the order of 1-1.5 arc-minutes for attitude and 1-2 fps (0.3-0.6 m/s) for velocity (one-sigma values). Intrinsic attitude errors of an ESG system are in the range of 1-3 arc-seconds (level) and 10-20 arc-seconds (heading or azimuth). Readout of these parameters is currently the limiting factor, resulting in 1-2 arc-minutes of total one sigma attitude error, using single speed resolvers for gimbal angle encoders. With multispeed resolvers or Inductosyns the attitude readout accuracy can be reduced to the order of 5-15 arc-seconds, consistent with the intrinsic attitude errors. Miniaturization of multispeed encoders should make them compatible with an inertial platform like SPN/GEANS. Hence, direct attitude accuracies from a precision ESG inertial platform within the next 2-3 years should be reducible by another factor of 5-10 to one, compared to the 1-2 arc-minutes currently available.

In addition to direct attitude stabilization from a gimballed ESG inertial platform, a new measure of flexibility has developed through the marriage of low cost strapdown inertial sensor assemblies, in one or more locations on an aircraft or ship, with a centrally located precision system. The technique of inertial slave alignment (attitude and velocity matching), similar to that used for air launched missile initialization, can marry the strapdown unit to the higher accuracy gimballed platform. Several development programs to provide this capability for radars and laser devices are currently underway. Accuracies on the order of 1-2 arc-minutes of absolute attitude are available. With upgrading of strapdown inertial sensors and slave align techniques, these accuracies should be reducible during the next few years to levels of 15-30 arc-seconds, one sigma. The slave align process also trims velocity and position errors of the strapdown unit and hence enhances its total inertial navigation and stabilization capability.

Packaging flexibility of the strapdown sensors offers very attractive options. For example, the H-478 series of Inertial Reference Units produced by Honeywell, which normally come in 4.0 x 4.5 x 12.3 inch (10.2 x 11.4 x 31.2 cm) packages, can be reduced

for critical volume applications to a sensor block containing three gyros, three accelerometers, and their temperature control (if required) in a package that's only $1.8 \times 4.5 \times 7.5$ inches ($4.6 \times 11.4 \times 19.1$ cm). This size package can readily be mounted directly on the rear of an antenna, providing direct stabilization with small lever arm corrections. The IRU electronic functions are then remoted to a more convenient location on the aircraft. Computing functions for the slaved strapdown unit may be performed either in the primary system's navigation computer or in a small mini- or micro-computer located with the IRU electronics.

The adaptability of this approach to motion compensation and sensor stabilization is almost unlimited. The costs of stabilizing additional sensors on an aircraft or ship are relatively small, once the proper master system has been provided for. Locations of sensors to be stabilized are similarly unrestricted - they may be mounted elsewhere within the fuselage, on or in the tail, or even on the wings or wingtips of an aircraft. Similarly, installation aboard ship is also very flexible, with remote strapdown sensors being usable throughout the vessel, on antenna masts, on weapon launchers or within turrets, etc.

The application of both high precision ESG inertial systems and lower accuracy strapdown units to the functions of motion compensation and sensor stabilization is expected to grow significantly during the 1980's, compatible with improving technologies for the various radar, sonar, laser, optical and electro-optical devices which require accurate pointing and stabilization.

GEO-SPIN™: PRECISION POSITIONING ON THE BATTLEFIELD

During the 1970's, inertial technology applications took a new and very challenging turn with the use of gimbaled inertial platforms for land positioning and survey tasks. The most rigorous of these applications, from the viewpoint of required inertial accuracies, is the land survey work. This includes three-dimensional position measurement in the 50 centimeter range, as already demonstrated by the GEO-SPIN™ system, as well as relative gravity measurement, including both vertical (anomaly) and horizontal (vertical deflection) components. The gravity measurements already performed have demonstrated amplitudes to the < 10 milligal level and vertical deflection accuracies of 2-4 arc-seconds, rms. By the end of this year, with improvements now being incorporated, the GEO-SPIN™ system should be demonstrating on-line positioning accuracies of less than 25 cm, rms, as well as gravity measurements of less than 1.5 arc-seconds, rms, (deflections), and 1-2 milligals (anomaly).

The operational techniques which permit the achieving of these accuracies include the use of periodic zero velocity updates (so-called "ZUPTs") to control the inertial system error growth. Typical intervals between ZUPTs are currently 3-5 minutes of time, with 20-60 seconds being spent in the zero velocity state at each ZUPT point. Because of ESG system stability, the intervals between ZUPTs can be increased for real-time battlefield positioning in the future.

The land survey and positioning role of inertial systems has been expanded to use both land vehicles and helicopters. In addition to accomplishing the aforementioned accuracies, inertial land survey offers quantum improvements in survey productivity, with factors of 10-20 to one already demonstrated, when compared to classical survey techniques. In other words, an artillery positioning survey, which would otherwise take several hours or longer to complete, can be done in only a matter of minutes using inertial survey equipment.

The high accuracy and stability of ESG inertial systems like GEO-SPIN™, combined with the low noise content of their inertial sensors (e.g., 1-2 cm of position uncertainty for GEO-SPIN™), offer major benefits to precision land survey. The current projections for GEO-SPIN™ measurement accuracies include 10-15 cm, rms, for position, < 1 milligal for gravity anomaly, and < 0.5 arc-second, rms, for vertical deflection of gravity (Reference 3).

For battlefield positioning, the advantage of closed-loop positioning is usually not available. Rather the task is to precisely locate a position, coming off a single reference point, or a pair of points in the case of a bearing or azimuth reference. This approach, known as open-loop positioning, results in less accurate positioning but still yields data in the 1-10 meter range, depending upon the interval between ZUPTs and distance from the reference point(s).

SYSTEM ERROR SOURCES

For ESG inertial systems like SPN/GEANS and GEO-SPIN™, calibration of the gyroscopes and accelerometers, and stability of the calibrated parameters thereafter, are essential to the high precision performance. To achieve the 0.1 nmph (0.19 kmph) accuracy, only once-a-year calibrations are required. The specified error budget values, including both calibration uncertainties and day-to-day, or runup-to-runup parameter shifts, are shown in Table 1.

TABLE 1. SPN/GEANS ERROR BUDGET
(One Sigma Values)

o Accelerometers:

Scale Factor	50 parts per million
Bias 50 micro-g's	
Misalignment Angle	14 arc-seconds

o Gyros:

G-Insensitive Drift	0.001 degree per hour
G-Sensitive Drift	0.001 degree per hour per g
G ² -Sensitive Drift	0.0002 degree per hour per g ²
Redundant Axis Torquing	0.001 degree per hour

The exceptional low g² characteristics for the gyro (and a similarly low value for the accelerometer) are important in field operations because they result in very low environmental sensitivity of the inertial components to vibration and shock inputs. Compared to conventional sensors in 1 nmph systems, these values are some 50 to 400 times smaller. Similarly, because the ESG gyros are operated in an inertially space-stable IMU (rather than a torqued local vertical mode), an important error source, gyro torquing has been virtually eliminated. The redundant axis torquing defined in Table 1 is at a very low level required to keep the redundant axis No. 2 of gyro 2 aligned to the No. 1 axis of gyro 1 (this because we have two two-degree-of-freedom gyros with four active axes, but only three orthogonal platform axes are needed for stabilization). As a result key elements of SPN-GEANS performance lie directly within the inertial sensors' design. These characteristics combine with carefully controlled thermal and magnetic environments within the IMU and electronic circuit designs with the necessary resolution, dynamic range, and stability to yield the specified overall system performance.

When continuous operation of SPN/GEANS is part of the scenario, then the system level performance can be improved by 2:1 or better. Combining this with premission calibrations (such as in shipboard or land vehicle applications) yields still further improvements. For example, when precisely positioning on land, a one-hour long series of accelerometer calibrations can reduce those errors in Table 1 to levels of 1-2 ppm (scale factor), 1-2 micro-g's (bias) and 1-2 microradians or 0.2 to 0.4 arc-second (misalignment angle). These parameters are then compatible with submeter positioning on the battlefield.

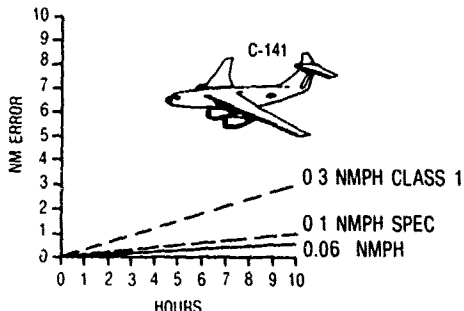
Higher order terms also become important when considering precise battlefield positioning. In the case of accelerometers, the second order nonlinearity of scale factor should be accounted for, especially in a space-stable system where accelerometers are continuously tumbling at Earth's rate through a 1g gravity field. As described in Reference 3 paper, this nonlinearity can be trimmed down to an uncertainty of 1-2 parts per million per g, using the same accelerometer calibration mentioned above. A noteworthy aspect of that calibration is that it can be done as a normal part of field operations with the inertial system installed in its vehicle. The entire operation is automatic once it is initiated by operator command.

Gyros in the ESG system can also be calibrated in the field although it is a longer process (currently 30 hours) and hence would take equipment out of service for a day or so. However, the good news is that even for the precise positioning on the battlefield, to levels discussed thus far, it appears unnecessary to calibrate the gyros more than once per year.

FIELD PERFORMANCE TEST DATA

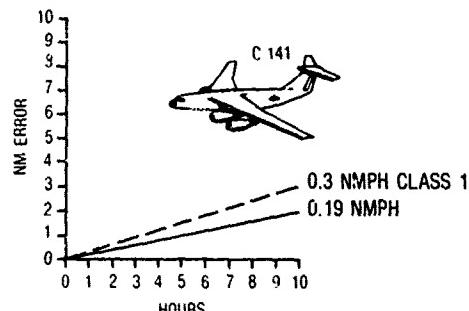
The SPN/GEANS and GEO-SPIN[™] systems have been extensively tested in the field. Flight tests of the aircraft INS have taken place beginning as far back as 1971. Many of these were performed at the Central Inertial Guidance Test Facility (CIGTF), located in the U.S. at Holloman Air Force Base, New Mexico. In the 1975-76 time period the SPN/GEANS EDM (Engineering Development Model) systems underwent formal flight verification tests by the U.S. Air Force at CIGTF. A summary of those flight tests is shown in Figure 2. The data presented therein primarily show long term flight performance (3-6 hour sorties). SPN/GEANS qualified at 0.06 nmph (0.11 kmph) CEP for six-hour and 0.10 nmph (0.19 kmph) CEP, for three-hour flights, all in the pure inertial mode-- in other words, no navigation aids such as doppler radar (velocity damping) and external position fixing were used. In the right side of the figure are shown the air start/air align performance results. Operating scenario for these sorties was a zero ground reaction time with the INS being initialized and aligned in the air, using APN-213 doppler radar for velocity initialization and CIRIS position fixing to provide convergence of the azimuth alignment solution. Results of air align flights were quite good-- far better than ever demonstrated previously by any other INS. These data and subsequent flights in B-52 bombers convinced the U.S. Air Force that air start/air align was a viable operating option for the SPN/GEANS INS.

VERIFICATION FLIGHT TESTS



NUMBER OF FLIGHTS 26
 PERFORMANCE 0.06 NM PH (CEP)
 VELOCITY <1.0 FT/SEC

AIR START/AIR ALIGN



NUMBER OF FLIGHTS 10
 PERFORMANCE 0.19 NM PH (CEP)
 VELOCITY <1.2 FT/SEC

FIELD OPERATING HOURS 980
 FLIGHT HOURS 268
 AVERAGE HOURS/FLIGHT 4.9
 NUMBER OF FAILURES 1 GROUND

FIGURE 2. HOLLOWAY AIR FORCE BASE

Although the performance results shown in Figure 2 express aircraft INS accuracy in commonly accepted terms, for certain types of tactical missions, shorter term position data are of interest, such as relative position error over any ten-minute period. In the battlefield situation, for example, this could be of interest in "seek and destroy" missions or in ones where a target is identified along with the attacking aircraft's position, at the beginning of a few minute period, and it is then necessary to precisely know the aircraft's position for the next 1-10 minutes. Short term position accuracy of this type involves the Schuler loop characteristics of an INS which cause cyclical errors, having an 84-minute period, to propagate at error rates 4-6 times greater than the long term characteristics of the INS. Using data obtained from the CIGTF verification tests, we analyzed these shorter term errors, specifically over periods of 1 and 10 minutes. This was done by taking the position error measurements for up to 25 flights, examining the data points obtained at 12-minute intervals and ratioing them back to 1 and 10-minute periods. This linearizing step appeared to be valid, and probably somewhat conservative, over these relatively short time increments. The results of that analysis are shown in Figures 3, 4, and 5. The radial errors shown in Figure 3 are actually rss combinations of the longitude and latitude errors of Figures 4 and 5, combined on a time increment basis. In other words, at T+2 hours the longitude errors from 24 flights at that point in time were combined with the respective latitude errors to obtain the rss radial error of 19 yards (17 meters) relative to the position at T+1 hour 59 minutes. It should be kept in mind that the errors plotted in Figures 3, 4, and 5 are pure inertial ones with no navigation aids used to trim INS position, velocity or attitude errors. For positioning over the battlefield, these values represent a worst case scenario for SPN/GEANS. Even so, they are 5-10 times better than those obtainable with other aircraft INSSs.

Where higher in-flight precision is needed, the SPN/GEANS data can be mixed via Kalman filtering with those from other sources, with the result that much smaller position errors will develop. For several applications, 25-50 meter, CEP, uncertainties have appeared to be easily available. As mentioned previously in this paper, combining SPN/GEANS with high precision DME or GPS-aiding, will result in real-time errors in the several meter category. Although actual field test data cannot be presented here, let it suffice to say that feasibility has been proven. This has already been found to be of interest in certain commercial geophysical applications, such as airborne gravity surveys. In time it may also be exploitable in the military battlefield situation.

For the motion compensation application, actual field test data cannot be presented here. However, laboratory tests have been performed using SPN/GEANS alone and SPN with a slave-aligned H-478 strapdown IRU. Results of several of these tests are shown in Figures 6-9. For SPN alone, the IMU was mounted on a test table and then rotated in azimuth in small increments. At each point a series of 30 measurements was taken so that noise data could be analyzed. The mean values of each set of 30 points are plotted in Figure 6. Note that all values are well under one arc-minute, with typical values in the 30-40 arc-second range. Figure 7 shows the measurement of noise or short term instability,

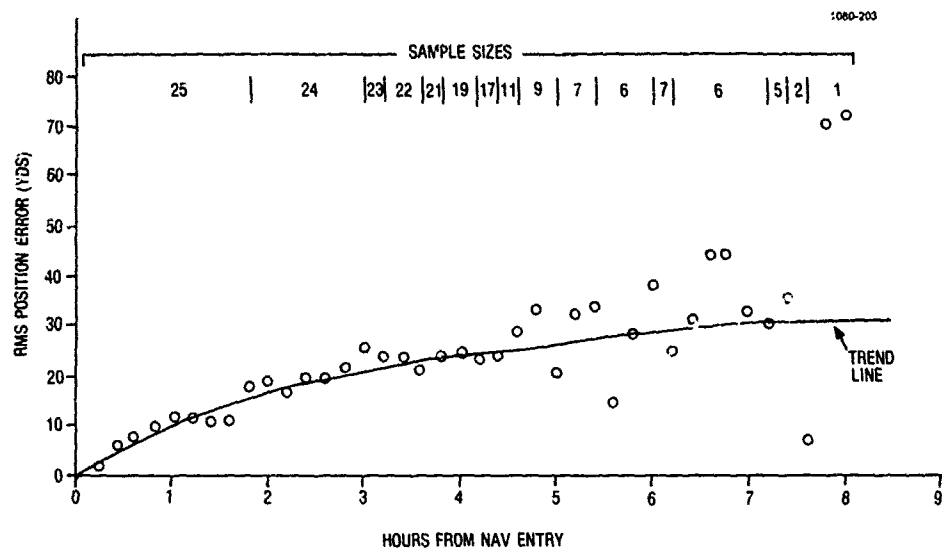


FIGURE 3. SPN/GEANS FLIGHT DATA SHORT TERM POSITION ERRORS
(RSS RADIAL ERROR) ONE MINUTE INTERVALS

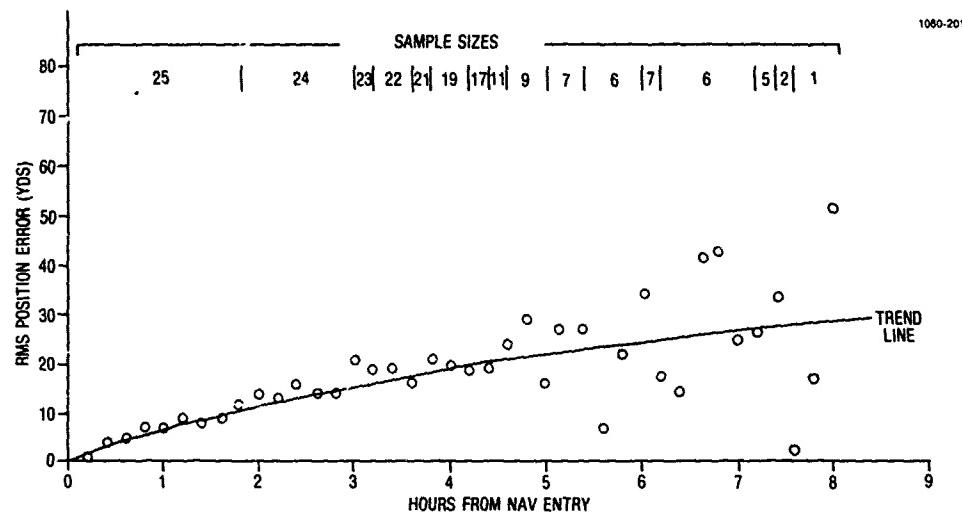


FIGURE 4. SPN/GEANS FLIGHT DATA SHORT TERM POSITION ERRORS
(DELTA LONGITUDE) ONE MINUTE INTERVALS

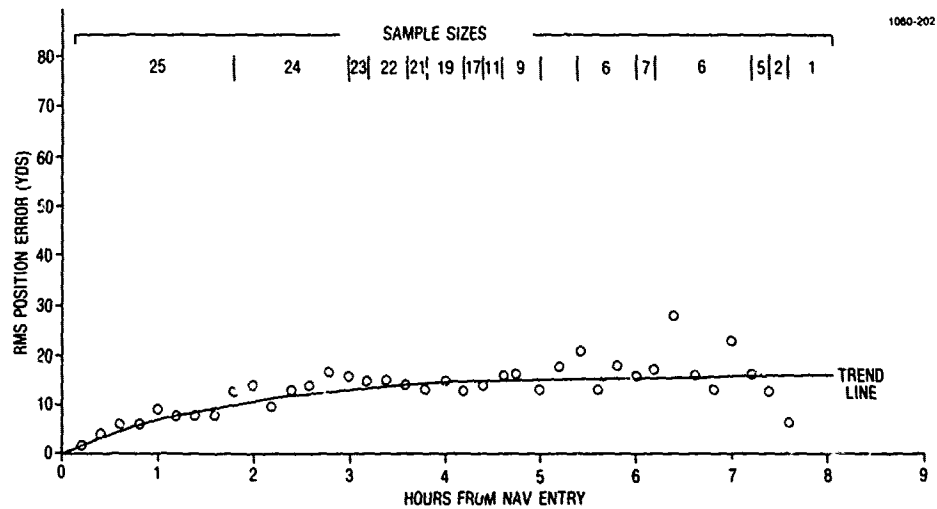


FIGURE 5. SPN/GEANS FLIGHT DATA SHORT TERM POSITION ERRORS
(DELTA LATITUDE) ONE MINUTE INTERVALS

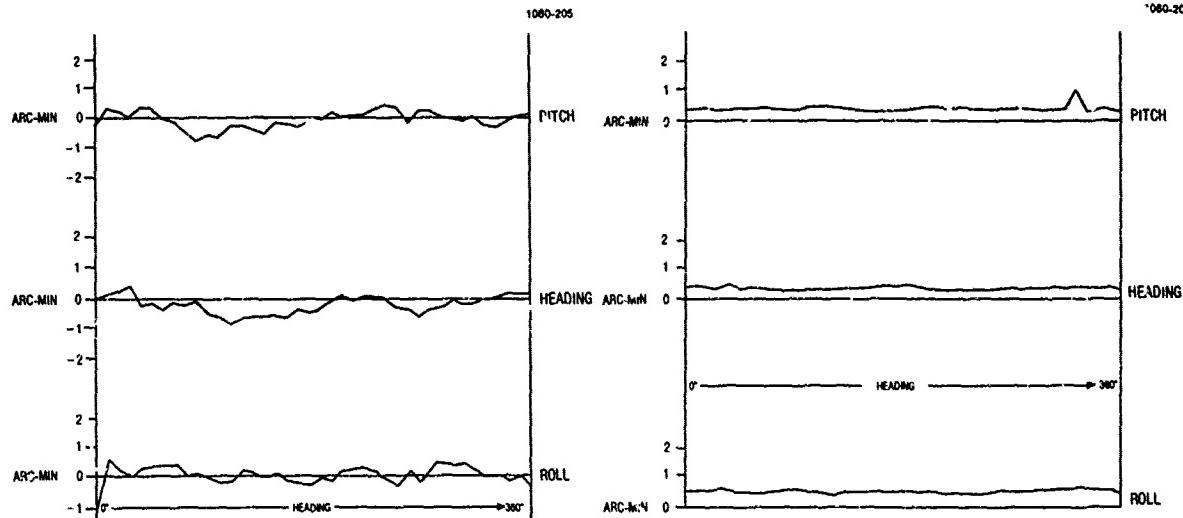
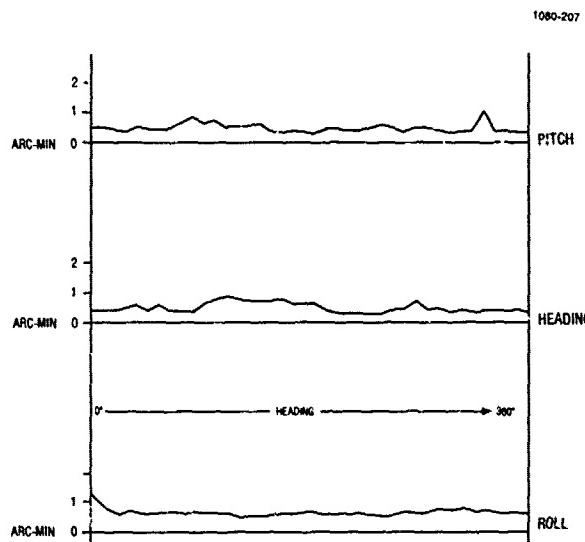
FIGURE 6. SPN/GEANS ATTITUDE ACCURACY -
ERROR MEANSFIGURE 7. SPN/GEANS ATTITUDE ACCURACY -
STANDARD DEVIATIONS

FIGURE 8. SPN/GEANS ATTITUDE ACCURACY - RMS ERROR

A/C HEADING ERROR (ARC-MINUTES) 0.73

Alignment 0.52
Tracking 0.51
Noise 0.07

A/C PITCH ERROR (ARC-MINUTES) 1.41

Alignment 0.62
Tracking 1.27
Noise 0.07

A/C ROLL ERROR (ARC-MINUTES) 1.10

Alignment 0.41
Tracking 1.02
Noise 0.07

FIGURE 9. H-478/SPN REMOTE MEASUREMENT SYSTEM DATA

expressed as the standard deviation of the 30 samples (roll, pitch, and heading) taken at each azimuth position. The typical values from this test were about 40 arc-seconds. The mean and standard deviation values were combined to obtain root-mean-square (rms) measures. These data are shown in Figure 8 with typical values being less than 60 arc-seconds. Figure 9 shows laboratory test results when an H-478 strapdown IRU was combined with (aligned to) a SPN/GEANS IMU. Again, roll, pitch, and heading data are displayed. Each set of data was analyzed in terms of an alignment error, a tracking error after the IRU was moved, and a noise error or data scatter. Note that the total errors were in the 60-90 arc-second (1-1.5 arc-minutes) range. Alignment and tracking were the most significant contributors with noise levels being relatively small. Subsequent field tests on H-478 type units have shown similar results, in terms of total errors, when slave aligning the strapdown unit to a master INS. These and other motion compensation data are discussed in the Reference 2 paper, along with estimated improvements in these performance levels during the 1980's.

Field positioning test data were reported very recently in the Reference 5 paper. Tests were performed on surveyed test courses in Florida and Wyoming. A wide variety of tests was run and the following characteristics evaluated:

1. Single, double, and four traverse runs over 30-63 km distances with four minute ZUPT intervals.
2. Double traverses over a 6 km distance with one minute ZUPTs.
3. Short term repeatability with a variety of system headings and survey directions using one minute ZUPTs.
4. ZUPT interval sensitivity (of special interest in battlefield positioning) during static tests with intervals varied from one to eight minutes.
5. Field heading sensitivity on an L-shaped test course (this had been an important limitation in earlier inertial positioning systems).
6. Helicopter double traverse runs over a 63 km test course using four minute ZUPT intervals, as well as both landed and hover ZUPTs.
7. Azimuth measurement accuracy in the field using a two-point positioning and inverse azimuth determination technique.
8. Coarse gravity measurements (deflections and anomaly) over a 63 km test course with four minute ZUPTs and on-line data reduction. (Earlier inertial positioning systems had only an off-line capability in determining gravity values.)

Detailed discussion of these data were covered in Reference 5. However the highlights of these tests were:

1. Land vehicle single traverses yielded 52-75 cm, rms, positioning (latitude, longitude, and elevation). Double traverses improved this to the 40-60 cm, rms, range. Open-loop errors were typically 4-6 meters. Figures 10 and 11 show typical data.
2. One-minute ZUPT survey data were in the 8-13 cm, rms, range.
3. One-minute ZUPT repeatability with respect to a common station was in the 1.6 to 4.1 cm, rms, range with 1.6 to 3.1 cm being most representative.
4. ZUPT interval sensitivity appeared to be about an 8.7 cm increase in rms uncertainty per minute (see Figure 12).
5. There was no discernible heading sensitivity after closure and smoothing of field test data.
6. Helicopter test data (landed ZUPTs) were as good as or better than those from land vehicle tests over the same course (see Figure 13).
7. Azimuth measurement accuracies were in the less than ten arc-seconds, rms, range.
8. Gravity measurements were 2-4 arc-seconds, rms, for vertical deflections and 5-9 milligals, rms, for anomalies, without using premission accelerometer calibrations.

Although these levels of performance are typically better than required for battlefield operations, the noteworthy point is that an inertial positioning system, such as GEO-SPIN™, which can deliver these levels of closed loop, real-time, smoothed data accuracies, should readily be capable of delivering open loop accuracies on the battlefield to the order of a few meters or so.

Run No.	RMS Position Error (cm)			Azimuth Error Arc-Sec
	Latitude	Longitude	Elevation	
1	100.6	81.4	37.0	-
2	105.2	74.0	63.0	-
3	56.4	74.2	54.0	4.4
4	41.0	51.5	62.0	7.6
5	50.6	57.5	82.0	9.4
6	31.7	25.6	56.3	13.1
7	35.2	35.0	51.0	13.1
8	29.1	58.1	51.6	10.9
9	120.3	21.3	114.0	15.1
10	47.5	32.5	36.0	6.7
Total RMS	70.0	55.0	64.0	11.0
Less Test Course Error	15.0	15.0	3.0	10.0
Net Error Versus Specification Values	55.0	40.0	61.0	1.0
Data Source: 4-Wheel Drive Vehicle Tests, Cheyenne Wyoming Survey Test Range	100.0	100.0	100.0	30.0

FIGURE 10. LAND VEHICLE FIELD ACCEPTANCE TEST DATA SUMMARY

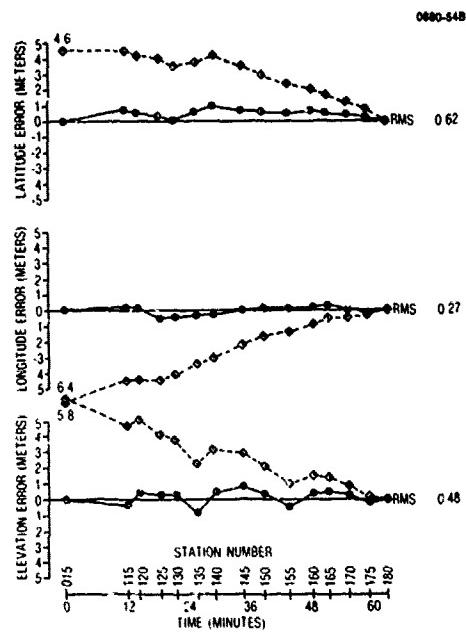


FIGURE 11. RAW AND SMOOTHED SURVEY DATA

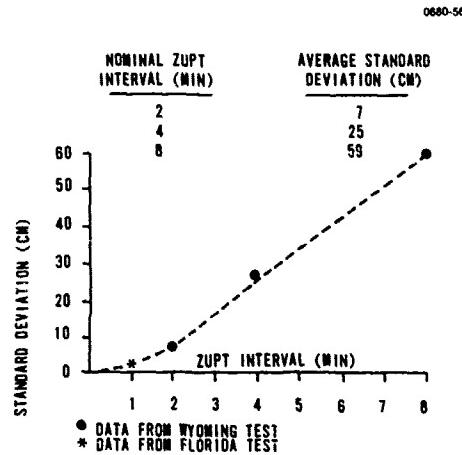


FIGURE 12. ZUPT INTERNAL DATA SUMMARY

Run No.	RMS Position Error (cm)	Latitude	Longitude	Elevation
1	64	*	54	
2	26	32	23	
3	42	73	19	
4	36	61	31	
5	66	56	52	
6	40	54	42	
7	48	98	58	
8	51	44	89	
9	45	67	55	
10	Not Applicable - Different Course			
11	35	153	27	
12	40	54	42	
13	91	128	54	
14	93	59	77	
15	40	56	60	
16	132	94	73	
17	84	93	29	
18	74	62	39	
19	42	58	34	
20	20	32	39	
Total RMS	64	79	52	
Less Test Course Error	15	15	3	
Net error	49	64	49	

*Invalid reference data used.

FIGURE 13. HELICOPTER WYOMING FIELD TEST DATA SUMMARY

HYBRID ESG INERTIAL SYSTEMS

Although systems like SPN/GEANS and GEO-SPIN™ do not rely upon other navigation aids for their highly accurate performance, there are situations where such aids can be put to good use to further enhance positioning precision. As a consequence, SPN has been operated in hybrid configurations with LORAN, TRANSIT Navigation Satellites, precision Distance Measuring Equipment (DME), and a variety of radars for both position fixing and velocity aiding (doppler radar). Shipboard configurations have used Electromagnetic (EM) Speed Logs for velocity damping. Preliminary studies have been performed to show the feasibility and benefits of using Global Positioning Satellite (GPS) with inertial systems. The results of one set of simulations, using SPN/GEANS as the INS, are shown in Figures 14-16. The scenario for this simulation was one where SPN operated pure inertial for five hours, was then updated by GPS for one hour, and again operated pure inertial for another 1.5 hours. A review of the figures shows that short-term position and velocity data were essentially controlled by GPS during the hour of integrated operation and SPN performance following that period was about 4:1 better in short-term position* and 2:1 better in velocity. Because of the interaction of attitude and position in the SPN equations and the presence of those parameters in the Kalman filter error states, SPN attitude errors were also improved during and after the GPS-aided interval.

In order to realize the fullest benefit of such hybrid system operation, it is necessary to use Kalman filtering in the system software mechanization. Many analyses and simulations have been performed over the years on Kalman filtering of hybrid inertial systems. However, reducing these to practice did not always meet with the predicted successes, at least in the early years. SPN/GEANS has enjoyed above average success in this regard. Operational Kalman filters have been used with the GEANS family of systems since 1972. Error state sizes included 7, 9, 10, 13, 17, 21, and 23 parameters. SPN has one of the most sophisticated airborne filters flying today, with 23 error states. It has been in use for over three years.

For ground positioning the GEO-SPIN™ operates in a dual mode-- one with pure inertial data adjusted linearly and with a least-squares filter, the other with a 21 state Kalman filter. Because of the low noise levels in GEO-SPIN™ and the need for further optimization of the filter, it has yet to surpass the pure inertial/least-squares filter in performance. However, it is anticipated that in the next year or so, the roles will be reversed and Kalman filtering will provide effective accuracy improvement on the surface as it has done previously in the air.

OPERATIONAL USE OF ESG INERTIAL SYSTEMS

A key question which arises when we speak of high precision performance is that of consistency. Will the system perform reliably with the desired accuracies? That's where the importance of design centering enters the picture. Many dollars have been expended in designing, analyzing, and testing the SPN/GEANS and GEO-SPIN™ electronic and mechanical designs to insure that adequate design centering does exist. This applies to electronic circuit, in the selection and rating of components, balancing of their operating parameters, worst-case circuit analysis, and the rigorous testing of the final circuits and assemblies. In the mechanical design realm, it includes the careful balancing of thermal parameters (temperatures, gradients, heat flows, etc.), shielding of magnetic fields (both internally and externally generated), and mechanical tolerancing to maintain dimensional integrity, reduce stresses, etc.

Design centering results in improved reliability or Mean-Time-Between-Failures (MTBF). For the ASN-101 with over 10,000 hours of field operation the mature field MTBF of 1,139 hours was demonstrated versus a prediction back in 1970 of 1,192 hours. Where fewer operating hours are obtained, a Reliability Growth Curve must be used to measure MTBF. The AN/ASN-131 demonstrated 604 hours MTBF in 2-1/2 years of operational flight testing in the 1975-78 time frame. This placed it well ahead of the expected field MTBF for the number of cumulative operating hours on the Reliability Growth Curve, whose ultimate predicted value was 1500 hours. For the current AN/ASN-136, the predicted MTBF is 1771 hours. Comparison of early operating data to the growth curve expectations, indicate that it should achieve this as a demonstrated value within the next few years.

Another operational factor is the environmental capability of an inertial system. A piece of precision equipment which cannot be used in the rugged extremes encountered on and over the battlefield is of little value to military forces. In the design of SPN/GEANS and GEO-SPIN™, the capability to withstand rugged environments was designed in from the beginning. Design characteristics for these equipments are shown in Figure 17. These parameters have been demonstrated in most cases by formal qualification testing. This has been complemented by in the field experience with testing from the cold and snow of Alaska, to the deserts of New Mexico and the hot, humid conditions of Florida. High latitude operation to the North Pole has also been demonstrated. Under all of these conditions the INE operated accurately and reliably.

*See earlier paragraph for discussion of short-term position errors versus long-term position error growth.

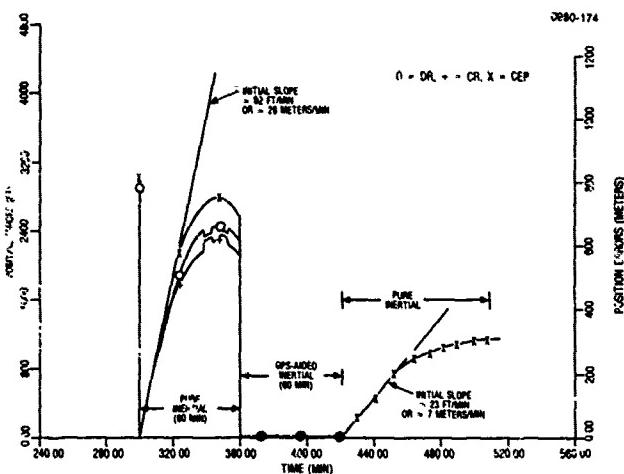
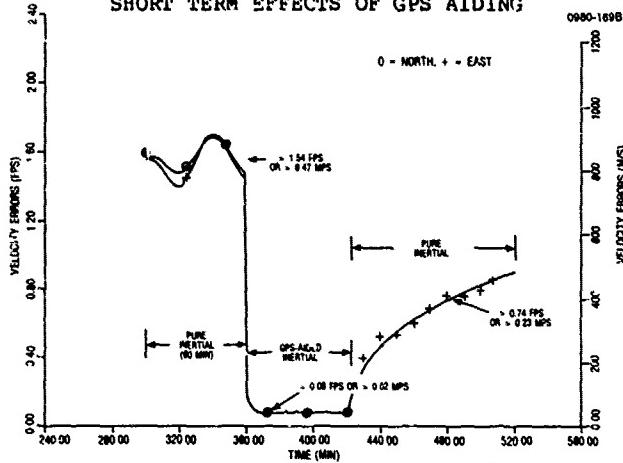
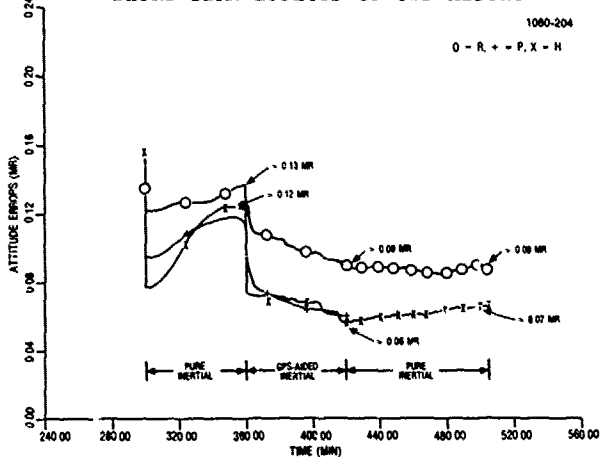
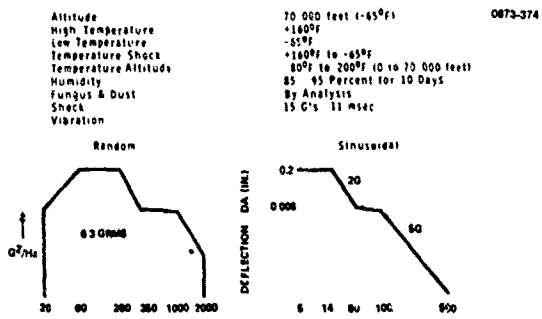
FIGURE 14. MISSION ANALYSIS - GPS/INERTIAL
SHORT TERM EFFECTS OF GPS AIDINGFIGURE 15. MISSION ANALYSIS - GPS/INERTIAL
SHORT TERM EFFECTS OF GPS AIDINGFIGURE 16. MISSION ANALYSIS - GPS/INERTIAL
SHORT TERM EFFECTS OF GPS AIDING

FIGURE 17. ENVIRONMENTAL REQUIREMENTS

When operating in the field, credibility in the performance of the equipment is enhanced if the operator has some means of knowing if it is functioning properly. In the SPN/GEANS and GEO-SPIN® equipments, this is provided by Built-In-Test-Equipment (BITE). It samples at least 69 different parameters during each computer cycle (32 times per second) and checks to ensure their values are within the proper tolerances. If any exceed allowable limits, the operator is alerted immediately by a BITE signal which appears on the CDU display. This signal will tell him not only that a malfunction has occurred, but also in which Line Replaceable Unit (LRU, meaning IMU or IEU) it is present. Thus he can quickly isolate the problem, replace the failed LRU, and put the system back into full operation. Average mean-time-to-repair/replace (MTTR) was demonstrated in a formal U.S. Air Force test program to be 20 minutes at the LRU level.

The ability to detect, isolate, and correct malfunctions is carried to the next maintenance level, that of the individual modules, also under automatic computer control. When a failed LRU is received at the depot or field maintenance shop, it can be evaluated, using a System Test Set (shown in Figure 18). LRU diagnostic programs are loaded aboard the test computer. The technician uses standard test equipment (oscilloscopes, voltmeters, etc.) under the direction of the computer to isolate the failure to the defective module or modules. This capability was also formally demonstrated for the U.S. Air Force with an MTTR of 1.15 hours being realized on the IMU and IEU with 23 different failures that were intentionally induced into the equipment. High skill levels are not required for these fault isolation and replacement operations. The procedures have been designed so that an E-5 level maintenance technician can perform them to the module level. Operational and E-3 personnel can handle the LRU level fault diagnosis and replacement.

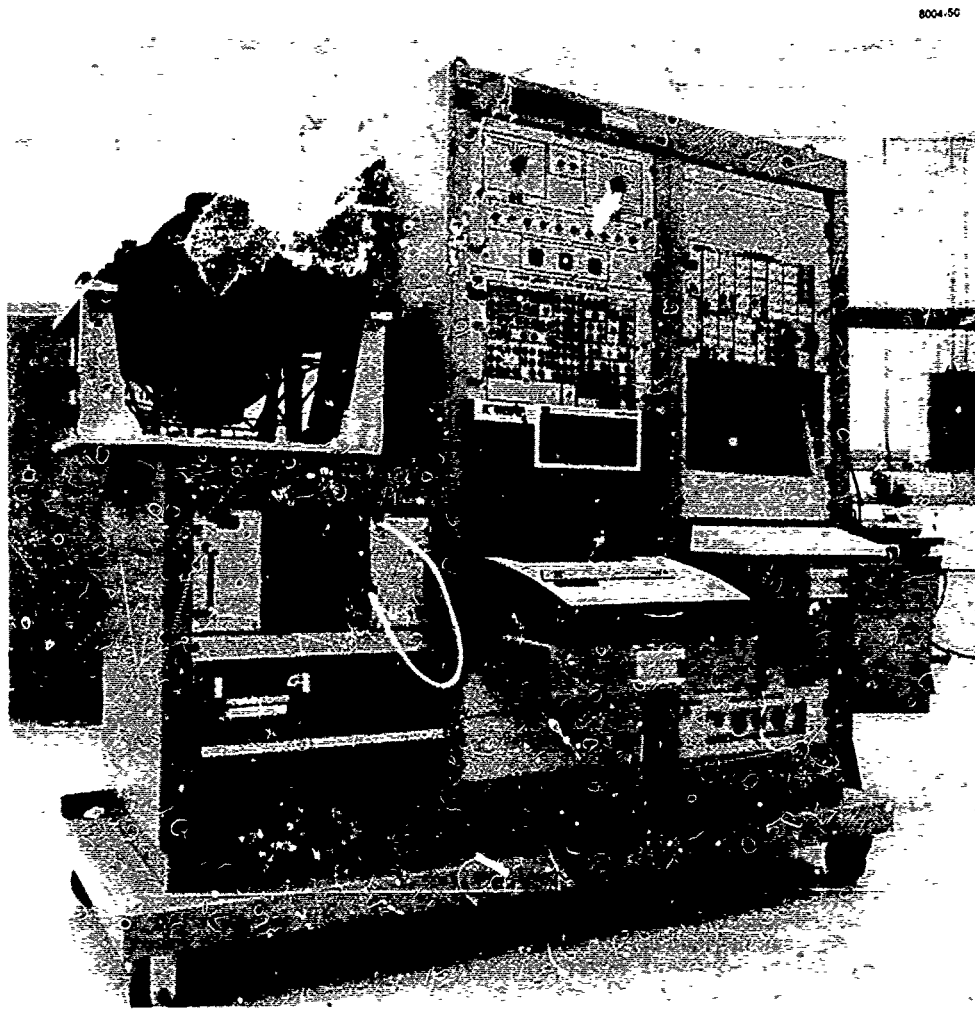


FIGURE 18. SPN/GEANS SYSTEM TEST SET

A final consideration for operational usefulness is that of calibration. The least desirable equipment is that which requires adjustment, tuning, or "tweaking" in the field. The SPN/GEANS and GEO-SPIN™ systems do not require any such actions. Rather, to meet the aircraft performance level of 0.12 nmph (0.22 kmph), CEP, requires only once per year self-calibration of the accelerometers, gyroscopes, and resolvers (gimbal angle encoders). This procedure is completely under automatic computer control and takes 42 hours to complete. With software improvements currently being developed this will be reduced to 28 hours. For GEO-SPIN™ operation on the battlefield, again the gyros and resolvers need be calibrated only once per year. Frequency of calibration of the accelerometers depends upon the desired accuracy. For closed loop positioning of 0.5 - 1.0 meter, rms, the day-to-day, cooldown shifts of accelerometer parameters are acceptable and no premission calibration is required. This should also apply for open-loop positioning in the range of 5-10 meters, rms. Four-minute ZUPT intervals are assumed. For closed loop accuracies much less than 0.5 meter, rms, or open loop accuracies in the 1-2 meter, rms, range, a premission accelerometer calibration may be required. This procedure takes one hour and can be performed with the normal system turn-on, warmup, and alignment procedure at the beginning of each operating period, extending the total system preparation time from one hour to two hours. With a feature known as gyro constant speed control, the GEO-SPIN™ can be operated for several days and still maintain the extra high precision performance (less than 0.5 meter, rms).

BATTLEFIELD APPLICATIONS - ON THE SURFACE

Because of high precision positioning and azimuth determination, and the ability to operate continuously for long periods of time, a wide variety of potential applications exist. These include:

1. Topographic surveying and positioning to establish useful reference points, routes, and common reference grids.
2. Artillery mobile observer positioning within minutes.
3. Artillery firing battery placement and firing reference azimuth determination within seconds or minutes of arriving at a firing position.
4. Positioning and initialization of ground launched missiles for tactical or intermediate ranges.
5. On-launcher, rapid placement, and initialization of weapons for "shoot and scoot" operations.
6. Guiding of lead vehicles in tank platoons, armored vehicle companies, etc., during cross-country movement, under bad weather, low visibility, or night-time conditions.
7. Positioning of visual or electronic listening posts for surveillance of enemy activities.
8. Rapid positioning of ground combat units (platoons, companies, and above) regardless of weather conditions, visibility, or familiarity with the terrain. For integrated ground and air operations, the hitting of friendly troops with close air support because of incorrect positions of either should be a thing of the past.

A very important feature of all of these applications is that they can be achieved without any electromagnetic radiation to or from the operating units. Thus, the possibility for achieving a self-contained, rapid strike capability is greatly enhanced.

AIRBORNE APPLICATIONS OVER THE BATTLEFIELD

Just as self-contained precision positioning can be achieved on the battlefield surface with GEO-SPIN™, so too can precision airborne positioning be obtained. Several potential applications of this capability are:

1. Highly accurate tactical reconnaissance missions can be flown without radiating from the aircraft for navigation purposes. Improved lane control, precision positioning during aircraft turns and other maneuvers (usually lost with more conventional, local vertical INSSs, can be achieved).
2. The SPN/GEANS can simultaneously navigate the aircraft and provide sensor stabilization or motion compensation for reconnaissance sensors such as radars, lasers, infrared, or electro-optical devices. Arc-minute or better pointing accuracy is available.

3. Low altitude precision navigation even under conditions of severe vibration and buffeting is attainable with SPN/GEANS whereas performance of other INSs tends to degrade under these conditions. The reason is that g-sensitive and g^2 -sensitive characteristics of gyros and accelerometers can be excited by these environmental disturbances with the result that performance is degraded, often by factors of 3-5:1 during the disturbance. Residual shifts can also occur which result in continued degraded performance even after the disturbance has been removed. The 50 to 400 times smaller coefficients in SPN/GEANS and GEO-SPIN™ yield the benefit of no performance degradation during and after such environmental exposures. This benefit has been proven operationally through flights in F-4 Fighter/Attack and P-3 ASW type aircraft.
4. In combined reconnaissance and strike operations, the precision of SPN/GEANS type inertial systems can result in more effectively and accurately controlled missions, thus enhancing a surgical strike capability with either conventional or nuclear weapons.
5. For helicopter operations in battlefield reconnaissance or control roles, airborne positioning accuracies of 1 to 50 meters, CEP, are achievable, depending on the scenario and navigation aids available to work with GEO-SPIN™ or SPN/GEANS. Since the inertial system provides continuous and hence instantaneous self-contained data, the use of "pop-up" and similar maneuvers for vehicle security is enhanced.

CONCLUSION

The high precision navigation and positioning accuracy now available with ESG Inertial Systems such as SPN/GEANS and GEO-SPIN™ offer a new dimension of self-contained capability to the battlefield commander. The equipment and software have been developed and all major hardware items are in production as standard U.S. Government Inventory items. The step that remains is to adapt these systems to specific military battlefield applications.

REFERENCES

1. Hadfield, Michael J., "Location, Navigation and Survey-Adaptability of High Precision ESG Inertial Systems in the 1980's," Institute of Electrical and Electronic Engineers PLANS 1978 Position Location and Navigation Symposium, San Diego, California, U.S.A., November, 1978.
2. Hadfield, Michael J., "Multi-function Inertial Precision: An ESG Systems Approach," 35th Annual Meeting of the Institute of Navigation, St. Louis, Missouri, U.S.A., June, 1979.
3. Hadfield, Michael J. "Critical Inertial System Characteristics for Land Surveying," The 1st International Symposium on Inertial Technology for Surveying and Geodesy, Ottawa, Canada, October, 1977.
4. Hadfield, Michael J. "GEO-SPIN": A Second Generation Inertial Survey Approach to Gravity Field and Positioning Measurements," Canadian Geophysical Union, Sixth Annual Meeting, Fredericton, New Brunswick, Canada, June, 1979.
5. Hadfield, Michael J., "Field Test Results on the GEO-SPIN™ ESG Inertial Positioning System," American Institute of Aeronautics and Astronautics Guidance and Control Meeting, Danvers, Massachusetts, U.S.A., August, 1980.
6. Hadfield, Michael J. "Use of an ESG Inertial Navigation system for Offshore Surveying," The Institute of Navigation National Marine Meeting, Linthicum Heights, Maryland, U.S.A. October, 1977.
7. Warzynski, Capt. Robert P., USAF, and Ringo, Ronald L. "The Evolution of ESG Technology," AGARD Conference Proceedings No. 116 on Inertial Navigation Components and Systems, Ueberlinger, West Germany, April, 1972.

GLOSSARY OF TERMS

DME	Distance Measuring Equipment; electromagnetic (microwave) or electro-optical (infrared and laser) equipment for precise range and range rate measurement.
ESG	Electrically Suspended Gyro; also known as Electrostatically Supported Gyro, wherein a spinning rotor is levitated in an electrical force field.
GEO-SPIN™	Earth Resource Related - Standard Precision Inertial Navigation/Survey System.
GPS	Navstar Global Positioning System; gives position accuracies of 30-40 feet (9-12 meters) in three dimensions, with receivers on moving bodies.
IPS	Inertial Positioning System; an inertial navigation system which has been adapted for precision position measurement on and over the Earth's surface.
IRU	Inertial Reference Unit; a strapdown inertial sensor package; also known as an ISA (Inertial Sensor Assembly); contains gyros and accelerometers with their associated electronic circuitry; designed to operate as a low accuracy INS in conjunction with a computer and control/display unit or in a slave-aligned mode in conjunction with a master INS, for higher precision position, velocity, and attitude measurement.
JTIDS	Joint Tactical Information Distribution System; provides a distributed digital communications and position location system.
MACS	Multiple Access Communication System.
PADS	Precision Azimuth Determining System; an application of first generation IPS equipment for survey of artillery firing positions.
PLRS	Position Location and Reporting System.
SPN/GEANS	Standard Precision Navigation Gimbaled Electrically Suspended Gyro Aircraft Navigation System.
ZUPT	Zero Velocity Update; a technique for stopping a vehicle and resetting velocity conditions in an Inertial Positioning System.

**THE POTENTIAL OF A MULTIFUNCTION
INFORMATION DISTRIBUTION SYSTEM (MIDS)
FOR POSITION LOCATION**

by
G. Hoefgen
STANDARD ELEKTRIK LORENZ AG
Stuttgart, Germany

1.0 THE BASIC PROCESS OF POSITION LOCATION

1.1 Introduction

The Multifunction Information Distribution System (MIDS) offers the potential for position location by multi-ranging. There are two versions of range measurements: one-way and two-way ranging. Both versions are applicable to a MIDS, but the basic feature is one-way ranging in order to keep transmissions low and to save capacity.

In general, the range R is determined as the product of propagation time τ between a transmitting source and a receiving user multiplied by the speed c of light ($R = \tau c$). Very precise synchronised clocks are necessary at the source as well as at the user to measure the propagation time with the required accuracy of some tenths of nanoseconds (e.g., 10 ns time error corresponds to 3 m range error).

All terminals participating in a MIDS net transmit messages at specified and known times. As a precondition thereof, the common system time among all users is established and maintained by suitable synchronisation procedures. The residual bias error of the clock can be further reduced by means of the position location process as described below. A requirement for developing the position location of a user is knowledge of the position and quality of each source to be used. That is realised by the fact that a great portion of all MIDS messages are position reports (P-messages) containing, among other information, position coordinates (latitude and longitude or relative coordinates), altitude, course, speed, position quality and time quality.

1.2 Passive Position Location

In the passive mode, position location of a user within the MIDS net is achieved in principle by listening to the P-message transmissions of a number of sources serving as reference positions to the user. The receive times of the P-messages are measured by the user terminals. The time difference between a source transmission and the user reception is as follows:

$$\Delta t_i = (t_u - \Delta t_{ub}) - (t_i - \Delta t_{ib})$$

wherein the source transmission time is composed of the true (system) time t_i and the source bias Δt_{ib} , and the user receive time is composed of the true time t_u and the user bias Δt_{ub} . Because there are no means to differentiate between source and user bias, the expression $\Delta t_b = \Delta t_{ub} - \Delta t_{ib}$ is used for the further considerations, and the true time difference becomes:

$$t_u - t_i = \Delta t_i + \Delta t_b \quad (1)$$

The measured time difference Δt_i , multiplied by the speed of light, represents a pseudo range, whereas the true range is:

$$R = (t_u - t_i) c = \sqrt{(x-x_i)^2 + (y-y_i)^2 + (z-z_i)^2} \quad (2)$$

wherein (x_i, y_i, z_i) is the position of the source in cartesian coordinates, and (x, y, z) represents the unknown user position.

In most cases, the terminals are not elevated very much with respect to each other, thus altitude calculations are difficult to make with sufficient accuracy.

Therefore the altitude is measured directly (e.g. with barometric altimeters) and the difference $\Delta z_i = z - z_i$ is put as a known value to the equation above. This results in an advantageous reduction of the calculation task from the three-dimensional space to the two-dimensional plane (x, y) .

In order to get a position fix of the user, at least the P-messages from three different sources (1, 2, 3) are necessary. The corresponding equations, formed by a combination of (1) and (2) are the following:

$$R_1 = \sqrt{(x-x_1)^2 + (y-y_1)^2 + \Delta z_1^2} = (\Delta t_i + \Delta t_b) c \quad (3a)$$

$$R_2 = \sqrt{(x-x_2)^2 + (y-y_2)^2 + \Delta z_2^2} = (\Delta t_i + \Delta t_b) c \quad (3b)$$

$$R_3 = \sqrt{(x-x_3)^2 + (y-y_3)^2 + \Delta z_3^2} = (\Delta t_i + \Delta t_b) c \quad (3c)$$

By means of these equations the variables x , y and Δt_b can be determined. Figure 1 shows geographically the same case.

The achievable time and position quality of the user depends on the time and position qualities of the sources. It also depends on the geometric relationships between the user and the sources. The latter one is known as geometric dilution of precision (GDOP). As sketched in Figure 2, the GDOP acts as an error amplification mechanism. In reality, of course, under the assumption of normally distributed range

errors, the position error figures are ellipses. Further parameters determining accuracy are discussed under the paragraphs 2.2 and 2.3.

1.3 Hierarchical Aspects

The aim of a MIDS is to be a nodeless system wherein each terminal would be permitted to range to others within the net. It has been proven, however, that such an interactive operation can become unstable [1]. The position location function, therefore, has to be based on a hierarchical principle. This principle is realised by distributing the information for position location in one direction only, from the centre outwards. There is a time centre (a terminal called time controller) and a position information centre.

These centres are characterised by definition to possess the highest possible time and position quality; they may be both incorporated in one terminal. The information flow is coupled with a quality degradation. That means that the time quality and the position quality of the user are at least one grade lower than the qualities of the sources used for position location.

For the operational use a set of quality figures ranging from 15 as the highest quality down to 0, has been defined to describe the time and position errors of the sources. The error values listed in Table 1 are standard deviations (1σ values). As far as the position quality is concerned, the error values represent the major axis of the error ellipse.

1.4 Round Trip Timing

For the passive mode of position location as described above at least three sources under good GDOP conditions are necessary to calculate the user position and the system time from the received P-messages. For the very first participants in a net and for those being responsible for very high time standards, the passive mode of operation is not feasible or not sufficient. In those cases a so called Round Trip Timing (RTT) method is applied. The RTT method is identical to a two-way ranging procedure. Figure 3. shows the function of the two possible versions (static and contention). In the static version, the interrogating terminal transmits a short message containing the address of the reference terminal at the interrogator's best estimate of the system time. The reference terminal measures the receive time t_R with respect to its own best estimate of system time and transmits a response message containing the receive time data after a known constant time delay T . The interrogator measures the time difference Δt between the transmission of the interrogating message and the reception of the response. That enables the interrogating terminal to calculate independently from each other the clock bias Δt_b and the (true) range R as follows:

$$\Delta t_b = \frac{T + t_R - \Delta t}{2} \quad (4)$$

$$R = c \cdot \frac{\Delta t + t_R - T}{2} \quad (5)$$

In the contention version the procedure is the same, except that the interrogations are addressed to a group of sources identified by their same time quality grade (Q_t).

The RTT process is very suitable to distribute the system time with the best achievable accuracy. This is also true for the range measurements, but this process cannot be used to establish position references by itself.

1.5 Position Reference Sources

The determination of the position of a user by ranging requires a minimum number of reference sources, the position of which is known. The very first participant forming a MIDS net or a single terminal cannot range to any other; it has to know its own position or obtain it through other means. The second participant can range to the first one and get a circular line of position but no fix.

Thus the second participant also has to obtain its own position by other means. The range measurement to the first terminal, if taken, can only help to improve the position accuracy under certain circumstances. A third participant may range to the first two and will get two position points as the crosspoints of the two range circles, but only one of the two is the correct fix, i.e. the position information derived from only two reference sources is ambiguous.

These considerations result in the basic rule that a minimum number of three reference sources with known position is necessary to achieve non-ambiguous position determination.

The basic (minimum three) position reference sources may be ground stations with inherently known precise position coordinates. If ground stations cannot be used operationally, airborne or shipborne terminals may become position reference sources. In these cases, the NAVSTAR GPS would be very suitable for the derivation of the actual position information of the terminals concerned with very high accuracy. There may be cases where users may want to navigate relatively to each other (RELNAV) without the necessity to know in absolute (geodetic) coordinates where they are. A relative grid, established from the minimum number of reference sources (e.g. by INS or other means), may serve this purpose.

2.0 PERFORMANCE CONSIDERATIONS

2.1 Techniques and Configurations

The basic nature of MIDS is information distribution with a message rate adapted for this main purpose. Depending on the operational environment the P-message rate may be as low as one per 12 s. Assuming that lower rates are not permitted at the position reference sources and further assuming that the system shall work with a number of reference sources down to the minimum, a mean time up to approximately

10 s will be needed for taking a position fix. That is of course an extremely long time, especially under the aspect of comparison with other systems for position location and navigation presently in operation (e.g. TACAN). On the other hand, MIDS offers the potential for range measurements with higher accuracies than present systems.

While the low P-message rate obviously does not affect the position location accuracy for stationary or very slowly moving users, the position of the dynamic user cannot be determined as the crosspoint of range circles. More complex techniques are required for medium and high dynamic users (aircraft, helicopters, fast vehicles).

The most commonly proposed solutions for dynamic users employ dead reckoning devices such as INS, Doppler or air data as external inputs to the Kalman filter [2], [3], [4], [5] in addition to the range measurements. These arrangements probably satisfy high accuracy requirements, but adequate results of investigations are still missing. The drawbacks obviously are the relatively long time (several minutes) to achieve full accuracy and the dependence on external sensors, i.e. the operation is non-autonomous, and the reliability is decreased when compared with an autonomous position location system using MIDS by itself. Another aspect of concern is the fact that several users (helicopters, vehicles) do not carry sensors as mentioned above to support dead reckoning.

To get an autonomous system, some investigations were also done without using external sensors [2], [6]. The simulation described in [2], however, is based on unrealistic assumptions (e.g. known initial position, speed and acceleration and constant speed and altitude during the whole simulated mission). For this reason the simulation cannot be accepted as representing the real environment and proving the system function. Another simulation, described in [6], was based on a model with 4 fixed reference ground stations and one aircraft under good GDOP conditions. The error generated during a 90° turn with 1.5°/s and 180 knots was up to 360 m which is unacceptable. As a conclusion, therefore, it seems to be impossible to achieve the required accuracy for high dynamic users with MIDS equipment only with a 12 sec update.

The problem of insufficient accuracy for a dynamic user equipped with a MIDS terminal only could obviously be solved, if the transmission times of the P-messages of the reference sources could be sent approximately simultaneous, e.g. within 50 ms. Precise position location is then possible by multi-ranging, and a simplified dead reckoner can be used to estimate the actual position by linear and quadratic extrapolation. Whether this method can be applied, depends on the finally selected signal structure and net management.

The following performance considerations mainly refer to accuracy. They are taken separately for the stationary case, which also includes slow moving users, and for the dynamic case. Although there does not exist a clear limit between the two user categories, a user velocity of about 3 m/s may be a reasonable value.

2.2 The Stationary Case

The processing of propagation times of the P-messages from the reference sources to the user is very simple for the stationary case. There is either no position change of the user, or the change is negligible during the maximum time interval (approx. 10 s) which is necessary to get a position fix.

Figure 4 shows a simplified functional block diagram of the user equipment for the stationary case. The source selection module is fed from the basic MIDS terminal signal processor with all P-message data and the corresponding propagation times Δt as observed with the user's own clock, i.e. including the time bias (Δt_b). Only the sources with better time and position qualities (Q_t, Q_p) than those of the user are suitable for further processing. Another decision criterium for the source selection is the geometric configuration between the user and the sources (GDOP). The selected source data feeds the fix calculation module. It provides the user's position (x, y) as well as the time bias (Δt_b) for correcting the clock and the time and position qualities (Q_t, Q_p) as inputs to the source selection module.

The achievable accuracy of the user position determination depends on the following parameters:

a) Source time and position qualities

As shown under paragraph 1.2, the user position is determined by propagation time measurements of the P-messages from reference sources, the position of which is known. The position errors of the sources as well as their clock errors (compared with true system time) form an integral part of the set of equations (3a to 3c) for the fix calculation. That means that the time and position qualities (Q_t, Q_p) of the reference sources directly transform into the achievable accuracy of the user position location, and the user time and position quality will be at least one grade lower as compared with the reference sources. As a basic rule for source selection, therefore, the user will range to those sources with superior qualities only.

b) Propagation time measurement accuracy

The measurement accuracy of the P-message propagation times from the sources to the user is dependent also from the following hardware and signal structure related factors:

At the source the timing accuracy of the P-message transmissions is dependent from the respective time controlled switching hardware. The time measurement accuracy of the received P-messages at the user depends on the signal bandwidth and the signal-to-noise ratio in addition to the performance of the respective time measuring circuitry.

c) Short term clock stability

Due to the fact that the update rate with a MIDS can come down to only one set of measurements per 10 s, a sufficiently high short term clock stability is required. A clock error in the order of 10^{-9}

(corresponding to 3 m range error during a 10 s time interval) seems to be adequate. Both, the source and the user clock errors contribute to the degradation of position location.

d) Geometric dilution of precision (GDOP)

As explained under paragraph 1.2, the position location accuracy achievable with a MIDS highly depends on the scenario. The source selection function, therefore, is a very important one. Only those sources with a good geometry in respect to the user are considered for the fix calculation. In general, the error contribution from the geometrical relationships will be the lowest possible, if the angular differences between the sources as observed from the user are around 90°. In contrast thereof, the error contribution gets to a maximum, if the angular differences tend to be 0° or 180°.

e) Propagation anomalies

The propagation time from the sources to the user may be altered due to irregularities in the atmosphere concerned. Although experience with TACAN indicates that the effect will be of minor importance, some attention should be given to it during the MIDS experimental evaluations.

Another potential error source is multipath propagation. In this case the maximum error is estimated to be equivalent to approximately half a chip length, i.e. 100 ns \approx 30 m, for multipath levels of 0 dB to -6 dB as compared with the direct signal.

f) Computational errors

According to the modern state of the art of computer technology, computational errors should be kept negligibly small.

All parameters mentioned above contribute to the resulting error of the position location of stationary users. In order to assess the achievable accuracy to some extent some simple examples were investigated theoretically. These examples only deal with the contribution of source time and position qualities, and the geometric dilution of precision (GDOP) to the resulting error. Thus, they are to be considered idealised.

For the passive mode of operation three sources R₁, R₂ and R₃ were used with position and time qualities of 15 each ($Q_p = 15$, $Q_t = 15$). The geometric angle between the three sources was changed from 90° to 180°. As result, Figure 5, Figure 6, and Figure 7 show curves of constant position qualities representing the accuracy under ideal conditions.

With active range measurements by means of the RTT method only two sources R₁ and R₂ are necessary for position location (ambiguity not considered). Figure 8 shows curves of constant position quality, whereby the position qualities of the sources are assumed to be 15 each. The time qualities of the sources are irrelevant for determining ranges by the RTT process.

It should be pointed out that the investigations described above do not consider the influence of the propagation time measurement accuracy, the short term clock stability, and the propagation anomalies, which will further degrade the finally achievable accuracy. Nevertheless, these simple examples very well show especially the geometric dilution of precision.

2.3 The Dynamic Case

The dynamic case of a MIDS application is characterised by fast moving users. During a 10 s time period, which may be needed to take one full set of measurements for position location, the user will change its position considerably, and the instantaneous position can no longer be determined as the crosspoint of circles representing the measured ranges. Thus a recursive filtering algorithm is to be used to estimate the present position by extrapolation from past measurements. In order to enable the filter to process position changes correctly during accelerative actions of the user as well, external dead reckoning devices such like INS, Doppler or air data are necessary as additional inputs to the filter.

A simplified functional block diagram of the user equipment for the dynamic case is shown in Figure 9. While the basic MIDS terminal is considered to be the same as in the stationary case, the simple fix calculation is replaced by the much more complex Kalman filter and the position data extrapolation. Both functions are realised as computer software.

The accuracy of position location of a dynamic user of course, is dependent from the same parameters as listed above for the stationary case. But, in addition to them, some more parameters degrade the achievable accuracy in the dynamic case:

a) User dynamics

Fast moving users such like aircraft, helicopters or even ground vehicles are characterised by their own velocity and acceleration as a function of time. While constant velocity is simple to be processed in the filter and normally does not significantly degrade the position location accuracy, special attention is to be given on the user's manoeuvres causing accelerations and variances thereof. As the filter needs time to adapt to these variances, the position location accuracy degrades as a consequence of kind, quality and rapidness of manoeuvres (depending on dead reckoner performance).

b) Dead reckoner performance

During the manoeuvres of a dynamic user, its dead reckoner acts as the sensor of the motion variances. Thus, the dead reckoner enables the MIDS user equipment to indicate the instantaneous position very closely to the true position. This path-following features of the dead reckoner is the basis for

maintaining accuracy during manoeuvres. Its inherent accuracy, therefore, influences the position location accuracy of a MIDS user terminal. The higher the dynamics of the user is, the more the influence of the dead reckoner will be. Best dead reckoner performances are achieved with INS, as reported in [4], while Doppler or air data are less powerful.

c) P-message rate

The rate of the received P-messages from the reference sources significantly influences the position location accuracy of a dynamic user. The higher the rate, the better the accuracy will be. The rate of approximately one P-message from one source within 12 s is considered as the minimum rate. Thus, the availability of only three reference sources transmitting at the minimum rate will be the worst case. Higher rates from the single sources or the possibility to use more than three sources will improve the situation, provided that a correspondingly higher processing speed is feasible.

d) Filter performance

The algorithm complexity of the Kalman filter also relates to the achievable accuracy. In order to process the inputs from an INS to the best possible extent, it is proposed to apply 15 to 18 filter states [3]. That results in a high degree of software complexity, and the drawback may be the limited capacity of the terminal computer within the required processing time of less than 3 s (comparable to P-message rate). Thus, a trade-off between filter complexity and position accuracy seems to be reasonable for the different user types.

Although comprehensive investigations on the accuracy of the MIDS position location are still missing, a computer simulation accomplished by MITRE presents very valuable results with a special scenario. The scenario as depicted in Figure 10 contains five MIDS ground reference stations (R_1, R_2, \dots, R_5) with inherently best position qualities (all $Q_p = 15$). Reference R_2 is considered to be the time reference ($Q_t = 15$), the others have the time quality $Q_t = 14$. The user is an aircraft at 500 feet altitude and with a constant velocity of 140 m/s (278 knot.). Its simulated straight flight in X-direction and back takes 37 minutes.

The user is equipped with an INS of moderate quality in addition to the MIDS terminal. The position quality, therefore, comes down considerably ($Q_p = 1$) at the end of the 26 minutes time period out of coverage from the reference stations. Further parameters of the simulation are 12 s P-report intervals, 4 s process time per observation and 30 ns receive time noise.

As a result of the simulation, Figure 11 shows the development of the position quality of the user during the five minutes flight (thick line in Figure 10) after re-entry to coverage of the reference stations R_1, R_2 , and R_3 .

3.0 CONCLUSION

The Multifunction Information Distribution System (MIDS) offers a great potential for position location and navigation. The position location will be accomplished by multi-ranging based on time-of-arrival measurements. Besides this preferred passive mode an active method (RTT, Round Trip Timing) providing range and time measurements most accurately and independently from each other will be feasible.

The achievable accuracy depends on the operational and physical environment and on the performance of the equipment used. For the stationary case, which is characterised by fixed or very slowly moving participants, the main parameters determining accuracy are source time and position qualities, propagation time measurement accuracy, short term clock stability, geometric dilution of precision (GDOP), and propagation anomalies. In the dynamic case characterised by fast moving users the accuracy will be further degraded by the user dynamics, the P-message rate, the filter performance, and the dead reckoner performance.

4.C ACKNOWLEDGEMENT

The author wishes to acknowledge the support from the MIDS Team, headed by J. Dominitz. Furthermore, he is grateful to E.A. Westbrook (The MITRE Corporation) and K. Kohler (Standard Elektrik Lorenz AG) for their theoretical investigations on system accuracy.

5.0 REFERENCES

- [1] E.A. Westbrook and R.C. Snodgrass, Relative Navigation by Passive Ranging in a Synchronous Time Division Multiple Access Data Net, The MITRE Corporation, MTR-2996, March 1975.
- [2] W.R. Fried, Principles and Simulation of JTIDS Relative Navigation, IEEE Transactions on AES, Vol 14, No 1, January 1978.
- [3] W.R. Fried and R. Loelinger, System Configuration and Algorithm Design of the Inertially Aided JTIDS Relative Navigation Function, NAECON Proceedings, 1979.
- [4] W.R. Fried, JTIDS Relative Navigation - Architecture, Error Characteristics and Operational Benefits, NAECON Proceedings, 1979.
- [5] Sanford Welt, Dynamic Simulator Test and Evaluation of a JTIDS Relative Navigation System, NAECON Proceedings, 1979.
- [6] E.A. Westbrook, A Layman's Guide to the JTIDS RELNAV System Simulator, The MITRE Corporation, WP-21150, 1 March 1977.

Table 1 Time and Position Quality (Q_t , Q_p)

QUALITY FIGURE	TIME ERROR (1σ) Nanosec.	POSITION ERROR (1σ) Meters
15	\leq 50	\leq 15
14	\leq 71	\leq 22
13	\leq 100	\leq 30
12	\leq 141	\leq 43
11	\leq 200	\leq 61
10	\leq 282	\leq 86
9	\leq 400	\leq 122
8	\leq 565	\leq 172
7	\leq 800	\leq 244
6	\leq 1130	\leq 345
5	\leq 1600	\leq 488
4	\leq 2260	\leq 690
3	\leq 4520	\leq 1378
2	\leq 9040	\leq 2755
1	\leq 18080	\leq 5510
0	$>$ 18080	$>$ 5510

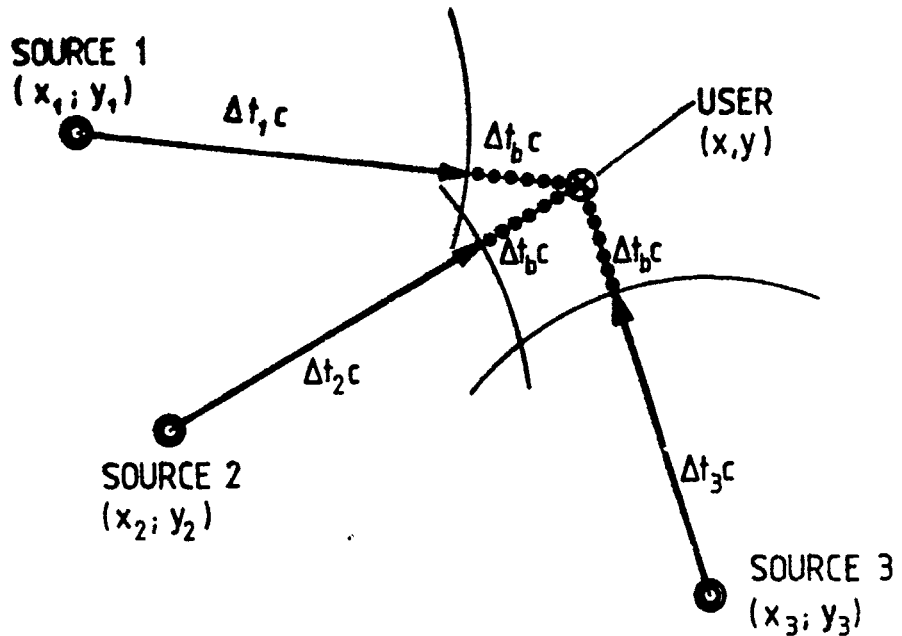


Fig.1 Position determination of a passive user by one-way ranging

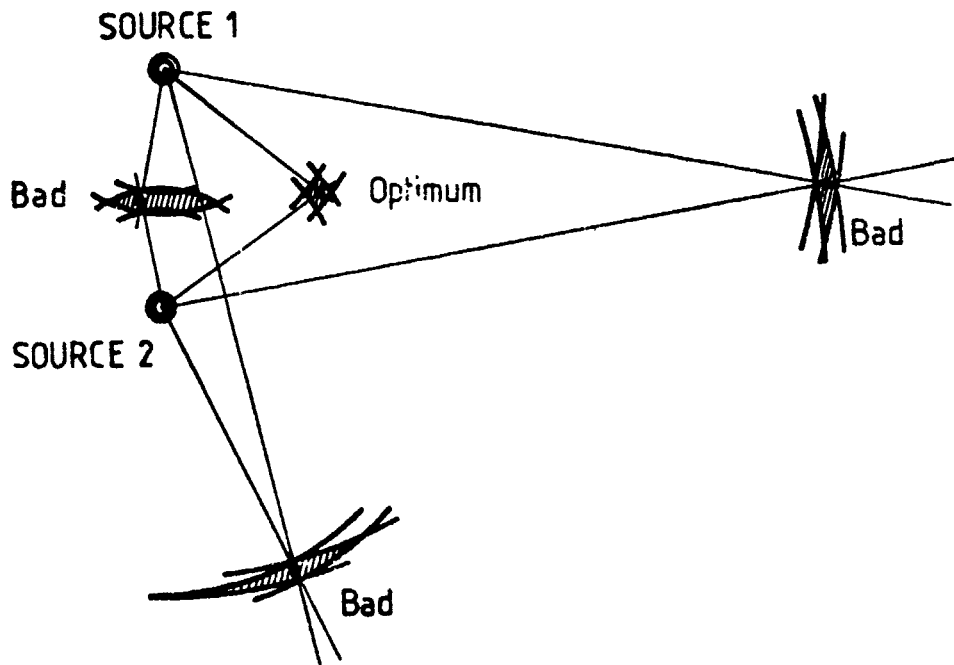
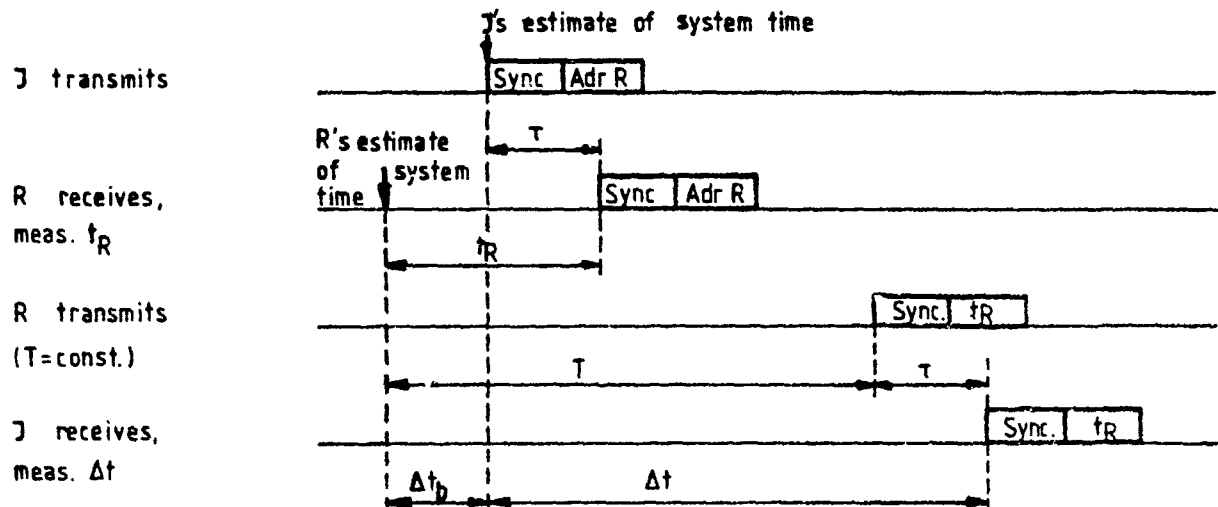


Fig.2 Geometric dilution of precision (GDOP)

STATIC VERSIONCONTENTION VERSION

(time quality TQ used as group address)

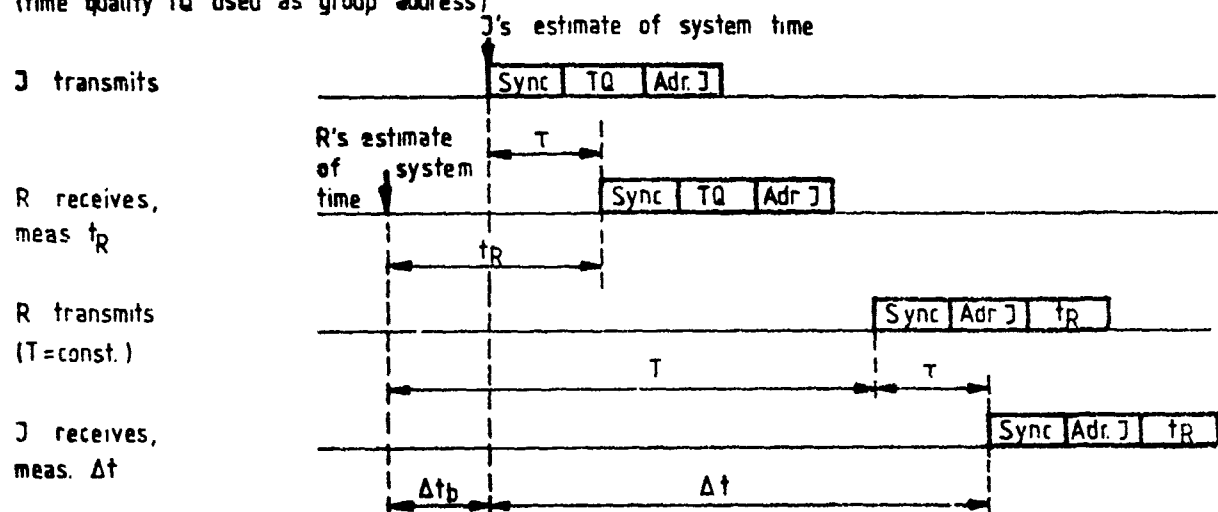


Fig.3 Round Trip Timing (RTT) between an Interrogator (I)
and a Reference Terminal (R)

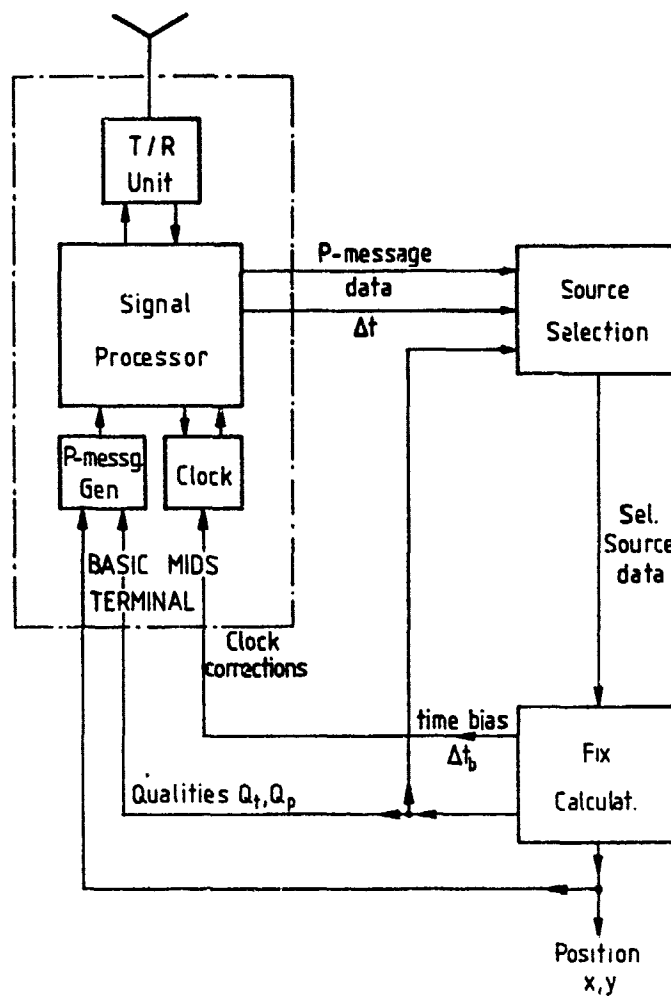


Fig.4 The MIDS user equipment functions for position location (stationary)

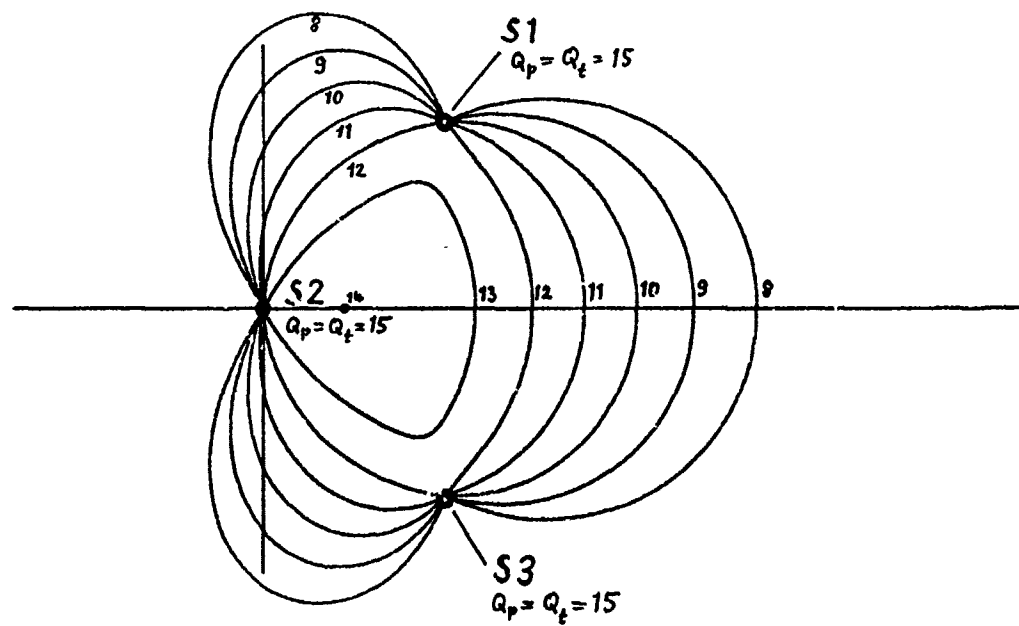


Fig.5 Position quality (Q_p) distribution for the passive mode of operation

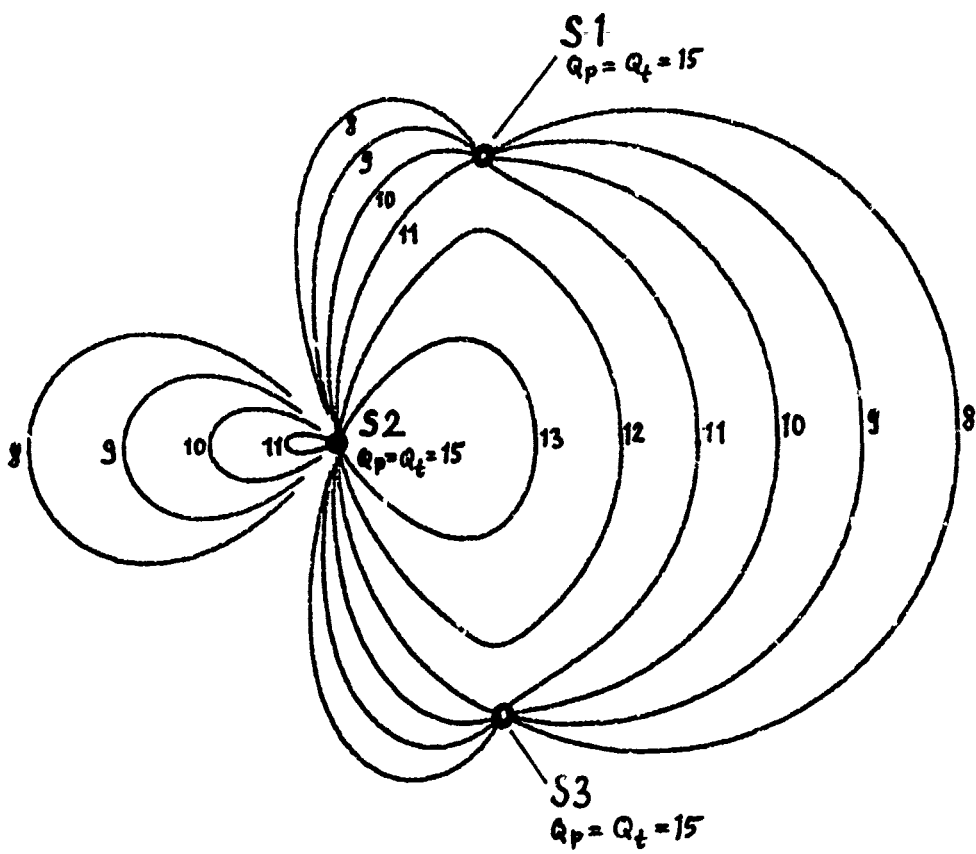


Fig.6 Position quality (Q_p) distribution for the passive mode of operation

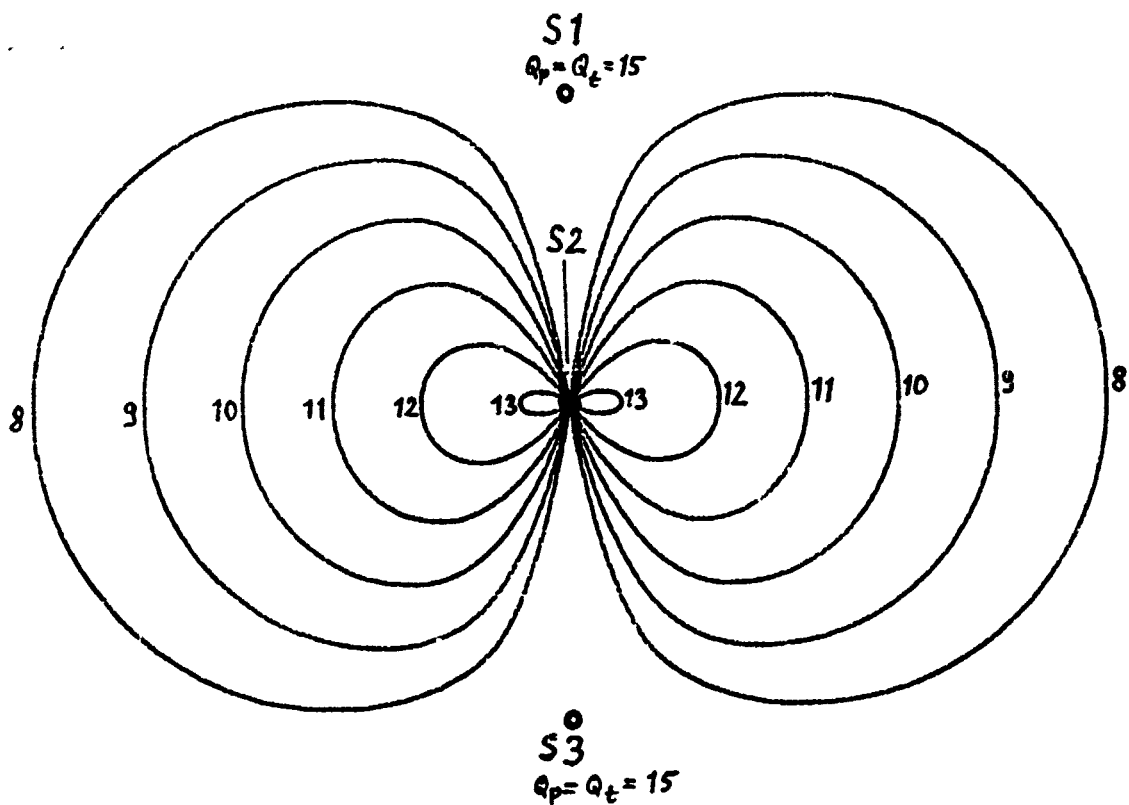


Fig.7 Position quality (Q_p) distribution for the passive mode of operation

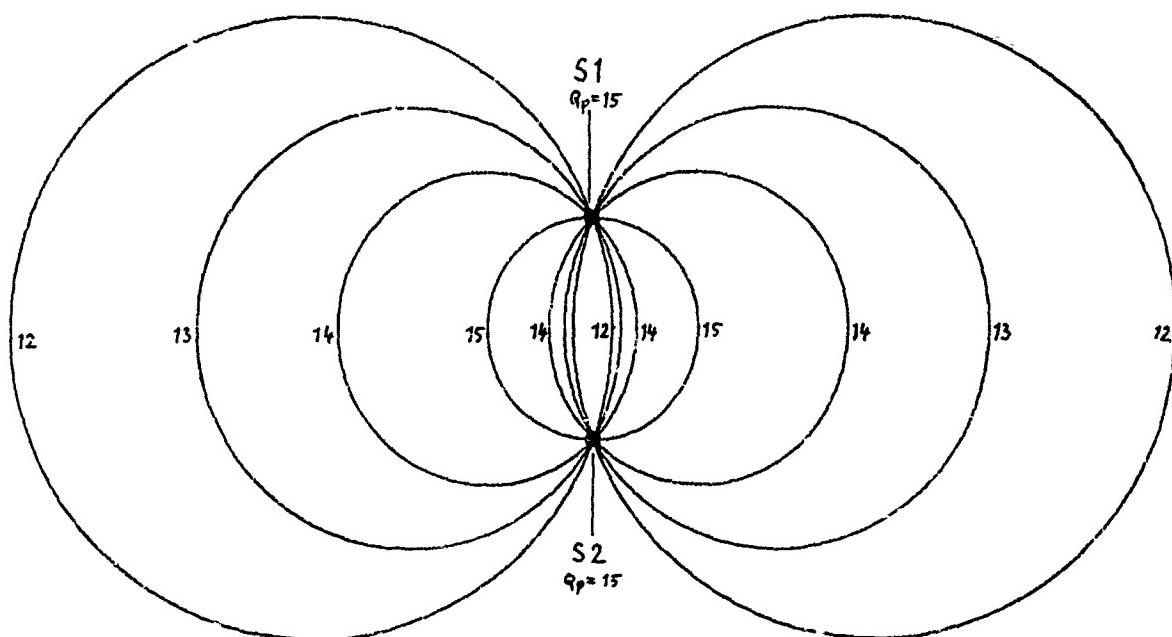


Fig.8 Position quality (Q_p) distribution based on RTT

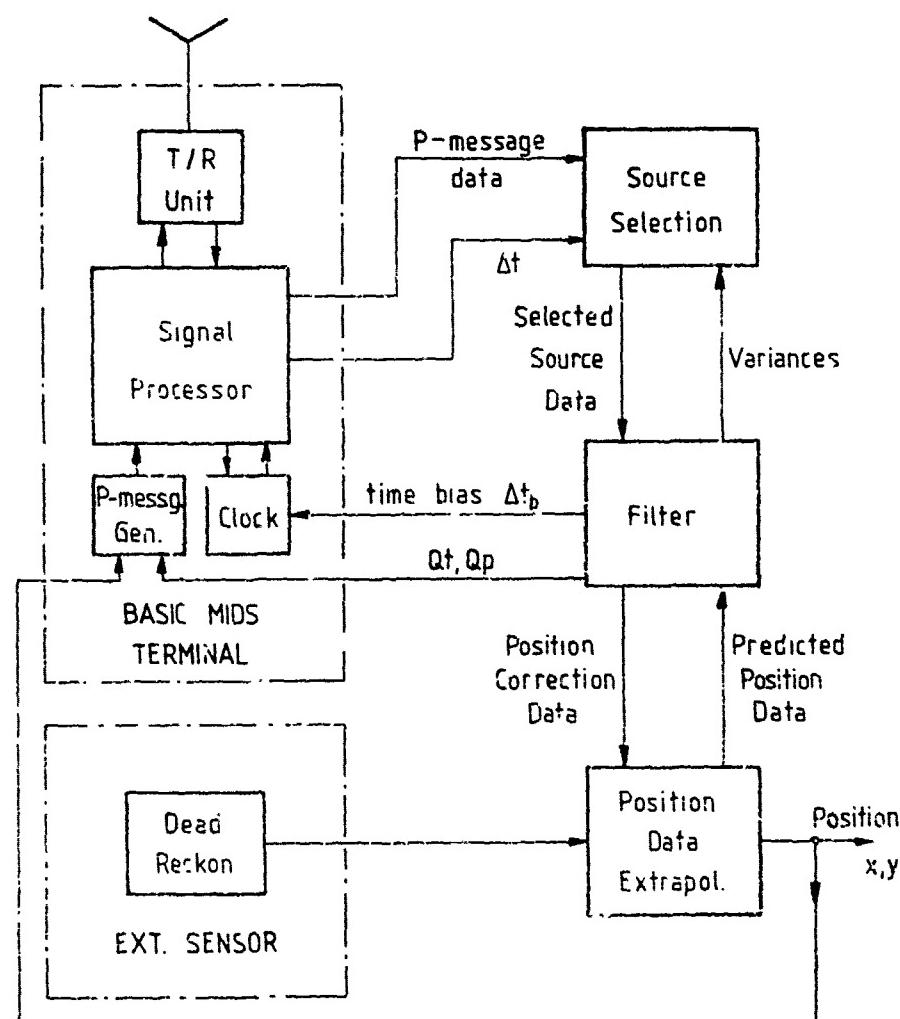


Fig.9 The MIDS user equipment fuctions for position location (dynamic)

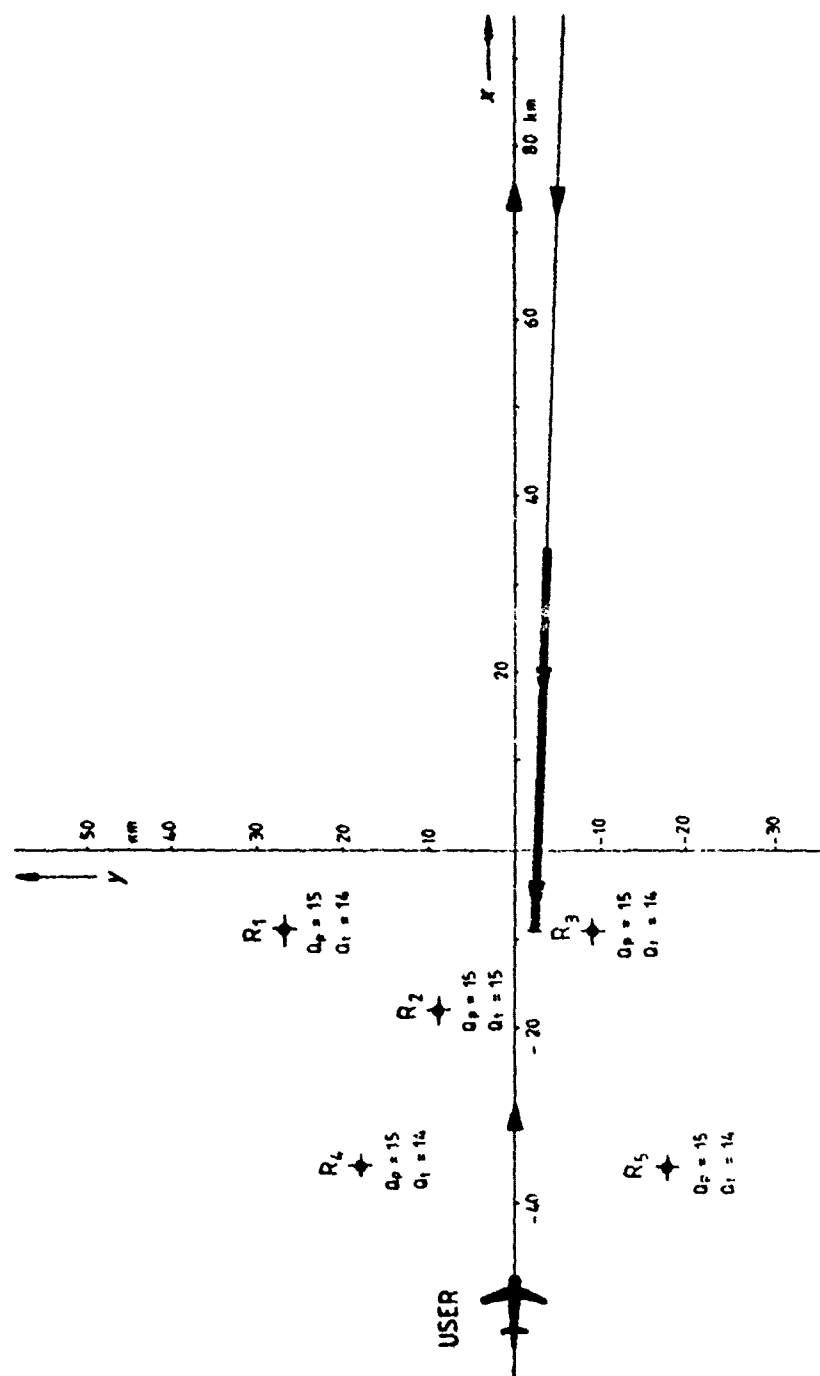


Fig.10 Dynamic model for computer simulation (by MITRE)

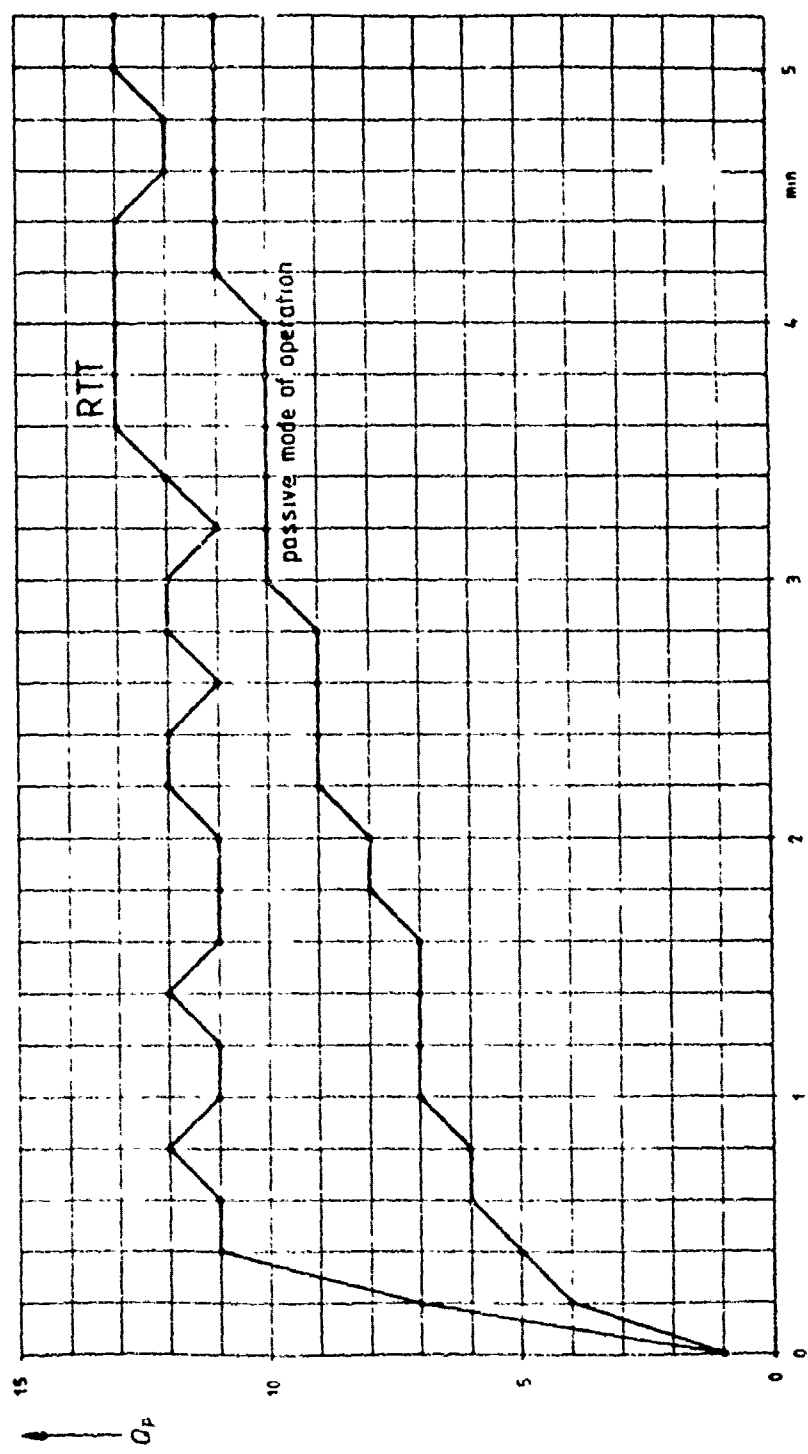


Fig.11 Airborne position quality (Q_p) development

**JTIDS DISTRIBUTED TDMA (DTDMA) TERMINAL DEVELOPMENT RESULTS
WITH EMPHASIS ON RELATIVE NAVIGATION PERFORMANCE**

by

J. Rubin and S. Welt
ITT Avionics Division
500 Washington Avenue
Nutley, NJ 07110 U.S.A.

SUMMARY

ITT Avionics Division has recently completed extensive laboratory testing of Advanced Development Model (ADM) terminals developed for the U.S. Department of Defense under the Joint Tactical Information Distribution System (JTIDS) Program. These terminals feature the advanced JTIDS Phase II Distributed TDMA (DTDMA) architecture. Further laboratory and flight tests are now in progress in U.S. Navy laboratories in San Diego, California.

The terminals developed under this effort include two Class 1 Command and Control terminals for installation aboard CVA ships and E-2C Command and Control aircraft, two Class 2 Tactical Fighter terminals for installation aboard F-14A fighter aircraft and one JTIDS Environment Simulator (JES) for use in simulation of multi-aircraft dynamic JTIDS RF environments and evaluation of terminal performance.

The functions performed by the C-N-I JTIDS Distributed TDMA terminals include secure and jam resistant digital voice, digital data, precision Relative Navigation, TACAN Navigation, and the IFF identification service. In addition, full interoperability with the JTIDS Phase I TDMA system is also provided.

This paper is essentially presented in two parts. Part one gives an overview of the basic DTDMA system. Additionally, descriptions of the basic terminals developed for the Class 1 and Class 2 application and the JTIDS Environment Simulator (JES) are provided. In the second part, the JTIDS Relative Navigation function is discussed. A brief REL NAV overview is provided and qualitative results of testing are presented.

INTRODUCTION

The Joint Tactical Information Distribution System (JTIDS) is a tri-service, multi-channel, multi-function system. During Phase I, a Time Division Multiple Access (TDMA) channel (JTIDS I) was introduced to handle total connectivity information distribution for digital communications and relative navigation. Distributed TDMA (DTDMA), the selected approach to JTIDS Phase II (JTIDS II), expands this capability by providing increased data rate capacity and additional C-N-I functions. The DTDMA channel architecture provides a structure which permits a single terminal to participate concurrently in multiple time-independent functions or networks which have the flexibility to be structured and organized in a manner to efficiently meet the broad spectrum of tactical information-distribution operational requirements. JTIDS II DTDMA is compatible with and includes the TDMA function of JTIDS I which becomes one of the channel structures available to system users.

PART I. DTDMA SYSTEM AND TERMINAL DESCRIPTION

Distributed TDMA Overview (1)

JTIDS II/DTDMA operates in Lx-Band (960 to 1215 MHz). It provides a system that combines spread-spectrum multiple-access command and control functions with conventional TACAN navigation and IFF identification service. Distributed TDMA is a technique that utilizes low duty cycle pulses, pseudo randomly distributed in the time-frequency-code (T-F-C) domain. This characteristic of pseudo-random time separation is a major feature of DTDMA. It permits flexible channel architecture and enhances channel access.

Conventional high duty cycle or continuous transmission methods operate in a "serial" mode wherein the message synchronization preamble is immediately followed by the data message. This ordering is used for each user in turn. In DTDMA both the synchronization and message signals from many terminals are dispersed in time (and frequency/phase code) resulting in interleaved or "parallel" transmissions from many sources. The DTDMA signal structure permits performance to be tailored to specific needs, thus resulting in a more consistent cost/performance relationship. Specifically, utilizing low duty cycle pulse techniques coupled with pseudo random time separation, DTDMA provides a communication architecture which can be tailored to the composition of the particular communication being sent. Rigid time separation is not required so messages are not constrained to any slot or fixed time duration. Consequently, a message uses only that portion of the system capacity which is actually required, permitting system resources to be used and reallocated with maximum efficiency.

The unique combination of low duty cycle pulse techniques operated within a discipline of full ambiguity (pseudo-random) of time-frequency-code provides a digital communication service that offers high levels of anti-jamming and low probability of exploitation coupled with powerful pseudo-noise access techniques which make real-time C³, anti-jamming (A/J) and low probability of exploitation (LPE) a practical reality.

Channelization Concepts. JTIDS II/DTDMA channelization and signal structure are based upon maximizing the utility of available ambiguities in time frequency and phase code. If all of the Lx-Band (T/F) space is subdivided into elemental T/F resolution elements they may be formed into T/F patterns which can be identified with specific RF transmission channels for use by selected terminals for specific functions.

The DTDMA channel architecture is modular in nature. At the macroscopic level we have The Meta Channel (MC), while at the microscopic level we have the Basic Event (BE). In between lie two important channel constructions called Basic Channel (BC) and Function Channel (FC). We proceed to a brief definition of these concepts, starting with the fundamental element.

Basic Event (BE). The fundamental building block, or smallest basic portion in the Time-Frequency-Code (T-F-C) space is called the Basic Event (BE). It is shown pictorially in Figure 1.

The Basic Event is uniquely associated with an event code that fully describes its signal and channel parameters. These event codes are generated at a 12.8 microsecond rate (78,125 times per second). Figure 2 shows a simplified example of PR event code usage.

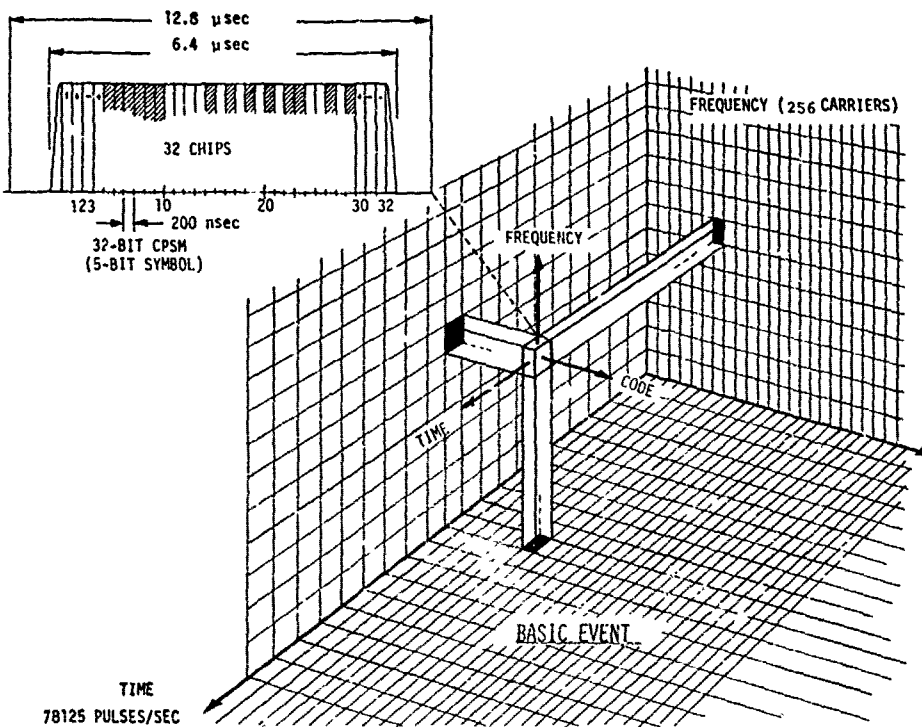
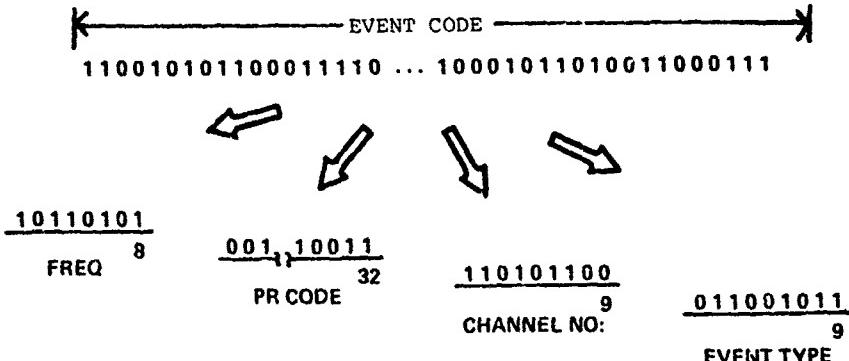


Figure 1. Basic Event

- SPECIFIC BINARY SUB GROUPS OF EVENT CODE ARE DESIGNATED FOR SPECIFIC FUNCTIONS



- ALL TERMINALS WITH SAME CODE OF DAY WILL INTERPRET THE SPECIFIC BINARY SUB-GROUPS IN AN IDENTICAL MANNER
- ALL TERMINALS WITH IDENTICAL TIME OF DAY AND INITIAL CODE WILL GENERATE IDENTICAL EVENT CODES FOR EACH EVENT INTERVAL

Figure 2. Pseudo-Random Event Code Usage

Meta Channel (MC). The contiguous stream of all BE's form by definition a Meta Channel. The MC may be viewed as the multiplexing of many T-F-C patterns each with mutually exclusive Basic Events. Different MC's are distinguished by different contiguous T-F-C patterns which then define different event codewords and in turn different BE's.

Basic Channel (BC). Of fundamental importance is the particular T/F channel denoted as the Basic Channel. The 78,125 events of the Meta Channel are subdivided into 512 Basic Channels. Therefore, each BC has an event rate of about 152.2 Hz (78,125/512). In general, these events may be divided and broadly classified as either source (Source of Communication, e.g., transmitting platform), synchronization events or message events. The BC concept also defines the "page" as that time for 512 BE or 6.5536 msec (512 x 12.8 microseconds). See Figure 3 for a pictorial description of the BC.

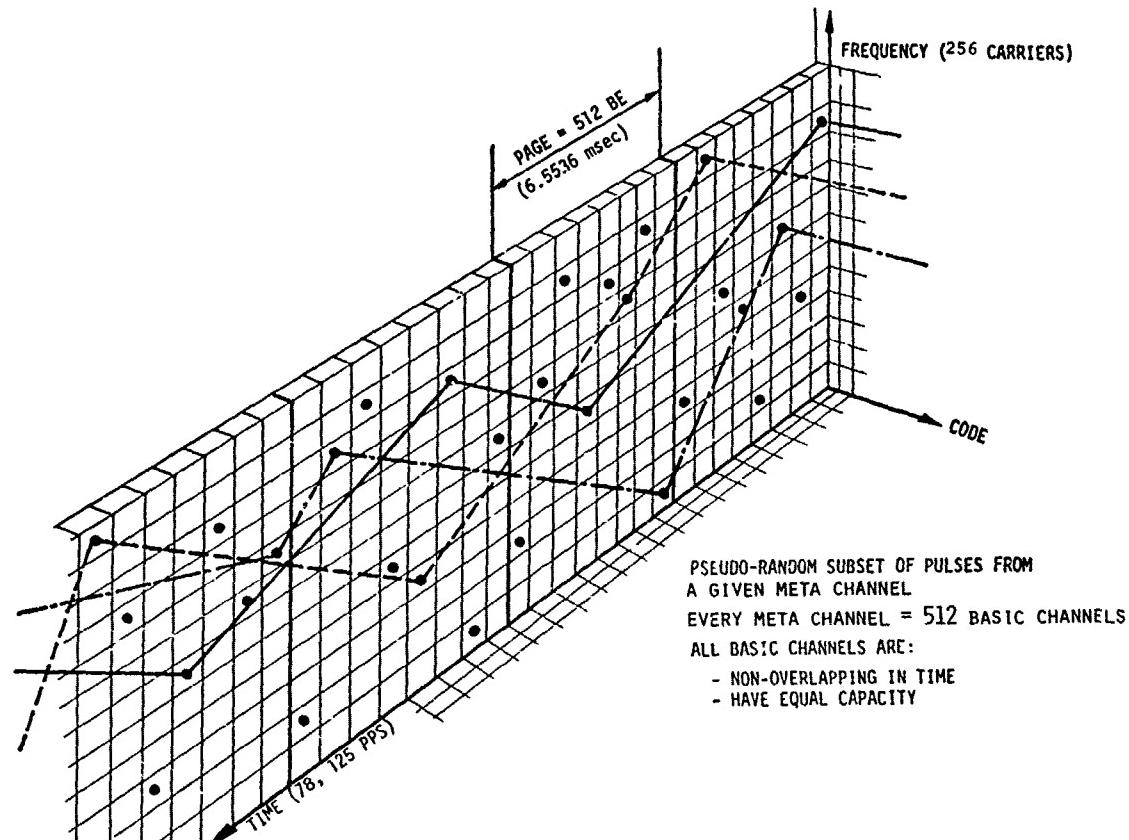


Figure 3. Basic Channel

Function Channel (FC). When a channel is designed to support a specific user function (i.e., Link-4A, Link 11, or High or Low Rate Digital Voice, etc.), it consists of sets of Basic Channels which are organized to support the required numbers of subscribers with a prescribed level of channel capacity. The totality of these building block channels is called a Function Channel (FC). A pictorial representation of the FC is shown in Figure 4. As indicated, there are 512 BC's available on each MC for use in construction of FC.

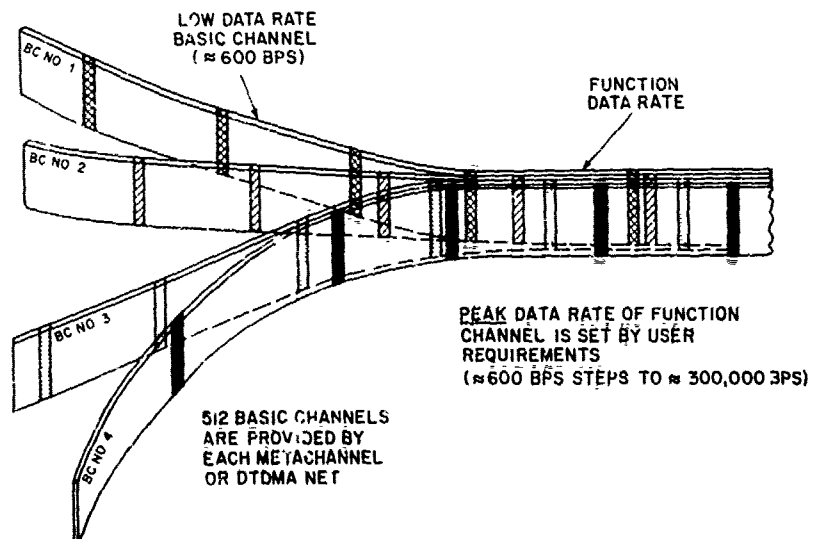


Figure 4. Composition of Function Channel (FC)

The multi-function C-N-I requirements of the host platform are generally met with a number of FC's operating within one or several MC's. Figure 5 shows the Function Channels operating on a single MC. As indicated the capacity of an MC is on the order of 300 KBPS. Specific terminal channel capacities are tailored to operational needs.

In this manner channels are constructed to meet C³ requirements. These channels are tailored efficiently in terms of access rate (message start (M) rate), data rate (number of basic channels) and composite channel grouping (composition of multi-function nets) for specific operationally driven communication needs.

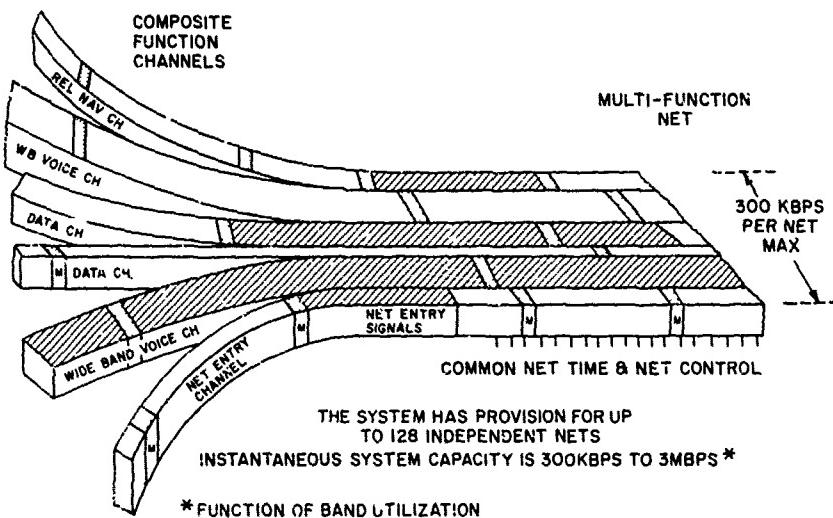


Figure 5. Composition of Multi-Function Net

Class 1 Command and Control Terminal Description (2)

The JTIDS Phase II Command and Control Terminal (Class 1) provides a functional repertoire developed from operational scenario analyses performed by the military and the JTIDS Joint Program Office. The platforms intended as candidates for the Class 1 include the CVA ships and the E-2C aircraft. It is anticipated that other command and control centers both airborne and surface based would be appropriate platforms.

The functional capability of the Class 1 ADM Terminal is summarized in Table 1.

TABLE 1. FUNCTIONAL CAPABILITIES CLASS 1/CLASS 2 TERMINALS

PARAMETER	CLASS 1	CLASS 2
Number of Nets	12	3
Power Output	1.0 kw	200/800 watts
Number of Rcvr.	4	2
Function:		
DTDMA		
Dig. Voice (15 KBPS)	3 channels	2 channels
Link-11	Full modes	Relay only
Link-4A	Yes	Yes
Coded Voice/Data (2.4 KBPS)	Yes	No
TADIL-B	Yes	No
Rel Nav	Yes	Yes
TDMA	Yes	Yes
TACAN	Yes	Yes
IFF	Yes	Yes
Data Rates:		
Xmit.	70 KBPS	50 KBPS
Rcv.	100 KBPS	70 KBPS

Several DTDMA command and control data channels are provided to handle digital data in a transparent manner for full compatibility with current NTDS/ATDS operations. The Link-4A (TADIL-C), Link-11, a surveillance reporting link, and TADIL-B, the U.S. Marine Corps' point-to-point data link, are provided. A TDMA channel provides interoperability with JTIDS Phase I terminals.

The TACAN interrogator function includes the standard Receive (REC), Transmit/Receive (T/R), and Air-to-Air (A/A) modes.

The IFF transponder function of the terminal is identical to that provided by the AN/APX-72 IFF set. Included are the AIMS Mark XII transponder modes (1, 2, 3/A, C and 4).

A simplified block diagram of the Class 1 Terminal is shown in Figure 6. A photo of the Class 1 ADM is shown in Figure 7.

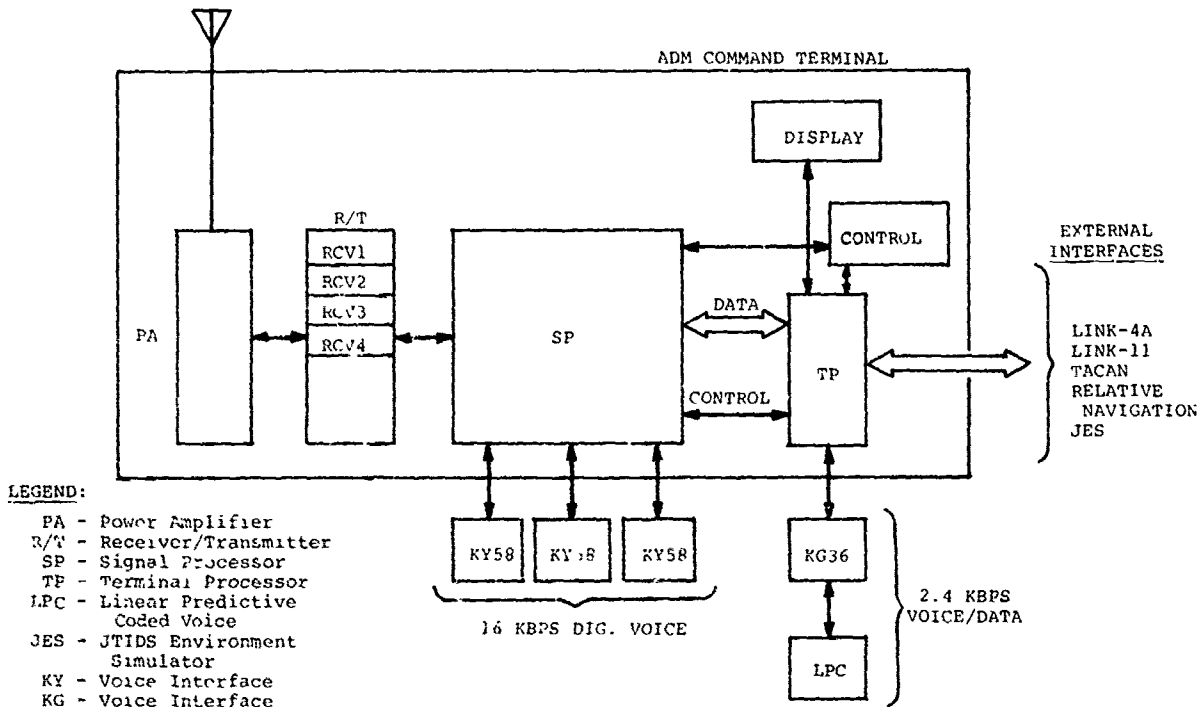


Figure 6. JTIDS Phase II PTDMA Command and Control Terminal, Block Diagram

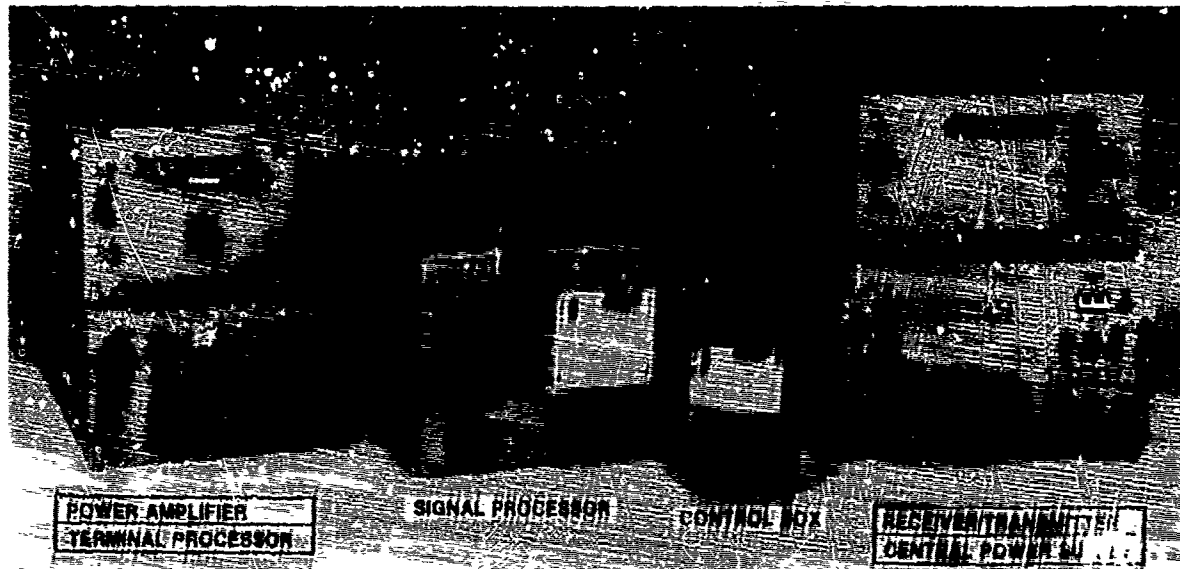


Figure 7. Class 1 ADM Photo

Class 2 Tactical Fighter Terminal Description (3)

The JTIDS II Tactical Terminal (Class 2) ADM functions represent a subset of those available on the Class 1 terminal as listed in Table 1. They were selected from operational scenario analyses performed by the U.S. Armed Forces and the JTFPS Joint Program Office.

Although not specifically limited to a single aircraft type, the U.S. Navy's F-14A was used as the candidate for defining representative operational requirements. The Tactical Terminal is also applicable to other platforms such as the F-4, F-15, F-16, F-18, and A-7.

The major advantage of the DTDMA architecture is that with reduced data rate requirements, the number of receiver channels can be reduced while still maintaining full anti-jamming protection. Thus, the Tactical Terminal needs only two receiver channels for JTIDS whereas the higher data rate Command Terminal has four receivers. Since each receiver channel includes not only an IF amplifier but also a frequency synthesizer, a spread spectrum pulse compressor/detector, and real-time digital controlling circuitry, the elimination of receivers without loss of anti-jamming protection is a significant cost and size savings. DTDMA further permits one to configure a single receiver terminal at lower data rates, while again maintaining full anti-jam protection. This single receiver approach is feasible for cost-effective austere platform requirements.

The simplified block diagram (Figure 8) shows that the Tactical Terminal has two time-shared receivers for JTIDS and TACAN and a dedicated IFF receiver, all serviced by a common RF front end. The transmitter's solid-state exciter and power amplifier outputs JTIDS, TACAN and IFF pulses each of which is appropriately shaped by the amplitude modulator. The output pulses are interleaved in real-time with a peak power of 200/800 watts for JTIDS and 800 watts for TACAN and IFF.

Figure 9 shows a photo of the ADM Class 2 Tactical Terminal.

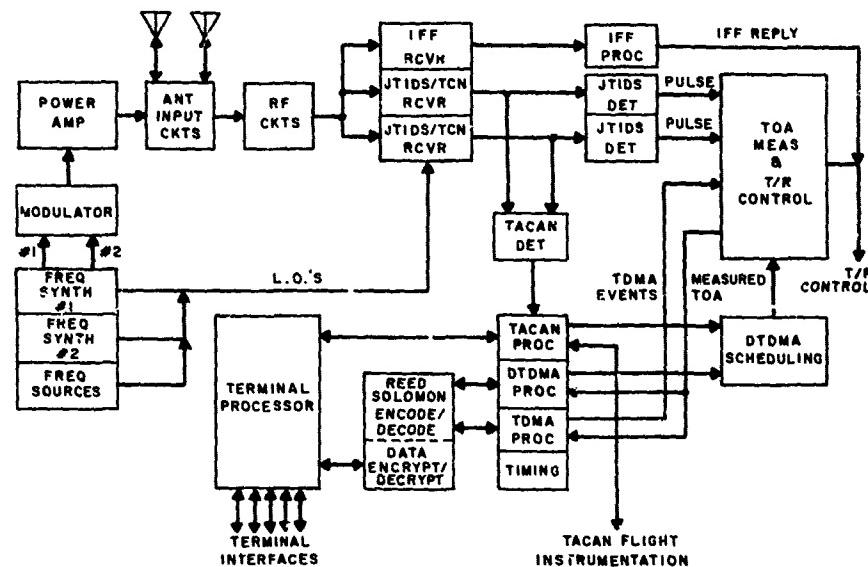


Figure 8. JTIDS II Tactical Terminal (Simplified Block Diagram)

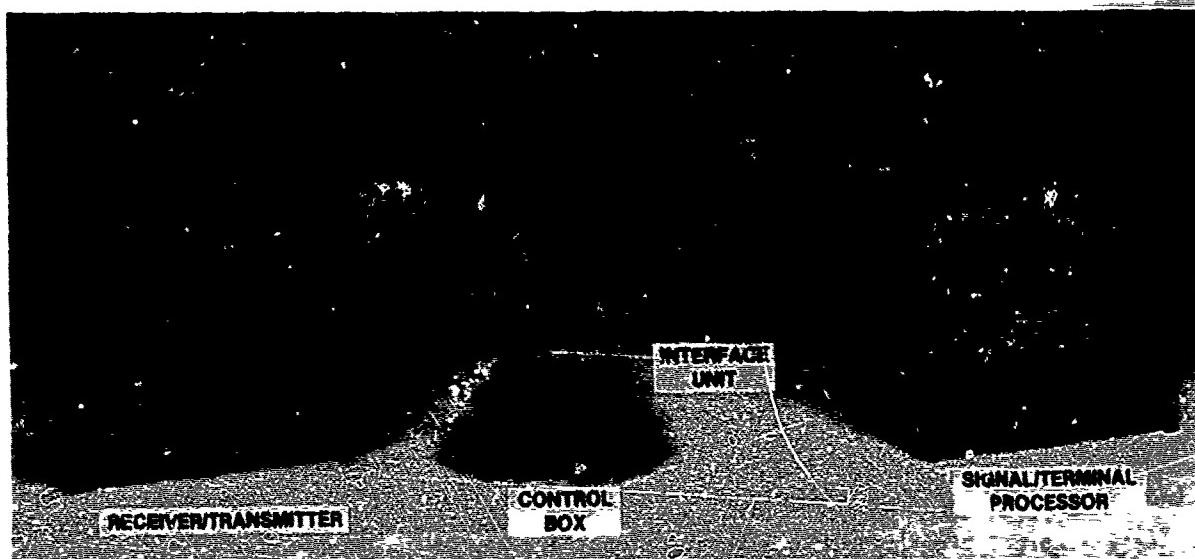


Figure 9. ADM Class 2 Tactical Terminal

JTIDS Environment Simulator (JES). The JTIDS Environment Simulator provides real-time dynamic simulation of the expected 300 KBPS JTIDS multi-net environment. In addition,

performance evaluation of up to three terminals under test is possible. The JES is basically a two part system. The first, the "simulator," consists of four independent RF transmitting sections. Two of these are for DTDMA use, the third is a TDMA output, and the fourth a random filler pulse output. In this manner a synthesized but full dynamic multi-netted JTIDS RF environment can be generated. The second major portion of the JES consists of the "evaluator." This section is essentially software driven and provides reference data for transmission by the JES for all DTDMA and TDMA functions. Via digital interfaces back from the terminals under test, full performance evaluation can be performed. Figure 10 is a simplified block diagram of the JES. Table 2 lists the functional capabilities of the JES and Figure 11 shows a photo of the unit.

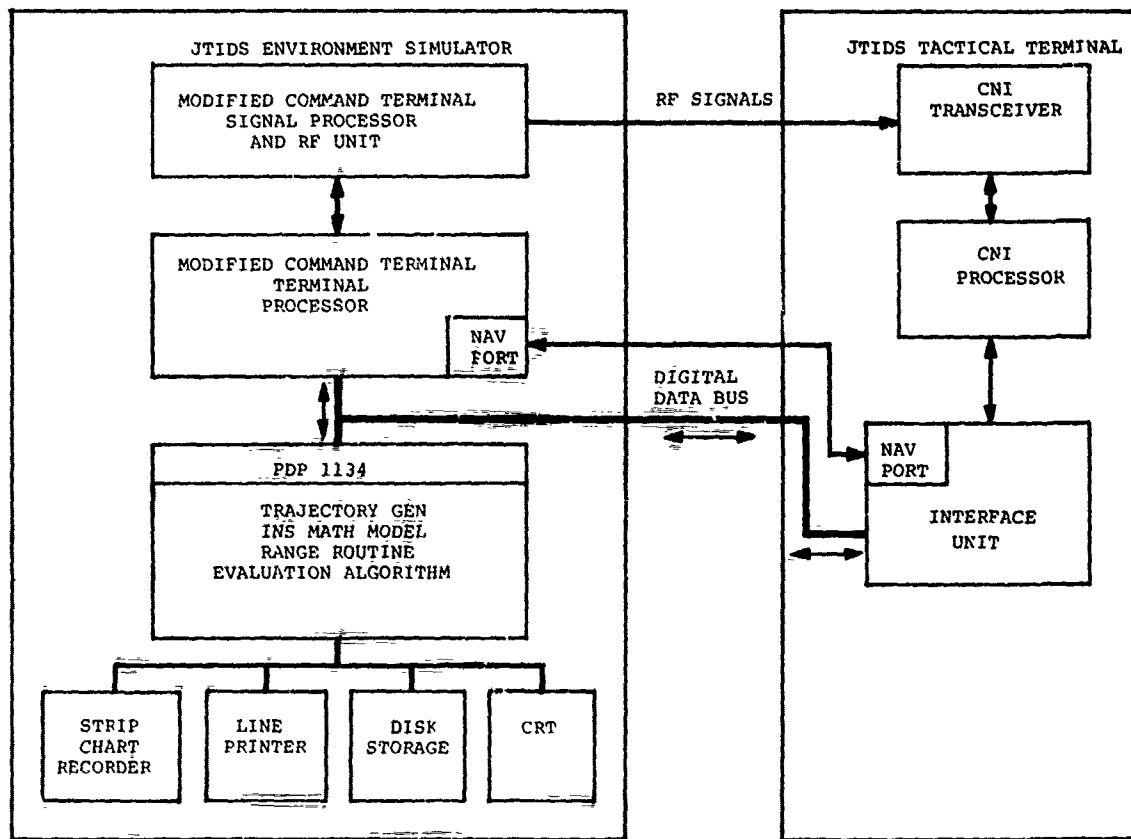


Figure 10. JTIDS Environment Simulator, Block Diagram

TABLE 2. JTIDS ENVIRONMENT SIMULATOR FUNCTIONAL CAPABILITIES

• Simulates RF Environment of 300 KBPS
JTIDS I (TDMA) 60 KBPS
JTIDS II (DTDMA) 120 KBPS
Random Filler Pulses 120 KBPS
• Operates Simultaneously with Three JTIDS Terminals
• Simulates 12 Independent Nets
• JTIDS I - Net Entry - Active
• JTIDS II - Net Entry - Active
- Link 4A
- Link 11
- Digital Voice (16 KBPS)
- Coded Data Channel (2.4 KBPS)
• Random Pulse Generation Up to 120 KBPS
• Performance Analysis in Real Time JTIDS I, JTIDS II, Link 4A, Link 11, Voice and Coded Data Channels
• Dynamic Motion Profiles for 191 Users
• Digital Voice Simulation
• Relative Navigation Simulation

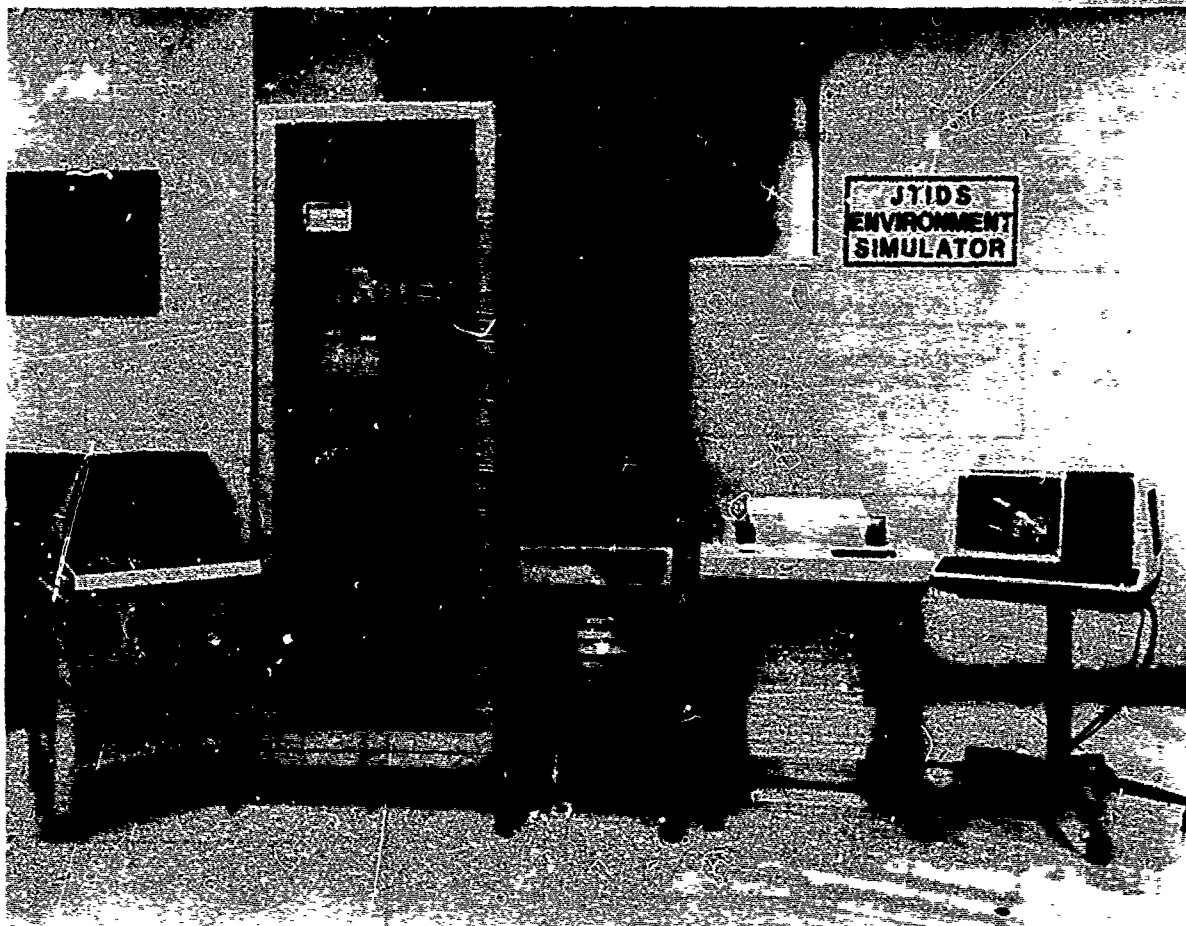


Figure 11. JTIDS Environment Simulator

PART II. RELATIVE NAVIGATION OVERVIEW AND TEST RESULTS

The following sections will describe the implementation of the basic Relative Navigation function in the ADM terminals. The dynamic JES simulation capabilities in the REL NAV area will also be treated.

Relative Navigation. The purpose of the Relative Navigation (REL NAV) function mechanized in the JTIDS terminals is to tie the operations of a tactical community of users to a common relative navigation grid while optimally blending the fast response and short term accuracy of self-contained dead reckoning navigation equipment with JTIDS derived position and status reports from multiple users.

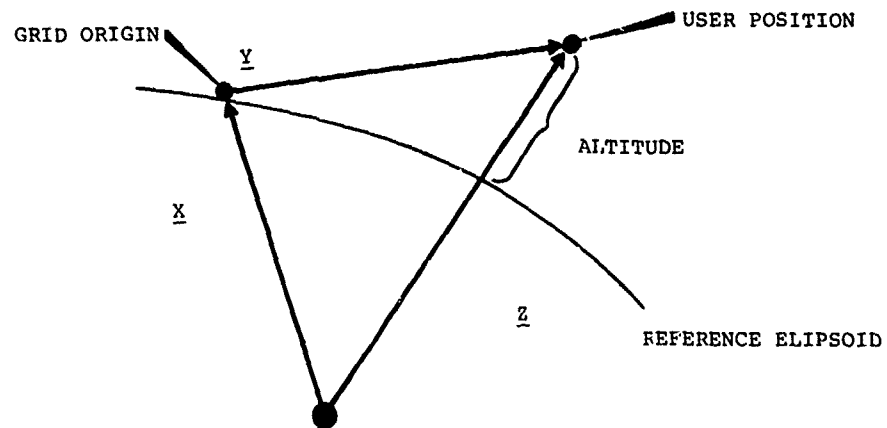
REL NAV System Description. Basic to the operation of the system is a stable relative navigation grid which provides compatible inter-operation for differing terminal types found in a highly inter-active tactical system. The location of the grid origin is defined by one moving user or two stationary users assigned to the role of Navigation Controller. All users, other than the Navigation Controller, continuously update their estimates of position and velocity in the relative grid as well as the location of the grid origin based on the time-of-arrival of JTIDS messages called Position and Status Report (P-Messages) received from other users.

Figure 12 illustrates the relationship between the relative and geodetic navigation vectors mechanized in the REL NAV algorithm. The vector navigation equation employed by all users is given by: $\underline{X} + \underline{Y} = \underline{Z}$.

Figure 13 illustrates the navigation grid which is defined as a tangent plane normal to the reference ellipsoid at the grid origin. The grid U, V, W coordinates are defined as U-grid east, V-grid north and W-grid altitude. The V-grid north axis is related to true north by a counterclockwise rotation, β , about the W-grid axis.

The REL NAV algorithm is implemented in software contained in the units Terminal Processor. The software is provided with received P-message data and the measured TOA of these messages from the Signal Processor (see Figure 6). The three primary software modules used to provide the REL NAV function are:

- (1) Kalman Filter
- (2) Source Selection
- (3) Dead Reckoner Data Processing



\underline{X} = Grid Origin Position Vector
 \underline{Y} = Relative Grid Position Vector of User
 \underline{Z} = Geodetic Position Vector of User

Figure 12. REL NAV Grid Definition

V-GRID NORTH TRUE NORTH

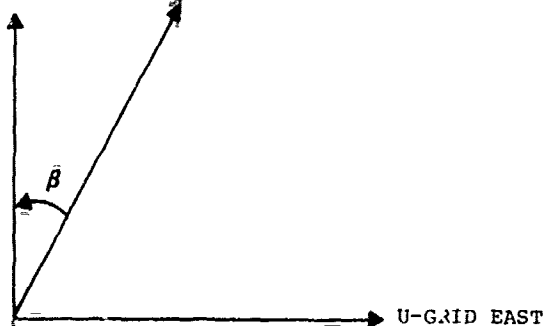


Figure 13. Tangent Plane Coordinates

Figure 14 illustrates a functional block diagram for REL NAV in a terminal equipped with an Inertial Navigation System (INS).

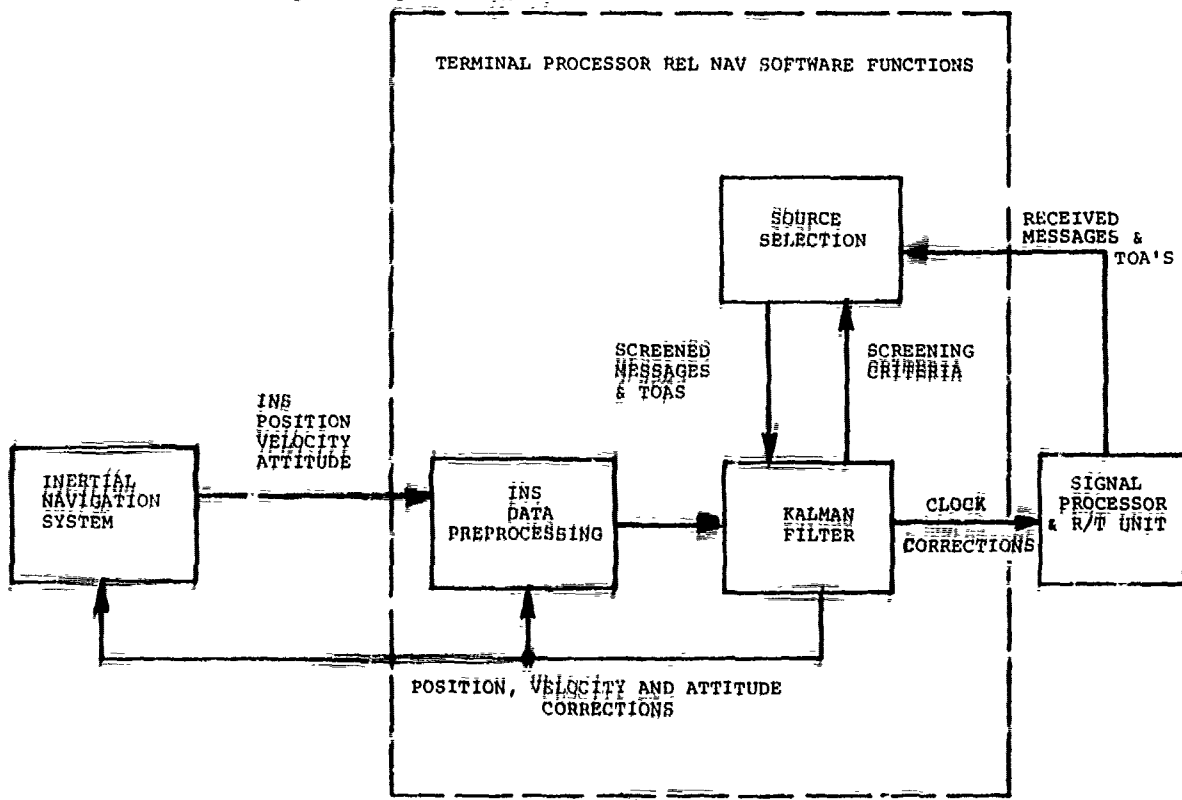


Figure 14. JTIDS REL NAV Functional Block Diagram

Initially, the terminal REL NAV software employs the INS position and velocity data to perform dead reckoning navigation in the geodetic coordinate system. As P-messages containing the relative grid and geodetic coordinates of members of the community are received, this data is screened using a "Source Selection Criteria." This software module is provided with an initial set of screening criteria from the Kalman filter module. Successfully screened P-message data and measured TOA's are then provided to the Kalman filter where this data is optimally mixed with INS data to provide estimates of:

- (1) Grid and Geodetic Position
- (2) Grid and Geodetic Velocity
- (3) INS Position, Velocity and Altitude Corrections
- (4) Clock Phase and Frequency Corrections
- (5) Revised Source Selection Screening Criteria

Essentially, the Kalman filter employs the P-message TOA as a range measurement which is compared with a computed value obtained from own position and position data contained in the received P-message. The difference between the measured range (TOA) and computed range is processed by the Kalman filter in order to provide estimates of the elements in the filter state vector. The Kalman filter covariance matrix elements are used to continuously revise the Source Selection screening criteria and to calculate estimated own position and time quality figures of merit which are transmitted to other users together with estimated position data in each unit's own Position and Status Report (P-Message).

In order to utilize a measured TOA as an indication of range between a transmitting and receiving terminal, all users must be in time synchronization to participate in the navigation community. This fact becomes obvious when it is noted that a measured TOA (pseudo-range measurement) contains the range data needed plus the clock offset between the two units. In the system organization, one unit is designated the Net Time Reference. This unit arbitrarily establishes the one clock used as the community standard. Other units designated as Geographic Position References provide absolute position inputs to the community and are either surveyed ground sites or possessors of independent high accuracy geodetic navigation systems.

The Time and Position References form the foundation of the absolute navigation grid which is extended beyond radio line-of-sight of these relatively few units by propagation of the position information available from them through navigating elements by means of the Relative Navigation function of the data link. This is carried out within a hierarchical organization for data interchange, based on the quality of time and position information available from each unit.

The establishment of such a hierarchy is intended to prevent circulation and amplification of errors and prevent system instability which has been found to occur in completely equalitarian user communities. The rank of each unit in the time and position hierarchies is indicated in the P-message by four quality fields. Each unit uses, discards, and weighs range measurements to other units based on the relative ranks of source and user. The algorithms for this choice and the algorithms used to determine the transmitted quality levels define the system organization, and are specified in the Source Selection function. Briefly, the organization is as follows. The Time Reference has the highest time quality. Position References have the highest geodetic position quality. In a purely Relative Navigation mode the Navigation Controller is selected as the arbitrary relative position reference for the remainder of the system. This unit arbitrarily establishes the relative grid origin and north orientation.

Within the hierarchy, the Navigation Controller has the highest relative position quality and highest azimuth quality.

Below the Time Reference and Navigation Controller there are two classes of user, Primary and Secondary. The designations relate to the use of active roundtrip timing (RTT) versus passive synchronization and the associated source selection logics. Within the two classes, source selection and qualities are based on estimated accuracy without reference to the class of operation.

Control of source-user relationships is based on the estimated accuracy of synchronization and position derived within the filter algorithms of each unit and reflected in the position and status reports (P-messages) by four data fields denoted: Time Quality (Q_t), Geodetic Position Quality (Q_{pg}), Relative Position Quality (Q_{pr}) and Relative Azimuth Quality (Q_{ar}). These fields indicate the latest estimate of the accuracy of the setting of the local clock (accuracy of time of transmission) and accuracy of the positions reported in that P-message.

One unit, designated the Net Time Reference, transmits a Q_t of 15, and does not adjust its terminal clock. Position Reference units are defined as units of accurately known geodetic position derived external to the relative navigation system. Position References transmit $Q_{pg} = 15$. The Navigation Controller defines the origin and orientation of the relative rectilinear planner (U,V) grid. A Navigation Controller transmits $Q_{pr} = 15$ and $Q_{ar} = 7$ and does not perform adjustments to relative grid position on the basis of TOA observations. However, a Navigation Controller may adjust his geodetic position and velocity on the basis of observations of messages from units of superior Q_{pg} including, but not limited to, Position References. Table 3 lists the various quality figures of merit used in the REL NAV system together with the values for each integer.

TABLE 3. TIME, POSITION, AND AZIMUTH QUALITIES
AND EQUIVALENT STANDARD DEVIATIONS

QUALITY LEVEL	GEODETIC POSITION σ_{pg}	GRID POSITION σ_{pr}	TIME σ_t	AZIMUTH σ_{ar}
	σ_{pg} (ft)	σ_{pr} (ft)	σ_t (nanosec)	σ_{ar} (mils)
15	<50	Nav. Cont.	Time Ref.	
14	<71	<71	<71	
13	<100	<100	<100	
12	<141	<141	<141	
11	<200	<200	<200	
10	<282	<282	<282	
9	<400	<400	<400	
8	<565	<565	<565	
7	<800	<800	<800	<1
6	<1130	<1130	<1130	<2
5	<1600	<1600	<1600	<4
4	<2260	<2260	<2260	<8
3	<4520	<4520	<4520	<16
2	<9040	<9040	<9040	<32
1	<18080	<18080	<18080	<64
0	>18080	>18080	>18080	>128

Initial net entry is an operation which is separate from the Relative Navigation Function which must precede instigation of any of the fine synchronization routines. Choice of Active or Passive shall be determined by assignment of the unit as Time Reference, Position Reference, Navigation Controller, Primary, Secondary or radio silent. RTT designates a Round Trip Timing process wherein the synchronizing unit transmits an RTT interrogation message addressed to another unit.

The interrogated unit responds with a message containing sufficient information to allow the synchronizing unit to properly compute the local clock offset. A continuing series of such RTT events are used to maintain clock offset and drift rate (frequency error) and estimated accuracy of synchronism. RTT synchronization is used by Position References, Primary Users, and Navigation Controllers.

Secondary users compute clock offset and drift from passive observations of a set of P-messages/TOA values from geographically separated sources. Passive synchronization requires no prior knowledge of own-unit relative grid or absolute geographic position other than an approximate initial estimate required to start recursive filter operations.

REL NAV Simulator. The performance of the REL NAV algorithm is a complex function of vehicle dynamics, RF signal environment and the quality and relative geometry of the available sources of P-messages. Several methods of testing the algorithm were considered and at an early phase of the program it was decided to use the computer controlled JTIDS Environment Simulator (JES) to provide real-time dynamic JTIDS RF and INS signals to stimulate the terminal as well as perform real-time performance analysis. Use of the JES facilitated integration and test of the REL NAV software and hardware consisting of the JTIDS receiver and Kalman navigation filter under a wide variety of signal environments, source geometrics and dynamic mission profiles.

Figure 15 illustrates a typical JTIDS terminal connected to the JES. The simulator is divided into two major hardware blocks: a modified JTIDS Terminal and a PDP 11/34 Digital Computer. The PDP-11/34 is programmed to provide the following functions:

- Trajectory Generation
- Inertial Navigation System (INS) Math Model
- Range Routine
- Real Time Performance Evaluation
- Post Simulation Evaluation

The modified JTIDS terminal contained in the JES performs RF signal management, accepts range data from the PDP-11/34 and transmits JTIDS position reports and Round Trip Timing Replies (RTTR's) to the Terminal under test.

The major units of the Terminal under test illustrated in Figure 15 are the Transmitter/Receiver Unit, Signal Processor Unit and Terminal Processor Unit. The Terminal Processor contains three REL NAV Software modules. The Navigation Port Interference Processor (NPIP) accepts inertial position, velocity, altitude and time marks from the simulated INS and preprocesses this data for the Kalman Filter. In addition, the NPIP module provides JTIDS Terminal Kalman Filter estimated position, velocity and attitude corrections to the JES PDP-11/34 Real Time Performance Evaluation Module. The Source Selection and Message Processing (SSMP) module screens all received valid position reports and selects the optimum reports for processing by the Kalman Filter.

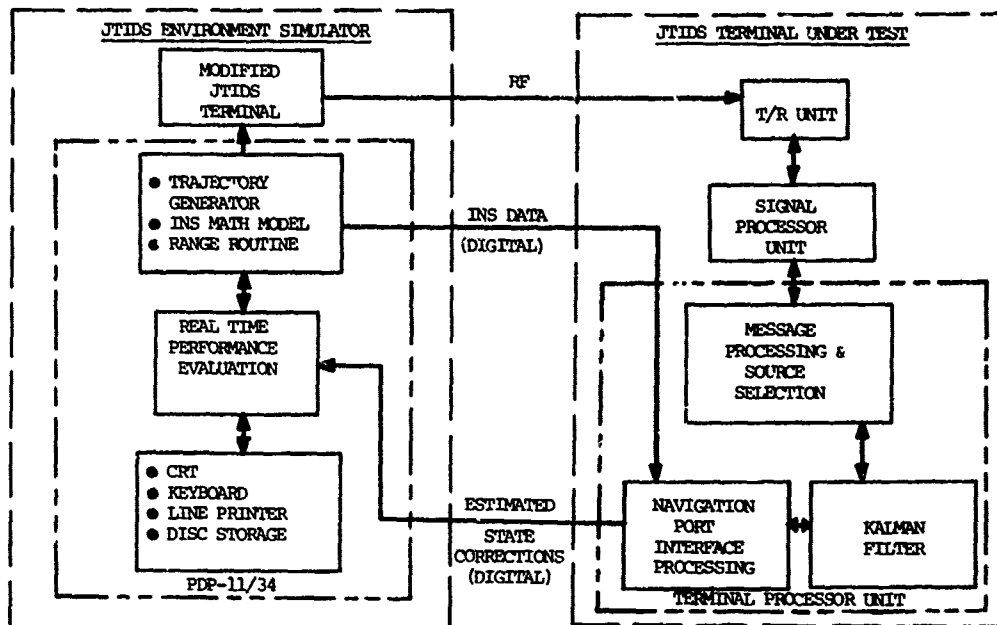


Figure 15. JES Dynamics Simulator and Terminal Under Test, Functional Block Diagram

The controlling function of the simulator is a trajectory generator. A complete simulation flight profile for the Terminal under test is defined with a set of initial conditions and segment data. The true trajectory generator is initialized with latitude, longitude, altitude, velocity, heading and flight path angle. Each segment of a mission is defined by its duration in multiples of computation intervals and the constant rate of change of aircraft velocity, heading and flight path during the segment. The Trajectory Generator updates the true vehicle state vector by numerically integrating a set of differential equations. The INS Math Model is provided with a set of true accelerations sensed by a perfectly aligned INS and computes a portion of the derivatives of a direction cosine matrix which is used to transform the true accelerations into a coordinate system for the simulated misaligned INS. In addition, the Trajectory Generator transforms the true geographic coordinates of the Terminal under test into Relative Grid Coordinates and provides these to the Range Routine. The mathematical equations programmed for the Trajectory Generator, INS Math Model, Range Routine and Evaluation software modules are given in Reference (4).

The JES provides both a real time test evaluation capability via the PDP-11/34 CRT Display and a more detailed post test evaluation analysis of data stored during the simulation. The real time evaluation display presents true (Trajectory Generator) and Terminal Under Test level position and velocity as well as the differences (errors) between the latter.

In addition, key output variables of the JES Trajectory Generator, INS Math Model and Range Routine as well as the estimated INS corrections of the Terminal under test are stored on the PDP-11/34 Disc for post simulation data analysis.

REL NAV Simulation Results. Figure 16 illustrates a typical test trajectory and source geometry that exhibits time varying geometrical dilution of precision (GDOP). The initial segment of the simulated mission consists of take-off and climb to 10,000 feet and cruise to the east at 800 feet per second. This is followed by a sequence of ninety degree, three (3) q turns which result in the rectangular pattern shown in Figure 16.

Figures 17 and 18 show the relationship between grid and geodetic level position navigation errors (rss) respectively for each segment of the trajectory and the expected rss level position errors obtained from the Kalman filter covariance matrix. These are the grid and geographic position quality figures of merit (Q_{pr} and Q_{pg}) respectively, which are inserted into the units own P-messages. The solid lines in Figures 16 and 17 are Q_{pr} and Q_{pg} while the dashed lines are the actual level position errors (rss). Two factors should be noted when examining Figures 16 and 17. The predicted position quality figures of merit exhibit discrete jumps. This is due to the fact that the discrete quality integers represent a range of values as listed in Table 3. Note that the actual rss system performance (dashed line) almost always lies below the predicted performance (solid line). In addition, note that the system predicted performance is more accurate in the north-east (upper right hand corner) of the box pattern due to the better GDOP where the difference in bearing of the two sources is ninety degrees. In the south-west (lower left hand corner) of the box pattern, the difference in bearing of the two sources is about forty degrees.

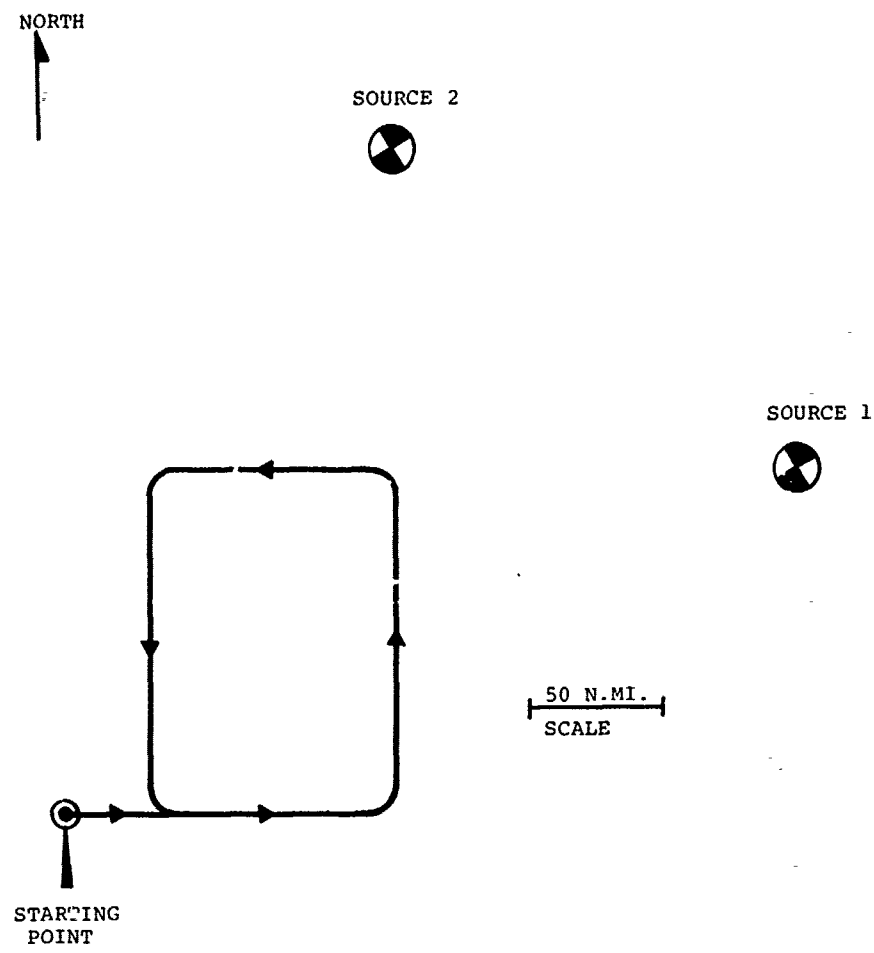


Figure 16. Dynamic Trajectory and Source Geometric

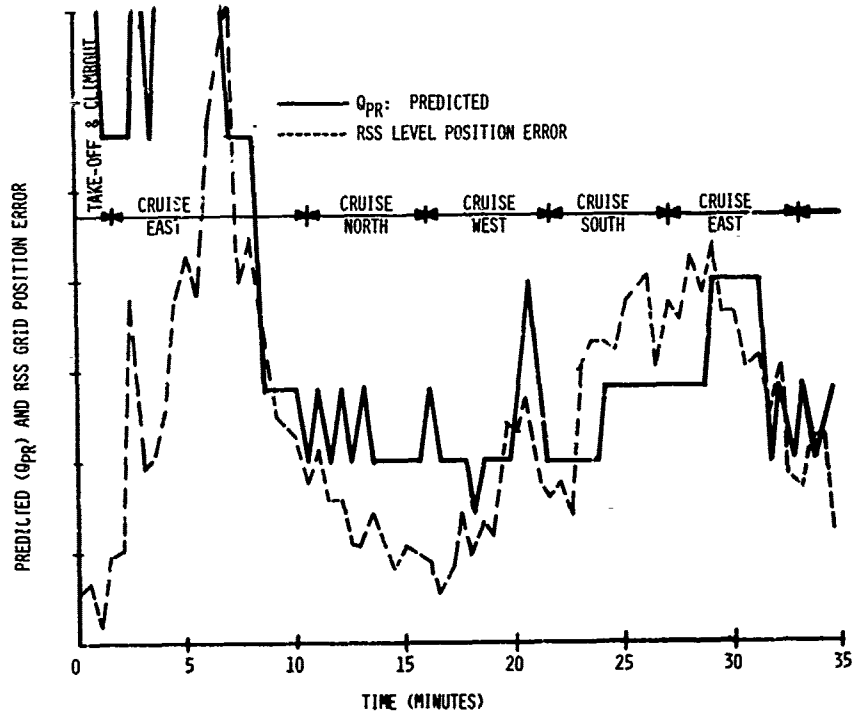


Figure 17. Grid Predicted (Q_{pr}) and RSS Grid Position Error Versus Time (Passive Sync)

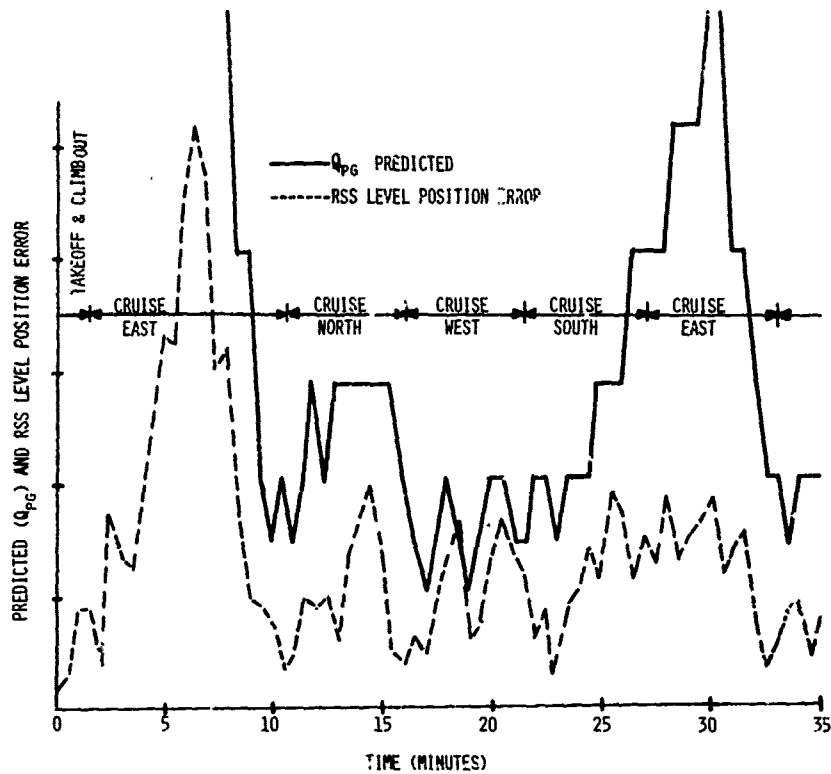


Figure 18. Geodetic Predicted (Q_{pg}) and RSS Level Position Error Versus Time (Passive Sync)

SUMMARY AND CONCLUSIONS

Extensive testing of the Command and Tactical Terminals were performed utilizing the JES to simulate highly dynamic and diverse RF environments. System performance limits were obtained with barrage and optimum jamming for active and passive net entry as well as for each communication function individually and various mixes of com/nav functions. Multi-net, multifunction tests were performed utilizing TDMA, DTDMA and TACAN waveforms simultaneously. In general, all key terminal parameters were demonstrated successfully. The systems and JES are currently located at the Naval Ocean Systems Center, San Diego, undergoing additional com/nav testing and integration with Naval shipboard and airborne Tactical Data System Command and Control computers.

Communication and Navigation System function design, integration, dynamic laboratory verification and transition to field test tasks were aided by using the dynamic real time simulation and evaluation capabilities of the JES. The computer-controlled JES furnished an effective method of bridging the gap and provided a smooth transition between system integration and field test phase of the program.

GENERAL REFERENCES

- (1) J. Rubin, "Distributed TDMA - An Approach to JTIDS Phase II," Principles and Operational Aspects of Precision Position Determination Systems. Presented at AGARD, July 1979.
- (2) J. Rubin and J. Heinen, "JTIDS DTDMA - Command and Control Terminal," Principles and Operational Aspects of Precision Position Determination Systems. Presented at AGARD, July 1979.
- (3) J. Rubin and J. Heinen, "JTIDS DTDMA Tactical Terminal," Principles and Operational Aspects of Precision Position Determination Systems. Presented at AGARD, July 1979.
- (4) Sanford Welt, "Dynamic Simulator Test and Evaluation of the JTIDS Relative Navigation System," presented at the IEEE National Aerospace and Electronics Conference, Dayton, Ohio, May 1979.

ACKNOWLEDGMENTS

The terminals described herein were developed under JTIDS Joint Program Office/Naval Air Development Center, Contract No. N62269-76-C-0105.

JTIDS DUAL GRID NAVIGATION USING TIME SYNCHRONIZED DATA LINKS

Robert C. Stow
Joel D. Reiss
Singer-Kearfott Division
150 Totowa Road
Wayne, New Jersey 07470
U.S.A.

SUMMARY

This paper represents a comprehensive survey of the fundamental theory, principal design considerations, and expected operational performance capabilities of relative navigation as developed by Singer Kearfott Division utilizing the JTIDS data link. Beginning with a description of the basic methodology of dual-grid (relative and geographic) hybrid navigation, the design of the relative navigation estimation algorithm is presented, with special emphasis on modeling considerations within the Relative Navigation Kalman Filter and the Observation Screening Algorithm. These considerations include requirements for global navigation, communities composed of mixed types of dead-reckoning units, and efficient usage of available data provided by the JTIDS data link.

Specific requirements for integration of the basic software design in a robust configuration are discussed, and expected performance levels within various community structures are presented. Most importantly, the application of this capability to operational problems in targeting and weapon delivery are discussed at length. Particular emphasis is placed on discussion of the generic effects of relative navigation errors on both targeting and weapon delivery.

1.0 INTRODUCTION

The essence of JTIDS relative navigation is the establishment of time synchronization and relative position, velocity, and dead reckoning sensor platform azimuthal correlation among the members of a mission or multi-member community. In this respect, no community member represents an independent entity, but rather is an integral part of a network of users linked together by a precise, high-capacity jam resistant digital RF data link. This data link implements an architecture which embodies various forms of Time Division Multiple Access (TDMA) techniques all requiring time synchronization for the basic communications function. This is required since communication channels are separated through time division where individual transmissions by each single member of the community are received by all other members (multiple access) without the need for specific addressing. Thus individual member receivers, having access to all community data link information, can screen for that data critical to its particular mission.

The only JTIDS terminal data link performance characteristic which must be specifically controlled for relative navigation is the accuracy of time synchronization and message TOA detection. With accurate net time synchronization and TOA detection coupled with position and status messages normally transmitted by individual members to support command and control functions, the relative navigation function is implemented with negligible added recurring cost to the basic JTIDS terminal cost. Since relative navigation is primarily a terminal software function, implementation only requires added terminal processor memory and an input/output interface with the vehicle on-board navigation subsystem. From a relative navigation point of view the network of JTIDS data link subscribers may be considered as one hybrid navigation system having distributed sensors. The relative grid provides a unique measurement base in which the precise exchange of each member's sensor data occurs. This same network allows for the distribution of geographic position data (e.g. GPS) and the mutual augmentation of different types of velocity or acceleration navigation sensors.

1.1 Technical Overview

As background to the material covered in this paper, a brief review of fundamental aspects of JTIDS relative navigation is presented. Following this discussion software algorithm structure and design sensitivities will be presented together with subsequent operational performance and application considerations.

1.1.1 Relative Navigation Operation

Relative navigation operation mechanizes hybrid relative navigation simultaneously in relative grid and geographic grid coordinates for each JTIDS community member. This is achieved using grid hierarchy source selection procedures programmed in each terminal processor which test for minimum acceptable qualities and geometric preferences associated with potential sources to be used for updates. The relative grid is defined to have the following properties:

- o The grid is a tangent plane grid with a sea level origin at the designated reference point. It is tangent to the surface of the earth at its origin.
- o The coordinate Frame is an Orthogonal frame with axes (U, V, W) and nominal orientation U-East, V-North, W-Up.
- o The grid azimuth angle, β , defines the angle between the grid V-axis and true north at the grid origin $\lambda_0^\circ, \phi_0^\circ$. (Figure 1)

Quality screening and geometry screening are done separately for both grid and geographic sources. Adherence to those procedures provides relative grid lock of all JTIDS community members in position, velocity, attitude and timing using JTIDS range and position report data. Also the presence of accurate geodetic sources will simultaneously result in high accuracy geodetic position, velocity and attitude. Achieving relative grid lock creates a correlation of user dead-reckoning equipment to the grid which maintains accuracy between range updates from other members. This is particularly important when considering the situation of a group of users becoming radio silent or when antenna shadowing is present during critical portions of a mission. Correlation of each user's dead-reckoning system to the relative grid permits accurate navigation during such periods of time. In the absence of accurate geographic updates, the community will also achieve relative grid lock and benefit from accurate relative knowledge.

Source selection procedures provide the community with an ordered way of performing both grid and geodetic updates. Geodetic updates are interwoven with grid updates in such a way as to maintain accurate performance in both geographic and relative frames. Sources for geodetic updates may be taken from fixed ground stations or mobile users that have good knowledge of geodetic positions.

Operation with or without fixed stations is provided by these procedures. Thus, relative performance (grid lock) can be achieved in a community of strictly mobile members. However, if fixed stations are available they can be incorporated into the community as a navigation controller and/or as geographic references, or participate as a user performing both geodetic and grid updates on other community members.

Selection procedures are such that community size may vary from two to an unlimited number of community members. To achieve mutual ranging and position reporting between community members, dual grid navigation reporting is accomplished in the position and status messages. Both relative grid coordinates and geodetic coordinates are formatted within position and status messages. Contained in a single message is the required data for either a geographic update or relative grid update. Therefore, the source selection procedures can consider each received position and status source selection procedure as the sole decision maker with regards to the quality and type of update a given user will perform.

Once having entered the grid community, each member transmits his estimated position and quality for others to observe. The qualities represent the system's statistical estimates of its own navigation errors and are assigned based predominantly on the JTIDS navigation filter's covariance matrix. They are used by other members in their observation selection logic in an effort to utilize the most accurate data. A separate quality is transmitted for geographic navigation accuracy and relative grid navigation accuracy. Each user terminal continually checks the validity of the filter covariance terms used to generate these qualities and associated observations as discussed in 2.2.3. If an invalid condition is detected the reported qualities are conservatively modified to reflect this condition.

In addition to the TDMA system derived range observations with a predicted range based on source and user-relative grid position data (TOA grid update), the filter is designed to process three other observation types. Each of these other three is related to the use of geographic navigation. They are:

- o Geodetic Fixes - Used when the actual current latitude and longitude of the vehicle is available from some on-board sensor.
- o Offset Geodetic - Used when the position of any arbitrary point (i.e., reported user location) in the relative grid is known also in geographic coordinates. User relative grid data is used with the reported source relative grid position to translate the source reference geodetic position to determine user aircraft geodetic position.
- o TOA Geodetic - Used when the reported geographic position of a TDMA equipped member is accurately known. This update is analogous to the TOA grid update with geodetic positions used in place of the relative grid positions from the source position and status messages.

1.1.2 Community Filter Organization and Navigation Kalman Filter Architecture

The achievement of a stable relative community based upon mutual data interchange demands the establishment of a specific observation protocol. This observation protocol is utilized to generate a hierachal relative navigation structure, which when used in conjunction with the other observation selection logic, serves to stabilize and order navigation performance. In this structure there are three classes of participating community members:

- o Navigation Controller
- o Primary User
- o Secondary User

A particular member's designation is seen by others only through his reported quality.

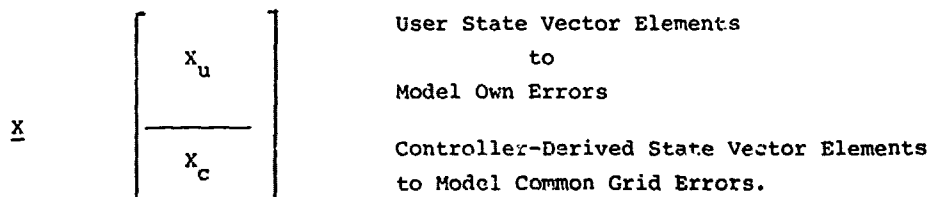
Since he is a community grid reference, the navigation controller is constrained to not perform any relative grid observations. His reported grid position quality is fixed at the maximum attainable value. Primary users are allowed to observe the navigation controller and other Primary or Secondary users provided that the member to be observed is of equal or higher relative position quality. Primary users will always use active TDMA system time synchronization and their reported relative position quality is constrained to be less than that of a nav controller. Active time synchronization is performed independent of the relative navigation function through the use of special round trip timing messages. Secondary users are constrained to observe only members with a higher quality than their own. Their maximum reported quality is constrained to be less than the maximum allowable reported quality of a Primary user. A Secondary user can utilize either active or passive TDMA system synchronization. Passive synchronization is performed by the relative navigation filter through simultaneous estimation of both relative position and clock bias errors based upon JTIDS message time of arrival (TOA) data. While operating in the passive synchronization mode, position messages can still be transmitted for others to observe. The reported qualities will be consistent with the level of synchronization achieved. Thus it is possible for a Secondary User, in either active or passive synchronization, to be observed by even a Primary user, provided the appropriate relative quality levels and other selection criteria are satisfied.

Relative navigation protocol does not significantly affect the geographic observation logic, where geodetic sources of greater than own quality are continuously screened for by all members including the nav controller. The offset geographic observation is the most affected since it relies on relative grid navigation quality.

The design of the software is centered about the Relative Navigation Kalman Filter (RNKF), a quasilinear Kalman Filter, whose estimation process must satisfy the following criteria to fulfill the dual grid navigation and the controller - dominated relative grid hierarchy:

- a) Correlation of error in relative position, velocity, and platform azimuth between the navigation controller and all other members must be achieved to ensure good relative navigation. Navigation controller errors in position, velocity, and azimuth are referred to as common grid errors.
- b) Estimation of errors in geographic positions, velocities and platform azimuth for all members including the navigation controller must be capable of being achieved to improve geographic accuracy and to limit relative grid drift in the geographic frame. Contrary to relative grid accuracy, geodetic accuracy is dependent upon accurate geodetic sources participating within the JTIDS community.

The design approach to the RNKF represents a suboptimal approximation to the modelling of significant grid dynamics. One approach, albeit an unworkable one, would be for each user to model pertinent error states of all other users. The suboptimal form of the relative navigation state vector which has proven most flexible in achieving the above two objectives has been the following, which has applicability to both communities containing members with common dead-reckoning equipment suit types and communities containing members with mixed dead-reckoning equipment suit types.



The size and contents of X_u and X_c to satisfy particular configurations of user and nav controller will be discussed in later sections of this paper.

1.2 Geneology

The current state of the art of relative navigation technology is the cumulative result of more than ten years of continuous development which has resulted in:

- o Successful demonstration of relative grid navigation through integration of TDMA data links with inertial navigation systems using aircraft and ground stations (1972).
- o Successful integration of at-sea navigation and highly accurate relative navigation, resulting in accurate control of a community of multiple aircraft and a helicopter carrier without need of ground stations (1973).
- o Tests of the tactical utility of relative navigation using Kearfott equipment in ASW and target handoff tests (1973-1974).
- o Demonstration of relative navigation using mixed inertial and non-inertial (Doppler) navigation communities (1975) with the consequent expansion of sensor models in the state vector.
- o Development and flight testing of secure AJ, LPI, JTIDS AN/URO-28 communications terminal suitable for installation on fighter aircraft (1976-1980) employing relative navigation.

2.0 SOFTWARE ALGORITHM STRUCTURE AND DESIGN

As a point of reference in the discussion of design features of the Relative Navigation algorithm design philosophy, it should be noted that the following requirements must be met:

- a) Full global navigation coverage.
- b) Dual grid state estimation (i.e. relative and geodetic navigation) to allow the separation and estimation of both grid and geodetic state elements (position, velocity, alignment) in a robust scheme, suitable for operational use.
- c) Application to a broad range of dead-reckoning types and mechanizations operating within communities containing either common or mixed reckoning types.
- d) Establishment and maintenance of the grid community hierarchical structure described earlier.
- e) Maximum utilization of the information transfer capabilities of the high capacity JTIDS data links in which relative navigation is imbedded.
- f) Ability to provide in-flight alignment of the attitude reference associated with the dead reckoning navigation subsystem for quick reaction aircraft initialization and take-off.

An important implication of these requirements is that, unlike prior applications of externally aided navigation, relative navigation represents a distributed estimation process, whereby each member takes maximum advantage of the estimates provided by the others to maintain a consistent solution in both grid and geodetic frames. This is achievable by careful calibration of both own and community error sources, a stable observation protocol, and full utilization of the data transfer capabilities of the JTIDS data link.

For purposes of this discussion, the Relative Navigation software algorithm will be constrained to include the following three computational functions:

- 1) Relative Navigation Kalman Filter (RNKF) in which the optimal stochastic estimation process resides, for both user and common grid states.
- 2) Observation source selection processing, which has the responsibility of choosing, from the set of all incoming JTIDS position and status messages from the community those which are to be used as input to the RNKF.
- 3) Navigation port input/output processing, which provides the interface between the RNKF and the subscriber dead-reckoning device.

These functions, of course, are imbedded within the larger domain of terminal software. A schematic of the relationship of the above functions including general data flow requirements is shown in Figure 2.

2.1 Relative Navigation Kalman Filter (RNKF) Modelling Considerations

As the core of the relative navigation processing function, the RNKF design presents fundamental questions as to the choice of states required for modelling. In keeping with the concept of recognizing potential drift characteristics associated with common grid errors, the state vector format of the RNKF will consist of a partitioned vector, divided into own (user) states, modelling the significant error contributors of the subscriber, and controller states, representing the significant grid dynamics of the navigation controller (i.e. common grid errors).

Because each dead reckoner type has different error contributors, the user state vector for each of the generic types considered must reflect the particular on-board D/R type. The software impact to provide the capability has been found to be small. Illustrated in Table I is a list of the significant error contributors for each of the generic dead reckoner types. Those elements checked represent errors which are modelled in the user own state vector.

Selection of controller states, in a similar manner, must reflect the controller dead reckoning type. Modelling of selected controller states by the user allows the user to separate its own error signatures from those of the controller in a mixed D/R community. In this way own user velocity and alignment states, which represent absolute geodetic rather than relative quantities can still be calibrated while maintaining grid lock. This feature is particularly important in an environment of both grid and geographic observation updates.

The foregoing discussions have outlined the general RNKF design philosophy. More specific solutions to the design requirements of the RNKF will now be outlined. Consider first the selection of states. The dual grid navigation requirement mandates the inclusion of both relative grid position, or functions thereof, and geodetic position states. Velocity states are also required. The choice of absolute or relative velocities is a matter of computational convenience, since they are derivable from each other by a linear transformation involving β , the grid azimuth angle, and grid drift velocity which are also modelled as states. The requirement for passive navigation requires the inclusion of states for clock bias and its time derivative. Baro altimeter error similarly requires a dedicated state.

The requirement for a common mechanization for varying dead reckoning sensor platform azimuth control applications requires a brief digression. The mechanization of any given stable sensor reference system will involve a transformation of acceleration or velocity from the platform frame of reference (PF) to the geodetic frame, an earth centered rotating (ECR) frame. An intermediate reference frame (RF) is defined, with origin at the vehicle and with angular velocity of its z (vertical) axis equal to a function of vehicle position, velocity, and specific platform mechanization. If $[C]$ represents the direction cosine matrix between ECR and RF, the following relationships between the elements of $[C]$ may be shown to apply:

$$\text{Geodetic Latitude } (\lambda) = \tan^{-1} \left(\frac{c_{33}}{c_{13} \cos \theta_A - c_{23} \sin \theta_A} \right)$$

$$\text{Geodetic Longitude } (\phi) = \tan^{-1} \left(\frac{c_{32}}{c_{31}} \right)$$

where θ_A is the offset angle of the RF from geodetic north given by:

$$\theta_A = \tan^{-1} \left(-\frac{c_{23}}{c_{13}} \right)$$

The general time solution of the $[C]$ matrix requires the knowledge of five terms of the $[C]$ matrix. By using quaternions to perform the direction cosine update five integrations can be eliminated. The following equivalence exists between the elements of the quaternion tensor and the direction cosine elements (Q_1, Q_2, Q_3, Q_4):

$$c_{11} = Q_1^2 - Q_2^2 - Q_3^2 + Q_4^2$$

$$c_{12} = 2(Q_1 Q_2 + Q_3 Q_4)$$

$$c_{13} = 2(Q_1 Q_3 - Q_2 Q_4)$$

$$c_{21} = 2(Q_1 Q_2 - Q_3 Q_4)$$

$$c_{22} = -Q_1^2 + Q_2^2 - Q_3^2 + Q_4^2$$

$$c_{23} = 2(Q_2 Q_3 + Q_1 Q_4)$$

$$c_{31} = 2(Q_1 Q_3 + Q_2 Q_4)$$

$$\begin{aligned} C_{32} &= 2(Q_2Q_3 - Q_1Q_4) \\ C_{33} &= -Q_1^2 - Q_2^2 + Q_3^2 + Q_4^2 \end{aligned}$$

where the following identity holds:

$$Q_1^2 + Q_2^2 + Q_3^2 + Q_4^2 = 1$$

Apparently, only four quaternion elements must be time propagated to achieve full knowledge of the direction cosine matrix [C]. By taking advantage of the above identity, however, it turns out that only three unique equations are required to fully represent the dynamics of geodetic latitude, longitude, and the azimuth angle of RF to ECR. Differences between specific mechanizations are accommodated in the time derivatives of these terms.

For an inertial dead reckoner, user states must include two more terms to specify the transformation between platform frame and an RF. These are represented as the verticality errors of the platform. This concludes the discussion of user states vector choice.

For the common grid (controller) states, a knowledge of the controller is required. For inertial controllers, it is known that error signatures will exhibit a sinusoidal Schuler characteristic. Thus, controller dynamics of inertial nav controllers are represented by a truncated Schuler mode, consisting of two pseudo tilt states, and two velocity error states. For non-inertial controllers, controller azimuth drift is a critical consideration, and controller velocity errors are modelled only as first order Markovian processes.

The final choice of state vector configuration, as a result of these considerations, is shown in Figure 3. It will be noted that a generalized 17-state filter will represent the model for a wide class of dead reckoning types, provided a small subset of states are varied to reflect the appropriate type (as indicated by the differences between the three columns of Figure 3.) The four controller state elements are varied depending on controller navigation subsystem type. Four of the thirteen user states are varied depending upon user navigation subsystem type.

2.2 Relative Navigation Filter Initialization and Timing

The proper operation of the RNKF estimation process requires the correct modelling of system dynamics and the accurate representation of system errors, as embodied in the filter covariance matrix. These requirements apply both for initialization of filter parameters (states and covariances) and for on-line response to changing system conditions. The basic source for own state covariance and state initialization is the navigation port with the on-board dead reckoning device. For controller states, appropriate data can be obtained either as initialization inputs or more flexibly from the data link position and states messages. In order to minimize loading requirements on the nav port and the data link, tuning data is usually represented by quality levels. A summary of representative nav port and data link parameters used for initialization is shown in Table II.

2.2.1 Controller State Modification Algorithm

It has been found from simulation, that in the case of poor quality inertial controllers doing geodetic updates, a large transient which propagates through the community can result. The characteristic of the transient is that a sudden change in controller grid drift results from a sudden calibration of controller geodetic velocity. Because the user maintains an estimate of inertial controller grid velocity error and tilt, any significant unmodelled change in those states will cause a transient which could be destructive (cause filter divergence) to the community. An algorithm has been developed which arrests this transient by adjusting both user's controller states and the corresponding on-diagonal elements of the covariance matrix. This adjustment can be made based upon reported controller qualities, one for velocity and one for tilt.

When controller geodetic velocity and tilt is improved as a result of doing geographic updates, typical filter performance reflects this improvement in its covariance matrix. Based upon the appropriate filter covariances the controller computes a quality for both grid velocity and tilt states. When a user recognizes an increase in reported controller qualities, the user responds by making the appropriate adjustments. When a decrease in quality level is observed no action is taken because the underlying assumption is that an update has not occurred and this reported deterioration is normal error growth of the controller's inertial navigator. In the case of a reported improvement in quality, the user reduces its estimate of controller velocity error and/or tilt in proportion to the percent change in reported quality between two successive values. The fact that the user is modelling controller error states, and not the state itself, makes this algorithm a valid procedure.

2.2.2 Design for Externally Aided Dead Reckoners

The system modelling procedure described earlier is based on the unstated assumption that the estimation of system errors resides exclusively within the RNKF. If the on-board subscriber navigation possesses a reset or update capability derived externally to

JTIDS, this fact must be integrated within the relative navigation estimation algorithm. Position reset is characteristic of an external position fix derived from flyover, GPS or some other geodetic position sensor. Position and velocity reset combines a position reset with a modification to D/R computed velocity. A total D/R state estimation reset is a case where there is an external estimation algorithm which models and estimates position errors, velocity errors, and dead-reckoner state errors such as platform tilts. An example of this latter reset type is that of a full Kalman filter mechanization.

Terminal relative navigation algorithm options in dealing with these resets may be addressed in terms of the nav interface data transfer. A Class I interface is one where no information concerning updates is passed to the RNKF. Conversely, a Class III interface is one where all magnitudes, signs, and times of estimated resets are made available. The former case suffers from performance limitations in that thresholds exist for position and velocity resets, beyond which filter performance degrades seriously. The Class III interface passes all relevant information, at the cost of greater complexity, with the RNKF altered in a deterministic manner to account for the magnitude changes in states due to external resets. The preferred solution, denoted by Class II, consists of a single bit passed by the subscriber to the RNKF specifying the time of reset. A weighted least squares algorithm, operating on reported dead reckoning velocity inputs, can be used to estimate the magnitude of the velocity change, and will modify RNKF covariances and velocity state values to stabilize filter performance. This provides a simple interface approach that can generally be applied to interface with all types of hybrid navigation subsystem mechanizations.

2.2.3 Operational Aspects of RNKF for Robust Performance

An operationally useful navigation algorithm requires certain self-adjusting features to account for improper observation data, an automatic reset capability in cases of long periods of validity failed observations, and accommodation to certain limitations of the quasilinear filter mechanization.

A reasonableness test for both grid and geographic observations is provided, based upon comparing observation residual magnitudes with expected errors based upon covariance magnitudes. Failed observations are not passed to the filter for processing. When a specified number of updates has failed, the filter will make the reasonable assumption that the solution has been lost, and will command a reacquisition of the relative grid, involving a reset of certain states and covariances based upon the on-board navigation subsystem indicated geodetic position and velocity.

Extended grid range observation processing along one axis (one-range update) may result in very large ratios between the covariance value along the cross range axis to along range covariance value. When this occurs the filter linearity assumptions become strained due to continued processing of observations nonlinearly related to position state elements. This could, if unchecked, cause problems in erroneous estimation of filter position corrections along the cross range axis. Special algorithms are thus provided to sense this condition and desensitize cross range corrections.

The result of these modifications to a standard Kalman Filter mechanization results in a flexible self-adjusting and stable algorithm suitable for operational use.

2.3 Observation Source Selection Processing

The determination of the optimum observation set for relative navigation processing is one of the critical factors in determining navigation performance. The screening and selection of a limited subset of possible observations from a large number of possible candidates is a particularly difficult analytical task for two primary reasons:

- o Any practical screening algorithm must be designed to operate in real time on the basis of a limited information set from each potential candidate.
- o The observation policy of each individual member is coupled through the mutual ranging procedure; hence, an observation policy which is optimal for any individual is not necessarily optimal for the community at large. That is to say that the community stability problem is intimately tied to the observation processing logic.

The observation source selection algorithm takes into account the subscribers own quality factors (as embodied in the state covariance matrix), and source reported grid, geographic, azimuth correlation and time quality levels provided in incoming position and status messages. Also considered is the role of the subscriber in the grid hierarchy and, in cases of TOA grid or TOA geodetic observations, the geometric relationship between the user and potential subscriber.

2.4 Navigation Port Interface Processing

As the principal conduit for data exchange between the RNKF and the on-board dead-reckoning device, the navigation port processing must be critically examined to assure compatibility with all possible types and mechanizations of such devices. In general, the on-board dead reckoner will provide the RNKF with position and velocity data, initialization data, and time/status data, depending on its type. The RNKF will provide hybrid state estimates and/or corrections, quality (covariance) data, as well as timing information for tagging of data transfer.

3. OPERATIONAL PERFORMANCE VARIATIONS WITH COMMUNITY STRUCTURE

JTIDS relative navigation provides each subscriber with the ability to optimize navigation performance simultaneously in both the geodetic grid and the relative grid for any given community structure and user dead reckoning equipment suit. Most if not all other radio aided navigation systems (i.e. LOFAN, OMEGA, GPS) control the effects of geometry and update source quality on navigation performance through the placement of high accuracy surveyed reference transmitters, placed in ideal geometry locations (or orbits). This is done to guarantee near optimum geometry and source quality to all users in the operational area of interest. These transmitters and user receivers are designed for dedicated support to only the navigation function. JTIDS transceivers are integrated within user avionics systems and are primarily designed to support anti-jam high capacity digital communications. One of the advantages of the time synchronized TDMA architecture is in providing wide distribution non-nodal communication links. An additional advantage is to provide highly accurate user to user range (or TOA) with each message transmission and reception. Precise position location and identification (PPLI) messages periodically transmitted by each user within a command and control net allow source positions time correlated with measured TDMA range data to be available to support each user's relative navigation processing function. However, these transmitting sources are not just dedicated to supporting the relative navigation function, but have a variety of mission objectives within the operational task force or command and control community. Although individual units can be stationed to provide optimized geometry within an optimized community structure this is not a requirement for the relative navigation processing function.

The relative navigation processing performed by each user seeks to optimize performance at each instant in time for any given community structure (geometry and source quality) and reports both geodetic and relative grid qualities to identify its estimation accuracy at each instant in time. Thus each user's relative and geodetic navigation performance will always be equal to or better than its on-board navigation system depending on the community structure within which it is operating. In good geometry high source quality situations extremely high accuracy is attained and is primarily limited by the highly accurate TDMA ranging accuracy. The processing is designed so that even a two member community with one nav controller and a single user with good relative bearing motion can achieve two dimensional position accuracy only six times the accuracy attained in a good geometry multiple source situation. The key to this processing technique is the integration of the JTIDS range data and position messages with the on-board dead reckoning nav system as discussed in section 2.

An important part of establishing an operational JTIDS community is to configure the community in such a way so that the desired navigation performance is achieved while still satisfying all platform mission requirements. Table III summarizes qualitatively the expected relative grid and geodetic grid performance (position, velocity, heading) for different types of JTIDS community configurations.

Relative grid performance in a community containing unsurveyed ground stations and performance in an all mobile community without accurate geodetic references shows accurate relative grid calibration which is only a function of geometry. The effect of ground stations has the advantage of eliminating grid drift. Grid drift for all mobile communities without geodetic references can be characterized as a translational and rotational drift error of the community with time in relating relative grid positions to true geodetic positions of each community member. At each instant in time the user to user relative position errors are small and bounded. However, the relative position errors between each user and an earth fixed point will tend to grow primarily with the geodetic drift characteristics of the navigation controller dead reckoning navigation subsystem. In an all mobile community with accurate geodetic references, accurate relative grid calibration is achieved and relative grid states converge to corresponding geodetic states to the accuracy of the geodetic references. When geodetic updates are introduced at some later time as opposed to being present during an entire scenario, accurate calibration of both relative and geodetic coordinates is achieved and relative grid coordinates approach geodetic grid coordinates through a fixed transformation offset. This offset is a function of the grid drift present during the time prior to entry of geodetic references.

Geodetic grid performance in a community containing unsurveyed ground stations and no geodetic references will exhibit improvement depending upon the most accurate member. In the case of inertial users, the gyrocompass mechanism permits further calibration of the inertial user dead reckoner and therefore leads to improved geodetic performance. In the case of an all mobile community without geodetic references, geodetic improvement is dependent on the most accurate member. This error is unbounded in that the community will tend to drift geodetically with the most accurate member. For the other two configurations defined in the table, accurate geodetic grid performance is achieved because of the presence of accurate geodetic references.

4. OPERATIONAL APPLICATIONS TO TARGETTING AND WEAPON DELIVERY

The level of improvement that JTIDS relative navigation can have on operational aspects such as targeting and weapon delivery depend upon relative navigation parameters such as grid translation and rotational drift, relative grid position accuracy, velocity accuracy, and azimuthal correlation. Azimuthal correlation and its relationship to grid rotational drift will be discussed first before discussing operational effects of relative navigation performance.

There are two characteristics which identify user dead reckoning platform azimuthal correlation. They are:

- o Azimuth correlation between all user platforms and the nav controller platform.
- o Azimuth correlation between all user platforms and the apparent rotational drift in relative grid.

The first characteristic is assured in the case of two or more fixed nav controllers or two or more position references. Furthermore, with either fixed nav controllers or position references, grid rotational drift does not exist. This first characteristic can also exist for all mobile member communities but with some degree of grid rotational drift present. In this situation the degree of user azimuthal correlation to the controller is dependent upon controller velocity magnitude and community geometry changes. If controller velocity magnitude is relatively slow, as is the case for a ship controller, then community geometry changes become the predominant affects and the second azimuthal correlation characteristic is seen. Grid rotation and azimuthal correlation are a function of community nav controller speed and community geometry change dynamics.

Illustrated in Figure 4 (Case 1) is a mobile member community with a fast moving controller which exhibits some degree of grid rotation. Because this controller travels a significant distance over a relatively short period of time, the distance traveled presents a reference line in time and space against which user platforms can align in azimuth their respective platforms (i.e., estimate relative grid azimuth). It is this mechanism which allows users to achieve azimuthal correlation to the nav controller ($\alpha \approx 0$) and each other. When azimuthal correlation is achieved relative to the controller, the user has determined its heading reference relative to the orientation of the controller defined grid (α) to within an accuracy of $\pm \alpha$. This is illustrated in the figure by each user's platform axes (x_1, y_1) being aligned with the controller platform axes (u_C, v_C). When the user accomplishes this alignment, estimated grid velocity direction is well known as shown in Figure 4. In this case navigation extrapolations in between updates are performed in the controller defined grid.

Figure 5 illustrates a similar situation (Case 2) but with a slow moving nav controller. Unlike the fast moving controller, the slow moving controller does not present a significant reference "line" against which users can align their platforms. In the absence of significant controller motion, lines in space which exist between other community members provide a reference against which users can align their platforms in azimuth. In this case the reference lines in space as seen by a user are effectively those perceived by the reported grid positions of other members. Since the reported positions are those of the rotated grid, a user achieves azimuthal alignment relative to the rotated grid. This is achieved in such a way that the error in estimating a user's own azimuthal alignment relative to the controller defined grid is in error by an amount equal to and opposite in sign to the grid rotation angle, α . For this case, the estimated velocity vector which is maintained in the u_C, v_C computational frame is rotated from the true velocity vector by an amount α . Therefore, user navigation extrapolation in between updates is truly done in a rotated frame.

Targetting error which results from a Case 1 situation is illustrated in Figure 6. In this scenario, user 1 performs a range (R) and bearing (θ) targetting operation and hands-off to user 2 grid target coordinates. As is illustrated in Figure 6, user 1 locates the target, T_1 , with a displacement error equal to its own grid position error (i.e., the difference between estimated and true grid positions). In response, user 2 computes a bearing angle to target, for weapon initialization purposes, based on its own estimated grid position and reported target coordinates. When user 2 actually points with this computed bearing angle from its true position, the look direction is parallel to the computed bearing direction. This leads to a user 2 estimated target position, T_2 , which is displaced from user 1's estimated target position by an amount equal to its own grid position error. Observing Figure 6 shows that the resultant targetting/weapon initialization error is the vector difference in user 1 and user 2 grid position errors. Therefore, the interesting result is that for Case 1 type grid rotation, targetting/weapon delivery errors are not proportional to grid rotation angle through target range but a function of cooperating user grid position errors.

Case 2 grid rotation provides a situation such that there are no targetting/weapon delivery errors. In this case, user 1 locates a target using range and bearing measurements. Assuming no instrument errors, the range measurement is equal to the true target range and the bearing angle is that measured relative to the platform axes (x_1, y_1). Since the platform axes are misaligned with respect to the computational axes (u_C, v_C) by an unknown amount, α , the computation of target coordinates in the computational frame effectively rotates estimated target position through an angle α or $-\alpha$ about user 1 estimated grid position. As was done in Case 1, user 2 computes a range and bearing angle to target based on its own estimated grid position and reported target position. This computation is done in the computational frame. As can be seen by studying Figure 7,

the user 2 computed target range is equal to the actual range. When user 2 actually points to the target it does so relative to its platform axes (x_2, y_2) which are misaligned from the computational frame by the same unknown amount as user 1; that is γ . In performing this operation a rotation back to the true target position is accomplished. Therefore when user azimuthal correlations are to the rotated grid, targetting/weapon delivery errors are reduced to zero. In this case, however, if the controller were to enter into targetting operations, it would not be correlated in grid azimuth to other members thus introducing pointing errors that are proportional to γ through target range. This situation could be alleviated if the nav controller were to make independent measurements on the community in order to estimate grid rotation angle. This aspect is not further explored here but is mentioned as a possible approach to addressing this situation.

As was discussed for Case 1 azimuth correlation when grid rotation exists, rho-theta targetting with weapon initialization and firing provides an impact error which is independent of target range when user azimuth is not correlated to grid rotation. This impact error is a function only of cooperating user grid position errors; that is estimated minus true grid position differences for both targetting and delivery aircraft. Because this error is fixed in both magnitude and direction (for a given set of conditions), the effective target pointing error will decrease as target range increases. In addition, effective pointing error will vary from zero to maximum value depending upon target direction relative to direction of impact error. Therefore, the effect of grid rotation, in this case, is not one of a true pointing error. These properties are illustrated in Figure 8.

Illustrated in Figure 8 are parametrical contours which are drawn relative to the user 1/user 2 baseline. In this figure, the baseline is shown vertical. User 2, which is the delivery aircraft, appears at the tangent point of the contours. User 1 may lie either above or below user 2 at a normalized distance of one. The parameter for these tangential contours is pointing error (n_p) normalized to grid rotation angle (γ). Radial direction outward from user 2 is target range (R_p) normalized to baseline distance (R_{12}). Therefore, moving outward along a radial shows that effective pointing error decreases with increased target range. The direction perpendicular to the baseline represents the direction of maximum along track target range error and zero pointing error. Therefore, as angle to target (θ_T) changes from zero to 90 degrees pointing error varies from zero to maximum.

When using a radar (range, bearing) for targetting operations, pointing error of the radar is a significant error contributor to the targetting process. Using the above properties can lead to the determination of a point at which the radar begins to contribute more error to the targetting process than grid rotation angle. During operational scenarios actual grid rotation angle will not be known, in general. However, knowledge of the basic sensitivities can help define the regions in which grid rotation has lesser impact on pointing error angle. Figure 3 shows that this region is forward of the user 1/user 2 baseline. Therein, radar azimuth errors will be the major (in this context) contributor to cross track targetting errors for targets forward of the baseline. As target direction begins to approach the general direction of the baseline, grid rotation and radar azimuth errors will both contribute but with different characteristics as a function of target range. The target pointing error due to grid rotation effects is constant and independent of target range whereas the target error due to radar azimuth errors is directly proportional to target range. Concentric circles whose centers lie at user 2 location and whose radii equal maximum range values are given also. These ranges represent the values required to achieve an effective pointing error under maximum cross track error conditions. In the evaluation of targetting performance if direction is not considered, then only targets appearing beyond the maximum range would be considered as satisfying a desired pointing error requirement. The region that lies outside the contour of constant pointing error ratio and inside the circle that is tangent to that contour represents the added area gained for accurate targetting when direction is considered.

Operational impacts of relative navigation are summarized in Table IV. This table illustrates in a qualitative way the impacts that the six listed relative navigation parameters have on operational functions such as targetting, weapon initialization and firing, and weapon guidance. Both multisensor and single sensor type targetting is considered. Multisensor targetting errors are considered for both rho-rho and theta-theta type targetting. Targetting/weapon delivery performance for both types of targetting combined with weapon guidance or weapon initialization and firing delivery techniques are addressed in this table. Single sensor targetting (rho-theta) and hand-off to a second member for weapon initialization and firing or weapon guidance is also addressed. The first four rel nav parameters of Table IV are now briefly reviewed. Grid translation and rotational drift effect the five operational functions in similar ways. That is, this parameter directly influences either target extrapolations or user rel grid navigation accuracy during periods of weapon guidance or during times prior to release for non-guided weapon. The effect of rel grid position accuracy is obvious in that any position error in the grid (or rotated grid) will be directly translated into weapon impact error. This effect is the same for all operational functions. Rel grid velocity accuracy effects extrapolation of target position during targetting operations and contributes to position error build-up during periods of time between target locate and weapon impact for both guided and un-guided weapons. This rel grid velocity error effects the five operational functions in similar ways as illustrated in Table IV. Errors in azimuthal correlation between members of a community will contribute to pointing errors which are a function of target range. As illustrated in Table IV, this pointing error may not exist depending on the type of targetting and weapon guidance. For instance if rho-rho

61

targetting (item 1) is chosen in combination with JTIDS multisensor guidance (item 3), the azimuthal correlation errors will not effect weapon impact accuracy.

The impacts of user azimuthal correlation to grid rotational drift on the operational functions listed are summarized in the last column of Table IV. Item four of the table summarizes case 1 discussed above which explained that the lack of user platform azimuthal correlation to the apparently rotated grid would yield a bound targetting error which is a function of user uncorrelated grid rotation error and the baseline between the two cooperating users. Item four of this table extends this result to include weapon delivery as well as targetting aspects. In this case, however, the combined result of both targetting and weapon initialization and firing yields an impact error which is equal to the targetting error. Case two discussed the situation of having complete correlation to the rotated grid and its impact on targetting. In this situation no targetting error exists. If rho-rho guidance is used in this case, the weapon will be successfully guided to target without any impact error. Beginning with item one, the impact of azimuthal correlation to grid rotation on performance of multisensor targetting combined with weapon initialization and firing or weapon guidance is summarized. For rho-rho targetting, this rel nav parameter has no effect in that target location is strictly a function of range measurements and user estimated positions. When this targetting is combined with weapon initialization and firing (item 2), impact error is proportional (less than 1:1) to target range when users are not correlated to grid rotation (Case 1). As we already explained if users are completely correlated to the rotated grid (Case 2), there is a zero impact error. When rho-rho targetting is combined with JTIDS guidance (item 3), azimuthal correlation to grid rotation does not effect impact error in that both targetting and guidance are functions of range measurements and user estimated positions only.

For item five, impact accuracy is proportional (less than 1:1) to target range. Recalling item 4 situation, targetting (rho-theta) error was a bounded error independent of target range. When JTIDS weapon guidance is used with rho-theta targetting as is the case in item 5, users will guide a weapon to a point that is related to the estimated target position by a rotation through θ . If Case 2 (i.e., azimuthal correlation to grid rotation) situation exists here, then weapon guidance will guide the weapon to estimated target coordinates (i.e., T_1 of Figure 7) which causes the true weapon impact point to agree with the true target location. However, if a Case 1 situation exists (i.e., no azimuthal correlation), the weapon will be guided to target coordinates, T_1 , of Figure 6. This will cause an impact error which is equal to the difference in Case 1 and Case 2 user 1 estimated target positions. Therefore, this mechanism causes an impact error which is less than the amount that would occur had the weapon been guided to true target position, T . In general, the notes indicating a less than 1:1 proportionality to target range address this mechanism.

Table IV also addresses the impact of azimuthal correlation to grid rotation on theta-theta type targetting. Entries in the table indicate similar type performance as described above, but on an item per item basis results differ from rho-rho targetting results.

One of the most important characteristics of JTIDS is its ability to provide users with accurately correlated time synchronization in parallel with relative position correlation. This feature is particularly applicable to the implementation of a variety of multi-platform target sensor correlation techniques.

5. CONCLUSIONS

JTIDS relative navigation provides a powerful integration of TDMA data link performance features with user navigation subsystem equipment on a multi-user community wide basis. An efficient and flexible relative navigation software algorithm structure and design allows broad application to all generic classes of navigation subsystem equipment likely to be found on any candidate host platform in which JTIDS terminals would be integrated. With proper control of the JTIDS community structure order of magnitude improvements can be realized in community navigation performance which in turn offer significant improvements in overall command and control, targetting and weapon delivery. In particular, performance effects were discussed and summarized for a variety of targetting, weapon initialization, and guidance techniques. It is observed that if targetting method and weapon delivery method are chosen appropriately then the effect of error producing rel nav parameters can be minimized or eliminated. In addition cooperative targetting and weapon delivery carried out by two or more units operating with JTIDS relative navigation should always improve the performance obtained. The level of improvement depends upon the community structure. With good geometry dramatic levels of navigation performance improvement can be attained in the range of one or two orders of magnitude. This tends to force overall targetting and weapon delivery performance to be paced by errors other than relative navigation accuracy such as targetting radars or weapon guidance sensors. The performance characteristics discussed in this paper are based upon over ten years of relative navigation development. This included extensive simulation analysis and numerous flight test programs which have clearly demonstrated both the technical feasibility and operational utility of relative navigation utilizing time synchronized TDMA data links.

REFERENCES

1. Steele, W. J., Schlenger, J.I., "JTIDS PROVIDES A RELATIVE NAVIGATION/COMMUNICATIONS APPROACH TO MULTI-SENSOR INTEGRATION", IEEE Position Location and Navigation Symposium, November, 1978.
2. Stow, R. C., "TACTICAL HYBRID NAVIGATION SCHEME FOR MIXED COMMUNITY COORDINATION", IEEE Conference, 1973.
3. Leondes, C. T., "PRINCIPLES AND OPERATIONAL ASPECTS OF PRECISION POSITION DETERMINATION SYSTEMS", AGARDograph No. 245, July 1979.

FIGURE 1. RELATIVE GRID AND GEODETIC GRID NAVIGATION

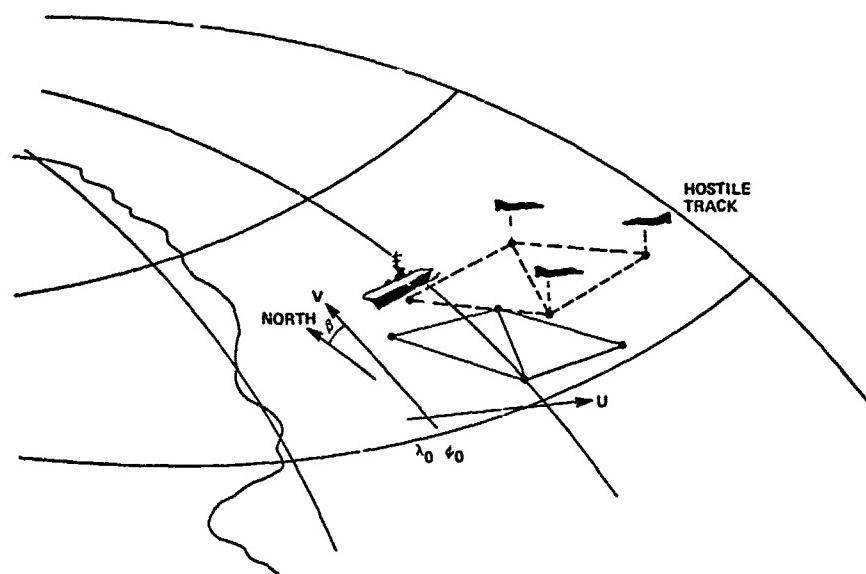


FIGURE 2. RELATIVE NAVIGATION ESTIMATION PROCESS

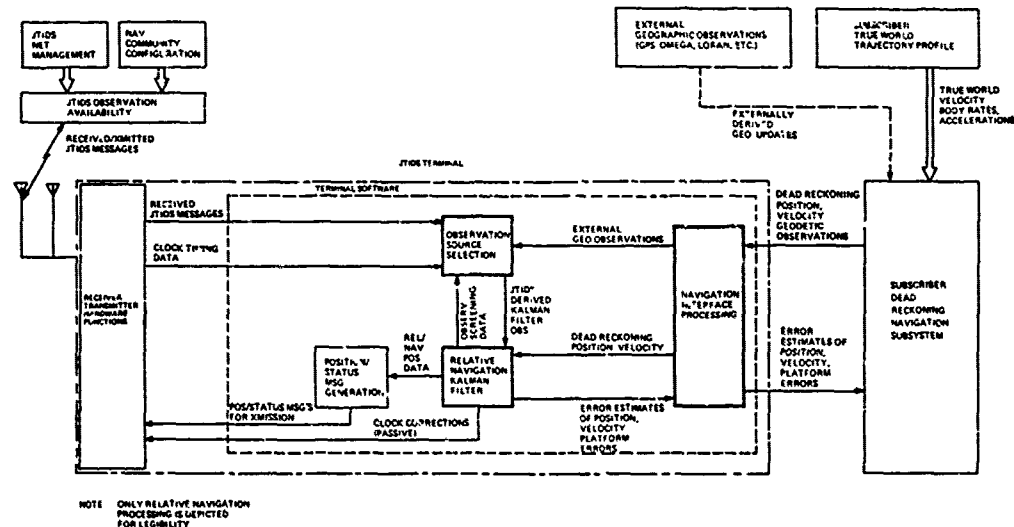


TABLE I. DOMINANT ERROR CONTRIBUTORS AND OTHER CANDIDATE STATE ELEMENTS

<u>INERTIAL</u>	<u>DOPPLER RADAR</u>
✓ TILT	✓ SCALE FACTOR
✓ HEADING	✓ TRACKER BIAS
GYRO BIASES AND SCALE FACTORS	✓ WATER MOTION
ACCELEROMETER BIAS & SCALE FACTORS	SHORT TERM NOISE
MASS UNBALANCE	BORESIGHT
DEFLECTIONS OF THE VERTICAL	
<u>AIR DATA COMPUTER (ADC)</u>	<u>ATTITUDE HEADING REFERENCE SYSTEM (AHRS)</u>
✓ SCALE FACTOR	✓ HEADING
BIAS	✓ AZIMUTH DRIFT
✓ WIND MOTION	TILT ERRORS AND TRANSIENTS
ANGLE OF ATTACK	
SHORT TERM NOISE	
<u>EM LOG</u>	<u>TDMA (PASSIVE MODE)</u>
✓ SCALE FACTOR	✓ CLOCK BIAS
BIAS	✓ FREQUENCY DRIFT
✓ WATER MOTION	THERMAL TRANSIENT
SIDE-SLIP ANGLE	
BORESIGHT	SHORT TERM NOISE

FIGURE 3. RELATIVE NAVIGATION FILTER STATE VECTOR CONFIGURATIONS

STATE ELEMENT	INERTIAL (PURE AND DOPPLER DAMPED) HYBRID INERTIAL	DOPPLER - AHRS HYBRID DAHRS	ADC-AHRS/EMLOG-GYRO COMPASS HYBRID ADC OR EMLOG*
1	ΔQ_1 QUATERNION	ΔQ_1 QUATERNION	ΔQ_1 QUATERNION
2	ΔQ_2 REPRESENTATION	ΔQ_2 REPRESENTATION	ΔQ_2 REPRESENTATION FOR
3	ΔQ_3 FOR GEO POSITION & AZIMUTH	ΔQ_3 FOR GEO POSITION & AZIMUTH	ΔQ_3 GEO POSITION & AZIMUTH
4	ρ_x	D_z AZIMUTH DRIFT	D_z AZIMUTH DRIFT
5	ρ_y } PLATFORM TILTS	EK DOPPLER SCALE FACTOR	EK ADC SCALE FACTOR
6	P_u GRID U POSITION	P_u GRID U POSITION	P_u GRID U POSITION
7	P_v GRID V POSITION	P_v GRID V POSITION	P_v GRID V POSITION
8	β GRID AZIMUTH ANGLE	β GRID AZIMUTH ANGLE	β GRID AZIMUTH ANGLE
9	E_h ALTITUDE ERROR	E_h ALTITUDE ERROR	E_h ALTITUDE ERROR
10	V_x X GEO VEL.	V_{wn} N, E WATER MOTION	V_{wn} N, E WIND OR WATER MOTION
11	V_x Y GEO VEL.	V_{we} OR DOP VEL BIAS	V_{we} N, E WIND OR WATER MOTION
12	B_c CLOCK BIAS	B_c CLOCK BIAS	B_c CLOCK BIAS
13	f_c CLOCK FREQ. ERROR	f_c CLOCK FREQ. ERROR	f_c CLOCK FREQ. ERROR

STATE ELEMENT	INERTIAL CONTROLLER	CONTROLLER STATES NON-INERTIAL CONTROLLER	FIXED STA. GROUND CONTROLLER
1	δ_{uc} } CONTROLLER	D_{zc} CONTROLLER AZ DRIFT	NONE
2	δ_{vc} } U, V PSEUDO TILTS		
3	EV_{uc} } CONTROLLER	EV_{uc} } CONTROLLER	
4	EV_{vc} } U, V VELOCITY ERROR	EV_{vc} } U, V VELOCITY ERROR	

TABLE II. QUALITY FIELDS AND DATA USED FOR INITIALIZATION OF THE FILTER MODEL

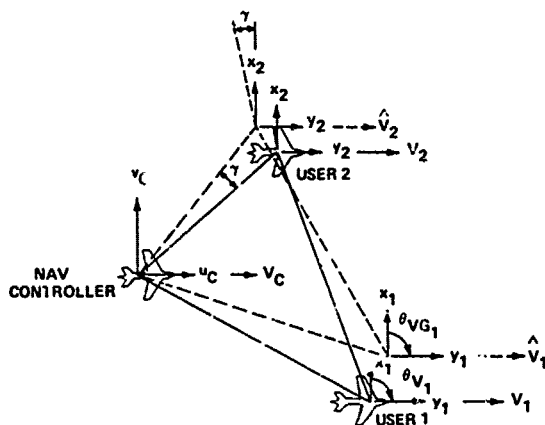
NAV PORT/FFP	INITIALIZED OWN STATE OR COVARIANCE MODEL
Q_p (POSITION QUALITY)	LAT, LON COV.
Q_v (VELOCITY QUALITY)	NORTH VEL, EAST VEL, TILTS COV.
Q_{HDG} (HEADING QUALITY)	GEODETIC HEADING COV.
Q_{D2} (DRIFT QUALITY)	AZIMUTH DRIFT COV.
NAV SUBSYSTEM TYPE	USER STATE MODEL OPTION
VELOCITY, POSITION	GEO POSITION AND VELOCITY STATES
WANDER ANGLE	QUATERNION STATES
DAMPING GAINS	DAMPING GAINS
PPLI - MESSAGE DATA	INITIALIZED CONTROLLER STATE OR COVARIANCE MODEL
Q_{pR} (SOURCE GEODETIC QUALITY)	GEO POSITION COV.
Q_{vR} (SOURCE GRID QUALITY)	GRID POSITION COV.
Q_{AR} (SOURCE AZIMUTH QUALITY)	GRID AZIMUTH COV.
GRID TYPE	CONTROLLER STATE MODEL OPTION
Q_{VC} (CONT. VELOCITY QUAL.)	GRID VELOCITY DRIFT COV.
Q_{VC} (CONT. VERTICALITY QUAL.)	GRID VERTICALITY COV.
Q_{DZC} (CONT. DRIFT QUAL.)	GRID AZIMUTH DRIFT COV.
Q_{SC} (CONT. AZIM. QUAL.)	GRID AZIMUTH COV.
$\lambda, \phi, \theta, P_U, P_V, h$	λ_0, ϕ_0 , GRID ORIGIN

TABLE III. JTIDS DUAL GRID SUBSCRIBER PERFORMANCE CHARACTERISTICS

JTIDS COMMUNITY CONFIGURATION	RELATIVE GRID			GEOSTATIC GRID		
	RELATIVE POSITION l_R, ϕ_R	RELATIVE VELOCITY v_{NR}, v_{ER}	RELATIVE READING	GEOSTATIC POSITION l_G, ϕ_G	GEOSTATIC VELOCITY v_{NG}, v_{EG}	GEOSTATIC HEADING
TWO OR MORE FIXED UNSURVEYED GROUND STATIONS WITHOUT GEOSTATIC REFERENCES	ACCURATE CALIBRATION WITHOUT GRID DRIFT			IMPROVEMENT OF ON-BOARD NAV SYSTEM DEPENDENT ON MOST ACCURATE GEOSTATIC COMMUNITY MEMBER ACCURACY IS BOUNDED.	ACCURATE CALIBRATION FOR INERTIAL USERS	ACCURATE CALIBRATION FOR INERTIAL USERS
ALL MOBILE COMMUNITY WITHOUT ACCURATE GEOSTATIC REFERENCES	ACCURATE CALIBRATION WITH GRID DRIFT			IMPROVEMENT DEPENDENT ON MOST ACCURATE MEMBER. ACCURACY IS UNBOUNDED.	IMPROVEMENT DEPENDENT ON MOST ACCURATE MEMBER	IMPROVEMENT DEPENDENT ON MOST ACCURATE MEMBER
ALL MOBILE COMMUNITY WITH ACCURATE GEOSTATIC REFERENCES	ACCURATE CALIBRATION WITH CONVERGENCE TO l_G, ϕ_G	ACCURATE CALIBRATION WITH CONVERGENCE TO v_N, v_E	ACCURATE CALIBRATION WITH CONVERGENCE TO GEOSTATIC HEADING	ACCURATE BOUNDED CALIBRATION	ACCURATE CALIBRATION	ACCURATE CALIBRATION
ALL MOBILE COMMUNITY WITHOUT ACCURATE GEOSTATIC REFERENCES INITIALLY FOLLOWED BY ENTRY OF GEOSTATIC REFERENCES	ACCURATE CALIBRATION WITHOUT GRID DRIFT WITH FIXED OFFSET* FROM l_G, ϕ_G	ACCURATE CALIBRATION WITH A FIXED OFFSET* FROM v_N, v_E BASED ON REL EGN OFFSET FROM GEO STATIC	ACCURATE CALIBRATION WITH FIXED OFFSET FROM GEOSTATIC HEADING	ACCURATE BOUNDED CALIBRATION	ACCURATE CALIBRATION	ACCURATE CALIBRATION

THIS FIXED OFFSET IS NOT FIXED FROM SCENARIO TO SCENARIO, BUT IS FIXED AS A RESULT OF A
FIXED TRANSFORMATION FOR A GIVEN SCENARIO

FIGURE 4. USER PLATFORM AZIMUTHAL CORRELATION FOR FAST MOVING NAV CONTROLLER



CASE 1 - AZIMUTHAL CORRELATION TO NAV CONTROLLER DEFINED GRID IN PRESENCE OF NON-ZERO GAMMA ANGLE.

v_c, v_1, v_2 = TRUE GRID VELOCITIES OF EACH RESPECTIVE COMMUNITY MEMBER.

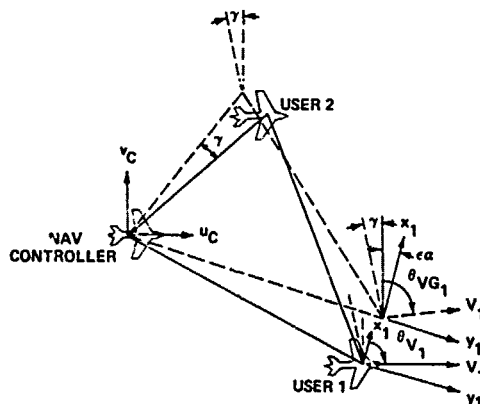
$v_c, \hat{v}_1, \hat{v}_2$ = ESTIMATED GRID VELOCITIES OF EACH RESPECTIVE COMMUNITY MEMBER.

$\epsilon\alpha_1 \approx \epsilon\alpha_2 \approx 0$ INDICATING CORRELATION OF USER'S PLATFORM REF. TO NAV CONTROLLER PLATFORM REF.

γ = APPARENT ROTATION OF COMMUNITY TRIAD BASED UPON ESTIMATED GRID POSITIONS RELATIVE TO NAV CONTROLLER.

$\theta_{VG_1} = \theta_{V_1}$ TRUE HEADING OF USER 1 VELOCITY VECTOR IN PLATFORM COORDINATES.

FIGURE 5. USER PLATFORM AZIMUTHAL CORRELATION FOR SLOW MOVING OR STATIONARY NAV CONTROLLER



CASE 2 - AZIMUTHAL CORRELATION TO ROTATED GRID ANGLE GAMMA

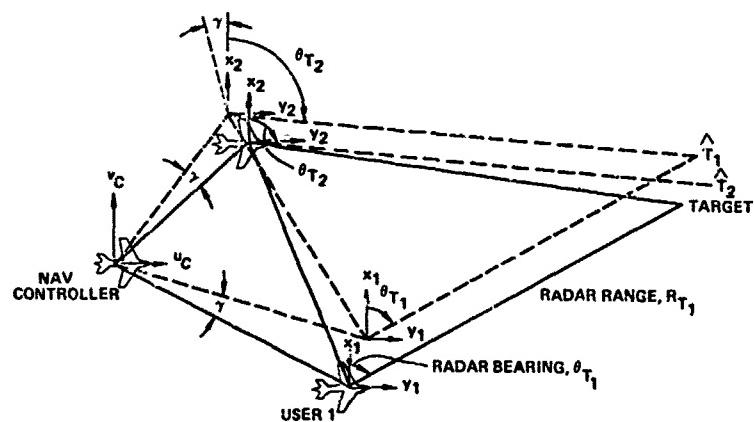
v_c = SMALL OR ≈ 0

$\epsilon\alpha_1 \approx \epsilon\alpha_2 \approx -\gamma$ INDICATING CORRELATION OF USER'S PLATFORM

REF. TO ROTATED TRIAD WITHOUT CORRELATION TO NAV CONTROLLER PLATFORM REF.

$\theta_{VG_1} = \theta_{V_1}$ TRUE HEADING OF USER 1 VELOCITY VECTOR IN PLATFORM COORDINATES.

FIGURE 6. RADAR (ρ/θ) TARGETTING BY USER 1 WITH HAND-OFF TO USER 2 FOR WEAPON INITIALIZATION AND FIRING (CASE 1)



CASE 1 - COMMUNITY AXIMUTHAL CORRELATION

$$\epsilon d_1 \approx \epsilon d_2 > 0$$

θ_{T_1} = TRUE TARGET RADAR AZIMUTH MEASURED RELATIVE TO
TRUE PLATFORM REFERENCE OF USER 1

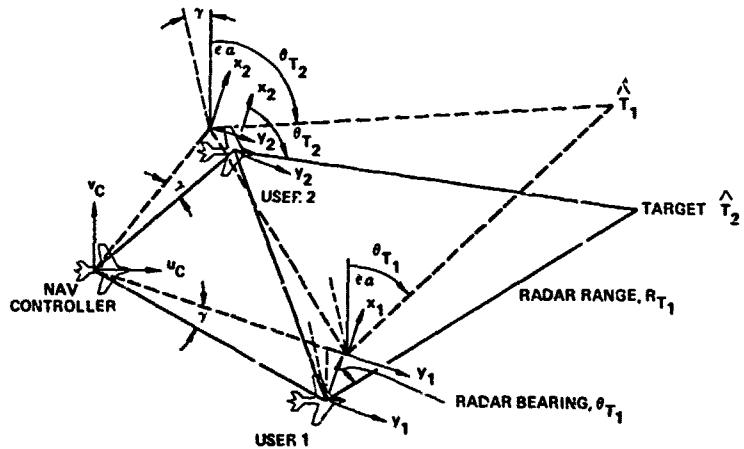
R_{T_1} = TRUE TARGET RADAR RANGE FROM USER 1

\hat{T}_1 = USER 1 ESTIMATED TARGET GRID POSITION

θ_{T_2} = COMPUTED USER 2 TARGET AZIMUTH RELATIVE TO
USER 2 PLATFORM REFERENCE

\hat{T}_2 = USER 2 DETERMINED TARGET POSITION AS REFERENCED
TO TRUE USER 2 PLATFORM REFERENCE

FIGURE 7. RADAR (ρ/θ) TARGETTING BY USER 1 WITH HAND-OFF TO USER 2 FOR WEAPON INITIALIZATION AND FIRING (CASE 2)



CASE 2 - COMMUNITY AXIMUTHAL CORRELATION

$$\epsilon d_1 \approx \epsilon d_2 \approx -\delta$$

θ_{T_1} = TRUE TARGET RADAR AZIMUTH MEASURED RELATIVE TO TRUE
PLATFORM REFERENCE OF USER 1

R_{T_1} = TRUE TARGET RADAR RANGE FROM USER 1

\hat{T}_1 = USER 1 ESTIMATED TARGET GRID POSITION

θ_{T_2} = COMPUTED USER 2 TARGET AZIMUTH RELATIVE TO USER 2
PLATFORM REFERENCE

\hat{T}_2 = USER 2 DETERMINED TARGET POSITION AS REFERENCED TO
TRUE USER 2 PLATFORM REFERENCE

FIGURE 8. GEOMETRY SENSITIVITIES FOR ρ/θ RADAR TARGETTING AS A FUNCTION OF UNCORRELATED GRID DRIFT

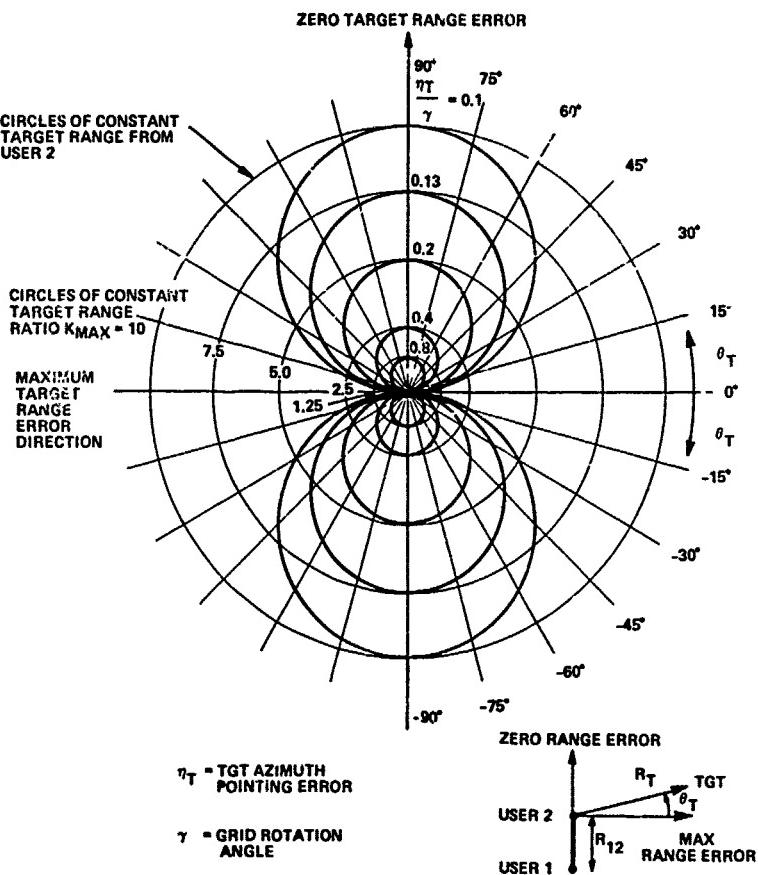


TABLE IV. OPERATIONAL APPLICATION TO TARGETTING AND WEAPON DELIVERY

TARGETTING, WEAPON INITIALIZATION AND GUIDANCE	GRID TRANSLATION AND ROTATIONAL DRIFT	REL GRID POSITION ACCURACY	FNL GRID VELOCITY ACCURACY	USER PLATFORM AZIMUTH CORRELATION TO OTHER USERS	USER PLATFORM AZIMUTH CORRELATION TO GRID ROTATIONAL DRIFT
1. MULTISENSOR TARGET CORRELATION • $\rho_1 - \theta_1$ TARGETTING • $\rho_1 - \theta_2$ TARGETTING	ONLY EFFECTS ACCURACY IN EXTRAPOLATION OF TARGET POSITION OVER TIME.	DIRECTLY EFFECTS ACCURACY WITH A BOUNDED ERROR INDEPENDENT OF GRID-ROTATIONAL-DRIFT PERFORMANCE.	ONLY EFFECT ACCURACY IN EXTRAPOLATION OF TARGET POSITION OVER TIME.	NO EFFECT DIRECTLY EFFECTS ACCURACY WITH TOT ERROR PROPORTIONAL TO TOT RANGE.	NO EFFECT EFFECTS ACCURACY WITH TOT ERROR PROPORTIONAL ($<1:1$) TO TOT RANGE.
2. WEAPON INITIALIZATION AND FIRING TO MULTISENSOR LOCATED TARGET.	EFFECTS ACCURACY AS A FUNCTION OF TIME BETWEEN TARGET LOCATE AND WEAPON FIRING.	SAME AS IN (1)	EFFECTS ACCURACY AS A FUNCTION OF TIME BETWEEN TARGET LOCATE AND WEAPON IMPACT*.	DIRECTLY EFFECTS ACCURACY WITH IMPACT ERROR PROPORTIONAL TO TOT RANGE.	EFFECTS ACCURACY WITH AN IMPACT ERROR PROPORTIONAL ($<1:1$) TO TOT RANGE WITH RHO-RHO TARGETTING. EFFECTS ACCURACY WITH A BOUNDED IMPACT ERROR PROPORTIONAL ($<1:1$) TO TOT RANGE WITH GRID ROTATIONAL DRIFT INDEPENDENT OF TOT RANGE WITH THETA-THETA TARGETTING.
3. WEAPON JTIDS C-IDANCE MULTISENSOR LOCATED TARGET.	EFFECTS ACCURACY AS A FUNCTION OF TIME BETWEEN TARGET LOCATE AND WEAPON IMPACT.	SAME AS IN (1)	SAME AS (2)	NO EFFECT ON WEAPON GUIDANCE	NO EFFECT FOR RHO-RHO TARGETTING. EFFECTS ACCURACY WITH IMPACT ERROR PROPORTIONAL ($<1:1$) TO TOT RANGE FOR θ/θ TARGETTING.
4. SINGLE SOURCE (ρ/θ_1) TARGET LOCATION AND HAND-OFF TO ANOTHER SOURCE (2) FOR WEAPON INITIALIZATION AND FIRING.	SAME AS IN (1) & (2)	SAME AS "IN (1)"	SAME AS IN (1) & (2)	SIMILAR EFFECT TO (1) & (2)	EFFECTS IMPACT ACCURACY WITH A BOUNDED ERROR INDEPENDENT OF TOT RANGE (FUNCTION OF USER GRID POSITION ERRORS ONLY.)
5. SINGLE SOURCE (ρ/θ_1) TARGET LOCATION AND HAND-OFF TO ANOTHER SOURCE (2) FOR WEAPON JTIDS GUIDANCE TO TARGET.	SAME AS IN (1) & (3)	SAME AS IN (1)	SAME AS IN (1) & (3)	SIMILAR EFFECTS TO (1) & (3)	EFFECTS IMPACT ACCURACY WITH A 1:1 BURN PROPORTIONAL ($<1:1$) TO TOT RANGE

LE SINTAC ET SES PERFORMANCES EN LOCALISATION

par

L.J. MILCEVIC

Directeur à la Division Systèmes Electroniques

THOMSON-CSF

116, avenue Aristide Briand

92220 BAGNEUX

FRANCE

et

JC. CHARAVIT

Ingénieur à la Division Systèmes Electroniques

THOMSON-CSF

M. RONSIN

Ingénieur Division Télécommunications

THOMSON-CSF

66, rue du Fossé Blanc

92231 GENNEVILLIERS

FRANCE

RESUME

Après un bref historique du SINTAC, on indique le principe de base de navigation. On décrit le matériel mis en oeuvre et on donne une analyse détaillée des sources d'erreurs dues à l'équipement et tout spécialement celles dues à l'horloge et à la période de resynchronisation. On examine aussi des erreurs dues aux multitrajets.

La localisation dans le SINTAC est faite par des mesures discontinues, la navigation continue est obtenue par un algorithme traitant les mesures de distance du SINTAC d'une part et des données de l'air et du cap du mobile d'autre part. L'algorithme utilisé est celui du filtrage de KALMAN.

Les résultats de simulation sont conformes aux prévisions : les erreurs vraies restent dans les limites de 10 à 20m pour des périodes de mesures de l'ordre de la seconde, période courante dans un trafic de densité moyenne.

On a cherché ici des résultats avec un système hybride minimal toujours disponible à bord d'un avion. Il est évident qu'en cas d'utilisation de système inertiel ces résultats ne peuvent qu'être supérieurs et surtout l'autonomie du système augmentée.

1. INTRODUCTION

Le programme SINTAC est dans la phase du développement exploratoire SINTAC 2, interopérable avec JTIDS, qui comprend 3 phases :

La première phase d'étude s'achève actuellement. Ses objectifs consistaient principalement à modifier le format d'émission pour assurer l'interopérabilité SINTAC/JTIDS et à réaliser une maquette émetteur/récepteur. Cette maquette constitue le banc d'essai qui permet de vérifier les performances sous différentes conditions de brouillage et de multitrajets. Le second intérêt de cette maquette est l'essai du logiciel associé à différentes fonctions. (figure 1)

La seconde phase prévoit la réalisation de plusieurs maquettes de terminaux SINTAC permettant des expérimentations en vol. Il sera ainsi vérifié :

- les performances opérationnelles du matériel et du logiciel dans les fonctions communication, navigation relative, identification.
- l'interopérabilité JTIDS/SINTAC.

Simultanément, quelques développements technologiques sont faits sur les points importants mis en évidence durant la phase 1.

La troisième phase se poursuivra à partir de 1983 par l'industrialisation du produit qui devrait aboutir à des livraisons de matériel série en 1987. Il est prévu de développer diverses classes de terminaux faisant dans la mesure du possible appel à des modules communs, le logiciel et la présentation étant adaptés au besoin spécifique.

Ce programme est susceptible de subir des modifications en fonction du développement du concept SINTAC 3 actuellement en examen.

2. GENERALITES

Dans le SINTAC la navigation est basée sur les distances entre les différents terminaux d'une communauté d'utilisateurs. Ce procédé présente quelques caractéristiques importantes quant à la précision de localisation.

- ces distances ne sont pas mesurées directement. Chaque utilisateur les déduit de la mesure du temps d'arrivée (TOA) d'un événement identifiable, émis par un autre terminal dont la position est connue.

- ces distances ne sont pas mesurées d'une manière continue. La mesure est faite avec une périodicité très variable pouvant atteindre 10 à 12 secondes. Entre deux mesures, l'utilisateur travaille par estimation au moyen d'un algorithme plus ou moins compliqué qui dépend de la vitesse de déplacement du porteur,

et des moyens d'estime disponibles.

- les références utilisées pour la localisation peuvent être fixes ou mobiles (cas de la navigation relative). L'événement identifiable peut donc être entaché de deux imprécisions : soit le moment de l'émission, soit la position de l'émetteur ou les deux simultanément.

- enfin, l'environnement physique n'est pas idéal, et comme dans tous les systèmes radio-électriques, les réflecteurs naturels ou artificiels donnent naissance à des multitrajets porteurs d'un signal d'erreur.

- les facteurs affectant la précision de llocalisation sont donc nombreux. Pour la «implification de l'exposé» ils ont été divisés en deux groupes :

- ceux affectant la précision sur la mesure du temps d'arrivée. Ils sont plus spécialement reliés aux performances du matériel et ils comprennent l'effet de l'environnement.

- ceux liés aux méthodes mises en œuvre pour utiliser cette information. Ils comprennent l'influence du logiciel du terminal utilisateur et des procédures de gestion de la communauté des utilisateurs.

3. LA MESURE DU TEMPS

L'imprécision sur la mesure du temps est le résultat de deux facteurs :

- le format du signal dans l'espace : c'est l'information fournie par le terminal émetteur et qui peut être altérée lors de la propagation sous l'effet des trajets multiples.

- le matériel mis en œuvre pour détecter le temps d'arrivée du signal précédent, et le mode de fonctionnement de ce matériel.

3.1. Le format du signal

Pour la navigation on utilise deux messages SINTAC particuliers :

- le message "P" ou message de position émis systématiquement par les participants, et le message "RTT" qui est un échange d'interrogation/réponse entre deux participants.

Dans les deux cas, le préambule donne lieu à une première mesure sommaire du temps d'arrivée. Cette mesure est affinée à l'aide des impulsions de synchronisation qui le suivent et qui fournissent le TOA. Dans le matériel expérimental de la phase 1 l'en-tête et le texte du message ne servent pas à la mesure du TOA. Leur utilisation est indirecte en ce sens que les deux sous-messages contiennent des informations utiles au traitement ultérieur du TOA :

- Position de l'émetteur et indices de qualité des horloges et de la navigation dans le cas des messages P.

- instant d'arrivée du message d'interrogation sans le cas de la réponse RTT.

Tous les constituants du message SINTAC (Préambule, Synchro, En-tête, Texte) sont composés d'une série d'impulsions dont les caractéristiques intéressantes en ce qui concerne la détermination de TOA sont leur nombre et leur forme

Le préambule comporte 16 ou 32 impulsions émises sur 8 fréquences différentes. La synchronisation comprend 4 ou 8 impulsions émises sur 4 ou 8 fréquences différentes.

Le fait que ces impulsions soient émises avec saut de fréquence a peu d'influence sur la précision intrinsèque de la mesure du TOA. Par contre cette particularité est intéressante dans la résistance au multitrajet.

Chaque impulsion d'une durée normale de 6,4 µs est étalée en spectre par une modulation MSK à 5 MHz. Le code utilisé pour la séquence d'étalement est sans influence sur la précision. Pour la partie du message qui nous intéresse il dépend uniquement du tirage d'une boîte chiffre. Cet aléa est connu des participants qui peuvent procéder à une corrélation entre la séquence émise et la séquence attendue. Le résultat de cette corrélation sera une impulsion fine d'environ 300 ns à 3 dB, encadrée de lobes secondaires. Cette forme détermine en grande partie la précision possible sur le TOA :

Elle permet d'obtenir une précision sensiblement égale au dixième du lobe soit environ 30 ns. Cette valeur correspond aux performances recherchées.

3.2. Matériel mis en œuvre

Le schéma fonctionnel du terminal est donné figure 2. Il comprend une chaîne émission/réception dont les opérations sont commandées par une logique de séquencement et dont les données sont traitées par un calculateur.

- Emetteur

Il comprend un modulateur suivi d'une chaîne de transposition de fréquence et d'un amplificateur de puissance ;

Le modulateur effectue le codage C.C.S.K. des symboles à transmettre, le cryptage de la suite binaire obtenue à l'aide d'un aléa fourni par la boîte chiffre, et la modulation MSK d'une porteuse.

Tous ces circuits sont à large bande et les dérives du temps de transit sont considérées comme négligeables dans la suite de cet exposé.

- Circuits de réception

Ils comportent les récepteurs nécessaires à l'acquisition du préambule et à la démodulation du texte du message.

Ces récepteurs sont sélectifs en fréquence et cette sélectivité participe à l'imprécision sur la mesure du temps.

- synthétiseur de fréquence

Il reçoit de la logique de séquencement les fréquences de chaque symbole et génère les oscillateurs locaux nécessaires aux transpositions.

Il n'intervient pas comme source d'erreur dans la mesure de distance.

- Horloge

Elle est pilotée par un oscillateur de bonne stabilité et fournit une heure absolue locale qui doit être réajustée périodiquement, par synchronisation avec les participants SINTAC ; il sera vu plus loin que c'est la principale cause d'erreur.

- Circuit de synchronisation et de démodulation

Ce dispositif effectue les opérations suivantes :

- reconnaissance du préambule du message à recevoir par corrélation des signaux provenant des récepteurs accordés sur les fréquences du préambule. Cette reconnaissance permet de connaître l'heure relative avec une précision de 100 ns environ.
- amélioration de la connaissance de l'heure relative grâce au circuit de synchronisation fine et lecture du TOA.
- extraction d'information, détection et correction d'erreurs.

Ce circuit joue un rôle important dans la mesure de distance.

Séquencement et traitement de l'information

Le dispositif de traitement des messages, reçoit le message à coder en provenance du calculateur, ou le message codé en provenance du récepteur.

Il effectue les opérations de routine :

codage, décodage, entrelacement, stockage, etc...

La boîte chiffre génère des lois pseudo-aléatoires nécessaires à la sélection des fréquences, des codes, et en général de tous les aléas utilisés dans le format de la transmission.

La logique de séquencement organise le déroulement des tâches au niveau de la récurrence. Elle reçoit du calculateur une série d'ordres définissant la fonction du terminal et commande la mise en action de tous les sous-ensembles précédents.

Tous ces dispositifs sont sans relation avec la précision sur la distance.

- Le calculateur

Le calculateur effectue les tâches suivantes :

- a) Gestion des échanges avec les organes extérieurs :
- b) Gestion des procédures des fonctions :

- entrée dans le réseau
- synchronisation
- localisation
- identification
- communication

c) Contrôle de fonctionnement du terminal.

Le calculateur effectue donc tous les traitements sur l'information "distance brute" que lui fournit le circuit de démodulation. A ce titre il intervient directement dans la précision de la localisation.

3.3. Méthode de détection utilisée

L'équipement détermine dans tous les cas l'arrivée de l'évenement (TOA) par rapport au début de la récurrence.

La détection du préambule du message est faite en utilisant un circuit comprenant des corrélateurs programmables et des lignes à retard. La somme des signaux corrélés permet de détecter une présence de préambule annonciatrice d'un message en initialisant le processus de synchronisation fine.

Le récepteur SINTAC utilise des corrélateurs numériques et l'échantillonnage se fait au rythme de 200 ns. Durant la détection du préambule, l'horloge d'échantillonnage a une phase quelconque par rapport à celle du terminal émetteur. (figure 3)

Par rapport au signal fourni par une corrélation analogique le signal numérisé présente une granularité au pas de 200 ns, introduisant une incertitude identique sur l'instant de détection du préambule avec un dispositif à seuil.

Le rôle du dispositif de synchronisation fine est de caler la phase d'horloge d'échantillonnage au centre du signal en sortie des corrélateurs. Dans le matériel phase 1 on utilise quatre impulsions dans le sous-message synchro. A chaque impulsion, l'erreur de phase est évaluée dans un corrélateur à deux voies à l'aide d'un procédé à avance/retard utilisant deux horloges déphasées de $\pm T/2$: lorsque le calage en phase est correct l'amplitude des échantillons à $+ T/2$ et à $- T/2$ est identique. Si les amplitudes sont inégales leur rapport permet de déterminer le signe et l'importance de la correction de phase à effectuer.

Le synoptique du dispositif de synchronisation fine est donné figure 4.

Le corrélateur à deux voies est échantillonné au rythme d'une horloge 5 MHz dont la phase est modifiable par le prépositionnement du diviseur D. Le prépositionnement est fourni par le contenu d'un accumulateur représentant la correction de phase. Cette correction est fonction de l'écart constaté lors du dernier échantillonnage, entre l'axe du signal corrélé et la phase de l'horloge. Le corrélateur donne les amplitudes des échantillons à $\pm T/2$ et la logique de correction détermine la variation de phase à appliquer en fonction de ces amplitudes et de l'algorithme de correction choisi.

Le début de la récurrence initialise le compteur C qui est attaqué par une horloge rapide (80 MHz) et qui définit le temps foulé avec une granularité de 12,5 ns.

Le compteur est arrêté par l'acquisition du préambule et indique l'heure d'arrivée dans la récurrence avec une incertitude d'environ 200 ns.

Simultanément, l'arrivée du préambule remet à zéro l'accumulateur, le diviseur D, et la logique de séquencement.

Après échantillonnage de chaque impulsion de synchronisation, le contenu de l'accumulateur est modifié. Après ce groupe d'impulsions, le contenu N du compteur et le contenu ΔN de l'accumulateur représentent la valeur corrigée de l'heure d'arrivée du message. Il est envisagé pour les maquettes de la phase 2 d'améliorer ce dispositif pour lui donner la qualité de poursuite de la synchronisation sur les impulsions de l'en-tête.

3.4. Précision de la mesure sur l'heure d'arrivée

La précision sur l'heure d'arrivée est influencée par les facteurs suivants qui sont symbolisés sur la figure 5.

- le dispositif de filtrage qui introduit un temps de retard dépendant des conditions d'environnement.
- la chaîne d'amplification qui dispose d'un limiteur dont le temps de transit dépend du niveau du signal.

Le dispositif de détection du préambule est composé de lignes à retard et d'un détecteur de seuil. Le retard étant introduit de manière numérique sa stabilité à long terme ne dépend que de celle de l'horloge.

Le détecteur de seuil introduit une quantification et un bruit dépendant du rapport Signal/Bruit, donc du niveau du signal. Nous verrons toutefois que les erreurs introduites lors de la détection sont réduites par la synchronisation fine.

- le dispositif de synchronisation a une précision qui dépend, du nombre d'impulsions de synchronisation disponible, de l'algorithme utilisé pour le traitement, de l'imprécision sur l'heure de début de récurrence, de la dérive du signal d'horloge. Il introduit également une quantification du fait de la numérisation du processus, et un bruit qui dépend, comme pour l'acquisition, du niveau du signal.

3.4.1. Effet du filtrage

Il est d'autant plus sensible que ces filtres sont à bande étroite. Ceci focalise l'attention sur les filtres en fréquence intermédiaire et sur le filtre vidéo fréquence.

Le filtrage en fréquence intermédiaire utilise un filtre de Bessel de bande passante 3 MHz qui introduit un temps de retard de 150 ns environ.

Une variation de la bande passante de 5 % sous l'influence de dérives à long terme (climatique, vieillissement), introduit donc une variation du temps de transit de ± 9 ns environ.

Le centrage du filtre par rapport à sa fréquence nominale a un effet négligeable sur la dérive du temps de transit.

Après détection le signal vidéo est filtré par un passe bas à 5 MHz introduisant un retard de l'ordre de 60 ns.

Une variation de la fréquence de coupure de 5 % introduit de même une dérive de l'ordre de 3 ns.

L'effet global du filtrage est ainsi représenté par une dérive possible de l'ordre de ± 10 ns. Il faut toutefois mentionner l'influence du filtre de réjection I.F.F. qui introduira sur les fréquences proches un effet additionnel, restant faible à cause du saut de fréquence.

3.4.2. Effet de la limitation

La figure 6 présente le résultat des mesures faites sur l'amplificateur limiteur de la maquette SINTAC. La dérive de phase est de l'ordre de 20° ce qui correspond à une variation du temps de transit inférieure à la nanoseconde.

3.4.3. Effet de la ligne à retard

La durée du préambule est de 416 µs. Le retard entre la première et la dernière impulsion est introduit au moyen d'un registre à décalage piloté par l'horloge du terminal. Même avec une stabilité minimale de 10^{-5} , la dérive sur le retard introduit reste négligeable.

Par ailleurs, tout le dispositif numérique étant synchrone il n'y a pas cumul des dérivés des temps de propagation dans les circuits logiques employés.

3.4.4. Influence du détecteur de seuil

Le temps d'arrivée "brut" du préambule (avant correction par la synchronisation fine) est influencé par le rapport signal à bruit présent au moment de la numérisation de l'information. On conçoit que pour le bon fonctionnement de l'interpolation ultérieure faite par le dispositif de synchronisation, il est nécessaire que le bruit reste faible devant la quantification de 200 ns. Autrement il serait possible d'avoir une erreur d'un pas sur le temps d'arrivée.

En limite de portée le récepteur travaille avec E/N_0 de 12 dB.

Pour un seuil placé à mi-amplitude, le jitter sur l'instant de passage d'une impulsion individuelle atteindra 40 ns à 1σ en supposant un temps de montée instantané de 200 ns.

Le bruit sur les 16 ou 32 impulsions de préambule étant décorrélé, le jitter sur le TOA de préambule est réduit dans un rapport de 4 à 6, ce qui permet de remplir la condition ci-dessus.

3.4.5. Dispositif de synchronisation

- Influence du bruit et de l'algorithme

Ce bruit provient, du bilan de liaison, qui détermine le E/N_0 , et de la quantification adoptée pour la corrélation numérique.

Dans le matériel expérimental phase 1, la quantification est faite en utilisant 3 bits ce qui correspond à un jitter du même ordre de grandeur que celui entraîné par le E/N_0 en limite de portée.

L'algorithme utilisé consiste à appliquer une correction partielle après chaque impulsion traitée.

La figure 7 montre l'évolution de l'erreur mesurée avec le dispositif actuel en fonction du rang de l'impulsion reçue :

On voit que pour un décalage systématique de 100 ns, les quatre impulsions de synchronisation laissent une erreur significative. On remarque également que la quantification est le phénomène aussi important que le bruit thermique et que l'ensemble donne une erreur d'environ 20 ns à 1 σ . En pratique, lorsque l'erreur initiale sur l'acquisition est fluctuante, l'algorithme réduit la dispersion à environ ± 20 ns après la quatrième impulsion, ce qui correspond à une valeur d'environ 10 ns à 1 σ .

L'ensemble de ces erreurs est résumé figure 8.

- Influence de l'horloge

L'horloge est constituée d'un oscillateur qui pilote une chaîne de comptage du temps.

A partir d'un instant de référence, le comptage du temps écoulé est entaché d'une erreur qui dépend de l'incertitude sur le comportement à long terme de l'oscillateur : Paramètre qui inclut généralement la tolérance sur la fréquence nominale, l'effet du vieillissement, et l'effet de l'environnement thermique.

A titre d'exemple, dans le cas d'un oscillateur donné à 10^{-7} pour une période de plusieurs mois, ce qui est une performance honnête pour du matériel embarqué, on s'aperçoit que l'erreur commise sur la mesure du temps est de 100 ns par seconde écoulée depuis l'instant de référence.

Cette erreur peut être réduite grâce à trois possibilités :

- augmenter la précision de l'oscillateur.
- remettre la chaîne de comptage du temps à l'heure plus fréquemment.
- évaluer et tenir compte de la dérive à court terme de l'oscillateur.

Le premier procédé ne fait que reporter la difficulté sur le composant au prix d'une augmentation du volume et du coût et des instruments de contrôle.

La combinaison des deux autres procédés est beaucoup plus efficace compte tenu des possibilités du matériel mis en oeuvre autour de l'oscillateur. (figure 9)

La remise à l'heure de la chaîne de comptage du temps se fait lorsque les informations en provenance de participants mieux synchronisés permettent de calculer l'erreur de synchronisation. Ceci est réalisable à l'aide d'un échange RTT ou à défaut en utilisant plusieurs messages P en provenance de participants connaissant leur position avec une précision compatible avec leur erreur de synchronisation.

Dans un échange RTT, le participant mesure l'heure d'arrivée du message et renvoie cette indication dans sa réponse émise à une heure connue. L'interrogateur dispose ainsi d'un jeu d'équations dont la résolution fournit le décalage horaire.

Les échanges RTT étant en général limités à une périodicité d'une centaine de seconde, la remise à l'heure est à elle seule insuffisante. Il est nécessaire de tenir compte de la vitesse de dérive à court terme de l'oscillateur.

Ce calcul de dérive peut être fait après deux échanges RTT et mis à jour à chaque échange successif. La correction, donnant la vitesse de dérive est utilisable jusqu'au prochain échange. Il est ainsi possible d'améliorer la connaissance de l'heure d'un à deux ordres de grandeur suivant la complexité de l'algorithme utilisé.

Les précisions ainsi obtenues sur la distance sont résumées dans le tableau figure 10.

On voit que l'horloge est le facteur prépondérant et que sa qualité sera fixée par la précision désirée sur le TOA et les contraintes possibles de silence radio.

Il faut noter que la fréquence de l'oscillateur pilotant l'horloge introduit une granularité sur la mesure du temps. Utilisant un comptage à 80 MHz cette granularité est négligeable.

3.5. Effet des multitrajets

Dans une liaison à fréquence fixe et compte tenu :

- de la durée du message,
- de la vitesse de déplacement du récepteur,

les phases des multitrajets affectant chacune des impulsions d'un message sont corrélées ce qui est un phénomène gênant. Par contre, le saut de fréquence décortèle ces phases ce qui est favorable puisqu'il permet une moyenne des erreurs instantanées introduites par le multitrajet.

Le multitrajet n'est gênant que dans la mesure où il n'est pas possible de faire une discrimination entre le trajet direct et l'onde réfléchie.

Le temps est le moyen le plus commode de faire cette distinction, le trajet direct arrivant toujours en premier.

Cette discrimination reste possible tant que les deux pics de corrélation restent séparés par au moins 300 ns. Dans ces conditions le seul effet du trajet parasite est une diminution d'amplitude du signal principal qui n'affecte pas le temps d'arrivée mesuré.

Lorsque la différence de trajet réduit la séparation à moins de 300 ns il n'est plus possible de distinguer les deux pics de corrélation. Le centre de gravité du signal composite est différent du signal direct, d'où erreur.

En première approximation pour un trajet réfléchi de retard Δt et de niveau P , le déplacement est de la forme :

$$\epsilon = \Delta t \times \frac{P}{1+P}$$

L'erreur commise est représentée sur la figure 11 en fonction du niveau du signal réfléchi. On remarque que pour un niveau de - 10 dB qui représente une valeur courante, l'erreur sur le TOA est de 50 ns.

4. INFLUENCE DES ALGORITHMES DE NAVIGATION

Les temps d'arrivée des messages qui sont extraits des circuits de synchronisation fournissent des distances instantanées entre terminaux qui se déplacent.

La localisation d'un terminal dans un repère absolu ou relatif nécessite le traitement de ces distances en tenant compte :

- des positions des émetteurs
- des temps écoulés depuis la réception des messages
- des incertitudes sur les mouvements des terminaux.

La localisation sera d'autant plus précise si toutes les informations fournies par d'autres moyens de navigation sont pris en compte. L'équipement des porteurs est variable mais il existe toujours des moyens de navigation minimaux qu'il s'agit d'exploiter au mieux, de façon à accroître les performances de la localisation au moindre coût.

L'algorithme de traitement que nous utilisons tient compte, en plus des données SINTAC :

- des données de l'air et du cap pour les avions
- des distances parcourues et du cap pour les véhicules et navires.

Les résultats que nous présentons concernent le programme pour avions.

4.1. Principe de la localisation à l'aide du filtre

Ce principe est illustré sur la figure 12a qui pour la simplicité de l'exposé, porte sur la navigation dans un plan.

Le terminal connaît initialement sa position avec une incertitude donnée. Il se déplace et si ne disposait que des moyens autonomes de navigation, son incertitude de position irait croissante.

Par contre, chaque information extérieure de distance fournie par l'équipement SINTAC lui permet de diminuer l'incertitude sur sa position dans le relèvement de l'émetteur.

La disposition des participants étant quelconque les relèvements successifs sont différents et le polygone d'incertitude se réduit peu à peu jusqu'à se trouver limité par la précision du plus précis des moyens de localisation disponibles.

L'initialisation du processus nécessite l'insertion de la position du terminal, ce qui est généralement possible au départ d'une mission. Si ce n'est pas le cas, la méthode classique de localisation qui est employée consiste à estimer le mouvement du porteur, pour reporter dans le temps la position des balises rencontrées successivement.

Une première localisation est obtenue par intersection des indications de la troisième balise avec celles obtenues par report de position des deux premières.

4.2. Les données du traitement

Les moyens disponibles comprennent ceux apportés par la communauté SINTAC et les données de l'air.

La communauté SINTAC fournit deux types d'information :

- les messages P, et les messages RTT.

Les messages P sont des messages de position émis par chaque participant sur la base d'un message chaque seconde pour les avions, ou d'un message toutes les deux secondes pour les stations au sol. Chaque terminal choisit aléatoirement une récurrence sur les vingt allouées chaque seconde pour l'émission de tels messages. Dans une récurrence donnée un terminal à l'écoute recevra ainsi l'émission de son plus proche voisin.

Le message P fournit, en plus de la mesure de distance, la position de l'émetteur, et la précision estimée sur la position et la synchronisation. Ces deux indications permettent au terminal récepteur de prendre ou non en compte l'information distance, compte tenu de ses propres incertitudes.

Le message RTT est un échange avec un participant mieux localisé que le demandeur. Il est déclenché par l'algorithme de localisation qui en juge la nécessité, avec toutefois une cadence plus lente que 100 secondes. L'échange procure l'erreur de synchronisation entre les deux participants.

Les autres données prises en compte sont le cap et les données de l'air qui comprennent :

- l'altitude barométrique
- le dérapage
- la vitesse air
- la vitesse verticale.

Pour les besoins de la simulation, chacune de ces informations a été modélisée pour apparaître avec la cadence, la valeur nominale, et les erreurs appropriées.

L'environnement terrestre doit être également modélisé. La forme terrestre est représentée par une ellipsoïde et l'influence du vent est prise en compte à l'aide d'un modèle comportant des rafales.

La localisation peut se faire :

- soit en absolu dans le repère des coordonnées terrestres.
- soit en relatif par rapport à un terminal désigné comme référence locale principale

Dans ce cas la grille de coordonnée est centrée sur ce terminal et son orientation est faite grâce à un autre terminal désigné comme référence secondaire puisque nous avons choisi de ne pas considérer les possibilités de la centrale inertie.

4.3. Le traitement de l'information

L'algorithme utilisé est celui du filtrage de Kalman.

L'état du système est représenté par un vecteur à onze dimensions qui sont :

- la position absolue : longitude, latitude, altitude.
- la position relative : coordonnées relatives Nord et Est.
- l'erreur d'alignement Nord de la grille relative.
- la vitesse de déplacement : vitesses Nord, Est et verticale.
- l'erreur de synchronisation : erreur de calage et vitesse de dérive.
- la perturbation due au vent : vitesse Nord et vitesse Est.

Les observations permettant de raffiner l'état du système sont constituées par les 8 mesures suivantes.

- le T.O.A. qui peut être explicité, soit dans le repère absolu, soit dans le repère relatif.
- l'altitude
- le cap et le dérapage
- les vitesses : vitesse propre et verticale
- l'erreur de synchronisation
- la dérive de la synchronisation.

4.4. Résultats obtenus

Ils sont présentés sur les figures 13, 14 et 15. La figure 13 montre l'évolution de l'erreur de synchronisation, la figure 14 montre l'évolution de l'erreur de position et la figure 15 l'erreur de la vitesse.

La situation opérationnelle prise en compte comprend 3 stations au sol et 3 stations en vol circulaire ; le terminal dont les paramètres sont examinés se déplace en ligne droite à vitesse constante.

On remarque qu'après deux échanges RTT, le synchronisme de l'heure est acquis avec une précision correcte.

Le premier message P n'a pas d'influence sur la courbe d'erreur de position puisque le paramètre représenté est le demi grand axe de l'ellipse de position : au premier message P le cercle d'incertitude se transforme en ellipse. Il faut attendre le second pour observer une diminution de l'erreur.

On remarquera également sur la figure 14 que certains messages P ont peu d'influence. Il s'agit de messages dont l'origine est orthogonale au grand axe de l'ellipse. Sur la même figure, la dérive de l'erreur est fonction de l'incertitude sur la vitesse ; comme on le constate en comparant avec la figure 15.

4.5. Problèmes posés par l'algorithme

Le logiciel utilisé est programmé en 32 bits simple précision, compte tenu des moyens qui seront mis en œuvre dans le matériel définitif. Ceci fournit 7 chiffres significatifs ce qui est faible vu la dynamique des grandeurs à traiter : rayon de la Terre comparé à la précision de la localisation.

Les équations ont donc été écrites sous une forme compatible avec cette précision pour éviter de masquer l'information utile par le bruit du calcul.

Certaines difficultés de traitement apparaissent lorsque la précision d'une nouvelle information est nettement supérieure à celle contenue dans l'état du filtre. Pour les évidem, lorsque cette situation existe, la précision de l'information est augmentée par paliers. Cette méthode double ou triple le volume des calculs, mais cette situation n'existe qu'après une initialisation ou une reprise de contact.

5. CONCLUSIONS

Les résultats obtenus par la simulation sont conformes aux prévisions. Ils confirment :

- d'une part, que l'amélioration des performances est liée à l'amélioration de la synchronisation qui donne le talon à l'erreur de synchronisation et donc à l'erreur de position.
- et d'autre part, que l'utilisation du procédé d'estimation est fondamental pour la précision de localisation dans le système. Les données minimales étant les données de l'air et le cap. Le système inertiel ne peut qu'améliorer les résultats et tout spécialement augmenter l'autonomie du système.

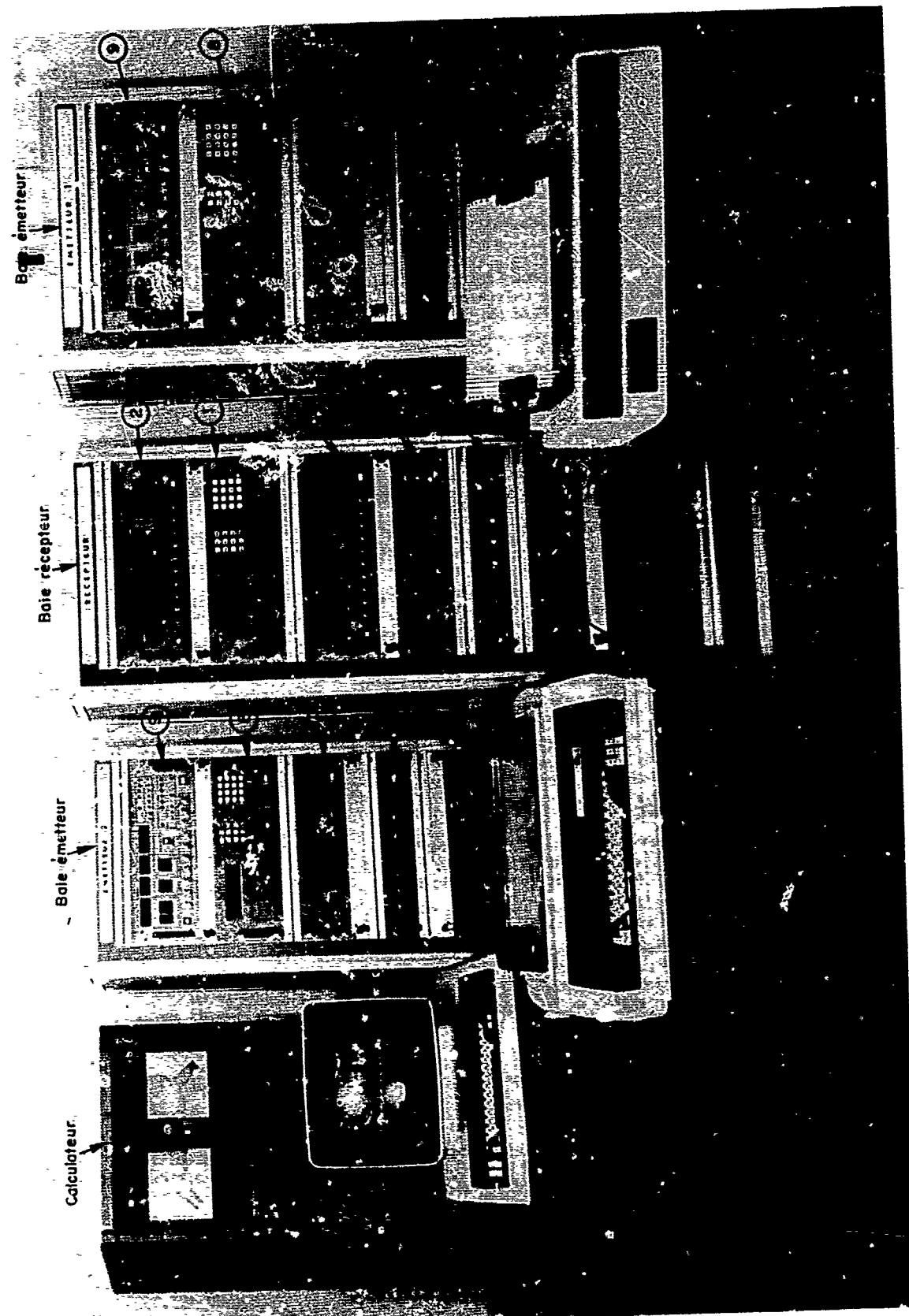


Fig.1 Ensemble maquette SINTAC II

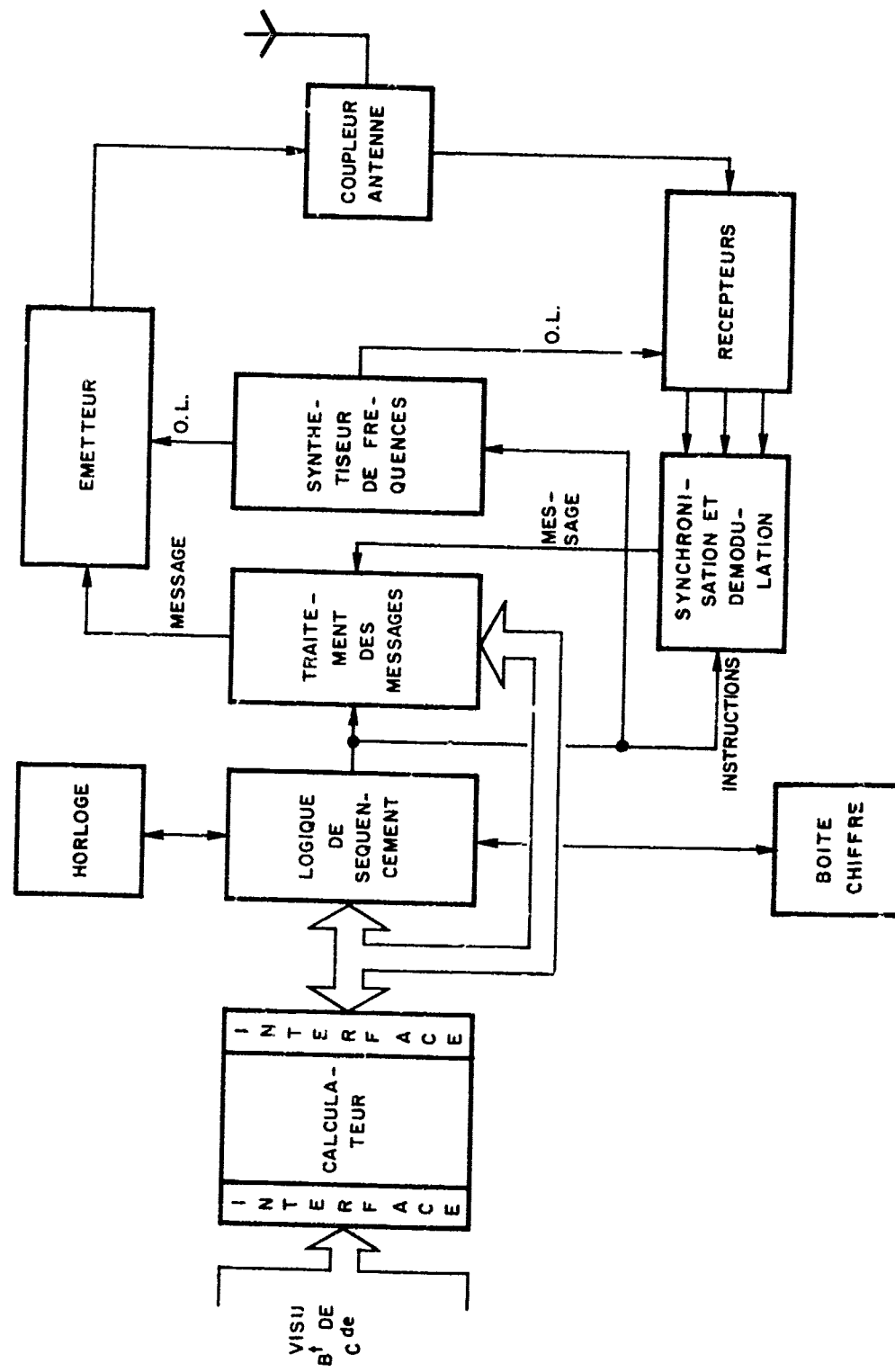
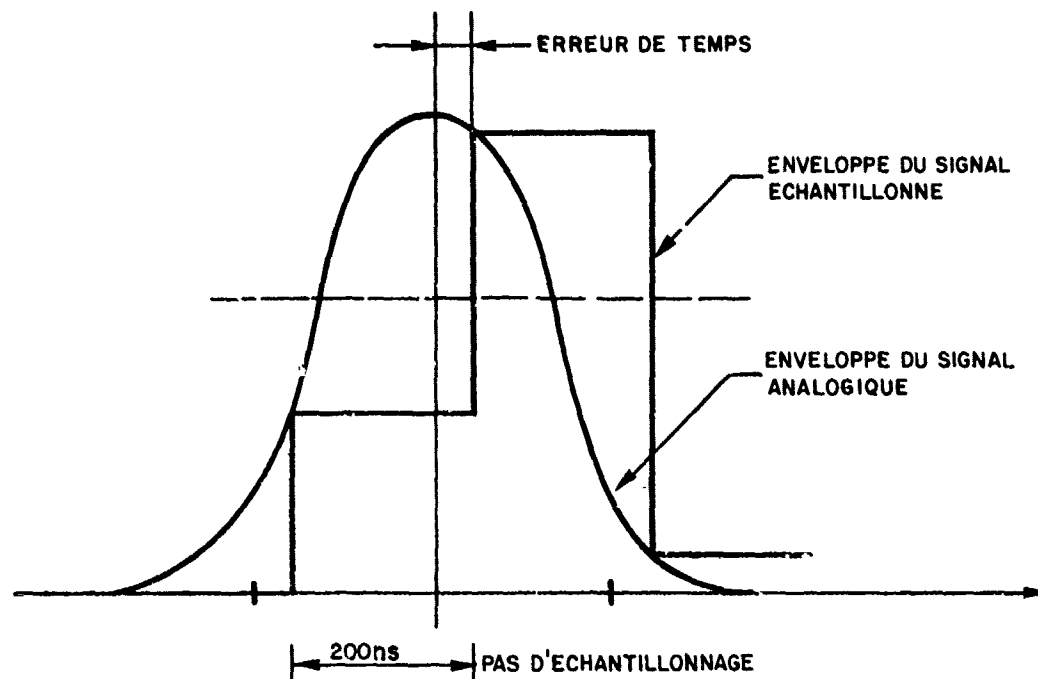
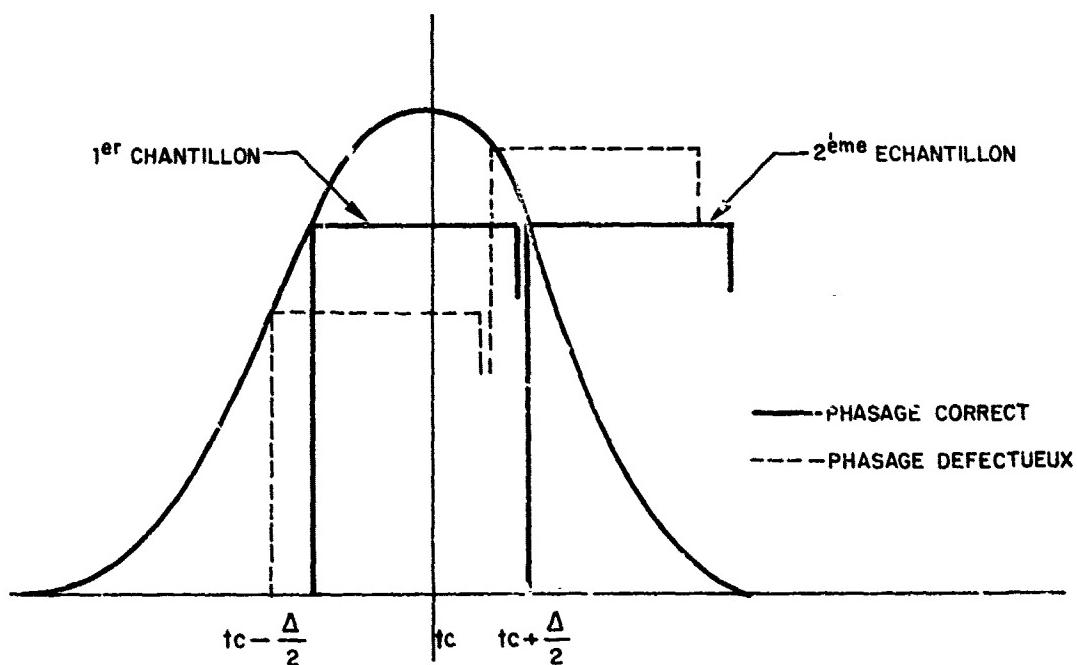


Fig.2 Schéma fonctionnel du terminal



a) SYNCHRO INITIALE



b) SYNCHRO FINE

Fig.3 Determination du TOA

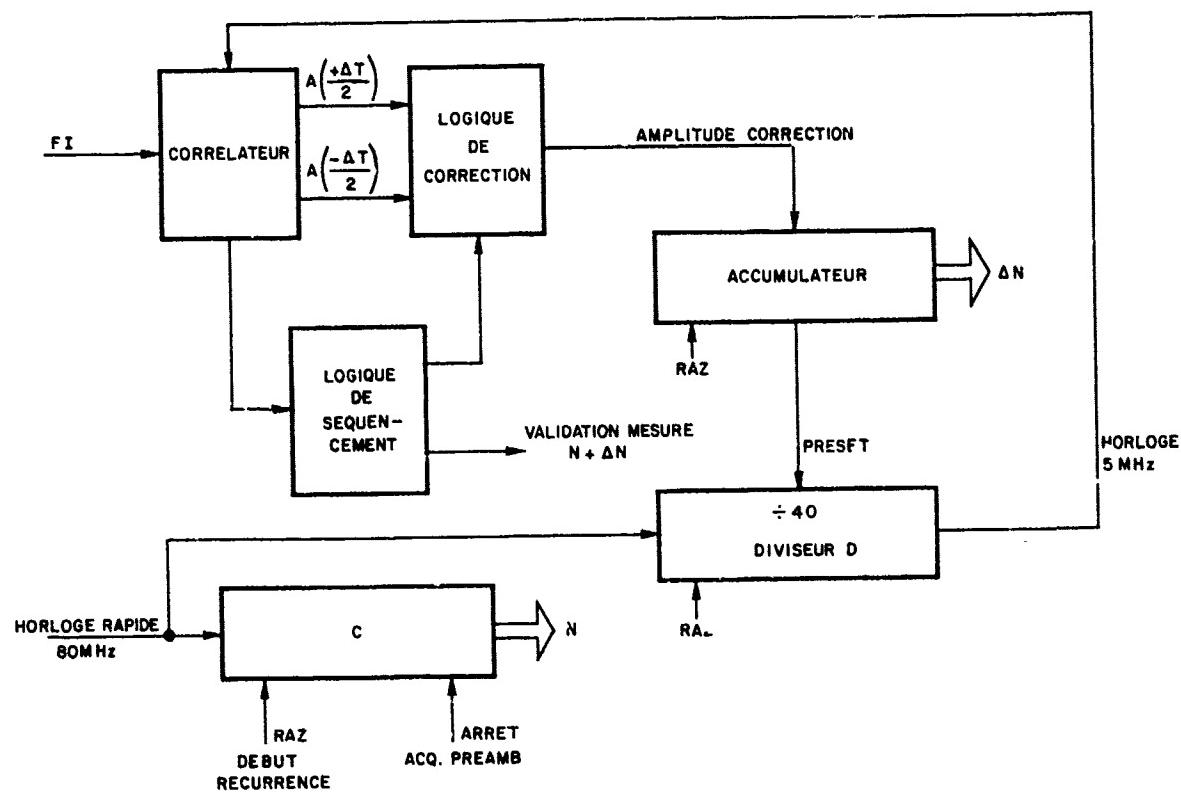


Fig.4 Circuit synchro fine

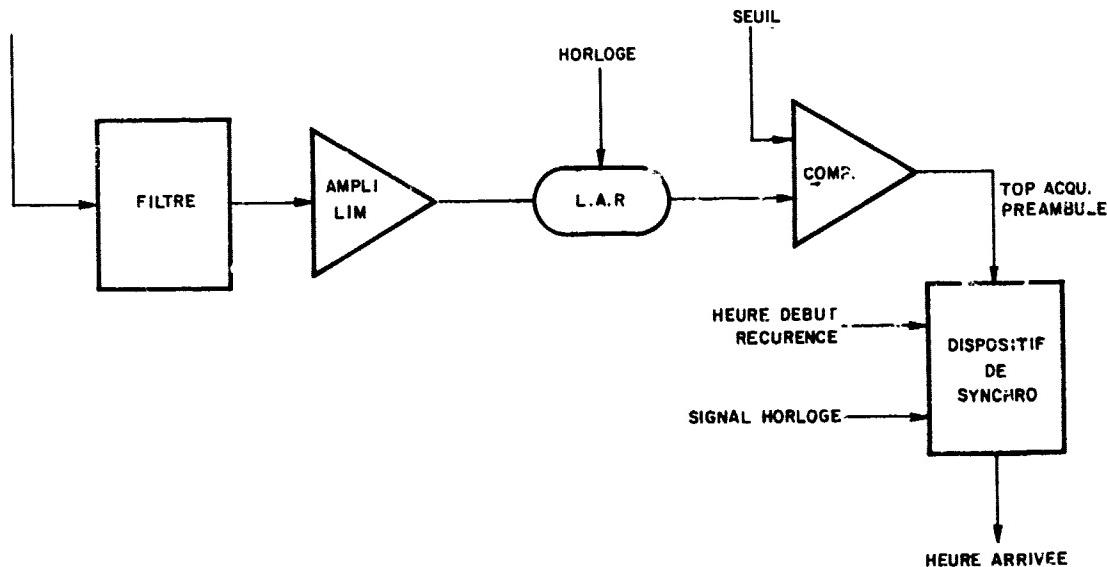


Fig.5 Mesure du TOA (facteurs d'erreur)

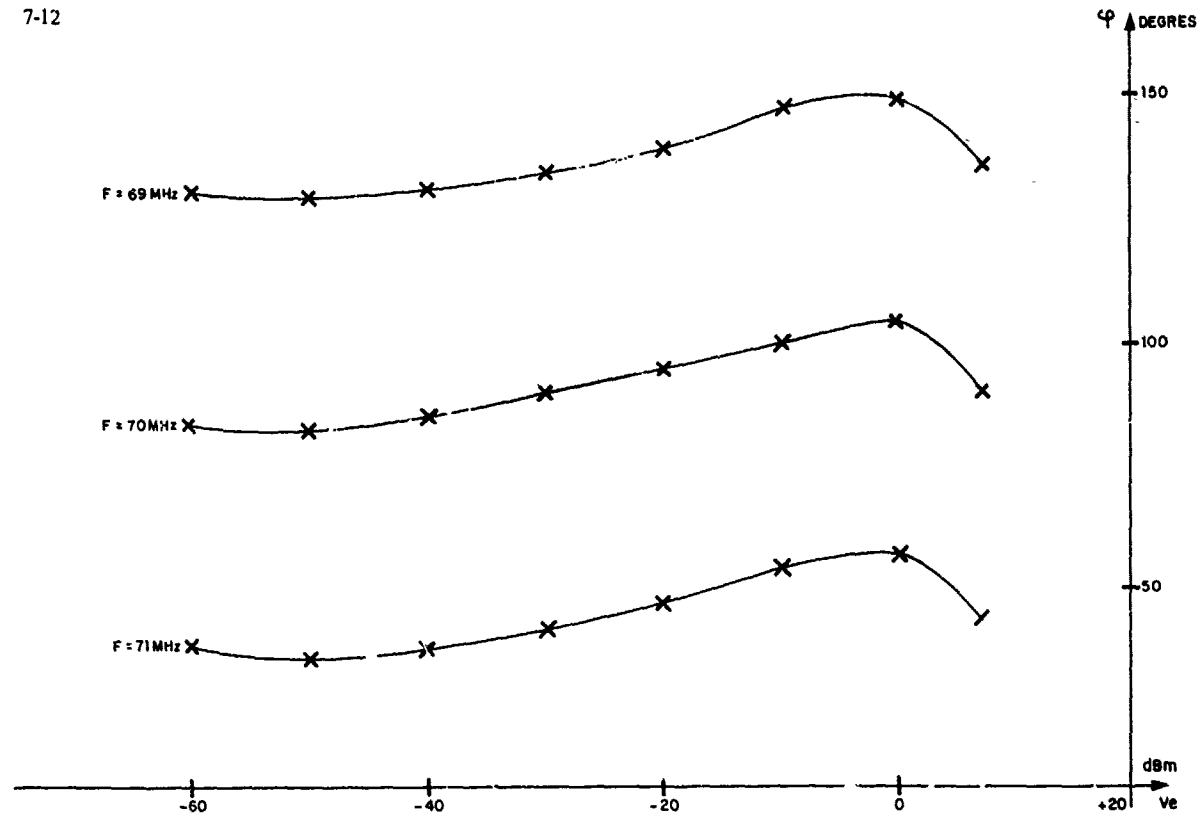


Fig.6 Effet du niveau HF

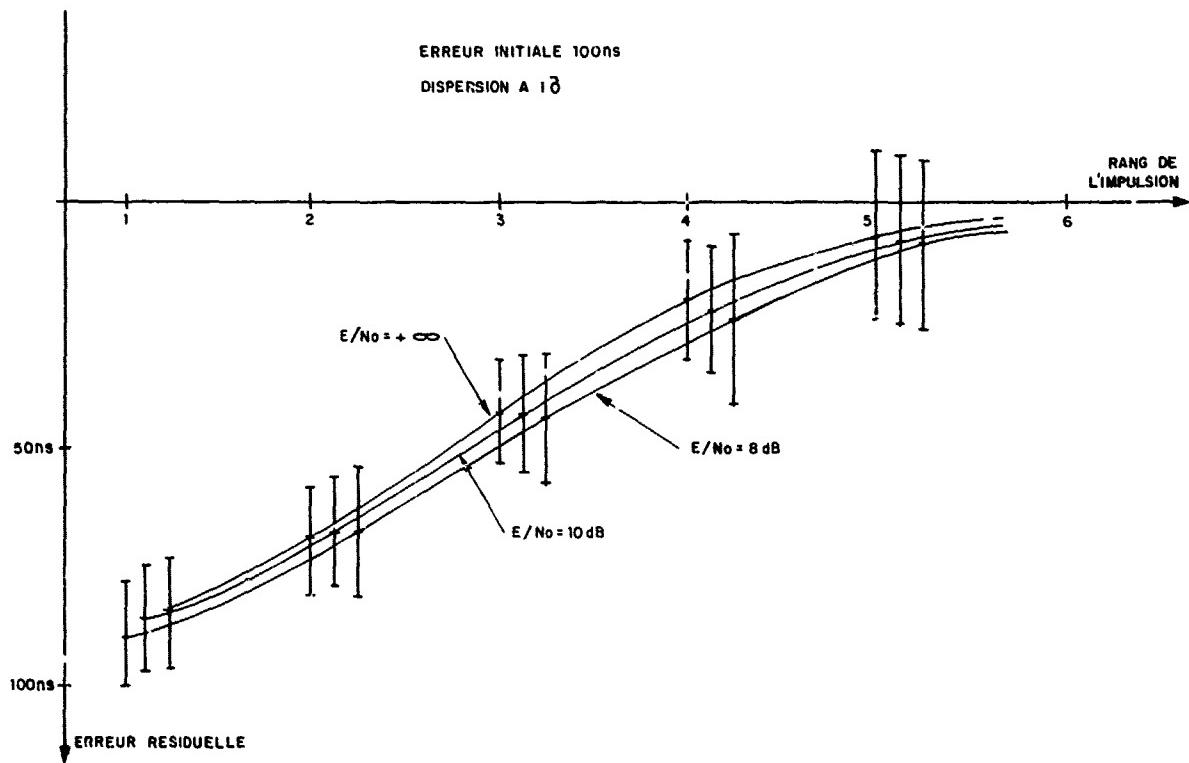


Fig.7 Algorithme de synchronisation

VALEURS EN ns ET A 13	FIXES	FLUCTUANTES
EFFET DU FILTRAGE	10	
EFFET DU LIMITEUR		NEGLIGEABLE
EFFET DE L'ACQUISITION		MASQUE
EFFET DE LA SYNCHRO		
BRUIT		20
ALGORITHME		10
TOTAL HORS HORLOGE	10	24

Fig.8 Recapitulatif des erreurs (hors horloge)

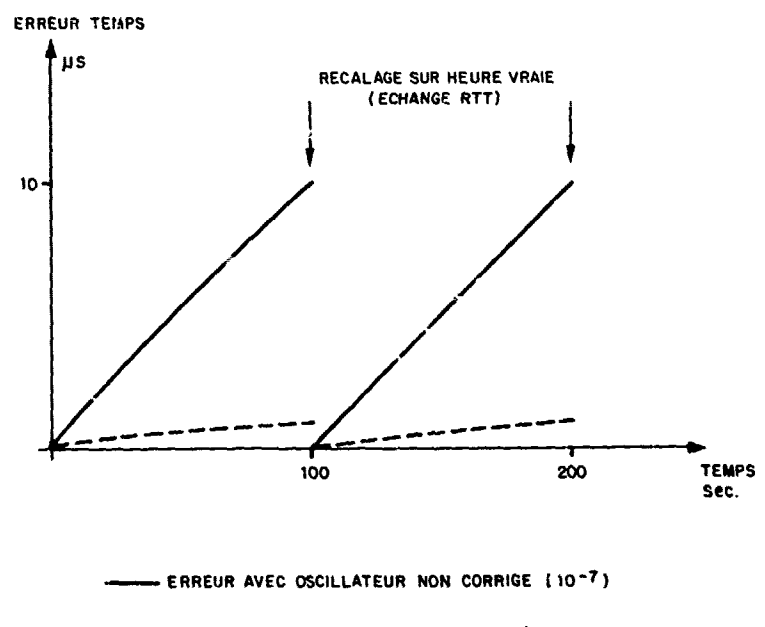
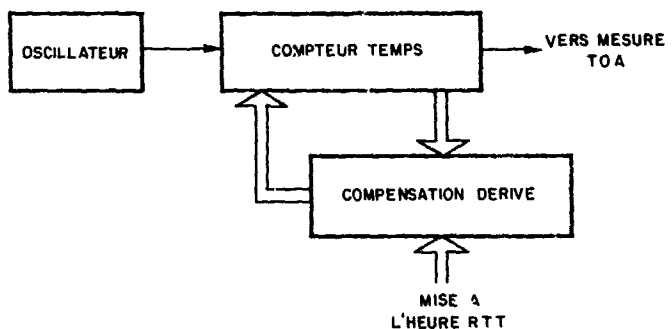


Fig.9 Compensation de la derive d'oscillateur

TALON DE PRECISION (ECHANGE RTT)		
T.O.A. INTERROGATION	($\sqrt{10 + 24}$)	26 ns
T.O.A. REPONSE	(10 + 24)	34 ns
TOTAL		45 ns

INFLUENCE HORLOGE (PERIODE DE 100 SEC)		
PILOTE A	10^{-8}	10^{-7}
DERIVE COMPENSEE A 1%	10ns	100ns
DERIVE COMPENSEE A 10%	100ns	1000ns

Fig.10 Precision globale sur TOA

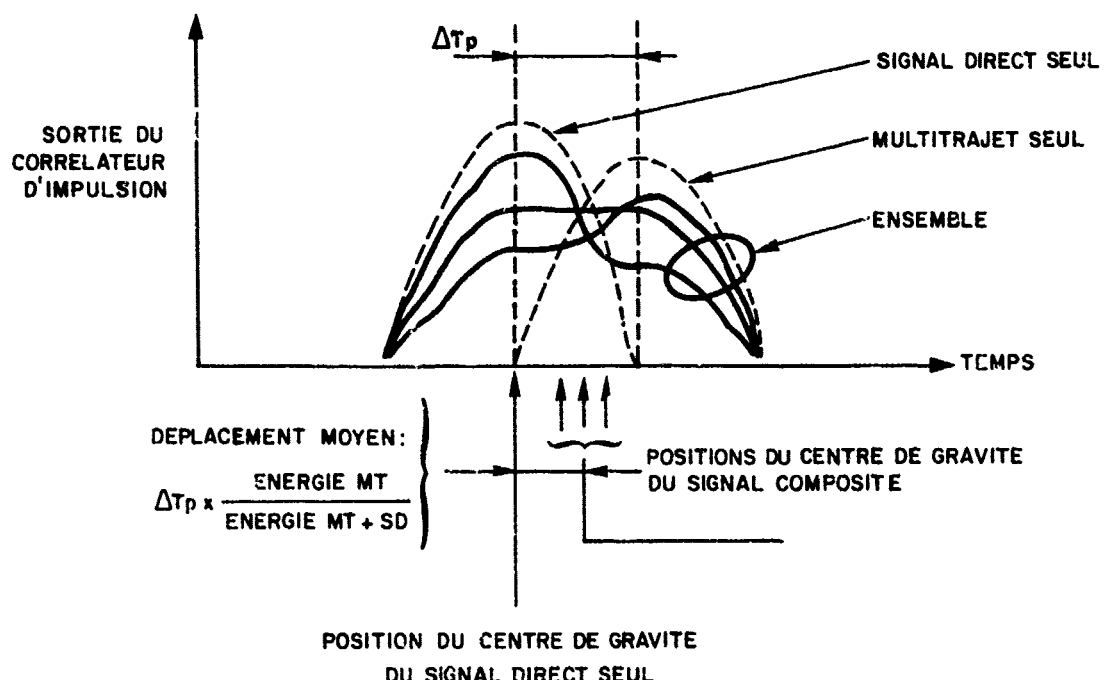
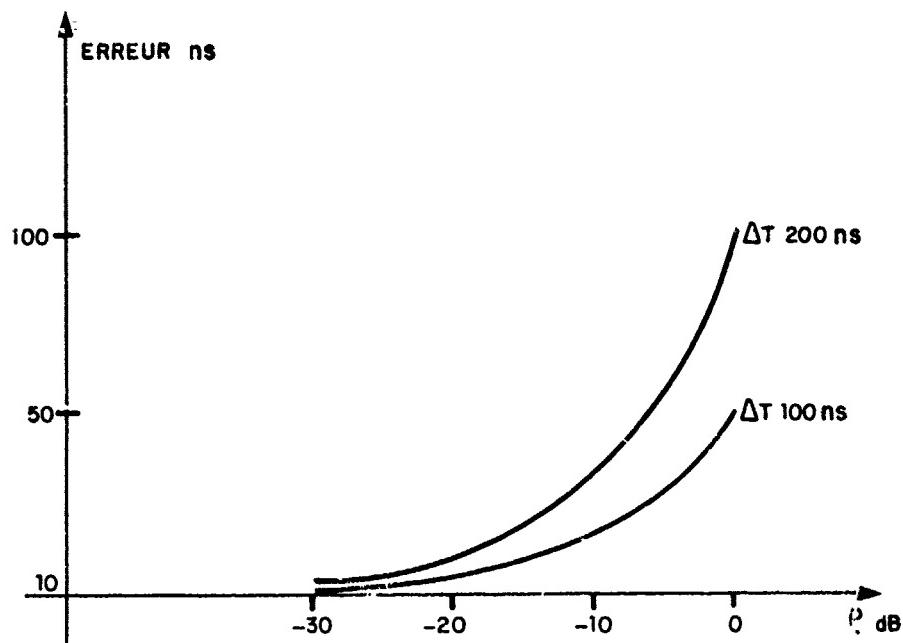
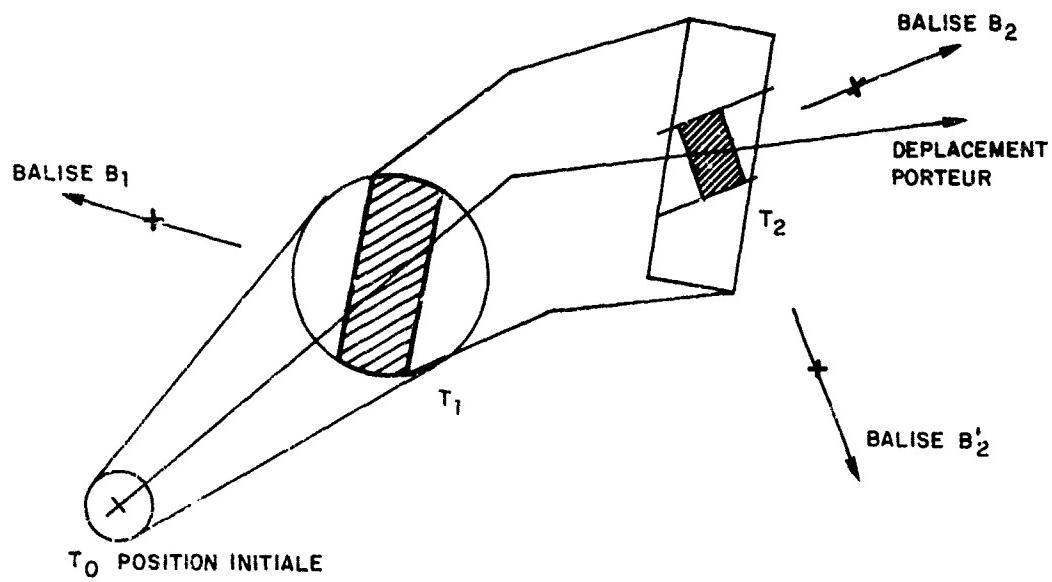
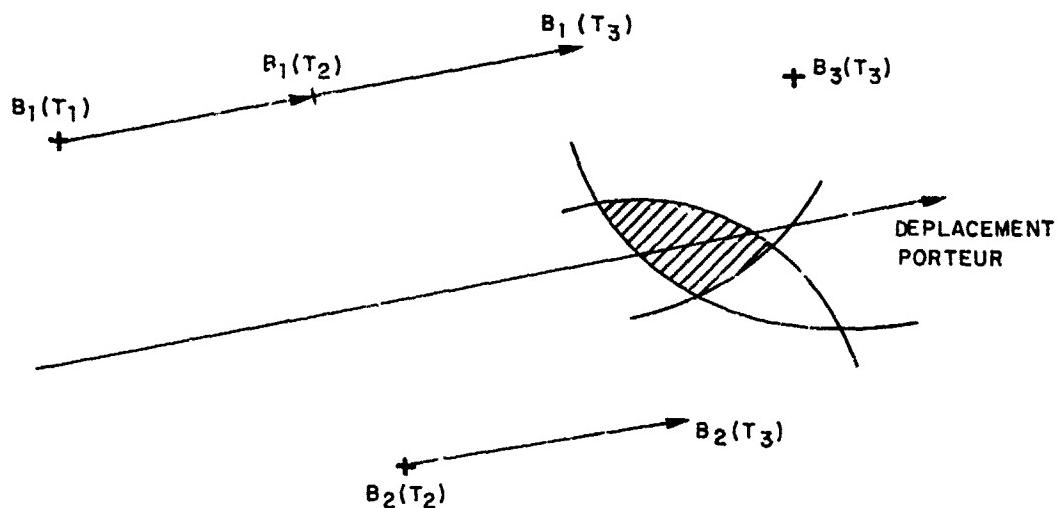


Fig.11 Effets des multitrajets



(a) - INITIALISATION



(b) - INITIALISATION

Fig.12 Algorithme de navigation

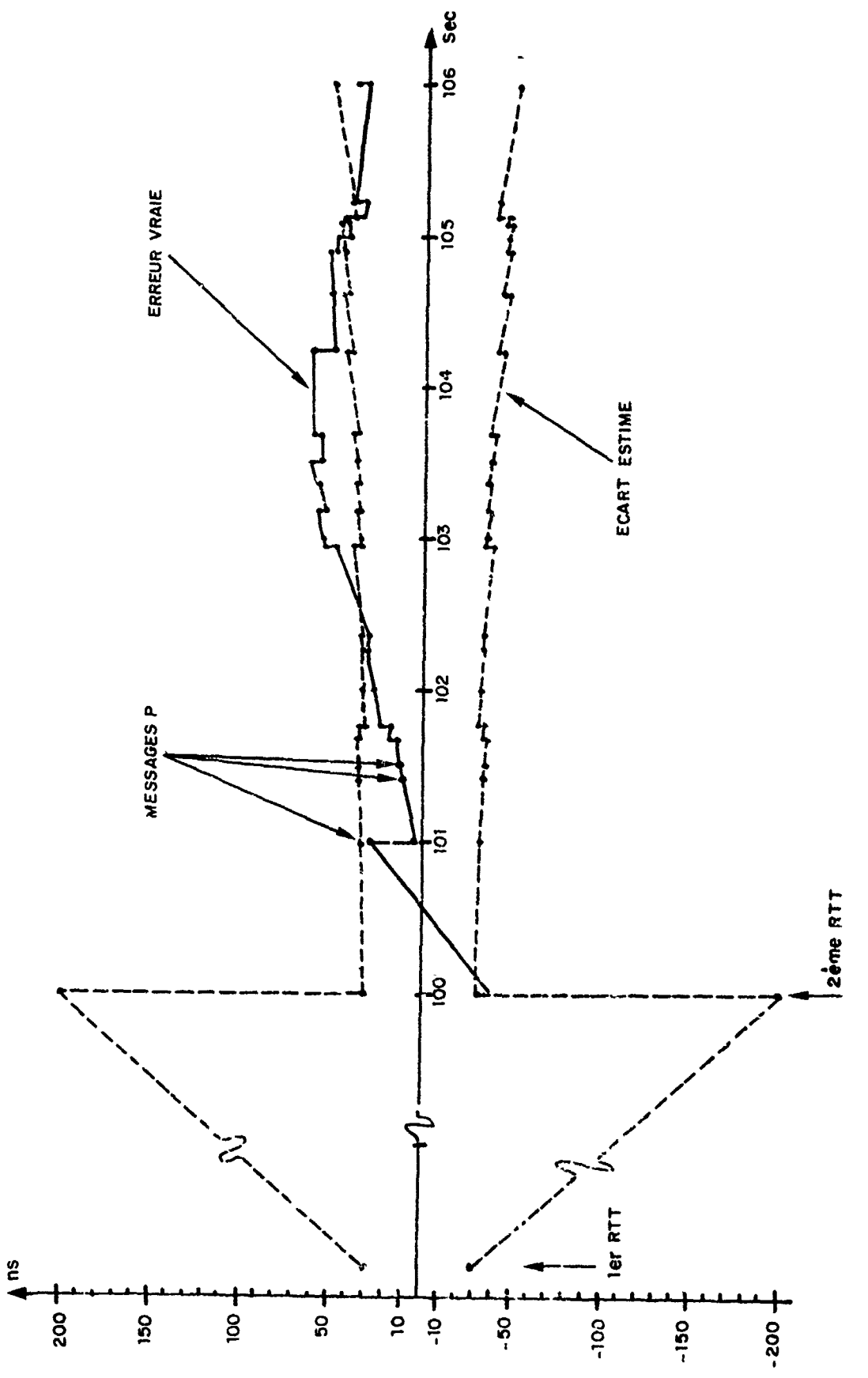


Fig.13 Erreur de synchronisation (horloge à 10^{-8})

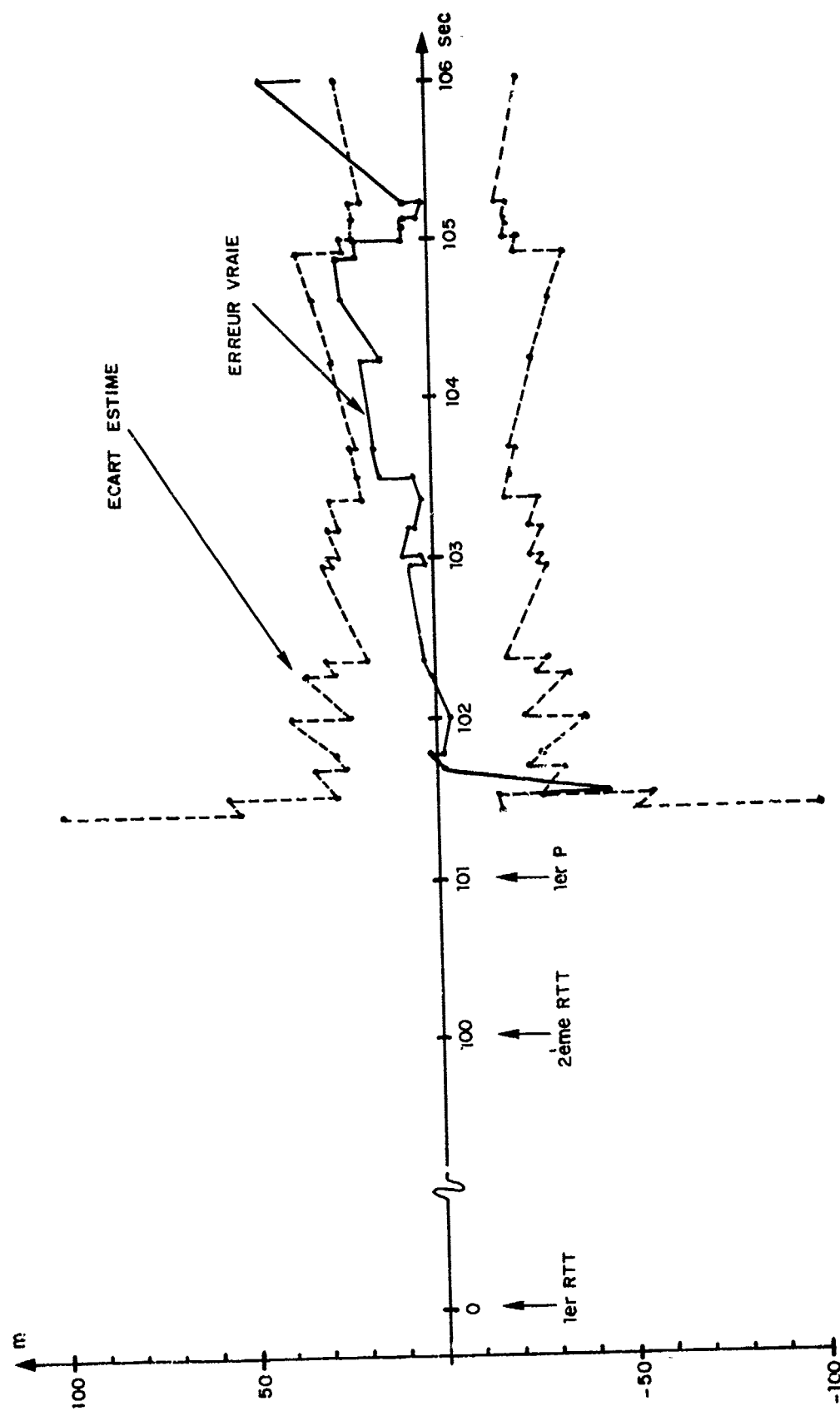


Fig.14. Erreur de position

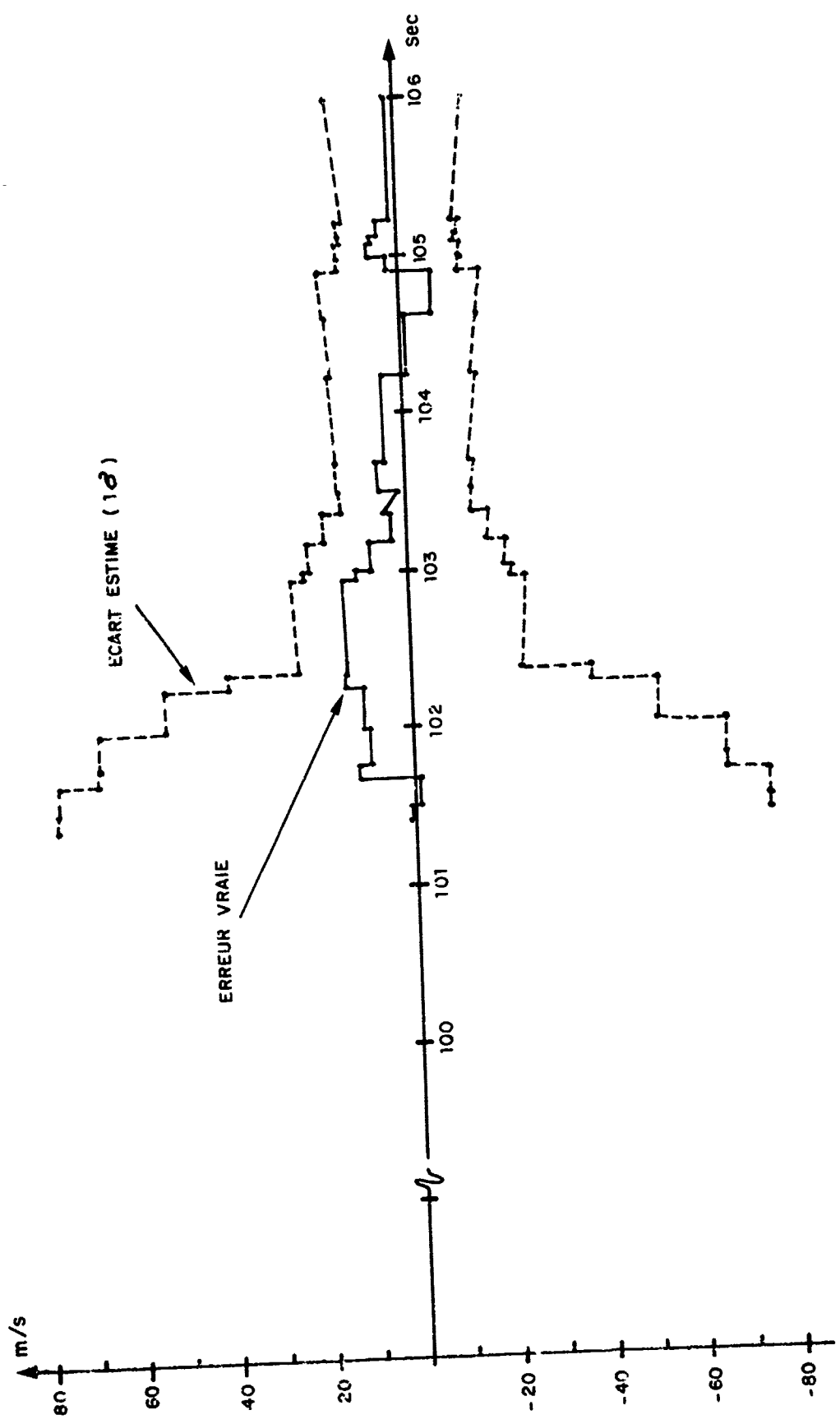


Fig.15 Erreur de vitesse (nord)

SINTAC AND ITS POSITIONING PERFORMANCES

by

Lj. MILOSEVIC
 Director at the Electronic Systems Division
 THOMSON-CSF
 116, avenue Aristide Briand
 92220 BAGNEUX
 FRANCE

and

JC. CHARAVIT
 Engineer at the Electronic Systems Division
 THOMSON-CSF

M. RONSIN
 Engineer at the Telecommunications Division
 THOMSON-CSF
 66, rue du Fossé Blanc
 92231 GENNEVILLIERS
 FRANCE

SUMMARY

After a short review of the SINTAC program, the information processing when the terminal is used in the navigation mode is described :
 The receiver of the SINTAC terminal provides a serie of distance information. It is shown that the major hardware errors are related with the terminal master oscillator and the interval between synchronization.
 The navigation processor includes a KALMANN filter which smoothes these data and reduces them using the craft bearing and the air data.
 Using the hardware limitation and the KALMANN algorithm, the results of the simulation program are given. The navigation errors are in accordance with the forecast. They are within 20 meters when the distance measurements occur with an average of 1 second. Such period being representative of the medium traffic. The goal was to show the performance achievable with the minimal system always available aboard an aircraft. When INS is added, these results could only be better and the requirement for active synchronization decreased.

1. INTRODUCTION

The SINTAC program is currently in the exploratory phase of JTIDS - interoperable SINTAC-2 which consist of 3 phases :

The first study phase is currently at its final stage. Its purpose was essentially to modify the transmission format to obtain SINTAC/JTIDS interoperability and to develop a brass-board of the transceiver. This brass-board is the test bench used to verify performances under various jamming and multipath conditions. The second purpose of the brass-board was to test the software associated to various functions (figure 1).

The second phase provides for the development of several advanced development models of SINTAC terminal to be used for flight experiments. This will provide for the verification of :

- operational performances of the software and hardware in the communication, relative navigation and identification functions,
- SINTAC/JTIDS interoperability.

Currently, a few technological developments are carried out on the major points which were evidenced during phase 1

The third phase will begin in 1987 and cover industrial manufacture of the product, leading to series equipment deliveries in 1987. It is currently planned to develop several terminal classes using, whenever possible, common modules, the software and physical aspects being adapted to each specific requirement.

This program could be modified according to the SINTAC-3 concept development currently under review.

2. GENERAL

In the SINTAC system, navigation is based on the measurement of distances between the various terminals of a group of users. This process has several major features as regards localization accuracy :

- the distances are not measured directly. Each user determines the distances from the measurement of the Time of Arrival (TOA) of an identifiable event generated by another terminal whose position is known.
- distance measurement is not continuous. Measurements are performed with a variable periodicity, up to 10/12 seconds.
- between 2 measurements, the user works on an estimate basis with a more or less complex algorithm according to the carrier velocity and to the available estimation facilities.
- references used for localization purposes can be fixed or mobile (e.g. relative navigation). The identifiable event can carry two types of inaccuracies : transmission time, transmitter position or both.
- finally, the physical environment : not ideal and, like in any other radio-electric system, natural or man-made reflectors generate multipath resulting in error signals.

Thus there are many factors influencing localization accuracy. To simplify the following discussion, these factors have been divided in two groups :

- factors influencing the accuracy of the time arrival of the measurement. These are more particularly related to the equipment performances and include the effects of the environment.
- factors related to the methods applied to use the information. These include the effect of the user terminal software and of the management procedure of the community of users.

3 TIME MEASUREMENT

The time measurement inaccuracies are the result of two factors :

- signal format in space : i.e. the information supplied by the transmitting terminal which may be altered during propagation by the effect of multipaths.
- the equipment used to detect the T.O.A. of the previous signal and the operation mode of this equipment.

3.1. Signal format

Two specific SINTAC messages are used for navigation purposes :

- the "P" or position message transmitted systematically by the participants and the "RTT" message which is a question/answer exchange between two participants.

- in both cases, the preamble is used for a first (coarse) measurement of the T.O.A. This measured value is further refined by the subsequent synchronization pulses which supply the T.O.A. In the experimental equipment of phase 1, the message header and text are not used to measure the T.O.A. These are used indirectly as the two sub-messages contain information useful for the subsequent processing of the T.O.A. :

- . transmitter position and quality indexes of the clocks and of navigation in the case of "P" messages.
- . time of arrival of the interrogation message in the case of the "RTT" answer

All the components of the SINTAC message (preamble, synchronization, header, text) consist of a series of pulses whose significant characteristics - as regards the determination of the T.O.A. - are their number and shape.

The preamble consists of 16 or 32 pulses transmitted over 8 different frequencies. Synchronization consists of 4 or 8 pulses transmitted over 4 or 8 different frequencies.

The fact that these pulses are generated with frequency hops is of little influence on the intrinsic accuracy of the T.O.A. measurement. On the other hand, this characteristic is of importance as regards resistance to multipaths.

Each pulse of a normal duration of 6,4 µs has its spectrum spread by a 5 MHz MSK modulation. The code used for the spreading sequence does not affect accuracy. For the section of the message we are concerned with, the code depends only of the result generated by an encryption box.

This random code is known by the participants who may perform a correlation between the transmitted sequence and the expected sequence. The result of this correlation is a thin pulse (approx. 300 ns at 3 dB), with secondary lobes on either side. This shape determines largely the potential accuracy of the T.O.A. :

It provides for an accuracy which is approximately equal to one tenth of the lobe, i.e. 30 n sec. This number corresponds to the expected results.

3.2. Equipment used

Figure 2 is the functional diagram of the terminal. The system consists of a transmit/receive chain whose operations are driven by a sequencing logic and whose data are processed by a computer.

- Transmitter

The transmitter consists of a modulator followed by a frequency transposition chain and a power amplifier. The modulator performs the C.C.S.K. encoding of the symbols to be transmitted, the encryption of the binary series obtained with a random sequence provided by the encryption box, and the MSK modulation of a carrier.

All the above are wide-band circuits and transit time drifts are considered as non significant in the following part of this document.

- Reception circuits

The reception sub-system consists of the receivers required to detect the preamble and to demodulate the message text.

The receivers are selective and their selectivity causes part of the inaccuracy of the time measurement.

- Frequency synthesizer

The timing logic gives to the frequency synthesizer the frequencies of each symbol and generates the local oscillators required to perform frequency transpositions.

The synthesizer causes no error in the distance measurement process.

- Clock

The clock is driven by a high stability oscillator ; the clock supplies an absolute local time which must be periodically readjusted by a synchronization process with the SINTAC participants ; later, we will show that this is the major cause of errors.

- Synchronization and demodulation circuit

This device performs the following :

- . detection of the preamble of the message to be received by a correlation of the signals from the receivers tuned to the preamble frequencies. This detection process provides the relative time with an accuracy of roughly 100 ns.

- . improvement of the knowledge of the relative time by the fine synchronization and T.O.A. read circuits.
- . information extraction, error detection and correction.

This circuit is significant in the measurement of distances.
Sequencing and data processing.

The message processing system receives the message to be coded from the computer or the coded message from the receiver

The unit performs routine operations :

- encoding, decoding, interleaving, storage, etc...

The encryption box generates the pseudo-random sequences required to select frequencies, codes and, generally, all the random factors used in the transmission format.

The sequencing logic receives from the computer a series of orders defining the terminal function and controls the activation of all the previous sub-assemblies.

All the above devices have no influence on distance accuracy.

- Computer system

The computer system performs the following tasks :

- a) - management of exchanges with external devices :
- b) - management of function procedures :

- . entry to network,
- . synchronization,
- . localization,
- . identification,
- . communications ...

- c) - terminal operation checking.

Thus, the computer performs all processing actions on the "coarse distance" information from the demodulation circuit. Thus, the computer has a direct influence on the localization accuracy.

3.3. Detection method used

In every case, the equipment determines the event arrival (T.O.A.) with respect to the beginning of the time-slot.

Message preamble detection is performed by a circuit including programmable correlators and delay lines.

The sum of the correlated signals provides for the detection of the presence of a preamble indicating a message, and the initialization of the fine synchronization process.

The SINTAC receiver uses digital correlators and sampling is done at the rate of 200 ns. During preamble detection, the sampling clock phase is undetermined with respect to the transmitting terminal phase (figure 3).

Compared with respect to the signal supplied by an analogic correlation, the digitized signal has a 200 ns quantum introducing the same uncertainty over the preamble detection time provided of the threshold device.

The function of the fine synchronization device is to set the sampling clock phase over the center of the correlator output signal. In the phase 1 equipment, there are four pulses in the synchronization sub-message. For each pulse, the phase error is evaluated by a two channel correlator, by means of an advance/lag process with $\Delta = T/2$ phase difference : when the phase setting is correct, the amplitude of samples at $\pm T/2$ and $\mp T/2$ are identical. If the amplitudes are not equal, their ratio is used to determine the sign and magnitude of the phase correction to be performed.

Figure 4 shows the synoptic diagram of the fine synchronization device.

The two channel correlator is sampled at the frequency of a 5 MHz clock whose phase can be varied by the presetting of the D divider. The presetting is supplied by the content of an accumulator representing the phase correction. This correlation is a function of the difference read during the last sampling operation between the correlator signal and the clock phase. The correlator supplies the amplitudes of the samples at $\pm T/2$ and the correction logic determines the phase variation to be applied as a function of these amplitudes and of the correction algorithm selected.

The beginning of the time-slot initializes the counter C which is driven by a fast clock (80 MHz) and which defines the time passed with a 12,5 ns quantum.

The counter is stopped by the acquisition of the preamble and indicates the time of arrival in the time-slot with an uncertainty of about 200 ns.

Simultaneously, the arrival of the preamble resets the accumulator, the divisor (D) and the timing logic.

After the sampling of each synchronization pulse, the accumulator content is changed.

After the pulse train, the content (N) of the counter and the content (ΔN) of the accumulator represent the corrected value of the message T.O.A. For the phase 2 advanced models, an improvement is considered to allow this device to track synchronization on the header pulse.

3.4. Accuracy of the T.O.A. measurement

Accuracy of T.O.A. is influenced by the following factors illustrated on figure 5 :

- filtering unit : causing a time - delay according to environment conditions.
- amplification chain : the transit time of the associated limiter depend on the signal level.

The preamble detection device consists of delay lines and of a threshold detector.

The lag being inserted numerically, its long term stability depends only on the clock stability. The threshold detector introduces a quantization and a noise depending on the S/N ratio, i.e. on the signal level. We will see that errors introduced during detection are lowered by the fine synchronization.

- The accuracy of the synchronization device depends on the following : number of synchronization pulses available, processing algorithm used, inaccuracy on the time of beginning of the T.O.A., clock signal drift. This unit also introduces a quantization resulting from the digitization of the process and a noise which, as in the case of acquisition, depends on the signal level.

3.4.1. Effect of filtering

This effect increases when the bandwidth of the filter decreases.

Consequently, the attention is drawn on intermediate frequency filters and on the video frequency filter.

The I.F. filtering consists of a 3 MHz Bessel type bandpass filter introducing a time delay of about 150 ns.

Thus, a 5% variation of the bandwidth caused by long term drifts (environment, aging) results in about ± 6 ns variation of the transit time.

The centering of the filter with respect to its nominal frequency is not significant on the transit time drift.

After being detected, the video signal is filtered by a 5 MHz low-pass filter causing a 60 ns delay.

A 5% variation of the cut-off frequency also introduces a 3 ns drift.

The overall effect of filtering is thus represented by a possible drift of ± 10 ns. However, we must mention the effect of the IFF rejection filter which will add an additional effect (remaining low due to the frequency hop) on the adjacent frequencies.

3.4.2. Effect of limitation

Figure 6 illustrates the results of the measurements carried out on the limiter amplifier of the SINTAC brass-board. The phase drift is about 20°, which corresponds to a variation of the transit time smaller than a nanosecond.

3.4.3. Effect of the delay line

The duration of the preamble is 416 μ s. The delay between the first and last pulses results from a shift register driven by the terminal clock.

Even with a minimum stability of 10^{-6} , the drift on the added lag remains negligible.

In addition, the numerical device being synchronous, there is no accumulation of propagation time drifts in the logical circuits used.

3.4.4. Effect of the threshold detector

The "coarse" time of the arrival of the preamble (before the correction by the fine synchronization) is influenced by the S/N ratio value at the time of information digitization. Thus, for the proper operation of the subsequent interpolation performed by the synchronization unit, the noise must remain small with respect to the 200 ns quantization. Otherwise, we could have on step/increment error on the time of arrival.

At its range limit, the receiver operates with a 12 dB E/N₀ ratio.

For a threshold at mid-amplitude, the jitter of the passage time of an individual pulse will reach 40 ns at 1 σ , assuming a 200 ns instantaneous rise time.

The noise of the 16 or 32 preamble pulses being decorrelated, the jitter on the T.O.A. preamble is decreased in a 4 to 6 ratio, thus meeting the above requirement.

3.4.5. Synchronization unit

- Effect of noise and algorithm

The noise results from the transmission features which determine the E/N₀ ratio, and of the quantization for the digital correlation.

In the phase 1 experimental equipment, quantization is done with 3 bits and corresponds to a jitter with a magnitude similar to the one caused by E/N₀ at the limit of the range.

The algorithm used applies a partial correction after each processed pulse.

Figure 7 illustrates the evolution of the error measured with the current device with respect to the rank of the pulse received.

The figure shows that for a systematic offset of 100 ns, the four synchronization pulses leave a significant error. Note also that quantization is comparable to thermal noise and that together these cause an error of about 20 ns at 1 σ . In practice, when the initial acquisition error fluctuates, the algorithm lowers the dispersion to about ± 20 ns approximately after the 4th pulse, i.e. corresponding to a value of about 10 ns at 1 σ . These errors are summarized on figure 8.

- Effect of the clock

The clock consists of an oscillator driving a chain of cascaded counters. The elapsed time counted comprises an error which depends on the uncertainty on the long term behaviour of the oscillator ; this parameter usually includes the tolerance of the nominal frequency, the effect of aging and the impact of the thermal environment.

For example, in the case of an oscillator with a 10^{-7} accuracy for a period of several months, i.e. a

good performance for on board equipment, we see that the error affecting the measurement of time is 100 ns for each second elapsed since the time reference. There are three possibilities to decrease this error :

- increase the accuracy of the oscillator,
- reset more frequently the time counting chain,
- evaluate and account the short term drift of the oscillator.

The first action only switches the problem to the component at the price of an increase of volume and cost and also to the verification instruments.

The combination of the two other possibilities is much more efficient when accounting for the capabilities of the equipment used with the oscillator (see figure 9).

Resetting of the time counting chain is performed when the information from the best synchronized participants provides for the computation of the synchronization error.

This can be carried out by an RTT exchange or with several P messages from the participants, knowing their position with an accuracy compatible with their synchronization error.

During an RTT exchange, the participant measures the message time of arrival and retransmits this indication in its reply transmitted at a known time. Thus, the interrogator has a set of equations whose solution gives the time offset.

The RTT exchange, being generally limited to a periodicity of 100 secs, time resetting itself is insufficient. The velocity of the oscillator short term drift must be taken into account.

This drift calculation can be effected after 2 RTT exchanges and updated at each successive exchange. The correction giving the drift velocity can be used until the following exchange. It is thus possible to improve the knowledge of the time by one or two orders of magnitude, according to the complexity of the algorithm used.

The resulting distance accuracy is summarized on the table of figure 10.

Thus, it appears that the clock is most significant factor and that its quality will be determined by the accuracy required for the T.O.A. and by the possible constraints of radio silence.

It must be noted that the frequency of the oscillator driving the clock causes a quantization on the measurement of time. With an 80 MHz counting, the above factor becomes negligible.

3.5. Effect of multipaths

In a fixed frequency link and taking into account :

- message duration,
- receiver motion velocity

the phases of the multipaths affecting each of the pulses of a message are correlated and this results in an interference. On the contrary hand, the frequency hop decorrelates these phases and that is favorable as it provides for an average of the instantaneous errors caused by the multipath.

The multipath interferes when it becomes impossible to discriminate between the direct path and the reflected wave.

Time is the best factor to use to perform this discrimination, the direct path signal being always ahead of the reflected signal.

This discrimination remains possible as long as the two correlation peaks are separated by 300 ns at least. Under these phase circumstances, the only effect of the interfering path is a decrease of the primary signal amplitude, with no effect on the measured T.O.A.

When the path difference reduces the separation to less than 300 ns, the two correlation peaks can no longer be discriminated. The center of gravity of the composite signal being different from the direct signal center of gravity, an error condition occurs.

As a first approximation for a reflected path with a Δt delay and a P level, the displacement is of the following form :

$$\epsilon = \Delta t \times \frac{P}{1 + P}$$

The resulting error is shown on figure 11 as a function of the level of the reflected signal. It must be noted that for a -10 dB level representing a usual value, the error on the TOA is 50 ns.

4. INFLUENCE OF NAVIGATION ALGORITHMS

The arrival times of messages extracted from the synchronization circuits supply instantaneous distances between moving terminals.

The localization of a terminal is an absolute or relative reference requires distance processing taking into account :

- transmitter positions,
- time elapsed since message reception,
- uncertainty on terminal movements.

The accuracy of localization will increase if all the information supplied by the other navigation facilities are taken into consideration - Carrier equipment is variable but there are always minimum navigation facilities which must be used in the best possible way, in order to improve localization performance characteristics at the lowest possible cost.

In addition to SINTAC information, the processing algorithm used takes into account :

- air data aircraft course,
- distances travelled and course for vehicles and ships.

The results shown concern the aircraft program.

4.1. Principle of localization with filtering

This principle is illustrated on figure 12 ; for the sake of simplicity, navigation is only considered on a single plane.

The terminal is initially aware of its position with a given uncertainty. As it moves, the terminal would suffer from an increasing position uncertainty if it could only use autonomous navigation facilities.

On the other hand, each external distance information supplied by the SINTAC equipment results in a lesser uncertainty as regards its position in the transmitter indication.

The participants being in any position, the different successive indications and the uncertainty polygon is progressively reduced until it is limited by the accuracy of the most accurate localization facility available.

The process initialization requires the introduction of the terminal position ; this is generally possible at the start of the mission. Otherwise, the conventional localization method used consists in estimating the carrier motion in order to report the position of beacons successively detected.

A first localization is obtained by intersecting the indications of the third beacon with those obtained by the position report of the two first beacons.

4.2. Data for processing

The data available comprise those from the SINTAC community and the air data.

The SINTAC community provides two types of data :

- P messages and RTT messages.

The P messages are position messages transmitted by each participant at the rate of one message per second for the aircraft or one message every two seconds for the ground stations. Each terminal selects randomly one time-slot among the twenty allocated each second to transmit these messages.

In a given time-slot, a listening terminal will receive the transmission of the closest terminal.

In addition to distance measurement, a P message provides the transmitter position and estimated accuracy of the position and synchronization.

The two indications allow the receiving terminal to take into account (or not take into account) the distance information, considering its own uncertainties.

The RTT message in an exchange with a participant whose location is better than the requestor's. The RTT exchange is triggered by the localization algorithm according to requirements and at a rate lower than 100 seconds. The exchange provides the synchronization error between the two participants.

The other data considered are the course and the air data including :

- barometric altitude,
- drift,
- air velocity,
- vertical velocity.

For modelization purposes, each of the above has been simulated to appear with the appropriate rate, nominal value and errors.

The ground environment must also be modeled. The shape of the earth is shown as an ellipsoid and wind effects are taken into account by a model with wind bursts.

Localization can be effected :

- absolutely, in the earth coordinates referential,
- relatively, with respect to a terminal designated as primary local reference.

In this case, the coordinate grid is centered on the terminal and its orientation effected with another terminal designed as secondary reference because we have decided that the inertia device would be considered.

4.3. Data processing

The algorithm used is the KALMANN filtering algorithm. System status is represented by an 11 - dimension vector as follows :

- absolute position : longitude, latitude, altitude
- relative position : relative coordinates, East and North,
- north alignment error of the relative grid,
- displacement velocity : vertical, north and east velocities,
- synchronization error : setting error and drift velocity,
- wind effect : north velocity and east velocity

Observations providing for the fine adjustment of system status are the 8 following measurements :

- the T.O.A. which can be used either in the absolute or in the relative reference system
- altitude,
- course and drift,
- velocities : own and vertical,
- synchronization error,
- synchronization drift.

4.4. Results

The results are illustrated on figures 13, 14 and 15. Figure 13 illustrates the evolution of the synchronization error, figure 14 shows the evolution of the position error and the evolution of the velocity error is

shown on figure 15.

The operational environment of this case consists of 3 ground stations and 3 stations in circular flight ; the terminal whose parameters are considered moves along straight line, at constant velocity.

It must be noticed that after two RTT exchanges, time synchronism is obtained with an adequate accuracy.

The first P message has no influence on the position error curve as the parameter shown is the half large axis of the position ellipsis : with the first P message, the uncertainty circle becomes an ellipse. A decrease of the error only occurs with the second P message.

It will also be noted (see figure 14) that some P messages have very little influence. Those messages are from an origin which is orthogonal with respect to the large axis of the ellipsis ; it can also be seen, when comparing figure 14 with figure 15, that the drift of the position error is a function of the speed uncertainty.

4.5. Algorithm related problems

The associated software is programmed in 32 bits simple precision, taking into account the facilities which will be used on the final equipment. This result in 7 significant digits, which is low considering the dynamic features of the values to be processed : earth radius compared with localization accuracy.

Thus, the equations have been written in a format compatible with this precision, to avoid masking the useful information by the computation noise.

Some processing problems arise when the accuracy of a new information is significantly better than the one contained in the filter status. To avoid those problems whenever this situation exists, the accuracy of the information is increased by steps. This process results in a two-to-threes-fold increase in the volume of computations but this only occurs after an initialization procedure or after recovering contact.

5. CONCLUSIONS

The results obtained with the simulation process are in accordance with the forecast. The results confirm:

- on one hand, that the improvement of performances is linked to the synchronization which provides the synchronization bias error and, thus, to the position error.

On the other hand, the use of the dead reckoning process is basic for the accuracy of localization in the system. The minimum data are the course and the air data. The inertia system can only improve the results and particularly to increase the autonomy of the system.



Fig.1 SINTAC II mode!

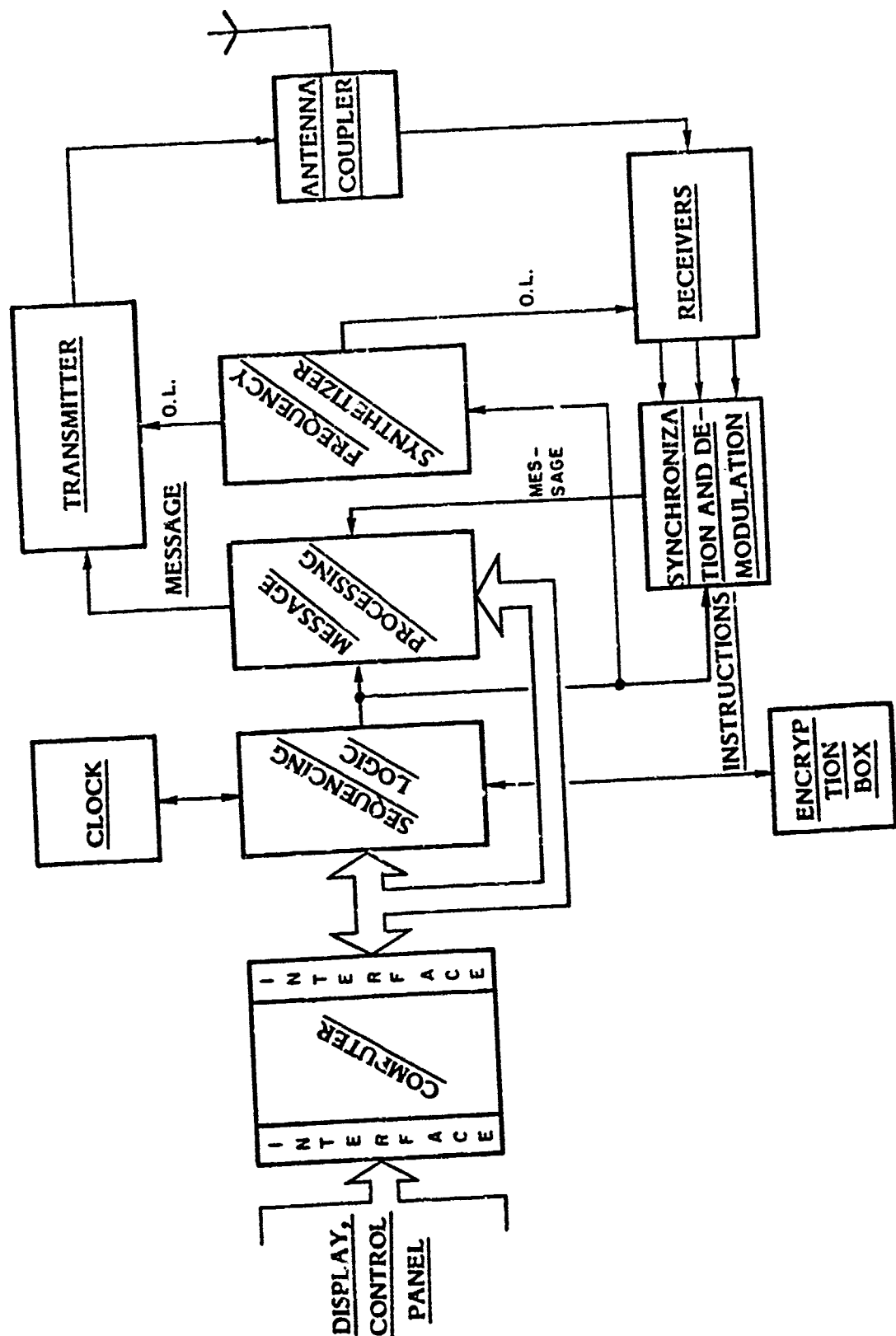


Fig. 2 Functional diagram of the terminal

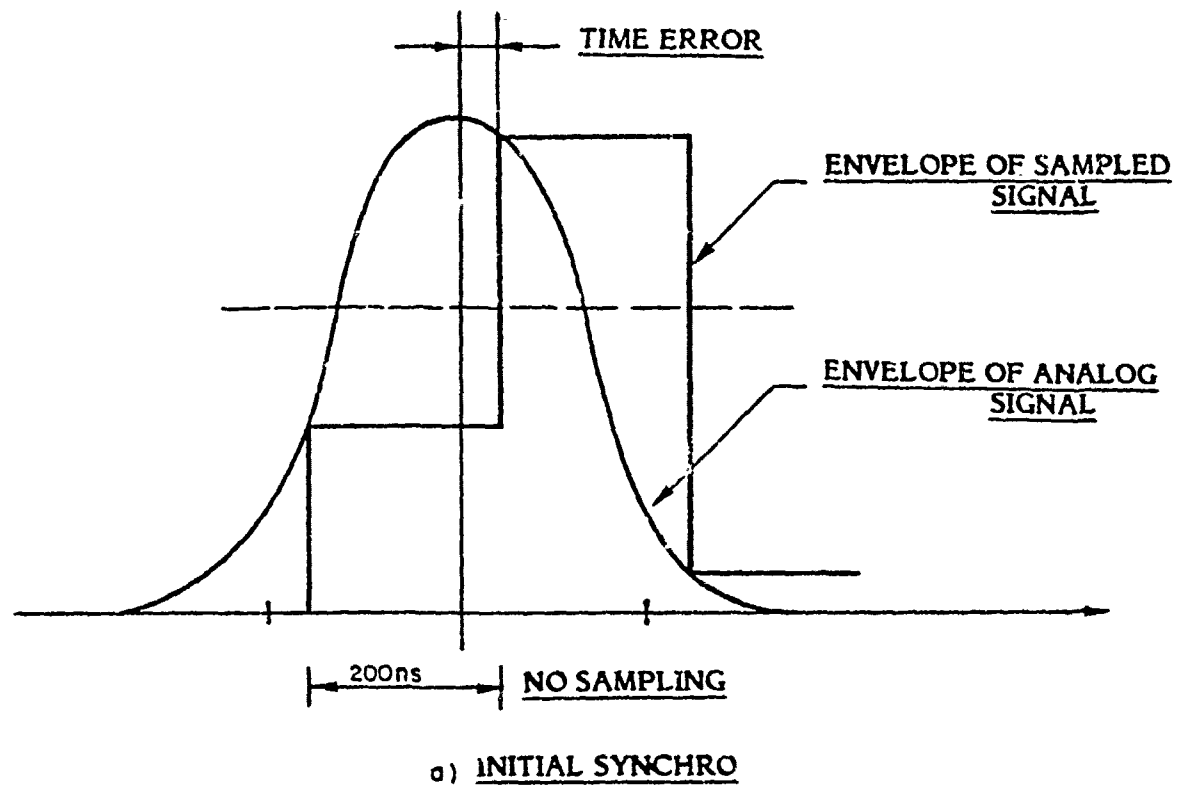
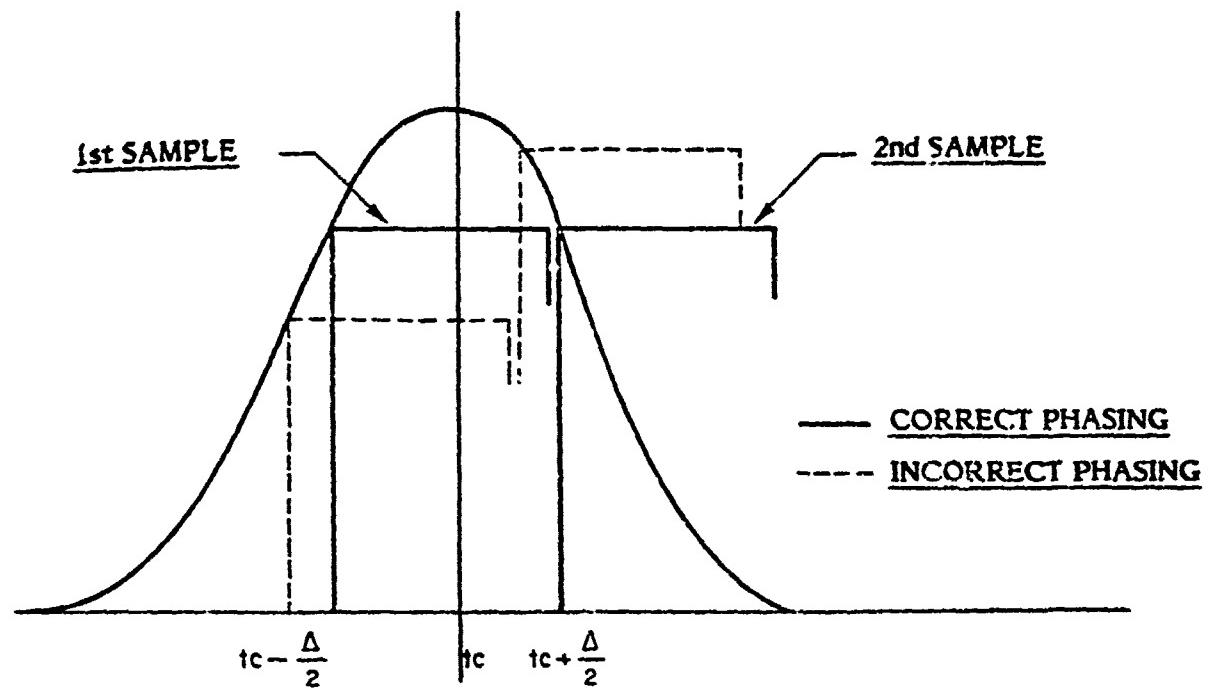
a) INITIAL SYNCHROb) FINE SYNCHRO

Fig.3 Determination of the TOA

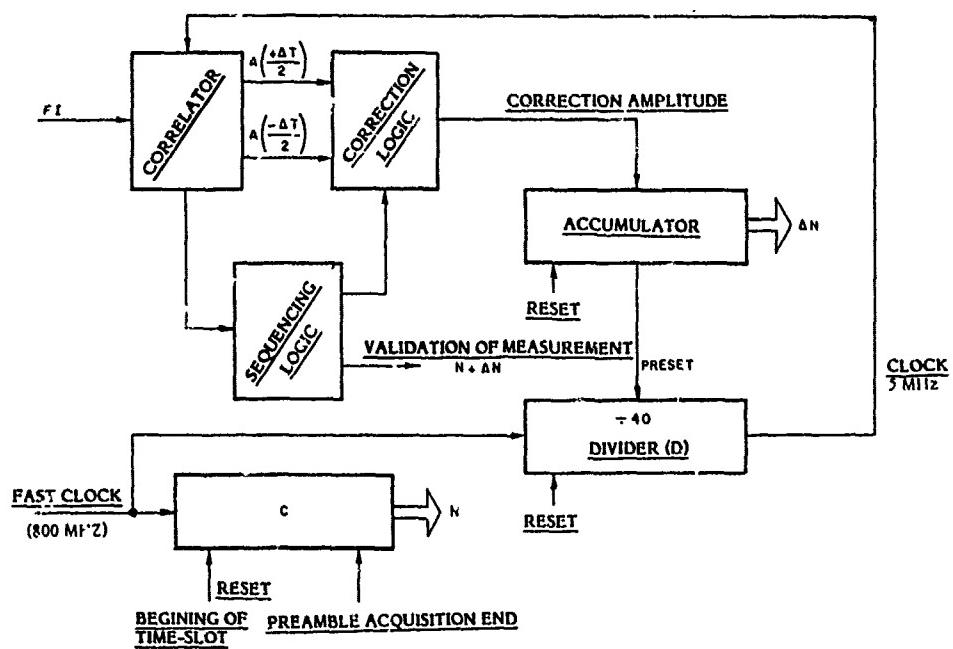


Fig.4 Fine synchronization circuit

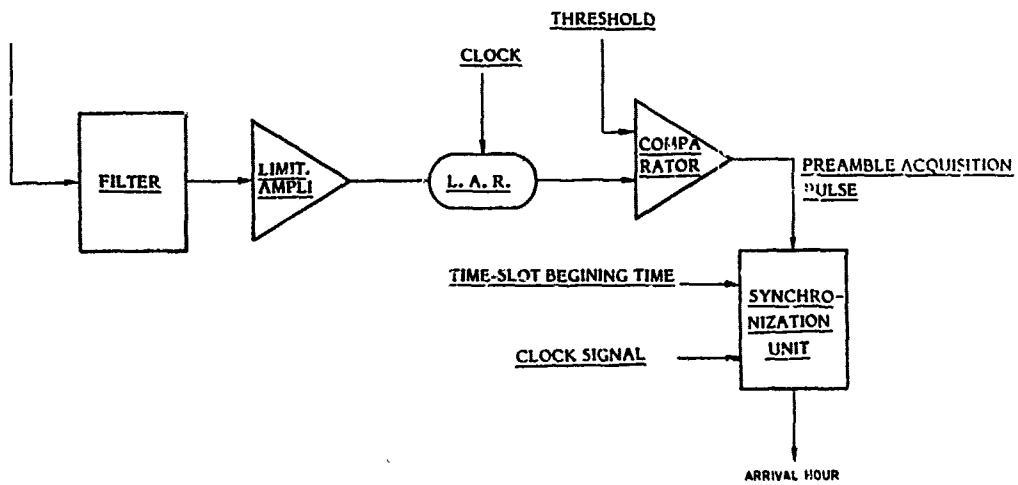


Fig.5 TOA measurement (error factors)

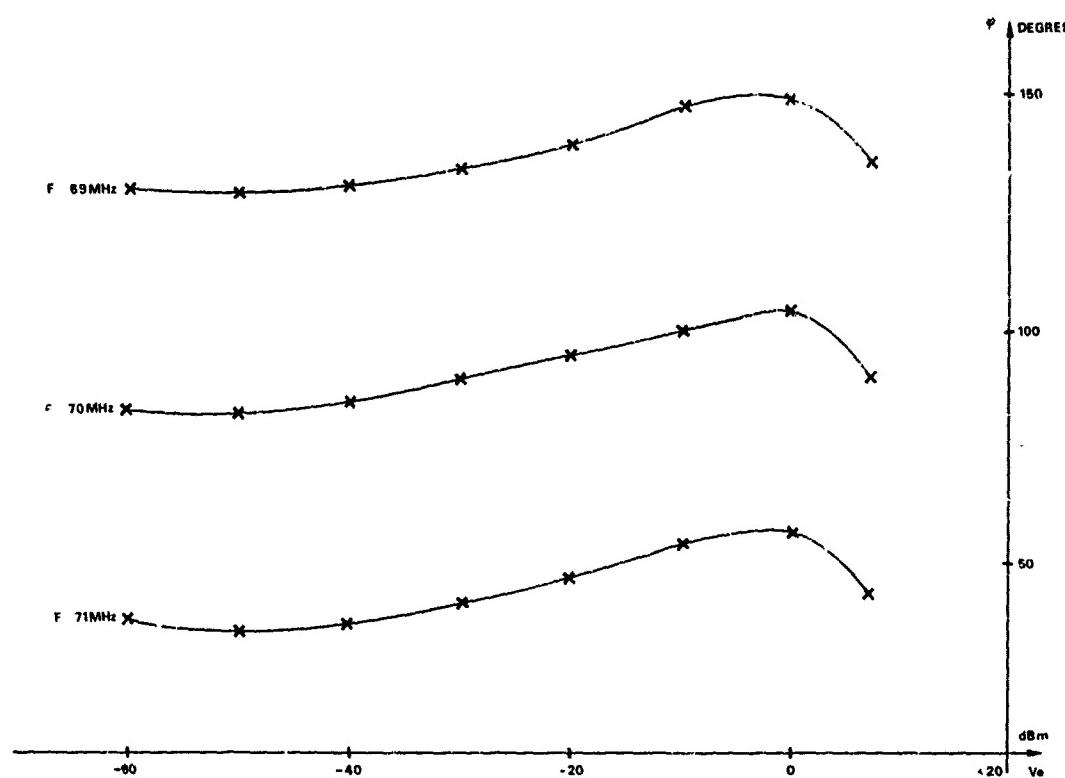


Fig.6 HF level effect

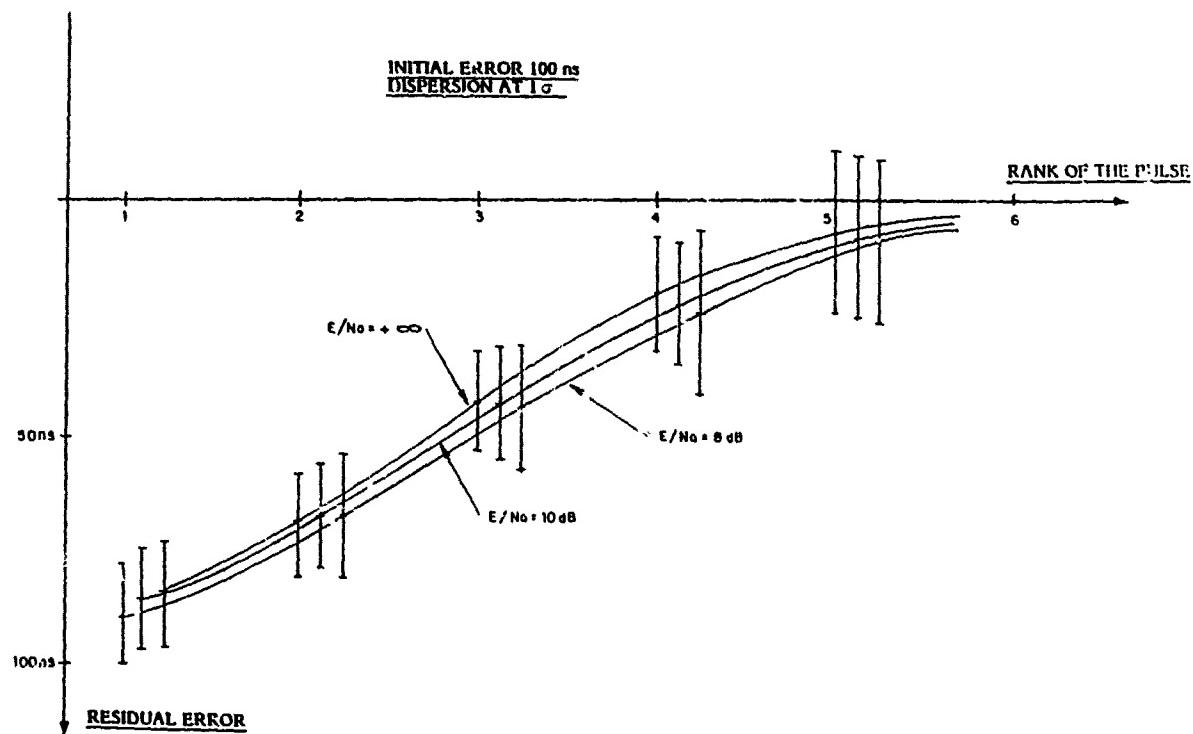


Fig.7 Synchronization algorithm

VALUES (in ns) AT 1 σ	FIXED	FLUCTUATING
EFFECT OF FILTERING	10	
EFFECT OF LIMITER	NOT SIGNIFICANT	
EFFECT OF ACQUISITION	MASK	
EFFECT OF SYNCHRO		
NOISE		20
ALGORITHM		10
TOTAL, OF CLOCK	10	24

Fig.8 Error table (off clock)

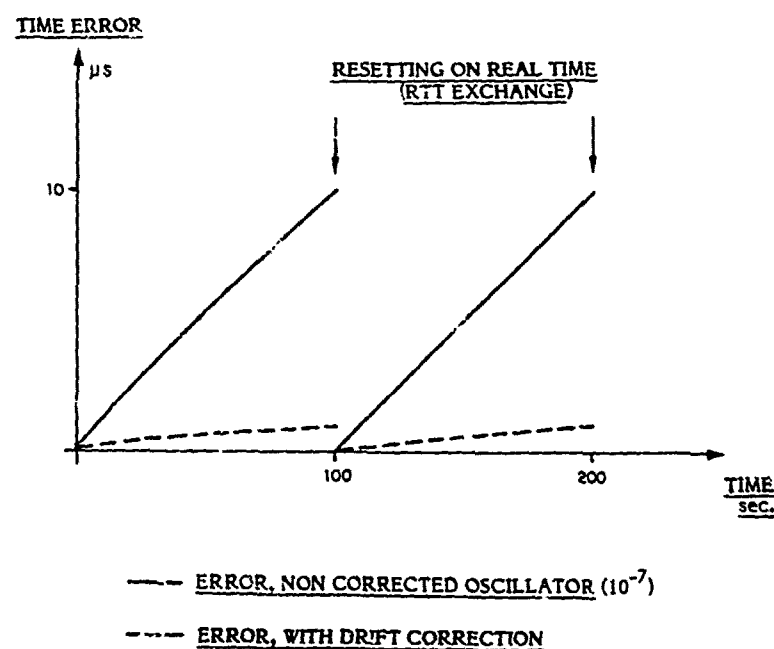
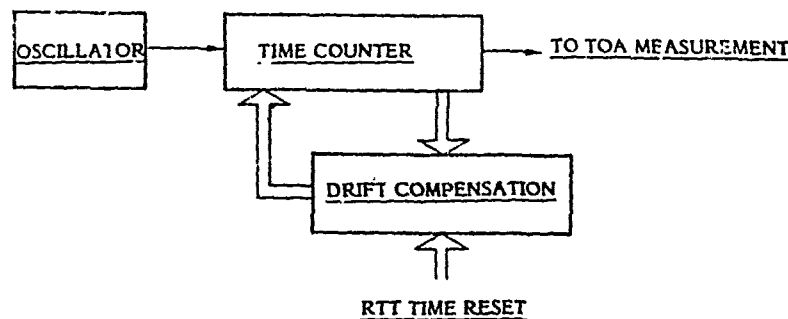


Fig.9 Compensation of oscillator drift

<u>ACCURACY REMAINDER (RTT Exchange)</u>		
T.O.A., INTERROGATION ($\sqrt{10 + 24}$)		26 ns
T.O.A., ANSWER (10 + 24)		34 ns
TOTAL		45 ns

<u>EFFECT OF CLOCK (100 sec. period)</u>		
PILOT A	10^{-8}	10^{-7}
1% COMPENSATED DRIFT	10ns	100ns
10% COMPENSATED DRIFT	100ns	1000ns

Fig.10 TOA overall accuracy

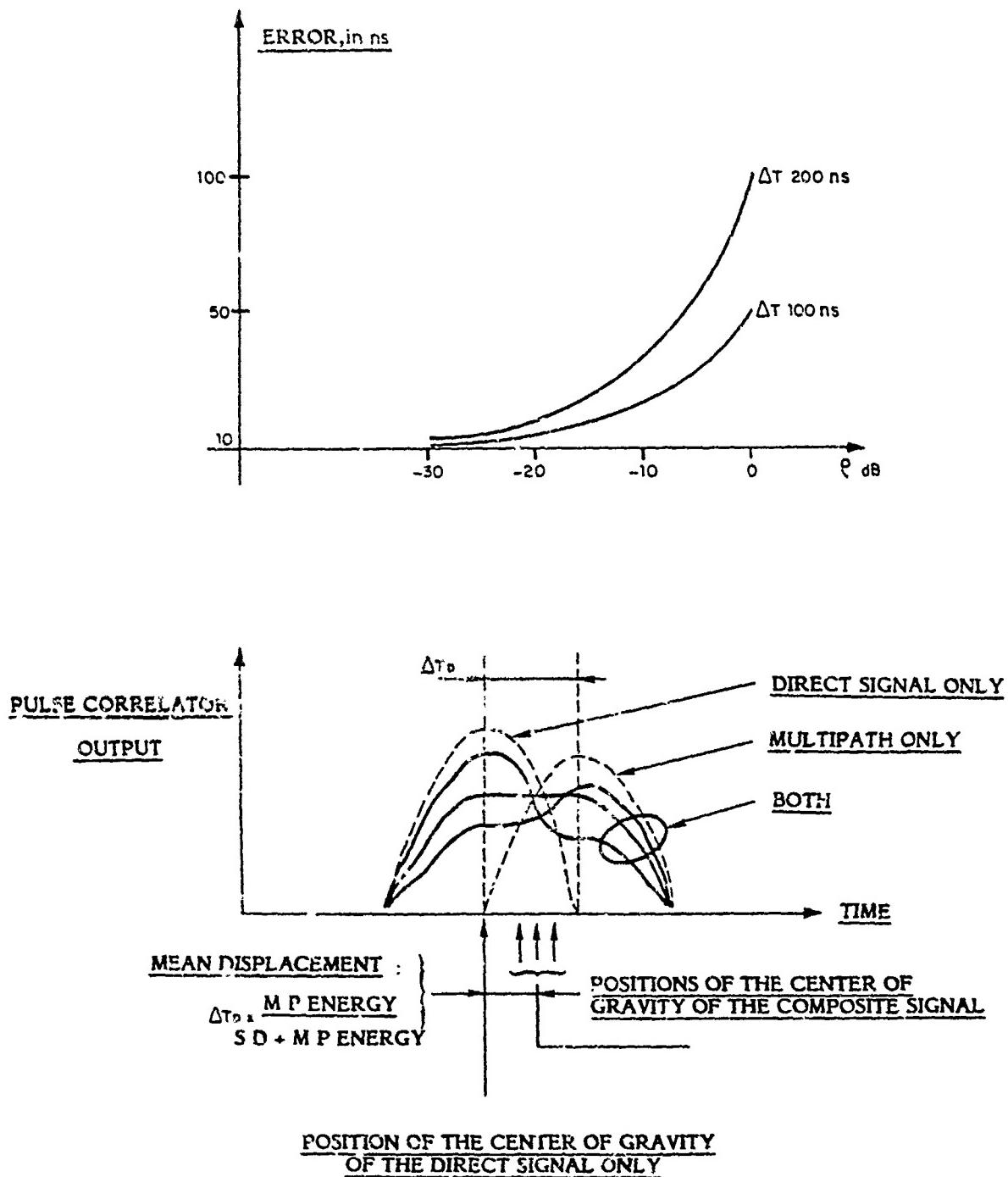
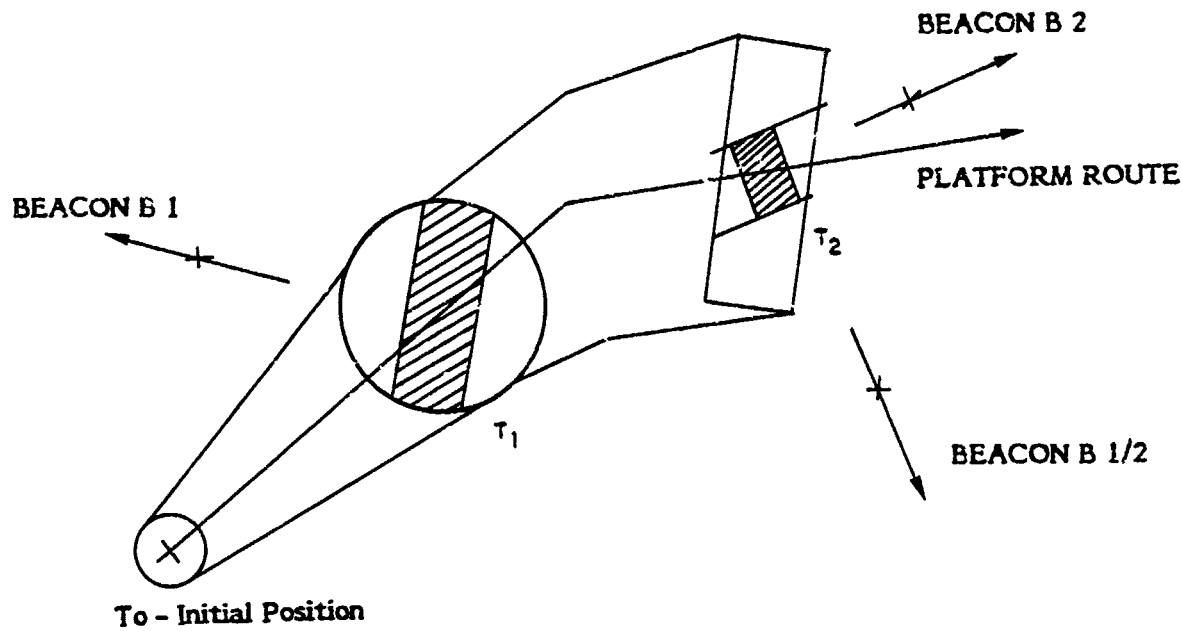
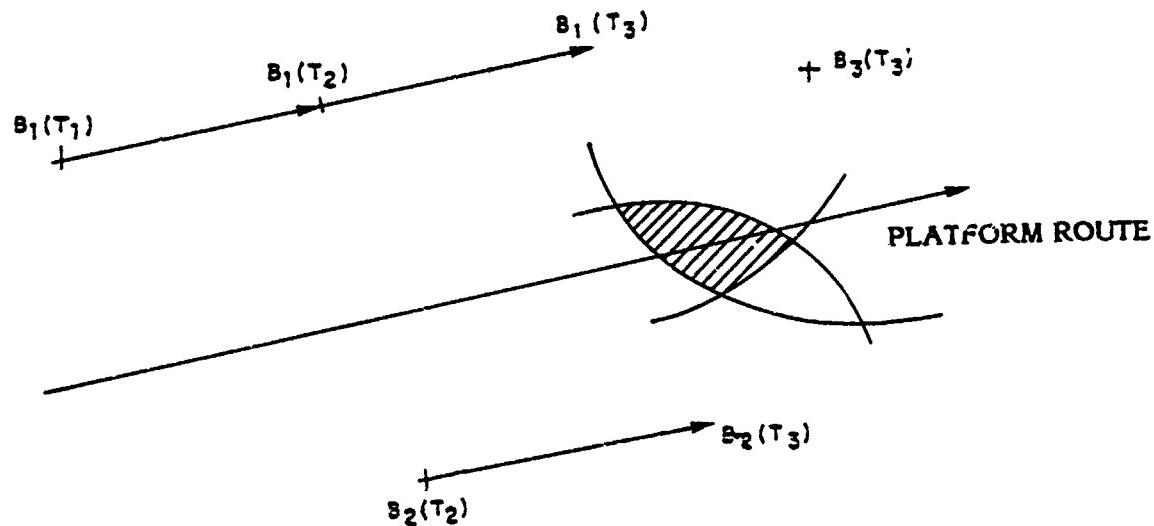


Fig.11 Effect of multipaths

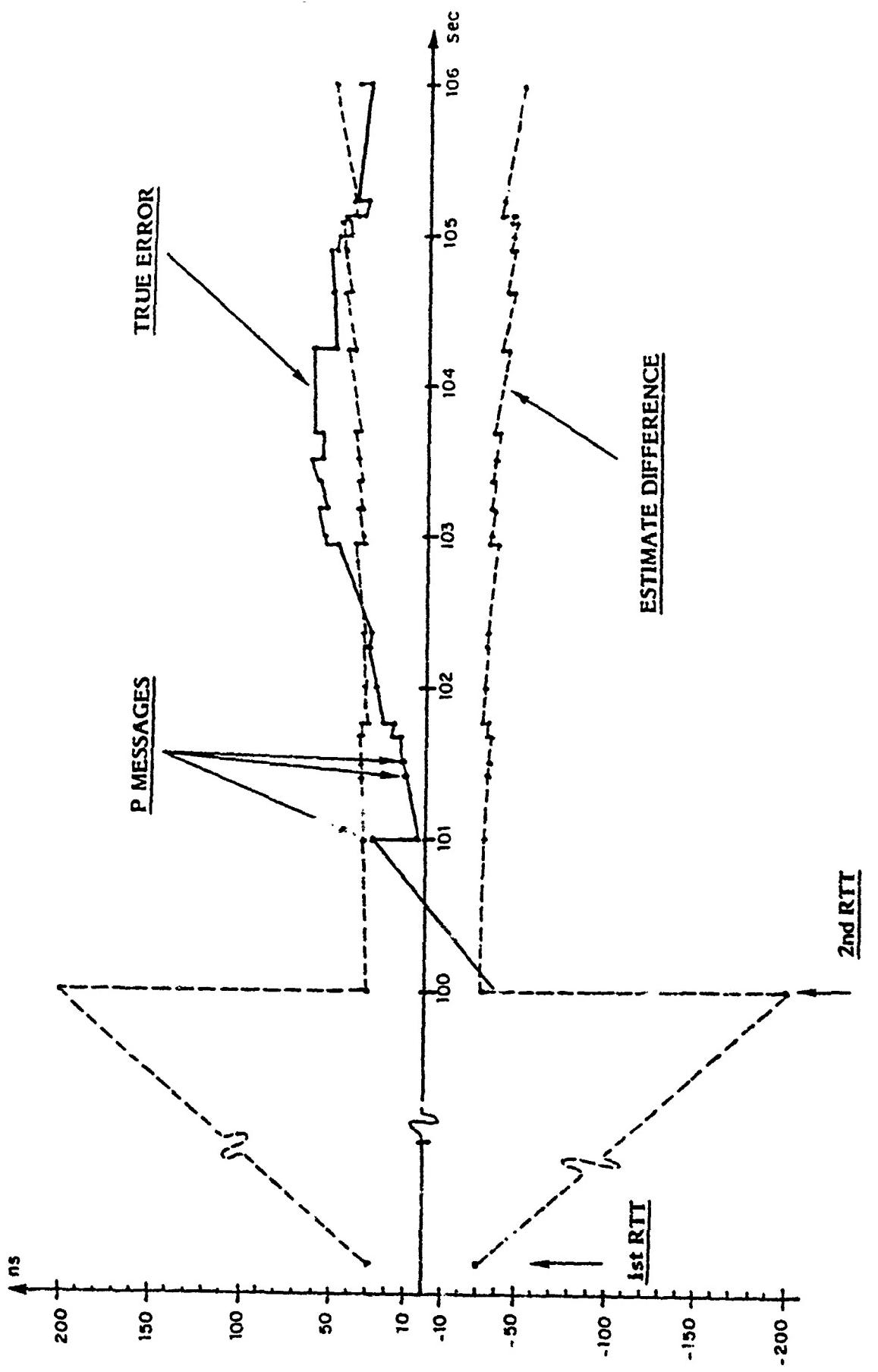


(a)- MAINTAINING



(b)- INITIALISATION

Fig.12 Navigation algorithm

Fig.13 Synchronization error (10^{-8} clock)

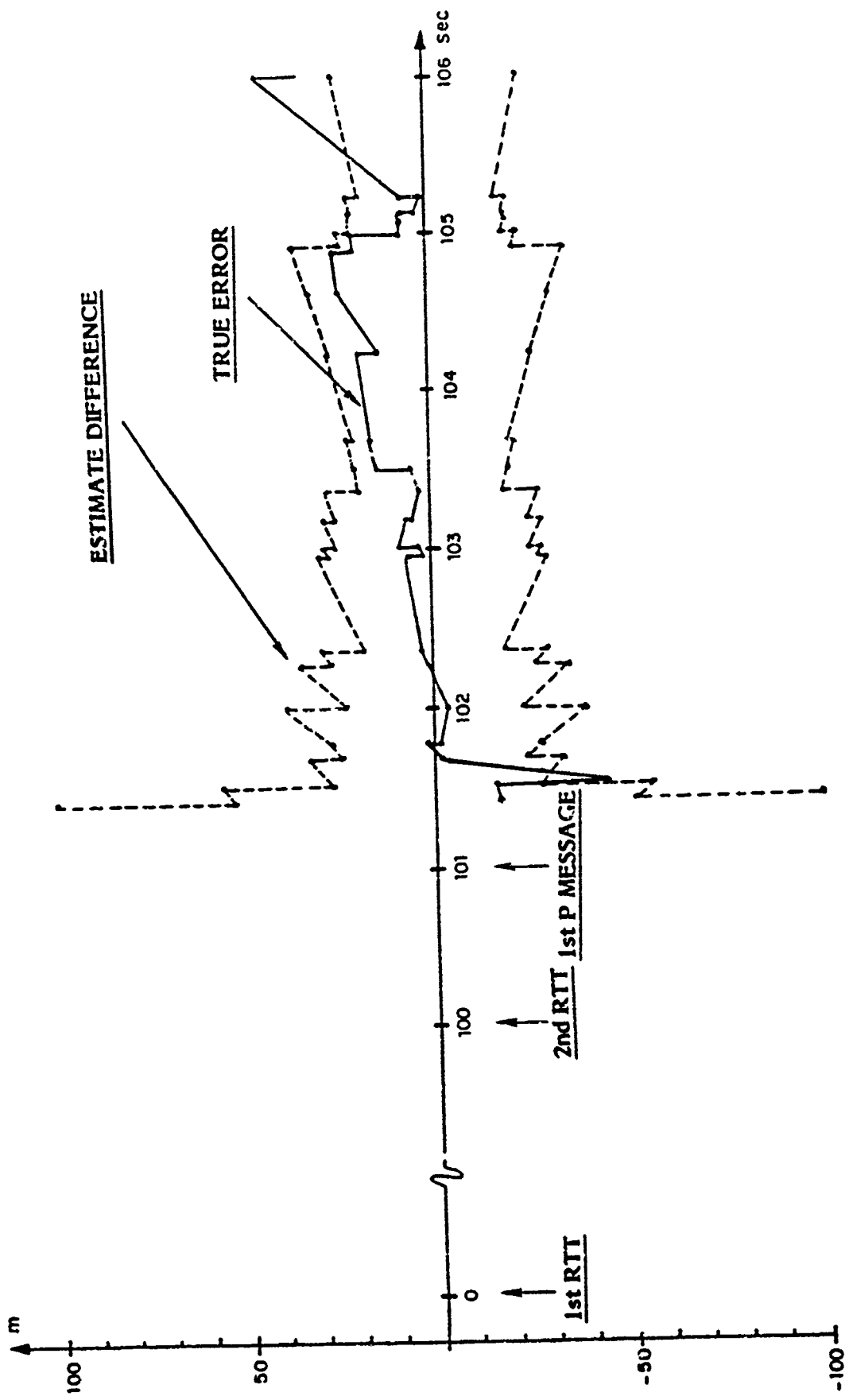


Fig.1-4 Position error

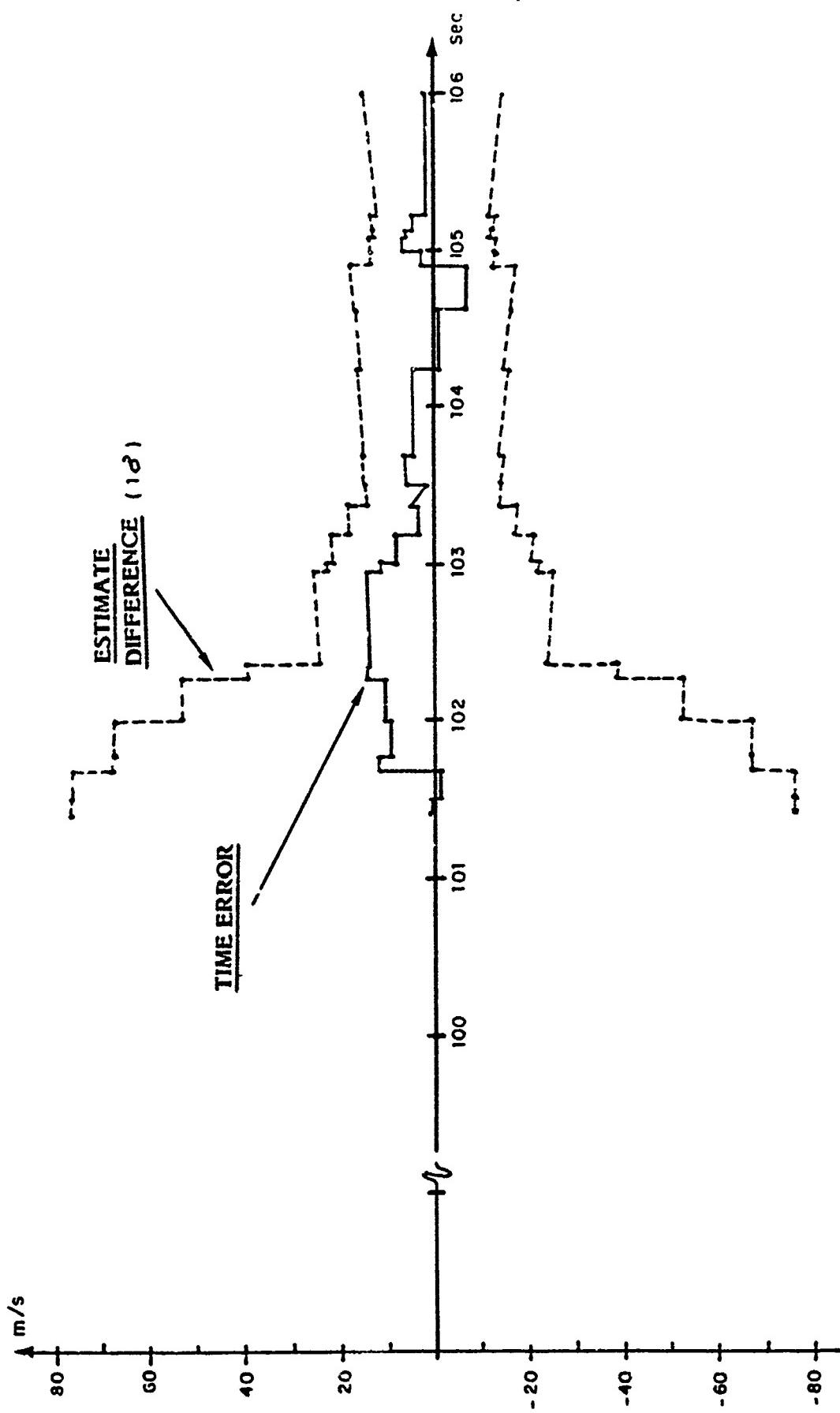


Fig.15 Velocity error (north)

NAVSTAR GPS PROGRAMME REVIEW

Wing Commander Hugh Coriat (RAF)
Headquarters Space Division (AFSC)
PO Box 92960, Worldwide Postal Center
Los Angeles, California 90009
USA

SUMMARY

This paper traces the origins of the Navstar Global Positioning System. It reviews briefly the activities and results of the first formal phase of the programme which set out to validate the GPS concept. It discusses the current activities which are focused on the full scale engineering development of the system. Finally, it looks ahead to the last phase of the programme: the system's operational deployment.

INTRODUCTION

Since the early 1960s, both the US Air Force and the US Navy pursued an extensive technology programme independently, to demonstrate the feasibility of developing a defence navigation satellite system capable of meeting the needs of a broad spectrum of users. The concept of a universal positioning and navigation system resulted from these combined technical efforts, which - in 1973 - led to the birth of a new programme designated the Navstar Global Positioning System (GPS).

Under the authority of the Department of Defence (DOD), the executive agency for the programme was vested in the US Air Force. It was given a charter to develop a system which would provide all authorised users anywhere on or near the surface of the earth, continuous and precise three-dimensional position, velocity and time. The GPS Joint Programme Office (JPO) at the US Air Force Systems Command's Space Division - in Los Angeles, California - was given this task.

Following very encouraging early test results, nine NATO nations signed a Memorandum of Understanding with the United States in 1978, to assist in the development of GPS. The JPO is, therefore, unusually joint in its nature, since it involves participation by the US Air Force, the US Navy, the US Army, the US Marine Corps, the Defense Mapping Agency, NATO and the US Department of Transportation which represents the interests of the Coast Guard and the civil navigator. The inclusion of a NATO Team so early in the technical development of a major project, represents a new and unique venture by the United States.

GPS CONCEPT

The GPS satellite constellation will be deployed so as to provide worldwide coverage that ensures any suitably equipped user access to at least four satellites at any time (Figure 1). Navstar satellites transmit navigation signals at two L-band carrier frequencies of 1575.42 MHz (L1) and 1227.6 MHz (L2). L1 is modulated by a Clear/Acquisition signal and a Precision signal, whereas L2 is modulated by a Clear/Acquisition signal or a Precision signal. In addition, these signals also contain satellite health data, constellation almanac, satellite ephemeris and clock corrections. Comparison of the delay between the two frequencies allows for the compensation of ionospheric propagation errors. Eventually, it is planned to deploy satellites which will have clear acquisition and precise signals on both frequencies.

USER SEGMENT

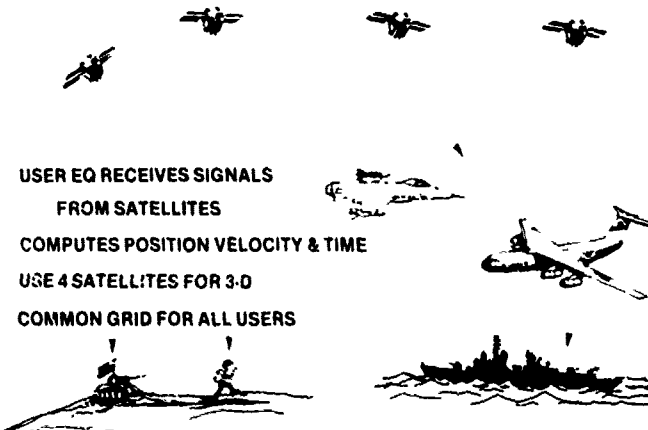


FIGURE 1

A Control Segment tracks satellites as they come into view, to enable it to predict satellite orbital positions, to provide satellite performance evaluation, and to calculate and update the navigation data being transmitted by the satellites. It performs this by completing three basic tasks (Figure 2). The satellite tracking is achieved by the monitor stations. A number of these passive unmanned facilities will be spread geographically around the world. The satellite ephemerides are then determined, and their future orbits and clock corrections predicted by the Master Control Station using the information provided by the monitor stations. Finally, the generated information used to predict the satellite's orbit is transmitted to the satellites by upload stations.

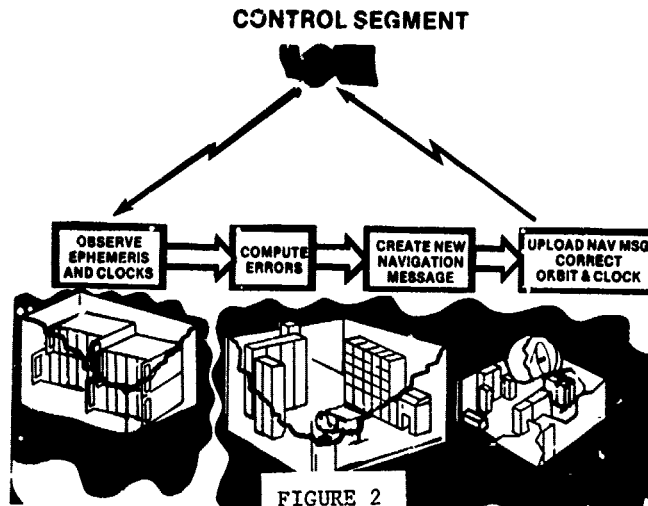


FIGURE 2

By using navigation signals from four selected satellites, a user's receiver can measure four independent pseudo-ranges and pseudo-range rates to the satellites. The user's receiver processor is then able to convert these measurements to three-dimensional position, velocity and time (Figure 3). Positions are calculated in the 1972 World Geodetic System (WGS 72), giving latitude, longitude and height relative to a fixed, earth centered uniform sphere or geoid. These coordinates can be converted by the receiver processor to any other coordinate system such as European Datum or Ordnance Survey of Great Britain. GPS-derived position and velocity information can be integrated directly into any weapon system or navigation computer.

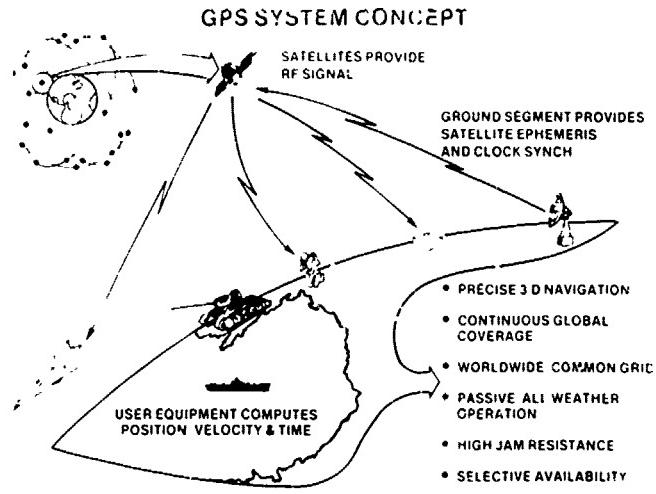


FIGURE 3

GPS CONCEPT VALIDATION (PHASE I)

The Phase I Navstar GPS constellation consisted of four satellites, optimized for coverage over the Yuma Proving Grounds in Arizona and San Clemente Island in California for approximately three hours each day. Satellites were launched from Vandenberg Air Force Base in California, by an Atlas booster equipped with an upper stage vehicle. The stage vehicles provided the propulsive force to boost the space vehicles to transfer orbit altitudes after Atlas burn-out.

The Phase I Control Segment consisted of a Master Control Station and an upload station, both located at Vandenberg Air Force Base, and four monitor stations located in Alaska, Hawaii, Guam and Vandenberg. The Air Force Satellite Control Facility at Sunnyvale, California supported all satellite operations requiring telemetry, tracking, and command (TT&C). The Naval Surface Weapons Center at Dahlgren, Virginia provided ephemeris analysis and predictions, when required.

To validate the GPS concept, four types of user equipments were developed. These included a high accuracy, high dynamic, four channel set; a high accuracy, medium dynamic, sequential set; a medium accuracy, low cost set; and a manpack (Figure 4). During Phase I, a total of 44 user equipments were developed by three manufacturers. In addition to being evaluated on a man's back, user sets were also assessed in a wide variety of host vehicles which included C-141 transport aircraft, P-3 maritime aircraft, UH-1 helicopter, F-4 fighter aircraft, amphibious landing craft, fast frigate, truck, jeep, van and armored personnel carrier.

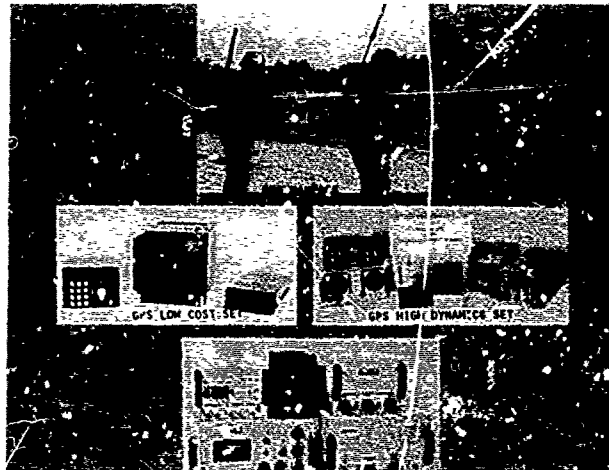


FIGURE 4

Approximately four years and \$365M after the first Defense Systems Acquisition Review Council (DSARC) authorised the implementation of Phase I of the programme, the GPS concept was validated beyond doubt. Some 650 missions were completed in a variety of host vehicles using GPS ground transmitters - the inverted range - deployed at Yuma Proving Grounds, and orbiting GPS satellites when these became available. Twenty-three major test objectives were pursued to validate the GPS concept and design, to demonstrate its military value and to define system cost (Figure 5). Comprehensive details of Phase I results are the subject of a separate paper (31st AGARD Symposium, Paper Number 31, Navstar GPS Field Test Results). Consequently, only a brief outline is given here for the sake of completeness.

GPS MAJOR TEST OBJECTIVES	
CONCEPT VALIDATION	
USABLE SIGNAL LEVELS	Demonstrate Military Value
3-D POSITION, VELOCITY AND TIME	COMMON GRID(GROUND SEA AIR)
TIME SYNCHRONOUS SATELLITES CONTROL USERS)	SHIPBOARD OPERATION
ACCURACY DEGRADATION DUE TO ALTITUDE, VELOCITY AND DYNAMICS	PROPELLER MODULATION
DESIGN VALIDATION	MANPACK PERFORMANCE
SIGNAL STRUCTURE AND MODULATION	FOLIAGE
ACQUISITION/REACQUISITION	JAMMING
COMPENSATION FOR ATMOSPHERIC PROPAGATION DELAY	LANDING APPROACH
MULTIPATH	RENOUVOUS
USER EQUIPMENT AMMING RESISTANCE	HAF-OF EARTH
SIGNAL AVAILABILITY TO UNAUTHORIZED USERS	STATIC POSITIONING
SYSTEM VULNERABILITY (ANALYTICAL)	CROSS COUNTRY NAVIGATION
PRECISE SATELLITE EPHEMERIS	Precision WEAPON DELIVERY

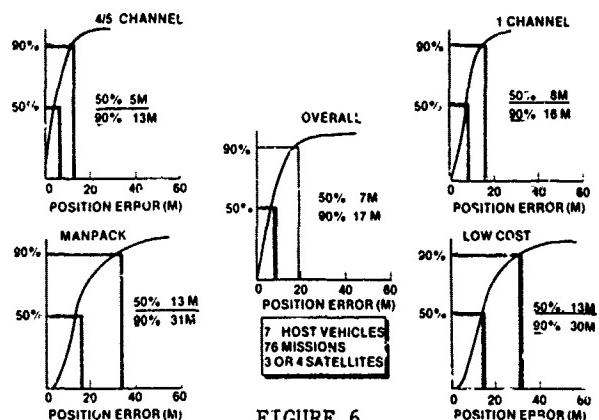
FIGURE 5-1

GPS MAJOR TEST OBJECTIVES (CONT'D)	
Demonstrate Military Value	INITIAL ESTIMATES OF RELIABILITY/MAINTAINABILITY
COMMON GRID(GROUND SEA AIR)	DEFINE SYSTEM COST
SHIPBOARD OPERATION	DESIGN TO COST GOALS
PROPELLER MODULATION	INITIAL LIFE-CYCLE COST ESTIMATES
MANPACK PERFORMANCE	
FOLIAGE	
JAMMING	
LANDING APPROACH	
RENOUVOUS	
HAF-OF EARTH	
STATIC POSITIONING	
CROSS COUNTRY NAVIGATION	
Precision WEAPON DELIVERY	
INITIAL ESTIMATES OF RELIABILITY/MAINTAINABILITY	
DEFINE SYSTEM COST	
DESIGN TO COST GOALS	
INITIAL LIFE-CYCLE COST ESTIMATES	

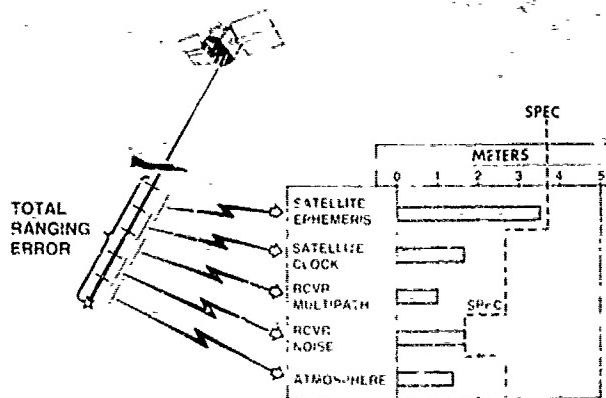
FIGURE 5-2

Navigation results obtained with high accuracy receivers suggested that the eventual performance of the next generation of user equipments and operational systems might have the potential to exceed expectations (Figure 6). An overall error of less than 10 meters (33 feet) (three-dimensional 50%) and 20 meters (66 feet) (90%) was obtained using all types of GPS sets on a wide variety of host vehicles. System error sources such as satellite ephemeris, satellite clock, multipath, receiver noise, and atmospheric delays were evaluated and found to be within budgetary allocations (Figure 7).

NAVSTAR GPS NAVIGATION PERFORMANCE (3-D POSITION ERROR)



ERROR BUDGET ALLOCATION



A number of operational system applications were demonstrated both within the objective environment of the Proving Grounds at Yuma, and in more subjective mission scenarios off range. Precision level and toss bombing by the F-4 using a high dynamic GPS set fully integrated with an inertial system, gave dramatic improvements in accuracy over conventional methods. Rendez-vous results between the C-141 and the F-4, the helicopter and the manpack, and between the P-3 and a landing craft, each steered by Navstar, displayed clearly its potential for enhancing any inter-Service or international operation. Low level navigation accuracies demonstrated during UH-1 helicopter flights and F-4 bombing approaches hinted at the system's potential to significantly improve a low flying aircraft's ability to acquire targets, or even to release weapons blind. Potential GPS applications are almost boundless; and only a few were briefly demonstrated during Phase I. These included long cross-country flights, harbour navigation in unprogrammed thick fog, photo-mapping, and static geodetic surveying.

Although a comprehensive assessment of the threat and vulnerability of GPS is beyond the scope of this paper, it is nonetheless a vital part of any concept validation, and the JPO addressed this area fully during Phase I. A few general comments can be made here to highlight techniques which might be available to secure system immunity from enemy countermeasures. In general, space vehicle designs will aim to increase satellite immunity, and to reduce the attacker effectiveness. Techniques available to achieve this might include nuclear and laser hardening of components; the selection of high orbits and carefully chosen orbital spacings to reduce kill probabilities; the selection of a resilient constellation to secure graceful system degradation; and a well-planned replenishment strategy to minimise the effect of losses. The dominant factor in this evaluation, however, is likely to be cost - as much for the attacker as the defender - for it will govern what each is able to do.

The Control Segment will probably be subjected to more familiar threats such as direct attack, sabotage and jamming. Hardening, redundancy of systems and encrypted spread spectrum telemetry and command links will provide valuable counters. However, probably the most effective countermeasure within this segment is likely to be the reduction of the frequency of satellite uploads, so that the system's capability is not heavily dependent on the survivability of the Control Segment. Figure 8 shows that the predicted accuracies of satellite operational clocks and ephemeris predictions should secure a graceful system degradation, such that 60 meters total system accuracy will be available some seven days after last upload.

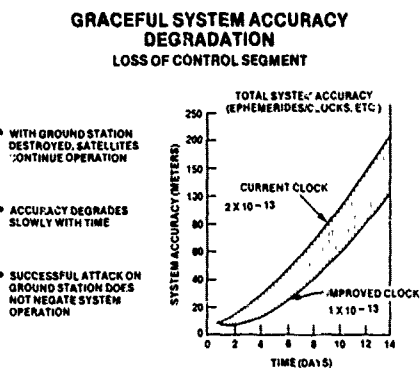


FIGURE 8

User Segment immunity can be secured through affordable electromagnetic pulse shielding, limited nuclear hardening, and spread spectrum techniques, but especially through the use of adaptive antennas and Inertial Measurement Unit aiding. There can be little doubt that GPS - along with any other navigation aid available - will either be exploited or hindered by the enemy. If it is exploited, we can limit its value to an enemy by the use of techniques which provide full system accuracy only to authorised users. If it is hindered, we can minimise the impact of mixing GPS with self-contained navigation aids. This, tied to the use of some or all of the counters described above, will still provide any user with significant improvement in capability, whatever the theatre.

Following the completion of Phase I, the JPO presented its findings to DSARC II. It recommended the development of a 24 satellite constellation deployed in three 10,900 nautical mile (20,200 Km) high circular orbits, 120° apart and inclined at 55° to the equator, with each satellite having a 12-hour period. The system was to provide an accuracy of 10 meters (33 feet) (SEP). The user equipment was to be developed competitively by two contractors, and two ground control stations were to be developed to secure system redundancy.

Based on the irrefutable evidence gathered during Phase I, and on an evaluation of the GPS potential in light of other defence priorities, the DSARC approved the programme transition from Concept Validation to Full Scale Engineering Development. With this approval, however, the Secretary of Defense issued a challenge to reduce projected overall system costs to make it more affordable. It was recognised that the estimated cost for development, acquisition and operation of the system constituted a major national commitment. It was also recognised, however, that a significant part of this investment could be offset by judicious phase-out or reduced use by the DOD of other less capable systems and equipments. Furthermore, it was recognised that the improved capabilities that Navstar could provide to nearly every facet of military applications, would far exceed the basic system cost in terms of increased military effectiveness. It was within this framework that the Full Scale Engineering Development of GPS began.

GPS FULL SCALE ENGINEERING DEVELOPMENT - PHASE II

Following a series of evaluations by the DOD, the Services, and the JPO, it became clear that a completely restructured GPS programme would have to be developed to meet the majority of the user's requirements, and remain within available funds. This restructured programme has now been defined, and is currently being implemented.

Within the Space Segment of the GPS system, significant economies were achieved by reducing the constellation from 24 space vehicles to 18. Studies had indicated that an 18 satellite constellation would still provide a very significant military capability, although as a result of poor satellite geometry, some deterioration of three-dimensional navigation accuracy would occur in certain predictable and limited geographic areas. This limitation creates so-called 'holes' or 'outages' in navigation accuracy performance. In mid-Northern latitudes, users will be affected over predictable short periods of time. For user whose altitude is known, and therefore where a three-satellite solution is achievable, these 'holes' will not be seen at all. Following extensive studies to evaluate all available options, an 18 satellite constellation with three space vehicles in each of six planes separated in longitude by 60° was selected. The satellite's inclination of 55° to the equator, and its 12-hour periods were retained (Figure 9).

The Navstar GPS 6 Plane 18 Satellite Configuration

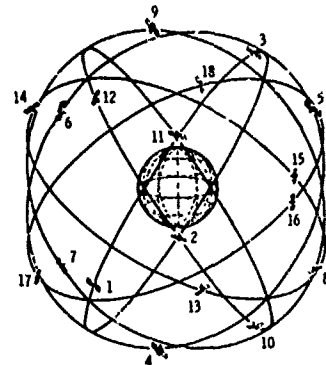


FIGURE 9

During Phase II, the GPS Control Segment at Vandenberg and the four monitor stations will be maintained to support User Segment Development Test and Evaluation, and Initial Operational Test and Evaluation. In parallel, the JPO is negotiating a three-part contract to continue operation and maintenance of the Phase I Control Segment; to upgrade the Phase I system; and to develop and implement the entire Phase II/III system. The JPO is evaluating a number of sites for the world-wide deployment of operational monitor stations.

User equipment developments were not affected by the programme restructure. Two contractors are currently in competition for the award of the GPS user equipment production contracts. A total of 54 user equipment sets are being developed by each contractor for thorough evaluation during Phase II. Approximately one year after the start of the system's full scale engineering development, the user equipment's System Design Reviews have been held. These covered a broad range of activities including set designs, schedules, control and display unit operations, system integration, navigation software, test planning and logistics. They will be followed by Preliminary Design Reviews in the summer and autumn of this year, and by Critical Design Reviews during the second half of 1981.

In order to enhance design-to-life cycle-cost, maximum commonality will be sought between user equipment for all host vehicles, and between GPS system elements. Basic system elements are likely to include two types of antennas, a Fixed Reception Pattern Antenna and a Controlled Reception Pattern Antenna; an antenna electronics control unit; one of three types of receiver processors according to the dynamics of the host vehicle; one of two control and display units; a flexible modular interface unit; and a power converter. A possible family of GPS user equipments resulting from Phase II designs is shown at Figures 10-11. These equipments will be designed to operate in some 30 different types of US host vehicles, and will be tested during Full Scale Development in eight vehicles.

SET TYPE	EXAMPLES HOST VEHICLE TYPE	BASIC SYSTEM ELEMENTS						HOST VEHICLE PEUAR LRS AND ACCESSORIES		
		FPA (F)	CRA (C)	ANTENNA ELECTRONICS	RECEIVER PROCESSOR (R1) OLD	RECEIVER PROCESSOR (R2) MMI	RECEIVER PROCESSOR (R3) MMI	CONTROL DISPLAY OTHERS	INTERFACE UNIT	VE PC AD
LOW DYNAMICS LRD	MANPACK	X	X	X	X			X		
	VEHICLE	X	X	X	X			X	X	
MEDIUM DYNAMICS MDT	HELICOPTER	X	X	X		X			X	X
	SURFACE SHIPS	X	X	X		X			X	X
HIGH DYN HDS MDT	HIGH PERFORMANCE AIRCRAFT	X	X	X			X		X	X
	SUBMARINE	X	X	X			X		X	X

NOTES:
(1) FPA = FIXED RECEPTION PATTERN ANTENNA
(2) CRA = CONTROLLED RECEPTION PATTERN ANTENNA

FIGURE 10

GPS COMMON FAMILY DESIGN CONCEPT

POSSIBLE FAMILY OF GPS USER EQUIPMENTS

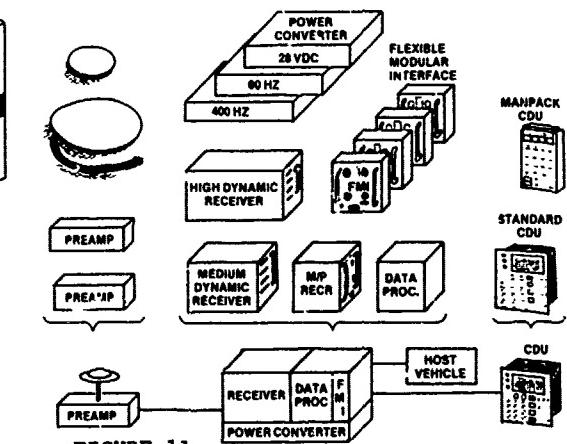


FIGURE 11

User equipment designs will incorporate a 'selective availability' feature which will deny the full system accuracy to non-authorised users, and will at the same time prevent spoofing. Access to the full system capability will require a 'key' which will be input either through the system's control and display unit, or through the data loader.

When available in early 1982, these equipments will be subjected to thorough and demanding tests. Development Test and Evaluation will last about one year and will include qualification/acceptance tests, combined environmental tests, and field tests. Initial Operational Test and Evaluation will follow. It will be performed over a period of nine months in a variety of host vehicles including M60 tank, UH60 helicopter, A6 attack aircraft, F16A fighter aircraft, P3C maritime aircraft, B52D bomber aircraft, CV64 aircraft carrier, and SSN submarine (Figure 12). Tests will be performed in an operational environment by operational users, and will include an evaluation of maintenance concepts. The Initial Operational Test and Evaluation programme is in itself a very ambitious venture, since it has to meet the differing, and often conflicting, needs of a very wide variety of users. A Joint Service Test Planning Group is responsible for the implementation of this phase of the programme. Test sites are in the process of being selected, and will probably include locations in the Southwest Continental US, and in Europe.



FIGURE 12

NATO INVOLVEMENT IN GPS

The future potential of Navstar GPS was clearly recognised by the majority of NATO nations. With this potential in mind, nine of the NATO nations signed a Memorandum of Understanding with the United States on 28 April 1978, agreeing to form a 'NATO' multi-national team to work within the US Navstar Joint Programme Office and assist in the development of GPS. This team arrived on site towards the end of 1978. The aims of the Memorandum are to allow the JPO to take account of NATO operational, technical and logistic requirements and problems in the development of the system, and of user equipment in particular, and to allow the NATO Team at Space Division to gather information for an assessment of the Navstar system from a NATO point of view, while contributing their own skills and expertise to the project. Although NATO nations have not yet committed themselves to the acquisition of Navstar GPS, they are following programme evolution closely to define their future requirements. NATO Team activities are centered on providing GPS information which will help the identification of these future national requirements. Furthermore, much effort is being devoted to evaluate the feasibility of developing a GPS user equipment standard amongst NATO nations, in order to further the goals of interoperability and standardisation. These efforts, so early in the development phase of the programme, are unique and offer real possibilities.

NAVSTAR AVAILABILITY

The availability of Navstar GPS to the civilian community is a subject which commands a great deal of attention amongst potential users. The problem is complex and hinges primarily - but not exclusively - on a conflict of interest between the need for some form of denial or degraded capability in order to preclude the full potential of Navstar being used against the United States or its allies, and the full exploitation of system's capabilities. In its deliberations, the DOD has attempted to achieve an equitable balance between national security and system utility. In establishing the level to which the system accuracy should be degraded, the DOD studied the national security implications of such a global capability. It worked closely with the Department of Transportation, the Federal Aviation Administration, the US Coast Guard, NASA, and other agencies of the Federal Government. It concluded that Navstar should be made available for civil use at an accuracy level that was consistent with national requirements. As a result, it decided that an accuracy of approximately 200 meters (656 feet)(SEP) would not seriously jeopardise national security in mid-1980s.

Several techniques, to implement this capability in the operational system, have been developed but not yet fully tested or evaluated. The operational procedures needed to provide adequate control and security of these techniques in all levels of conflict are currently being analysed. The DOD did recognise that the outcome of their policies might impact the future civil use of GPS. For this reason, it wished to ensure that all interested parties were kept informed of progress. A US Federal Radio Navigation Plan currently being formulated by the DOD and DOT jointly, is seen as a key stone of the policy.

GPS OPERATIONAL DEPLOYMENT (PHASE III)

Following a successful DSARC III, planned for the fall of 1983, the full production and operational deployment of the GPS will begin. The operational GPS constellation will be deployed in the Space Shuttle instead of the Atlas system. Insertion of the space vehicles from Space Shuttle altitudes into final orbits will be achieved by Payload Assist Modules (Figure 13). The number of GPS satellites which will be launched on a single mission by the Shuttle will depend on its cargo configuration. Figure 14 shows a shared configuration in which two GPS space vehicles are carried. Satellite lifetime is expected to be seven and a half years with a six-year mean mission duration. The constellation will be deployed so as to give a two-dimensional navigation capability by end of 1985, and a three-dimensional navigation capability of 16 meters (52 feet) (SEP) by end of 1987.

NAVSTAR SPACECRAFT IN PAM-D CRADLE

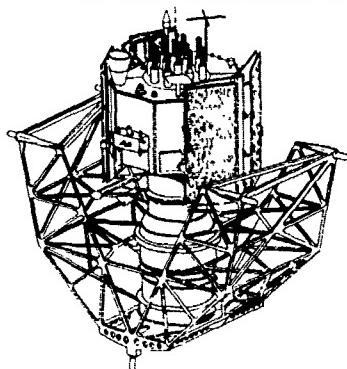


FIGURE 13

GPS LAUNCH SYSTEM PHASE III

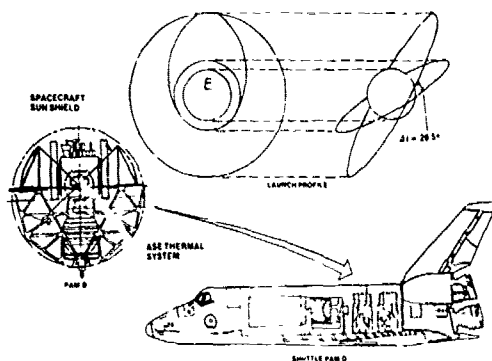


FIGURE 14

The existing Control Centre at Vandenberg will become the Initial Operations Control Centre capable of handling up to 18 space vehicles. This will eventually be superseded by the Navstar Operations Centre at a location which has not yet been defined. Monitor stations will be deployed so as to provide full tracking of the GPS constellation.

The Phase III user equipment contractor will be selected from competing Phase II contractors. A source selection will determine who is selected, and will be based on an assessment of Initial Operational Test and Evaluation results, technical performance, life cycle cost, commitment to support cost control, production and management capabilities, and manufacturer's previous experience.

A follow-on Phase III contractor - needed to secure a second supply source - will be selected from US or NATO contending manufacturers. The criteria for selection has not yet been defined; but having been selected, the follow-on manufacturer will be qualified by the winner of the Phase II competition, and will eventually produce user equipments to the winner's design. The timing of all activities described in this paper is shown at Figure 15.

In the seven short years of its existence, GPS has commanded serious attention as much from its proponents as its opponents. Forceful arguments have been voiced by both, often objectively, but occasionally with less tangible logic. What is clear, however, is that the technology needed to implement the validated GPS concept is available. What is not so clear is how much of this technology is affordable. Navstar has brought many new challenges which have been met successfully, even though a few years ago these might have appeared somewhat formidable. More challenges need to be faced in the years ahead to exploit the system's full potential; a potential which reaches far beyond the mere POSITIONING capability, which its title suggests.

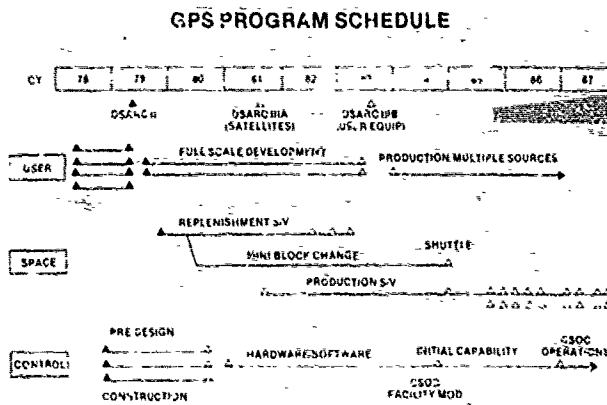


FIGURE 15

The system's ability to improve target acquisition and weapon delivery capabilities as well as its ability to enhance nearly every aspect of warfare - particularly in an inter-Service environment - has already been demonstrated clearly. Indirectly, such a global system is also forcing us to address in a practical way, many elusive goals which we have sought to implement over the years, such as: Joint Service procurement, interoperability, standardisation, and international collaboration. Navstar GPS offers us a worthy challenge; it deserves continued and serious attention from its ever-widening circle of potential users.

REFERENCES

1. Honorable Gerald P. Dinneen, STATUS AND PLANS FOR THE NAVSTAR GLOBAL POSITIONING SYSTEM, Statement by Assistant Secretary of Defense for Communications, Command, Control and Intelligence, before the Subcommittee on Transportation, Aviation and Communications of the Committee on Science and Technology, House of Representatives, The 9th Congress, Second Session, 21 April 1980.
2. NATO Navstar GPS Team, NAVSTAR - A SINGLE NAVIGATION SYSTEM FOR NATO, NATO's Fifteen Nations, Feb-Mar 80, Volume 25, Number 1, Pages 32-36.
3. Colonel Don Henderson and Wing Commander Hugh Coriat, STATUS REPORT ON THE GLOBAL POSITIONING SYSTEM, Navigation - Journal of the Institute of Navigation, Spring 1980, Volume 27, Number 1.
4. NAVIGATION - Journal of the Institute of Navigation, Summer 1978, Volume 25, Number 2.

ABBREVIATIONS USED IN TEXT

DOD	Department of Defense
DOT	Department of Transportation
DSARC	Defense Systems Acquisition Review Council
GPS	Global Positioning System
JPO	Joint Programme Office
MHz	megahertz (one million hertz)
MOU	Memorandum of Understanding
NASA	National Aeronautic and Space Administration
NSWC	Naval Surface Weapons Center
PAM-D	Payload Assist Module - D
SD	Space Division
SEP	Spherical Error Probable
SV	Space Vehicle
WGS	World Geodetic System

NAVSTAR FIELD TEST RESULTS

BY

Colonel Robert L. Peterson (USMC)
Deputy Program Manager
HQ SD/YEM
POB 92960
Worldway Postal Center
Los Angeles, California 90009

SUMMARY

Since the early 1960s, the U.S. Navy and U.S. Air Force have pursued actively the concept of navigation using radio signals transmitted by space vehicles whose positions in space are accurately known. The impetus for such a space-based navigation system was the broad spectrum of military users for whom precise, global navigation is required. Navstar Global Positioning System (GPS) is under development by the United States Department of Defense (DOD) and will provide a world wide three-dimensional accuracy of 10-20 meters when operational in the late 1980s. The system has just completed the Concept Validation Phase of the development cycle and approval has been given to enter the Full Scale Development (FSD) Phase of the program during which pre-production user equipment will be developed and tested. This paper describes the most significant user equipment tests conducted during the Concept Validation Phase. These tests demonstrated that a 10-20 meter accuracy is achievable and a very precise navigation capability has a wide range of military applications.

INTRODUCTION

Since the early 1960s the United States has pursued actively the concept of navigation using radio signals transmitted by space vehicles whose positions in space are accurately known. The impetus for a space-based navigation system is the broad spectrum of military and civilian benefits realizable from highly precise world-wide navigation and positioning. Transit was the first such system to become operational and is still widely used for maritime navigation and for surveying purposes; however, it does not meet the Services' requirements in the out years.

The Services' requirement for a continuously available, three-dimensional capability resulted in the Navy's TIMATION program and the Air Force's 62IB effort. These parallel development programs for a space-based navigation system attracted the attention of the Deputy Secretary of Defense who, in April 1973, issued a memorandum designating the Air Force as the executive Service for a joint development effort which would feature the best aspects of the TIMATION and 62IB programs. In addition, a system would be developed to meet the unique navigation and positioning requirements of all Department of Defense Agencies. Thus the Navstar Global Positioning System was born with the stated objective of providing a very precise position/navigation system in three dimensions, plus time, that will also be used for weapon delivery. In addition, a secondary objective is to stop the proliferation of navigation equipment since Navstar is envisioned as replacing many existing types of navigation aids such as Transit, Omega, VOR and TACAN.

SYSTEM DESCRIPTION

The Navstar GPS Phase I program has three distinct segments as follows:

Space Segment-

Navstar GPS is a space-based navigation system that is capable of providing highly accurate, three-dimensional position and time information to suitably equipped users anywhere on or near the Earth. In its final Phase III operational configuration, Navstar will deploy six planes of satellites in circular 20,200 kilometer orbits. Each plane will contain three space vehicles for a total of eighteen satellites on-orbit. The Phase I & II constellation consists of only five satellites in orbits designed to optimize coverage over the user equipment test locations in the southwestern United States.

The Navstar satellites transmit a composite signal at two L-band frequencies. One is for acquisition and coarse navigation and one is for precise navigation. In addition to the navigation message, the signal contains satellite ephemeris information, atmospheric propagation correction data and satellite clock bias information. The dual frequency transmissions permit determination of the signal delay resulting from passage through the ionosphere.

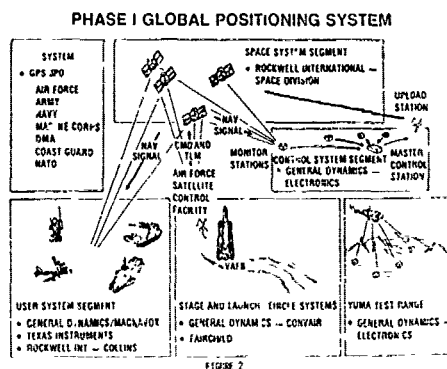
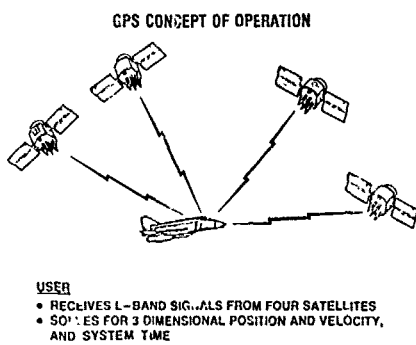
Control Segment-

Four ground-based Monitor Stations located in Alaska, Guam, Hawaii and Vandenberg Air Force Base in California passively track the satellites as they come into view. The Master Control Station, also at Vandenberg AFB, collects the ranging data from the Monitor Stations and generates the navigation message. This information, plus clock bias, is uploaded to each satellite on a daily basis.

User Equipment Segment-

The Navstar User Set consists of a receiver and navigation processor which require signals from at least four satellites to solve for the user's three-dimensional coordinates and system time (see Figure 1). The position solution is computed in World Geodetic Survey-72 coordinates and can be converted to any convenient reference system or units such as local datum latitude/longitude and military grid reference system. In high dynamic vehicles such as fighter aircraft, the GPS User Set may be supplemented by an Inertial Measurement Unit (IMU) to maintain navigation accuracy during high acceleration maneuvers. Such a combination is referred to as an Aided User Set.

The entire Phase I system is depicted in Figure 2 and the characteristics of the operational system are listed in Figure 3.



NAVSTAR GLOBAL POSITIONING SYSTEM CHARACTERISTICS

- CONTINUOUS GLOBAL COVERAGE
- PRECISE POSITION & VELOCITY IN 3 DIMENSIONS & TIME
- WORLDWIDE COMMON GRID
- PASSIVE & ALL WEATHER OPERATION
- UNLIMITED NUMBER OF AUTHORIZED USERS/SELECTIVE DENIAL
- HIGH JAM RESISTANCE

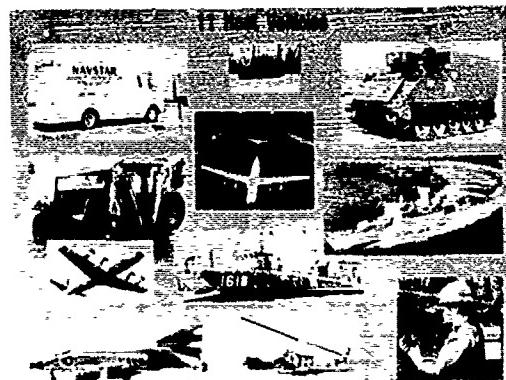
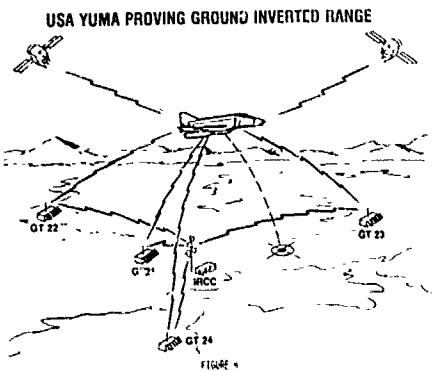
FIGURE 3

THE FIELD TEST PROGRAM FOR NAVSTAR USER EQUIPMENT

Following approval for the Navstar GPS program in December 1973, the system entered the Concept Validation Phase (Phase I) of development. Advanced Development Model user sets were developed during this phase to meet the requirements of high and medium dynamic users plus a manpack small enough to be carried by a foot soldier. The fundamental difference between the sets is the number of receiver channels. For high dynamic users, a four or five channel set is required which simultaneously receives navigation information from four satellites and provides real-time positioning of the vehicle. Medium dynamic user sets utilize a single channel to sequence between four satellites, updating the position solution approximately once every eight seconds. The manpack also uses a single channel sequencing receiver. In addition, a low cost, single channel/single frequency receiver was developed as a TACAN replacement. Testing of the sets developed by three contractors began at the U.S. Army Yuma Proving Ground (YPG) in the southwestern United States on 15 March 1977 and is continuing at a lower level of activity.

Because Navstar testing commenced prior to the launch of any space vehicles (six are now in orbit), a ground system called the Inverted Range (IR) was installed at YPG to simulate signals from four Navstar satellites. The system consists of four Ground Transmitters (GTs), each simulating a Navstar satellite, and the Inverted Range Control Center (IRCC) which monitors the GTs and maintains time synchronization among them. The IRCC can also control a combination of GTs and satellites during what is termed as hybrid testing. In addition, three ground-based laser trackers, which comprise the Precision Automated Tracking System (PATS), were installed to accurately determine the trajectory of the test vehicle for comparison with the GPS navigation solution. The lasers track optical reflectors mounted on the test vehicles to an accuracy of less than 1.0 meter position error and 0.1 meters per second velocity error. Figure 4 shows the concept of the Inverted Range. As satellites became available, they were used in conjunction with the GTs. Finally, accuracy by satellite only was tested when four satellites were in orbit.

Phase I testing was conducted with user equipment representing a wide dynamic range. These vehicles are shown in Figure 5 and the number of test missions completed are shown in Figure 6. The 651 test missions represent one of the most extensive Concept Validation exercises ever completed by the United States DOD. In preparation for approval to proceed from Concept Validation into FSD, test data were collected to satisfy the twenty-two Major Field Test Objectives listed in Figure 7. This paper will present samples of data from the more significant user equipment test objectives completed in Concept Validation of the system.



PHASE I TEST MISSIONS

MAR 77 - MAY 79

C141 TRANSPORT	77	M35 TRUCK	63
F4J FIGHTER	118	MOBILE TEST VAN	106
P3B PATROL	47	ARMORED PERSONNEL CARRIER	17
UH1 HELICOPTER	70	M151 JEEP	25
FRIGATE (FF1076)	14	MAN	91
LANDING CRAFT	23		
TOTAL 851			

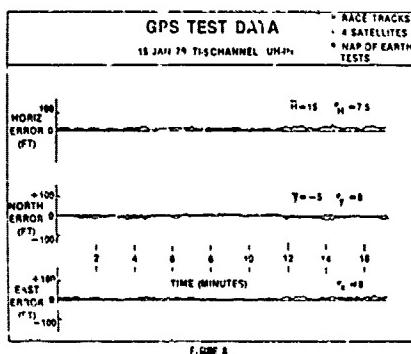
FIGURE 6

MAJOR FIELD TEST OBJECTIVES	
NAVIGATION ACCURACY	THREAT PERFORMANCE
1 POSITION ACCURACY	13 JAMMING RESISTANCE
2 VELOCITY ACCURACY	14 SELECTIVE AVAILABILITY
3 EFFECTS OF DYNAMICS ON ACC	ENVIRONMENTAL EFFECTS
DEMONSTRATIONS OF MILITARY VALUE	15 PROP & MOTOR MODULATION
4 PRECISION WEAPON DELIVERY	16 COLLAGE ATTACHMENT
5 LANDING APPROACH	17 MULTIPATH REJECTION
6 RESCUEOUS	18 IONOSPHERIC AND TROPOSPHERIC CORRECTION
7 PHOTOMAPPING	SYSTEM CHARACTERISTICS
8 MAP-OF-EARTH OPERATIONS	19 SATELLITE CLOCK AND EPHEMERIS ACCURACY
9 STATIC POSITIONING	20 ACQUISITION AND REACQ TIME
10 COMBINED OPERATIONS	21 TIME TRANSFER
11 CROSS, COUNTRY	22 SIGNAL LEVELS AND SIGNAL STRUCTURE
12 SHIPBOARD OPERATIONS	

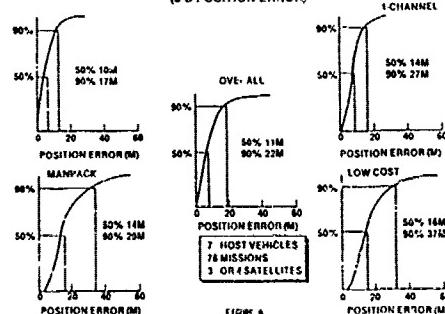
FIGURE 7

NAVIGATION ACCURACY

Navigation accuracy was determined by comparing the GPS user set solution with the real position of the vehicle as determined by the laser trackers. Since all vehicle and laser data are time synchronized, post processing provided difference plots in the X, Y & Z axes as shown in Figure 8. Difference plots were aggregated to demonstrate the navigation performance as shown in Figure 9. Sample performance data are shown for the different types of Advance Development Models of user equipments on the various vehicles while using only satellite signals for positioning and navigation.

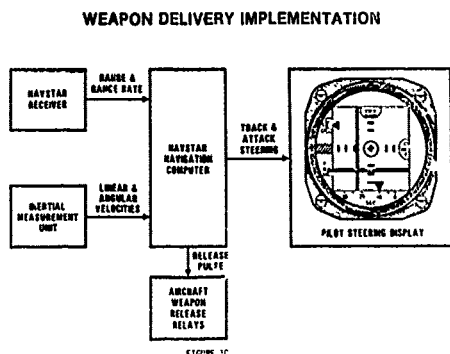


NAVSTAR GPS NAVIGATION PERFORMANCE (3 D POSITION ERROR)

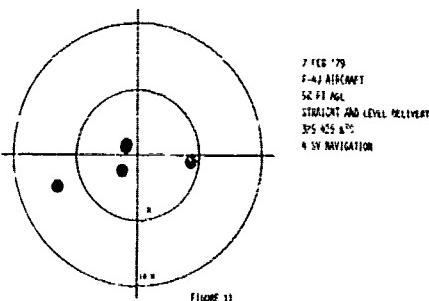


WEAPON DELIVERY

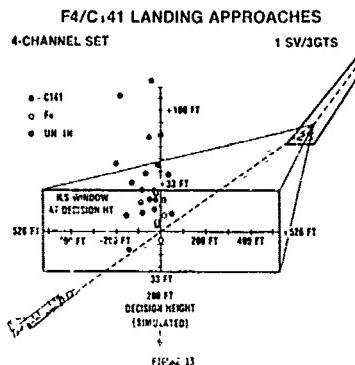
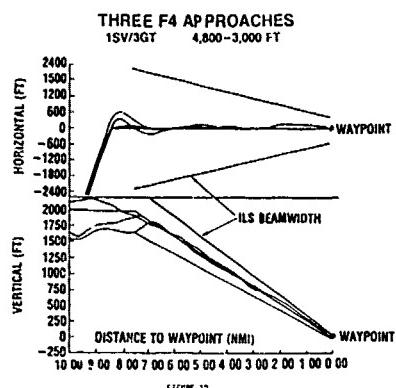
The F-4 aircraft and MK-82 freefall bombs were used to evaluate Navstar in the weapon delivery role. Figure 10 illustrates the implementation in the aircraft. Target coordinates were entered into the Navstar computer by the operator. Using information from both the inertial unit and the Navstar receiver, the Navstar computer generated steering and weapon release data. The pilot's steering display provided azimuth steering corrections and an indication of time to go for the release. The Navstar computer generated the automatic release pulse when the correct solution was reached. Deliveries were made from high (10,000 feet), medium (5000 feet) and low (200 feet) altitudes. Loss deliveries from low altitudes were also made. Figure 11 shows an actual plot of bomb impacts around the selected target coordinates during a representative mission.



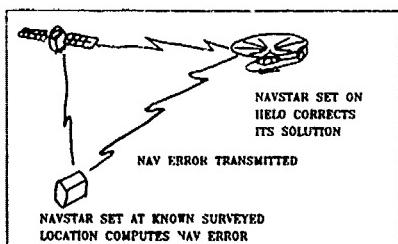
GPS BOMBING RESULTS

**LANDING APPROACH**

Navstar aircraft user equipment incorporates the capability to enter three-dimensional waypoints into computer memory so that steering information (range, bearing, time to go) can be computed from one waypoint to the next. This information is used to drive a pilot's steering display which can display horizontal and vertical deviation from the intended flight path between subsequent three-dimensional waypoints. If key landing approach positions are entered as Navstar waypoints, the pilot is provided with a self-contained landing approach aid that is independent of ground equipment or controllers. Test missions of this concept were flown by the F-4. Figure 12 shows the actual approach path of the aircraft as compared with the existing Instrument Landing System (ILS) beamwidth. Similar tests were conducted with the C-141 aircraft and the UH-1 helicopter. Figure 13 illustrates the point at which each approach terminated as compared with the imaginary ILS window at the decision height. These approaches were flown using one satellite and three GTs. Tests conducted using satellites only showed a greater deviation in the Z axis but still acceptable as an approach aid where higher than precision minimums are acceptable.



The need to provide a higher degree of accuracy for precision approaches than that available by Navstar (10-20 meters) led to the concept of differential navigation. Figure 14 illustrates this concept. A Navstar receiver is located on a surveyed point where X, Y & Z system errors can be identified. These errors are data linked to aircraft operating in the same geographical area and therefore, subject to the same errors. The X, Y & Z errors obtained from the reference receiver are subtracted from the aircraft receiver solution thereby improving the position accuracy of the aircraft. Results of the differential navigation tests for 11 January 1980 are shown in Figure 15. As noted on the chart, regardless of geographical Navstar system error, the corrected solution was less than three meters in the X, Y & Z axes. Figure 16 shows actual UH-1 helicopter landing approach results using differential navigation where fifty percent of the landings terminated in a box six meters by ten meters square.

NAVSTAR DIFFERENTIAL NAVIGATION

NAVSTAR GPS FIGURE 14 AS OF DATE: 11 JAN 80

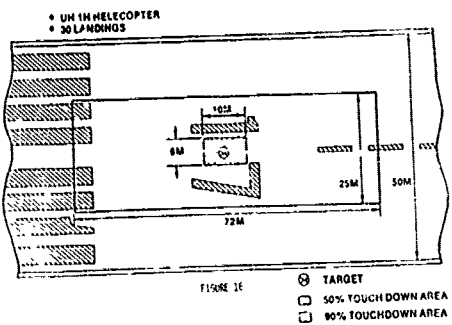
DIFFERENTIAL NAV RESULTS

11 JAN 80 4 SATELLITES TRADE

PARAMETER	CORRECTION OPS		CORRECTED SOLN. IN CHD
	X	Z	
X	2m	2.6m	
Y	2m	2.7m	
Z	1m	2.7m	
MEAN	—	—	0.29m
SD	—	—	0.35m
MAX	—	—	0.39m

FIGURE 15

GPS Δ NAV APPROACHES
(LAGUNA AIRFIELD)

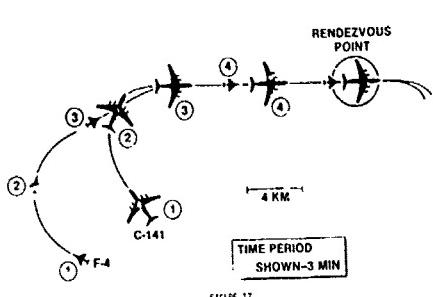


RENDEZVOUS

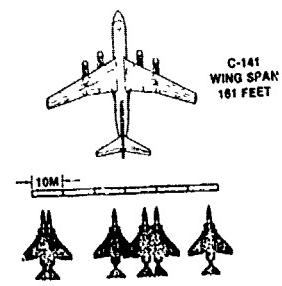
The Navstar GPS user equipment operator is able to input a moving waypoint into the system. This is accomplished by identifying a starting position (latitude/longitude), time, direction and velocity to the system. Subsequently, any user can get bearing and distance information to the moving waypoint merely by inserting the four parameters into his own set. This moving waypoint feature can be employed to effect a rendezvous between GPS equipped vehicles. For this test, the C-141 and F-4 aircraft were used; however, the same capability exists for any combination of GPS equipped vehicles.

Figure 17 shows the flight profile for the F-4/C-141 rendezvous test. Both aircraft were attempting a rendezvous on a moving waypoint using only information provided on the pilot's steering display. The C-141, arriving at the moving waypoint ahead of the F-4, flew a position right on the three-dimensional waypoint. The F-4 then flew a blind rendezvous on the moving waypoint (C-141) using a thousand feet of vertical separation for safety reasons. Figure 18 shows the results of these tests which demonstrated that the F-4 could fly a blind rendezvous and terminate within the wingspan of the C-141.

F-4/C-141 RENDEZVOUS FLIGHT PROFILE



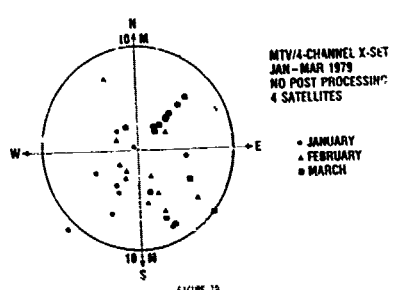
AIRBORNE RENDEZVOUS DATA
1 SV/3G1S
19 OCT 78
LATERAL ERROR AT POINT OF CLOSEST LONGITUDINAL APPROACH



STATIC POSITIONING

The purpose of this test was to determine the static accuracy of Navstar GPS for surveying purposes without the use of post processing. This test, therefore, represents the real-time survey accuracy of the system for tactical purposes. A high dynamic receiver was installed in an instrumented test van for this test. Shown in Figure 19 is a scatter diagram of the position accuracy of the system during tests conducted during January, February and March of 1979. Figure 20 is a breakdown of the data showing the number of days testing was conducted, i.e., RMS errors in the X, Y & Z axes and the probable spherical error.

REAL-TIME STATIC POSITIONING TEST RESULTS



REAL-TIME STATIC POSITIONING TEST RESULTS

4 SATELLITES MTV/X-SET JAN-MAR 1979

MONTH	NO OF TEST DAYS	POSITION ERRORS (M)			SEP
		RMSX	RMSY	RMSZ	
JAN	9	5.06	4.99	8.26	9.39
FEB	12	2.72	4.00	5.62	6.33
MAR	14	3.76	4.53	3.78	6.22

FIGURE 20

CROSS COUNTRY

The P-3 aircraft, equipped with medium dynamic and low cost user equipment sets, was selected for the cross country navigation evaluation. An overwater route from Hawaii to the San Francisco area was used to compare Navstar accuracies with other on-board navigation systems. Figure 21 shows the flight profile for this test. The west to east flight profile was used to take maximum advantage of the test satellite constellation visibility. About half the flight was conducted using a three satellite solution. Accurate navigation using three satellites is possible by entering the users altitude which, in effect, replaces one of the satellites in the solution computation. Navstar results compared favorably with the on-board Omega, inertial and TACAN navigation systems. When crossing the Air Defense Identification Zone (ADIZ) off the west coast of the United States, air traffic control radars could not detect any error between the GPS equipped P-3 and the ADIZ fix that was being used as a waypoint.

SHIPBOARD OPERATIONS

Shipboard accuracy tests began in December 1978 aboard a U.S. Navy Landing Craft Utility (LCU) on an instrumented test range off San Clemente Island, California. These trials were conducted with both the high and medium dynamic user equipment sets during a period when only three satellites were available. The input of sea level altitude eliminated the need for the fourth satellite. For this test, the "truth" reference was a Motorola miniranger system installed at four surveyed positions on the island (see Figure 22). This system was evaluated against the laser trackers at YFG and was determined to be accurate to within a meter.

P3 NAVSTAR OVER-WATER FLIGHT
1-CHANNEL Y AND 2 SETS 12 MARCH 1979 3/4 SATELLITES

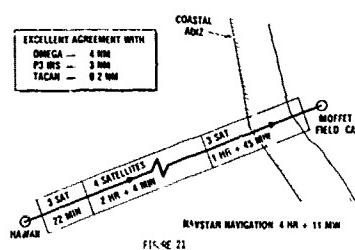


FIGURE 21

LCU NAVIGATION ACCURACY TEST PROFILE

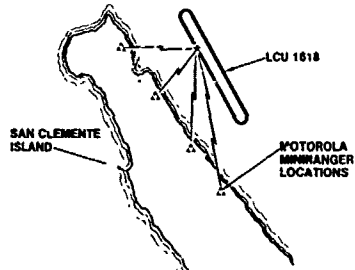


FIGURE 22

Figure 23 is the plot of the high and medium dynamic set performance for 13 December 1978 while navigating with three satellites. As shown, both sets were navigating to an accuracy of about ten meters during periods of good satellite geometry. After about eighty minutes, the satellite Geometric Dilution Of Precision (GDOP) increased as the satellites clustered at high elevation angles. This was predictable for the three satellite test constellation and will not occur with the eighteen satellite operational constellation. When the GDOP improved, the sets again navigated to about a ten meter accuracy. Figure 24 is a photo of the Control Display Unit of the high dynamic set (left) and the medium dynamic set (right) during the navigation trials. Both sets were operating independently at the time. Note the agreement between the two solutions.

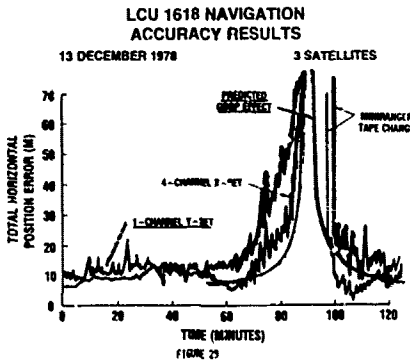


FIGURE 23

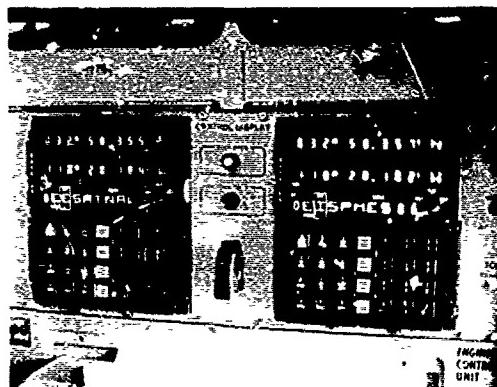
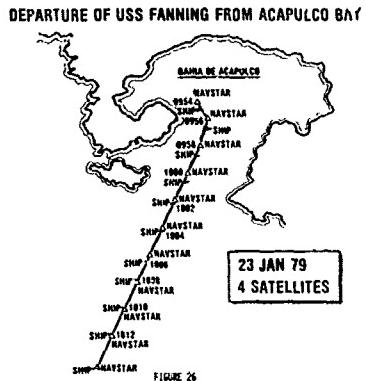
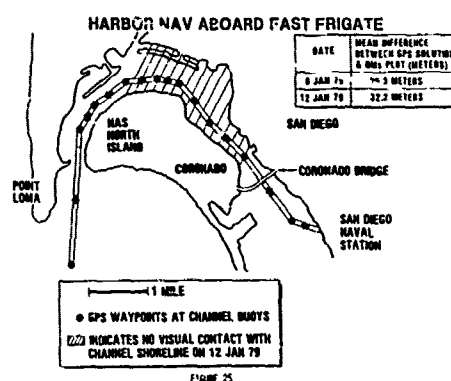


FIGURE 24

Harbor navigation aboard the fast frigate, USS Fanning (FF 1076), was accomplished by entering the positions of the channel buoys in the San Diego Harbor as Navstar waypoints. Voice commands from the Navstar operator to the bridge provided the ship's navigator with GPS steering information from one waypoint to the next. In addition, the navigator maintained a plot of visual fixes (accurate to about 20 meters) for purposes of comparison with the Navstar solution. Figure 25 shows the Navstar waypoints utilized and the mean difference between the GPS solution and the navigator's plot for the testing conducted on 12 January 1979. The hash-marked area was transited under low visibility conditions due to heavy fog, during which time Navstar was used almost exclusively for navigation.

During the latter part of January 1978, the USS Fanning embarked on a ten-day, round-trip cruise between San Diego and Acapulco, Mexico with the Navstar equipment and test team aboard. Although no reference trajectory for the ship's precise track was available, it was demonstrated that Navstar could provide continuous, real-time, navigation information during extended cruises. In addition, the cruise marked the first time that four-satellite navigation was accomplished in a part of the world other than an area in the southwestern United States. Figure 26 is a portion of the ship's navigation chart marked with Navstar (triangles) and visual (circles) fixes, showing its track out of the Bay at Bahia De Acapulco, Mexico.



PARADROPS

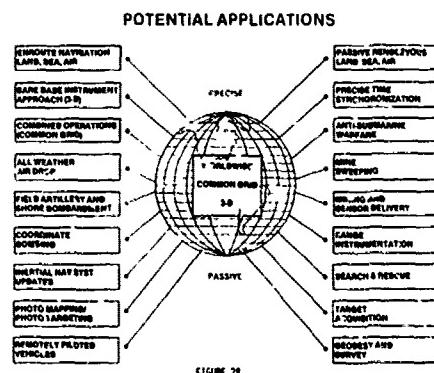
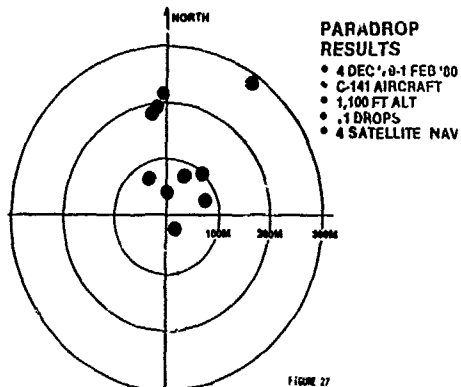
Although not required for Concept Validation, paratroop tests were conducted using the C-141 aircraft. The calculated release point for the drop, based upon altitude, wind and parachute characteristics, was entered as a Navstar waypoint. A cockpit steering display provided azimuth corrections as well as a release point indication to the pilot. Crewman aboard the C-141 executed a manual release of the parachutes upon command. Results of these trials are shown in Figure 27.

OPERATIONAL APPLICATION

The end use for the Navstar GPS system, from a U.S. DOD viewpoint, is to improve the effectiveness of the U.S. and allied military forces. Cost benefit studies show that accurate positioning and navigation enhanced significantly almost all land, sea and air missions. The aggregate improvement for such a wide range of applications results in a large force multiplier. It is beyond the scope of this paper to discuss in detail potential GPS applications, however, Figure 28 illustrates some of the mission areas where military effectiveness is improved dramatically. Civilian applications are equally impressive.

CONCLUSIONS

A great deal of Navstar testing has not been included in this paper because it was the intent of the author to restrict the scope to recent significant user equipment accomplishments for which data are readily presentable. The testing accomplished to date has met or exceeded almost every expectation or goal of the program. In the main, this impressive test record is attributable to the determined professional effort by the government, military, civilian and contractor personnel involved in the Navstar Concept Validation. The results presented represent, in distilled form, the contractor and government personnel, who believe in the vast potential of Navstar GPS and who are working to create a revolutionary improvement in navigation capability for military and civilian users worldwide.



ESTIMATION OF STRAPDOWN SENSOR PARAMETERS FOR
INERTIAL SYSTEM ERROR-COMPENSATION

by

Dr.D.K.Joos
U.K.Krogmann

Bodenseewerk Gerätetechnik GmbH
Postfach 1120
D-7770 Überlingen, Germany

SUMMARY

The performance of an inertial navigation system (INS) is largely affected by a number of important error-sources, where most of which are related to the instruments used. This particularly applies to strapdown-systems.

The paper describes laboratory test procedures to determine static and dynamic parameters of the gyro and accelerometer measurement model.

It is shown, that a proper rate-test and a multiposition test with respect to earth-rate and gravity-vector are well suited to ascertain static parameters with sufficient accuracy. Optimal parameter values are retrieved from measured test-data applying regression analysis techniques. It is shown, how uncertainties in parameter estimates can be determined from actual measurement residues.

The verification of major dynamic performance parameters of interest (i.e. anisoinertia torque, angular acceleration term) by appropriate test procedures utilizing a 3-axes test-table is shown.

Applicability and feasibility of the proposed test-procedures is demonstrated utilizing the Modular Strapdown System (MSS).

Test-configuration and sequence as well as processing of test-data including collection and reduction are described. Significant MSS error-parameters are extracted and evaluated applying iterative linear regression techniques. The corresponding software-structure is described.

The results obtained confirm the usefulness of the developed test-procedures and software for calibrating a strapdown-system with sufficient accuracy. Moreover it can be stated that the software-package exceeds its pure calibration function. It proved to offer a considerable potential to analyse a strapdown-system as well as the test-equipment.

1. Introduction

The objective of INS-Testing is usually devoted to demonstrate basic system navigation accuracy.

The performance of an inertial navigation system is largely affected by a number of important error sources, where most of which are related to the instruments used. This particularly applies to strapdown-systems.

Recent advances in sensor technology have provided instruments capable of determining angular rates and acceleration with high accuracy over a broad spectrum of dynamic conditions.

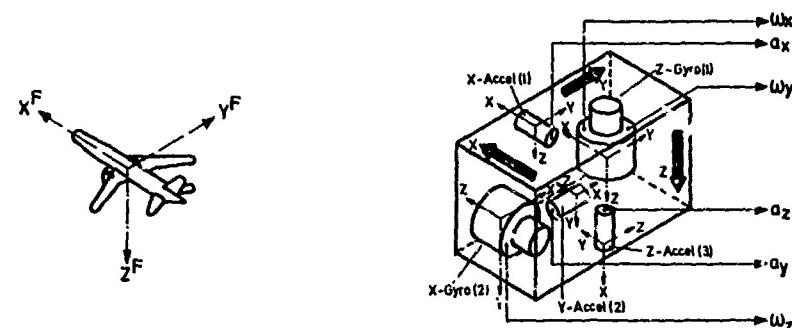
To fully utilize this potential requires accounting for several instruments- and system effects, which otherwise would cause considerable navigational errors. To accomplish this, precise laboratory measurement and identification of important parameters are necessary. Such sensor performance information represents the basis for the calibration of error-compensation algorithm included in the Strapdown-Inertial-System software.

2. Strapdown Sensor-Error-Models

Utilization of the inherent capabilities of todays inertial instruments requires accounting for several sensor- and system-effects, which otherwise would cause considerable navigational errors.

The extent of the parameter compensation becomes evident considering the sensor-error-models. The procedures described in the following are used for the calibration of a system containing two-axes dynamically tuned gyros with electrical caging as sensors for the angular rate.

In Figure 1 the sensor arrangement of the strapdown inertial measuring unit (IMU) with respect to vehicle-axes is shown. Furthermore the measurement equations for the two sensitive axes of the Z-gyro (1) are represented in tabulated form. Beside the desired rate term these equations contain a number of perturbing signal components. Some are determined by the imperfection of the sensors and their mounting (e.g. bias, mass-unbalance, misalignment etc.) and others are due to physical reasons (anisoinertia, angular acceleration, etc.).



Z - GYRO (1)		Measured Error - Terms
Y - Axis	X - Axis	
$\frac{M_x}{H} = (1+DSF_y) \cdot$	$-\frac{M_y}{H} = (1+DSF_x) \cdot$	Scalefactor
$\cdot [w_y]$	$\cdot [w_x]$	Desired Rate Term
$+ \alpha_{yx} \cdot w_z - \alpha_{yz} \cdot w_x$	$+ \alpha_{xz} \cdot w_y - \alpha_{xy} \cdot w_z$	Misalignment
$- m \cdot a_y + q \cdot a_x + n \cdot a_y \cdot a_z$	$- m \cdot a_x - q \cdot a_y + n \cdot a_x \cdot a_z$	Accel. Dep. Terms
$+ \frac{C-A}{H} \cdot w_z \cdot w_y - \frac{A}{H} \cdot \dot{w}_x - \frac{C}{H} \cdot \dot{a}_y \cdot w_y$	$+ \frac{C-A}{H} \cdot w_z \cdot w_x - \frac{A}{H} \cdot \dot{w}_y - \frac{C}{H} \cdot \dot{a}_x \cdot w_x$	Dynamic Terms
$+ b_y]$	$+ b_x]$	Bias

Fig.1: Error-Model of a dry tuned 2-axes Strapdown-Gyro

In order to extract the useful information w_x, w_y, w_z from the measurable torquer signals M_y/H and M_x/H a compensation of static and dynamic error components in the measuring equations is necessary as shown in Figures 2 and 3 for gyro 1.

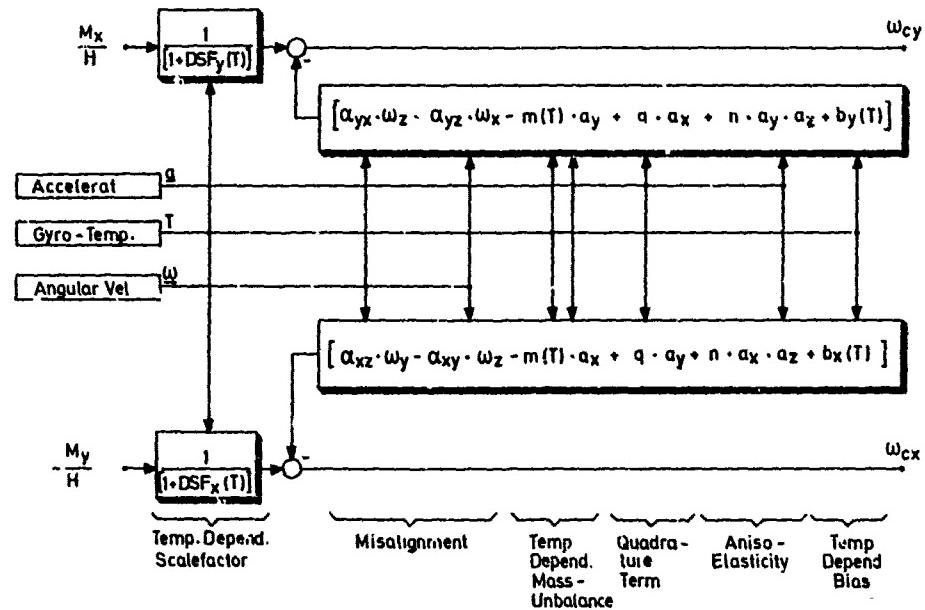


Fig.2: Compensation of static Gyro-Errors

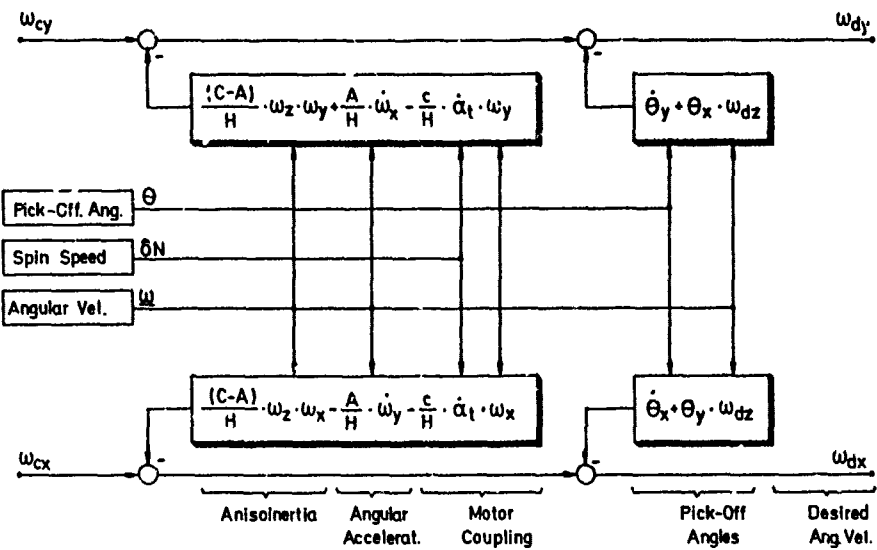


Fig.3: Compensation of Dynamic Errors

For compensating the unwanted terms the parameters of the error-model and the exact inertial rates as well as the acceleration components of the sensor block must be known.

The parameters of the error-model are determined by appropriate tests as described in the following. Due to the fact that some parameters are temperature-dependent, these tests have to be performed at various sensor temperatures.

The exact inertial angular rates and accelerations will only be available after compensation. For this reason only the uncompensated sensor signals can be used for the error compensation.

For the compensation of the dynamic components (Figure 3) the pickoff angles of the gyros and the rotor speed are also measured.

Regarding single-axis pendulous accelerometers considered here the corresponding linearized error-model for the x-accelerometer as well as the corresponding compensation block-diagram is shown in Figure 4. Fortunately full compensation of all error terms is not necessary in any application. Depending on the individual requirements means for proper compensation have to be implemented after careful analysis.

$$\frac{U_x}{SF_x} = (1+DK_x(T)) [a_x + \epsilon_{xz} \cdot a_y - \epsilon_{xy} \cdot a_z + KQ_x \cdot a_x^2 + B_x(T)]$$

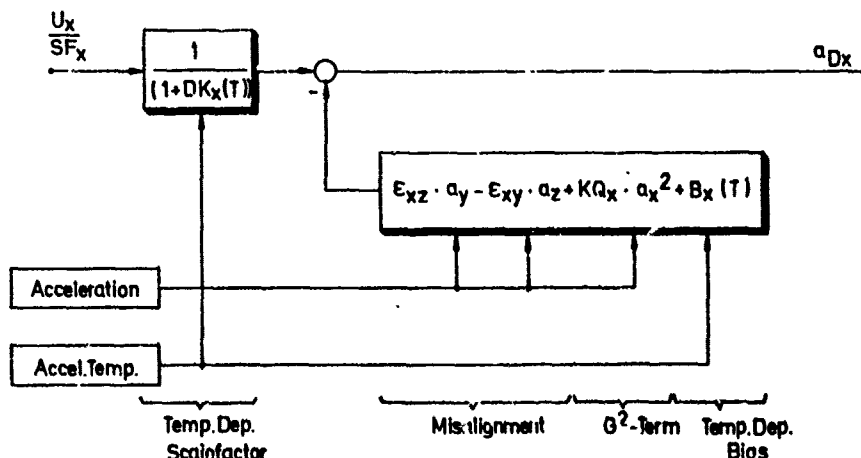


Fig.4: Compensation of Accelerometer-Errors

3. Determination of Gyro-Parameters

3.1 Test-Objective

The objective of laboratory tests to be performed is twofold:

- determination of static parameters
- verification of dynamic parameters

With respect to the first item two different types of tests have to be distinguished:

- rate-test to determine those parameters excited by external rates
- multi-position static test to determine all remaining parameters excited by external acceleration.

To accomplish this, a three-axis test-table is considered here as the main test-equipment.

3.2 Parameters for the Compensation of Static Errors

3.2.1 Rate-Test

The objective of the rate test is to determine
scale-factor

and

misalignment-errors.

Performing this task requires commencing through the following sequence of steps:

- adjust test-table sequentially in 3 positions, where in each position one of the three IMU main-axes is aligned to the local vertical
- rotate test-table CW and CCW about the vertical axis of the table with constant rate by 360°
- in each position integrate measured torquing-signals over a full period for CW- and CCW-rotations
- compute the differences of integrated signals for CW and CCW rotations.
These differences are proportional to scale-factor and misalignment errors.

As shown in Figure 5 the sensor block is arranged in test-position 1 on a test-table with respect to earth-rate and gravity-vector.

Following the sequential steps the resulting differences of the integrated signals for CW and CCW-rotations are shown in Figure 5 for test position 1.

From Figure 5 it also becomes ultimately evident, that in this testposition 1 the misalignments α_{xy} and α_{yx} become observable by an introduced table rate ψ_3 .

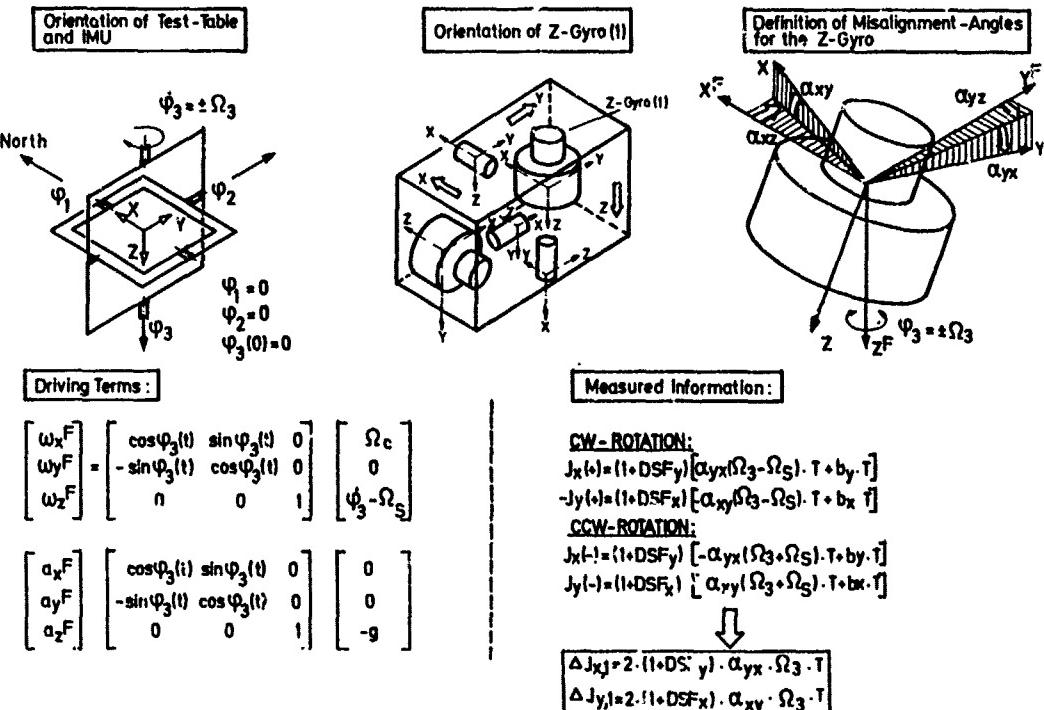


Fig.5: Rate - Test - Position 1

Figure 6 shows the three test positions required for the determination of the static parameters of the Z-gyro (1) according to the rate test procedure specified herein. In addition the determining equations for the scale-factor and alignment errors are listed.

Further positions and rotations about other axes of the test table provide redundant measuring information for the unknown parameters (see Figure 7). These then can be determined optimally in a least square sense applying linear regression techniques as described for the following multi-position test:

In order to determine possible non-linearities of the scale factor the tests must be performed at various rotation rates of the test-table.

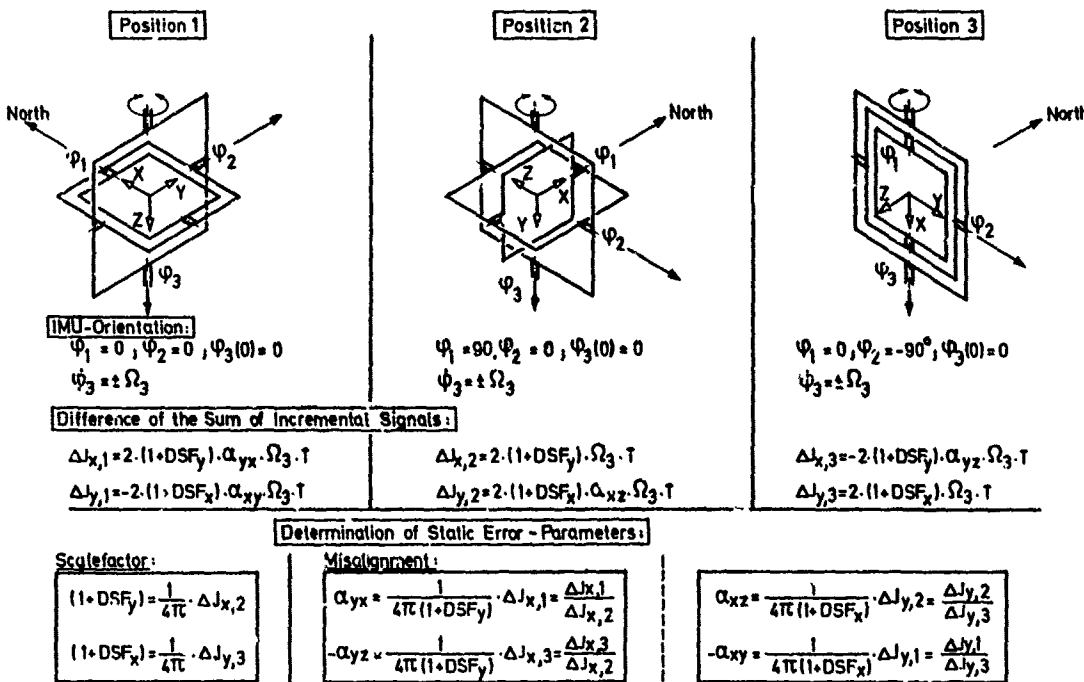


Fig.6: Static-Error-Parameters from a 3-Position Rate-Test

3.2.2 Multi-Position Static Test

The objective of the multi-position test is to determine the following gyro parameters excited by external acceleration:

- mass-unbalance
- quadrature term
- anisoelasticity.

Furthermore the bias drift is determined simultaneously.

To accomplish this, the following test procedure is appropriate:

- perform multi-position test by orienting the IMU in a number of predetermined positions with respect to earth-rotation and gravity-vector
- measure gyro torquer-signals over a predetermined period of time
- perform linear regression analysis to determine the best estimate for the error-parameter vector in a least squares sense.

Again only gyro 1 is considered in the following:

For the multi-position-test it is assumed that the scale-factor and misalignment-errors have been determined through the rate-test.

Figure 7 shows the individual orientations of the sensor block for the full 24-position-test. The three main positions are identified by the fact that each sensor block axis is oriented once in the north, east and vertical direction.

Each main position includes 8 test positions. They result from the stepwise tilting of the sensor-block by respectively 45° about the axes of the test table as shown in Figure 7. Different components of the earth-rotation and the gravity-vector are thus always acting along the sensor-block axes ($\omega_x, \omega_y, \omega_z$ resp. a_x, a_y, a_z) thus exciting corresponding error-terms in the measurement equations.

If "n" positions are generally considered, the measurement model according to equation (4.12) will result, for instance, for the Y-axis of gyro 1 (see also Figure 1).

$$\frac{1}{(1+DSF_y)} \cdot \begin{bmatrix} \frac{M_x}{H}(1) \\ \frac{M_x}{H}(2) \\ \frac{M_x}{H}(n) \end{bmatrix} - \begin{bmatrix} \omega_y(1) & \omega_z(1) & -\omega_x(1) \\ \omega_y(2) & \omega_z(2) & -\omega_x(2) \\ \omega_y(n) & \omega_z(n) & -\omega_x(n) \end{bmatrix} \cdot \begin{bmatrix} 1 \\ \alpha_{yx} \\ \alpha_{yz} \end{bmatrix} = \begin{bmatrix} -\alpha_y(1) & \alpha_x(1) & \alpha_y(1) \cdot \alpha_z(1) & 1 \\ -\alpha_y(2) & \alpha_x(2) & \alpha_y(2) \cdot \alpha_z(2) & 1 \\ -\alpha_y(n) & \alpha_x(n) & \alpha_y(n) \cdot \alpha_z(n) & 1 \end{bmatrix} \cdot \begin{bmatrix} m \\ q \\ n \\ b_y \end{bmatrix} + \begin{bmatrix} v(1) \\ v(2) \\ v(n) \end{bmatrix} \quad (3.1)$$

Known From Rate-Test	Torquer Signals In Diff. Positions	Determined From Test-Table Position
Known From Rate Test	Determined From Test-Table Position	Unknown Parameter-Vector

<u><u>Z</u></u>	<u><u>A</u></u>	<u><u>x</u></u>	<u><u>v</u></u>
Measurement-Vector	Measurement-Matrix	Parameter Vector	Measurement Noise

Lin Regression-Model:
$$\underline{\underline{Z}} = \underline{\underline{A}} \cdot \underline{\underline{x}} + \underline{\underline{v}}$$

Assuming that the individual measurements are statistically independent, this is an equation in the form of a linear regression model:

$$\underline{\underline{Z}} = \underline{\underline{A}} \cdot \underline{\underline{x}} + \underline{\underline{v}} \quad (3.2)$$

An optimal estimate $\underline{\underline{x}}$ of the parameter vector $\underline{\underline{x}}$ in the sense of minimum error squares can be determined as follows:

$$\hat{\underline{\underline{x}}} = (\underline{\underline{A}}^T \underline{\underline{A}})^{-1} \cdot \underline{\underline{A}}^T \cdot \underline{\underline{Z}} \quad (3.3)$$

If $\underline{\underline{x}}$ is an m -dimensional vector, it is necessary that $\underline{\underline{A}}$ must include m linear-independent row-vectors to ensure full observability of $\underline{\underline{x}}$.

The following applies to the variance of the optimally estimated value $\underline{\underline{x}}$ if the individual measurements have equal variances σ^2 :

$$\text{VAR}(\hat{\underline{\underline{x}}}) = \sigma^2 \cdot (\underline{\underline{A}}^T \underline{\underline{A}})^{-1} \quad (3.4)$$

An unbiased estimate for σ^2 can be computed from the residues of the measured values:

$$(3.5)$$

$$\hat{\sigma}^2 = \frac{\underline{\underline{w}}^T \underline{\underline{w}}}{N - M}$$

with

$$\underline{\underline{w}} = \underline{\underline{z}} - \underline{\underline{A}} \cdot \underline{\underline{x}}$$

N = number of positions (measurements)

M = number of unknown parameters

For a subset of 8 positions that are specially marked in Figure 7 the quantitative regression-model is indicated in Figure 8. The acceleration- and rate-values of the test position 4 can for instance be readily explained by means of the gyro orientation shown in Figure 8. In this respect the test position 4 is derived from the main position 1 by the rotation $\psi_1 = 135^\circ$.

The observability of the parameter vector of equation (3.1) by means of the selected 8 positions is ensured because the determinate derived from four arbitrary rows of the A-matrix (Figure 8) is not equal to zero. There exist therefore four linear independent row-vectors of A.

If the measurement matrix A according to Figure 8 is now used in equation (3.4) the variance of the optimally estimated value \hat{x} for the parameter vector x is shown in Figure 9 together with that for the full 24-position-test.

Supposing that the torquer signals of the gyros in the individual positions are measured with an accuracy of $0.01^\circ/\text{h}$ (i.e. measurement noise $\sigma^2 = (0.01^\circ/\text{h})^2$) the accuracies of the estimated parameters result as shown in Figure 9.

With the exception of the anisotropicity coefficient the measurement noise is reduced by the 8-position test.

Main Position Nr	Initial Position of the Three Axis Test Table	IMU-ATTITUDE			
		$\varphi_1(\text{Roll})$	$\varphi_2(\text{Pitch})$	$\varphi_3(\text{Yaw})$	
1		0°	0°	0°	
		45°	0°	0°	
2		90°	0°	0°	
		135°	0°	0°	
3		180°	0°	0°	
		225°	0°	0°	
		270°	0°	0°	
		315°	0°	0°	
2		0°	-90°	-90°	
		0°	-5°	-90°	
3		0°	0°	-90°	
		0°	45°	-90°	
		0°	90°	-90°	
		0°	135°	-90°	
		0°	180°	-90°	
		0°	225°	-90°	
		90°	0°	90°	
		90°	45°	90°	
		90°	90°	90°	
		90°	135°	90°	
		90°	180°	90°	
		90°	225°	90°	
		90°	270°	90°	
		90°	315°	90°	
Measurement Sum of the Incremental Sensor Signals					
Measur Time 10 Min					
Const rate $\pm 0.1, 0.3, 1, 3, 10 \text{ deg/sec}$					

Fig.7: Summary of Test - Positions

Model for the 8-Position-Test:
 $\text{Lat} = 45^\circ, \Omega_E = \Omega_E \cos 45^\circ = \Omega_E \sin 45^\circ$

$$\frac{1}{\Omega_E + D\dot{\Omega}_E y} \begin{bmatrix} M_{(I)} \\ M_{(II)} \\ M_{(III)} \end{bmatrix} = \begin{bmatrix} 0 & -1 & -1 \\ -\frac{1}{2}\sqrt{2} & -\frac{1}{2}\sqrt{2} & -1 \\ -1 & 0 & -1 \\ -\frac{1}{2}\sqrt{2} & \frac{1}{2}\sqrt{2} & -1 \\ 0 & 0 & -1 \\ 0 & 1 & -1 \end{bmatrix} \begin{bmatrix} 1 \\ d\dot{y}_x \\ d\dot{y}_z \end{bmatrix} + \begin{bmatrix} 0 & 0 & 0 & 1 \\ \frac{1}{2}\sqrt{2} & 0 & 0 & \frac{1}{2}\sqrt{2} \\ 0 & -\frac{1}{2}\sqrt{2} & 0 & -\frac{1}{2}\sqrt{2} \\ 0 & 0 & -1 & 0 \\ 0 & 0 & 0 & 1 \end{bmatrix} \begin{bmatrix} m_x \\ m_y \\ m_z \\ b_y \end{bmatrix}$$

$Z(t)$

$\text{Lat} = 45^\circ$
 $\Omega_E = \Omega_E \cos 45^\circ = \Omega_E \sin 45^\circ$
Main Position No.1

$\psi_1 = 135^\circ$
 $\psi_2 = \psi_3 = 0$

North
 East
 Local-Vert (Down)
Test-Position No.4
2-GYRO (II)

Fig.8: Regression-Model for Multi-Position-Test

8-Position-Test			
$\text{Var}(\hat{x}) = \sigma^2 \cdot$	$\begin{bmatrix} 0,36/g & 0 & 0 & -0,06/g \\ 0 & 0,5/g^2 & 0 & 0 \\ 0 & 0 & 2/g^4 & 0 \\ -0,06/g & 0 & 0 & 0,14 \end{bmatrix}$	$\sigma(\hat{m}) = 0,006^\circ/\text{h}/\text{g}$ $\sigma(\hat{q}) = 0,007^\circ/\text{h}/\text{g}$ $\sigma(\hat{n}) = 0,014^\circ/\text{h}/\text{g}^2$ $\sigma(\hat{b}_y) = 0,004^\circ/\text{h}/\text{g}$	
	24-Position-Test		
	$\text{Var}(\hat{x}) = \sigma^2 \cdot$	$\begin{bmatrix} 0,125/g & 0 & 0 & 0 \\ 0 & 0,125/g & 0 & 0 \\ 0 & 0 & 0,7/g^4 & 0 \\ 0 & 0 & 0 & 0,04 \end{bmatrix}$	$\sigma(\hat{m}) = 0,004^\circ/\text{h}/\text{g}$ $\sigma(\hat{q}) = 0,004^\circ/\text{h}/\text{g}$ $\sigma(\hat{n}) = 0,008^\circ/\text{h}/\text{g}^2$ $\sigma(\hat{b}_y) = 0,002^\circ/\text{h}/\text{g}$

Fig.9: Covarianve-Analysis Results for one Gyro-Axis

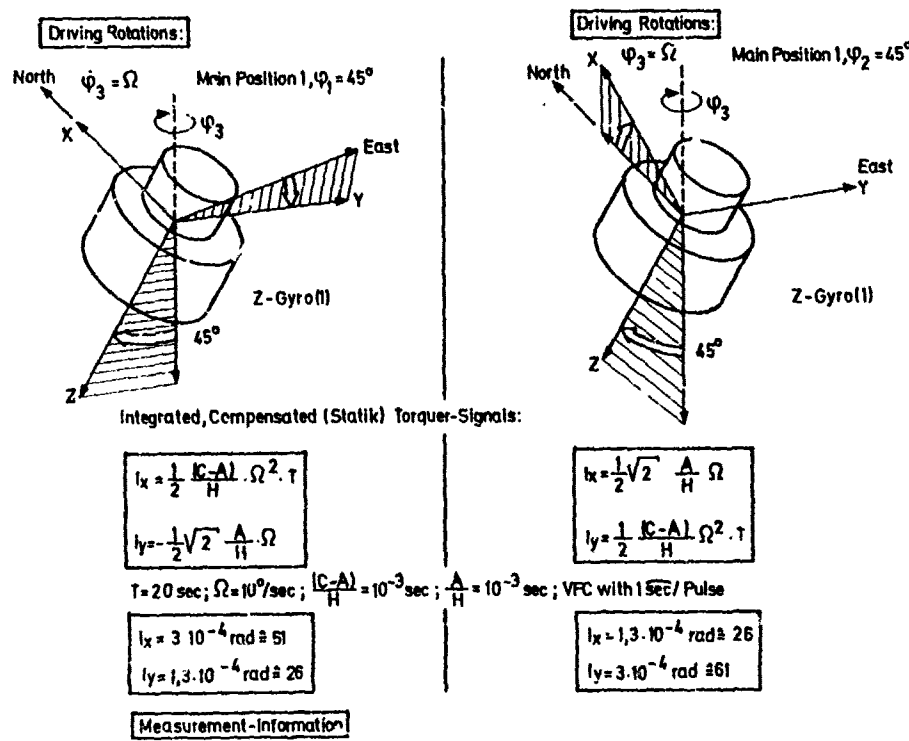


Fig.10: Verification of Anisoinertia and Angular-Acceleration Term

3.3 Dynamic Parameters

3.3.1 General Remarks

As shown in Figure 3, the following dynamic effects have to be taken into consideration:

- angular acceleration term
- anisoinertia term
- motor coupling

For simultaneous harmonic motions about the spin axis and about one of the input axes there further occurs the socalled pick-off-rectification effect which is taken into account for the compensation according to Figure 3 by measuring the pick-off angles. Due to the large bandwidth of the gyro caging loops, for aircraft applications the pick-off angles are small and therefore rectification-effects are often negligible. For this reason a compensation is often not required. As can be seen from Figure 6 no particular parameter is involved in the compensation of pick-off angle effects.

The parameters of the three above mentioned components are determined by the design of the gyro. They can be measured with a slide-gauge, so to speak and are not subject to considerable changes from gyro to gyro. For this reason it is therefore not appropriate to speak of sensor error parameters here. The gyro manufacturer can indicate these parameters accurately. A dynamic test is rarely performed for verifying the manufacturing data.

The motor coupling term should not be further considered here as its verification requires special measurements in the frequency domain to discern it from the frequency-independent anisoinertia-term. This goes beyond the scope of this paper.

For the two other components various procedures are contemplated in the following where the application of which is based on the available test equipment.

3.3.2 Anisoinertia-Term

Again only gyro 1 (z-gyro) is considered in the following.

The general measurement equations show that this term can be excited by simultaneous angular rates ω_z and ω_x respectively ω_z and ω_y .

For verifying (C-A)/H the sensor block is oriented as shown in Figure 10 and rotated about the vertical axis of the test table (γ_3) with a step angular rate for a duration of T seconds. The thus generated angular rates ω_z and ω_y respectively ω_z and ω_x excite contributions in the torquer signals Mx/H and My/H generated by (C-A)/H.

If these torquer signals are compensated for the known static error portions and integrated the signals I_x and I_y shown in Figure 10 will result.

Let us assume that these integrated values are available as pulse sequences at the output of voltage/frequency converters with a pulse weight of 1 arcsec.

For $T = 20$ sec, $= 10^0/\text{sec}$ the number of generated pulses for typical values (C-A)/H is readily measurable so that (C-A)/H can be verified as shown in Figure 10.

If + 1 pulse is assumed as uncertainty, the accuracy for the determination of (C-A)/H is in the order of 2%.

The parameter A/H determining the angular acceleration term is also excited during this test. The reason is the angular acceleration phase necessary to obtain the constant table rate. Its measuring accuracy is approximately 4% for the assumed test conditions. Another test method is described in paragraph 3.3.3.

Two further procedures for the verification of (C-A)/H are presented in Figure 11 using sinusoidal or uniform angular rates.

In this respect it is always assumed that the measured torquer signals are compensated for the other error-model portions which are assumed to be known.

For sinusoidal excitation about the Y and Z-axis (spin-axis of the z-gyro (1) of the sensor block) the torquer signal Mx/H contains besides the nominal term the portions proportional to (C-A)/H shown in Fig. 11.

The latter can be considered as error ω_y in the measurement of ω_z . The portions are independent of the frequency of the excitation signals as long as it is smaller than the bandwidth of the caging loops. For typical value of (C-A)/H = 10^{-3} sec the rectified portion causes a drift of $\Delta\omega_y = 0.02^0/\text{h}$ per $1^0/\text{sec}$ amplitude of the angular rate input.

The motor coupling is also excited by ω_z if the frequency of the test signals is not smaller than 1 - 2 Hz.

Figure 11 shows an alternative possibility for the verification of (C-A)/H. The sensor block is tilted on the test table about the X-axis through 45^0 so that for γ_3 -rotations about the vertical axis of the test table angular rates ω_y and ω_z of the sensor block will occur.

For constant positive and negative rates $\dot{\varphi}_3 = \pm \Omega$ the x-torquer signal is recorded. The sum of both torquer signals contains as useful information the portion $(C-A)/H$. This leads with the numerical values shown in Figure 11 to an amount of $6^\circ/h$ for the sum of the torquer signals. This value can be readily measured with a suitable test equipment.

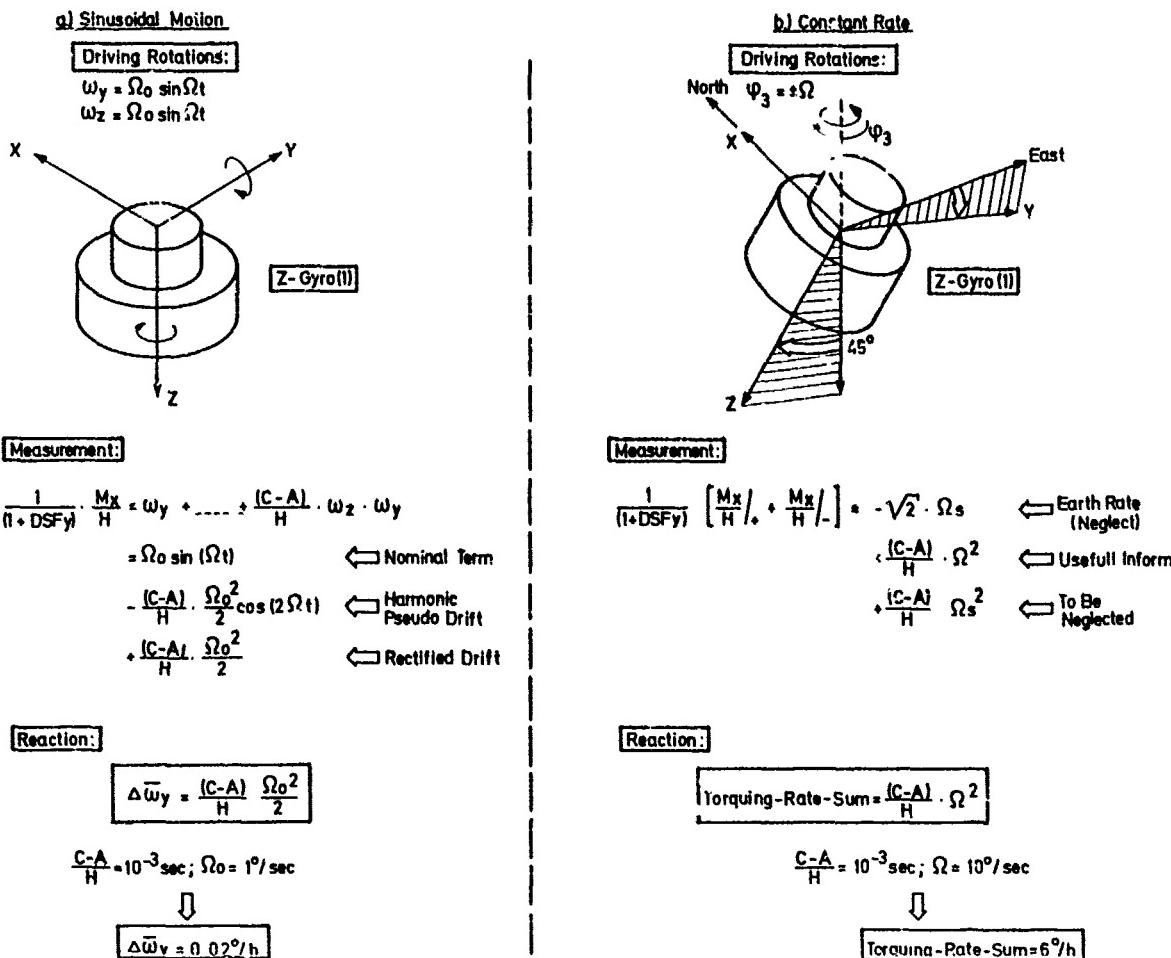


Fig.11: Verification of Anisoinertia-Term

3.3.3 Angular-Acceleration Term

As shown in paragraph 4.3.2, during the tests indicated in Figure 10 information is also obtained about the parameter A/H which determines the angular-acceleration term. In order to excite this term in the x-torquer signal of the z-gyro an angular acceleration $\dot{\omega}_x$ is necessary. In this basis Figure 12 shows two further test-possibilities. In Figure 12 this term is excited by a sinusoidal rate about the x-axis.

The compensated torquing signal M_x/H contains a part ω_y according to $A/H \cdot \Omega_0 \cdot \Omega \cdot \cos(\Omega \cdot t)$. Together with the nominal sinusoidal rate ω_x measured by the torquing-signal M_y/H this gives rise to a pseudo-coning motion. This in turn causes a rectified drift about the third axis (heading-drift $\dot{\psi}$) which might be observed directly or from resultant velocity errors in the full inertial navigation system.

An alternative more direct method is shown in Figure 12. A step-rate-input about the x-axis produces an observable averaged y-axis rate output $\bar{\omega}_y$, which is $7^\circ/\text{h}$ for a step-rate-input of $10^\circ/\text{sec}$, averaged over a time interval of 5 sec. Again this apparent y-axis drift could be observed directly or reduced from resulting velocity errors. Here the velocity error is caused by the averaged error rate $\bar{\omega}_y$, entering the schuler-loop as an impulse-perturbation.

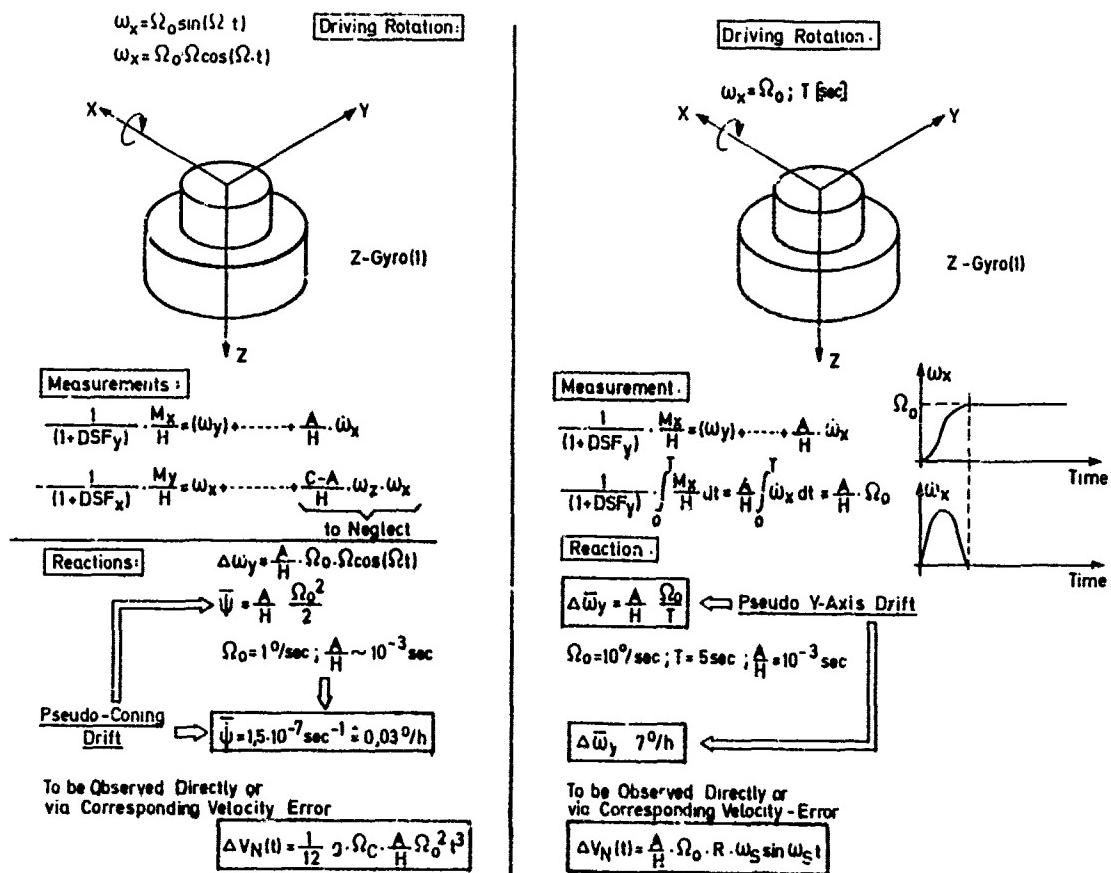


Fig.12: Verification of Angular-Acceleration-Term

4. Determination of the Accelerometer Parameters

The parameters of the accelerometers can also be determined by a multi-position test as described in paragraph 3.2.2 for the gyro.

For this purpose a linearization of the measurement equation (see Figure 4) is however required. The linearization provides the following error-model for the x-accelerometer:

$$\frac{U_x}{S_{Fx}} - a_x = D K_x \cdot a_x + e_{xz} \cdot a_y - e_{xy} \cdot a_z + K \theta_x \cdot a_x^2 + b_x \quad (4.1)$$

Figure 13 shows the linear regression model for a 6-position test. For this test those 6 positions of the 24 general positions are selected in which each surface of the sensor block is pointing once on downward direction. These positions are specially marked in Figure 13. Looking at the measurement matrix shown, it contains at least five linearly independent row-vectors so that the parameter vector is observable.

It results from the variances computed according to (3.4) and shown in Figure 14 for the elements of the parameter vector that the measurement noise σ^2 is already reduced performing the 6-position-test. The variances are computed supposing a measurement-noise of $\sigma^2 = (10^{-4} g)^2$. As in the 24-position test more redundant information is available, the parameters can of course be determined more accurately, namely by the factor $\sqrt{24/6} = 2$.

The variances of the 24-position test apply similarly to all three accelerometers.

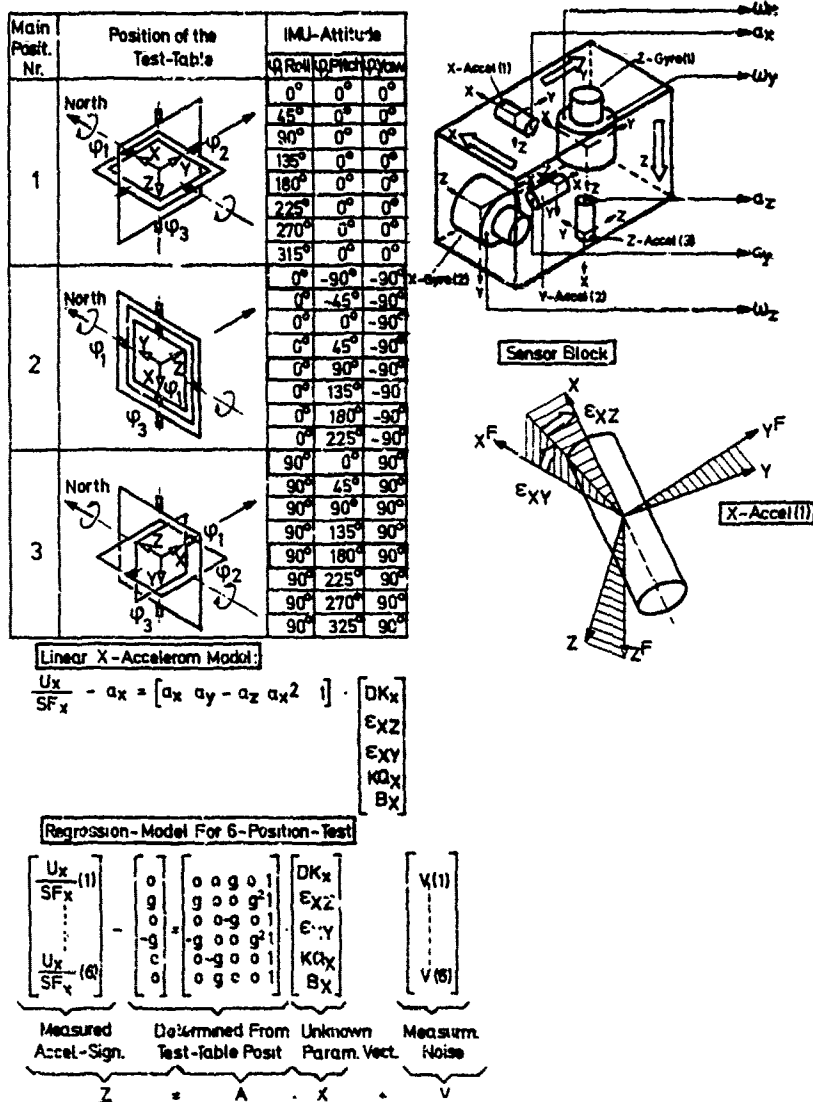


Fig.13: Accelerometer Regression-Model

6-Position-Test

$$\text{Var}(\hat{x}) = \sigma^2 \cdot \begin{bmatrix} 0,5/g^2 & 0 & 0 & 0 & 0 \\ 0 & 0,5/g^2 & 0 & 0 & 0 \\ 0 & 0 & 0,5/g^2 & 0 & 0 \\ 0 & 0 & 0 & 0,75/g^4 & -0,25/g^2 \\ 0 & 0 & 0 & -0,25/g^2 & 0,25 \end{bmatrix} \rightarrow \begin{aligned} \sigma(D\hat{K}_x) &= 0,71 \cdot 10^{-4} \\ \sigma(\epsilon_{XZ}) &= 0,71 \cdot 10^{-4} \\ \sigma(\epsilon_{XY}) &= 0,71 \cdot 10^{-4} \\ \sigma(K\hat{Q}_x) &= 0,87 \cdot 10^{-4}/g \\ \sigma(B_x) &= 0,50 \cdot 10^{-4}/g \end{aligned}$$

24-Position-Test

$$\text{Var}(\hat{x}) = \sigma^2 \cdot \begin{bmatrix} 0,125/g^2 & 0 & 0 & 0 & 0 \\ 0 & 0,125/g^2 & 0 & 0 & 0 \\ 0 & 0 & 0,125/g^2 & 0 & 0 \\ 0 & 0 & 0 & 0,3/g^4 & -0,1/g^2 \\ 0 & 0 & 0 & -0,1/g^2 & 0,075 \end{bmatrix} \rightarrow \begin{aligned} \sigma(D\hat{K}_x) &= 0,35 \cdot 10^{-4} \\ \sigma(\epsilon_{XZ}) &= 0,35 \cdot 10^{-4} \\ \sigma(\epsilon_{XY}) &= 0,35 \cdot 10^{-4} \\ \sigma(K\hat{Q}_x) &= 0,54 \cdot 10^{-4}/g \\ \sigma(B_x) &= 0,27 \cdot 10^{-4}/g \end{aligned}$$

$\sigma^2 = (10^{-4} g)^2$

Fig.14: Covariance for the x-Accelerometer

5. Application of Test-Methods to Calibrate the Modular-Strapdown-System (MSS)

5.1 Introductory Remarks

So far test-procedures have been described and treated in general. The following paragraphs are dealing with the application of these procedures for a particular system. First of all this system is briefly described.

With respect to potential applications in guidance and control of aircrafts, an experimental strapdown navigation system has been developed and built within the scope of the German Future Aircraft Technology Research Program (ZTL).

The following requirements have been established

- evaluation of the attitude angles and angular velocities in digital form
- autonomous alignment
- flexibility with respect to matching different accuracy categories by modular structure
- medium accuracy navigation performance of the experimental system
- possibility to update the system by external navaids.

For calibration purposes the MSS has been submitted to various position- and ratetests at IABG test facilities in Munich. It is the objective of the following paragraphs to demonstrate the applicability and feasibility of the proposed test-procedures to evaluate the basic system parameters of a strapdown system.

5.2 Description of the MSS

5.2.1 Inertial Measurement Unit (IMU)

The Figure 15 shows the inertial measurement unit (IMU), consisting of two parts: the electronic box, containing the caging loops, power amplifier V/F converters etc., and the inertial sensor unit with two dynamically tuned two degrees of freedom Teledyne gyro SDG5 and three Systron Donner accelerometers SD 4833A-1PX. Figure 16 gives a closer view of the sensor unit.

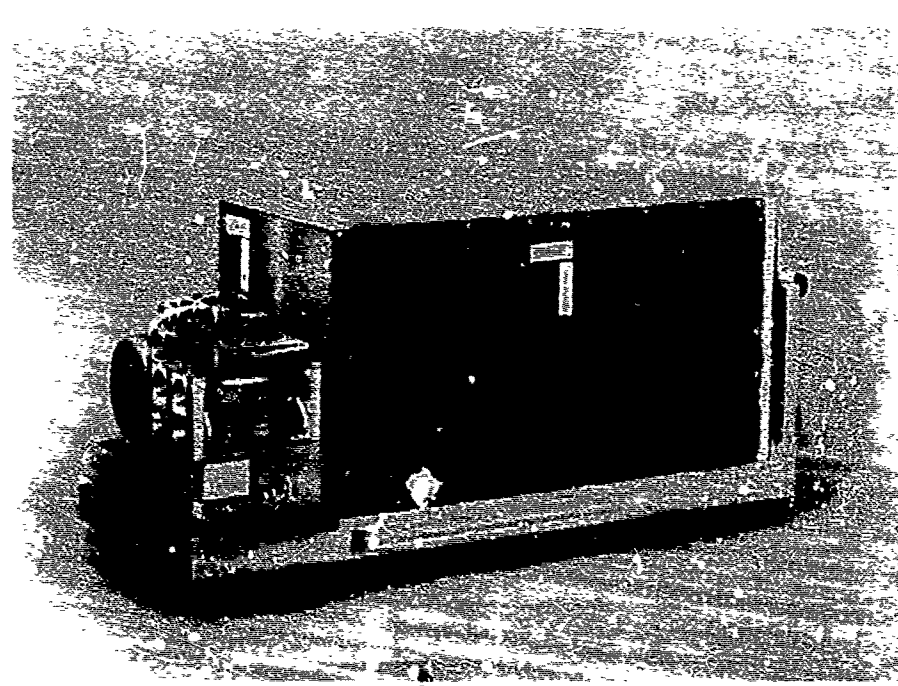


Fig.15: Inertial Measurement Unit of the Strapdown System



Fig.16: Sensor Unit

5.2.2 Error Model of the MSS

The error model for a single gyro resp. accelerometer has been discussed in the previous chapters. From these equations the whole error model of the MSS has been deduced and is presented in Figure 17, as far as the static error parameters are concerned.

Gyro 1

$$\frac{M_x}{H} = [1+DK_1(t)] \left[w_x + a_{xz} w_y - a_{xy} w_z - \text{mITI}_x \dot{q}_x + \dot{q}_y \ddot{q}_x + \dot{q}_z \ddot{q}_y + b_x(t) \right]$$

$$\frac{M_y}{H} = [1+DK_2(t)] \left[w_y + a_{yx} w_z - a_{yz} w_x - \text{mITI}_y \dot{q}_y + \dot{q}_x \ddot{q}_y + \dot{q}_z \ddot{q}_x + b_y(t) \right]$$

Gyro 2

$$\frac{M_z}{H} = [1+DK_3(t)] \left[w_z + a_{xy} w_x - a_{xz} w_y - \text{mITI}_z \dot{q}_z + \dot{q}_x \ddot{q}_z + \dot{q}_y \ddot{q}_x + b_z(t) \right]$$

Accel. 1

$$\frac{U_x}{H} = \left\{ 1+DK_X(t) \right\} \left[a_x + \epsilon_{xx} a_y - \epsilon_{xy} a_z + KQ_X \cdot a_x^2 + B_X(t) \right]$$

Accel. 2

$$\frac{U_y}{H} = \left\{ 1+DK_Y(t) \right\} \left[a_y + \epsilon_{yy} a_z - \epsilon_{yz} a_x + KQ_Y \cdot a_y^2 + B_Y(t) \right]$$

Accel. 3

$$\frac{U_z}{H} = \left\{ 1+DK_Z(t) \right\} \left[a_z + \epsilon_{zz} a_x - \epsilon_{zx} a_y + KQ_Z \cdot a_z^2 + B_Z(t) \right]$$

Fig.17: Sensor Error Model of the Modular Strapdown System

5.2.3 Accuracy Requirements upon the Tests

Prior to the tests it is necessary to specify how accurate the error parameters have to be determined to meet the demands put on the system performances. A common figure of merit for inertial navigation systems is the navigation accuracy expressed in nautical miles per hour.

From system analysis it is well known how single error sources propagate through the system. For the medium accuracy of the MSS it was stated that the uncompensated part of each significant error source should not exceed the limit of 1 nm/h. From this statement some dozens requirements upon the accuracy of determining the error parameters by static tests have been deduced.

The most important results are summarized in Table 1 and 2. The values shown refer to an aircraft with an assumed velocity of 400 kn.

ERROR	NOTATION	ACCURACY	UNITS
BIAS	B_X, B_Y	$3 \cdot 10^{-4}$	G
SCALEFACTOR	DSF	$3 \cdot 10^{-4}$	
	α_C	$3 \cdot 10^{-4}$	G/G^2
MISALIGNMENT			
LEVEL	α_{XY} α_{YX}	$1 \cdot 10^{-4}$	RAD
AZIMUTH	α_{XZ} α_{YZ}	$2,5 \cdot 10^{-3}$	RAD

Table 1: Accuracy Requirements upon Accelerometer Parameters

ERROR	NOTATION	ACCURACY	UNITS	NOTE
BIAS	B_X, B_Y	0,016	°/H	NAV MODE
	B_X, B_Y	0,025	°/H	ALIGN MODE
	B_Z	0,08	°/H	NAV MODE
SCALEFACTOR	DSFK	$3,9 \cdot 10^{-4}$	-	CIRCULAR
MISALIGNMENT				FLIGHT
LEVEL	α_{XY} α_{YX}	$4,6 \cdot 10^{-5}$	RAD	CIRCULAR
AZIMUTH	α_{XZ} α_{YZ}	10^{-3}	RAD	FLIGHT
Z-AXIS	α_{ZK} α_{ZY}			NOT CRITICAL
MASS UNBALANCE				
GYRO 1	M^1	0,7	°/H/G	ACCEL. FLIGHT
GYRO 1	M^1	0,1	°/H/G	ALIGN MODE
GYRO 2	M^2	0,2	°/H/G	STATION. FLIGHT
QUADRATURE				
GYRO 1	Q^1	0,7	°/H/G	ACCEL. FLIGHT
GYRO 2	Q^2	1	°/H/G	NOT CRITICAL

Table 2: Accuracy Requirements upon Gyro Parameters

5.3 Test Configuration

The philosophy of calibrating a strapdown system by tests consists basically in submitting the system to accurately known accelerations and angular velocities, observing the system output quantities, comparing them with the well defined input quantities and explaining the differences by the influence of various system error sources.

In Fig. 18 a schematic view of the testconfiguration is shown how it has been built up at IASG Munich. The IMU of the Strapdown System is fixed to the inner gimbal of the three axis test table. The test table is driven by the Interdata 8/32 Computer and is capable to orientate the IMU deliberately with respect to earth gravitational and rotational vector. Furtheron it is possible to rotate the IMU with very accurate constant angular velocity.

From the IMU leads a data link to the MSS navigation computer MIDI. By DMA the preprocessed data are transmitted to the Interdata 8/32 Computer and are recorded then together with the relevant data from the 3 axis test table on magnetic tapes.

The main processing of the test data runs off line on a IBM 370 Computer at Bodenseewerk in Überlingen.

In the sequel the essential features of the tests are described in more detail.

5.3.1 Three Axis Test Table

The three axis test table type 53 W from Contraves-Goerz Corporation is described in /3/.

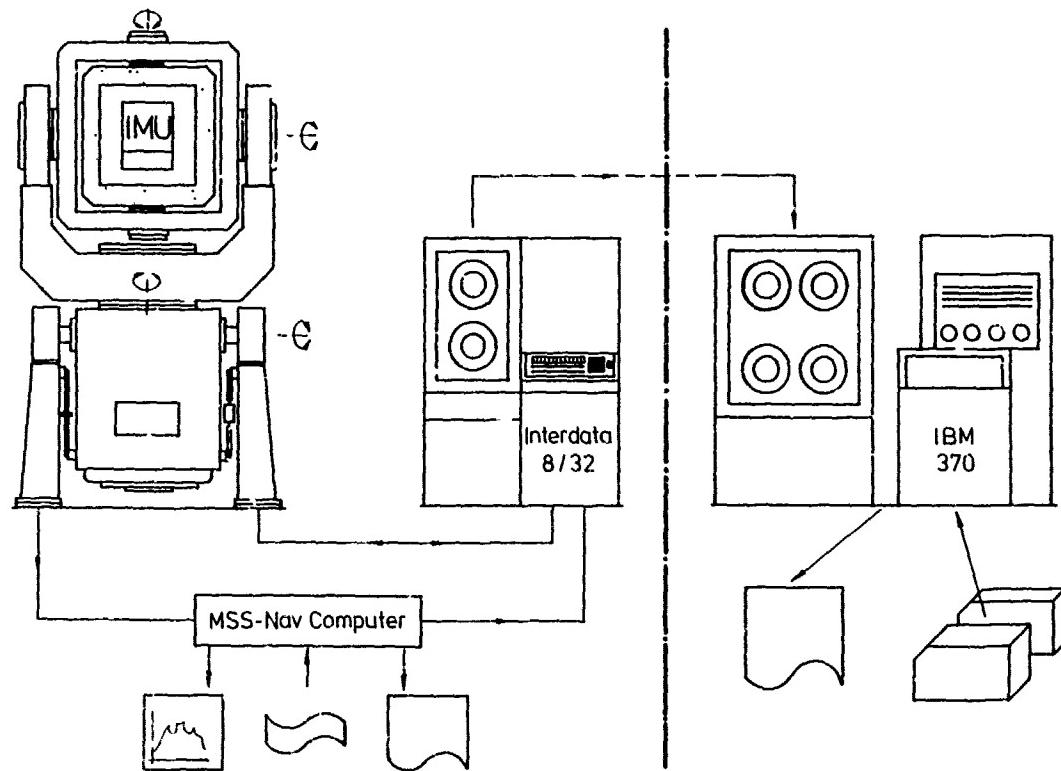


Fig.18: Testconfiguration

Data Transmission and Recording

The gyroscopes and the accelerometers torquer currents are measured by the voltage dropping at scale resistors. The voltages in turn are converted in the IMU by Voltages-to-Frequency-Converter into puls trains. In the navigation computer the pulses are accumulated and read out at constant time intervals. While navigating, the computer updates every 20 msec the quaternions, and every 100 msec an updating of the navigation occurs. In the test configuration, shown in Fig. 19, the accumulated increments are transmitted every 200 ms via DMA to the Interdata computer. The navigation computer drives also an eight channel analogue recorder, which serves as a quick look instrument as it allows to observe continuously sensor signals and various navigation quantities.

Besides the pure sensor signals all relevant data are transmitted and recorded together with the reference data from the test table on magnetic tapes. In Table 3 the content of a data telegram is listed.

As a plausibility check the Interdata computer looks at the navigation position coordinates and interrupts the trial if the drift exceeds a given value.

The test records are finally sent to the Bodenseewerk at Überlingen where the processing of the test data with the IBM 370 computer starts.

SENSOR SIGNALS

- 3 ANGULAR INCREMENTS
- 3 VELOCITY INCREMENTS
- 2 GYRO TEMPERATURES
- 4 GYRO PICK OFFS

NAVIGATION COMPUTER DATA

- 4 QUATERNION ELEMENTS
- 3 ATTITUDE ANGLES
- 3 VELOCITIES
- 2 POSITION COORDINATES
- 1 ALTITUDE

FLIGHT SIMULATOR DATA

- 3 ATTITUDE ANGLES
- 1 ANGULAR RATE

Table 3: Content of a data telegram

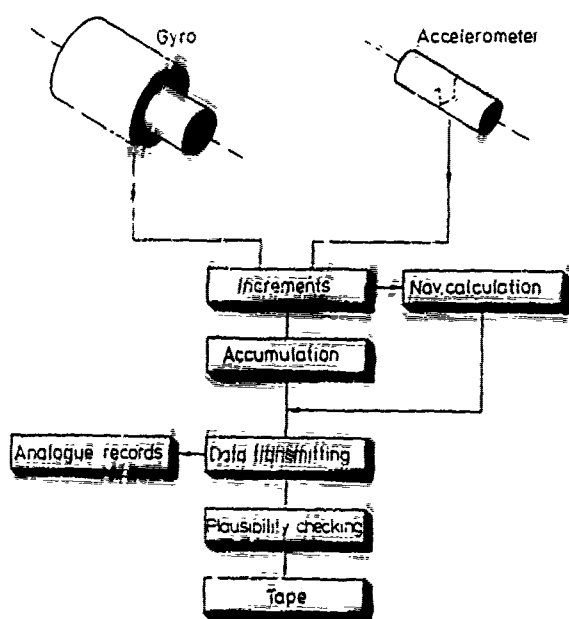


Fig.19: Read out and Record of Test Data

5.4 Test Procedures

5.4.1 24-Position-Static-Test

The 24-position-test is used for determining the parameters of the acceleration dependent error terms of a gyro (cf. 3.2.2)

- mass unbalance
- quadrature term
- anisoelasticity
- bias

The same procedure is used to calibrate the accelerometer parameters (cf. 4)

- bias
- scale factor
- misalignment of the sensitive axes
- acceleration square term

The 24-position-test is characterized by positioning the IMU in 24 different orientation relative to the gravitation vector. The test starts with the first main position shown in Fig. 7.

For 10 minutes the sensor signals are read out, transmitted to the Interdata computer which in its turn completes the MSS data by sampling the attitude angles of the three axis test table and adding them to the MSS data. All data were temporary recorded on a disc.

After ten minutes the orientation of the MSS is automatically changed by 45 degree until all eight positions belonging to a main position are completed. The trial is finished by writing the disc data on a magnetic tape.

5.4.2 Rate Test

The rate test is used to determine the parameters of the angular velocity error terms of the gyro

- scale factor
- misalignment of the sensitive axis.

The rate test is characterized by rotating the IMU about its three axis with accurately known angular velocities.

Similarly to the 24-position-test, the main orientations are defined in Figure 7. In each main orientation the IMU is rotated clockwise and counterclockwise with constant angular velocities 0, 0.1, 0.3, 1, 3, 10 Deg/h about the vertical axis of the three axis test table.

The measurement time is 36 sec in all cases. Start and stop of the rotation is however outside the measuring intervals in order to avoid dynamic effects.

Data read out and recording is identical to the 24 position test.

5.5 Determination of the Error Parameters

5.5.1 Processing of the Test Data

The continuous recording of the whole set of test data as shown in Table 3 with a sampling period of 200 msec generates a great amount of data, only a minor part of which is needed for the calibration process. The major part is not yet used, but is reserved for a deeper analysis of the overall system performance of the MSS later on.

A data reduction process is carried out with the aim to get the measurement vectors for the following linear regression processes. A survey of handling the test data is presented in Fig. 20. The main steps of data processing are:

- retrieving the information from the tapes
- change into physical units
- plausibility checking of the data
- data reduction by accumulating the sensors increments
- determining the basic statistics of the data
- generating the measurement vectors
- selection of one of the preprogrammed error models
- performance of the linear regression
- determining the confidence intervals
- printing of the results

In the sequel these steps are described in more detail.

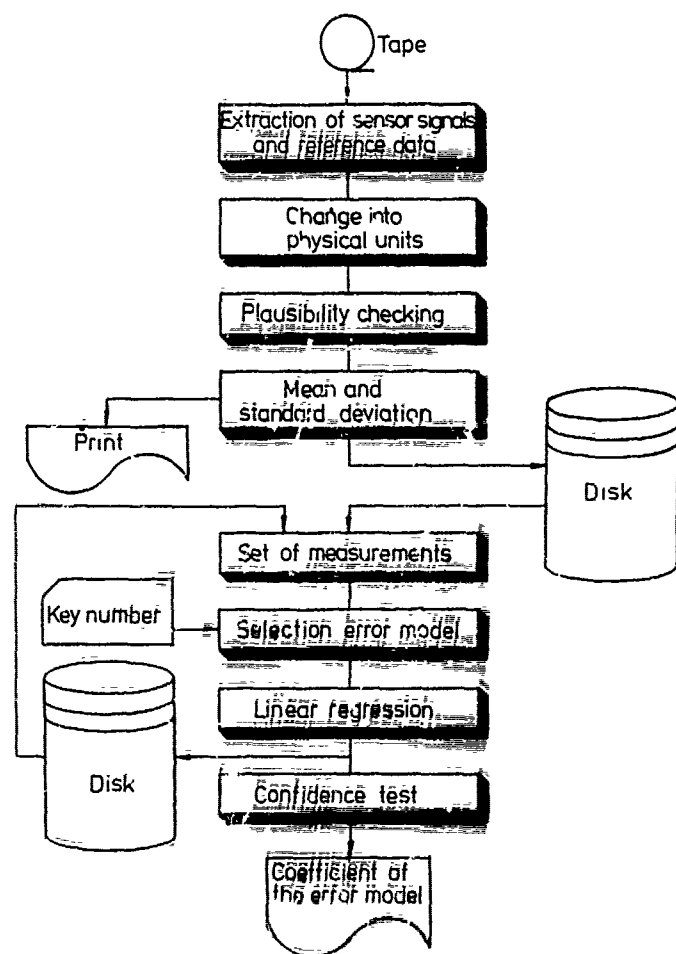


Fig.20: Processing of the Test Data

5.5.2 Data Reduction

A data file begins with a header which contains the marginal information about the test such as date, trial no., initial conditions, applied angular velocity etc. This information is printed as a header.

The data telegrams are then read out, piece by piece. Each time the sensor increments and the attitude of the test table are extracted, non relevant informations are omitted. The sensor outputs from each telegram are compared with corresponding values derived theoretically from the attitude resp. angular velocity of the three axis test table. When a preselected tolerance (e.g. 10 percent) is surmounted, the content of the data telegram is supposed to be not plausible and is therefore omitted. This plausibility checking is principally thought as an aid for preserving the results from errors in the data transmission.

Within one trial all sensor increments are accumulated, the mean value, the mean square value, and the standard deviation of the mean value are derived.

The mean values of each trial of ten minutes are arranged in an array which serves as a measurement vector for the following linear regression process. In this way the data of the 24-position-test are reduced to 6 vectors (three gyros and three accelerometer axis) with 24 elements, the data of the rate test are reduced to 3 vectors with 27 elements. For further processing these vectors are stored on a disc memory.

5.5.3 Evaluation of the Error Parameters

5.5.3.1 Linear Regression

For estimation of the error parameters the linear regression method (least square adjustment) is applied, as described in paragraph 3.2.2.

For application of linear regression to the rate- and 24-positions-test, the error model from Figure 17 has to be adapted to equation (3.2). This is done by

- linearizing the error model equation and neglecting higher order terms (cf. chap. 5.5.3.2)
- introducing the values of the gravity acceleration a_g and angular velocity ω_i from test conditions into the equation
- integrating the error model equations over the measurement time.

As an example, the resulting set of measurement equations for the gyro x-axis is shown in (5.1).

X Axis Gyro Error Model.

$$-\frac{My}{H} = [1 \cdot DSF_x(T)] [\omega_x + \alpha_{xz} \omega_y - \alpha_{xy} \omega_z - l_m(T) \alpha_x - l_q \alpha_y + l_n \cdot \alpha_x \cdot \alpha_z + b_x(T)] \quad (5.1)$$

X Axis Gyro Measurement Model for Linear Regression $\mathbf{z} = \mathbf{Ax} + \mathbf{v}$

$$\begin{bmatrix} z_1 \\ \vdots \\ z_n \end{bmatrix} = \begin{bmatrix} l_{x1} & l_{y1} & -l_{z1} & -j_{x1} & j_{y1} & j_{xz1} & T_1 \\ \vdots & \vdots & \vdots & \vdots & \vdots & \vdots & \vdots \\ \vdots & \vdots & \vdots & \vdots & \vdots & \vdots & \vdots \\ l_{xn} & l_{yn} & -l_{zn} & -j_{xn} & j_{yn} & j_{xzn} & T_n \end{bmatrix} \cdot \begin{bmatrix} DSF_x \\ \alpha_{xz} \\ \alpha_{yz} \\ l_m \\ l_q \\ l_n \\ b_x \end{bmatrix} \quad \begin{array}{l} \text{scale factor} \\ \text{misalignment} \\ \text{misalignment} \\ \text{mass unbalance} \\ \text{quadrature term} \\ \text{anisoelasticity} \\ \text{bias} \end{array} \quad (5.3)$$

Abbreviations

$$T_1 = \int_0^{T_1} \omega_x dt, \quad l_{xi} = \int_0^{T_1} \omega_y dt, \quad l_{zi} = \int_0^{T_1} \omega_z dt \quad (5.4)$$

$$z_i = \int_0^{T_1} (-My/H - \omega_x) dt \quad (5.5)$$

$$j_{xi} = \int_0^{T_1} \alpha_x dt, \quad j_{yi} = \int_0^{T_1} \alpha_y dt, \quad j_{xzi} = \int_0^{T_1} \alpha_y \alpha_z dt \quad (5.6)$$

Singularities

Care must be taken on singularities of the inverting process of the $(A^T A)^{-1}$ matrix.

Singularity occurs when a column of the A matrix is zero or numerically near zero. Then the corresponding error parameter is not observable, the linear regression fails. In this case the nonobservable error parameters have to be omitted and the regression has to be done with the reduced error model (cf. chapter 5.5.3.3).

5.5.3.2 Iterative Linear Regression

The application of the linear regression in a straightforward way, will not yield the result wanted, as the accuracy of the parameters determined will be very different.

To obtain optimal results, the covariance matrix $(A^T A)^{-1}$ has been analysed in detail in paragraph 3.2.2. The result for the gyro x-axis is presented schematically in Fig. 21. In the rate test as well as in the 24-position test only certain parameters can be determined with sufficient accuracy. The other parameters are either not observable or only observable in a linear combination with some others, or they are observable with only insufficient accuracy. Similar results apply for the accelerometer x-axis shown in Fig. 22.

An optimal use of all information is attained when the effects of those parameters which are not only scarcely observable are corrected by preprocessing the measurement vector \underline{z} . The vector of the known parameters then is reduced by these parameters.

This procedure can be done iteratively. The principle is shown in Fig. 23. The single steps are as follows:

1. Determining of DSF, α_{ij} , α_{ik} by the rate test data
2. Correcting the 24-position-test data by DSF, α_{ij} , α_{ik} effects from step 1
3. Determining of m, q, n, b, with preprocessed data from step 2.
4. Correcting of the rate test data by m, q, n, b effects from step 3
5. Repeating the procedure at step 1 with data from step 4

Test	Main Position	Parameter of the Gyro Error Model						
		DSF _x	α_{xz}	α_{xy}	m ^t	q ^t	n ^t	b _x
Rate Test	1							
	2							
	3							
	1+2+3							

Test	Main Position	Parameter of the Gyro Error Model						
		DSF _x	α_{xz}	α_{xy}	m ^t	q ^t	n ^t	b _x
24 Position Test	1							
	2							
	3							
	1+2+3							

[■] Determinable with sufficient accuracy

[■■■] Determinable with unsufficient accuracy

[] Not observable

1. Observable only as linear combination

Test	Main Position	Parameter of the Accel. Error Model				
		DK _x	ϵ_{xz}	ϵ_{xy}	ϵ_{Q_x}	B_x
24 Position Test	1					
	2					
	3					
	1+2+3					

[■] Determinable with sufficient accuracy

[] Not observable

Fig.21: Observability of the
Gyro x-Axis Parameters

Fig.22. Observability of the
Accelerometer x-Axis
Parameters

Preprocessing of the Test-Data

The knowledge of known effects or parameters allows the correction of the raw gyro test data, denoted for this purpose as vector \underline{W}' , in the following manner (see Fig. 27):

In first step the raw data \underline{W}' are corrected by multiplying them with the best known scale factor SCF.

In the second step the effect of the other known error parameters, arranged in the partial correction vector \underline{x}_c^*

(5.7)

are calculated by the expression $A^* \underline{x}_c^*$ and subtracted from scaled data $\underline{W}' \cdot \text{SCF}$. The star in \underline{x}_c and A denotes the omitting of the elements corresponding to the scale factor error DSF as this parameter has to be treated separately.

The resulting vector

$$\underline{z}(n) = \underline{W}' \cdot \text{SCF}(n-1) - A^* \underline{x}_c^*(n-1) \quad (5.8)$$

is now the basis measurement vector for subsequent linear regression. The result of the regression has then to be interpreted as iterative improvement of the scale factor $\text{SCF}(n-1)$ and the correction-vector $\underline{x}_c(n-1)$.

Temperature Compensation

The preprocessing procedure serves also to correct the test data for temperature effects.

As can be seen from the gyro manufacturer's data sheet, scale factor, mass unbalance and bias show a linear temperature dependance. By known temperature coefficients these effects can be accounted for. For this purpose the gyro temperature is continuously measured and recorded with each data telegram and accounted for in the preprocessing procedure.

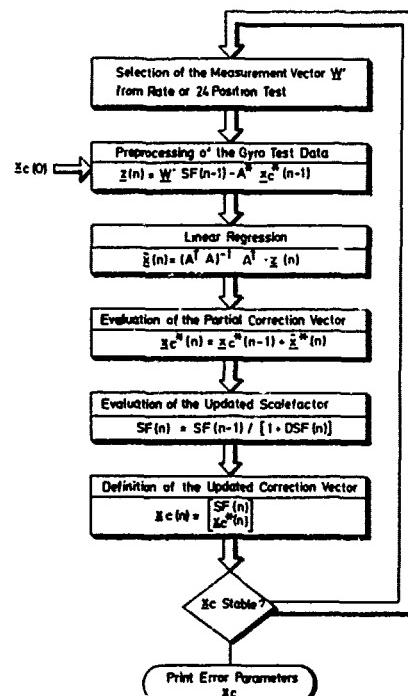
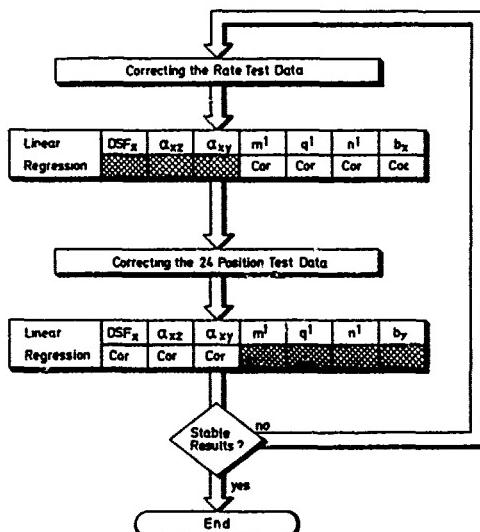


Fig.23: Optimal Use of all Test Data by Iterative Linear Regression

Fig.24: Preprocessing of the Test Data

Solution for Nonlinearities

The linear measurement model (5.2) was deduced from the error model (5.1) by neglecting the nonlinear higher order error terms such as

$$DSF_x \cdot (-ma_y + qa_x - na_x a_z + b_x)$$

The gyro performance data show that under certain conditions this expression may correspond to a drift in the order of $0.1^\circ/h$, so that the neglection assumption will not hold and a pure linear regression will give false results.

The iterative application of the linear regression discussed above yield a solution of this problem, as in a second iteration runn for which the linearity assumption is surely valid, the false parameters are corrected automatically.

Scale Factor for the Real Time Error Compensation

In the linearized error model (5.2) the scale factor error DSF can only be determined as coefficient to the input angular velocity of the three axis table. For the real time error compensation procedure in the navigation computer, the scale factor has however to be applied to the angular velocity measured by the strapdown gyros. This problem is also solved by the iterative linear regression. As is shown in Fig. 24, by the preprocessing procedure the scale factor is indeed applied to the gyro output and not to the input angular velocity of the three test table.

Variation of the Error Models

The linear regression software system contains the option to use several different error models. By selection of a key number the complete error model from Fig. 17 can be substituted by an reduced or by an extended error model.

The use of error models in which single error parameters are omitted is necessary when test data are processed for which one or several parameters are not observable. For these cases the calibration software allows to compensate fully the effects of the canceled error parameter in the frame of the preprocessing procedure.

But also for judging the importance of the single error parameters it is very useful to be able to omit or to add single error terms in the error model.

Confidence Test

A very helpful means for judging whether an error parameter is significantly different from zero or not is a statistical confidence test.

A test of the hypothesis that the estimated value of the error parameter in the regression error model is significantly different from zero can be checked by comparing the value of the parameter x_i to its standard deviation G_{xi} , derived from (3.5).

Under the assumption that the measurement noise is normally distributed the random variable

$$t_i = x_i / G_{xi} \quad (5.9)$$

obeys a Student t-distribution.

Therefore $100.(1-q)\%$ confidence limits for x_i can be defined by

$$x_i \pm t_i(n-m, 1-q/2). \quad (5.10)$$

$n-m$ = degree of freedom

n = number of measurements

m = number of parameter determined

$(1-q/2)$ = percentage point of the t-distribution.

For the 24 position test and for the rate test the value t_i is found to be approximately 2 for 95% confidence limits and 23 degrees of freedom.

The parameter values from the linear regression are now said to be significant different from zero, if

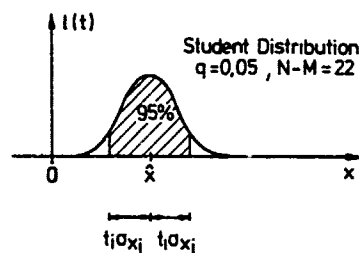
$$\frac{x_i}{2 \cdot G_{xi}} > 1 \quad (5.11)$$

Not significant values defined by

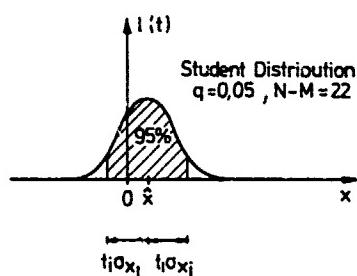
$$\frac{x_i}{2 \cdot G_{x_i}} \leq 1 \quad (5.12)$$

don't play any important role provided, that the confidence limits are smaller than stated in the accuracy requirements.
This situation is illustrated in Figure 25.

Parameter is significantly different from 0:



Parameter is not significantly different from C:



Software Test

In order to test the complete software that was written in FORTRAN IV and further to test whether the subroutines for the matrix inversion are sufficient accurate a set of sensor error parameters were arbitrary defined. With the help of the error model, fictitious sensor signals were generated and fed to the computer program.

The values of the sensor parameters which were evaluated by the calibration software were in accordance with the original values in the order of $5 \cdot 10^{-7}$.

References

- /1/ D.K.Joos
Comparison of typical gyro errors for strapdown applications DGON-Symposium
Gyro-Technology, Sept. 1977, Stuttgart, Germany
- /2/ P.J.Donoghue, L.B.Cotter
Test and evaluation of a dry tuned strapdown-gyroscope in a system environment,
DGON-Symposium, Gyro-Technology, Sept.1977, Stuttgart, Germany.
- /3/ H.Bertler
Test-facilities and procedures for strapdown-systems, DGON-Symp. Gyro-Technology
Sept. 1978, Bochum, Germany
- /4/ P.Eykhoff
System identification, J.Wiley and Sons, London, 1974
- /5/ Kendall M., Stuart A.
The advances theory of statistics
Charles Griffin and Company Ltd. London 1963
- /6/ D.K.Joos, U.K.Krogmann
Identification and Determination of Strapdown Error-
Parameters by Laboratory Testing.
Advances in Inertial Navigation Systems and Components,
AGARDograph (Ed.H.Sorg), to be published in 1980.

List of Symbols:

$\alpha_{ij}, \alpha'_{ij}$	misalignment of ith-sensor axis about jth-axis
m	mass-unbalance coefficient
q	quadrature coefficient
n	anisoelasticity coefficient
$C-A_H$	anisoinertia coefficient
C	rotor polar moment of inertia
A	rotor transverse moment of inertia
H	angular momentum
a_i	acceleration along ith sensorblock-axis
ω_i	angular-rate about ith sensorblock-axis
b_i	gyro bias about ith sensorblock-axis
DSF_i	scalefactor error of ith sensorblock-axis
DK_i	i-accelerometer scalefactor-error
KQ_i	quadratic error-coefficient of i-accelerometer
KC_i	cubic error-coefficient of i-accelerometer
KR_i	cross-coupling coefficient of i-accelerometer
B_i	bias of i-accelerometer
α_t	motor phase angle
M_i	torque about ith gyro axis
U_i	output-voltage of i-accelerometer
T	temperature
t_i	t-distributed testvariable

EVALUATION D'UN SYSTEME DE NAVIGATION HYBRIDE A GYROLASERS "SEXTAN"

D.Regnault, Service Essais/Equipements, Centre d'Essais en Vol, BP No.2,
 91220 Brétigny sur Orge, France
 J.Leclerc, Crouzet SA, 25 rue Jules Védrines, 26027 Valence, France
 B. de Salaberry, SFENA, Aérodrome de Villacoublay, 78140 Vélizy Villacoublay,
 France
 J.P.Pradoux, SV2 Crouzet-SFENA, 204 Rond Point du Pont de Sèvres,
 92516 Boulogne, France

I - PRÉSENTATION DE L'EXPOSE

Depuis 1972, avec le soutien de la DRET, SFENA étudie et développe le gyromètre laser en liaison avec la Société QUANTEL pour l'aspect Recherche.

Très tôt des marques d'intérêt des Services Officiels de tutelle de la Délégation Générale de l'Armement sont apparues. Prolongeant l'action de la DRET, le STEN puis le STTE et les Etats-Majors des trois armes ont soutenu l'action industrielle.

De ce fait, courant 1978, les réalisations expérimentales de gyromètres laser ont permis d'obtenir des performances compatibles des premières applications envisagées. SFENA avait, en outre, une grande expérience des accéléromètres de précision et disposait d'un modèle, qui associé au gyrolaser lui permettait de réaliser des Centrales d'Altitudes et de Vitesses.

D'autre part, à cette époque, CROUZET possédait la connaissance des systèmes de navigation pour hélicoptères et avions, les techniques d'hybridation permettant d'optimiser les performances d'un système hybride Inertie-Doppler ainsi qu'un capteur magnétique statique pouvant servir à la détermination du cap initial.

Toutes les conditions étaient donc réunies en 1978 pour que CROUZET et SFENA confient à leur filiale commune SV2, la direction d'un programme de réalisation et d'expérimentation d'un système de navigation hybride : Inertie Sans Plate-forme - Doppler. Adapté aux hélicoptères armés de la prochaine génération, ce système appelé SEXTAN a été développé avec le soutien du STEN et du STTE.

L'exposé qui va suivre a pour but de présenter les méthodes et moyens mis en oeuvre au cours des essais en laboratoire et pendant les essais en vol pour valider et vérifier les performances du système.

Les résultats de l'évaluation seront également donnés.

II-PRÉSENTATION DU PROGRAMME SEXTAN

Le programme SEXTAN qui vise l'équipement des hélicoptères armés de nouvelle génération volant à très basse altitude en vol tactique, permet d'offrir des systèmes ayant des performances très élevées à des coûts compatibles avec l'économie générale des projets européens.

Pour répondre à ces contraintes, SV2, CROUZET, SFENA ont réalisé un système utilisant une centrale à gyrolaser de performance modeste et par conséquent économique, associée à un radar Doppler.

Dans ce système hybride les performances à court terme seront imposées par la centrale inertielles et celles à long terme par le radar Doppler.

Le schéma fonctionnel d'un tel système permet de préciser les composants fondamentaux de SEXTAN : Planche 1

- Une centrale de navigation hybride comportant :
 - . trois gyrolasers
 - . trois accéléromètres
 - . un calculateur assurant les fonctions :
 - plate-forme virtuelle (c'est-à-dire effectuant le calcul des altitudes et des vitesses en axes porteur à partir des mesures gyrométriques et accélérométriques)
 - hybridation Inertie-Doppler et Inertie-Baro
 - navigation
- Un radar Doppler.
- Un ensemble de capteurs de pression assurant la stabilité du système dans le plan vertical.
- Un magnétomètre statique triaxial permettant d'obtenir, entre autres, un alignement rapide du système en cap.
- Un poste de commande et de visualisation.
- Des équipements périphériques tels que :
 - . l'indicateur de navigation,
 - . l'indicateur cartographique,
 - . l'indicateur de vol stationnaire.

- Planche 2 :**
 Le plan de développement des systèmes SEXTAN se déroule suivant trois phases :
 - une phase expérimentale qui correspond à SEXTAN I,
 - une phase prototype qui correspond à SEXTAN II, pour laquelle les équipements développés seront disponibles pour les essais en vol au début de 1982,
 - une phase série débutant en 1983.

III- PRÉSENTATION DU SYSTÈME EXPÉRIMENTAL SEXTAN I

Le détail du plan de développement de SEXTAN I apparaît sur cette planche. On peut distinguer les étapes suivantes : Planche 3

- spécifications, définition et modélisation de l'ambiance et des capteurs de fin 1977 à mi 1978,
- réalisation des équipements et mise en place des moyens d'essais en laboratoire de mi 1978 à mi 1979,
- intégration et recette d'août 1979 à novembre 1979,
- essais en vol de décembre 1979 à juin 1980.

Planche 4 :

Les principaux objectifs de SEXTAN I étaient de vérifier en vol le comportement des gyrolasers et de mettre au point tous les algorithmes du système de navigation hybride inertie à composants liés - Doppler, sans pour autant, développer dès ce stade les matériels prototypes spécifiques.

C'est pourquoi le système expérimental a été conçu en recherchant une grande souplesse de mise au point et en utilisant au maximum des équipements existant dans nos sociétés.

Les capteurs inertIELS ont été regroupés dans un boîtier appelé Unité de Mesure Inertielle (UMI).

La fonction calcul a été répartie dans deux équipements :

- Un calculateur universel UMP 7800 SFENA qui par sa puissance de calcul, sa souplesse de programmation et ses outils logiciels se prête bien à ce genre d'expérimentation.
- Un calculateur de navigation Nadir CROUZET - cet équipement qui a été retenu pour les hélicoptères de l'Aviation Légère de l'Armée de Terre Française (ALAT) a été simplement adapté à cette expérimentation.

IV - ORGANISATION DES ESSAIS EN LABORATOIRE

Les études et les essais du système SEXTAN ont été menés de façon à réduire au maximum le temps de vol nécessaire à la mise au point du système de façon à privilier les voies d'évaluation.

La planche 5 présente la méthodologie des essais pendant les diverses phases du développement.

Sur cette figure, on distingue les trois grandes étapes de la vie du projet :

- Les études théoriques qui, après l'établissement d'un logiciel de référence, permettent de définir le logiciel qui sera embarqué.
- La vérification de ce logiciel au sol.
- Les essais en vol.

Détaillons chacune de ces étapes :

Planche 6 :
 Le logiciel de référence établi au cours de la première phase d'étude est l'outil informatique de base pour les simulations et la mise au point du système. Il est destiné à simuler le logiciel qui sera embarqué et dont il sera l'image. Il est donc réalisé pour simuler sur un calculateur scientifique puissant les possibilités du calculateur embarqué et tient donc compte de sa vitesse d'exécution, des cadrages de mots, des erreurs de troncature etc...

Il a été mis au point en tenant compte :

- des algorithmes résultant des études théoriques qui ont suivi l'établissement des spécifications du système,
- des trajectoires synthétiques établies à partir d'enregistrements de paramètre de vol effectués sur hélicoptère,
- des modèles d'erreurs de tous les capteurs du système.

Après cette mise au point, le logiciel embarqué est à son tour créé et validé en laboratoire avec le maximum d'éléments réels du système et en montant l'Unité de Mesure Inertielle sur un simulateur deux axes (Table GOERZ) : Planche 7

Dans une première phase, l'UMI est calibrée par des mouvements et des positionnements axe par axe. À l'issue de cette phase, les paramètres d'erreurs des capteurs (biais, facteurs d'échelle, calages des trièdres de mesure) sont calculés et les termes de compensation correspondants sont introduits dans le logiciel.

Dans une seconde phase, on fait exécuter à la table des mouvements simulant les divers types de vol et les résultats sont comparés à ceux obtenus dans les simulations précédentes.

Les sorties des capteurs enregistrées au cours de ces dernières simulations peuvent être réutilisées pour un traitement en centre de calcul afin de faciliter l'analyse des divergences éventuelles entre les deux types de simulation.

V - ESSAIS EN VOL

Les essais en vol du système SEXTAN I avaient pour but de qualifier sur hélicoptère :

- la technologie du gyromètre laser,
 - le concept du "strapdown",
 - le système hybride Inertie-Doppler dans le cadre du choix du système de navigation pour le programme HAC;

Ces essais se sont déroulés au Centre d'Essais en Vol de Brétigny (CEV), de décembre 1979 à juin 1980 et ont comporté 60 heures de vol pour 46 vols. Deux phases ont été réalisées :

- une première phase de mise au point constructeur,
de 42 heures de vol (34 vols)
 - une deuxième phase d'évaluation officielle
de 18 heures de vol (12 vols)

La responsabilité de la phase mise au point incombe à l'industriel. Le CEV apporte son soutien à l'industriel par ses moyens d'essais : - aéronef
- moyens de mesure
- moyens de traitement et son expérience des essais en vol.

La responsabilité des vols d'essais et du programme d'essais sont du ressort du CEV. Les programmes des vols sont préparés en collaboration avec l'industriel. La phase d'évaluation officielle est entièrement du ressort du CEV.

V-1 Moyens

.Planche 8 :

Le système SEXTAN a été installé sur le SA 330 "PUMA" n° 1024. Cet hélicoptère de la classe 4 à 6 tonnes qui n'est pas totalement représentatif de ce que sera l'HAC et ceci en particulier pour ce qui concerne les vitesses d'évolution, présente l'avantage de faciliter l'emport d'installations d'essais complexes. Il est déjà équipé pour des essais de systèmes de navigation.

Les différents éléments de SEXTAN ont été implantés comme le montre la planche 9.

- le calculateur UMP 7800 et l'UMI, sous le plancher de la partie cargo,
 - le radar Doppler sous l'hélicoptère est calé à 0° par rapport à la référence horizontale,
 - le calculateur Nadir et l'indicateur de navigation, en partie centrale de la planche de bord,
 - les deux indicateurs de vol stationnaire, sur les parties droite et gauche de la planche de bord, un devant chaque pilote,

- L'installazione

Planche 10 :

- le Nadir en banquette
 - l'IDN

- et les deux

Cette photo montre la partie cargo avec à gauche au premier plan l'installation de mesure, au centre et en bas la soute contenant l'UMP et l'UMI.
Au fond à gauche le pupitre expérimentateur et au fond au centre le siège du bras.

Au fond a gauche
Blanche 13 :

Cette vue de la soute nous permet de distinguer l'UMI et l'UMP 7800.

Les moyens embarqués pour les essais de SEXTAN permettent :

- de contrôler le fonctionnement en vol du système,
 - d'obtenir une trajectoire de référence,
 - de réaliser l'acquisition des paramètres nécessaires aux simulations faites au sol et au calcul des performances.

La planche 13 présente le synoptique complet de l'installation embarquée sur le PUMA.

- . la centrale "strapdown" composée de l'UMI et de l'UMP 7800,
- . les autres équipements faisant partie du système SEXTAN, c'est-à-dire principalement le Nadir recevant les informations en provenance d'un Doppler DECCA 80, d'un boîtier capteurs de pression et de température, d'un magnétomètre. Le Nadir fournit d'autre part à l'IDN et l'IVS les informations de navigation et de pilotage,
- . l'installation de mesure.

la trajectoire de référence est obtenue à partir d'une centrale inertIELLE à plate-forme Litton 51 associée à une caméra de verticale. Un calculateur universel assure l'acquisition d'une liaison DMA (Direct Memory Access) avec l'UMP 7800 du système SEXTAN.

Les paramètres acquis sont :

- d'une part les paramètres capteurs et senseurs (gyromètres, accéléromètres, Doppler, capteurs de pression, magnétomètre)
- d'autre part les paramètres "système" tels que attitudes, cap, position, vitesse.

Ce calculateur assure également la gestion d'une liaison numérique série à destination d'un enregistreur magnétique pour les traitements au sol.

Les contrôles en vol sont faits à l'aide :

- de la face avant du Nadir,
- d'une visualisation numérique,
- d'un enregistreur papier.

V-2 Essais de mise au point

Les essais de mise au point ont comporté quatre phases : Planche 14

- La première a concerné l'intégration du système sur l'hélicoptère, la mise au point des chaînes d'acquisition de données, les essais sol et l'obtention d'un fonctionnement correct en vol. Cette phase dura deux mois et comporta trois vols.
- La deuxième phase était consacrée à la vérification du fonctionnement et des performances de la plate-forme virtuelle ainsi qu'à la mise au point de l'autocompensation du magnétomètre.
Cette phase dura deux mois et comporta quinze vols.
- La troisième phase qui permit la vérification et l'optimisation de l'hybridation inertie-Doppler comporta cinq vols échelonnés sur un mois.
- Au cours de la quatrième et dernière phase avant les vols de recette, le fonctionnement de la boucle baro-inertIELLE fut vérifié par l'utilisation d'une station de trajectographie sol à laser appelée STRADA. Cette phase qui comporta également des vols de synthèse et de prérecette dura un mois et comporta onze vols.

Au cours de ces vols, la bande magnétique enregistrée à bord est traitée par le CEV pour obtenir une bande magnétique compatible avec le centre de calcul de l'industriel.

Pendant la période de mise au point, le traitement des informations contenues sur la bande fournie par le CEV est schématisé sur la planche 15.

Partons de l'ordre d'essais en vol. En fonction de l'avancement des essais, un profil de vol est déterminé afin d'améliorer la perception des imperfections du système. Par exemple, un virage à plat comportant N tours permet de mettre en évidence l'erreur résiduelle sur le facteur d'échelle du gyro de cap.

La dernière version du logiciel embarqué est incorporée dans les équipements et le vol exécuté.

L'enregistrement effectué permet de régénérer en centre de calcul la trajectoire réellement suivie par l'hélicoptère. Il est alors possible à l'industriel soit de vérifier le comportement des capteurs en comparant les informations fournies par ceux-ci aux caractéristiques de la trajectoire, soit de vérifier le comportement du système par comparaison des informations données par SEXTAN à celles de la centrale de référence. Des simulations avec des logiciels modifiés sont également possible avant d'essayer ceux-ci en vol.

Les modifications apportées au système au cours de la mise au point ont été mineures. Seul le logiciel a été concerné car ces modifications n'ont porté que sur des valeurs de constantes comme :

les constantes de temps des boucles d'hybridation ou les coefficients caractérisant les gyromètres.

V-3 Essais d'évaluation

Après la phase de mise au point, s'est déroulée la phase d'évaluation officielle qui a comporté 18 heures de vol en 12 vols au cours du mois de juin 1980 : planche 16.

Ces vols se sont répartis en :

- 4 vols de navigation tactique caractérisés par de nombreuses évolutions en vitesse et en altitude à très faible hauteur,
- 8 vols de navigation "type convoyage".

L'évaluation a comporté également une régulation de cap afin de déterminer l'erreur de cap initial du système en fonction du cap d'alignement.

. Planche 17 :

L'exploitation de ces essais d'évaluation a été réalisée par le centre de calcul du C.E.V.

Les données brutes provenant de l'enregistrement sur hélicoptère subissent un prédé-pouillement destiné à les rendre assimilables par le centre de calcul équipé d'un IBM 3031.

Ce prédépouillement consiste :

- en un transcodage pour les enregistrements magnétiques
- en un dépouillement permettant d'extraire les données de recalage des photographies.

A partir des paramètres position et vitesse de la centrale Litton 51 enregistrés à bord, d'un modèle d'erreur en vitesse de la centrale à inertie et de photos de verticale de points géodésiques survolés, une référence de navigation est élaborée. Ceci-ci permet de connaître, à tout instant du vol, la position à quelques dizaines de mètres près et la vitesse à 0,3 kt près.

La comparaison entre la trajectoire de référence et la trajectoire fournie par le système SEXTAN permet le calcul des performances du système. Les résultats sont édités sous forme de graphiques, de listing et de statistiques.

V-4 Résultats

Du point de vue qualitatif le comportement du gyrolaser sur hélicoptère a été excellent.

. Planche 18 :

Il est possible de le résumer ainsi :

60 heures de vol en 46 vols
170 heures de fonctionnement
Pas de panne
Pas de fonctionnement marginal.

. Planche 19 :

Les performances obtenues au cours de l'évaluation sont regroupées sur cette planche en comparaison avec les objectifs visés.

La durée d'alignement mesurée a été inférieure à une minute et ceci sur plus d'une centaine d'alignements réalisés dans des conditions très variées y compris avec des vents travers de 25 kt et des rafales de 35 kt.

COMMENTAIRES DES RESULTATS

CONFIDENTIEL DEFENSE

VI - CONCLUSION

La parfaite réussite des essais en vol SEXTAN I montre que les différents concepts mis en oeuvre dans cette expérimentation :

- le gyromètre laser,
- les techniques inertielles à composants liés,
- les systèmes hybrides de navigation

sont actuellement bien maîtrisés par SV2 CROUZET-SFENA.

En particulier le fonctionnement du gyromètre laser sur hélicoptère est excellent.

D'ores et déjà les résultats obtenus avec le système expérimental sont compatibles avec les objectifs fixés pour le programme HAC.

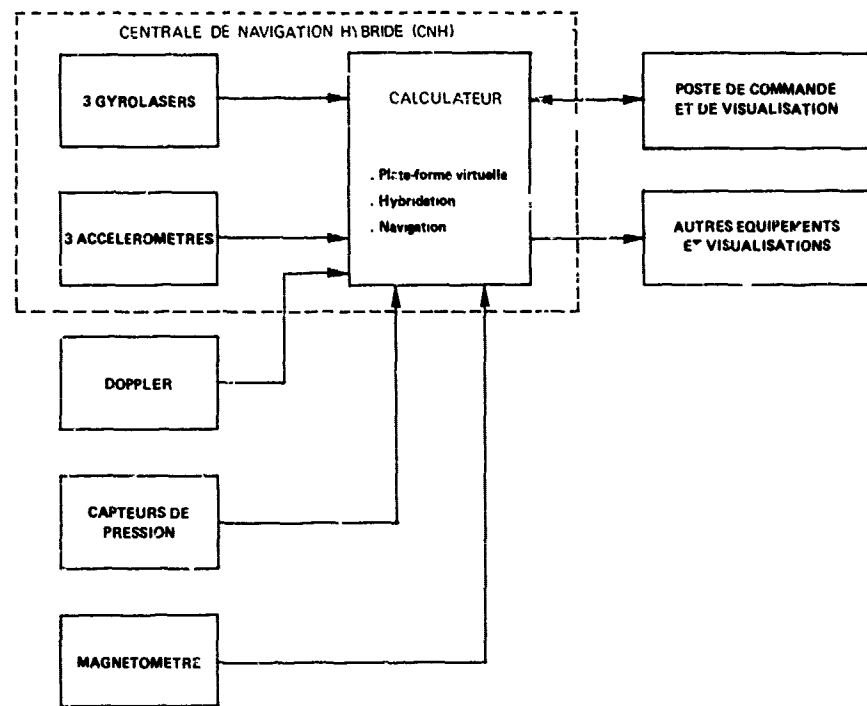


Fig.1 Synoptique fonctionnel SEXTAN

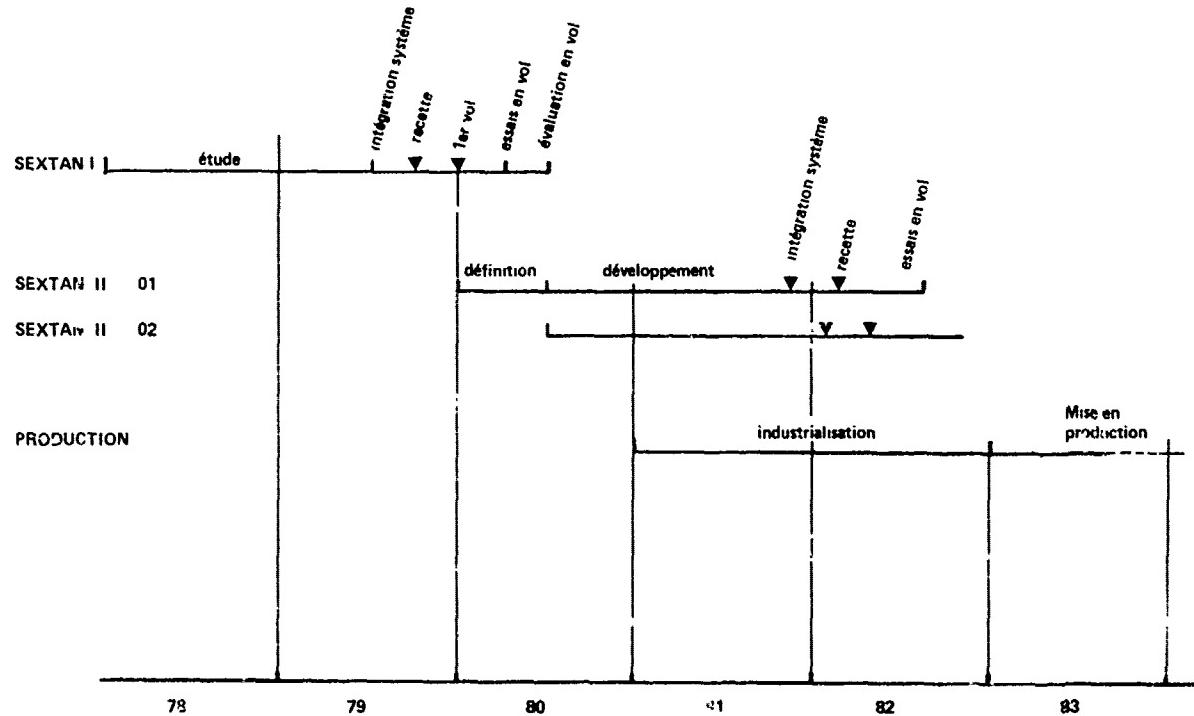


Fig.2 Plan de développement SEXTAN

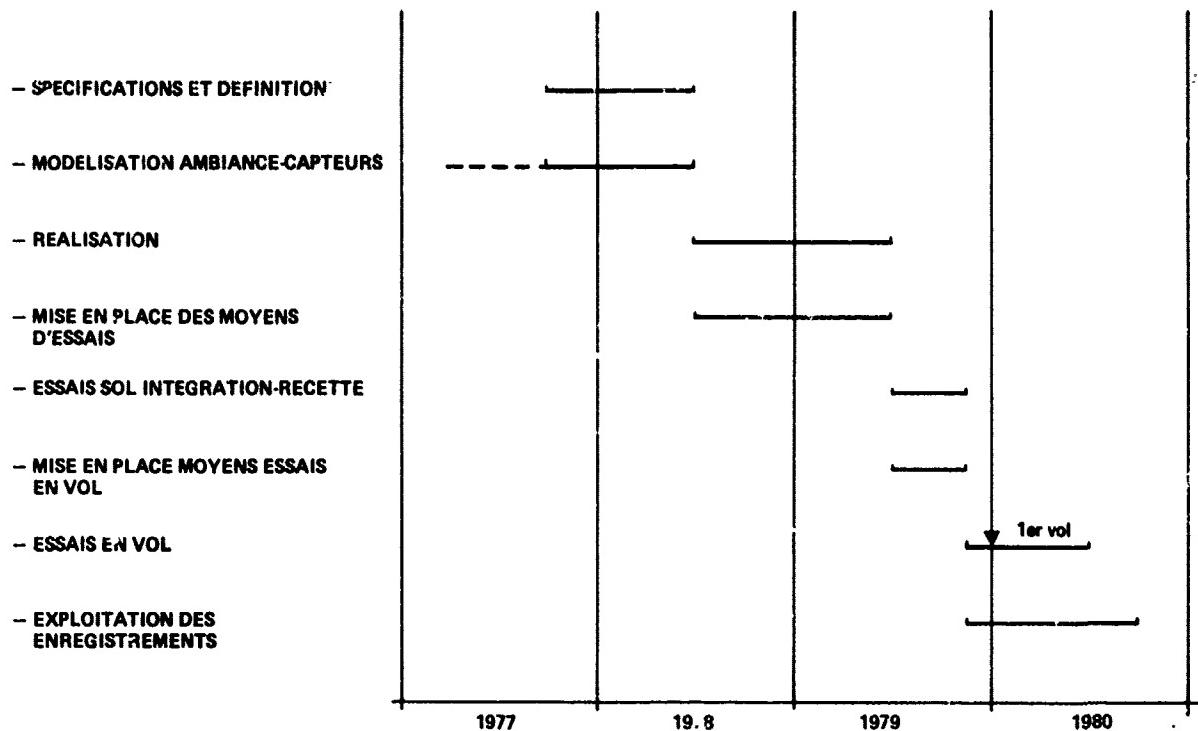


Fig.3 Plan de développement SEXTAN I

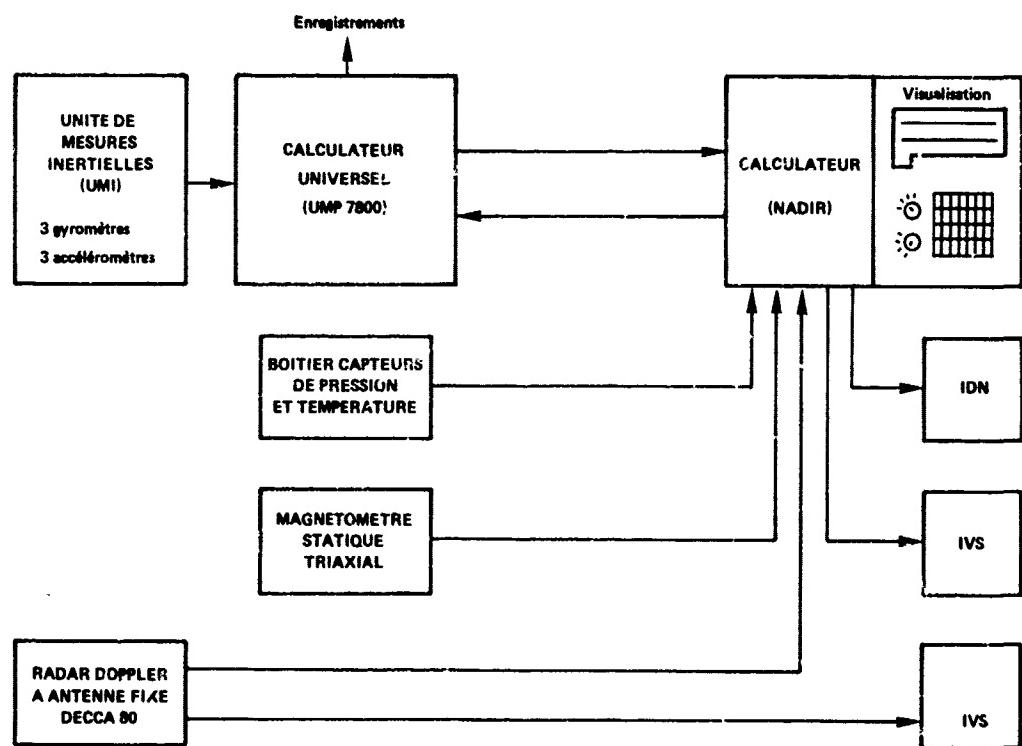


Fig.4 Synoptique SEXTAN I

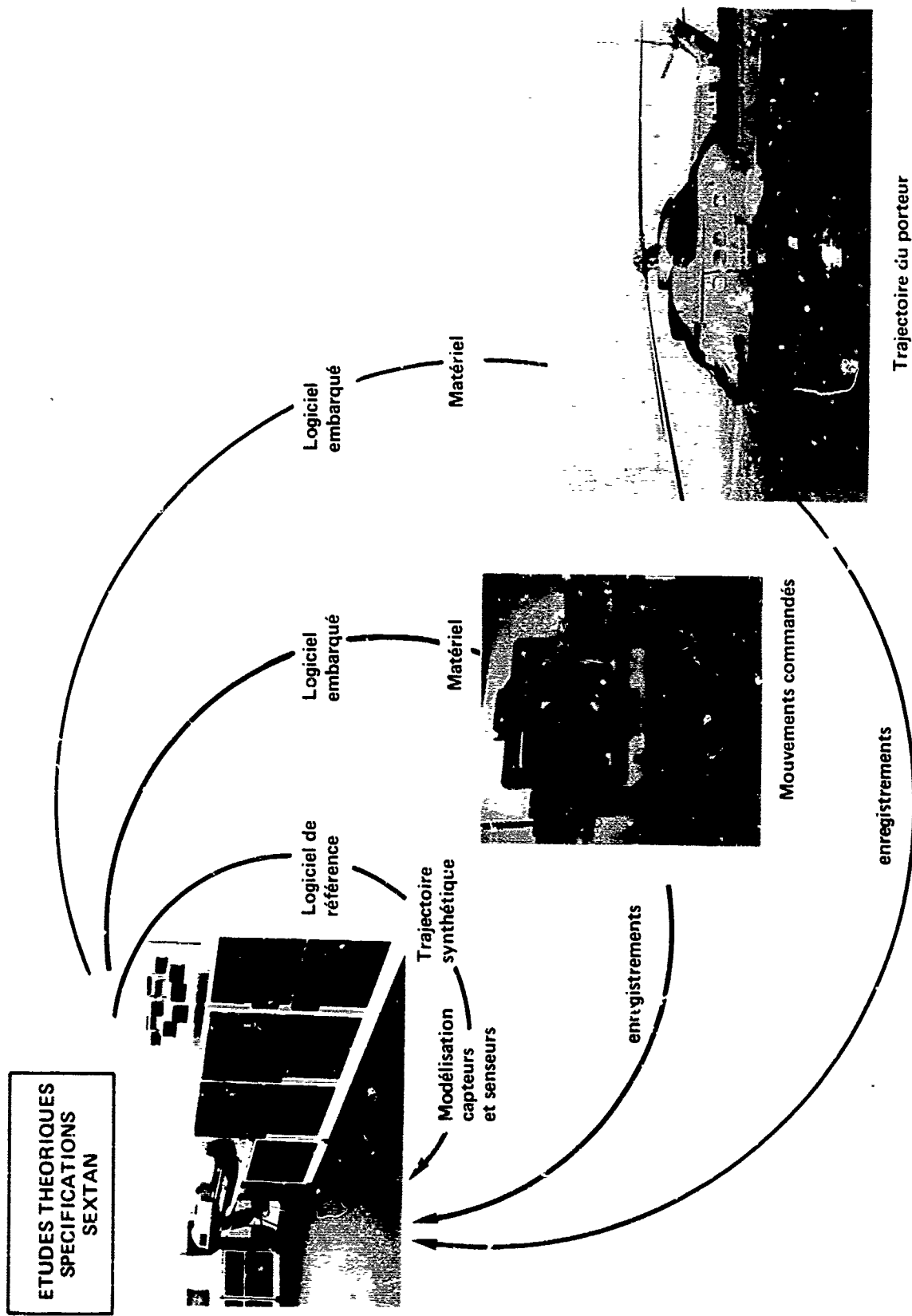


Fig.5 Méthodologie des essais

Trajectoire du porteur

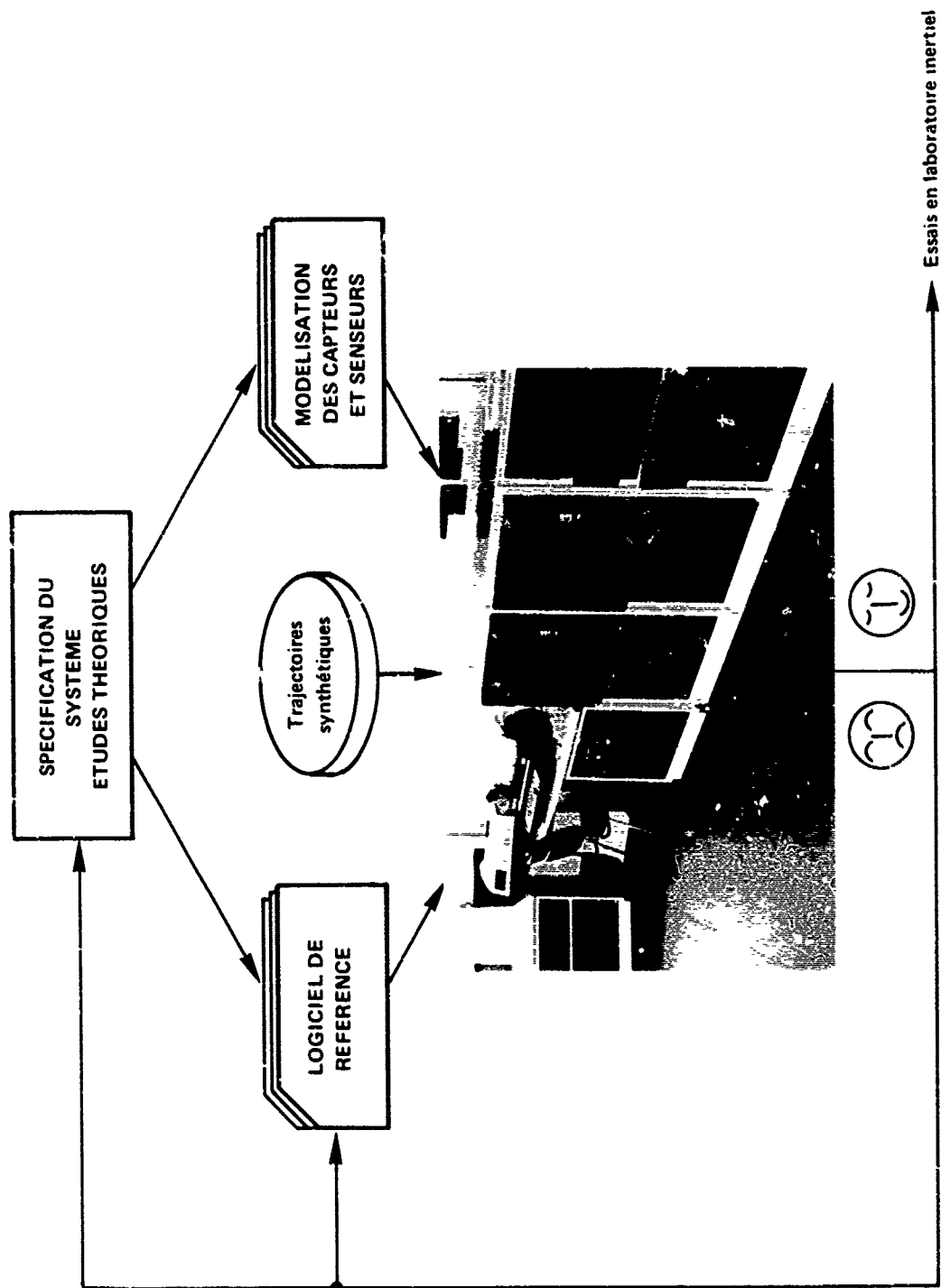


Fig. 6 Etudes et validation du logiciel de référence

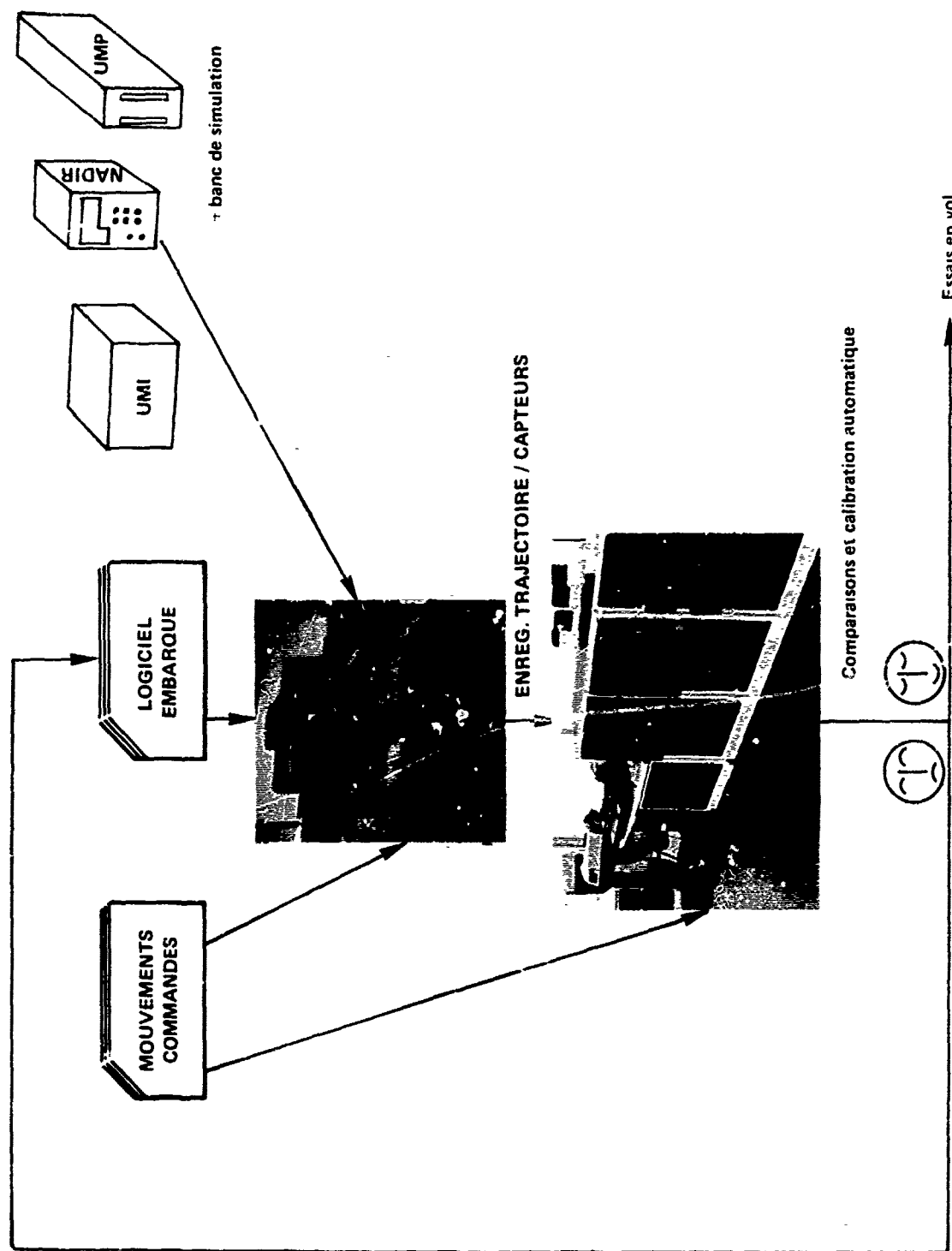


Fig. 7 Validation du logiciel embarqué

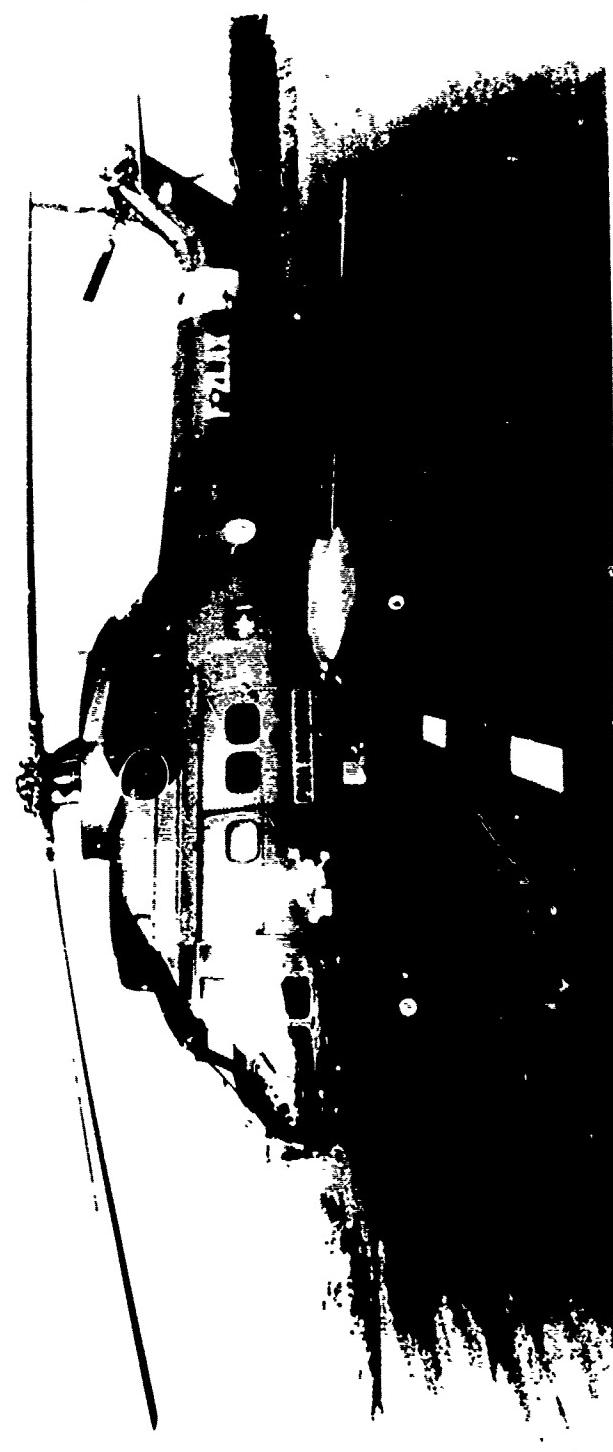


Fig.8 Hélicoptère PUMA du CEV

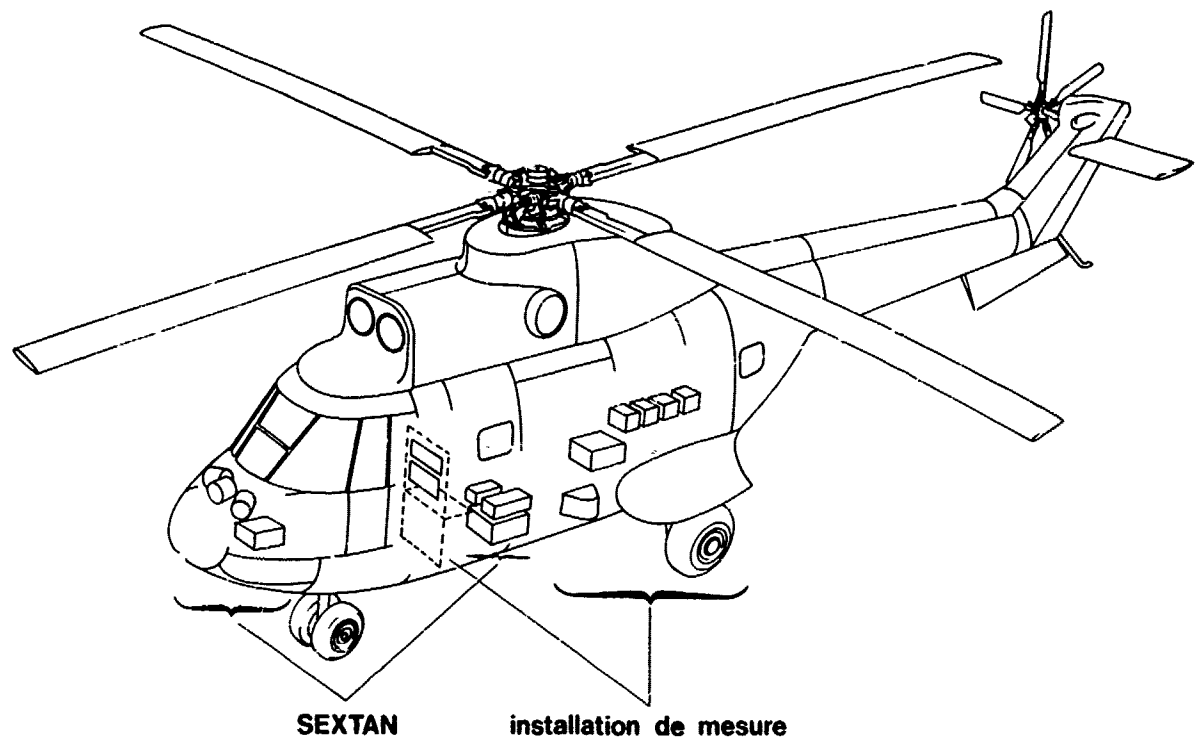


Fig.9 Implantation de l'installation a bord du PUMA

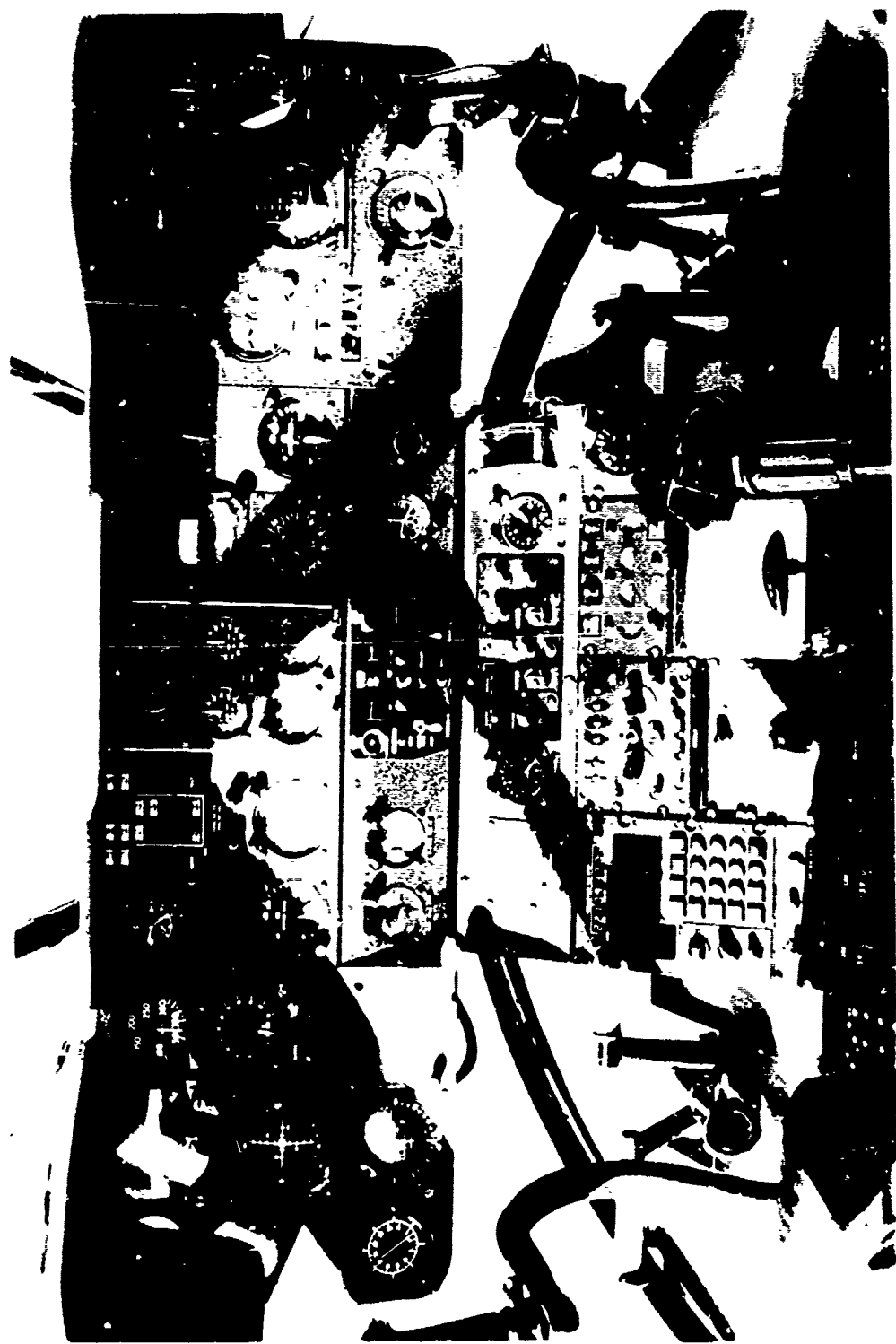


Fig.10 Calculateur Nadir SEXTANT I en planche de bord



Fig.11 Installation d'essai SEXTAN I sur PUMA CEV

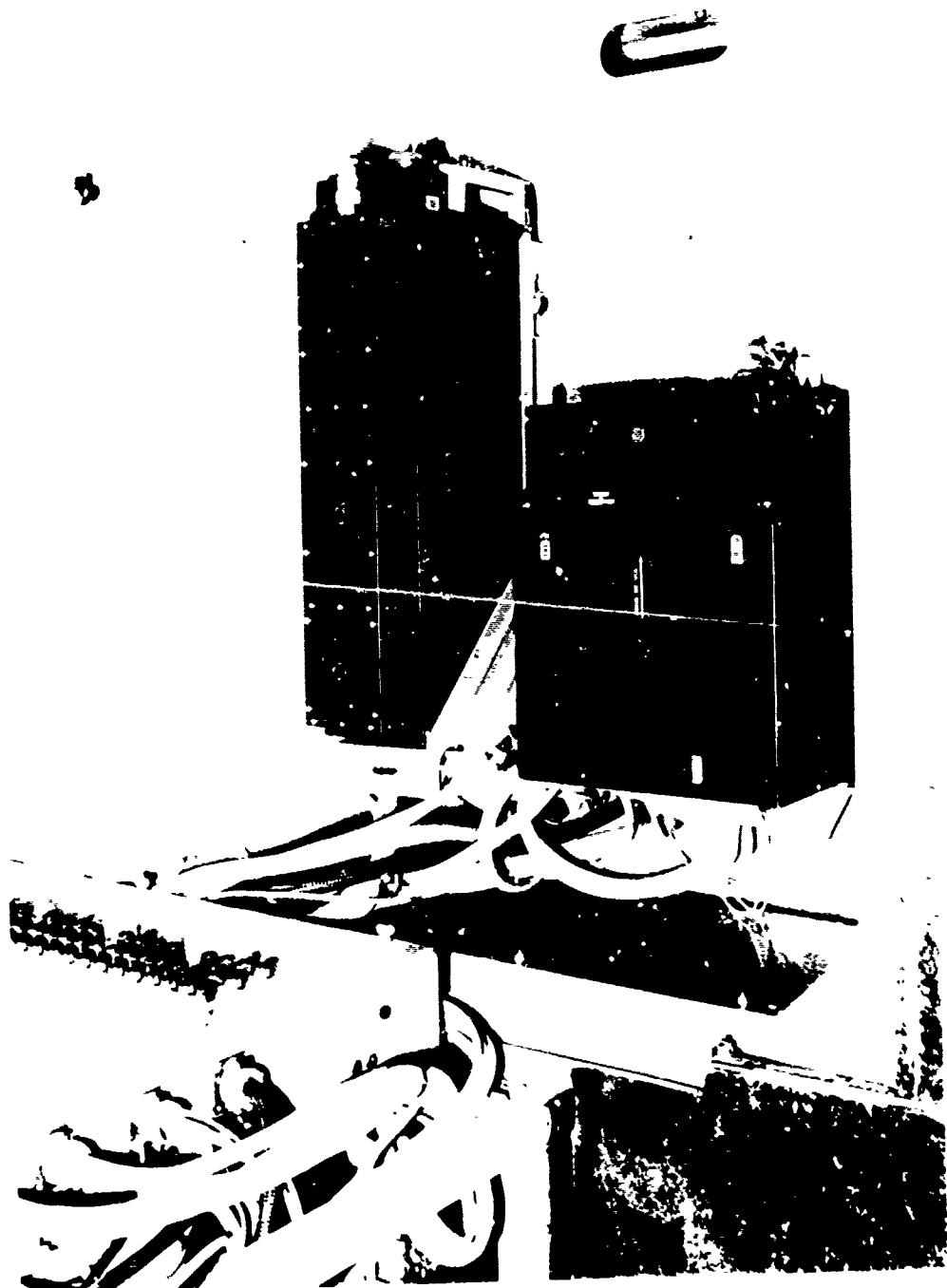


Fig.12 Unité de mesure inertielle et calculateur UMP 7800

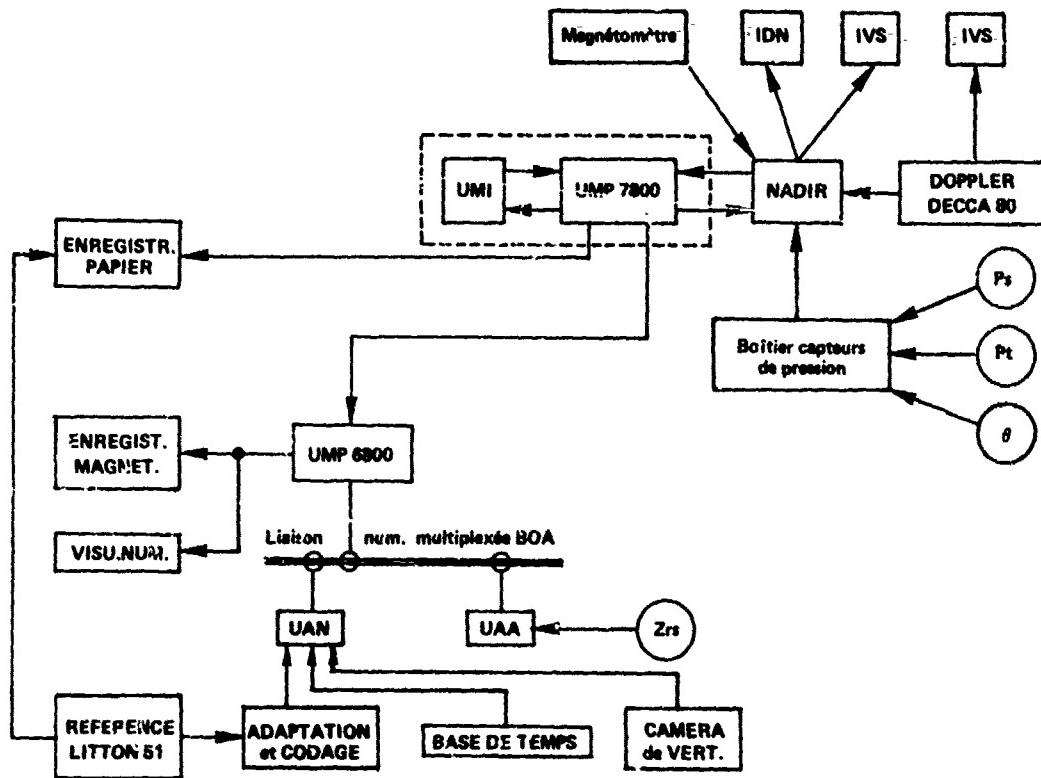


Fig.13 Synoptique de l'installation d'essai sur PUMA au CEV

- INTEGRATION - MISE AU POINT SOL OBTENTION D'UN FONCTIONNEMENT CORRECT EN VOL	3 VOLs	2 MOIS
- PLATE-FORME VIRTUELLE ET AUTOCOMPENSATION DU MAGNETOMETRE	15 VOLs	2 MOIS
- HYBRIDATION INERTIE-DOPPLER	5 VOLs	1 MOIS
- HYBRIDATION BARO-INERTIELLE VOLS DE SYNTHESE	11 VOLs	1 MOIS
	34 VOLs	

(42 h) de décembre 1979 à mai 1980.

Fig.14 Essais de mise au point

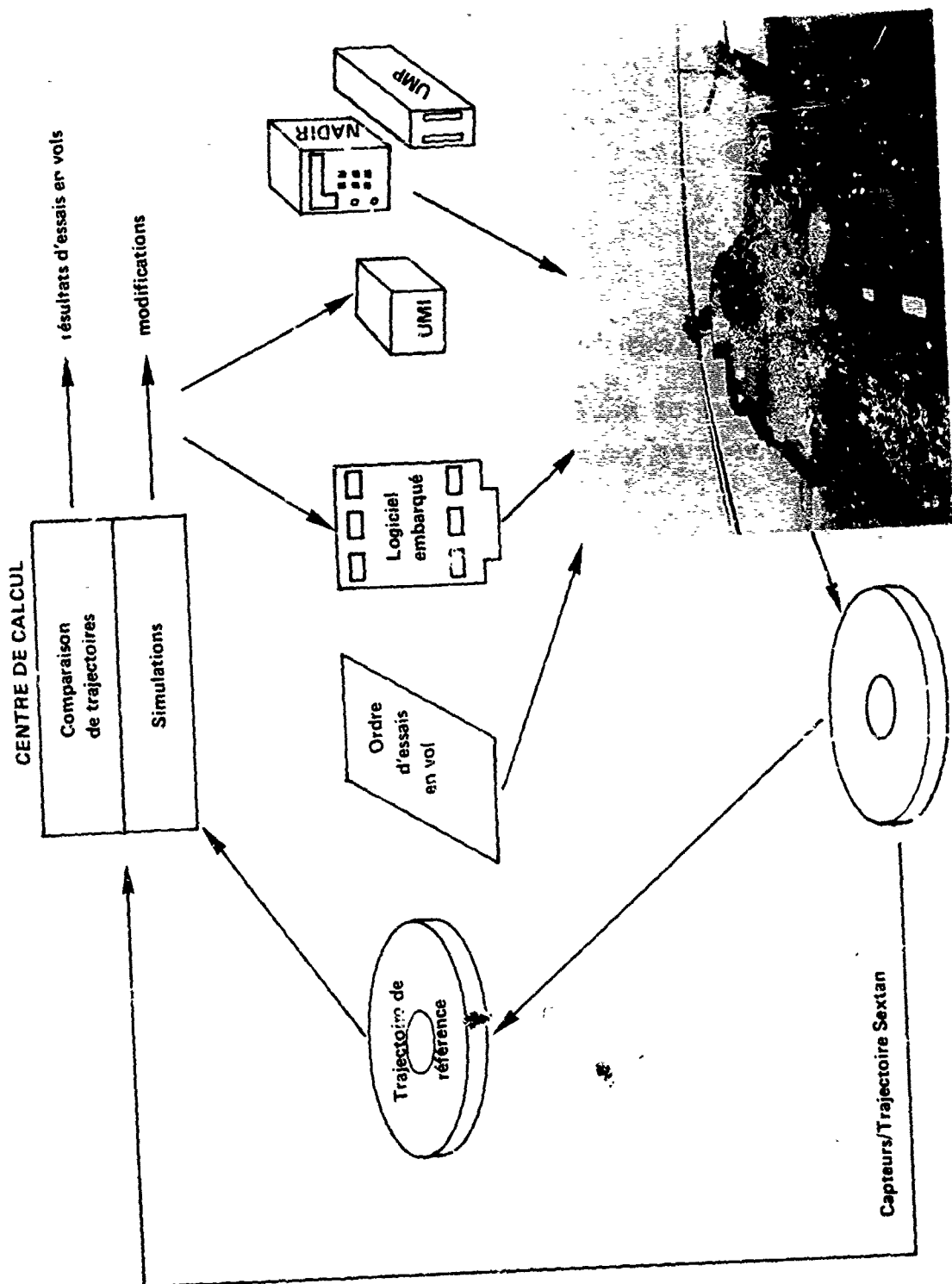


Fig. 15 Traitement de l'information lors des essais en vol
phase constructeur

• 18 HEURES DE VOL (12 VOLS)

4 VOLS DE NAVIGATION TACTIQUE

8 VOLS DE NAVIGATION "TYPE CONVOYAGE"

• 1 REGULATION DE CAP.

1 MOIS
(Juin 80)

Fig.16 Essais d'évaluation

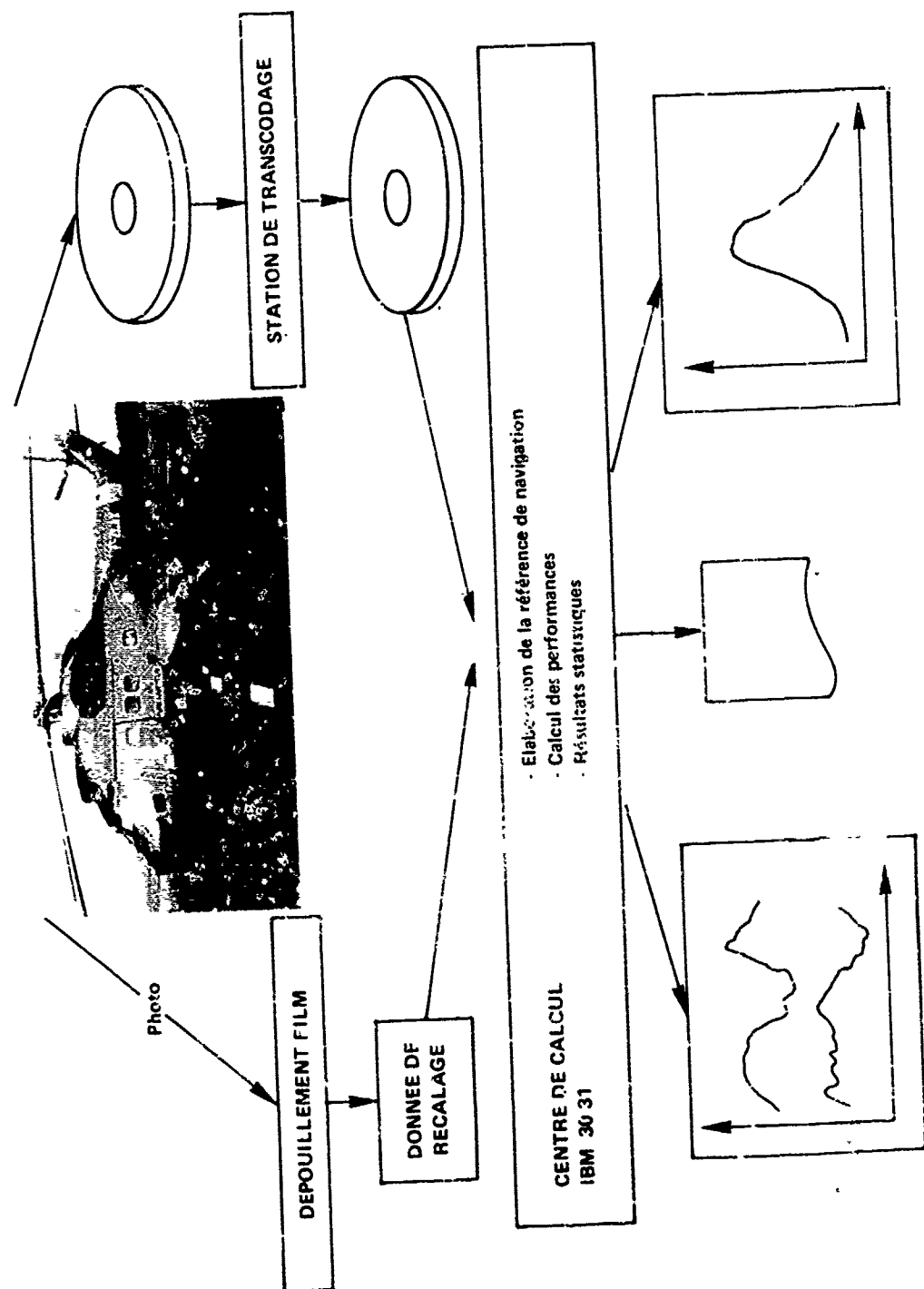


Fig.17 Traitement de l'information lors des essais en vol
phase d'évaluation

- **60 HEURES DE VOI. EN 46 VOLS**
- **170 HEURES DE FONCTIONNEMENT**
- **PAS DE PANNE**
- **PAS DE FONCTIONNEMENT MARGINAL**

Fig.18 Comportement du gyrolaser sur hélicoptère

**FLIGHT TEST RESULTS
OF AN
ADVANCED DEVELOPMENT MODEL
RING LASER GYRO NAVIGATOR (RLGN)**

Kenton L. Bachman
Communication Navigation Technology Directorate
Naval Air Development Center
Warminster, PA 18974 USA

SUMMARY

A flight test program has been conducted by the Naval Air Development Center to demonstrate the performance capability and reliability potential of an Advanced Development Model (ADM) Ring Laser Gyro Navigator (RLGN). The resultant performance of the RLGN in an A-7E and P-3C aircraft is described. Flight test results have demonstrated that the RLGN successfully met all position, velocity, and reaction time requirements. During a year and a half of nearly continuous Navy laboratory and flight tests there have been no failures, maintenance actions or calibrations required or performed on the RLGN system.

I. INTRODUCTION

The emergence of the Ring Laser Gyroscope (RLG) as an ideal rate sensor for strapdown inertial navigation system applications has stimulated widespread interest within the navigation/guidance user community. The laser gyro presents a technological opportunity to overcome cost, reliability, and performance deficiencies encountered with current operational airborne inertial systems used for navigation, weapon delivery, and flight control. The postulated advantages of a laser strapdown inertial system encouraged the establishment of an advanced development program under Naval Air Systems Command sponsorship in 1976 for the design, fabrication, test and evaluation of a Ring Laser Gyro Navigator (RLGN).

This paper addresses briefly the requirements leading to the formulation of an advanced development program for the RLGN. It describes in some detail the functional description of the RLGN including key hardware and software design features. Principal emphasis is given to a discussion of the flight test program in an A-7E and P-3C aircraft, and the resultant navigation and reliability performance. Effects of high latitude on system alignment and navigation will be discussed. Finally, a brief look at the proposed follow-on Full Scale Development (FSD) of a second generation Carrier Aircraft Inertial Navigation System (CAINS-II) applicable to all Navy carrier aircraft will be given.

II. RLGN REQUIREMENTS

Current operational inertial navigation and guidance systems for tactical aircraft and missiles have, to a significant degree, deficiencies in reliability, life cycle costs, and reaction time. These problems are compounded by the pressures to develop and procure numerous inertial system types and configurations tailored for specific applications across the Department of Defense (DoD) user spectrum. This expensive proliferation and the principal equipment shortcomings are due in part to limitations of the electromechanical technology now employed in gimbaled inertial reference units. An exception to this general situation is the Navy developed Carrier Aircraft Inertial Navigation System (CAINS). This gimbaled system using conventional sensors is deployed on several Navy aircraft, notably the F-14, A-2C, S-3A, and A-6E, and some later F-4 aircraft models. However, the stringent environmental performance requirements placed on this system have adversely affected system reliability resulting in a high cost of ownership.

Present and future aircraft inertial navigation system requirements indicate a need for durable, reliable, and low cost-of-ownership inertial systems capable of operating for extended periods without calibration or maintenance. Strapdown inertial navigation systems employing the RLG are now showing that they can meet these requirements.

Strapdown systems provide all the information and outputs normally provided by a gimbaled inertial system, and in addition provide body rate information for aircraft flight control systems. This information is presently supplied by separate angular rate sensors that are not part of the navigation system. In the strapdown configuration, the angular rate and linear acceleration sensors are "strapped" to the airframe and sense the total dynamic input from the airframe motion.

The RLG, with an inherent digital output and essentially unlimited input capability, provides an ideal solution for the strapdown gyro dynamic range problem. Present accelerometers are for the most part directly applicable to the strapdown configuration. Because the accelerometers are not physically stabilized by a gimbal system, their outputs must undergo a computer coordinate transformation from vehicle coordinates to geodetic coordinates. Thus, a portion of the gimbaled inertial navigation system complexity

(gimbals, resolvers, synchros, and associated electronic circuits) is shifted to the more reliable, lower-cost computer. With the introduction of high-speed, low-cost inertial processing units and semiconductor memories, any cost penalties associated with the strapdown computation requirement have been virtually eliminated.

III. ADVANCED TECHNOLOGY LASER GYRO PROGRAM

In a series of directives dating from 1974 the Office of the Secretary of Defense/Under Secretary of Defense for Research and Engineering (OSD/USDR&E) provided guidance to the Service Secretaries for the establishment and operation of an Advanced Technology Demonstration Laser Gyro Program. This program evolved from highly successful Navy exploratory development efforts in laser gyro technology and prototype system development dating back to the late 1960's. The Navy was named executive agent for this effort and a program office was established within the Naval Air Systems Command in 1976. The general objective of the program was to demonstrate the military utility of laser gyros for aircraft navigation, and missile guidance applications. Specific program objectives were to (1) validate the cost, reliability and suitability of RLG's for aircraft navigation and missile guidance systems and (2) to make recommendations on these factors to the Department of Defense (DoD) prior to a commitment into Full Scale or Engineering Development. Pursuant with these program objectives, an Advanced Development Model (ADM) RLGN was developed to assess the reliability, maintainability, and performance factors in a full military environment.

The Naval Air Development Center (NAVAIRDEVGPN) was assigned lead laboratory responsibility for the development, test and evaluation of this system. A contract was let with Honeywell Inc. in 1976 for the design and fabrication of the system to specifications drawn up by NAVAIRDEVGPN. The equipment underwent acceptance tests in January 1979 and was delivered to the Navy in February of 1979.

Performance goals for the RLGN advanced development system were selected to be compatible with the requirements of production inertial navigation equipment in military applications. A summary of the major goals is presented in Table 1. Reliability/maintainability goals established to achieve life-cycle cost goals include a MTBF of 2500 hours for the INU, sensor replaceability without system level recalibration and no regularly scheduled system calibration requirement.

TABLE 1

RLGN ADM PERFORMANCE GOALS	
Reliability	2500 hours MTBF (INU)
Position Accuracy	1 nmi/hr [1.85 Km/HR] CPE rate
Velocity Accuracy	3 ft/s, [0.91 M/S] $\frac{^{\circ}}{^{\circ}}$ per axis
Altitude Accuracy	2.5 arc min (RMS)
Heading Accuracy	3.0 arc min (RMS) and 0.02 deg/hr 1,
Acceleration Capability	10 G's each axis
Rate Capability	400 deg/s each axis
Reaction Time (-54° to +71°C)	less than 10 minutes
Calibration Inertial	>1 year
Test Provisions	BITE, incl sensors

IV. RLGN SYSTEM DESCRIPTION

The ADM RLGN consists of an Inertial Navigation Unit (INU), Control Display Unit (CDU), Mode Select Unit (MSU) and battery. The RLGN INU is packaged in a 3/4 ATR long case and was designed to withstand the typical military environmental ranges for temperature, altitude, vibration and shock as well as typical mission flight profiles. The RLGN Control Display and Mode Select units are commercially available equipment. The INU provides position, velocity and attitude information to the CDU. The INU consists of three orthogonal body-mounted laser gyros and three accelerometers, a digital computer, I/O electronics, sensor electronics and a power supply. Figure 1 shows a block diagram of the ADM INU and external interfaces.

The RLGN utilizes three Honeywell GG 1342 laser gyros to sense incremental angular displacement about the attitude and heading axes. The GG 1342 utilizes the integral block discharge tube configuration and body dither for lock-in compensation. The geometry of the gyro body is a 50 degrees isosceles triangle with a 34.5 cm path length. The laser gyro is designed for operation with a 0.63 micron (visible red) wavelength and has a pulse quantization of 2 seconds of arc. The salient performance characteristics of the RLGN laser gyros are summarized in Table 2.

The RLGN utilizes three Systron Donner Model 4841 accelerometers. The 4841 is a low-cost, inertial-grade, electrically servoed accelerometer designed for strapdown applications in aircraft and missiles. The main performance characteristics of the RLGN accelerometers are shown in Table 3.

The output from the laser gyros are roll/pitch/yaw angular increments. The gyro electronics control the gyro operation and provide gyro performance independent of temperature and dynamic conditions. The accelerometer electronics convert the accelerometer analog output into digital pulses. The gyro and accelerometer misalignment numbers, scale factors, biases and thermal compensation coefficients are stored in a special

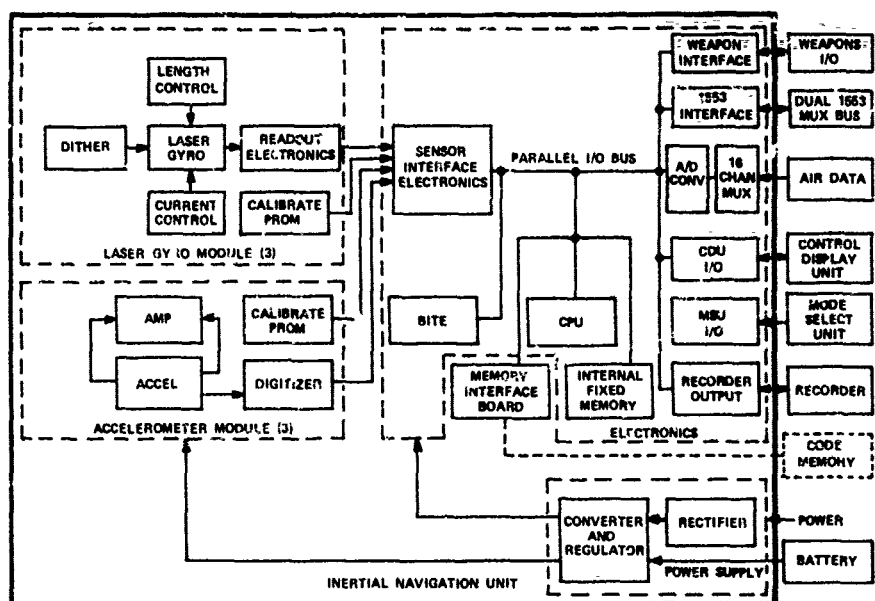


FIGURE 1. BLOCK DIAGRAM OF THE ADM INU AND EXTERNAL INTERFACES.

TABLE 2

RLGN LASER GYRO SALIENT CHARACTERISTICS			
Parameter	X	Axis Y	Z
Gyro Bias (deg/hr)		(0.007°/hr - spec value)	
Gyro Scale Factor Linearity (PPM)	3.1	2.5	1.1
Gyro Random Walk (deg./hr)	0.0011	0.0013	0.0050

TABLE 3

RLGN ACCELEROMETER SALIENT CHARACTERISTICS			
Parameter	X	Axis Y	Z
Bias Stability (μ G)	3	16	17
Scale Factor Linearity (%)	0.0012	0.0014	0.0009

Programmable Read Only Memory (PROM). These parameters are transferred into system memory during alignment. Built In Test (BIT) capabilities are incorporated in the RLGN to detect failures in the gyros, accelerometers, power supply and processor. Continuous BIT is operational during all power-on modes and additional BIT can be initiated during stand-by modes of operation.

All inputs and outputs to the digital computer are transmitted over a parallel I/O bus. The sensor electronics provide counting and data transfer control functions to transfer sensor outputs to the computer memory. The air data sensor provides barometric altitude in either digital or analog form to stabilize the INU's vertical loop. The CDU displays position and velocity components from the computer and allows the operator to insert display mode select commands and initialization data. The MSU provides the means for selecting system operating modes (on, off, standby, align and navigate). The I/O electronics contain provisions for formatting data for a digital tape recorder and for interfacing with other aircraft system for experimental purposes. Under normal test conditions, the INU would operate from the internal semiconductor (PROM/ROM) memory. An external core memory interface, used for test and checkout only, allows for software/memory checkout and modifications but is not required for normal flight operations. An additional feature of the RLGN is the provision of a MIL-STD-1553A digital multiplex bus interface. The mux bus is capable of controlling the RLGN modes of operation and interrogating the data bus. Provisions are available to control the RLGN from either the mux bus or the CDU.

The inherent digital character of the RLG has made possible extensive use of Built-in-Test (BIT) for performance monitoring, failure detection and malfunction isolation. Each laser gyro, for example, outputs seven "health" signals that can provide an indication of performance degradation before a failure occurs. In the RLGN, BIT signals are also brought out for the accelerometers, power supplies, central processor, timing and

control, and interface functions. From a maintainability point of view, recalibration is minimized through use of systematic error compensation performed in the processor. Each laser gyro has its own PROM (Programmable Read Only Memory) containing known error coefficients that are read into computer memory at system turn-on. Thus, gyros may be replaced readily without the need to perform system recalibration, obviating the need for sophisticated test equipment in the field.

V. RLGN TEST PROGRAM

The RLGN was delivered to NAVAIRDEVcen in February 1979 after successfully completing acceptance testing at the contractor's plant. The acceptance testing included temperature tests at -65°F, 0°F, 100°F, and 135°F (-54°C, -18°C, 38°C and 57°C); random vibration tests in the frequency spectrum of 15 to 2,000 Hz and at test levels of 0.01 and 0.4 g²/Hz along each axis; voltage and frequency variation tests; Scorsby tests; altitude tests; and Electro Magnetic Interference (EMI) tests. The cumulative CEP rate of the RLGN for these tests (excluding navigation errors during actual vibration) was 0.67 nautical miles/hour (1.24 km/hr); the rms velocity errors were 1.85 feet per second (0.56 m/s) in the north channel and 1.45 (0.44 m/s) feet per second in the east channel.

A program plan was originally formulated to progressively test and evaluate the RLGN through a series of baseline tests in the laboratory and a mobile van, followed by flight tests in a P-3C aircraft to obtain accurate position and velocity performance, and finally by flight tests in a high performance aircraft. However, the potential user community's immediate concern centered on the operability of a strapdown laser gyro navigation system in a high performance fighter/attack environment. To satisfy this need, NAVAIRDEVcen initiated A-7E test program plans in January 1979.

VI. A-7E FLIGHT TEST PROGRAM

The objective of the A-7E flight test program was to demonstrate the performance capability of the RLGN in a dynamic flight environment, simulating close air support and surface attack profiles. In particular the aims of the flight tests were to show:

- a. Performance accuracy of the RLGN in a high dynamic flight environment
- b. Reliability potential
- c. Performance stability without recalibration
- d. Reaction time

ALIGNMENT TESTS

Prior to commencing actual flight tests a series of alignment tests were conducted to determine the optimal alignment time and to ascertain whether there was any difference between alignment direction, and power source; i.e., ground power cart vs. aircraft engine power. The results indicated that 5.5 minutes was the preferred alignment time. (Two and one-half and one minute alignments were also performed during the flight tests because of the desire for fast reaction performance data.) The results also showed that generally the alignments were as good if not better with the engine running. Therefore, it was concluded that the A-7E flight tests would be conducted using engine power for system alignment. Finally, the tests showed that one gyro (X-gyro) appeared to have a slightly better gyrocompassing ability than the other (Y-gyro). This tended to indicate that the X-gyro was of somewhat better quality than the Y-gyro.

FLIGHT TEST DESCRIPTION

A total of 47 flights were conducted of approximately one and a half hours duration. The approach taken was to progressively explore more of the flight envelope as the testing progressed. Once the total flight envelope was established, an ensemble of identical flight profiles was conducted to demonstrate actual RLGN system performance. Figure 2 illustrates a typical flight profile.

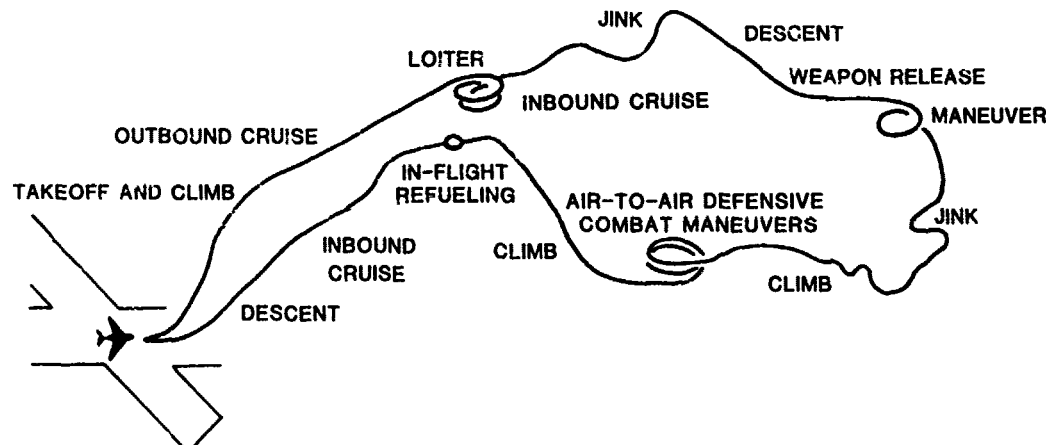


FIGURE 2. TYPICAL FLIGHT TEST PROFILE.

The aircraft was operated within standard NATOPS limits at various attitudes and altitudes. Maneuvers required ranged from the relatively benign to the high G profiles encountered in air to air combat engagements and weapons delivery applications. The former included: Circular, Racetrack, and Figure-8's all flown at standard rates of turn or less. The latter maneuvers included Jinking, Immelman, Split "S", Wingover and High "G" Pull-Up and Roll profiles. The aircraft flew at test altitudes ranging from 200 feet (61 meters) for the low level visual checkpoints to 25,000 feet (7,750 meters) during the high dynamic maneuvers. Speeds ranged from 200 knots (103 m/sec) Indicated Air Speed (IAS) to 0.98 Indicated Mach Number (IMN) during high speed dives. A maximum of 6 G's was pulled during the 540° wind-up maneuver.

For each of the 47 flights, quantitative data on system performance was obtained by comparing the RLGN position output with known geographic coordinates of previously selected ground checkpoints. Reference checkpoint data was obtained by direct overflight of previously selected TACAN stations for the outbound and inbound legs. Checkpoint data in the maneuver area was obtained by direct low level (61 meters) overflight of the Cape May NJ Coast Guard helicopter landing pad. Terminal velocity and position was also recorded after the aircraft was parked on the NAVAIRDEVCECEN landing apron.

FLIGHT TEST RESULTS

The results of the flight tests are summarized in Table 4 as a function of alignment time. The main criterion used in evaluating system performance was the Circular Probable Error as a function of time in navigate mode (CPE per hour). The CPE rate is defined as the median of an ensemble of radial position error rates. Thus for the data shown, there is a 50% probability that the radial position error divided by the elapsed time in the navigate mode shall be less than or equal to the CPE rate shown. The CPE rate is the standard figure of merit used to evaluate the Navy's Carrier Aircraft Inertial Navigation System (CAINS) equipment. The CPE rate was computed for each flight using the RLGN position error derived from ground checkpoints, TACAN checkpoints and low level visual checkpoints in the operating area. Typically each flight included 4-7 visual fly-over checkpoints at Cape May, NJ, 3 ground checkpoints (including closeout) and 3 TACAN checkpoints outbound and 3 inbound.

For the A-7 tests, the RLGN was not instrumented to adequately determine velocity performance due to the nature and objective of the program. Nevertheless, a gross estimate of system velocity accuracy was obtained from examining the RLGN closeout velocity readings when the aircraft came to a stop and the velocity reference was zero. Table 4 also includes the RMS closeout velocity error for the 5.5 and 2.5 minute alignment times. (There was no closeout data recorded for the 1 minute alignments.)

TABLE 4

SUMMARY OF RLGN A-7E FLIGHT TEST RESULTS			
Alignment Time (Min)	No. of Flights	CPE Rate (nmi/hr) [Km/hr]	Close Out RMS Velocity Error (fps) [m/s]
5.5	21	0.74 [1.37]	VN 5.3 [1.6] VE 4.1 [1.3]
2.5	20	1.30 [2.41]	VN 5.8 [1.8] VE 4.0 [1.2]
1.0	6	1.64 [3.03]	---

While individual error plots are not shown in this paper, an inspection of error propagation during each flight revealed no discernable change in system performance as a result of the maneuvers flown. These observations tend to demonstrate that, on the basis of using position accuracy as the performance criterion, the RLGN is insensitive to the type of airborne maneuvers that were performed during the A-7E flight tests.

It was also noticed from an inspection of individual error plots that latitude errors were usually larger, often considerably so, than the corresponding longitude errors. This may be due to the initial heading error after alignment causing a cross coupling of earth rate into the north-south (latitude and north velocity) channel. This heading misalignment consists of a gyro drift rate random bias and wide band (white) noise. In the case of gimbaled system the bias portion of the initial heading error, which during the gyrocompass alignment becomes strongly correlated with the east gyro bias, remains correlated during the entire flight. This correlation causes a partial cancellation between the east gyro drift and heading error. In a strapdown system, however, depending on the aircraft attitude during the flight this correlation may either disappear or actually change sign and become detrimental.

A-7E FLIGHT TEST CONCLUSIONS

All the objectives of the A-7 flight test program were successfully demonstrated. Position accuracy and reaction time were within the specified performance goals and there were no system failures, maintenance actions or calibrations required. Nearly all the flights were conducted following alignment under aircraft engine power. This is considered a positive factor from an operational readiness aspect. Further, on the basis of examination of the data, error propagation was apparently not affected by the

high dynamic fighter/attack environment nor by the immediacy of transitioning into high dynamics right after takeoff. The performance of the RLGN with reduced reaction time (viz 3.0 min and 1.5 min) makes it a viable candidate for navigation system applications where reaction time is at a premium.

VII. P-3C FLIGHT TEST PROGRAM

The objective of the P-3C flight test program was to determine RLGN velocity and position performance from a series of flight profiles designed to thoroughly exercise all channels of the system. Recalling that the A-7E aircraft was not instrumented to record velocity information during flight, the P-3C aircraft, on the other hand, utilized specifically designed test instrumentation to record RLGN data and time synchronize it with the P-3C reference inertial system and the ground radar tracking station. Thus it was possible to extract through post flight data reduction and analysis, a very accurate time description of RLGN velocity and position errors.

The reference P-3C inertial system used in these tests was the AN/ASN-84. Ground tracking of the aircraft was provided by a modified Nike-Hercules radar system with a specified accuracy of 0.2 mil rad. in azimuth and elevation and 10 yards (9.14 meters) in slant range. The flight tests were conducted over the Chesapeake Test Range of the Naval Air Test Center, Patuxent River, Maryland. At select times during the flight test series, the aircraft was flown over the Cine-Theodolite course to verify the accuracy of the reference radar data.

TEST EQUIPMENT DESCRIPTION

A simplified block diagram of the aircraft test instrumentation and interface is presented in Figure 3. Its operation may be briefly described as follows: The Telemetry Receiver receives an IRIG-B reference time signal from the Range Radar Station and synchronizes the real time clock of the Time Code Generator. The Time Code Generator then provides timing signals to the RLGN Tape Recorder Interface Unit. This unit formats and controls the output of the RLGN data and provides a synchronized time recording on the data Tape Recorder. (Up to 68 data items from the RLGN can be recorded on the Tape Recorder.)

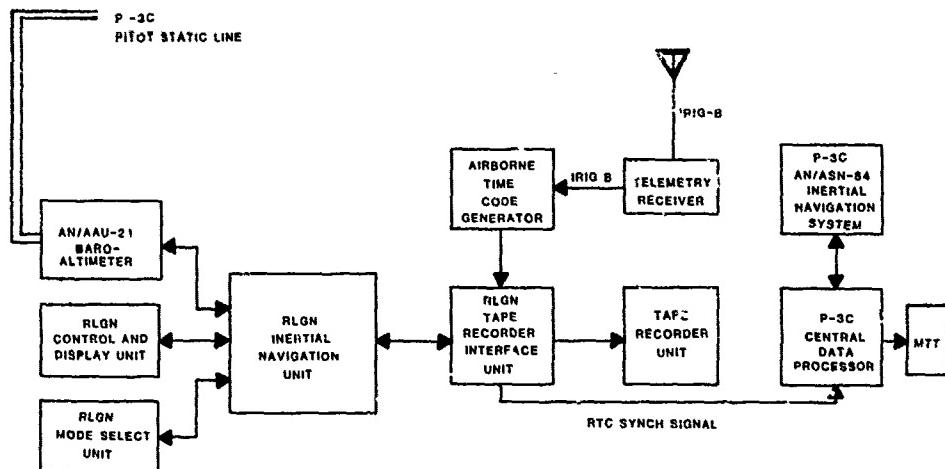


FIGURE 3. RLGN INSTRUMENTATION SYSTEM.

In addition the Tape Recorder Interface Unit supplies a synchronizing signal to the real time clock of the aircraft Central Data Processor. This assures time synchronization of the RLGN and AN/ASN-84 data with the range radar data.

The aircraft Central Data Processor receives and processes data from the AN/ASN-84 inertial system and formats the selected data variables for recording on the Magnetic Tape Transport (MTT) unit. The Baro-Altimeter provides altitude information to stabilize the vertical loop of the RLGN.

As part of the equipment installation, a radar transponder was installed on the aircraft to provide an accurate position reference for tracking by the radar station. The transponder was located in very close proximity to the RLGN and AN/ASN-84 inertial systems, which were located in line and adjacent to each other.

FLIGHT TEST DESCRIPTION

The P-3C flight program consisted of flight scenarios ranging from the relatively benign to the more complex as encountered in typical Anti-Submarine Warfare (ASW) mission profiles. There were three basic flight scenarios: Extended Figure Eights, Clover Leafs, and Ladder Patterns. The last two are primarily ASW mission profiles that have both a practical and analytical significance; analytical in the sense that they exercise almost continuously both horizontal channels of the RLGN thereby providing a good test of the system mechanization. The extended Figure 8 pattern included

a straight and level leg of approximately 40 miles [74.0 Km.] in the North-South direction and 30 miles [55.5 Km.] in the East-West direction. This leg permitted acceleration or deceleration of the aircraft as specified in the test plan.

Alignment times used were the same as used previously in the A-7E flight tests, i.e. 2½ and 5½ minutes. Most of the system alignments were performed using the aircraft Auxiliary Power Unit (APU) with the engine turned off. There were a few flights in which the system was aligned under engine power because of failures with the APU.

A total of 38 data flights were scheduled providing a mixture of alignment directions, alignment times, and flight profiles. Typical flight time under range radar coverage was two hours. Immediately prior to the data flight, both the RLGN and the AN/ASN-84 were ground aligned. The AN/ASN-84 alignment time was 20 minutes thereby providing a well aligned reference system. Alignment of the RLGN was initiated during the final 2½ or 5½ minutes. Both systems were then switched to the navigate mode together and the aircraft was ready for take-off.

DATA REDUCTION AND ANALYSIS METHODS

The data reduction and analysis techniques used in the A-7E flight tests were relatively straightforward since only RLGN position and close out velocity data were recorded. By contrast, the techniques used in the P-3C flights were more complex because of the wealth of information gathered from the different reference sources, i.e., RLGN, AN/ASN-84, radar, and cine-theodolite, and the desire to establish accurate time histories of system error propagation during flight.

Principal emphasis in the data reduction scheme was placed on an accurate determination of velocity error. Statistical means were used to separate the velocity error from true RLGN velocity.

Reference 1 describes a Forward-Backward Kalman Smoother computer program that was developed to generate accurate reference velocity information against which the RLGN velocity was compared. For these tests radar-aided AN/ASN-84 position information was selected as the reference. Basically, this reference was formed by differencing the AN/ASN-84 and radar position information and then filtering and smoothing the difference to form an estimate of AN/ASN-84 velocity error. This estimate was then subtracted from the raw AN/ASN-84 velocity information to provide a velocity reference for the RLGN. This reference velocity was in turn subtracted from RLGN velocity to provide an estimate of RLGN velocity error. A block diagram of this scheme is given in Figure 4.

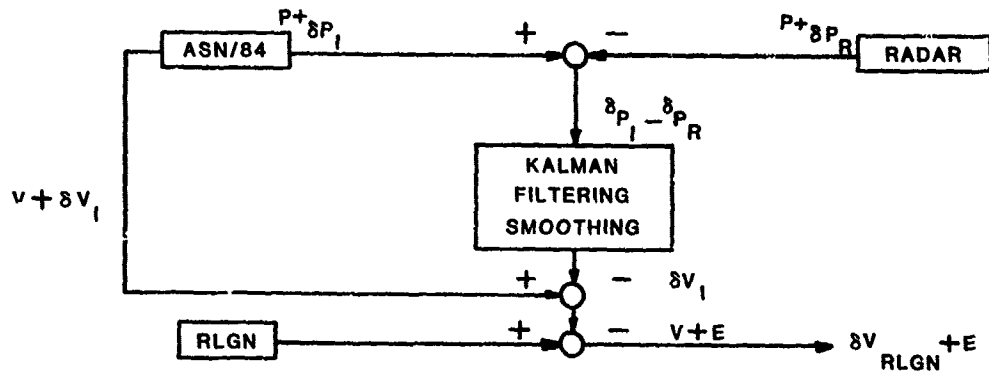


FIGURE 4. VELOCITY REFERENCE FOR ADM RLGN.

The same program can be used to estimate position, misalignment, and heading errors but these were not used at this time. Rather, position calculations were made by differencing the RLGN and radar derived position.

FLIGHT TEST RESULTS

The P-3C flight tests were still in progress at the time this paper was written. Hence the test results reported herein provide the first, albeit abbreviated indication of RLGN velocity performance using this technique. Additional test results will be provided in the oral version of this paper.

There have been a total of 32 test flights to date. All of these flights used the extended Figure 8 profile; the Clover Leaf and Ladder patterns were scheduled later. The following table summarizes the results obtained to date.

Figure 5 illustrates the cumulative position error over all the flights. Note that the majority of the flights are less than (1NM/HR [1.85 KM/HR]) CPE rate.

Of the 32 flights to date, 10 have been reduced for velocity error. The 10 flights selected represent a cross section of alignment direction, time, and flight direction thus providing a good composite velocity error description. Figure 6 illustrates the combined north and east velocity distribution for these flights. Note that the velocity

TABLE 5

SUMMARY OF RLGN/P-3C FLIGHT TEST RESULTS	
Total Flight Time	179 HR
Average Navigate Time	2.3 HR
Total Number of Flights	32
Number of System Failures	0
Number of Maintenance Actions	0
Number of System Calibrations	0
Total CPE Rate	0.84 NM/HR [1.55 KM/HR]
RMS North Velocity Error	2.62 FT/SEC [0.80 M/SEC] (10 Flts)
RMS East Velocity Error	2.26 FT/SEC [0.69 M/SEC] (10 Flts)

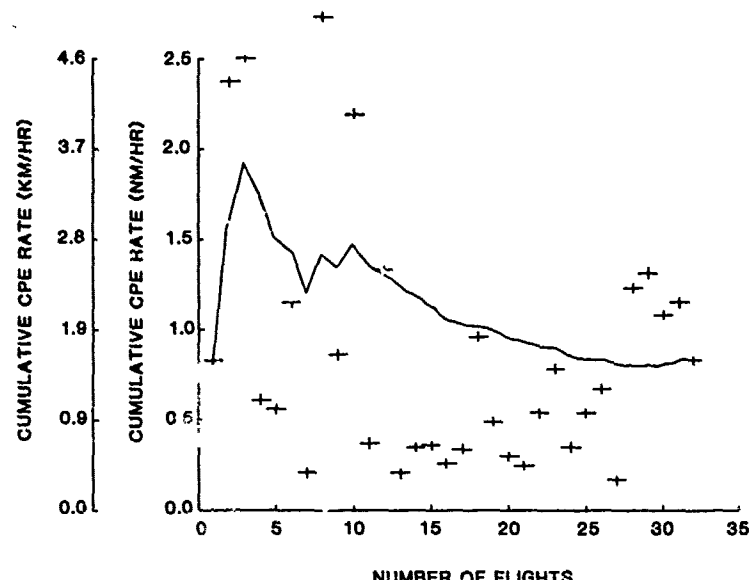


FIGURE 5. RLGN POSITION ACCURACY.

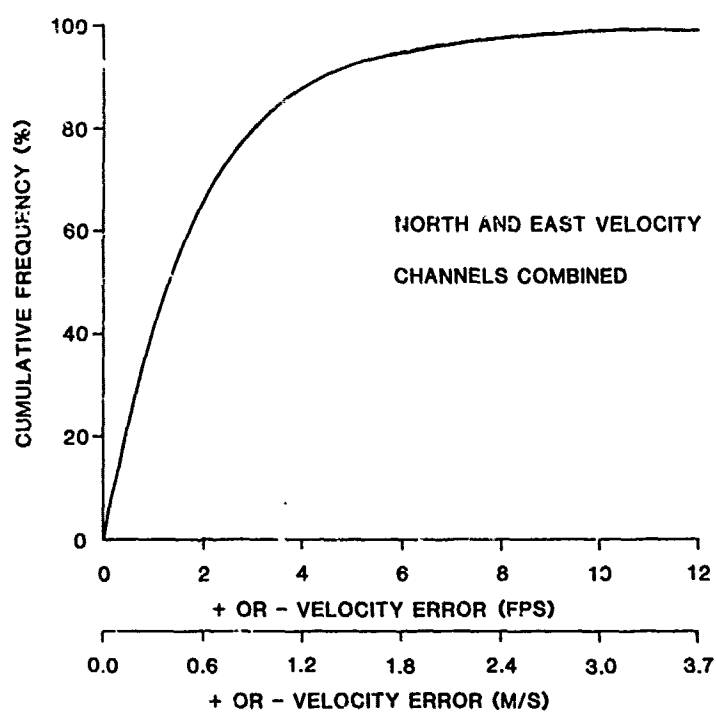


FIGURE 6. COMBINED NORTH AND EAST VELOCITY DISTRIBUTION.

errors for approximately 90% of the flights were less than 4 ft/sec [1.22 m/sec]. The average horizontal velocity error per channel was 2.45 ft/sec [0.75 m/sec]. This is well below the specified velocity error of 3 ft/sec [0.91 m/sec] RMS.

VIII. HIGH LATITUDE TESTS

The flight test schedule was interrupted in early July 1980 to conduct a series of high latitude flight tests on the system. The objective of these tests was to determine the alignment time and resultant position accuracy at a location where the effective earth rate sensed during alignment was significantly reduced. Keflavik, Iceland at a latitude of 64° north was selected as the most suitable location.

The ground alignment tests consisted of performing a series of alignments with the aircraft pointed at each cardinal heading. The system was repeatedly aligned for 15 minutes (at 15 minutes the alignment filter gains reduce to zero) while recording both horizontal sensed earth rate components. From these values true heading was computed and plotted as a function of alignment time. The criteria used for selecting the aligned time was the time when the RMS azimuth error reached and stayed within three (3) arc min. From these tests a 7.5 minute reaction time was selected. It is noted that an alignment time of 5.5 minutes was selected using the same criteria for the tests conducted at the Naval Air Development Center where the latitude is 40° North. In-flight position data only was recorded as there was no radar range tracking facilities available. On-top position indications were obtained from TACAN stations and non-directional radar beacons. Flight test altitudes varied from 200 feet [61 meters] for the on-top position fixes to 5000 feet [1500 m] during the airways portion. The resulting position accuracies achieved during these tests are shown in Figure 7. The total CPE rate was 0.73 NM/HR [1.35 Km/HR] for the five (5) flights.

RLGN HIGH LATITUDE FLIGHT TESTS

KEFLAVIK, ICELAND

ALIGN DIRECTION	FLIGHT DIRECTION	FLIGHT TIME (HRS)	CPE RATE (NM/HR)
NORTH	EAST-WEST	2.5	0.50
NORTH	EAST-WEST	2.8	0.76
EAST	EAST-WEST	2.9	0.76
NORTH	NORTH	3.8	0.53
EAST	ROUND ROBIN	4.0	0.93

TOTAL CPE RATE (50TH PERCENTILE) = 0.73 NM/HR

NOTE: 7.5 MIN ALIGNMENT TIME USED IN ALL FLIGHTS

FIGURE 7. RLGN HIGH LATITUDE FLIGHT TESTS.

IX. CAINS II

The successful test program on the Advanced Development Model (ADM) RLGN has now prompted the Naval Air Systems Command to initiate procurement planning for the Full Scale Development (FSD) of the next generation Carrier Aircraft Inertial Navigation System (CAINS). The CAINS II FSD program is expected to be based upon the proven RLG strapdown design demonstrated in the RLGN test program. CAINS II is expected to become standard equipment for all Navy carrier aircraft requiring self-contained inertial navigation capabilities.

It is noted that the recent selection by the U.S. Marine Corps of a laser navigation system for the AV-8B Vertical/Short Take-Off and Landing (V/STOL) aircraft was influenced by the successful RLGN development program. The favorable impact of RLG strapdown system technology has been further demonstrated in the commercial aviation market with the contract award by Boeing Co. for laser inertial reference systems on their new model 757 and 767 airplanes, and most recently by Airbus Industries for the A-310 airplane.

CONCLUSIONS

While flight tests in the F-3C aircraft were still in progress, it can be said that up until this time, all the test objectives of the A-7E and P-3C flight test programs have been successfully demonstrated. Position, velocity, and reaction time accuracies were all within specified performance goals. As important if not more so, there have been no system failures, maintenance actions, or calibrations in 18 months of nearly continuous Navy tests. The system has a total of 950 operating hours including 300 in the A-7E and P-3C aircraft.

In view of the fact that this was an Advanced Development Program on prototype equipment, the test results clearly represent significant progress in advancing RLG strapdown technology for both military and commercial avionics applications.

REFERENCES

1. NAVAIRDEVCECEN Technical Memorandum: 401TM 80-RLGN-001

**JTIDS RELATIVE NAVIGATION
TEST AND EVALUATION**
by
Lawrence Newman and Patrick J. Finnegan
COMMUNICATION AND NAVIGATION TECHNOLOGY DIRECTORATE
NAVAL AIR DEVELOPMENT CENTER
Warminster, Pennsylvania 18974

Summary

JTIDS performs precision range measurement, position data interchange, and data processing functions which form the basis of its relative navigation capability. JTIDS relative navigation establishes a universal tactical grid, solves the grid lock problem, improves on-board navigation systems' accuracy and shares community navigation resources. An extensive test program has been conducted to measure the performance of the advanced development model of JTIDS. This paper describes the test program, flight scenarios, data analysis, and general results of this effort.

I. INTRODUCTION

Navigation is based on the ability to assign coordinates in a definable grid system to platforms or other objects of interest. JTIDS, the Joint Tactical Information Distribution System, has this inherent capability by virtue of its precision range measurements, position data interchange, and data processing features. JTIDS is a tri-service program to develop an integrated communications, navigation and identification system.

The Class II ADM-Phase I JTIDS terminal was designed to provide secure communications among cooperative tactical elements operating in a hostile electromagnetic environment. Its TDMA (Time Division Multiple Access) communications architecture supports not only inter-unit data exchange but also permits measurement of time-of-arrival (TOA) between cooperative members. When precision TOA measurements are made available to on-board processors of inertial subsystem data, a synthesis is possible to support tactical navigation requirements. The rel nav function provides the synthesis in a software ensemble of modules which were designed to provide geodetic and grid navigation information in terms of position, velocity, and attitude.

JTIDS also disseminates its navigation data to the entire tactical community, thereby providing an essential consistency of position location to each of its elements. This consistency, applies not only to the positions of each member but to all data derived in the community from on-board sensors and fleet tactical data interchange systems. This permits the acquisition of precise fire control solutions based on sensor data derived from multiple platforms and stations, i.e., data "fusion".

JTIDS relative navigation is designed to operate with a minimal dependency on sources of accurate absolute geographic position. However, once the participants in the relative navigation community have accurately established their relative position (i.e., their displacements from one another), they can share their geographic navigation resources and thus improve the absolute position accuracy of members equipped with less precise geographic position references. In essence, the relative navigation grid can be used to relay the geographic position of the better equipped members.

II. JTIDS TEST PROGRAM AT NAVAIRDEVcen

The JTIDS development program plan provided for an evolutionary development in two phases. Phase I was the development of the basic digital jam-resistant information distribution system with relative navigation, TACAN and identification capabilities. Equipment developed in this phase was required to be capable of operating without degrading TACAN or other existing CNS systems. Phase II is the extension of the accomplishments of Phase I. Equipment developed in Phase II is designed to have greater capacity and flexibility while maintaining compatibility with TACAN and interoperability with the Phase I equipment. In addition the Phase II equipment incorporates an IFF transponder function consistent with the ICNI concept.

The Phase I test program conducted at NAVAIRDEVcen was part of the Navy's Test and Evaluation program designed to provide the technical data base necessary to make recommendations for the technology/system to be integrated into Navy platforms. In addition, these bench and flight test results are being provided to both developmental and operational test representatives of the various services in order to support independent evaluations of system performance with respect to their specific requirements.

The JTIDS Test and Evaluation Program is based upon requirements, system characteristics, and issues identified in JTIDS development program documents. These documents identify the system features which are required to alleviate current information system deficiencies. That is, JTIDS must enhance operational capabilities in the following areas: orderly transition, connectivity, range, relay capability, survivability and reconstruction, system capacity, flexibility, low error probability, jamming resistance, information security, low probability of signal intercept and exploitation, passive operation, relative navigation, net entry, identification capability, message format compatibility, electromagnetic compatibility, joint and combined operational capability, multiple netting and unformatted digital data. These enhanced capabilities will be provided to the user with a reaction time equal to, but preferably better than present data link systems.

Among the critical issues to be addressed in the test program was the following:

Does JTIDS enhance the correlation of multiple designated targets as a result of its employment?

-The ability of JTIDS relative navigation to enhance TDS grid lock thereby eliminating multiple designations of the same target will be evaluated.

In response to this issue, the Navy has conducted an extensive bench and flight test of the JTIDS relative navigation function.

III. Bench Tests

The major objective during the bench or laboratory phase of testing was to verify that the equipment operated according to the characteristics identified in the Phase I Class 2 Performance Specification and to perform sensitivity analyses in areas of operation which corresponded to technological issues or design risks.

The AN/URQ-28 model JTIDS was designed to interface with the ASN 90/91 Inertial Navigation System. The JTIDS terminal accepts inertial data via the navigation port and estimates errors in own ship position, velocity and tilt based upon messages received from communication net participants. The terminal determines these corrections as a result of comparisons of message time of arrival (TOA) or slant range with the range indicated by position data in received messages. Range differences in the compared values are attributed or assigned to various error sources (states).

These corrections to position, velocity and tilt values are then output via the Relative Navigation Port.

Special software was loaded into the ASN 90/91 computer in order to provide the required inertial data in a format compatible with the Relative Navigation Port. The software utilized did not process or correct inertial position information based up AN/URQ-28 terminal corrections.

The port consisted of an input and an output serial 50 KHz channel. Each channel consisted of a differential data line, a pair of control ("ready") lines, a deadreckoner time mark discrete, and a common pair of 50 KHz clock lines. Input and output words (20 bits each) are exchanged via the port until the total 36 words (18 input, 18 output) are transferred during each navigational computation cycle.

The relative navigation function was first examined using static tests on the bench utilizing carefully attenuated signals transmitted among those terminals situated in the laboratory. These tests exercised the JTIDS relative navigation interfaces, the NADC designed data recording capability, and basic relative navigation functions and modes which provided the necessary level of confidence to proceed on to flight test operations.

IV. FLIGHT TESTS

The primary objective of the flight test program was to evaluate terminal communication and navigation performance in a dynamic environment. Specifically, performance characteristics such as navigation accuracy which cannot be completely evaluated in a static configuration were examined with the aid of accurate tracking radars.

Upon completion of initial bench test AN/URQ-28 terminals were installed in three cargo-type aircraft: a C-121, a P-3A and an RH-53. Palletized JTIDS test installations consisted of the following equipments:

- Terminal Equipment Group -

- AN/URQ-28 R/T unit
- Mode Control Unit
- Switchable Filter Assembly
- Interim Secure Data Unit

- Terminal Interface Equipment -

- Display Unit Processor
- CRT Display
- Tactical computer set AN/ASN-91
- CAN D/S Converter terminal

- Ancillary Equipment -

- Inertial Measurement Set AN/ASN-90
- Air Data Computer

The JTIDS installation configuration is shown in Figure 1. Each aircraft was equipped with the instrumentation shown. Ground stations did not require an Inertial Measurement System.

The following equipment was used to collect data during the flight tests:

- Digital Incremental Tape Recorder (Kennedy 1708)
- Tape Recorder Interfaces (NADC design and fabrication)
- Time Code Generator

Aircraft utilized during flight tests were chosen based on the following requirements:

- Flight dynamics consistent with AN/ASN 90/91 Inertial System operational characteristics.
- Sufficient space for palletized installation of terminals and test equipment and in-flight monitoring of equipment performance by engineering personnel.

- Flight endurance in excess of four hours to provide efficient use of test ranges as well as meet navigation accuracy test duration requirements.
- Characteristics which enable evaluation of operation with a cross section of user types (e.g. multipath, rotor blade interference, etc.).

V. DATA RECORDING AND PROCESSING

Data recorded for analysis included grid and geodetic navigation parameters as estimated by the AN/URQ-28 in addition to the raw inertial navigation position data during all but 17 of 106 tests.

The following group of data processing programs were developed in order to analyze the AN/URQ-28 performance during flight tests:

TCOPY - creates a permanent file of data.

ODRCFIL - accesses file created by TCOPY and creates a file which is used by the REL/NAV Dump Program. This program searches files for JTIDS control word blocks and IRIG-B time tags each record. There are two versions of this program, to be used with the appropriate tape recorder interface type (P-message vs. no P-message).

NADCMF - this program accesses data from the files created by ODRCFIL and writes to a file PLOTIA. In addition, this program prints out the Kalman cycle data of the AN/URQ-28 terminal. Data is selected from one $\frac{1}{4}$ second cycle, one $\frac{1}{2}$ second cycle, and every 16 second cycle.

KXPLOTF - reads data contained in PLOTIA files, prints tables and generates printer plots of position and navigation qualities, filter states and covariances.

DAPLOT - reads data contained in PLOTIA files and plots Kalman cycle data. Qualities, states and covariance are output to a 7-track tape which drives a 753 CAL COMP plotter.

P-MSG - this program accesses either permanent files or flight types directly and prints contents of P-messages exchanged during test (both transmitted and received).

In addition, a data reduction program was developed to assist in quantifying the accuracy of the AN/URQ-28 rel nav function as well as its ability to navigate geodetically and in the grid in terms of position, velocity and attitude estimates.

The Rel Nav Data Reduction Program (RNDRP) shown in Figure 2, utilized as a post-flight evaluation program, was composed of multiple subprograms which process time-tagged radar tracking information and rel nav data to obtain quick-look results, filtered results, smoothed results, and community analysis (inter-unit) results. With the aid of this tool, it was possible to assess the grid and geodetic position, velocity, and attitude estimates of the rel nav filter.

Data acquisition was accomplished with a Digital Incremental Tape Recorder. Inputs to the recorder were provided by the digital tape recorder interface unit which accumulates performance data from the JTIDS display unit processor and reference data from the time code generator. The magnetic tape records generated were processed on the ground by NAVAIRDEV/CEN computer facilities. The on-board digital clock system provided the exact time of each processing sequence. These reference clocks, located at each test site and in each aircraft, were synchronized via the IRIG-B time code received over UHF radio during all flights. During flights on the NAVAIRTESTCEN - NASA (WALLOPS) tracking range all test participants were synchronized to range time.

VI. FLIGHT SCENARIOS

A test flight normally consisted of an inertial ground alignment period followed by a 5 minute period of tape data recording while the aircraft remained stationary at a surveyed point near the end of the runway. This period of recording provided an estimate of the inertial alignment quality. Upon completion of the stationary inertial position recording, the aircraft would take off and enter the tracking range vicinity. Upon acquisition of beacon tracking by the NATC and/or NASA-WALLOPS island radars, an additional 5 minutes of inertial position data were accumulated prior to initiation of the specific AN/URQ-28 test to be conducted. Similarly, each test ended with a 5 minute recording of inertial position data with the terminal in the "no update" navigation mode. These periods of no update processing allowed the establishment of boundary conditions or reasonable inertial system performance assessment at the start and finish of each AN/URQ-28 test. The final 5 minute period of no update processing also indicated the rate at which position accuracy would deteriorate should no other JTIDS terminal be available. Each test covered a span of approximately 30 minutes with the result that each flight tape represented between 40 and 45 minutes of flight time.

The first flight test of the AN/URQ-28 occurred on 11 Oct 1978. These early tests involved three JTIDS terminals, two of which were operated as ground stations. One ground station was located in the JTIDS laboratory at NAVAIRDEV/CEN. The other ground station was installed in a van and located at a distance of approximately 12 miles from NAVAIRDEV/CEN. This configuration of two ground stations separated by 10 to 15 miles was utilized for flight tests designed to verify functional operation of terminal capabilities and establish confidence in equipment performance. Two hundred test hours were accumulated between 11 April 1979 and 4 May 1979. 14 test flights were performed which resulted in acceptable system performance based upon "mark-on-top" checks which demonstrated order of magnitude consistency between system reported position and actual position. These system demonstrations provided sufficient indications that system performance warranted initiation of radar-tracked performance tests.

Testing at the NATC/NASA-WALLOPS ISLAND tracking range commenced on 26 June 1979 and continued until 28 September 1979. Exercises conducted during this period involved up to 3 aircraft and two ground

stations. Figure 3 shows the trajectories flown, location of JTIDS ground stations and location of tracking radars.

During the three month period of testing, a total of 81 exercises were performed during a total of 31 range test days. The average length of an exercise was 40 minutes, including a five minute period of boundary condition data collection at the beginning and end of each exercise.

A series of runs were designed to exercise the relative navigation algorithms in various geometries, community configurations and system modes. The following is a summary description of some of these runs.

Exercise A

With both ground stations acting as navigation controller (NC), Point Lookout being the net time reference (NTR) and relative grid origin (RGO), a single aircraft is flown in trajectories 1, 4, or 5 and receives updates in Mode 1 (active). The runs are 45 minutes long with 5 minutes in No-Kalman-Update mode, 35 minutes in Kalman update (TOA's are processed to update grid), and the last 5 minutes in No-Kalman-Update mode again. The run begins with a sync reset

These runs portray performance with good geometry conditions, good system time (active mode, round trip timing) and serves as a baseline performance run. It is indicative of a scenario wherein permanent ground sites with surveyed positions are used to establish the grid for aircraft or other platforms entering the community. With two ground stations there should be minimum grid translation and rotation.

Exercise B

This is the same as (A), but the run begins with a sync and a nav reset. The added nav reset restores the Kalman filter covariances to their initial (large) values which have the effect of weighing the measurements more heavily.

As a result, the filter will update relative position, relative velocity, etc. in larger steps. This is expected to shorten the convergence (grid acquisition) time, but depending on circumstances, could produce an overshoot and subsequent oscillations in the filter's estimates i.e., the difference between (A) and (B) may be likened to underdamping and overdamping, respectively.

Exercise C

This is the same as (A), but passive. This is, therefore, the baseline passive run for the rel nav series and should exhibit performance somewhat less effective than (A), because system time will be an added unknown to be estimated (i.e. no RTT).

Exercise D

With both ground stations acting as secondary users initial relative position quality was set to zero ($Q_{PR} = 0$). Two aircraft, flown in trajectory 1, 2, or 4, transmit actively to the passive ground stations, one aircraft is NC and NTR and the other is a primary user. Point Lookout ground station is the grid origin. The 5/35/5 Kalman update timing is used as in (A).

This is the "flying baseline" wherein an aircraft squadron brings the grid to a new user (e.g. ship, ground site). The new user must attempt to locate itself in the grid held by the aircraft. This should be rather difficult to do since the aircraft in this run must establish their own grid first (see Exercise E). Of interest here would be the level of grid drift acquired by the two ground stations, the accuracy of their estimated positions, and the amount of grid rotation.

Exercise E

This is a modification to (D) in that the exercise is preceded by an Exercise (A). This allows the flying baseline segment of the new run to begin with good qualities in the aircraft rather than zero quality. It is likened to the situation where aircraft leave their base having acquired the grid and "carry" the grid to a new community (ops area).

Thus, Exercise (E) is an intricate run wherein the ground stations start as NC's to allow the aircraft to acquire the grid (each aircraft performs as in Exercise(B)) and then switch to users after reinitialization so that they may attempt to pick up the grid from the aircraft. Of interest here is how effectively the aircraft maintain their qualities after the switch, the interaction of ground geo and air rel updates, grid rotation, and positioning accuracy.

Exercise F

This is a modification to Exercises (B). Two aircraft are active users as in a simultaneous run (B). After acquiring good position qualities, one aircraft departs the area on a constant heading and continues until transmission ceases. After reinitialization the aircraft returns and reacquires the grid. The exercise is, thus, a demonstration of performance phenomena when leaving and when entering the community.

Exercise G

This is a three aircraft flying grid run. One aircraft is acting as NC and NTR and the other two are primary users. The two ground stations are primary users too. All terminals are active and start with zero relative position quality, but at surveyed sites.

Here the aircraft must establish the grid with the ground stations as in a battle group. Relative position accuracy will be of interest as will the logic governing the interchange of multiple range

updates among participants, grid rotation, and the accretion of rel and geo qualities.

Exercise H

This is the same as (G) except that one aircraft is NC and a separate aircraft is NTR. Performance here will be compared to (G).

Most of the above exercise were conducted, but time, weather, aircraft, and system availabilities did not permit the completion of the total program.

VII. SUMMARY OF TEST RESULTS

By count, the predominant Class II terminal configuration tested was an actively synchronized user. Most of these cases included a single mobile member, the C131, P3A, or RH53, flying in the vicinity of two other JIIDS ground stations - one at Pt. Lookout and the other at Crisfield, some 25 miles away, across the Chesapeake Bay. The airborne unit under test was typically time synchronizing (via RTT) to the net time reference (time base controller) defined usually at Pt. Lookout which was also located at the grid origin. Both Pt. Lookout and Crisfield were also usually navigation controllers and geodetic position references.

The multi-aircraft test scenarios were designed to ascertain relative navigation performance between multiple independently navigating members. This environment is the most complicated to analyze due to the asynchronism of rel nav data among members. It is also the most important of test scenarios due to their resemblance to actual operational conditions; especially when out in an open-ocean with an absence of stationary ground stations to "anchor" the grid.

Basically, the rel nav function has as its goal the development of a tactical reference frame that is stable rotationally, translationally, and one in which relative position, relative velocity, and relative heading errors can be reduced to zero. The demonstrated system performance, which is classified, was considered to be both satisfactory and effective.

VIII. GLOSSARY OF TERMS

ACTIVE (Mode) - Mode in which the determination of own platform grid position using TOA measurements is enhanced by the added feature of RTT.

GEODETIC POSITION REFERENCE - Option, for those members of the community with high quality knowledge of own geodetic position, to identify this fact to the community of users by setting its transmitted geodetic quality (Q_p) to the highest value allotted.

KALMAN UPDATE - TOA (range) measurements are compared to the slant range computed between transmitting and receiving platforms based on their JTIDS-indicated positions. The relative navigation algorithm is based on the classic Kalman filtering technique which computes weighting factors which, when multiplied by the slant range difference, provides an update to indicated position and a calibration of internal error sources.

NAVIGATION CONTROLLER (NC) - Each relative navigation community selects one of its members as the relative grid origin (RGO) and identifies this fact to the community by setting its transmitted relative position quality (Q_{pR}) to the highest value allotted.

NAVIGATION RESET - Operator option (or built-in software reasonableness test option) to set the Kalman filter covariances to their initial (highest) level which results in relatively heavy weighting factors applied to the slant range difference.

NET TIME REFERENCE (NTR) - Each relative navigation community selects one of its members as the master time reference and identifies this fact to the community by setting its transmitted time quality (Q_t) to the highest value allotted.

QUALITY - Each member of the community transmits a measure of its JTIDS rel nav relative position, geodetic position, time, and azimuth qualities to be used by the recipient platform's Kalman filter in weighting the slant range differences.

PASSIVE (Mode) - Mode in which RTT is not available so that clock error calibration relies solely on multiple slant range difference measurements as processed by the Kalman filter.

PRIMARY USER - A member of the community who is not a navigation controller and is operating in the active mode.

ROUND TRIP TIMING (RTT) - Option of transmitting and then receiving back one's own signal as a means of precisely determining clock errors and thereby refining TOA (slant range) measurements.

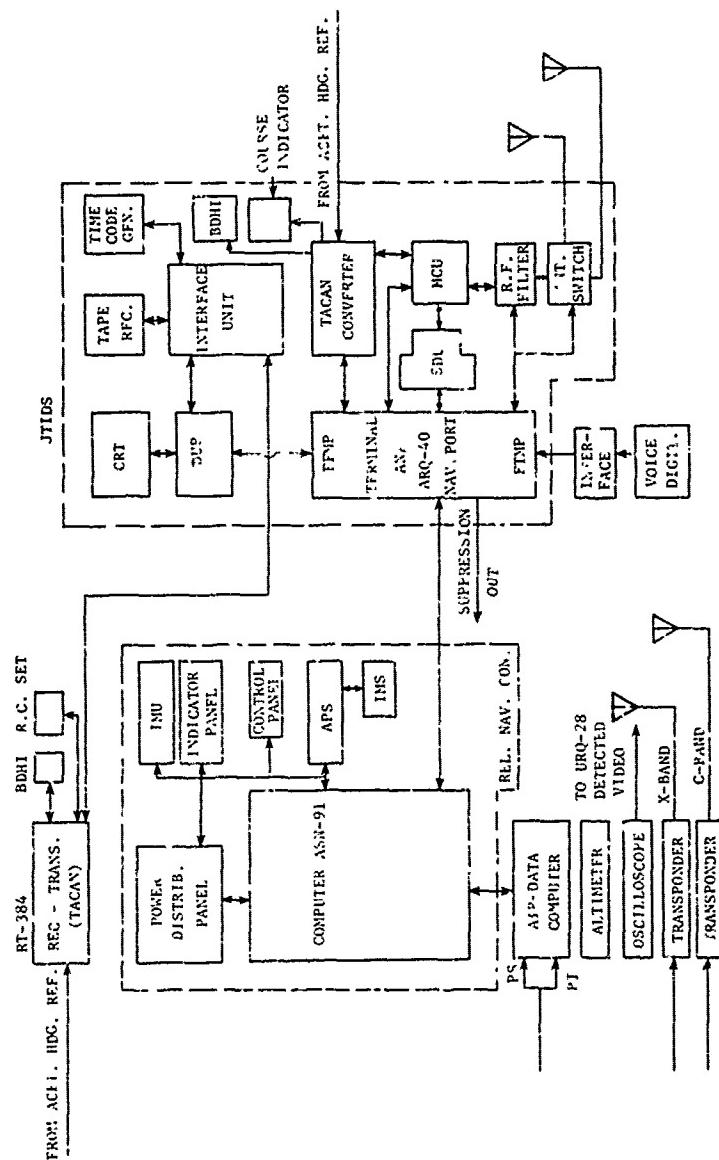


FIGURE 1. JTIDS INSTALLATION CONFIGURATION

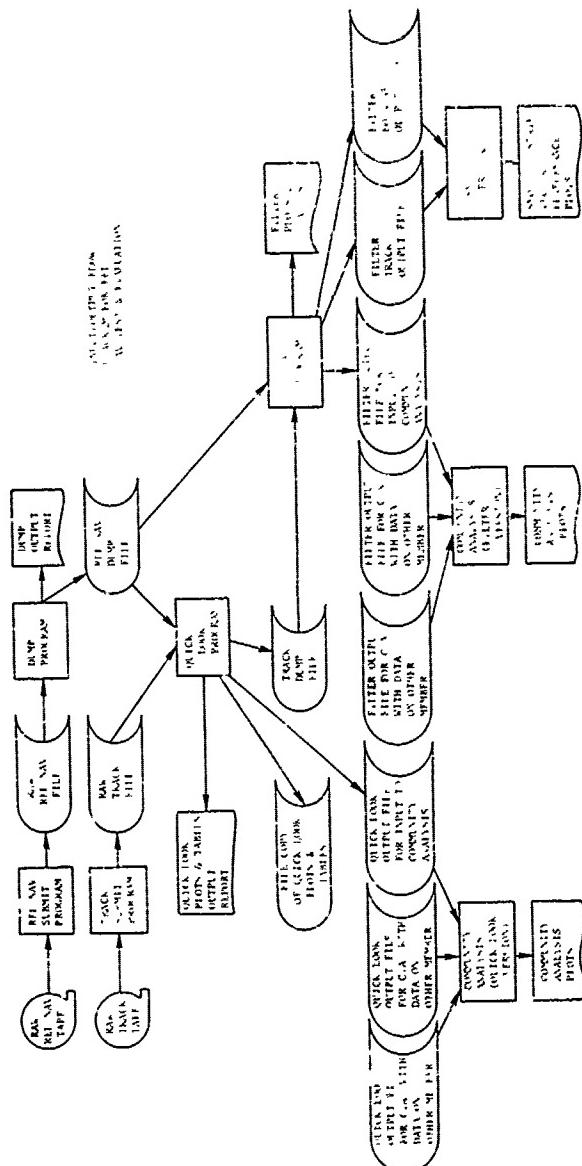


FIGURE 2. DATA REDUCTION PROCESSING FLOW

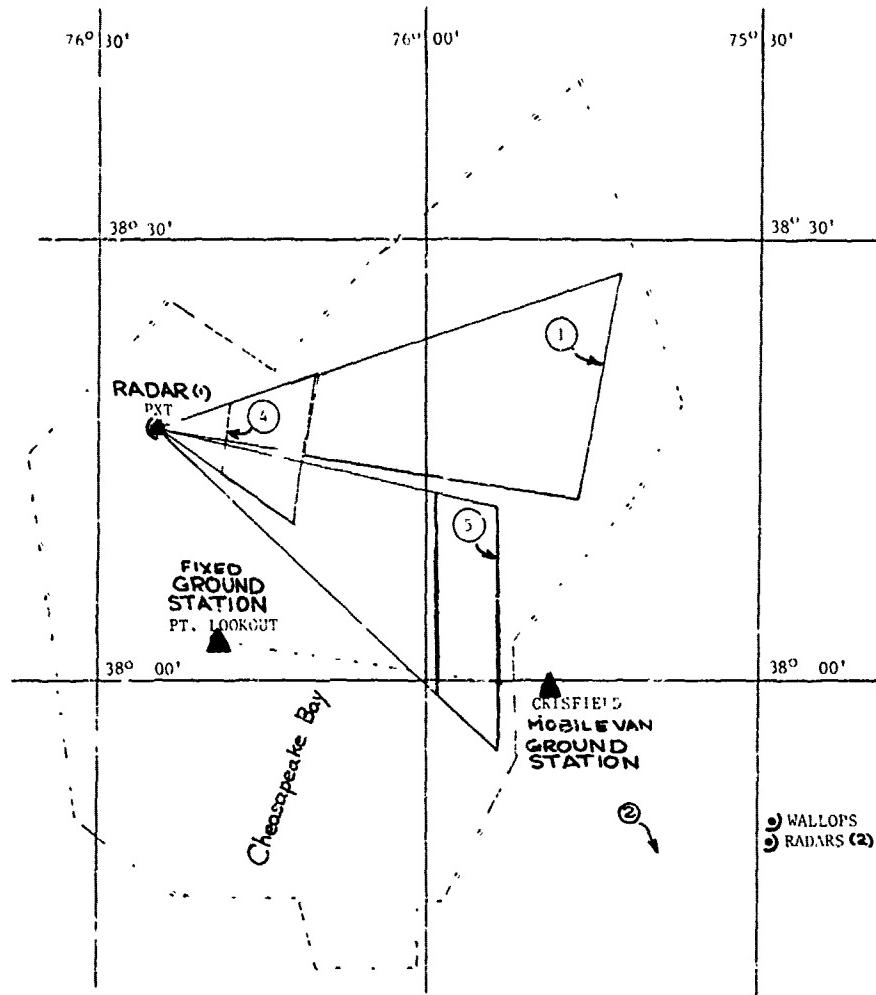


FIGURE 3.
RADAR TRACKING RANGE TRAJECTORIES

INTEGRATED NAVIGATION SYSTEMS BASED ON MULTIPLE DME

by

Ulrich Brokof
Karlheinz HurrassDeutsche Forschungs- und Versuchsanstalt
für Luft- und Raumfahrt e. V.
Institut für Flugführung
3300 Braunschweig, Germany

SUMMARY

In order to be able to cope with the growing air traffic at present and also in future, it is necessary to increase the navigation accuracy of aircraft. One possible solution might be the use of several DME ground stations simultaneously, or subsequently.

This paper describes two integrated navigation systems. Both systems consist of a self-contained dead-reckoning system which is constantly aided by distance measurements, down to different DME ground stations. The first dead-reckoning system is based on the true air speed as well as the heading of the aircraft. The second one is an inertial navigation system.

The integration of the dead-reckoning systems and the DME-system is carried out by means of a Kalman filter. The DME interrogator is constantly switched over to frequencies of five different ground stations.

Both integrated systems were tested during test flights made by the jet aircraft HFB 320. A tracking radar was used for determining reference trajectories in order to check the self-diagnosis of the Kalman filter.

A comparison between the two systems shows that extremely high navigation accuracies can be obtained, too, by the dead-reckoning system which is less expensive.

1. INTRODUCTION

The standard short range navigation system used in air traffic today is VOR/DME. It is very likely that this system will be still in use for some decades. At present almost all aircraft are equipped with VOR receivers and DME interrogators.

The navigation accuracy is limited essentially by the azimuth error of the VOR. The standard deviation of this error is nearly 2 degrees. A larger distance between an aircraft and a ground station will lead to a considerable position error.

Owing to a constant increase of air traffic the number of airways is rising, too. In order to prevent the collision risk becoming greater, it will be necessary to increase the navigation accuracy. It was already shown that a relatively simple integrated system may improve the navigation accuracy of the VOR/DME system [8]. This was a dead-reckoning system based on true air speed (TAS) and heading which was aided by DME measurements.

The multiple DME measurements were now also used to aid an inertial navigation system (INS) which is more sophisticated than the TAS navigation system. Both systems are tested by flight tests. The test results were checked by using a tracking radar. The reference positions of the tracked flight path were compared with the flight path positions of the two navigation systems.

2. DESCRIPTION OF THE MULTIPLE DME AIDED TAS AND INS NAVIGATION SYSTEM

The flight path of the simple TAS/heading and the more sophisticated INS system is generated by dead-reckoning. Due to their specific system errors their flight paths will deviate from the true flight path. Therefore, both systems are aided by DME measurements to different ground stations. The DME data are measured by one DME interrogator which is constantly switched over to frequencies of different ground stations (multiple DME). The integration of the two navigation systems with the DME measurements is done by means of a Kalman filter.

The Kalman filter enables the estimation of DME biases which refer to the individual stations and to the DME interrogator. The filter is designed for five different stations which will be exchanged along the flight path by other stations.

Because of the combinations of TAS, heading and ground data (DME) it is also possible to estimate the wind velocity components in the case of the simple TAS navigation system.

3. ERROR MODELS

The position errors of the simple dead-reckoning system using TAS and heading are caused by

1. uncertain determination of TAS,
2. uncertain heading and side slip angle, and
3. unknown wind conditions.

Taking into account these error sources and additionally the biases of the DME ground stations, the following system equations are obtained:

$$\begin{bmatrix} \dot{f}_x \\ \dot{f}_y \\ \dot{k} \\ \Delta\dot{\theta} \\ \dot{w}_x \\ \dot{w}_y \\ \Delta\dot{D} \end{bmatrix} = \begin{bmatrix} 0 & 0 & v_x & v_y & 1 & 0 & 0^T \\ 0 & 0 & v_y & -v_x & 0 & 1 & 0^T \\ 0 & 0 & 0 & 0 & 0 & 0 & 0^T \\ 0 & 0 & 0 & 0 & 0 & 0 & 0^T \\ 0 & 0 & 0 & 0 & 0 & 0 & 0^T \\ 0 & 0 & 0 & 0 & 0 & 0 & 0^T \\ 0 & 0 & 0 & 0 & 0 & 0 & 0^T \end{bmatrix} \cdot \begin{bmatrix} f_x \\ f_y \\ k \\ \Delta\theta \\ w_x \\ w_y \\ \Delta D \end{bmatrix} + \begin{bmatrix} v_{rx} \\ v_{ry} \\ 0 \\ \theta_r \\ w_{rx} \\ w_{ry} \\ 0 \end{bmatrix}.$$

The state elements f_x and f_y are the position errors in eastern and northern direction. For simplicity the model is shown here in an x, y-coordinate system. The computer program is actually worked out for geographic coordinates.

k represents the scale factor error of true air speed, $\Delta\theta$ the heading error and w_x and w_y the wind velocity components in eastern and northern direction. ΔD is a subvector comprising the systematic errors (biases) of five DME ground stations.

The system matrix contains the velocity components v_x and v_y calculated from true air speed and heading.

Random errors, such as turbulence, for example, which are influencing v_x and v_y are represented by v_{rx} and v_{ry} . The heading error has been modelled as random walk. The power density of θ_r has been chosen in such a way that a heading drift of ($\sigma =$) 2.75 °/h may occur. It has been assumed that the wind velocity will change as random walk, too. The power densities which were adopted for w_{rx} and w_{ry} cause the wind velocity to change by 4 m/s during about 10 minutes.

These noise inputs have already been chosen for many test flights across North Germany. They have turned out to be realistic values.

When using the inertial navigation system as onboard sensor the state vector contains the following elements:

- $\Delta\lambda, \Delta\phi$: the position errors in eastern or northern direction respectively,
- $\Delta v_x, \Delta v_y$: the velocity errors in eastern and northern direction,
- α, β, γ : the platform misalignment angles,
- ΔD : the subvector which comprises the systematic errors of the five DME ground stations.

The inertial navigation system was of the type LN3. A block diagram of the error model is given in Figure 1. This error model contains the SCHULER loops, earth rate-, velocity- and acceleration couplings. The gyro drifts are modelled as random walk process.

Both navigation systems are aided by DME measurements. The measurement data which are needed for the Kalman filter are differences between the original DME observations and the computed distances between the dead-reckoning position of the aircraft to the corresponding DME ground station.

The covariance matrix of the measurement noise is one-dimensional:

$$R = |\sigma_D|^2.$$

DFVLR had obtained a large number of DME data from preceding test flights. The comparison of these data with simultaneously measured and converted precise tracking radar data allowed to determine σ_D . In Figure 2 typical DME errors are plotted. In this case the mean value is 0.02 nmi, the standard deviation is 0.06 nmi (≈ 100 m). In agreement with this example, the biases of the other tests were always smaller than the σ -values of the

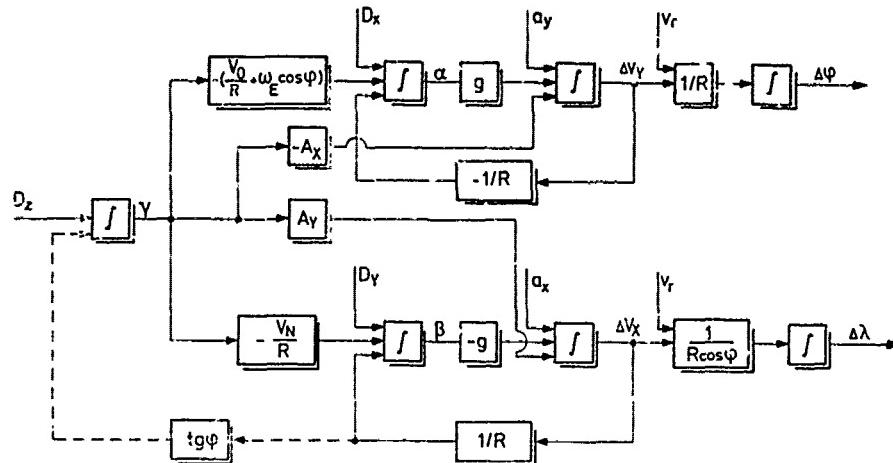


Figure 1: Block Diagram of the Error Model for the Inertial Navigation System.

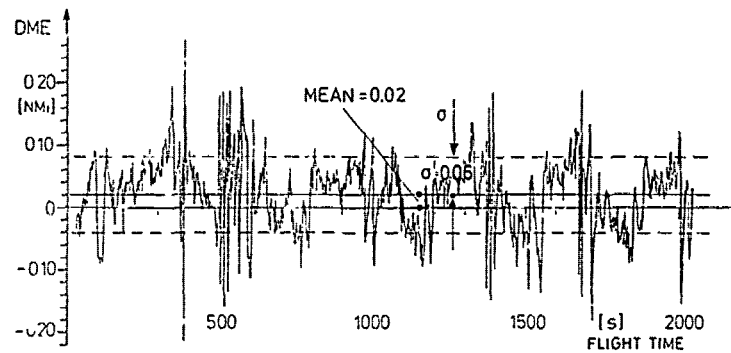


Figure 2: Plot of DME Errors.

random errors. Tests made by other organisations proved that the standard deviation of the systematic errors of different DME ground stations is approximately 150 m [5].

The numerical values which have been used in the error models are summarized in Table 1.

ONBOARD SENSOR	SYSTEM NOISE	POWER DENSITIES
Dead-reckoning with TAS, heading and wind	<ul style="list-style-type: none"> random velocity errors random heading errors (random walk input) random change of wind velocity components (random walk input) 	$1 \text{ [m}^2\text{s}^{-1}\text{]}$ $6.35 \cdot 10^{-7} \text{ [s}^{-1}\text{]}$ $3.2 \cdot 10^{-2} \text{ [m}^2\text{s}^{-3}\text{]}$
Inertial Navigation	<ul style="list-style-type: none"> random gyro drift (random walk input) accelerometer noise velocity noise 	$0.846 \cdot 10^{-11} \text{ [s}^{-1}\text{]}$ $0.2 \cdot 10^{-4} \text{ [m}^2\text{s}^{-3}\text{]}$ $0.05 \text{ [m}^2\text{s}^{-1}\text{]}$

Table 1: Numerical Values for the System Noise.

4. OPERATION OF THE KALMAN FILTER

Before starting the estimation process of the Kalman filter initial values have to be set for state elements, as well as for their covariances. These values for the covariances are listed in Table 2.

NAVIGATION SYSTEM AND MEASUREMENT SOURCES	STATE ELEMENT	STANDARD DEVIATION (1σ)
Dead-reckoning with TAS, heading and wind	position f_x, f_y scale factor $k' = 1 - k$ heading $\Delta\theta$ wind velocity w_x, w_y	5000 [m] 0.03 3 [deg] 40 [$m s^{-1}$]
Inertial Navigation	position f_x, f_y alignment angles α, β alignment angle γ for azimuth	5 m 0.01 [deg] 0.1 [deg]
DME ground station	distance bias D	150 [m]

Table 2: Initial Values when Starting the Kalman Filter Estimation Process.

The initial values of the state elements are zero. Only the initial values of the DME biases were set to 200 m which refers to the onboard equipment.

During the alignment procedure of the INS-system the test aircraft was positioned on a well surveyed point. Therefore, the initial position error for the INS system was set to 5 m.

The linear relation between the measurements and the state elements of the Kalman filter is represented by the measurement matrix M . For the simple dead-reckoning system (TAS, heading) this matrix is

$$M_{TAS} = \begin{vmatrix} \frac{\delta D}{\delta x}, \frac{\delta D}{\delta y}, 0, 0, 0, 0 \\ 1, 0, 0, 0, 0 \\ 1, 2, 3, 4, 5 \\ \text{position} \end{vmatrix}.$$

The first two elements of the measurement matrix are the derivatives of the DME distance D between the aircraft and the ground station which was just used in eastern (x) and northern (y) direction. The figure '1' on the right side of M takes into account the systematic error of the ground station. This coefficient is an approximation of

$$1/\cos\gamma \approx D/\sqrt{D^2 - \Delta H^2}.$$

It is only valid for small elevation angles γ from the station to the aircraft.

The position of the coefficient '1' in the measurement matrix changes according to the ground station, i. e. first position for first ground station, etc.. The filter is designed for a maximum number of five ground stations.

Whenever an aircraft leaves the covering range of the ground station, a new one has to be selected. The elements of the state vector and the covariance matrix corresponding to the new station have to be initialized again. In the covariance matrix the non-diagonal elements of the additional station have to be changed to zero.

The measurement matrix M_{INS} for the INS Multi DME system is only slightly different from the simple navigation system. It contains one zero element more according to the state vector:

$$M_{INS} = \begin{vmatrix} \frac{\delta D}{\delta x}, \frac{\delta D}{\delta y}, 0, 0, 0, 0, 0 \\ 1, 0, 0, 0, 0 \\ 1, 2, 3, 4, 5 \\ \text{position} \end{vmatrix}.$$

The cycle time of the Kalman filter is 2 seconds. The DME station in use is changed every 2 seconds, too.

In the case of the simple dead-reckoning system the mechanization of the Kalman filter is of the closed loop type: the results are immediately used by the dead-reckoning system. The advantage of this mechanization is that no great position errors will occur due to a strong wind, for example. It is also important with respect to the linearization of the measurement equation, especially with respect to the first two elements of the measurement matrix.

For the INS system an open loop filter is used. The updated position of the aircraft is determined by adding the estimated position errors to the position determined by the INS system. For calculating the first two elements of the measurement matrix as well as for calculating the measurement values for the Kalman filter the updated INS positions are used.

During time intervals when no DME observations are available all elements of the measurement matrix are set to zero. In this case the navigation procedure continues by using all elements in the state vector which were estimated by the Kalman filter.

When the position of the aircraft is near the ground station, position errors of the aircraft have great influence on the first two elements of the measurement matrix because of nonlinearity. If therefore the elevation angle between the ground station and the aircraft is greater than 18° ($1 : 3$) the measurements to that station are omitted.

5. DESCRIPTION OF THE TEST AIRCRAFT

In order to test the navigation systems some test flights were made by the HFB 320 (Hansa Jet) test aircraft of DFVLR in Braunschweig. During these tests the flight path of the aircraft has been tracked by a tracking radar. The comparison of the radar position with the positions of the navigation systems allows to check the accuracy which may be achieved.

A digital computer (Honeywell) as well as a magnetic tape recorder were part of the test equipment of the HFB 320. The computer was mainly used for collecting the flight data and for storing them on magnetic tape. The most important data were the following:

- time,
- true air speed (TAS),
- heading,
- INS velocity components,
- VOR/DME frequency,
- DME reading.

All data were stored 10 times per second (data rate 5 s^{-1}). The computer was also used for automatically selecting the VOR/DME frequencies. Either a Collins 860 E-3 or King KDM 7000 was used as DME onboard equipment.

The calculations for dead-reckoning and the Kalman filter calculations were made off-line because the necessary programs had been written for the central computer SIEMENS 7.755 of DFVLR. The relation between CPU-time of the computer and flight time was less than $1 : 28$. This relation was obtained for the simple dead-reckoning system including all computations which are not necessary in the case of on-line computation. On-line computation is planned for future tests. The programs will then be extended in order to test area navigation procedures.

6. FLIGHT TEST RESULTS

The flight path of a typical test flight is presented in Figure 3. This flight covers a distance of about 700 km. The flight time was nearly 106 minutes. A total number of 10 different ground stations was used during the flight.

The DME measurements to the different ground stations which were obtained during the flight are summarized in Figure 4. It shows the DME distances as a function of flight time. During take-off only two or three stations could be received. The measurements of 5 different stations which are provided in the Kalman filter are available after 10 minutes. The exchange of one station by another new one is indicated by arrows. During the landing phase the altitude is decreased. Therefore, only less than 5 stations can be received again.

The navigation accuracy which was achieved during the first part of the flight (1000 s) is shown in Figure 5 and Figure 6. In Figure 5 the covariances (2σ -values) and the position errors of the north-south components are plotted, while Figure 6 shows the equivalent values for the east-west components. The continuous lines are estimated 2σ -

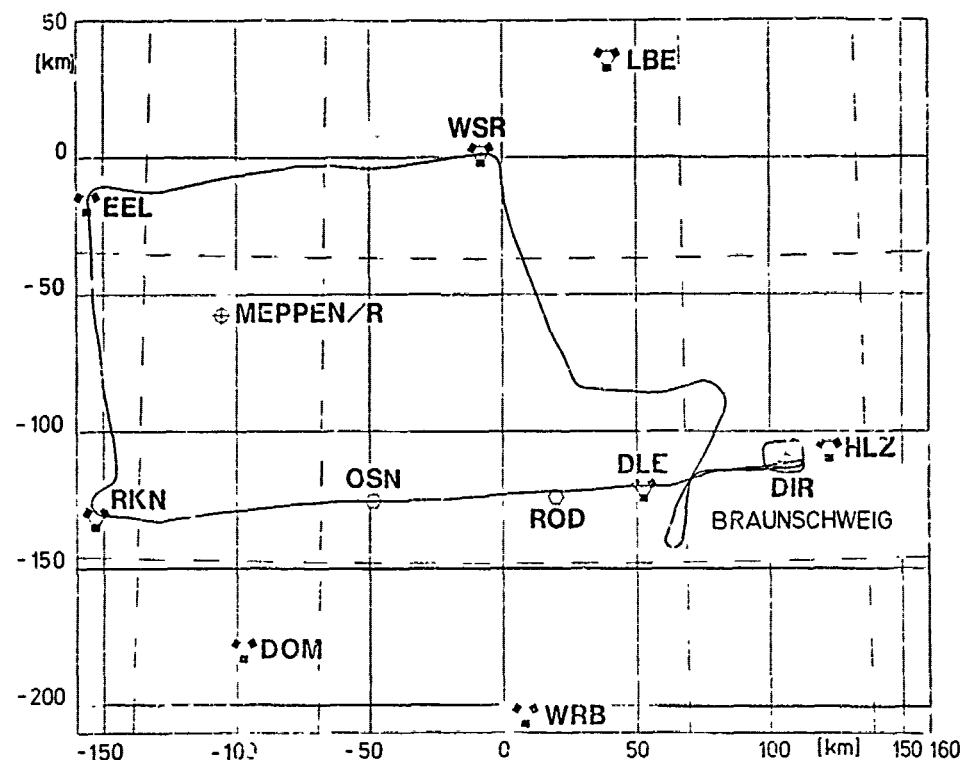


Figure 3: Total Flight Path of the Multi DME Test Flight.

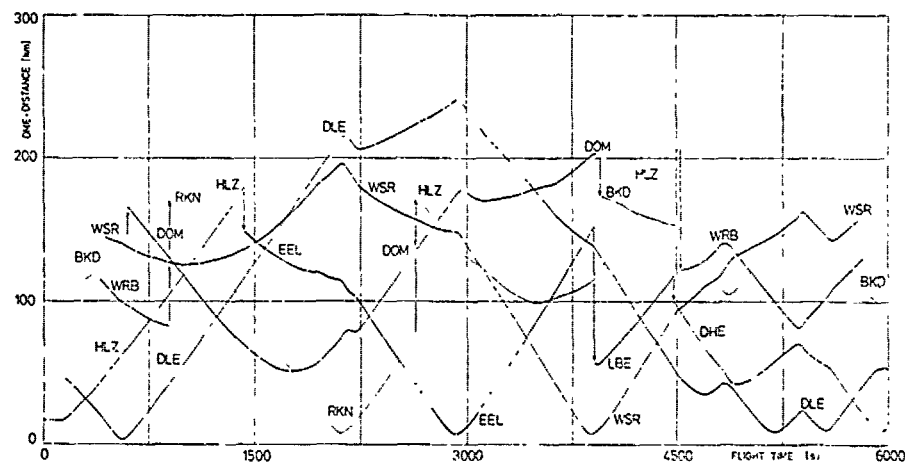


Figure 4: DME Measurements Achieved during the Test Flight.

values. They have been calculated from the covariance matrix of the Kalman filter algorithm. The asterisks and dots represent the differences between the tracking radar positions and the positions which were determined by the integrated navigation systems.

Five minutes after take-off, when reaching an altitude of 4500 ft, the DME distances to 5 different DME stations could be measured. After this time the east and north components of the 2σ -standard deviation had decreased from 5000 m to 200 m concerning the simple dead-reckoning system.

The estimation process for the INS system accuracy is different. Starting from position errors of 5 m the standard deviations increase during the climbing phase to 200 m and then decrease to 100 m (2σ). Figures 5 and 6 show the rapid improvement of the navigation accuracy every time when the signals of a new DME can be received especially during the climbing phase.

The deviations of the flight path positions of both navigation systems from the real flight path were identified by tracking radar measurements (DIR/RCA). The data sequence of the radar corresponds to one observation in 10 seconds. The deviations from both navi-

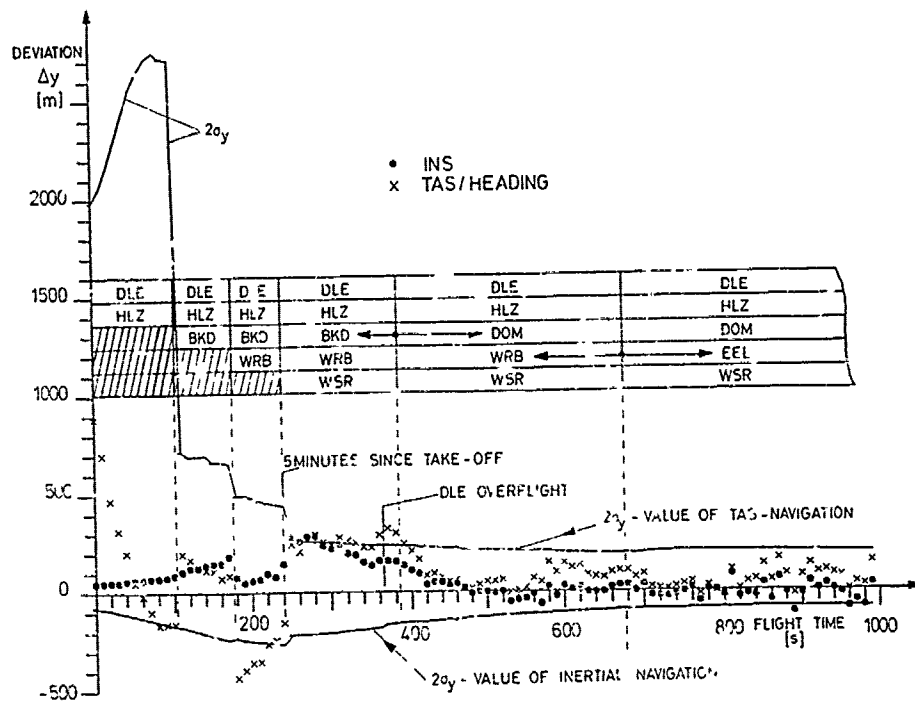


Figure 5: Navigation Accuracy of Both Multi DME Navigation Systems during the Initial Part (1000 s) of the Test Flight (North-South Component).

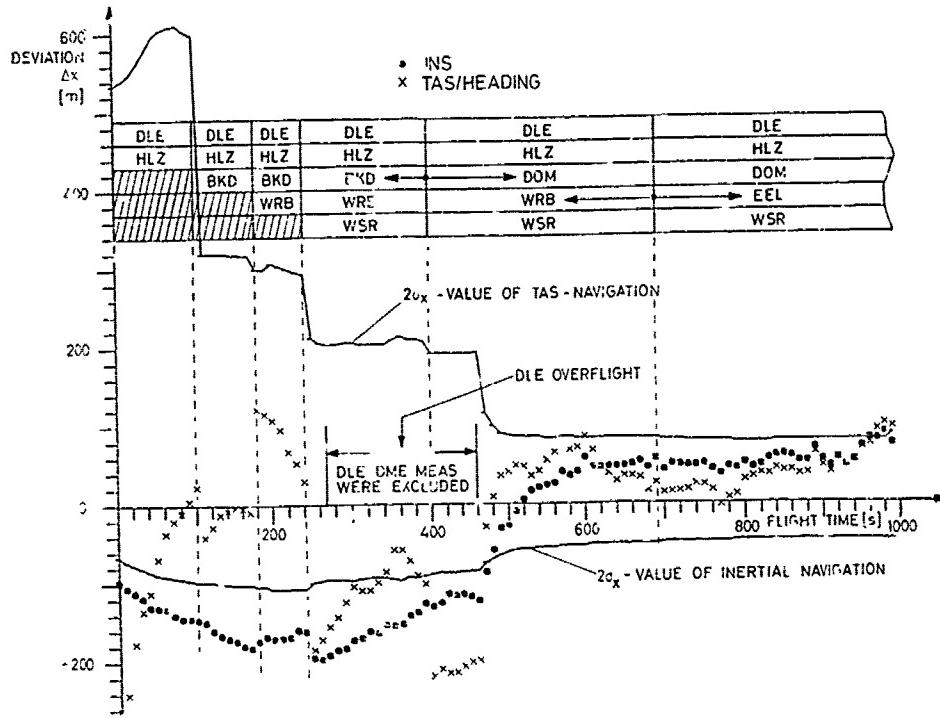


Figure 6: Navigation Accuracy of Both Multi DME Navigation Systems during the Initial Part (1000 s) of the Test Flight (East-West Component).

gation systems are normally well within the 2σ -boundaries, except for the inertial navigation system. Here, during the climbing phase of the aircraft, the deviations exceed the 2σ -boundaries. This effect is very probably due to an error in the INS equipment, which was detected in a short time interval during take-off of the aircraft.

In Figure 7 the flight path is plotted in a small region near the Braunschweig airfield. The dots are the positions which were determined from the DME aided simple dead-reckoning navigation system. The asterisks are the plotted positions of the tracking radar.

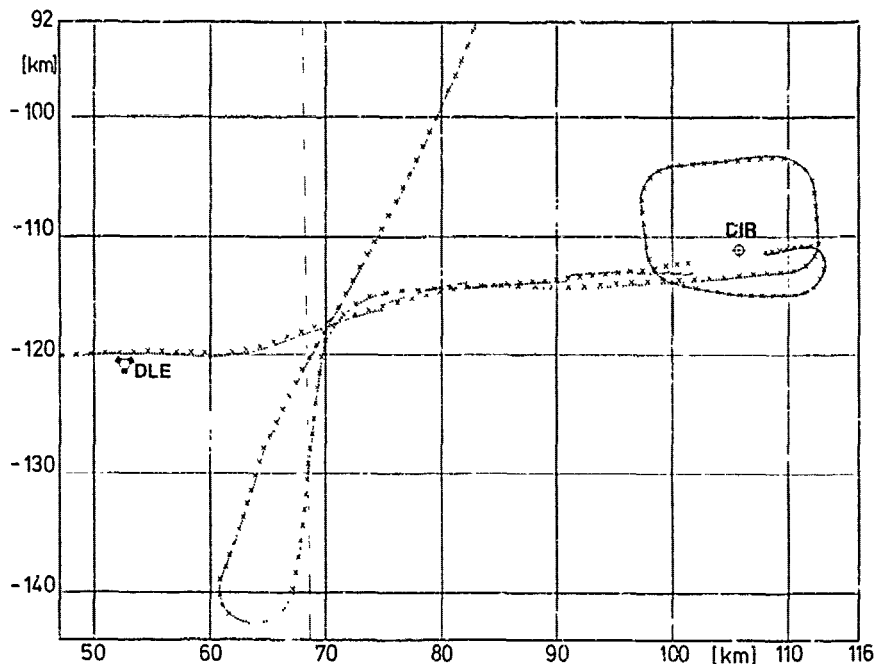


Figure 7: Flight Path of the Simple Dead-Reckoning Navigation System (TAS/Heading) Compared with Tracking Radar During Take-Off and Approach.

The comparison of both flight trajectories gives an impression of the increasing navigation accuracy shortly after take-off and the navigation accuracy during the approach to Braunschweig airport.

Although the altitude of the aircraft during approach and therefore the number of receivable DME stations has decreased to less than 5, the accuracy of the simple navigation system is only slowly decreasing. This effect is due to the well determined wind velocity components and the other state elements of the filter.

The estimation of the individual bias errors of the different DME stations is very important. It is necessary that the DME onboard equipment is carefully calibrated, otherwise the estimated systematic errors of the different DME stations will include a common distance bias which is due to the onboard equipment. Figure 8 shows the estimation process

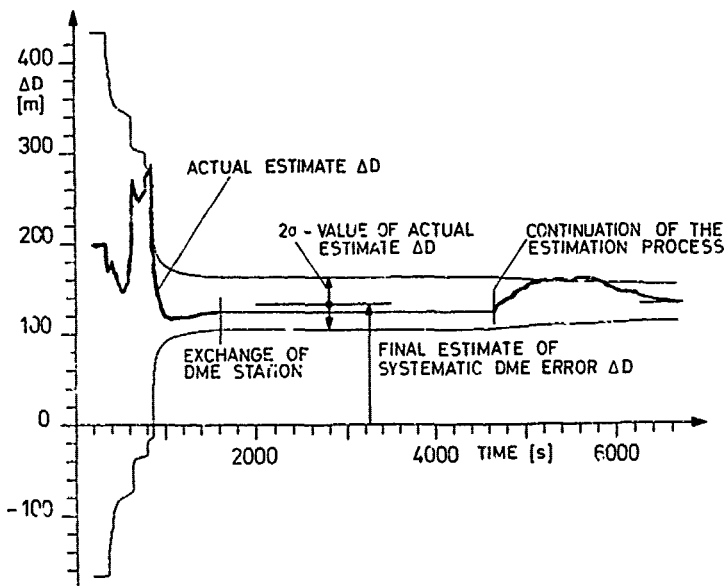


Figure 8: Estimation Process for the Systematic Distance Error of DME Station Hehlingen (HLZ).

for the systematic error of the DME station Hehlingen. The estimation is starting with a DME bias of 200 m. This value is caused by the onboard equipment. From experience the bias of an individual DME station may deviate by 300 m (2σ -value) from the initial value. During the flight now the systematic DME error will be determined more and more precisely. After 1600 s of flight time the station of Hehlingen is exchanged by another station. The estimates of ΔD and σ are stored because of a possible later use of the station. This takes place after 4600 s when the aircraft returns to the Braunschweig region.

The estimation procedure for the systematic error corresponds to a weighting process of the systematic errors of different stations to get a unique and optimized solution for the aircraft position. It is not the result of a calibration procedure by means of a precise reference.

The estimated biases of the DME ground stations are listed in Table 3. The biases of

No	DME STATION	DME STATION BIAS			
		TAS - NAVIGATION ΔD	$\sigma_{\Delta D}$	INS - NAVIGATION ΔD	$\sigma_{\Delta D}$
1	BRUENKENDORF (BKD)	- 123	14	- 76	12
2	DORTMUND (DOM)	68	10	75	9
3	ELBE (LBE)	11	38	120	24
4	HEHLINGEN (HLZ)	- 66	10	- 44	9
5	HELGOLAND (DHE)	58	12	50	11
6	LEINE (DLE)	55	6	41	6
7	WARBURG (WAR)	76	14	42	13
8	WESER (WSR)	14	8	16	7
9	EELDE (EEL)	- 170	10	- 178	10
10	REKKEN (RKN)	28	14	13	13

Table 3: Systematic Errors of DME Stations Reduced by the Systematic Component of 200 m Caused by the Onboard Equipment.

the stations Eelde and Rekken are influenced by a datum difference between the geodetic systems of Germany and Netherland which is approximately 50 m. The biases determined with the TAS navigation system are more reliable because of INS system errors during some parts of the test flight.

In previous tests DME measurements were simulated in such a way that the distances from a known flight path to different DME stations were computed. Then a random normally distributed error as well as an individual systematic error were added. The same filter, which was now used to determine the station biases from real measurements, estimated the biases very closely to the simulated input values by using the simulated measurements. This gives an indication that the systematic errors which were obtained here, are close to reality.

7. ADVANTAGES AND DISADVANTAGES OF BOTH INTEGRATED NAVIGATION SYSTEMS

The integration of the simple navigation system based on TAS and Heading as well as the more sophisticated INS navigation system with multiple DME measurements in a way which was shown in this paper has turned out some important advantages:

- The estimated and achieved position accuracy is better than 100 m (1σ) concerning the simple TAS system and better than 50 m (1σ) concerning the INS.
This is a great improvement in comparison with the VOR/DME or with TACAN, which are used for short range navigation today.
- The navigation is not interrupted if no DME signals are available.
- In case of the TAS navigation system the wind is continuously estimated and thus available onboard the aircraft. For the INS system the wind may be calculated by using TAS and velocity data from the INS.
- Both systems are suitable for precise area navigation.

Disadvantages for the integration procedure are

- the necessity of an additional computer and the required interface, and

- the necessity of coordinate inputs of the geographic positions for the DME ground stations into the computer. This means more work load for the pilot, if there is no device for automatic entering of these data.

With regard to the necessary digital computer the following has to be stated: during the last few years, the computer development has made great progress, i. e. the computers have become smaller, less expensive and more efficient. It is very probable that all aircraft will be equipped with a computer within the next few years. Then it will be possible to make the calculations for the Kalman filter. This is also true for small general aircraft which then may use the simple TAG navigation system. With such a system they will be able to navigate nearly as precise as greater aircraft with their more expensive systems.

8. REFERENCES

- [1] KAYTON, M. and FRIED, W.R., "Avionics Navigation Systems", New York, 1969.
- [2] GELB, A. (Ed.), "Applied Optimal Estimation", MIT Press, Cambridge, 1974.
- [3] HURRASS, K. and WINTER, H., "A High Precision Reference System for Aircraft Position and Velocity Measurements", DGON-Vierteljahresmitteilungen II/I'1, 1976.
- [4] HURRASS, K., "Some Investigations on DME Overall Accuracy and Navigation Accuracy", Internal DFVLR-Report, IB 153-79/03.
- [5] LATHAM, R., "Aircraft Positioning with Multiple DME", NAVIGATION: Journal of the Institute of Navigation, Vol. 21, No. 4, 1974.
- [6] CARLSON, N.A., "Fast Triangulation Formulation of the Square Root Filter", AIAA Journal, Vol. 11, No. 9, Sept. 1973.
- [7] WINTER, H., "Experiences in Flight Testing Hybrid Navigation Systems", ASARD Lecture Series No. 82, May 1976.
- [8] BROKOF, U. and HURRASS, K., "A Simple Integrated Navigation System Based on Multiple DME", NAECON Proceedings, Dayton, Ohio, May 1979, pp. 591 to 599.

DYNAMIC PERFORMANCE ANALYSIS OF
NAVSTAR/GPS NAVIGATION FILTERS

by

Michael John Dymant

Canadian Marconi Company, 2442 Trenton Ave., Montreal Canada

Dr. David Feseng Liang

Defence Research Establishment Ottawa, Ottawa, Canada

SUMMARY

A versatile Kalman filter has been developed for stand-alone navigation in Canadian Marconi Company (CMC) NAVSTAR/GPS receivers. The filter is designed for implementation in Class B (4-channel) and Class D (2-channel) receivers, and optimally incorporates height information from the aircraft baro-altimeter. The gain and covariance update rates can be reduced without performance degradation when certain conditions are satisfied. A U-D factorization similar to that of Bierman's design is used in a single precision Fortran form. Matrix sparseness and block triangularity are taken advantage of when possible. Computation burden has been assessed on CMC receiver microprocessors and compared with more conventional algorithms.

1.0 INTRODUCTION

This paper addresses real-time performance capabilities of a Navstar Global Positioning System Receiver equipped with a Kalman navigation filter. The results presented are derived from detailed simulation. RSS position and velocity error performance is examined in light of required processing power.

The Kalman Filter is implementable in Canadian Marconi Company Class B (4-channel) and Class D (2-channel) receivers, and can process baro-altimeter data into the solution if the vehicle is properly equipped. The filter provides a navigation solution for stand-alone or reversionary navigation and is superior in performance and CPU loading compared to other position fixing algorithms.

Filter performance is verified by Monte Carlo simulation to determine dynamic sensitivity and the effects of GDOP degradation and satellite outages. The benefits of baro-altimeter aiding are explored.

Under certain conditions, it is found that gain calculation can be slowed or suspended for periods of a few minutes without significant performance degradation. This allows the navigation computer to perform background tasks more efficiently.

2.0 SYSTEM OVERVIEW AND DYNAMIC MODEL SIMULATORS

Dynamic filter analysis was performed using a detailed simulation of nominal and stochastic system models. Canadian Marconi Company and the Canadian Department of National Defense have developed the Navstar Generalized Receiver Simulator, or NGRS.

The NGRS is a library of Fortran programs which enables a detailed analysis of GPS concepts and software. Twenty-four satellites are simulated dynamically, using nominal orbital ephemerides. The receiver simulator is designed to have user-selectable options to increase flexibility. Several hundred error coefficients and statistical values have been identified and are programmed to enhance truth model accuracy. The simulator attempts to make simulated measurements as close to reality as possible, so that eventual flight testing will not result in costly surprises. The receiver can be programmed to be sequential, simultaneous or single frequency. Data rate, jamming and satellite switch-over are all options which are user selectable.

The NGRS is divided into 3 major entities:

- 1) GPS Constellation - 24 satellites modeled in terms of ephemeral data.
- 2) GPS Data Link - The atmosphere through which the signals penetrate.
- 3) GPS Receiver - A dual frequency receiver simulated to be capable of supplying broadcast ephemeris and raw measurements.

Major error sources are presented accounting for random, correlated and bias characteristics. The important information about each of those random variables is contained in Table 2-1. Measurement statistics for the navigation filter are derived from this table.

With stand-alone navigation of the nature addressed here, incomplete (discrete) observations and sub-optimal filter structure render many error sources only weakly observable. Two error sources which directly affect filter performance and can be easily estimated are receiver oscillator drift and baro-altimeter bias.

Crystal oscillator stability is affected by such environmental factors as thermal gradients, vibration, G-force deformation and electrical variations. The Allan variance for crystal oscillators indicates that frequency drift has a characteristic similar to a random walk over short periods of time.

The detailed clock error model is presented in Appendix 1. The baro-altimeter error model is described in Appendix 2.

The measurement sequence for the 4-and 2-channel receivers is detailed in Figure 2-1. The sequential receiver time multiplexes its channels through the four satellite constellation by reacquisition. It has a slower data rate than the 4-channel receiver. During satellite switching, both configurations make use of the baro-altimeter measurement at a higher rate.

Nominal Characteristic	Correlation Parameter	1σ Magnitude	Comments
Satellite Clock Drift Prediction	Random Walk	0.2 m	Per Hour
Ephemeris Prediction	Bias	2.7 m	RSS
Other	Uncorrelated	0.7 m	
Ionospheric Residual	First Markov	200 km	3.0 m
Tropospheric Residual	First Markov	100 km	2.0 m
Other	Uncorrelated	0.5 m	
Multipath	"A," "B," "C"	1.0 m	Reducible
Oscillator Drift	Random Walk	1.8 m	Per Minute
Pseudo Range Accuracy	Uncorrelated	1.5 m	
Pseudo Range Rate Accuracy	Uncorrelated	3.2 m/sec	
Receiver Calibration	Bias	1.0 m	Reducible
Other	Uncorrelated	0.5 m	
Baro-Altimeter Bias	First Markov	100 km	5.0 m Elevation

Table 2-1. Nominal Navstar Error Sources

The flight generator simulates an aircraft flying in a northward direction and undergoing 2, 5 and 10g manoeuvres periodically. As aircraft attitude is not processed with a stand-alone GPS receiver, antenna offset becomes unimportant. A 3-dimensional point mass is therefore described by a spliced third order polynomial. Vehicle jerk is the driving term, constrained by the particular flight characteristics of a given airframe. Simulated flight duration is 500 seconds. The satellite constellation visible for most of this time is shown in Figure 2-2.

3.0 DEVELOPMENT OF KALMAN FILTER

3.1 General Kalman Filter Structure

The Canadian Marconi Company (CMC) Navstar receivers provide discrete pseudo range and range-rate measurements at fixed intervals. As a stand-alone navigation system, the dynamics of the vehicle are not continuously observable. Therefore, the system state equation is described by the following linear stochastic equation

$$\underline{x}_k = \Phi(t_k, t_{k-1}) \underline{x}_{k-1} + \Gamma_k \underline{w}_k \quad (3-1)$$

and the measurements to be filtered are represented by the non-linear equation

$$\underline{y}_k = h(\underline{x}_k) + \underline{v}_k \quad (3-2)$$

where the state \underline{x} is an n-vector, the measurement \underline{y} an m-vector, the state noise sequence \underline{w} an r-vector, the measurement noise \underline{v} an m-vector. Γ and Φ are, respectively n x r and n x n matrices.

\underline{w} and \underline{v} are assumed to be zero-mean Gaussian noise processes with covariances Q and R, respectively.

The best state estimate $\hat{\underline{x}}$ as given by the extended Kalman filter is:

$$\hat{\underline{x}}_k^+ = \hat{\underline{x}}_k^- + K_k (\underline{y}_k - \hat{\underline{y}}_k^-) \quad (3-3)$$

where

$$\hat{\underline{x}}_k^- = \Phi(t_k, t_{k-1}) \hat{\underline{x}}_{k-1}^+ \quad (3-4)$$

$$K_k = P_k H_k (H_k P_k H_k^T + \underline{r}_k)^{-1} \quad (3-5)$$

$$\hat{\underline{y}}_k^- = h(\hat{\underline{x}}_k^-)$$

and

$$H_k = \left. \frac{\partial h(\underline{x}_k)}{\partial \underline{x}_k} \right|_{\underline{x}_k = \hat{\underline{x}}_k^-} \quad (3-7)$$

K_k , H_k and P_k are the filter gain, measurement and covariance matrices respectively, and the error - covariance equations are represented by

$$P_k^- = \Phi(t_k, t_{k-1}) P_{k-1}^+ \Phi^T(t_k, t_{k-1}) + \Gamma_k Q_k \Gamma_k^T \quad (3-8)$$

$$\text{and } P_k^+ = (I - K_k H_k) P_k^- \quad (3-9)$$

3.2 Dynamic System Model

One application of Navstar receivers under development at CMC is for high and medium dynamic (2-10g's) aircraft requiring reversionary or self-contained stand-alone navigation.

It has been shown (1) that vehicles capable of sustained accelerations (radial or linear) will have smaller RMS position and velocity errors if these accelerations are estimated. Hence, the first nine states of the Navstar receiver filter are 3 components each of position, velocity and acceleration. The acceleration is treated as a random walk with a power spectral density q_1 obtained from Monte Carlo simulations to minimize filter transients for specific vehicle acceleration characteristics.

System errors which are unobservable over short periods of time include satellite ephemeris and satellite clock drift prediction residuals, ionospheric and tropospheric residuals, and the receiver biases. The ionospheric delay is minimized by performing a dual frequency phase measurement. The tropospheric delay is minimized by an empirically determined model resident in the receiver computer. Receiver biases are reduced by self-calibration circuitry. For a dynamic receiver, the above-mentioned residuals cannot be effectively separated from the pseudo range and pseudo range rate measurements. Estimation of these errors is not deemed practical in a real-time implementation.

The receiver oscillator drift is significant and must be estimated. From sensitivity analyses was found that the crystal oscillator drift characteristic can be effectively modelled by a random-walk frequency offset with power spectral density (PSD) q_{CAT} .

A baro-altimeter input provides enhanced performance with a stand-alone navigation system during times of a satellite switchover or when only 2 or 3 satellites are available. The baro-altimeter model selected is height-adaptive and distance correlated (first order Markov). Results of performance analysis with and without the baro-altimeter are presented in Section 5.0.

The state vector \underline{x} is therefore:

$$\underline{x} = \begin{bmatrix} x \\ y \\ z \\ \cdot \\ x \\ \cdot \\ y \\ \cdot \\ z \\ \cdot \\ x \\ \cdot \\ y \\ \cdot \\ z \\ \cdot \\ c\Delta t \\ \cdot \\ c\Delta t \\ B \end{bmatrix} \quad \begin{array}{l} \text{Position in earth fixed cartesian coord. (m)} \\ \text{Velocity (m/sec)} \\ \text{Acceleration (m/sec}^2\text{)} \\ \text{Oscillator errors (m, m/sec)} \\ \text{Baro-altimeter bias (m)} \end{array} \quad (3-10)$$

The state transition matrix Φ of Eq. (3-1) is given by (I is 3×3)

$$\Phi(t, t_{k-1}) = \left[\begin{array}{ccc|cc} 1 & \Delta t I & 1/2\Delta t^2 I & 0 & 0 \\ 0 & I & \Delta t I & 0 & 0 \\ 0 & 0 & I & 0 & 0 \\ \hline 0 & 0 & 0 & 1/\Delta t & 0 \\ & & & 0 & 1 \\ & & & 0 & 1 e^{-\Delta t/\tau_B} \end{array} \right] \quad (3-11)$$

The discrete form of the power spectral density matrix is:

$$\Gamma_k Q_k \Gamma_k = \left[\begin{array}{ccc|cc} \frac{\Delta t^5}{20} q_1 I & \frac{\Delta t^4}{8} q_1 I & \frac{\Delta t^3}{6} q_1 I & 0 & 0 \\ \frac{\Delta t^4}{8} q_1 I & \frac{\Delta t^3}{3} q_1 I & \frac{\Delta t^2}{2} q_1 I & 0 & 0 \\ \frac{\Delta t^3}{6} q_1 I & \frac{\Delta t^2}{2} q_1 I & q_1 \Delta t I & 0 & 0 \\ \hline 0 & 0 & 0 & \frac{\Delta t^3}{3} q_2 & \frac{\Delta t^2}{2} q_2 \\ & & & 0 & 0 \\ & & & 0 & k \end{array} \right] \quad (3-12)$$

where

$$k = q_B (1 - e^{-2\Delta t/\tau_B}) \quad (3-13)$$

q_1 = vehicle jerk power spectral density (m^2/sec^5)

q_2 = clock drift power spectral density (m^2/sec^3) = q_{CAT}

q_B = barometric noise power spectral density (m/sec)

τ_B = correlation time constant of baro-altimeter

and Δt = discrete measurement interval

3.3 Measurement Models

The Navstar measurements consist of the pseudo ranges and pseudo range-rates from four satellites. In principal, a solution for position in three dimensions only requires three pseudo range measurements. However, it is difficult to obtain receiver oscillator synchronization due to the presence of time delay between the receiver and satellites. For this purpose, four range measurements are incorporated to determine the time delay between the user and the synchronized satellites. The receiver pseudo-range measurement from the i th satellite is described by the equation:

$$R_i = ((x_i - x)^2 + (y_i - y)^2 + (z_i - z)^2)^{1/2} + c\Delta t + v_{Ri} \quad (3-14)$$

where (x, y, z) are components of the user position, (x_i, y_i, z_i) are the components of the i th satellite position, and v_{Ri} represents a zero-mean Gaussian noise process of the i th pseudo range measurement. The term $c\Delta t$ represents receiver oscillator synchronization error.

The pseudo range-rate measurement to the i th satellite has the form

$$\dot{R}_i = \frac{(x_i - x) \dot{(x_i - x)} + (y_i - y) \dot{(y_i - y)} + (z_i - z) \dot{(z_i - z)} + c\dot{\Delta t} + v_{RRi}}{((x_i - x)^2 + (y_i - y)^2 + (z_i - z)^2)^{1/2}} \quad (3-15)$$

where v_{RRi} is a zero-mean Gaussian noise process of the i th pseudo range-rate measurement.

Since R_i , \dot{R}_i and h are nonlinear they can be implemented in the form of the extended Kalman filter, where the measurement matrix H_R is obtained by taking the partial derivatives of Eqs. (3-14) to (3-16).

The generic barometric altimeter is modeled as (Appendix II):

$$h = (x^2 + y^2 + z^2)^{1/2} + B - R_c - \Delta h + v_B \quad (3-16)$$

where

h = baro-altimeter measurement

B = baro-altimeter bias

R_c = geocentric ellipsoid height

Δh = height of the user position above the ellipsoid

v_B = measurement noise residual

4.0 REAL-TIME IMPLEMENTATION OF KALMAN ESTIMATION ALGORITHMS

The conventional sequential discrete Kalman filter can be implemented with reasonable ease by most computer processors. Its algebraic simplicity and computational efficiency have contributed significantly to its wide spread application. However, it is well recognized that the Kalman filter can be numerically unstable due to the asymmetric of its covariance update equation.

$$P_k^+ = (I - K_k H_k) P_k^- \quad (4-1)$$

Under certain conditions, the above subtraction operation can cause the covariance matrix P_k to be asymmetric, which then leads to numerical instability.

To alleviate this problem, several alternatives have been proposed in the literature. Some of these methods are summarized as follows:

a) Stabilized Kalman Algorithm (2)

In order to ensure that P_k be non-negative definite, one popular approach is to rewrite Eq. (4-1) in a quadratic formulation

$$P_k^+ = (I - K_k H_k) P_k^- (I - K_k H_k)^T + K_k R_k K_k^T \quad (4-2)$$

However, Eq. (4-2) above requires almost three times as many arithmetic operations as that given by Eq. (4-1).

b) Carleson Square Root Formulation (3)

In this formulation, the error covariance matrices are represented in terms of their upper triangular square roots. Namely,

$$P_k^- = S_k^- S_k^{-T}$$

$$\text{and } P_k^+ = S_k^+ S_k^{+T}$$

where matrix S_k is unique and assures that the P_k generated will always be symmetrical and positive semi-definite. This square root filter formulation provides twice the effective precision of the conventional forms (4) but its disadvantage lies in that n square roots are necessary for each sequential measurement update.

c) Bierman U-D Factorization Algorithm

This method, of which Carleson's is a special case, factors the covariance matrix as follows:

$$P_k^- = U_k^- D_k^- U_k^{-T}$$

$$P_k^+ = U_k^+ D_k^+ U_k^{+T}$$

where U_k and D_k are, respectively upper triangular and unity diagonal matrices. This formulation is numerically and computationally superior. It has all the advantages of the square root formulation without the need of computing square roots.

In addition, the transition matrix, noise covariance matrix, and measurement matrix can be further exploited to enhance computation efficiency and to minimize its storage requirements.

After one observation is processed, with single precision CPU times of all filters analysed are tabulated below.

	50 μ sec +, -	70 μ sec x	70 μ sec *	1 msec /-	CPU Time μ sec
1. Conventional Kalman	258	270	1	0	31870
2. Stabilized Kalman	714	666	1	0	82390
3. Carleson Square Root	336	426	24	12	60300
4. Bierman U-D	300	414	12	0	44820
4a. Optimized U-D	180	221	12	0	25310

Table 4-1

Comparison of the baseline algorithms (Nos. 1-4) seems to indicate that the conventional Kalman is the most efficient. The question with it's use relates to numerical stability in a single precision formulation. The U-D formulation runs second in efficiency, with roughly 40% degradation in execution time. In single precision, it reflects comparable accuracy of the conventional Kalman equations in double precision format. Positive definiteness is better guaranteed, however. By taking advantage of the sparseness of H and unity diagonals in the U matrix, Bierman's algorithm has been made more efficient. From the table, overall efficiency has been increased by 43% from Bierman's standard formulation. It is also 20% more efficient than the conventional Kalman algorithm.

The U-D formulation is suitable for adaptation to covariance propagation. Between measurements, the covariance matrix propagates as

$$P_k^- = \Phi_k P_{k-1}^- \Phi_k^T + R_k Q_k R_k^T$$

Since $P_{k-1}^+ = U_{k-1}^+ D_{k-1}^+ U_{k-1}^{+T}$

Then: $P_k^- = (\Phi_k U_{k-1}^+) D_{k-1}^+ (\Phi_k U_{k-1}^+)^T + R_k Q_k R_k^T$

Φ_k is upper triangular and, except with the (12, 12) component, the diagonal has unity value. The upper triangular portion of P_k is computed taking advantage of matrix structure and the sparseness of Φ_k , D_{k-1} and Q_k . The product is factored into U_k and D_k in preparation for the data processing portion. Bierman proposes a modified Gramm - Schmidt algorithm whose form does not lend itself easily to matrix structure exploitation. For this reason the above algorithm has been selected.

Several formulations were made computationally efficient, accounting for sparseness of Φ and Q , and the special structure of U and D , noting that only the upper triangular portion of P_k need be formed. The four methods are examined in Table 2. Three of the four methods must perform the factorization of P_k into U_k and D_k . The modified weighted Gramm - Schmidt method propagates only U and D .

	+/-	x	+	/-	CPU Time usec
1. MWGS	902	907	1	11	119640
2. $\Phi(U D U^T)^T + Q$	869	960	1	11	121720
3. $(\Phi U) D (\Phi U)^T + Q$	741	841	24	11	108600
4. $(\Phi U) D (\Phi U)^T + Q$ (OPT)	650	751	12	11	96910

Table 4-2

The fourth method is a modification of the third in that the product ΦU is done explicitly to account for zero and unity multiplication. Storage is minimized because if multiplication is done by backward recursion, U can be overwritten. Method three is 9% more efficient than the modified weighted Gramm - Schmidt algorithm recommended by Bierman. The trick used in method four is 19% more efficient than the MWGS. As well, storage is reduced because U is overwritten.

The consuming portion of the covariance propagation lies in the factorization of the fully reconstructed upper triangle of P_k . The algorithm in the optimized form results in 286 subtractions, 352 multiplications and 11 divisions. Relative CPU time of 39710 for this portion means that 40% of the computation is dedicated to the task of factorization if method four is used.

5.0 DYNAMIC PERFORMANCE ANALYSIS

To verify filter performance and optimize the sub-optimal model statistics (jerk power spectral density) etc, NGRS was used with the flight dynamics generator mentioned in Section 2.0. Results are presented here which enabled the examination of filter sensitivity to vehicle dynamics, geometry, satellite outages, altimeter aiding and fixed gain implementation. Many simulations were performed using Monte Carlo runs, however this was not an extensive Monte Carlo analysis. Only a few of the most illustrative examples are included.

5.1 Vehicle Dynamic Sensitivity

Figures 5-1 to 5-4 are typical sample traces that indicate simulated performance of a vehicle subject to the flight scenario outlined in Figure 5-1. Several characteristics are obvious from these traces.

The baro-altimeter contributions to filter transient error is only marginal for both classes of receiver. This is largely a function of which direction the acceleration vector points.

Velocity and position transients for the sequential receiver are significantly higher than those of the simultaneous receiver. Figure 5-5 illustrates that the stand-alone Class B receiver is much better suited for high dynamic ranges. This figure is based on several Monte Carlo traces. The Class B receiver demonstrates a smaller velocity transient than the Class D. Position error transient, however, is largely insensitive over the entire dynamic range.

Figure 5-5 indicates that for negligible dynamics, the Class B and D receivers will exhibit similar performance.

5.2 Effects of GDOP and Outages

Geometric dilution of precision, or GDOP, is a useful figure for assessing the quality of the 4 satellite geometry.

Figures 5-1 to 5-4 indicate that position fixing with high GDOP results in larger RSS position and velocity error, and overall noisier filter results with the 2-channel sequential receiver. The 4-channel receiver demonstrates larger RSS position and velocity error with smoother filter results. The large steady state position errors are due to the sub-optimal nature of the filter, which passes unestimated biases (i.e., ephemeris errors) through the filter. These manifest themselves as a position error bias. GDOP can be used roughly as a multiplying factor to estimate how these biases further degrade position error.

Satellite signal jamming or delayed switchover will increase dynamic transients and cause long term drift errors without baro-altimeter or other aids. This is the effect of two problems. Firstly, the fourth satellite, if missing, will cause a geometrical weakness in the position fix. This will be critical when vehicle dynamics are present. As an example, assume that the satellite closest to the zenith is jammed or obscured. A vertical manoeuvre will result in poor observability for the remaining measurements. Hence large vertical position transients will occur. The second problem associated with satellite outages has to do with oscillator drift. The more stable the oscillator, the better the reduced-coverage performance will be. Figures 5-1 to 5-4 indicate that the sequential receiver drifts significantly in position after about 1.5 minutes due to poor observability and oscillator drift (e.g., Figure 5-1a, 350-490 sec). The 4-channel receiver exhibits much better RSS position error characteristics over this time period. This is because of the more abundant measurement information. Velocity error degrades only marginally over 90 seconds for both receiver configurations.

Two satellite position fixing, although not illustrated here, is possible for short periods of time with an augmented system, if vehicle altitude is known.

5.3 Altimeter Aiding

Altimeter aiding with a reduced satellite complement will significantly improve the accuracy of a 2-channel sequential receiver. Sustained navigation capability with only 3 satellites is possible, as the baro-altimeter bias is time correlated. The filter then reaches a somewhat degraded steady state condition.

An altimeter cannot be jammed and will provide a much more extensive navigation capability until the full 18 satellite constellation is deployed.

Altimeter aiding of a 4-channel simultaneous receiver does not provide short term benefits, but will serve to keep long term oscillator drift in check (<10 minutes). No significant position and velocity performance improvement is visible in Figure 5-2.

5.4 Fixed Gain Performance

Provided that the filter plant and measurement statistics remain constant, the Kalman filter steady state condition can be approximated by the discrete matrix Riccati equation ($P_k^+ = P_{k-1}^+ = P^*$):

$$P^* + (P^*H^T(HP^*H^T + R)^{-1}H - I) (\Phi P^*\Phi^T + RQ\Phi^T) = 0$$

under normal conditions becomes a function of the geometry matrix H . The row elements of H represent the satellite-to-user direction cosines, coordinated in the earth-fixed cartesian frame. H varies continuously with relative motion between the receiver and satellites, or discontinuously with satellite switchover. The gains used to process the innovations at steady state are

$$K^* = P^*H_k^T R^{-1}$$

By taking advantage of the fact that H_k changes slowly over several minutes (for mach 2 flight, maximum direction cosine change is approximately 1°/minute) it has been found that the updating rate of gain computation can be effectively slowed down without significant loss in precision. The advantage is that computer loading can be significantly reduced under normal flight conditions.

Several schemes are possible to implement this technique. One method is to bypass totally the filter covariance propagation and gain calculation for sustained periods of time (say 5 minutes). A compromise method would refresh gains at a 50% level by fully processing every other measurement. There exists a practical reduction level which optimizes CPU loading without seriously degrading navigation performance (6).

Figure 5-6 indicates fixed gain performance for a 2-channel sequential receiver provided with baro-altimeter input. The interval of interest is from 200 to 440 seconds. The normal filter covariance at 350 seconds begins to grow to a higher steady state level. The trace of the fixed gain technique uses covariance and gains which are last updated at 220 seconds. Hence the covariance does not grow until the propagation and gain update recommences at 430 seconds. The position traces use the same initial random number seed. Note that with 4 satellite coverage, the traces are somewhat similar. However after 350 seconds, when the fixed gain covariance begins to deviate rapidly from the normal gain covariance, position error degrades somewhat.

It can be concluded that the fixed gain technique shown, while extreme in its implementation, shows promise in reducing CPU loading under normal (4 satellite) operating conditions. The receiver could easily mechanize the fixed gain scheme by monitoring satellite outages and reverting to full gain computation under reduced sensor complement. This is especially attractive for 4-channel receivers because of the number and frequency of available measurements.

6.0 CONCLUSION

This brief analysis shows that a 12 state sub-optimal Kalman filter can be implemented and operated real-time in 2- and 4-channel CMC Navstar receivers. The algorithm is numerically stable in single precision U-D form, and makes optimum use of storage area.

Dynamic performance has been verified by Monte Carlo simulation. Sensitivity analyses of Class B and D receiver designs indicate similar RSS position and velocity error for low dynamic applications (< 1g) and superior 4-channel performance for medium and high dynamic applications. The baro-altimeter does not contribute significantly to dynamically induced transients.

During satellite switchover, the baro-altimeter input results in significant accuracy benefits as sustained 3 satellite navigation is possible. The filter produces a somewhat degraded steady state condition.

Finally, by taking advantage of certain steady state properties of the Kalman equations, gain computation can be performed at a reduced rate, freeing the navigation computer for background tasks. Further developments will include adaptive filtering to assure filter statistics are realistic. Fixed gain rules will be formulated and verified by simulation, so that navigation computation may be optimized without significant performance degradation.

REFERENCES

- (1) Wolfe, C. A. - "Navstar/GPS Navigation Analysis and Algorithm Development Study" Orincon Corp., La Jolla, CA 30 Nov., 1976
- (2) Bieman, G. J. - Factorization Methods for Discrete Sequential Estimation", Academic Press, New York, 1977
- (3) Carleson, N. A. - "Fast Traingular Factorization of the Square Root Filter", AIAA J. 11, No. 9 1973
- (4) Kaminsky, P. G. - "Square Root Filtering and Smoothing for Discrete Processes", PhD. Dissertation, Dept. Aero. & Astro, Stanford U.
- (5) Dymant, M. J. - "Navstar Generalized Receiver Simulator "Canadian Marconi Co., Internal Report (1979)
- (6) Damoulakis J. N. - "A GPS-HDUE System Configuration with Increased Processing power on Range and Range-Rate Measurements", Texas Instruments Incorporated Dallas, Texas

APPENDIX 1 - RECEIVER CLOCK ERROR MODEL

To provide a realistic model of the GPS receiver crystal oscillator errors, a second order stochastic model is used. The two error sources are: Frequency offset, modeled as a random walk with Gaussian white noise driving term of power spectral density Φ_w ; and crystal oscillator G sensitivity, a deterministic error proportional to the projection of the vehicle acceleration vector onto the crystal g-sensitive axis:

$$\dot{c\Delta t} = c\Delta t' + (\underline{a} \cdot \underline{l}_{sa}) S_{cr} \quad (1)$$

where

$c\Delta t$ - frequency offset error (m/sec) - the loop VCO reference frequency

S_{cr} - crystal acceleration sensitivity ($m/sec)/(m/sec^2) = sec$

\underline{a} - vehicle acceleration vector (m/sec^2)

\underline{l}_{sa} - crystal oscillator direction cosine

$\dot{c\Delta t}'$ - frequency drift-induced frequency offset

The plant is modeled as

$$\dot{\underline{x}} = F\underline{x} + Gw + Ha \quad (2)$$

where $\underline{x}^T = (c\Delta t, \dot{c\Delta t}')$ is the state

w - white noise driving term

$a = \underline{a} \cdot \underline{l}_{sa}$ - effective acceleration

and

$$F = \begin{bmatrix} 0 & 1 \\ 0 & 0 \end{bmatrix} \quad G = \begin{bmatrix} 0 \\ 1 \end{bmatrix} \quad H = S_{cr}$$

The output of the system is

$$\underline{y} = Ax + Ba \quad (3)$$

where

$\underline{y}^T = (\dot{c}_{at}, \dot{c}_{\dot{at}})$ is the effective state

$$A = \begin{bmatrix} 1 & 0 \\ 0 & 1 \end{bmatrix} \quad B = \begin{bmatrix} 0 \\ S_{cr} \end{bmatrix}$$

APPENDIX 2 - BAROMETRIC ALTIMETER MODEL

The generic barometric altimeter model to be described will be for a point-mass P. Consider first the measurement of a height h_g above sea level, provided isobaric surfaces are parallel to the geoid. The observation is then:

$$h_g \approx R_c + h - \Delta h \quad (1)$$

where the approximation is due to the fact that neither R_c nor R_n are perpendicular to the geoid. R_c is geocentric ellipsoid radius, R_n is geodetic prime vertical radius of curvature. The geoidal undulation Δh can be described by an autocorrelation function as being distance correlated. Therefore, 3 specific error sources exist:

1. Difference between sea-level and the reference ellipsoid (undulation)
2. isobaric fluctuations
3. noise in measurement of height (encoding)

Including all sources, the height is modeled as

$$h_g = |\underline{P}| - R_c - \Delta h + B + V_B \quad (2)$$

where

h_g - the measurement
 R_c - geocentric ellipsoid height
 h - height of P above the ellipsoid
 B - exponentially correlated bias which reflects undulation and isobaric fluctuations
 V_B - measurement residual
 Δh - geoidal undulation (or initial sea level bias)

Now

$$|\underline{P}| = (x^2 + y^2 + z^2)^{1/2} \quad (3)$$

$$\dot{B} = (-1/\tau_B) B + w_B \quad (4)$$

where

$$\begin{aligned}
 E(B(t_0)) &= 0 & E(V_B) &= 0 \\
 E(B(t_0)^2) &\sim \sigma_B^2 & E(V_B^2) &= \sigma_H^2 \\
 E(w_B) &= 0 & E(\Delta h) &= 0 \\
 E(w_B(t) w_B(t + \tau)) &= \phi_B \delta(\tau) & E(\Delta h^2) &= \sigma_{\Delta h}^2
 \end{aligned}$$

are the associated statistics.

The discrete version of (4) is necessary for simulation and estimation purposes

$$\phi(t_k, t_{k-1}) = e^{-(t_k - t_{k-1})/\tau_B} \quad (5)$$

The solution to (4) is

$$B(t_k) = \bar{e}^{(t_k - t_{k-1})/\tau_B} B(t_{k-1}) + \int_{t_{k-1}}^{t_k} \phi(t_k, s) w_B(s) ds \quad (6)$$

The statistics of $B(t_k)$ are as follows:

$$E(B(t_k)) = 0$$

$$E(B(t_k)^2) = e^{-2\Delta t/\tau_B} \sigma_{B_0}^2 + \int_{t_{k-1}}^{t_k} e^{-2(t_k-s)/\tau_B} \Phi_B ds \quad (7)$$

$$= e^{-2\Delta t/\tau_B} \sigma_{B_0}^2 + \sigma_w^2 (1 - e^{-2\Delta t/\tau_B})$$

$$\sigma_{B_0}^2 = (10)^2 \text{ (m)}^2$$

$$\sigma_w^2 = 2.7^2 + (.0035h)^2 \text{ (m)}^2$$

Simulation is performed as follows:

$$h_{Bk} = (x_k^2 + y_k^2 + z_k^2)^{1/2} - R_{ck} + B_k + v_{Bk} \quad (8)$$

where $h_k = (x_k^2 + y_k^2 + z_k^2)^{1/2} - R_{ck}$ is true height above the ellipsoid

$$B_k = e^{-\Delta t/\tau_B} B_{k-1} + \sigma_w (1 - e^{-\Delta t/\tau_B})^{1/2} w_1 \quad (9)$$

$$v_{Bk} = \sigma_h w_2 \quad (10)$$

and initially,

$$B_{k0} = (\sigma_{B_0}^2 + \sigma_{\Delta h}^2)^{1/2} w_3 \quad (11)$$

The correlation time is computed from the correlation distance

$$S_B = \frac{x_{corr}}{v_{horiz}} \quad (12)$$

where $x_{corr} = 100,000 \text{ m}$ is the correlation distance
 v_{horiz} = horizontal velocity

The random number generator computes independent zero mean and unit variance Gaussian numbers

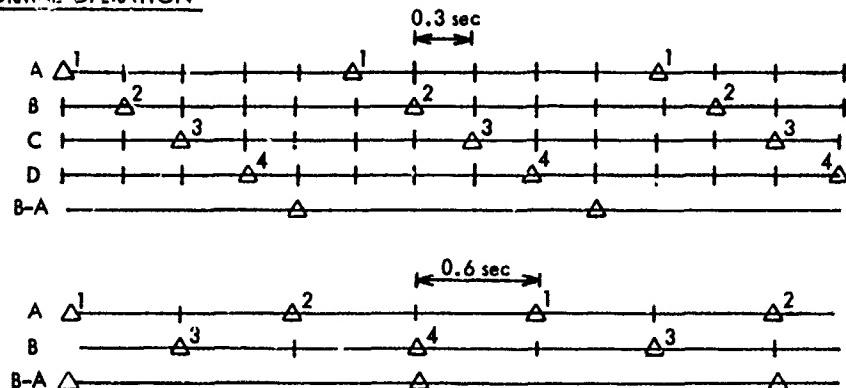
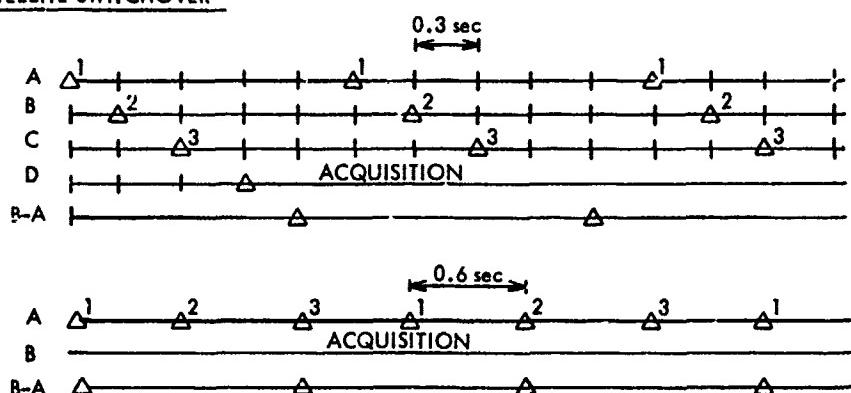
NORMAL OPERATIONSATELLITE SWITCHOVER

FIGURE 2-1 - 4 AND 2 CHANNEL RECEIVER MEASUREMENT
SEQUENCE, NORMAL OPERATION MODE AND
SATELLITE SWITCHOVER MODE.

— PSEUDO RANGE RATE
△ — PSEUDO RANGE

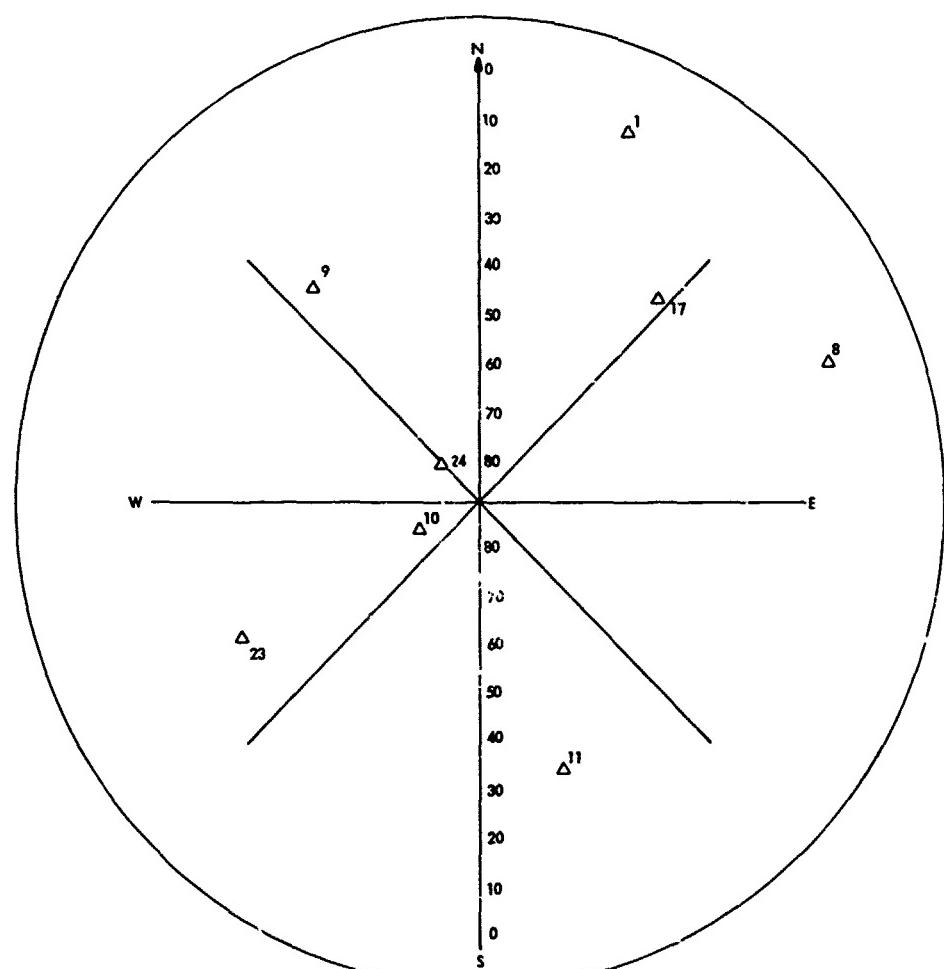


FIGURE 2-2
SATELLITE CONSTELLATION

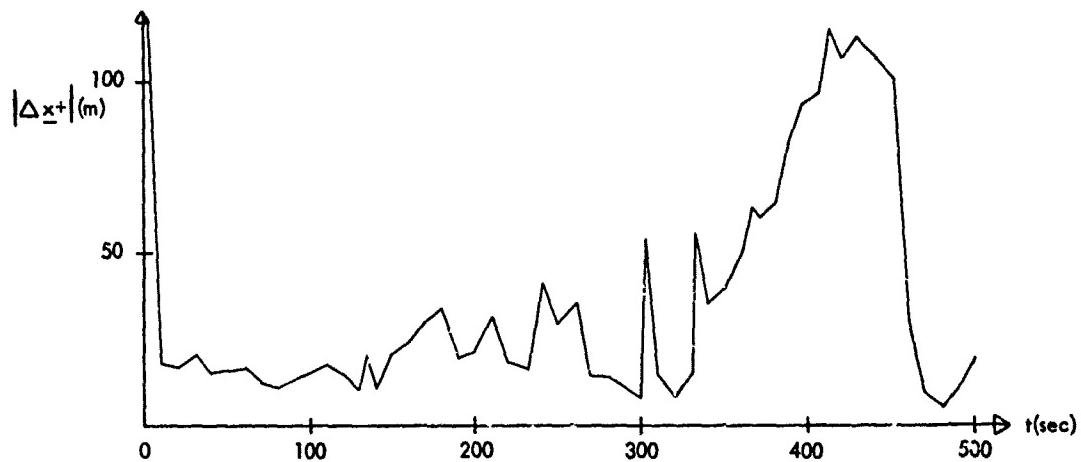


FIGURE 5-1a : RSS POSITION ERROR WITHOUT BARO-ALTIMETER
2 CHANNEL SEQUENTIAL RCVR

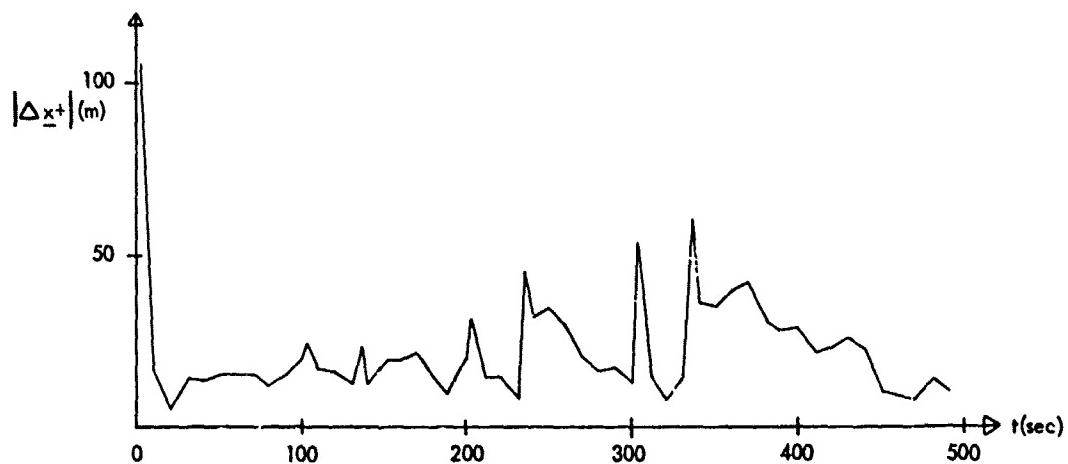


FIGURE 5-1b : RSS POSITION ERROR WITH BARO-ALTIMETER
2 CHANNEL SEQUENTIAL RCVR

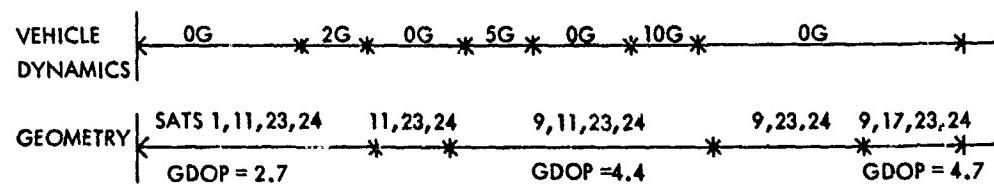


FIGURE 5-1c :FLIGHT SCENARIO

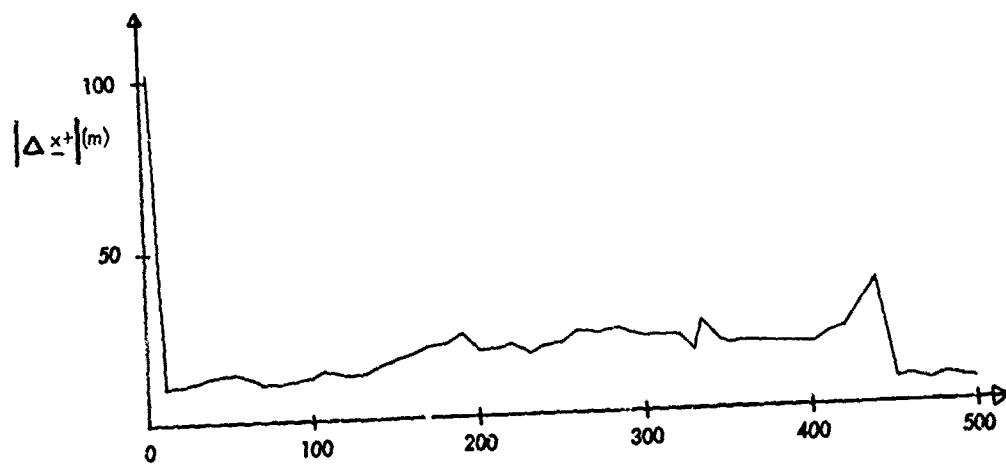


FIGURE 5-2a : RSS POSITION ERROR WITHOUT BARO-ALTIMETER
4 CHANNEL RCVR

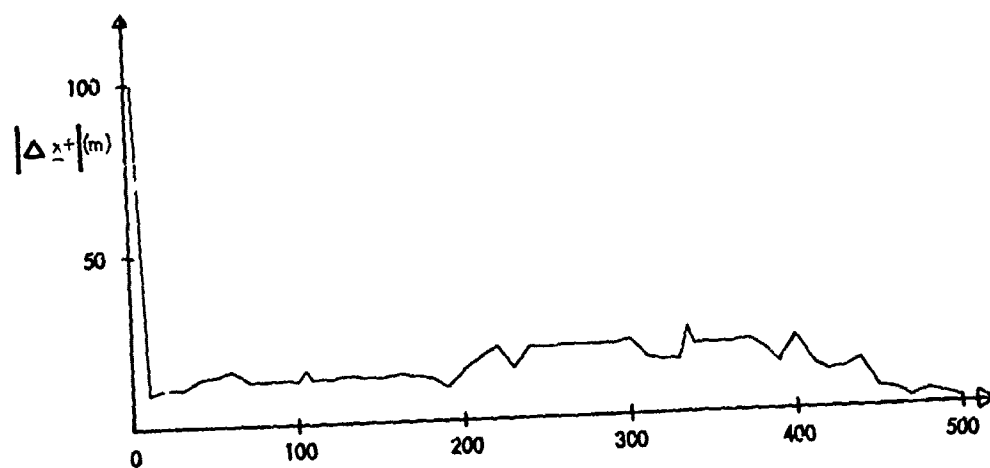


FIGURE 5-2b : RSS POSITION ERROR WITH BARO-ALTIMETER
4 CHANNEL RCVR

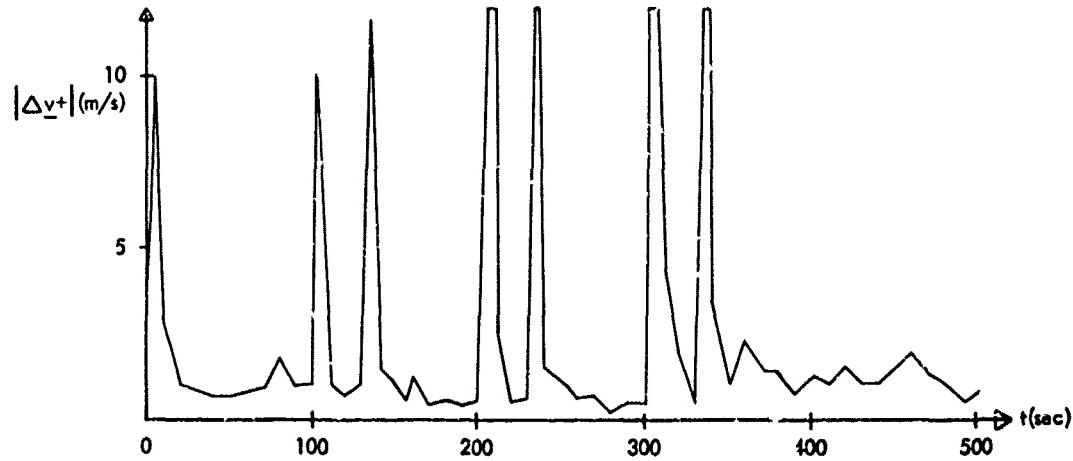


FIGURE 5-3a : RSS VELOCITY ERROR WITHOUT BARO-ALTIMETER
2 CHANNEL SEQUENTIAL

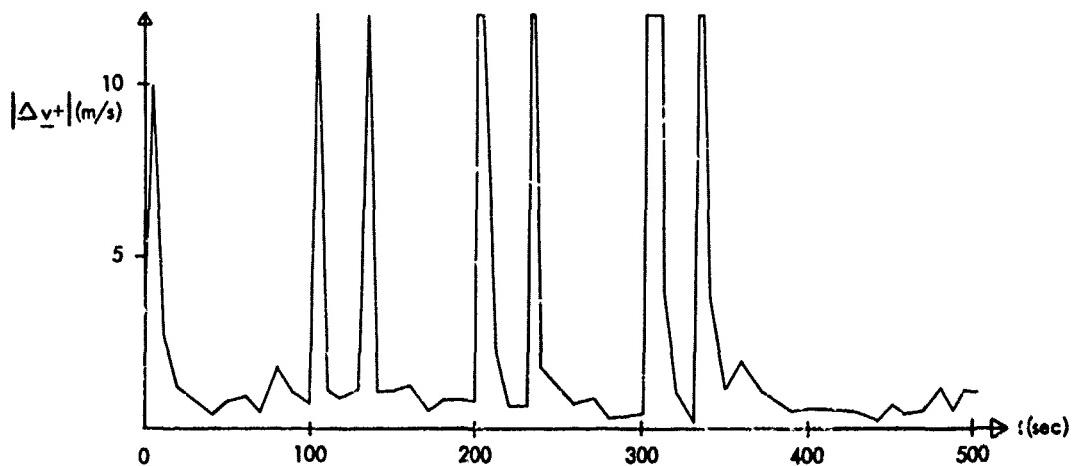


FIGURE 5-3b : RSS VELOCITY ERROR WITH BARO-ALTIMETER
2 CHANNEL SEQUENTIAL

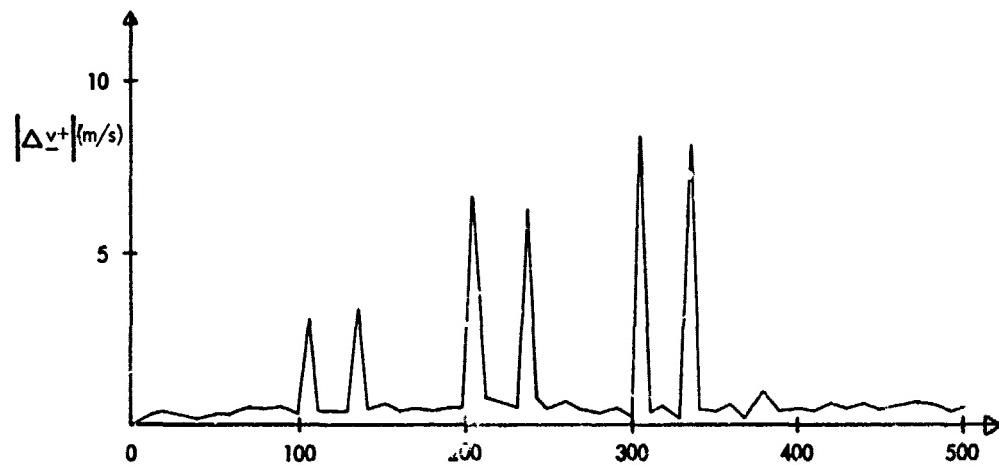


FIGURE 5-4a: RSS VELOCITY ERROR WITHOUT BARO-ALTIMETER
4 CHANNEL RCVR

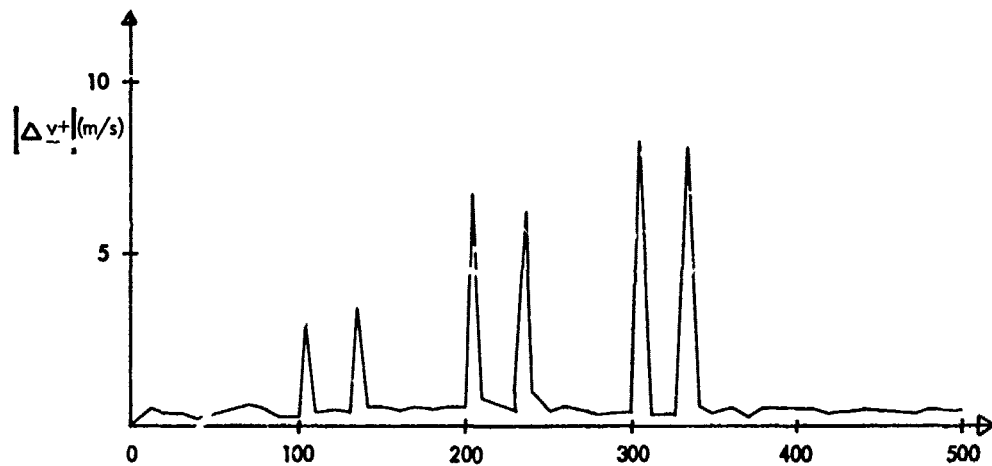


FIGURE 5-4b: RSS VELOCITY ERROR WITH BARO-ALTIMETER
4 CHANNEL RCVR

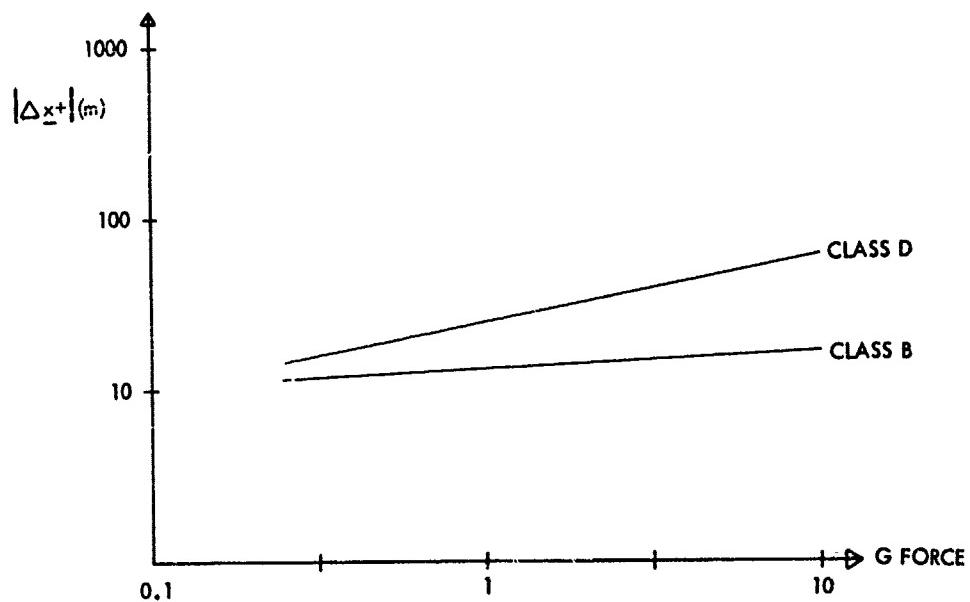


FIGURE 5-5a : DYNAMIC POSITION TRANSIENT

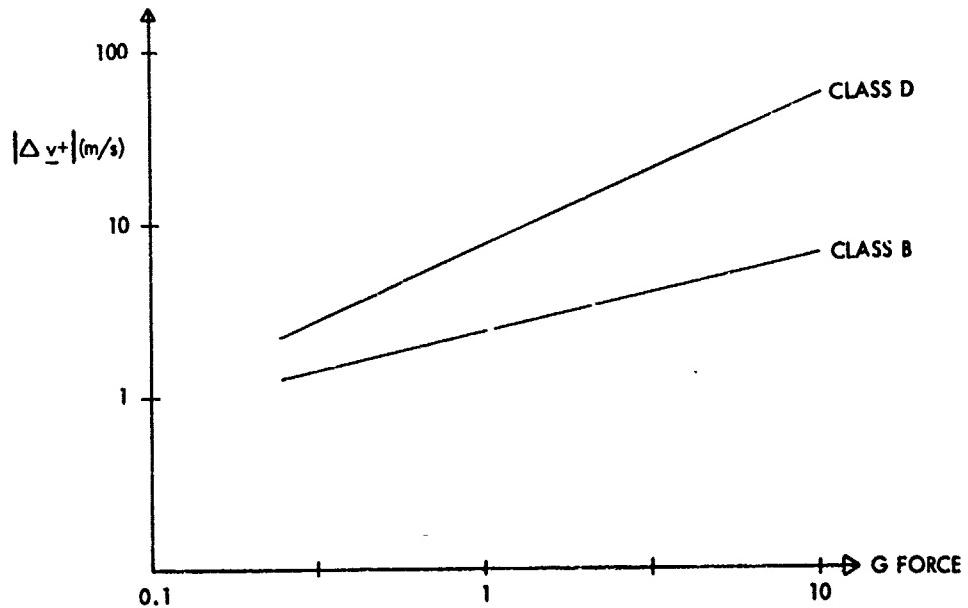


FIGURE 5-5b : DYNAMIC VELOCITY TRANSIENT

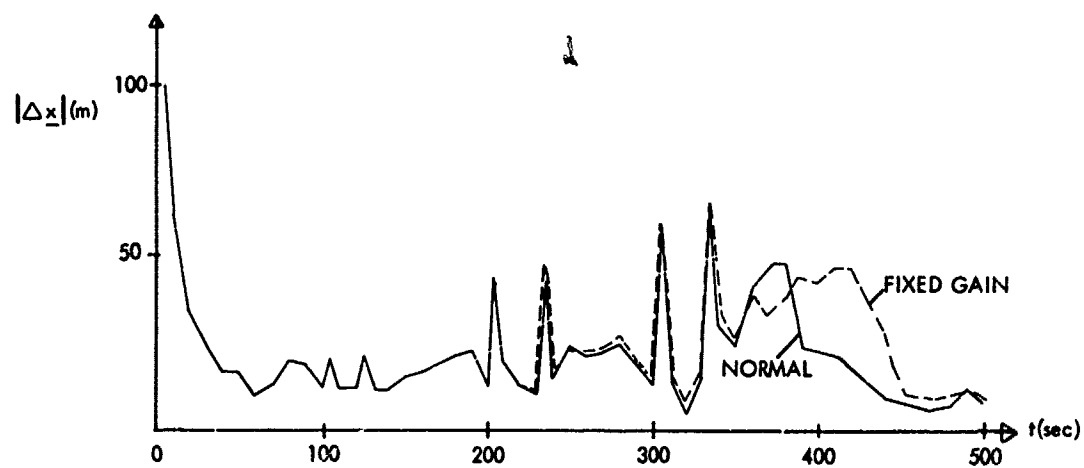


FIGURE 5-6a FIXED GAIN PERFORMANCE - POSITION ERROR

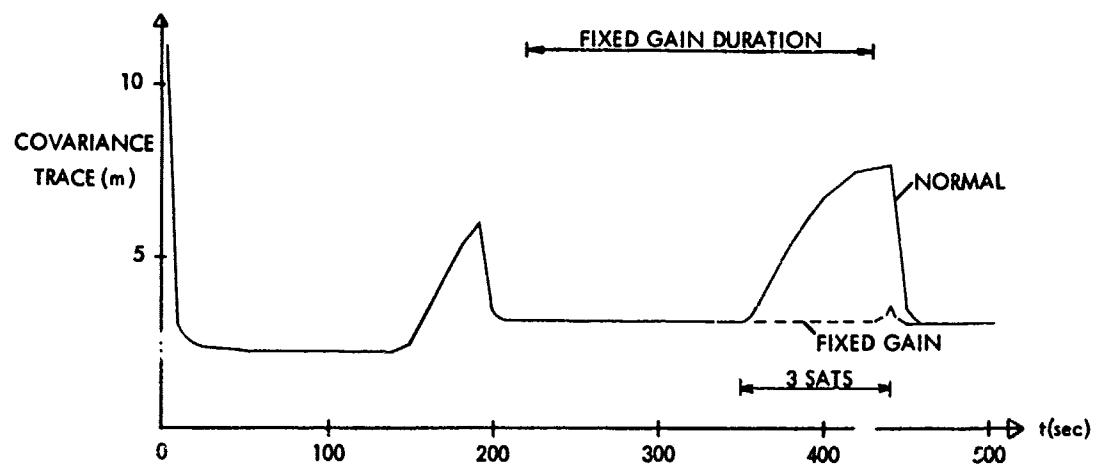


FIGURE 5-6b FIXED PERFORMANCE - COVARIANCE TRACE

**RAPID ALIGNMENT OF AIRCRAFT STRAPDOWN INERTIAL NAVIGATION SYSTEMS
USING NAVSTAR GLOBAL POSITIONING SYSTEM (GPS)**

by

Robert W. Tafel, Jr.
General Engineer
Code 4011
Naval Air Development Center
Warminster, PA 18974
USA

David Krasnjanski
Navigation Systems Engineer
Code 4011
Naval Air Development Center
Warminster, PA 18974
USA

SUMMARY

This paper investigates the use of the GPS navigation satellite system as a reference for the in-air alignment of a strapdown inertial navigation system (INS). A Kalman filter covariance simulation program is used to determine the optimal alignment performance which can be achieved with a hybrid INS/GPS configuration. The sensitivity of in-air alignment to resut interval and choice of observable is discussed. The impact of various flight profiles upon the effectiveness of the alignment mechanism is evaluated. The alignment sensitivities determined in the optimal study are then used to develop a suboptimal alignment filter suitable for mechanization in an airborne computer. The trade-off between filter size and alignment speed and accuracy is shown. Finally the recommended filter is compared to the optimal filter over a range of alignment conditions in order to demonstrate its effectiveness.

LIST OF SYMBOLS

A_E	east vehicle acceleration
g	earth's gravitational acceleration
L	latitude
δp_N	north position error
R_e	earth's radius
V_E	east velocity
δv_N	north velocity error
a_n	north accelerometer error
ϵ_a	azimuth gyro error
ϵ_e	east gyro error
ρ_D	angular velocity about the local vertical axis induced by motion across the earth's surface ($(V_E \tan L) / R_e$)
$\delta \theta_E$	east tilt error
$\delta \psi$	azimuth error
Ω	earth's rate of rotation
ω_N	angular velocity about the north axis induced by rotation of the earth and by motion across the surface of the earth ($\Omega \cos L + V_e / R_e$)

BACKGROUND

Inertial navigation, being a form of dead reckoning, can only be as good as the initialization which precedes it. When this initialization, or alignment, must be performed aboard a moving ship a source of reference velocity or position information is required from which the inertial error signals can be calculated. At present only attack aircraft carriers, equipped with a SINS (Ship Inertial Navigation System), possess a reference accurate enough to permit rapid and accurate aircraft INS alignment. Deck time required to align an INS to a nominal 2 km/hr CPE (circular probable error) rate navigational accuracy ranges from 7 to 10 minutes.

The SINS information is transferred to the aircraft INS via an RF (radio frequency) data link. The data link information is not secure; and during conditions of radio silence, it is replaced by umbilical cables which provide a direct electrical link to the SINS. However, these cables are cumbersome to use; they require the aircraft to remain stationary throughout INS alignment; and they are often in short supply aboard ship.

In the absence of an accurate reference source, as would be the case in the event of SINS failure or where the aircraft is to be launched from a non-carrier aviation ship or where the INS is to be aligned in flight, present alignment techniques will not suffice. The backup to SINS onboard a carrier and the primary navigation system aboard ships other than carriers is a gyrocompass/EM (electro-magnetic) log. This system cannot align an INS in a practical length of time. The accuracy of doppler radars, used as a velocity reference for in-air alignment, is severely limited over water so that the alignment required for 2 km/hr unaided inertial navigation cannot be achieved.

The Naval Air Systems Command has tasked the Naval Air Development Center to develop new INS alignment techniques which can overcome the problems described above. The objectives of these new techniques include the decrease in reaction time of aircraft aboard carriers for alert operations related to fleet air defense, the provision of a secure and jam-proof RF alignment technique, the development of an alternate alignment capability which can supplement the SINS aboard aircraft carriers thereby increasing reliability, and the development of an alignment technique to be used aboard ships, such as destroyers and amphibious assault ships, which may be host to V/STOL (Vertical/Short Take-Off and Landing) aircraft or INS-equipped helicopters.

A potential RF alignment reference presently under advanced development is GPS. It is a navigation satellite system which will provide accurate position, velocity, and time nearly continuously on a world-wide basis. In this application it would be used to provide position and velocity reference information for the in-air alignment of an aircraft INS. By enabling in-air alignment GPS would decrease the reaction time for carrier aircraft, provide a redundant alignment capability to SINS, provide the primary alignment reference for aircraft aboard non-carrier ships without requiring the installation of expensive navigation equipment aboard the ship, and permit INS alignment restarts in flight.

The evaluation of GPS as an INS alignment reference will be approached in the following manner. The first step will be to simulate an alignment filter utilizing GPS to align an INS. The simulation study will be devised to assess the maximum alignment speed and accuracy which can be obtained from an optimal INS/GPS combination. The sensitivity of the alignment process to variations in the aircraft trajectory will be examined to discern what limitations might exist to the in-air alignment process. Since an operational airborne computer cannot handle a complete mechanization of the error propagation of an INS/GPS combination, the final phase of the simulation study will involve the design of a suboptimal alignment filter which will approximate the optimal performance within the constraints of computer memory loading and cycle time. The alignment filter thus defined will be implemented in hardware, and a feasibility demonstration will be conducted in which the simulated performance will be verified and the efficacy of the approach proved. The results of the demonstration will then lead to recommendations as to how this alignment approach can be introduced into the fleet. This paper addresses the simulation study leading up to the definition of the INS/GPS alignment filter.

DESCRIPTION OF SIMULATION

A Kalman filter covariance analysis program was used to simulate the optimal combination of an INS with the GPS. The GPS error model is shown in Table I. It was obtained from the GPS Joint Program Office (JPO), and it represents the errors associated with a fully operational satellite system.* Measurements are taken simultaneously from four satellites. Each satellite has associated with it a three dimensional position error and a clock error consisting of a phase bias, frequency bias, and a phase random walk. Errors associated with the GPS receiver onboard the aircraft include signal propagation errors and a receiver clock error comprising phase bias and phase random walk errors and frequency bias and frequency markov (exponentially correlated) errors. Measurement error noise was not included as part of the JPO model; however, reference (1) pointed out that some error would exist due to quantization effects in the GPS receiver. Consequently measurement noise is included in Table I as representative of a minimum level of error.

The RLGN (ring laser gyro navigator) was selected as the strapdown INS to be aligned because it is representative of a maturing laser gyro technology. An advanced development model RLGN, built by Honeywell, Inc., is presently being evaluated at the Naval Air Development Center (reference (2)). The RLGN has been selected as the INS for the AV-8B V/STOL aircraft, and a commercial version of the RLGN has been designated by Boeing for the 757 and 767 series transport aircraft. The error model for the RLGN is shown in Table II (obtained from Honeywell, Inc.). The gyro random walk is characteristic of laser gyros and the small value for gyro scale factor errors is indicative of the fact that a strapdown INS gyro is not isolated from aircraft dynamics. Vertical deflection is included as an accelerometer error because unmodelled deflections of the local vertical will cause components of gravity to erroneously appear in the horizontal acceleration channels of the INS.

Table III shows a set of standard test conditions under which the simulation study was performed. The initial INS errors were those which would be present at the completion of a caging/coarse alignment mode. The aircraft was assumed to be flying north at a constant speed of 180 m/s. At the commencement of in-air alignment the aircraft turned counterclockwise at a standard rate of turn. Simultaneous measurements of range rate to four GPS satellites were used for Kalman filter resets at a 1.8 sec interval. The aircraft was flying in the mid latitudes in order to average the effect of latitude upon alignment efficiency, and the geometry of the satellites with respect to the aircraft was set at the median value of all possible configurations world-wide as measured by GDOP (Geometric Dilution Of Precision). In the analyses which follow each parameter was varied separately, with the others held constant, in order to establish alignment sensitivities. If no mention is made of a particular parameter, it may be assumed that its value was that shown in Table III.

*Note: Recent funding cuts to the GPS program have reduced the number of satellites for a full capability system. This change is not expected to affect the results in this paper.

Table IV shows the navigation requirements placed upon the RLGN by the Navy in reference (3). In order to achieve these accuracies the alignment requirements shown in the table must be met. These alignment error specifications were used as the criteria to establish when an in-air alignment had been completed.

OPTIMAL INS/GPS IN-AIR ALIGNMENT

Alignment of the inertial measurement unit (IMU) is accomplished in a strapdown system through determination of the coordinate transformation between the IMU coordinates (body coordinates) and geographic coordinates (local level coordinates). Inertial position and velocity errors may be estimated almost immediately through direct comparison with a reference source, but tilt and azimuth errors are usually estimated indirectly through their effects on INS velocity and position errors. The speed and accuracy of tilt and azimuth error estimation is determined partly by how long it takes the misalignment errors to propagate into measurement error and partly by how easily the misalignment error can be separated from sensor error. Figure 1 shows a simplified block diagram of error propagation in one channel of an inertial navigation system. The solid line shows the error propagation path for conventional gyrocompassing (nulling of earth rate sensed around the east axis). Azimuth error is two integrators removed from velocity error and three integrators removed from position error. Consequently the effect of azimuth error takes longer than any other alignment parameter to be manifest as a velocity and position error. It is usually the last alignment parameter to be estimated correctly, and so it determines INS alignment time.

Another path (dashed line) does exist for the propagation of azimuth error into velocity error. If azimuth is in error, acceleration and its integrals (velocity and position) will not be properly resolved into geographic coordinates. The effect of this pointing error can only be seen when the INS experiences acceleration. A comparison of the two alignment mechanisms is shown in figure 2. In straight flight the velocity is constant, and gyrocompassing is the mechanism by which azimuth error is estimated. When the aircraft turns, its velocity vector changes direction and the resultant centripetal acceleration (nearly $1g$) permits pointing error to be the dominant alignment mechanism. The improvement in azimuth alignment afforded by pointing error is dramatic. There is a 15:1 improvement in alignment time and a 10:1 improvement in steady state alignment accuracy. Alignment speed is increased because pointing error feeds directly into the velocity integrator, thus making azimuth error more quickly observable. Alignment accuracy is improved because pointing error must be distinguished from accelerometer error whereas gyrocompassing error must be distinguished from gyro error. The signal to noise ratio of pointing error (vehicle acceleration multiplied by azimuth error versus accelerometer error) is approximately an order of magnitude greater than the signal to noise ratio of gyrocompassing (earth and transport rates multiplied by azimuth error versus east gyro error).

Pointing error cannot affect velocity error any sooner than the second iteration of the error dynamics. The first iteration propagates the INS/GPS errors in response to the aircraft dynamics sampled at zero time (aircraft flying straight and level). The second iteration propagates them in response to aircraft dynamics sampled at some later time wherein the direction of the aircraft velocity vector has changed thus making the effect of pointing error observable at the velocity level. It is apparent that the rapidity with which errors are propagated and error resets are performed could affect alignment performance. The effect of two reset/iteration intervals were investigated. A 1.8 sec interval was chosen as typical of existing alignment algorithms, and an 18 sec interval was chosen to examine the potential for reduced timing burden on the navigation computer. These intervals are combined in three different regimes in figure 3. The solid line shows alignment response when errors are propagated through the Kalman filter at an 18 sec interval and every propagation is followed by a reset. The dashed line regime retains a reset interval of 18 sec but it samples aircraft dynamics and propagates errors ten times more frequently. The dotted line shows resets as well as error propagation proceeding at the higher rate. It can be seen that the accuracy of the first estimate of azimuth error diminishes as either the length of time over which errors are propagated is reduced (dashed line) or as the net change in aircraft dynamics between resets becomes smaller (dotted line). Although the observability of pointing error is initially smaller at the shorter reset/iteration intervals, the speed with which estimation begins and continues more than compensates for this. The 1.8 sec reset/iteration interval provides the fastest and smoothest overall response. For this reason it was used in the rest of the optimal simulation study in order to obtain finer precision in the investigation of alignment sensitivities.

Since INS misalignments affect velocity before they affect position, the choice of combining INS information with GPS information at the velocity level (range rate observable) or at the position level (range observable) could affect the performance of in-air alignment. As figure 4 indicates, the range rate observable provides a significantly faster alignment than does the range observable. This holds true for azimuth, tilt, and velocity error estimations. However, the sensitivity of the range rate calculation to INS position error is low, and the effect of this weak coupling is illustrated in figure 5. It shows that the estimation of INS position error proceeds much slower than the estimation of the other inertial errors and that the steady state position accuracy does not approach the accuracy inherent in the GPS range measurement. A method by which the speed of estimation could be brought into consonance for all of the inertial errors would be to process one range observation at the beginning of alignment (time zero) and then process range rate observations thereafter. The effect of this scheme is shown in figures 6 and 7. The one range observation reduces INS position error (figure 6) to an insignifi-

cant level in terms of long term navigation. The subsequent range rate measurements quickly estimate velocity error so that the position error actually is less affected by velocity estimation than when range observations were processed exclusively. At the level of azimuth misalignment (figure 7) there is virtually no difference in the alignment response even though processing of range rate observations was delayed by one reset interval. The response at the tilt and velocity levels is similar. Two other methods of combining range and range rate observations were examined--simultaneous measurement of range and range rate or alternating measurements of range and range rate, but neither of them provided significantly different alignment response. The scheme of one range observation followed by range rate observations was selected for use in this study.

The observability of pointing error is dependent upon the strength of the acceleration signal which drives it. In turns this acceleration is directly proportional to the rate at which the aircraft turns. Figure 8 shows the sensitivity of INS alignment to turn rate. The times required to align the INS to specified accuracy in tilt and in azimuth are both plotted. The first item of note is that, in contrast to gyrocompassing, pointing error has such a strong effect on velocity error that azimuth error is no longer the last alignment parameter to be estimated. At a standard rate turn of $3^{\circ}/sec$, it takes seven times longer to align in tilt than it does to align in azimuth. As turn rate is increased and the centripetal acceleration grows larger, the alignment time decreases. At turn rates in excess of $4.5^{\circ}/sec$ azimuth alignment time is at the absolute minimum of two iteration intervals (3.6 sec).

Under operational conditions an aircraft may not always turn at the beginning of in-air alignment. Since the speed of tilt error estimation (vertical alignment) determines overall NS alignment time when the aircraft turns at time zero, the effect upon vertical alignment of delaying the start of the turn will be examined. Figure 9 shows the response of vertical alignment to straight flight and turns. Vertical alignment is delayed in turns because both tilt error and pointing error feed directly into the velocity integrator. The greater magnitude of the pointing error signal causes azimuth error to be estimated first at the expense of tilt error estimation. In straight flight gyrocompassing error does not directly affect velocity; therefore, tilt error is readily observable and is estimated more rapidly. Since tilt error estimation is quicker in straight flight, overall NS alignment time may be reduced by delaying the start of the turn. In figure 10 the time of vertical alignment and azimuth alignment is plotted as a function of time before turn for a range of turn rates. It can be seen that vertical alignment time is generally improved by delaying the turn. For turns delayed beyond 20 seconds the entire vertical alignment is performed before the turn even begins, thus explaining the insensitivity of vertical alignment to turn delays beyond that time. Azimuth alignment also benefits somewhat from delayed turns, but for a different reason. No azimuth error estimation takes place during the short straight flight segments illustrated here because gyrocompass error has had no time to propagate into velocity error. However when turns are initiated after a period of straight flight in which tilt error has been reduced, the observability of pointing error is enhanced over that which prevails for turns begun at time zero. The effect is only seen at the lower turn rates where the centripetal acceleration driving function for pointing error is low. At the higher turn rates, and at the lower rates for turn delays beyond 10 seconds, the ratio of pointing error to tilt error is so high that no azimuth alignment improvement is seen. Figure 11 shows the effect upon INS alignment of turn rate and when it is initiated. Tilt error determines alignment time for turn delays of up to 16 seconds. At 16 seconds a minima occurs where vertical alignment time and azimuth alignment time are equal. Beyond 16 seconds azimuth alignment determines INS align time. The sensitivity of alignment time to turn rate is most apparent in the region where tilt error dominates. As turns are increasingly delayed the sensitivity to higher turn rates diminishes, so that beyond 30 seconds delay the process is insensitive to rates of $3^{\circ}/sec$ or greater. In this region azimuth alignment occurs in the minimum 3.6 seconds after start of turn, and INS alignment time virtually becomes a function of when the pilot turns the aircraft.

Two other parameters related to turn rate were examined for their effect on in-air alignment. The direction of turns was found to be insignificant. Clockwise and counter-clockwise turns were flown across the range of turn rates. Only occasionally did the clockwise turn exhibit a faster alignment time, and then it was by less than two seconds. The sensitivity of alignment to aircraft heading was also evaluated. Alignments under the standard test conditions were conducted for the cardinal and inter-cardinal headings. A comparison of the alignment response at the best and worst headings is shown in figure 12. Alignments at low turn rates appear to be more affected than alignments at high turn rates, but in no case is the delay in alignment greater than 5.4 seconds. The initial aircraft heading, therefore, has no appreciable effect on in-air alignment.

Besides turn rate, the other factor which determines centripetal acceleration is aircraft velocity. Figure 13 shows the sensitivity of the INS alignment parameters to variations in aircraft velocity. Vertical alignments are unaffected by velocity changes; however, azimuth alignments are decidedly affected. The decrease in velocity, especially at the lower turn rate limit, significantly reduces the strength of the centripetal acceleration. As a result the coupling of azimuth error into velocity error via pointing error is weakened, and azimuth alignments are delayed. Because azimuth alignment times are increased at lower velocities but vertical alignment times remain unaffected, it follows that azimuth alignment time will begin to determine INS alignment time at shorter delays in the start of turning. This can be seen in figure 14 where a nominal aircraft velocity of 180 m/s (representative of fixed wing aircraft) is compared to a velocity of 46 m/s (representative of rotary wing aircraft). It can be seen that at lower speeds and lower turn rates INS alignment time is significantly delayed. At the other extreme the effect is much less apparent. At the low speed azimuth dominance of alignment time

begins between zero and 10 seconds delay in turns, the time increasing as turn rate increases. Even when azimuth alignment does control, a relative improvement in INS alignment time is observed for delays between 10 and 20 seconds. Pointing error is still relatively more observable at longer delay times because of the more rapid estimation of tilt error afforded by straight flight. Beyond delays of 20 seconds, vertical alignment to specified accuracy is completed; and azimuth error estimation alone determines INS alignment time.

Acceleration in straight flight may also be used to generate a pointing error signal. Figure 15 compares the effectiveness of linear acceleration to that of centripetal acceleration. Under the standard conditions of a 3°/sec turn rate flown at 180 m/s a centripetal acceleration of approximately $1g$ is generated. The direction of the centripetal acceleration is out the left wing of the airplane. As the aircraft turns, an acceleration sinusoidally varying between 0 and $1g$ appears in the north and east navigation channels. The alignment time for this situation is shown as the dashed line of figure 15. The solid line shows the alignment time for a range of linear accelerations between 0 and $1g$. The variable nature of the acceleration caused by turning permits a better separation of tilt error and azimuth error, and thus permits a faster alignment than does constant linear acceleration in just one direction. The comparison was performed at different headings and with deceleration instead of acceleration, and the results were the same.

Table V shows the effect of various other conditions upon in-air alignment--initial conditions, aircraft location, and satellite geometry. All test conditions were held to those of Table III except where noted. Table V shows first the in-air alignment time and then the values of the various inertial errors at the end of alignment. Alignment time varied by less than two seconds from the standard in all cases. In addition none of the INS errors were significantly degraded at the time of completed alignment. It was concluded that in-air alignment was insensitive to the conditions evaluated.

SUBOPTIMAL INS/GPS IN-AIR ALIGNMENT

The previous section has shown the maximum alignment performance which may be obtained from a hybrid combination of GPS with the RLGN. This performance was achieved because all of the errors affecting the hybrid system were correctly modelled within the Kalman filter. It is impractical, however, to include the full error model in an operational filter; therefore, a subset of the full error model must be selected which, by accounting for the major error sources, still permits nearly optimal alignment performance. The approach taken in this study was to lump all of the inertial sensor errors and the GPS errors into equivalent biases and white noise (random walk). The filter was tuned (optimized) for a standard rate of turn flown at cruise speeds of a jet aircraft. Table VI shows various candidate suboptimal filters. The 15 state filter represents the initial lumping of error states into gyro, accelerometer, and GPS biases and random walks. The 12 state filter deletes the equivalent gyro biases and lumps their effect into the gyro random walk terms. The 9 state filter deletes accelerometer bias and creates a random walk term which feeds into INS velocity error. The random walk term can be expressed in either aircraft coordinates (the coordinates of the sensor error) or in geographic coordinates (the coordinates in which the effect of the error is felt). The 7 state filter deletes the GPS error states and expresses all GPS errors as an equivalent measurement noise.

The performance of these filter formulations is shown in figure 16. A 3.34 sec reset/iteration interval was chosen for this evaluation because the GPS receiver allocated for the subsequent feasibility demonstration operated at that cycle time. Range rate measurements preceded by a single range observation were chosen because of the faster alignment times which were achieved with this reset regime during the optimal study. The rest of the test conditions were those of Table III, so that the filters were evaluated under the conditions for which they had been optimized. In figure 16 it can be seen that gyro bias errors have no effect upon INS alignment time because their deletion causes no delay in alignment. This is because alignment proceeds so rapidly when pointing error is the azimuth alignment mechanism, that gyro error does not have time to propagate into velocity error where its effect could be observed. Since gyro bias error cannot be observed and estimated even in the optimal case, its deletion will cause no deleterious effects. The performance of the 9 state filters suggests that accelerometer errors do have time to propagate into velocity error and can affect alignment. Expressing accelerometer error as an equivalent random walk does compromise INS alignment somewhat, although the effect is seen only in that region in which tilt error estimation determines overall alignment time. Faster tilt error estimation is achieved when accelerometer random walk is expressed in aircraft coordinates because the true coupling of the sensor error into geographic coordinates is accounted for in the suboptimal formulation. The 7 state filter was also examined, but alignment time exceeded three minutes and it was concluded that GPS phase and frequency bias errors could not be discarded in an operational filter.

In view of the results shown in figure 16 the 9 state filter with accelerometer random walk error expressed in body (aircraft) coordinates was selected for further evaluation. It was felt that the degradation in system alignment for short delays in turning was an acceptable price to pay for the deletion of three more error states. The performance of this filter over a range of conditions for which it was not optimized is shown in figure 17. The solid lines define the performance envelope for optimal alignments. The limits represent the best and the worst alignment performance which can result from arbitrary combinations of turn rate and aircraft velocity sampled over the range of values used in the optimal study. The cross hatching shows the performance envelope of the 9 state suboptimal filter over the same range of possible trajectories. Except for

turns initiated within 20 seconds of the start of alignment, the suboptimal filter performs virtually as well as the optimal. This indicates that the suboptimal filter is not sensitive to excursions away from the specific values of speed and turn rate to which its performance was tuned.

Although range rate is the preferred observable, there are times when it may not be available and range will have to be used instead. Figure 18 shows the degradation in alignment time which might result. In the optimal case, where all of the INS/GPS error sources are estimated, range alignments lag range rate alignments by approximately one minute. The figure also shows that the suboptimal filter matches optimal performance reasonably well when processing range observables. In figure 19 the performance envelopes for range rate and range observables as processed by the suboptimal filter are compared. As in the optimal case range alignments on the average tend to lag range rate alignments by one minute. Suboptimal range alignments also show a higher sensitivity to variations in flight trajectory, as evidenced by the wider performance envelope. Figure 20 shows a comparison of the effect of the range and range rate observables upon the angle through which the aircraft must turn in order to accomplish in-air alignment. In the steady state the required angle for range rate alignments varies between 6° and 36°. These minimum angles can be obtained by delaying the start of the turn for at least 30 seconds after the commencement of in-air alignment. The previous figure showed that this approach would also result in the shortest alignment time as well. In the case of range alignments the angle of turn required to complete alignment is much greater. Although range rate alignments should impose no constraints upon the pilot because the required turn angles are likely to occur during normal maneuvers after take-off, range alignments quite likely will require that specific maneuvers be flown by the pilot in order to accomplish in-air alignment.

Linear acceleration provides another mechanism by which pointing error can be generated, but it affects the INS sensors differently than does centripetal acceleration. In a coordinated turn the net acceleration (centripetal acceleration and gravity) is along the normal axis of the aircraft. The suboptimal filter is tuned for turns, and this is reflected in the value of z axis accelerometer random walk error which is over four times larger than the x and y accelerometer random walks. The distribution of accelerometer errors is different under linear acceleration. More error appears in the x and y axes and less in the z axis. The effect of three values of linear acceleration upon an alignment filter tuned for turns is shown in figure 21. The filter's overly optimistic model of level axis accelerometer error has resulted in an underdamped system response. Tilt error initially decreases, then increases for a time before finally settling down to steady state. The level of tilt error at which this "hump" occurs determines whether the INS remains aligned after the first drop in tilt error (0.2g), whether the INS loses its initial alignment (0.4g), or whether alignment is not achieved at all within the first five minutes (0.8g). Figure 22 shows the time during which the RLGN is aligned for a range of linear accelerations from 0.05g to 1.0g. These results were obtained using range rate as the observable. Range alignments could not be accomplished in less than five minutes for any value of linear acceleration within this range.

CONCLUSIONS

The previous analyses have demonstrated that GPS is an accurate RF navigation reference which can be used to rapidly and accurately align a strapdown inertial navigation system in flight. A 9 state suboptimal alignment filter has been developed which closely matches optimal alignment performance over a wide range of flight conditions. The alignment filter has been shown to be insensitive to geographic position or satellite geometry; therefore, it has world-wide applicability. The insensitivity of INS/GPS alignments to initial conditions means that the technique can be used aboard carriers where accurate coarse alignment is possible or it can be used aboard other types of ships where the initialization might be less accurate. This study has shown that the primary azimuth alignment mechanism is pointing error. This mechanism may be activated by either aircraft turns or linear acceleration. The observability of pointing error is affected by speed, turn rate, and linear acceleration. The magnitudes of these parameters encountered during ordinary flight are sufficient to provide a rapid INS alignment; consequently, in-air alignment does not constrain aircraft reaction time by requiring specific flight maneuvers. It is concluded that the alignment filter described in this paper, processing a single range observable followed by range rate observables at an interval of 2-4 sec, will enhance the capability of Naval aviation to accurately navigate on a quick reaction basis. The thrust of this study has been directed toward rapid alignment and subsequent unaided inertial navigation, but there is little reason why GPS could not be used to continually update the INS as long as it were available. Even better unaided inertial navigation can be obtained when alignments are extended beyond the minimum times shown in this study.

REFERENCES

- (1) Orincon Corp., "Final Report NAVSTAR/GPS Navigation Analysis and Algorithm Development Study", 1976, OC-R-76-0564-1
- (2) Bachman, K. L., "Flight Test Results of an Advanced Development Model Ring Laser Gyro Navigator (RLGN)", presented at 31st Guidance and Control Panel Symposium, London, U.K., 14-17 Oct 1980
- (3) NAVAIRDEVCECEN Specification No. 607-DS-75-02, "Specification for the Advanced Development Model of the Ring Laser Gyro Inertial Navigation System"

TABLE I
GPS ERROR MODEL

<u>Error Source</u>	<u>Standard Deviation</u>	<u>Correlation</u>
<u>Satellite Position Error</u>		
X, Y, Z Bias	1.5 m	
<u>Satellite Clock Error</u>		
Phase Bias	0.9 m	
Frequency Bias	0.00015 m/s	
Phase Random Walk	0.00290 m/ $\sqrt{\text{sec}}$	
<u>Propagation Error</u>		
Atmospheric Delay Markov	2.4 m	30 min
Multi-Path Markov	2.4 m	20 sec
<u>Receiver Clock Error</u>		
Phase Bias	304.8 m	
Frequency Bias	0.3 m/s	
Frequency Markov	3.0 m/s	
Phase Random Walk	0.3 m/ $\sqrt{\text{sec}}$	2 hr
<u>Measurement Error Noise</u>		
Range	1.5 m	
Range Rate	0.015 m/s	

TABLE II
RLGN ERROR MODEL

<u>Error Source</u>	<u>Standard Deviation</u>	<u>Correlation</u>
<u>Gyro Error</u>		
Bias	0.157 mrad/hr	
Random Walk	0.035 mrad/ $\sqrt{\text{hr}}$	
Scale Factor	5.0 ppm	
Input Axis Misalignment	0.024 mrad	
Turn-on Transient	0.122 mrad/hr	15 min
<u>Accelerometer Error</u>		
Bias	0.568 mm/s ²	
Scale Factor	200.0 ppm	
Input Axis Misalignment	0.024 mrad	
Vertical Deflection	0.024 mrad	46 km

TABLE III
STANDARD TEST CONDITIONS

<u>Initial INS Errors (1σ)</u>	
North, East Position Error	1.8 km
North, East Velocity Error	0.3 m/s
North, East Tilt Error	0.52 mrad
Azimuth Error	0.03 rad
<u>Flight Profile</u>	
Velocity	180 m/s
Heading	0°
Linear Acceleration	0 m/s ²
Turn Rate	3°/sec ccw
Time Before Turn	0 sec
<u>Geometry</u>	
Latitude	40°
Satellite GDOP	MEDIAN
<u>Kalman Resets</u>	
Reset/Iteration Interval	1.8 sec
Observable	One range, then range rate

TABLE IV
ALIGNMENT EVALUATION CRITERIA

<u>Characteristics</u>	<u>Requirement</u>
<u>Navigation Performance</u>	
Heading Error	0.87 mrad RMS + 0.35 mrad/hr 1σ
Roll and Pitch Error	0.73 mrad RMS
Position Error Rate	1.9 km/hr CPE rate
X, Y, Z Velocity Error	0.9 m/s RMS
Reaction Time	3-5 min
<u>Alignment Performance (1σ)</u>	
North, East Position Error	< 0.2 km
North, East Velocity Error	< 0.03 m/s
North, East Tilt Error	0.097 mrad
Azimuth Error	0.87 mrad

TABLE V
MISCELLANEOUS INS ALIGNMENT SENSITIVITIES

<u>Initial INS Errors (1σ)</u>	<u>Standard</u>	<u>Poor Coarse Align</u>	<u>High Latitude</u>	<u>Bad GDOP</u>
North, East Position Error (km)	1.8	9.3	1.8	1.8
North, East Velocity Error (m/ σ)	0.3	10.3	0.3	0.3
North, East Tilt Error (mrad)	0.52	34.9	0.52	0.52
Azimuth Error (rad)	0.03	0.09	0.03	0.03
<u>Geometry</u>				
Latitude (deg)	40	40	87	40
Satellite GDOP	MEDIAN	MEDIAN	MEDIAN	90th PCT
<u>Parameter</u>				
In-Air Align Time (sec)	36.0	37.8	36.0	37.8
<u>INS Errors At End of Alignment (1σ)</u>				
North Position Error (km)	0.002	0.002	0.002	0.002
East Position Error (km)	0.002	0.002	0.002	0.003
North Velocity Error (m/s)	0.008	0.008	0.008	0.008
East Velocity Error (m/s)	0.005	0.005	0.006	0.009
North Tilt Error (mrad)	0.096	0.090	0.096	0.091
East Tilt Error (mrad)	0.076	0.067	0.076	0.068
Azimuth Error (mrad)	0.129	0.120	0.131	0.115

TABLE VI
CANDIDATE RLGN/GPS SUBOPTIMAL FILTERS

<u>Characteristics</u>	<u>Initial Conditions (1σ)</u>				
<u>Error States</u>	<u>15</u>	<u>12</u>	<u>9</u>	<u>9</u>	<u>7</u>
1,2. N, E Position Error (km)	1.9	1.9	1.9	1.9	1.9
3,4. N, E Velocity Error (m/s)	0.3	0.3	0.3	0.3	0.3
5,6. N, E Tilt Error (mrad)	0.52	0.52	0.52	0.52	0.52
7. Azimuth Error (rad)	0.03	0.03	0.03	0.03	0.03
8. GPS Range Bias Error (m)	304.8	304.8	304.8	304.8	-
9. GPS Range Rate Bias Error (m/s)	3.0	3.0	3.0	3.0	-
10,11. X, Y Acc. Bias Error (mm/s^2)	0.655	0.655	-	-	-
12. Z Acc. Bias Error (mm/s^2)	2.78	2.78	-	-	-
13,14,					
15. X, Y, Z Gyro Bias Error (mrad/hr)	0.157	-	-	-	-
X, Y Acc. Random Walk ($\text{m/s}/\sqrt{\text{hr}}$)	-	-	0.15	-	0.15
Z Acc. Random Walk ($\text{m/s}/\sqrt{\text{hr}}$)	-	-	0.67	-	0.67
N, E Acc. Random Walk ($\text{m/s}/\sqrt{\text{hr}}$)	-	-	-	0.25	-
X, Y, Z Gyro Random Walk (mrad/ $\sqrt{\text{hr}}$)	0.035	0.035	0.035	0.035	0.035
GPS Range Random Walk ($\text{m}/\sqrt{\text{sec}}$)	0.905	0.905	0.905	0.905	-
GPS Range Rate Random Walk ($\text{m/s}/\sqrt{\text{sec}}$)	0.051	0.051	0.051	0.051	-
<u>Kalman Resets</u>					
GPS Range Measurement Noise (m)	0.9	0.9	0.9	0.9	0.9
GPS Range Rate Measurement Noise (m/s)	0.015	0.015	0.015	0.015	0.015
Reset/Iteration Interval (sec)	3.84	3.84	3.84	3.84	3.84
Observable	Range or Range Rate for all filters				

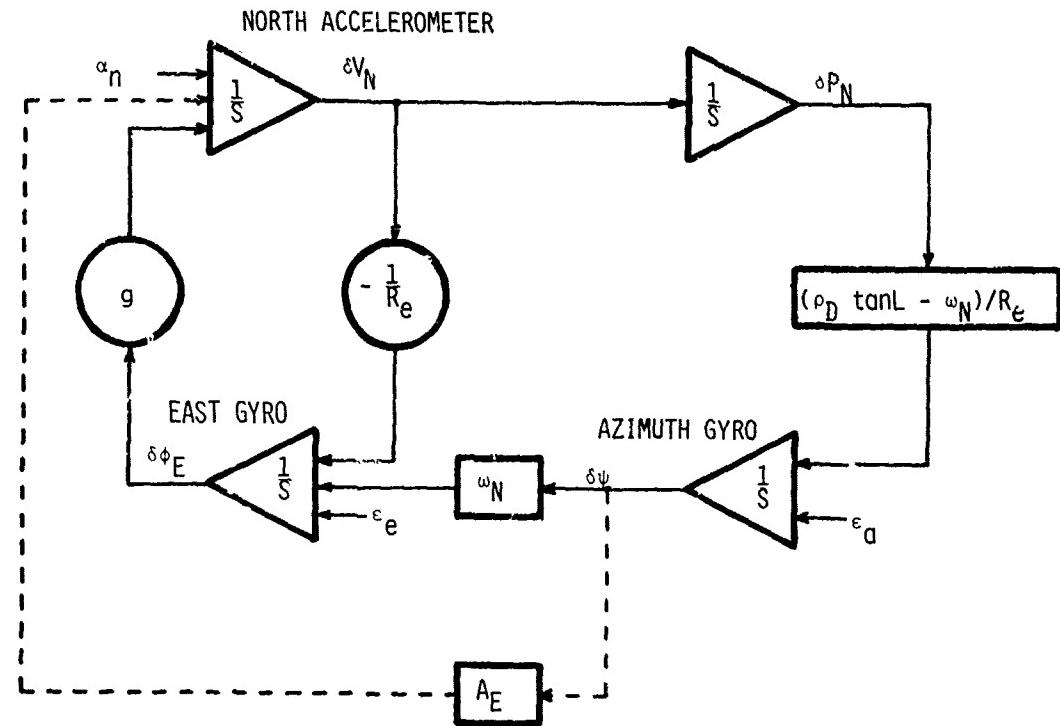


FIGURE 1. SIMPLIFIED INS BLOCK DIAGRAM

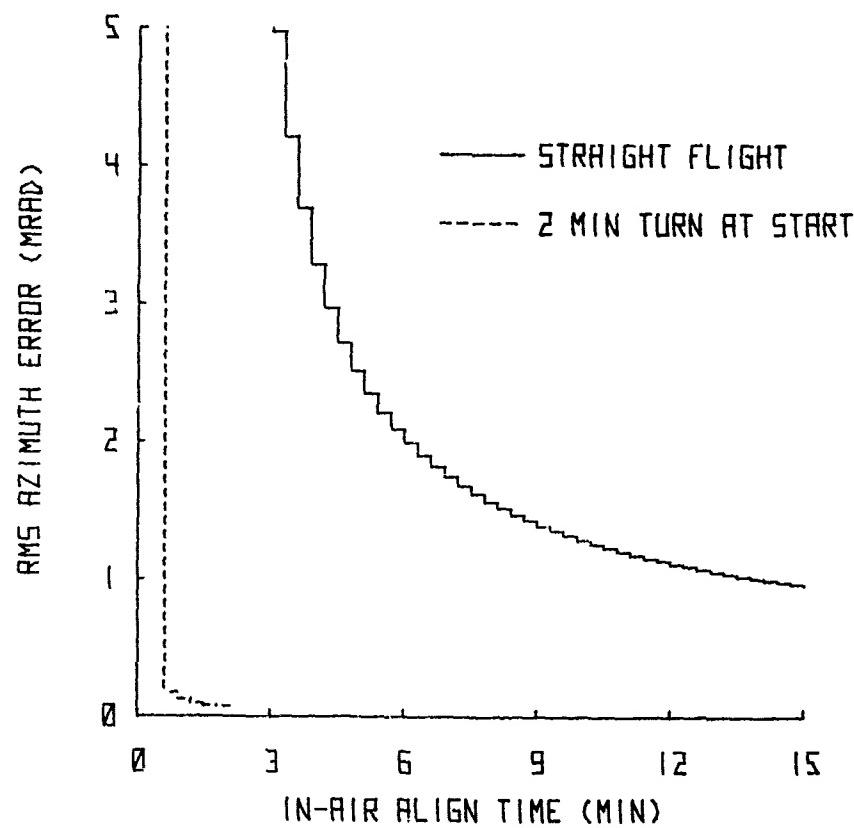


FIGURE 2. EFFECT OF TURNS ON INS AZIMUTH ALIGNMENT

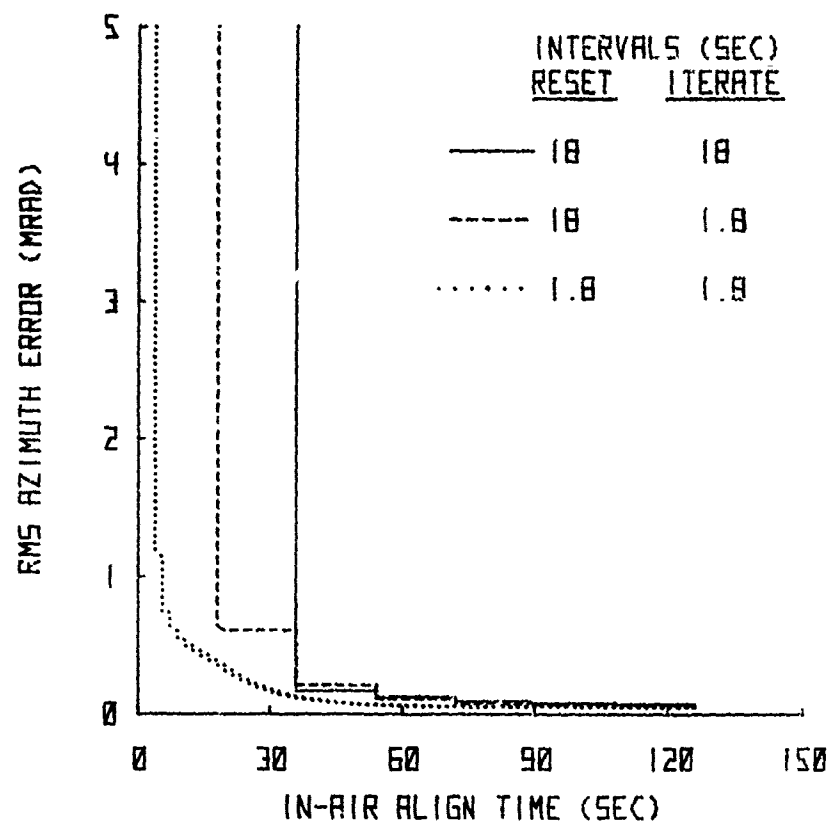


FIGURE 3. EFFECT OF RESET/ITERATION INTERVAL ON INS AZIMUTH ALIGNMENT

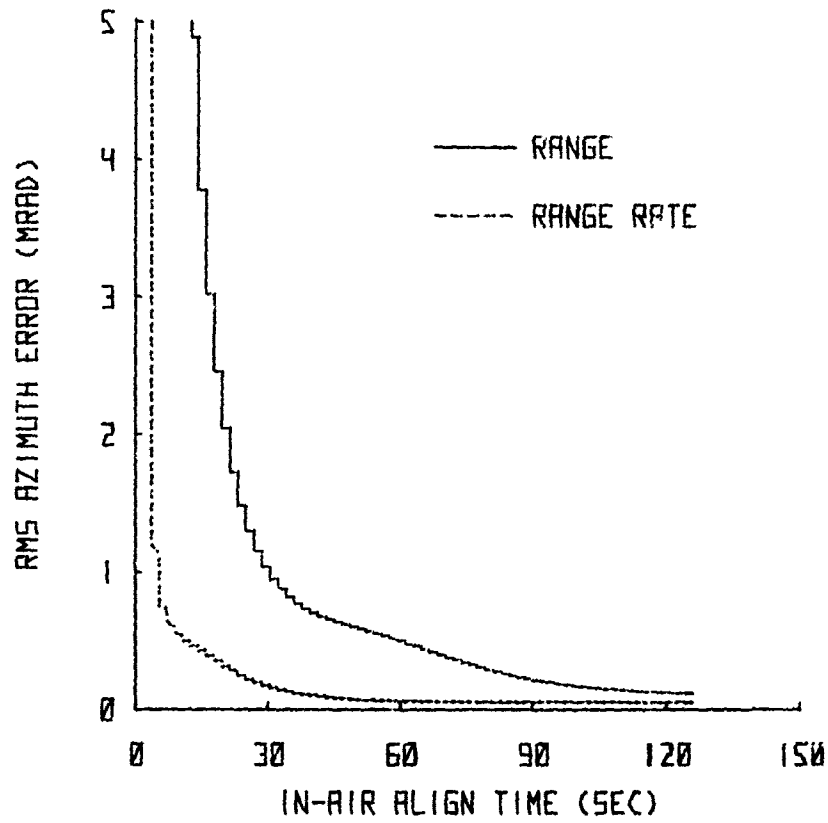


FIGURE 4. EFFECT OF OBSERVABLE ON INS AZIMUTH ALIGNMENT

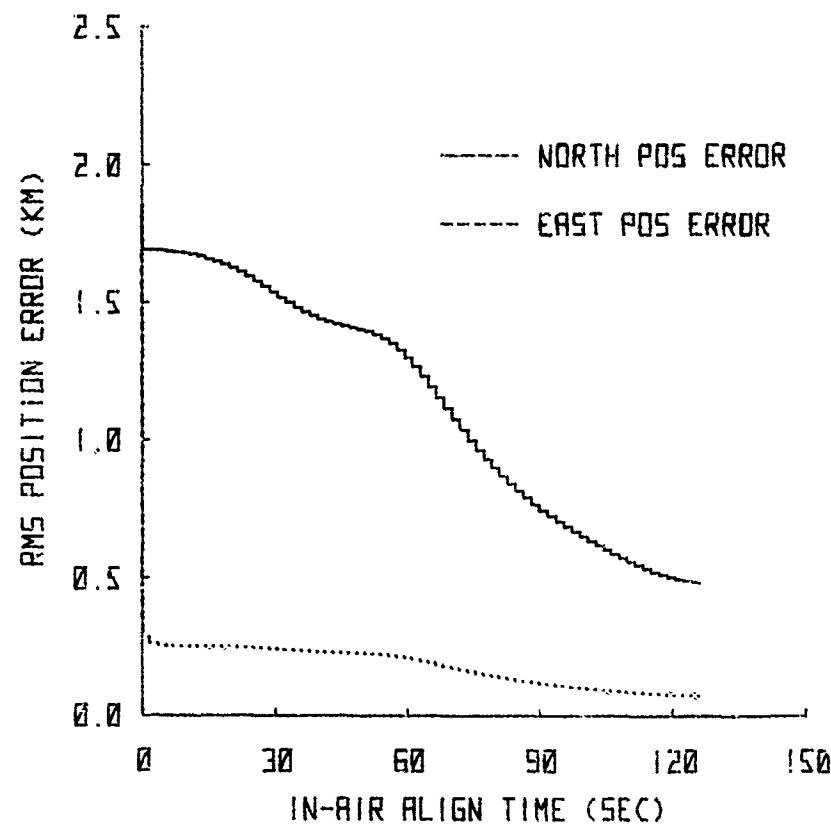


FIGURE 5. EFFECT OF RANGE RATE OBSERVABLE ON INS POSITION ERROR ESTIMATION

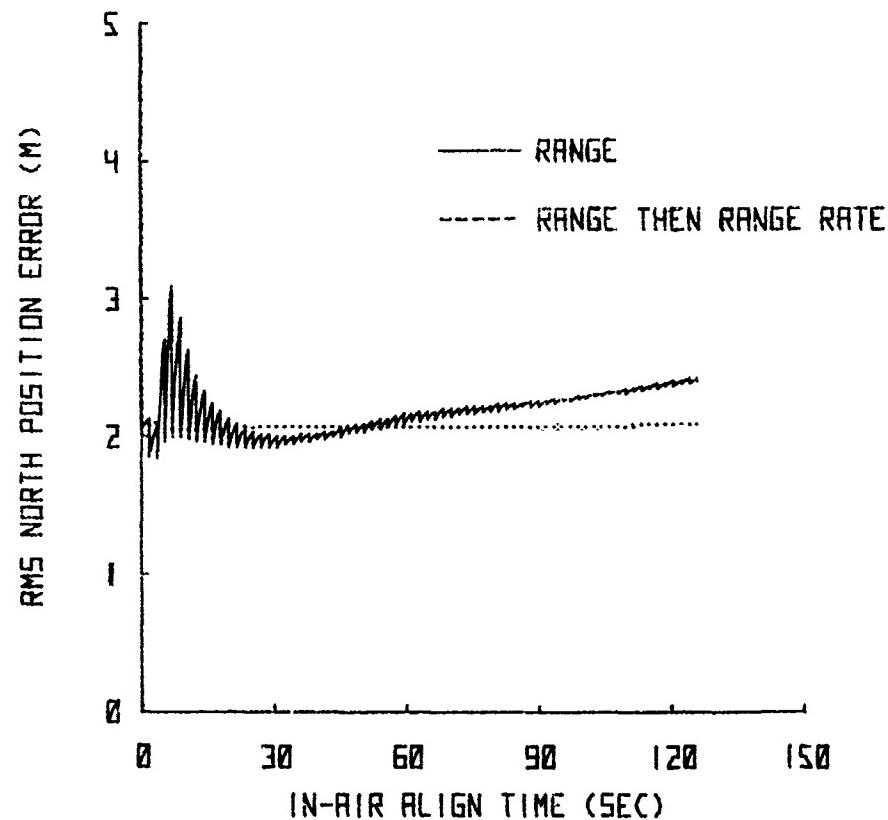


FIGURE 6. EFFECT OF COMBINATION OF RANGE AND RANGE RATE OBSERVABLES ON INS POSITION ERROR ESTIMATION

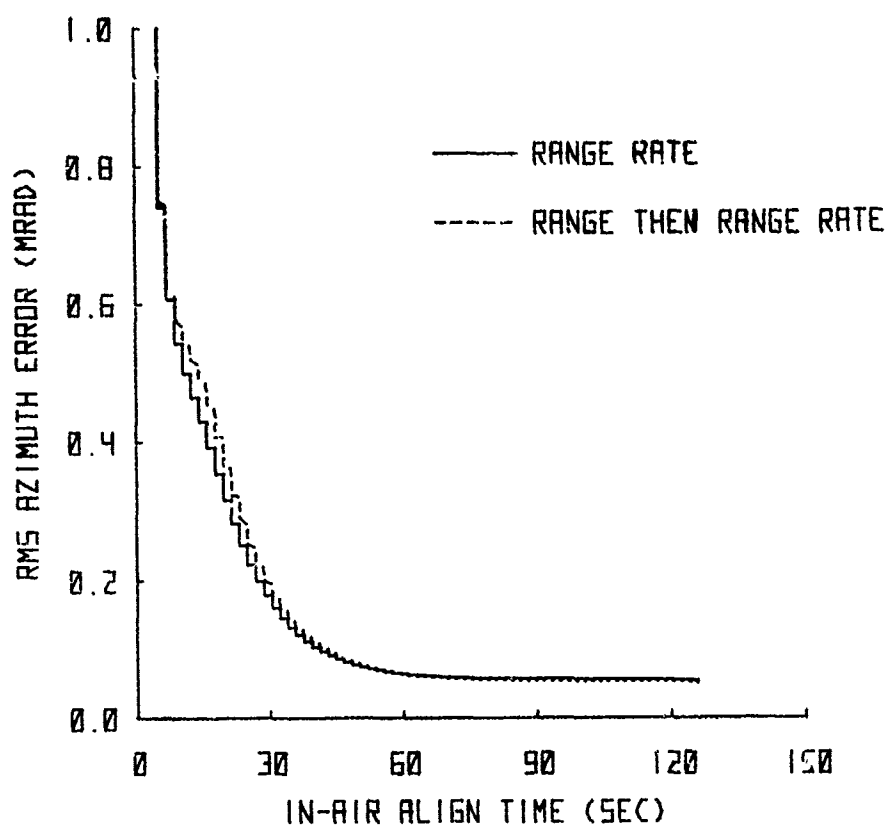


FIGURE 7. EFFECT OF COMBINATION OF RANGE AND RANGE RATE OBSERVABLES ON INS AZIMUTH ALIGNMENT

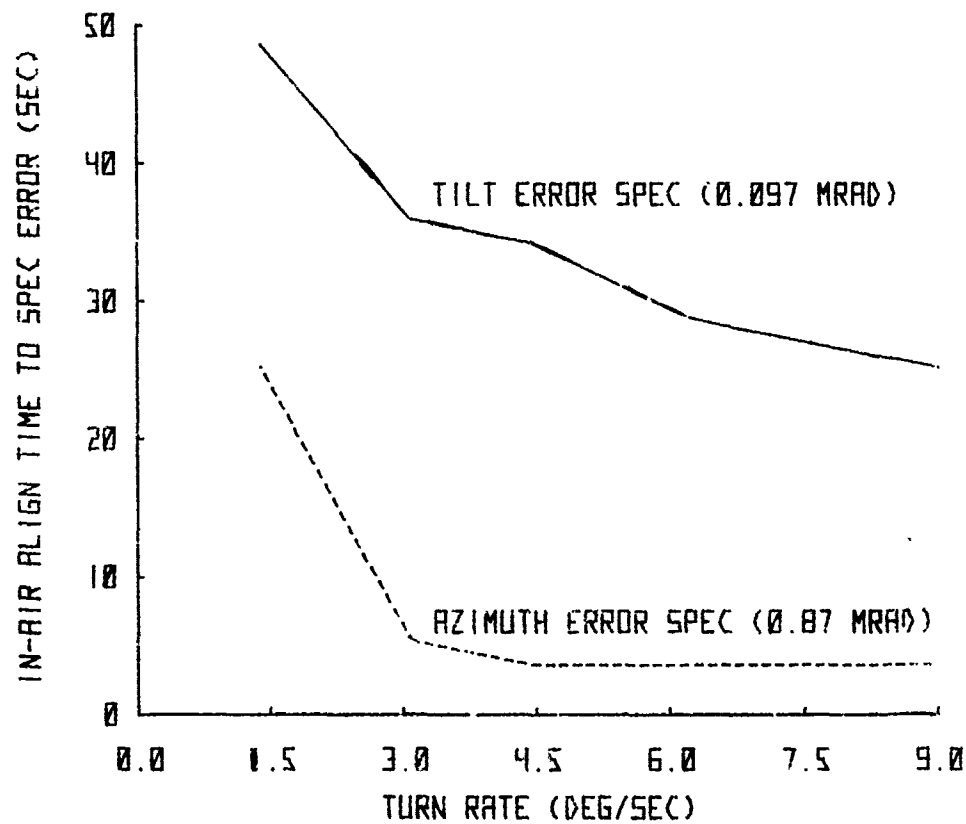


FIGURE 8. SENSITIVITY OF INS ALIGNMENT PARAMETERS TO TURN RATE

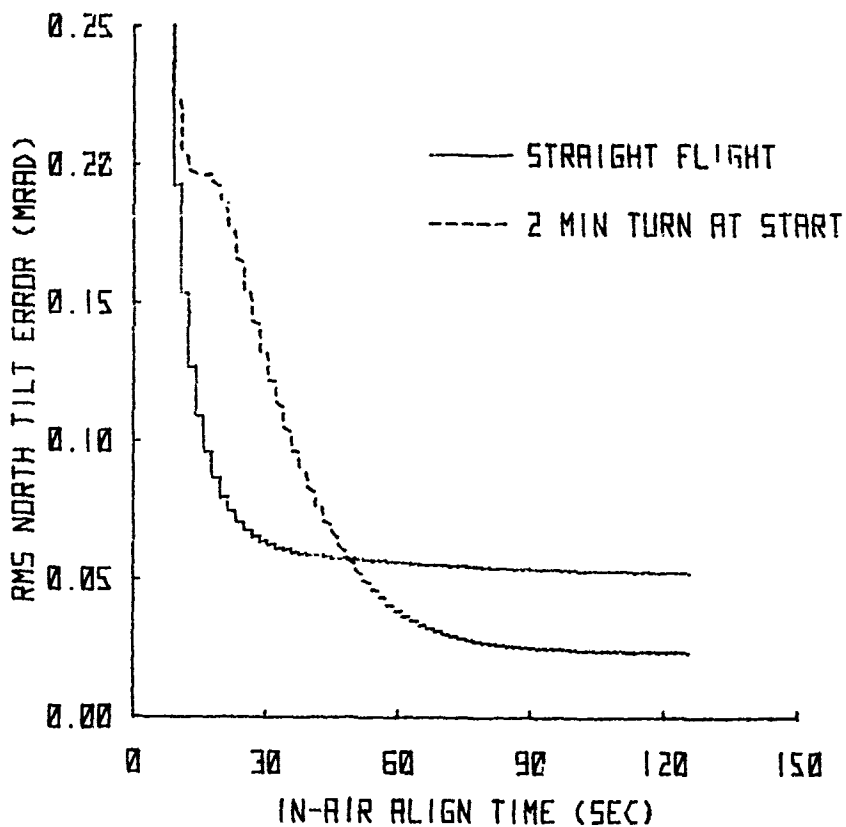


FIGURE 9. EFFECT OF TURNS ON INS VERTICAL ALIGNMENT

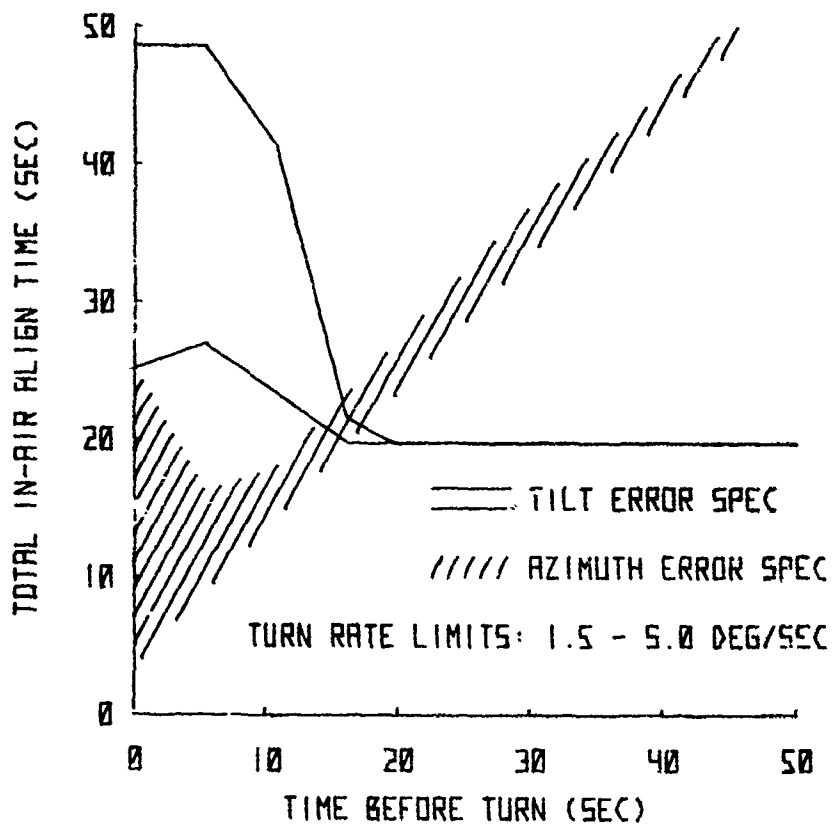


FIGURE 10. SENSITIVITY OF INS ALIGNMENT PARAMETERS TO TURN DELAY

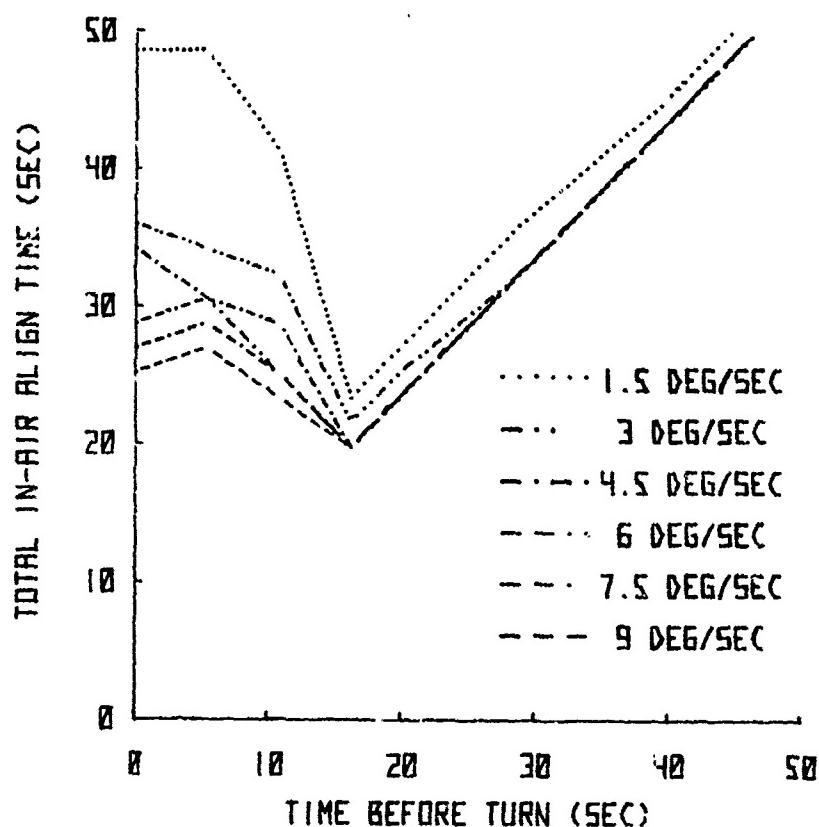


FIGURE 11. EFFECT OF TURNS ON INS ALIGNMENT

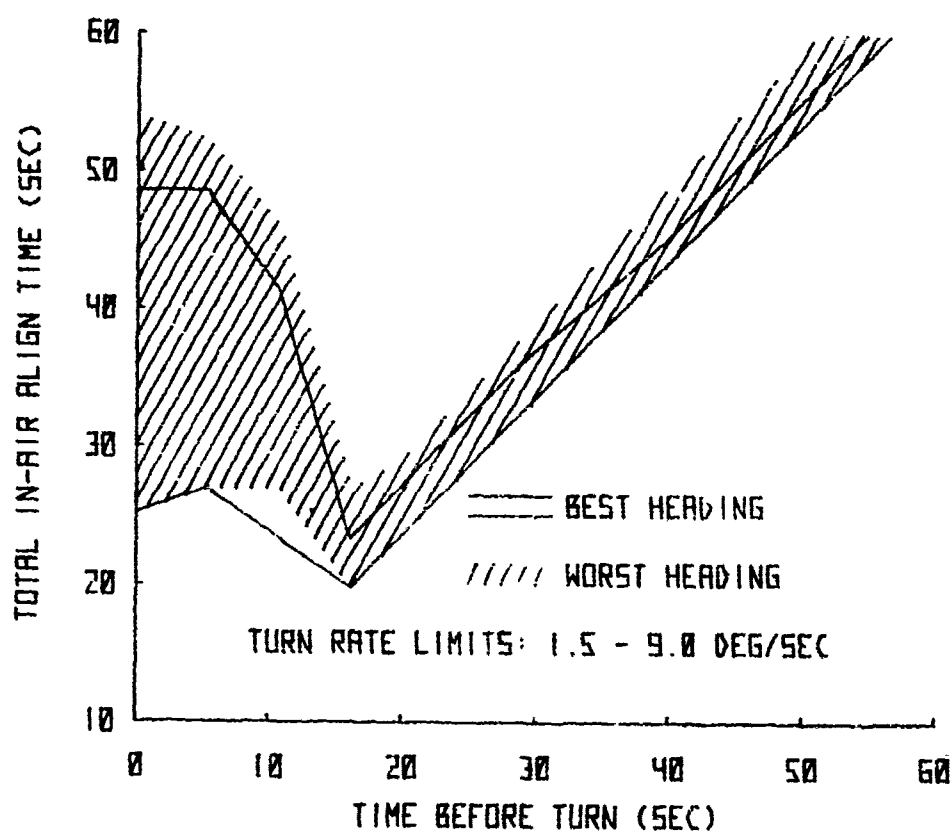


FIGURE 12. EFFECT OF HEADING ON INS ALIGNMENT

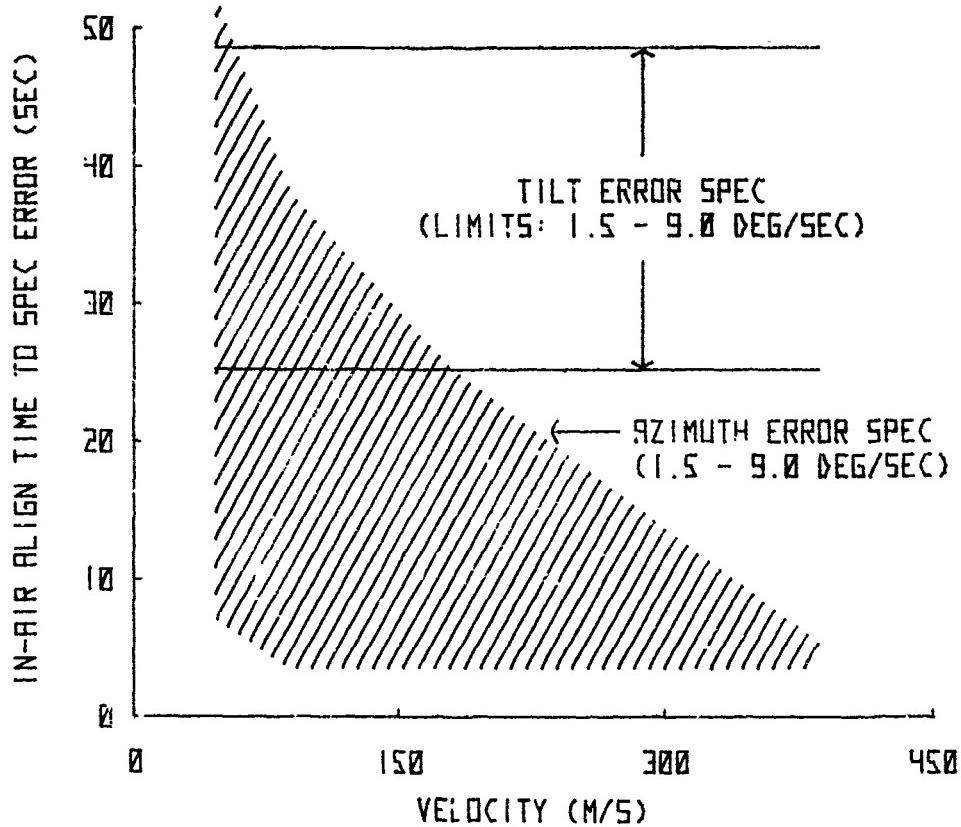


FIGURE 13. SENSITIVITY OF INS ALIGNMENT PARAMETERS TO VELOCITY

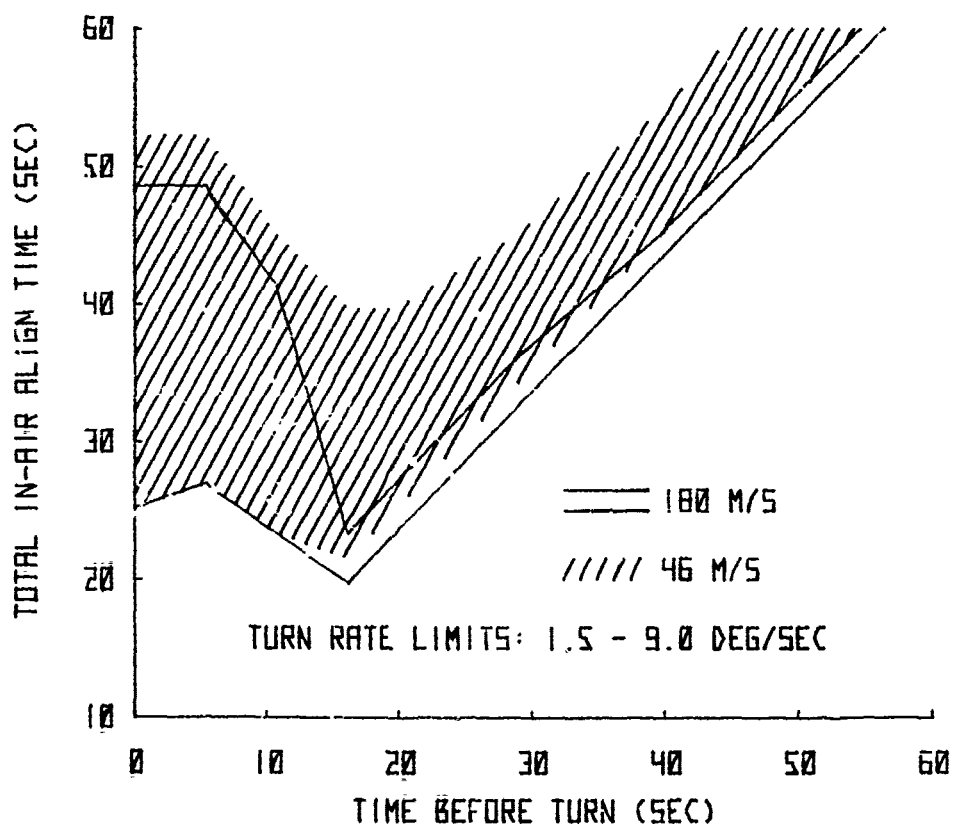


FIGURE 14. EFFECT OF VELOCITY ON INS ALIGNMENT

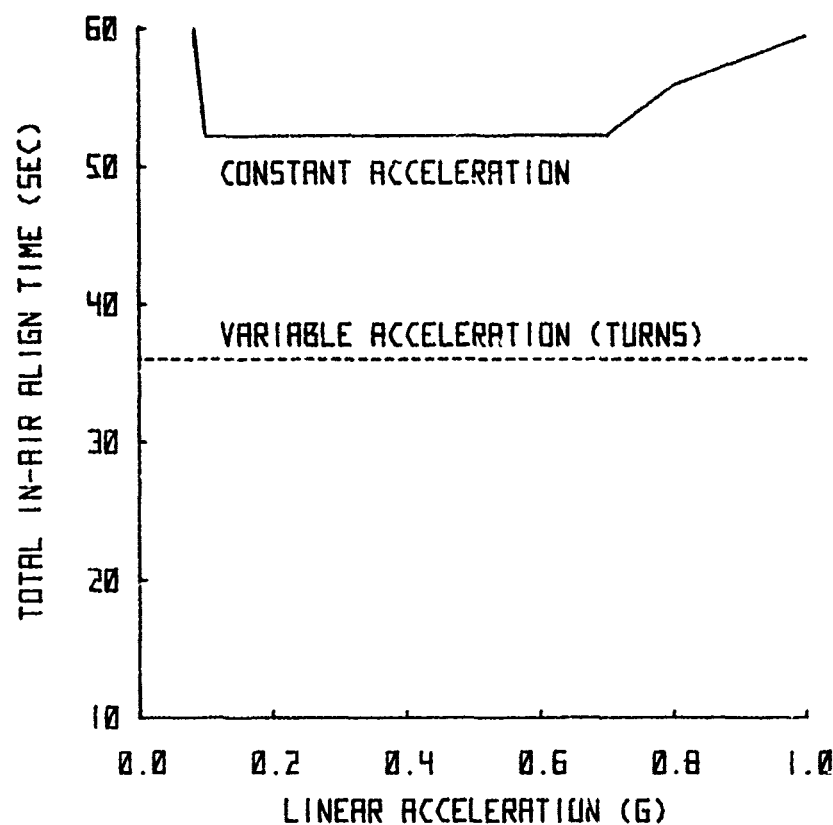


FIGURE 15. EFFECT OF LINEAR ACCELERATION ON INS ALIGNMENT

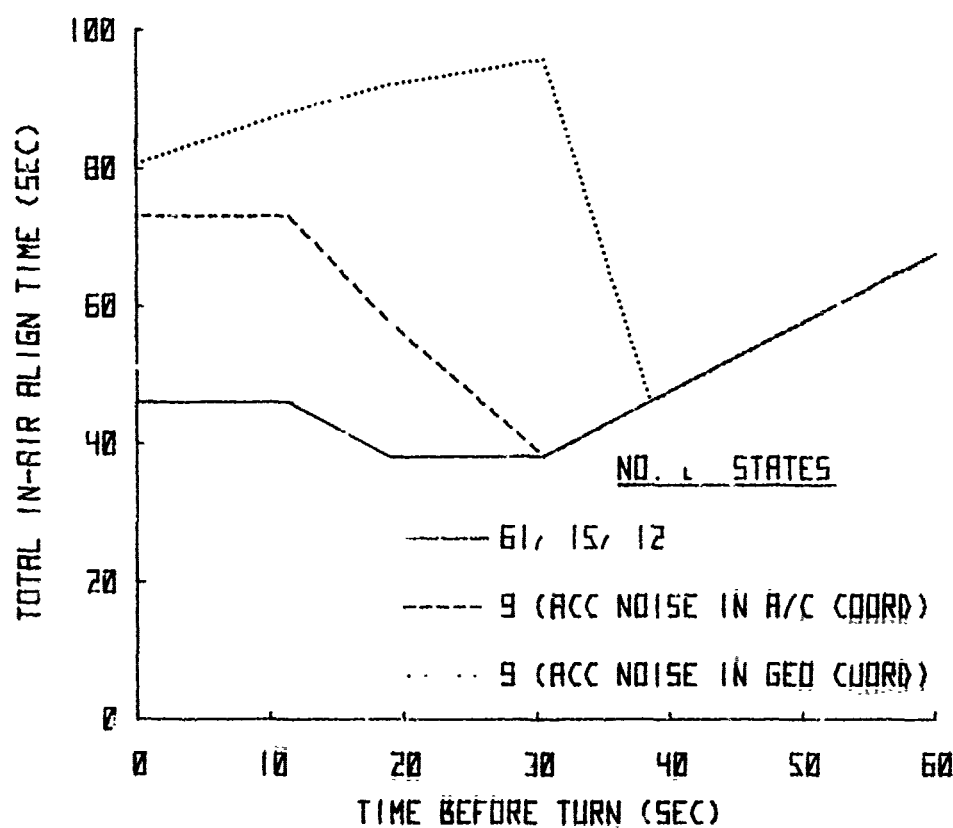


FIGURE 16. EFFECT OF SUBOPTIMAL FILTER STATES ON INS ALIGNMENT

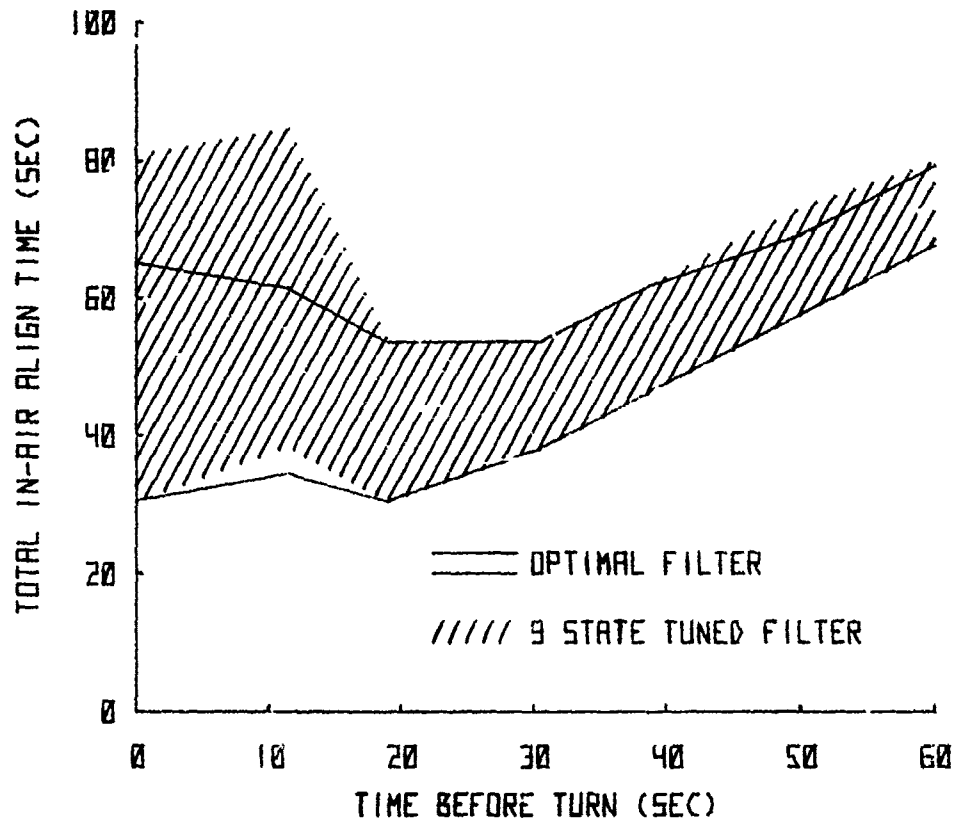


FIGURE 17. COMPARISON OF OPTIMAL AND SUBOPTIMAL RANGE RATE INS ALIGNMENTS

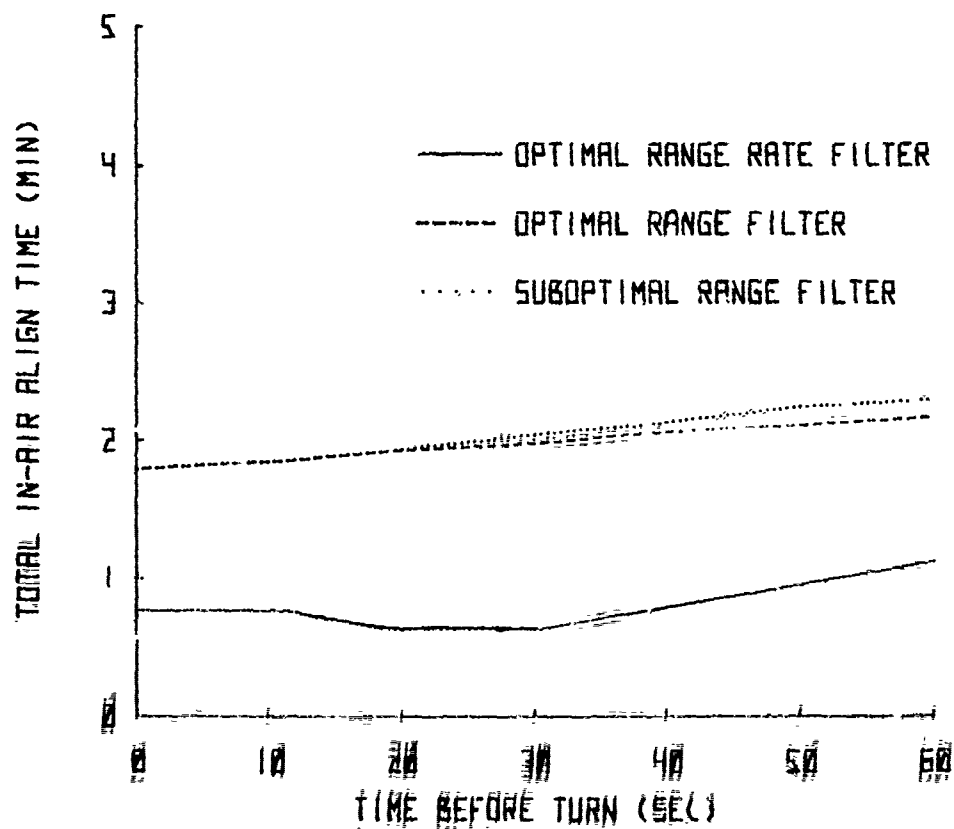


FIGURE 18. EFFECT OF OBSERVABLE ON OPTIMAL INS ALIGNMENT

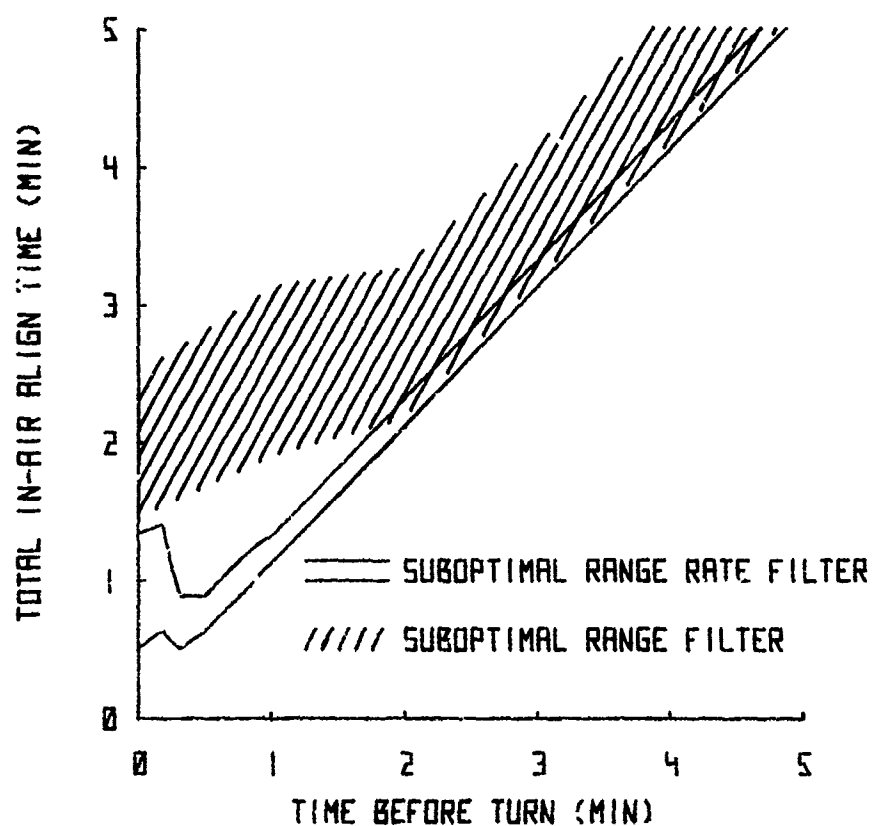


FIGURE 19. EFFECT OF OBSERVABLE ON SUBOPTIMAL INS ALIGNMENT

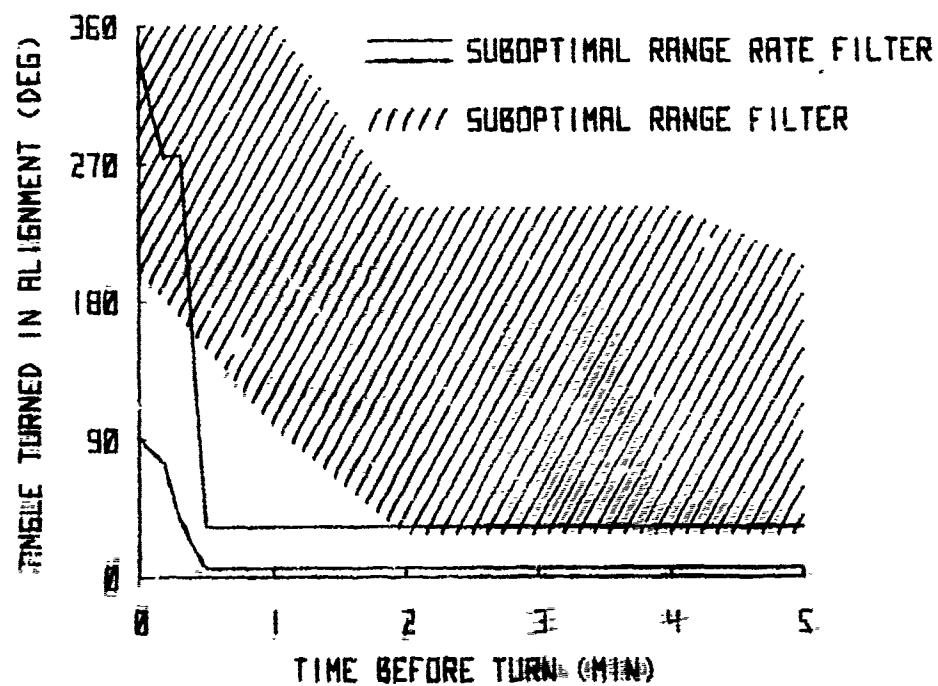


FIGURE 20. EFFECT OF OBSERVABLE ON ANGLE TURNED DURING SUBOPTIMAL INS ALIGNMENT

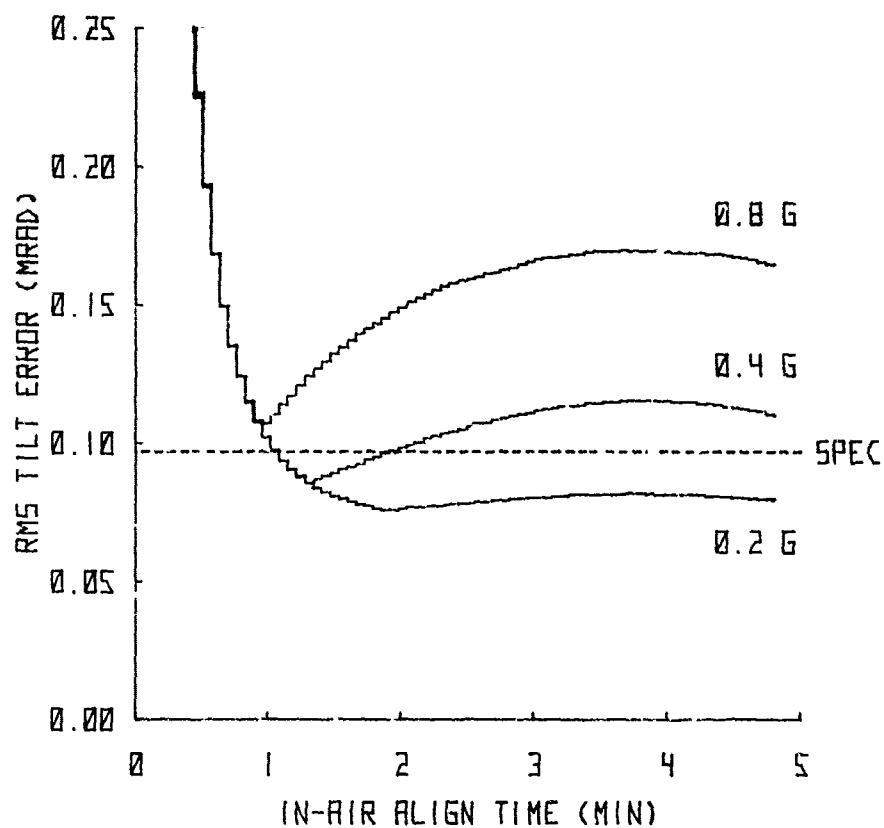


FIGURE 21. EFFECT OF LINEAR ACCELERATION ON SUBOPTIMAL INS VERTICAL ALIGNMENT

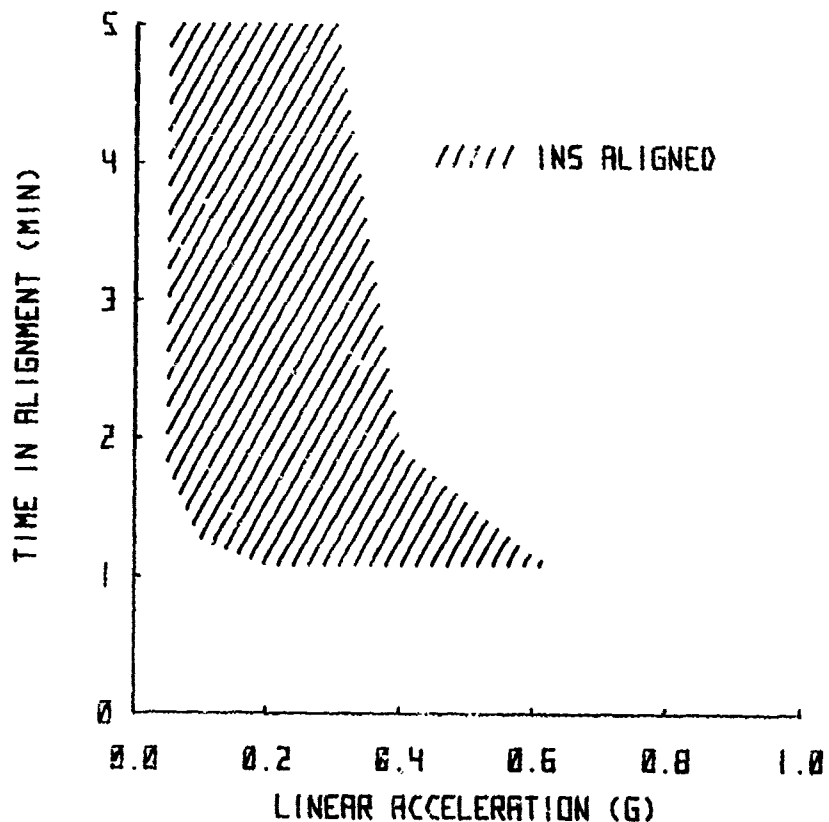


FIGURE 22. EFFECT OF LINEAR ACCELERATION ON SUBOPTIMAL INS ALIGNMENT

NEW NAVY PROGRAMS FOR DEVELOPMENT OF INTEGRATED INERTIAL SENSORS

Charles R. Abrams
 Manager, Advanced Flight Control Systems
 Robert J. Skoyle
 Manager, Advanced Navigation Systems
 U. S. Naval Air Development Center
 Warminster, PA 18974 USA

SUMMARY

This paper describes new concepts in sensor redundancy and subsystem integration being developed by the U.S. Navy for navigation/flight control functions and other using subsystems under the sponsorship of the Naval Air Systems Command in Washington, DC. The major emphasis is on a reduction in the number of required sensors, by the use of skewed configurations and functional integration. Substantial improvements in reliability and maintainability are anticipated from both the reduction in sensor complement and the introduction of ring laser gyros. Survivability is enhanced by the dispersion of redundant units.

Major issues discussed within this paper include the data management software for skewed rate sensors and accelerometers that have been developed, validated in the laboratory, and verified in flight tests. Status of planned system hardware, software, and flight testing for an Advanced Development Model (ADM) of an Integrated Inertial Sensor Assembly (IISA) to supply inertial data for flight control, weapon delivery and navigation are also presented.

INTRODUCTION

The evaluation of redundant flight control systems as typified by current fly-by-wire systems has been the impetus for new approaches to sensor redundancy. In addition, the number of subsystems that require inertial data, both redundant and non-redundant, has resulted in a proliferation of inertial sensors that tend to contribute significantly to the weight and cost of the aircraft.

Recent advances in solid state rate sensors, strapdown and skewing algorithms, Redundancy Data Management System (RDMS) concepts, and high speed microprocessors have created the potential for integration of the sensors and software into a set of strapdown units with the capability of providing redundant inertial data for navigation, flight control, weapon delivery, and display functions. The use of two strapdown Weapon Replaceable Assemblies (WRAs) incorporating skewed rate sensors and accelerometers will have the capability of providing the two fail-operational performance required by current and future high performance aircraft. The implementation of an Integrated Inertial Sensor Assembly will act as a surrogate for the separate dedicated sensors used in current aircraft, and will greatly reduce the sensor complement and improve reliability.

APPLICATIONS

I. The Advanced Skewed Sensory Electronic Triad (ASSET) Concept

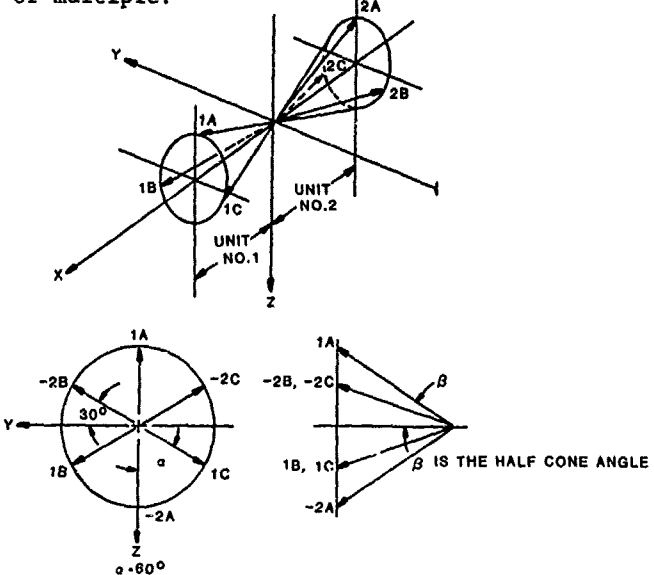
In order to satisfy redundancy and reliability requirements for flight control, multiple rate sensors with the same maximum rate capability have historically been oriented with their input axes coaxial with one another. An alternate approach takes advantage of vector sensor configuration rules which specify that three single-axis rate sensors could have their input axes skewed in any orientation with respect to each other or to the vehicle axes, to completely specify the angular velocity of the vehicle. The only restriction is that the input axes do not lie in the same plane. Prototype versions of this advanced rate sensor system have been configured with six sensors skewed with respect to each other so that if any three fail, none of the remaining input axes would be co-planar. One such prototype version has been developed, tested and flown successfully. This prototype system, known as ASSET, consists of a unique array of angular rate sensor and an associated RDMS.

The ASSET system provides a cost-effective alternative to the conventional redundant sensor approach by utilizing six rate sensors to provide two fail-operational capability, whereas the conventional, in-line approach utilizes twelve sensors for a quad-redundant system (e.g., F-18). All ASSET sensors are identical, while the in-line approach typically uses sensors of different range capabilities to measure roll, pitch, and yaw rates. The ASSET system utilizes a dispersed sensor array and is therefore a survivable configuration, whereas the conventional approach packages the four coaxial sensors within one box.

A. Redundancy Data Management System

A digital RDMS was developed for use with six rate sensors arranged in a skewed Cone Configuration as shown in Figure 1. The RDMS was primarily designed for use with a Digital Fly-By-Wire (DFBW) system for advanced fighter/attack aircraft. However, the software program in its entirety, or the concepts incorporated in the software, can also be applied to other sensory systems of an aircraft. Specifically, the system is designed

to provide a satisfactory estimate of the angular rates in the presence of sensor failures, either single or multiple.



NOTE: If the sensor axes in Unit No. 2 are viewed in a negative direction, the conic orientation is obvious.

Figure 1. Cone Configuration

1. Types of Failures

Temporary (Transient) Failures

A transient failure is defined as a sensor output that momentarily exceeds a value that could possibly be produced by aircraft motion.

Permanent Failures

A permanent failure is defined as an anomaly of the sensor output not expected under normal service conditions. Permanent failure anomalies include one or more of the following characteristics:

- a. Continuous sensor output bias, with no input, including hardover failures.
- b. Random short-term excursions (for several computational cycles).
- c. Periodic long-term, large-amplitude errors.
- d. Dynamic response errors.
- e. Scale factor errors.
- f. Failures to zero.

2. Subroutines

The system is designed to provide satisfactory rate information with noise superimposed on the sensors' output signals. In addition, the RDMS is designed to include a Filter Routine (FR) that could be used to satisfactorily diminish the effect of a slowly changing sensor bias on the performance of a fighter/attack aircraft. The FR can be bypassed if the RDMS is used with a set of sensors whose bias does not vary as a function of environmental change, or time.

A sensor Self-Test Routine (STR) is also included so that dynamic failures can be detected during ground check-out of the sensor system. When called, the STR compares the sensor outputs to predetermined limits which define a failed sensor.

An Executive Program controls the sequence in which the major subroutines are called as shown in the flow chart given in Figure 2. First the Executive Program is initialized. It then calls and stores the latest outputs from each of the six sensors for later use by the various subroutines. After this operation, the Executive Program calls up the Self-Test Routine, the Filter Routine, the Transient Failure Removal Routine (TFRR), the Sensor Voting Computational Routine (SVCR), and the Failure Isolation Computational Routine (FICR) as required. The following sections briefly describe the functions of the system.

The FR, which uses the sensor outputs if STR is not called, is mechanized to minimize the error caused by environmentally induced, or time dependent, bias change.

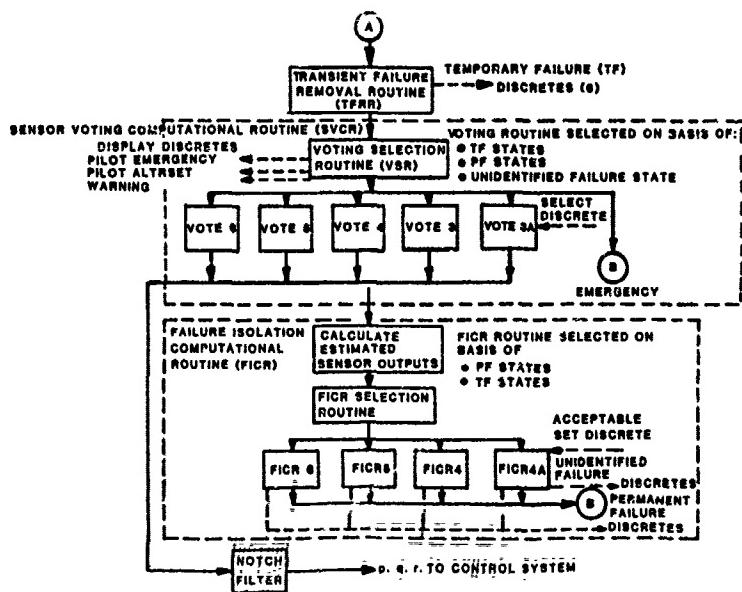


Figure 2. Redundancy Data Management System

In operation it essentially washes out the output of the sensor when the pilot's command to the control stick is zero (in-detent). The time constant of the washout is adjusted to a value consistent with acceptable aircraft handling qualities. When a command is applied (control stick out-of-detent), the sensor output is the sum of the last value of the output of the rate sensor when the command was applied, the change from the time the command was applied, and the predicted change due to continued environmental disturbances.

After filtering, the TFRR, which falls in the class of a passive in-line model monitor, places the sensor in a failed category if the latest value of a sensor output is unreasonable compared to the previous value of the estimate of the angular rate along the sensor axis. When a sensor is in the TF category, its output cannot be used in subsequent calculations for one iteration. At the completion of the TFRR operation, the filtered sensor output data is used by the SVCR and the FICR if four or more sensors have not failed.

The SVCR and TFRR accept information from the FICR which indicates that a permanent failure has occurred. When a sensor is placed in this category its output cannot be used to determine rate for all future iterations. The SVCR provides angular rate signals along roll, pitch, and yaw axes with the structural vibrations superimposed. With each iteration the SVCR detects the poorest performing sensor, inhibits the use of its output signal, and then resolves the information obtained from the remaining sensors, to provide full, pitch, and yaw signals. Isolation of a failed sensor takes place within the FICR routine and is indicated by the generation of a permanent failure discrete. Permanent failures are determined only after a number of iterations are complete. With this mechanization, the control system can be provided, at a high speed, with data free of transients and failed sensor outputs, and the FICR can function at a slower speed. The slow speed, non-time critical operation of the FICR need not be performed every iteration. In addition, improvement is gained in the reliability of sensor failure isolation because several iterations can be used to identify a failure, thus minimizing the number of false alarms and missed failures. If programmed correctly, the SVCR performs the recovery portion of coverage with 100% efficiency.

3. Failure Thresholds

Many production analog comparison monitoring systems are implemented so that the difference between the output of coaxial sensors is compared to a threshold. This threshold is often selected as the product of the allowable scale factor discrepancy (tracking error) and the maximum output range of sensors. When the difference exceeds the threshold, both sensors are then disengaged from the control system. Unfortunately, with a typical tracking error of 4% and a maximum range of 250°/sec, the threshold is set as high as 10°/sec. In addition, for numerous systems the threshold is adjusted to much higher levels to eliminate nuisance trips (false alarms) that are generated by momentary high level transient signals on the sensor output. For DFBW applications, where safety, mission completion, and accuracy are of paramount concern, an elevated value of threshold increases the probability of the system NOT detecting a failure and then using this failed sensor to generate a dangerous control output.

The failure thresholds must be adjusted properly so that the RDMS detects and isolates failures satisfactorily, and so that false alarms don't degrade the reliability of the system. This is one of the most critical problems to be overcome in applying a RDMS to DFBW systems. As failure thresholds are reduced, the probability of isolating failures is increased; however, false alarm and false isolation probability is increased and the reliability of the system is diminished. As thresholds are increased,

low magnitude failures are not isolated and the system performance will ultimately degrade. At best, adjusting the thresholds requires a compromise between these parameters.

Two features were incorporated into the RDMS to rectify these problems. First, the TFRR was introduced to adequately deal with the momentary outages which have historically caused nuisance disconnects. Second, within the SVCR and the FICR, two paths were incorporated for detecting and isolating failures. One was primarily designed to detect and isolate bias failures and the other was primarily designed to detect and isolate scale factor failures and failures to zero. The characteristics of these two paths are summarized in Table 1. As presently adjusted, when the Estimated Sensor Output (ESO) is greater than $5^\circ/\text{sec}$, the RDMS estimates the Scale Factor Error (SFE). Below $5^\circ/\text{sec}$, bias errors are estimated. This $5^\circ/\text{sec}$ crossover was selected to both minimize errors in the estimate of scale factor and in the estimate of bias, when rates were more or less than the crossover respectively.

Table 1. Two Paths of Failure Detection Within FICR

FAILURE DETECTION	'BIAS' PATH		'SCALE FACTOR' PATH	
	For ESO< $5^\circ/\text{SEC}$	For ESO> $5^\circ/\text{SEC}$	For ESO> $5^\circ/\text{SEC}$	For ESO< $5^\circ/\text{SEC}$
Form	Cross-Channel Comparison Monitoring		Cross-Voter Comparison Monitoring	
Type	1. Sensor Output Bias 2. Periodic Long-Term Large-Amplitude Errors 3. Hardover Failures 4. Failures to Zero		1. Scale Factor 2. Dynamic Response 3. Hardover Failures 4. Failures to Zero	

4. Comparison Monitoring

For the coaxial sensor configuration, as used in the F-18, the total number of sensors needed for n fail-operational capability with comparison monitoring is $3(n + 2)$. Specifically, the two fail-operational requirement imposed on DFBW rate sensor systems requires the installation of twelve rate sensors.

For skewed sensor systems, the total number of sensors required for n fail-operational capability, with comparison monitoring, is $(n + 4)$. Specifically, a two fail-operational requirement requires the installation of only six rate sensors for the generation of pitch, roll, and yaw information. Table 2 summarizes the requirements for both coaxial and skewed systems.

Table 2. Sensor Requirements for Coaxial and Skewed Systems (Comparison Monitoring)

OPERATIONAL REQUIREMENT	TOTAL NUMBER OF COAXIAL SENSORS REQUIRED	NO. OF TOLERABLE FAILURES		TOTAL NUMBER OF SKEWED SENSORS REQUIRED
		COAXIAL	SKEWED	
1 Fail-OP	9	1 per axis	any 1	5
2 Fail-OP	12	2 per axis	any 2	6
3 Fail-OP	15	3 per axis	any 3	7

NOTE: Assume Coverage = 1.0

Comparison monitoring can be performed prior to flight as well as during in-flight periods without disturbing the operation of the control system. During pre-flight checkout, certain failure modes such as scale factor failures and failures-to-zero are not detectable using the comparison technique. However, for in-flight phases of operation, it is the most efficient of the two generic monitoring schemes (i.e. comparison monitoring and in-line monitoring). There are various techniques for comparison monitoring viz:

a. Cross-Channel Comparison Monitoring

With cross-channel comparison monitoring, all of the sensor outputs are weighted similarly in the detection process. For example, the monitoring 'law' could be implemented so that the output signal of each sensor is compared to the average of the outputs of other sensors. If the absolute value of the difference is greater than a fixed threshold, the sensor is considered failed. In cases where more than one difference exceeds the threshold, the failure detection law could also include restrictions whereby only the sensor associated with the largest difference could fail.

b. Cross-Voter Comparison Monitoring

Using the same sensor information as the cross-channel monitor, the cross-voter comparison monitoring technique compares the output of the sensors to a selected 'best' output, which in many schemes is the median. It then uses that information to detect failures. The cross-voter law must 'decide' which is the best signal BEFORE the detection process is complete. For this reason, it is more prone to error than cross-channel comparison.

c. Output Comparison Monitoring

Another comparison monitoring scheme is estimated output comparison monitoring. It uses an estimate or 'model' of the sensor output, derived from other sensed information and/or control commands applied to approximations of the aircraft equations of motion. This estimate of sensor output is used as an 'extra' input in the development of cross-channel comparison monitoring techniques and cross-voting techniques. It can reduce the number of sensors needed to satisfy particular fail-operational requirements.

5. In-Line Monitoring

In-Line Monitoring can be active or passive for sensory systems as well as for other electronic and electromechanical equipment. Usually, this monitoring technique requires that additional equipment be added to the system to perform this function. If performed perfectly, that is, the probability of detecting a failure is 100%, only $3(n+1)$ in-line sensors are necessary for an n fail-operational capability. For skewed sensor systems, $(n + 3)$ sensors are needed for an n fail-operational capability; this is shown in Table 3. Because the monitoring technique does not rely on operation of the other redundant sensors, it is independent of past failure history of the other sensors. This characteristic is advantageous in the implementation of skewed sensor configurations where the coverage depends on the orientation of the remaining sensors after a failure occurs. A key advantage of this technique over comparison monitoring is that it can be designed to detect catastrophic simultaneous failures caused by enemy fire.

Table 3. Sensor Requirements for Coaxial and Skewed Systems (In-Line Monitoring)

OPERATIONAL REQUIREMENT	TOTAL NUMBER OF COAXIAL SENSORS REQUIRED	NO. OF TOLERABLE FAILURES		TOTAL NUMBER OF SKEWED SENSORS REQUIRED
		COAXIAL	SKEWED	
1 Fail-OP	6	1 per axis	any 1	4
2 Fail-OP	9	2 per axis	any 2	5
3 Fail-OP	12	3 per axis	any 3	6

NOTE: Assume Coverage = 1.0

a. Active In-Line Model Monitoring

With the active in-line model monitoring technique (also often called self-test), excitation is applied to the sensor or its associated circuitry. Its output response to the excitation is then compared to a model of the expected output from the device. Signals introduced may be high-frequency or static bias. In many instances, these excitations are used to check for a failure that may be difficult to detect by comparison monitoring, such as anomalies in a sensor time constant. To perform this type of test during a flight, a gyro may have to be taken "off-line" if the sensor response to the test excitation degrades aircraft control characteristics.

b. Passive In-Line Model Monitoring

The passive model monitoring technique covers the case where measurements of sensor parameters, sensitive to failure, are made during the sensor operational period. These measurements could include the sensor outputs (to ensure output is reasonable), the temperature of the environment surrounding the sensor, and voltage excitation. Such measurements are usually about 75% effective in detecting sensor failures.

From Table 3, it is evident that for a highly developed in-line monitoring system where the coverage approaches 1.0, the use of 6 skewed sensors has the potential for three fail-operational performance.

B. Flight Test Validation

The ASSET and RDMS concepts were validated by closed loop control of an EA-6B aircraft during actual flight. Aircraft performance was measured by control response testing using both the ASSET and the production orthogonally mounted rate gyros. There were essentially no differences in aircraft control performance when augmented by these

two separate rate sources. In particular,

a. There were no aircraft transients generated by the use of ASSET failure detection and isolation algorithms. This fact was adequately demonstrated by inserting failures both before and during a given set of maneuvers, and then comparing ASSET rates with the production gyro rates. There were no transients observed in the data, nor were any felt by the flight crew.

b. Tracking accuracy was not degraded after isolation of a failed ASSET sensor. This function was consistently demonstrated by direct comparison of ASSET rates with production rate gyro outputs before, during, and after failure detection and isolation by the RDMS.

c. Rate sensor dispersion introduced no undesirable characteristics into ASSET system performance.

C. Computer Requirements

The digital computer utilized for the ASSET Program was a version of the Singer SKC-3100. It is a general purpose airborne machine containing a 16K (14K PROM/2K RAM) memory, a 16 bit instruction word, a 19 bit data word, and is capable of performing 300K operations per second based on a 4:1 ratio of add to multiply. Based on this computational capability, the software required to execute the unskewing algorithms and RDMS is extremely modest and is given in Table 4.

Table 4. Computational Estimates

SENSOR	MEMORY(WORDS)			MAX TIME TO EXECUTE (MSEC)
	INSTRUCTIONS (ROM)	CONSTANTS (ROM)	RAM	
Rate	1600	600	175	4.5
Accel.	(same as rate)	200	100	4.5

Total (rate + accel.) = 2675 words

For advanced high speed microprocessors with higher throughputs, the execution time would be reduced accordingly.

II. Integrated Inertial Sensor Assembly (IISA) Concept

The IISA system employs redundant arrays of laser gyros and linear accelerometers in strapdown assemblies that, along with associated power supplies, electronics and digital processing provides a highly dependable source of inertial sensor data. The IISA concept is predicated upon the use of strapdown sensors that meet the stringent reliability requirements and signal characteristics required for the next generation fly-by-wire flight control system and are of sufficient quality to achieve navigation accuracies of 1 nautical mile per hour (1.85 km/hr). The feasibility of providing accurate navigation performance with a strapdown inertial navigator, employing laser gyros, has been demonstrated in lab, van and flight tests. For flight control applications, laser gyros have the inherent characteristics to provide the proper output signal with the required accuracy, bandwidth and stability over the dynamic environment of military aircraft within seconds of system turn on. Further, laser gyros offer other advantages in that they are more adaptable for redundancy than two degree of freedom sensors, afford rapid reaction from cold temperatures, offer high reliability and long operating life, and offer low maintenance since system recalibration is not required.

In order to explore this new capability and achieve the benefits for the next generation aircraft, the U.S. Navy has embarked on an advanced development program to demonstrate the IISA concept.

The IISA program was initiated by the Naval Air Systems Command in FY 77 through a series of exploratory development efforts to define performance goals and study trade-offs among IISA candidate configurations. Key requirements were established by the Navy to direct the system synthesis. These requirements included high reliability and minimum size and weight to enable the system to be incorporated in Vertical Short Take-Off and Landing (V/STOL) aircraft as well as future Conventional Take-Off and Landing (CTOL) aircraft, fail-operational/fail-operational/fail-safe fault tolerance for flight control signals to be compatible with future Navy fly-by-wire control requirements, dual-redundant WRAs for survivability (i.e. IISA should not suffer loss of function after one 23 mm shell hit on the aircraft skin), directly usable digital flight control signals and triple-redundant flight control computers to enable direct interface with future DFBW systems, and performance accuracies compatible with the most stringent requirements of the conventional navigation and flight control systems being replaced by IISA.

Primary goals, identified for each IISA function, are summarized in Table 5. These goals provided a basis against which candidate IISA configurations were evaluated and compared.

Table 5. Summary of IISA Goals

FUNCTION	PRIMARY GOAL	RATIONALE
Mission	Navy/Marine Corps Advanced Aircraft.	Future Multimission Aircraft Requirement
Navigation	1 NM/HR (1.85 KM/HR) CEP Position Accuracy with 5 min reaction time.	Anti-Submarine Mission; Low Level Missions
Weapon Delivery	3 FPS (0.9M/SEC) Time Average RMS Velocity Accuracy	Bombing Accuracy
Flight Control	0.01 DEG/SEC, 1 σ Body Rate Measurement Accuracy with 1 Min Reaction Time	Stability
Reliability	Probability of Loss of Control Due to IISA less than 1×10^{-7}	Safety of Flight
Maintainability	0.008 Maintenance Manhours per Operating Hour	F-18 Maintenance Experience
Survivability	Survive 23 mm Hel T Projectile	Simultaneous Failures
Operational Flexibility	Employ Modular Design	Applicability to Numerous Advanced Aircraft

A. IISA Candidate Configurations

Fifteen candidate IISA systems were configured to satisfy the original goals that are presented in Table 5. These candidates represented a wide range of variation relative to the quantity of WRAs, the quantity of sensors within each WRA, and the geometry of sensor input axes. Because of this wide variation, the group of candidates represented a comprehensive base from which an optimum IISA configuration was selected. A preliminary evaluation of these fifteen candidates was performed relative to functional reaction time, performance, reliability, redundancy management, physical characteristics, producibility (risk), software, environment, maintainability, survivability, weight, and life cycle costs.

Based upon this evaluation three candidate IISA configurations were defined for detailed trade-off analyses to enable selection of the most desirable configuration for development and test of an ADM. The three candidate IISA configurations which were defined for analysis included a dual tetrad, a dual skewed triad, and a triple orthogonal triad.

The block diagrams of each of these three sensor configurations, presented in Figures 3 to 5, show the sensors, digital processors, and external data bus interfaces. The navigation computer is common to each configuration although the software and memory requirements would differ. A brief description of the three candidates is given below.

1. Dual Tetrad

This candidate contains two WRAs; each WRA has four sensor axes. Three of the axes are orthogonal and are aligned with the aircraft primary axes while the fourth axis is skewed at an angle of 54.7 degrees with respect to each of the other axes. The gyro and accelerometer axes are collinear. The two WRAs are installed in the same orientation within the aircraft.

Each WRA provides a complete navigation function and all of the flight control signals. The navigation outputs are transmitted to aircraft system mission computers via dual MIL-STD-1553 data busses. The flight control outputs are transmitted to three flight control computers via triple redundant data busses. Sensor signal select for flight control is performed within the IISA.

2. Dual-skewed Orthogonal Triad

This candidate consists of two WRAs. Each WRA has three sensor axes with gyro and accelerometer axes collinear. The sensor axes are at 54.7 degrees with respect to the aircraft yaw axis; however, one of the WRAs is rotated 180 degrees about the aircraft yaw axis so that no more than two sensor set axes are coplanar. The WRAs are physically the same.

Each WRA provides a complete inertial navigation function and all of the flight control signals. The navigation outputs are transmitted to aircraft system navigation computers via dual MIL-STD-1553 data busses. The flight control outputs are trans-

mitted to three flight control computers via triple redundant data busses. Sensor signal select for flight control is performed within the IISA.

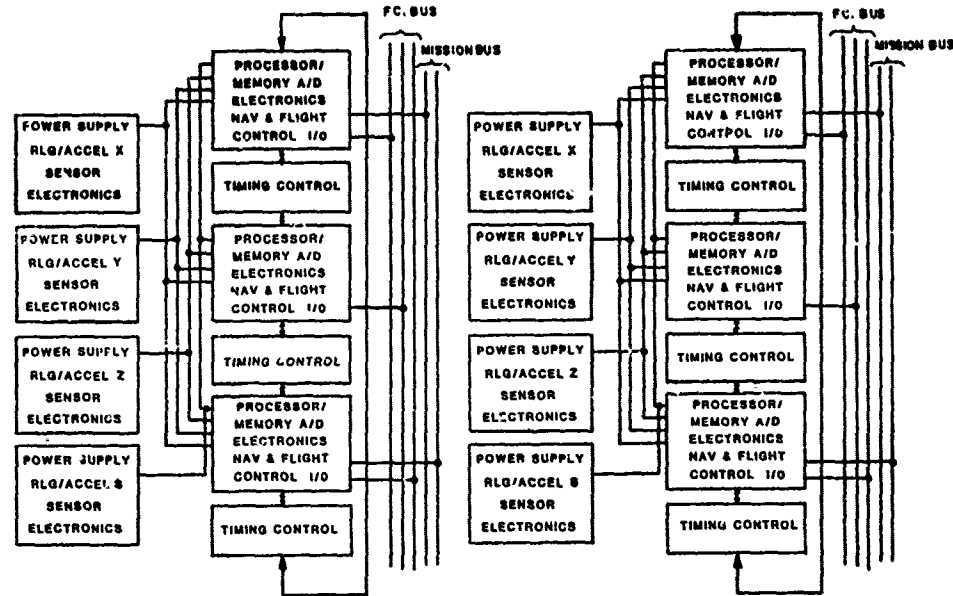


Figure 3. Dual Tetrad

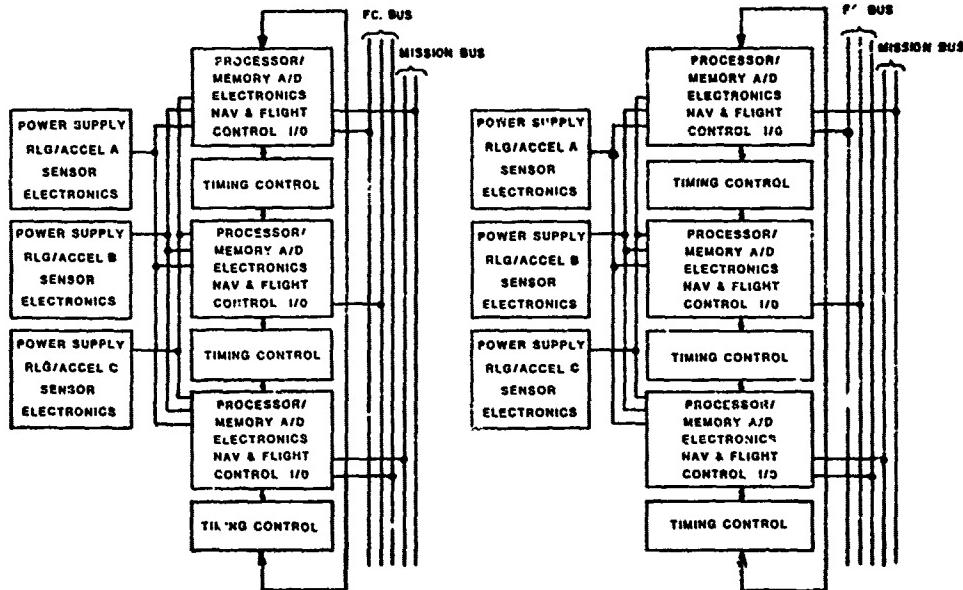


Figure 4. Dual Skewed Orthogonal Triad

3. Triple-Orthogonal Triad

This candidate has three WRAs. Each WRA has three sensor axes that are aligned with aircraft axes; gyro and accelerometer axes are collinear. The three WRAs are installed in the same orientation within the aircraft.

Each WRA provides a complete inertial navigation function and all of the flight control signals. The navigation outputs are transmitted to the aircraft's navigation system's computers via dual MIL-STD-1553 data busses. Flight control outputs are transmitted via triple redundant data busses to flight control computers. Sensor signal select is performed in the flight control computers.

B. Performance Analysis

Computer simulation performance analyses of the three candidate configurations

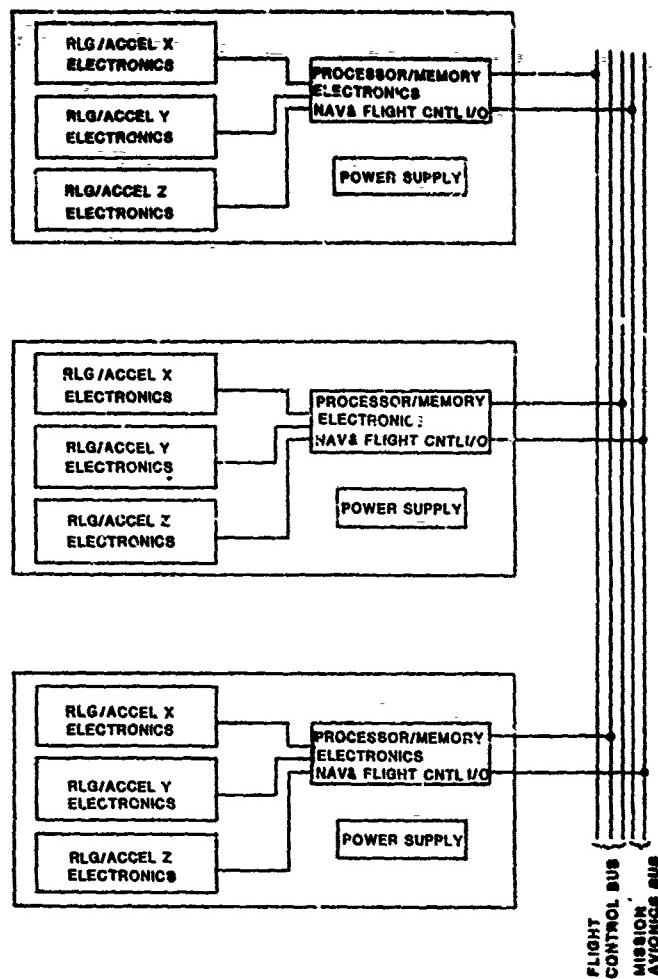


Figure 5. Triple Orthogonal Triad

were performed using representative mission profiles and error models. The three profiles, over which the IISA candidate configurations were evaluated, describe the following missions: (1) Anti-Submarine Warfare (ASW); (2) Surface Attack (SA); and (3) Close Air Support (CAS). The three scenarios were converted to computer program profile input data comprised of a time history of translational and rotational accelerations and thrust angular rates. Two sets of error model coefficients were evaluated. These coefficients were selected from representative 1978 ring laser gyro strapdown inertial system technology. The initial simulation data led to the conclusion that the use of error coefficients from the two selected error models resulted in errors that exceeded the goals set for IISA, particularly in velocity and heading. Therefore, additional simulation data was prepared and an error model that was improved relative to the first two error models was used. The ASW flight profile was utilized because it was judged to be as severe as any based on the results of the previous simulations performed.

The results of this simulation using the dual skewed configuration are presented in Table 6. It may be noted that the use of the improved error coefficients resulted in IISA output errors that were all acceptable and, in addition, provided a margin. The performance margin (difference between goal and simulated capability) has been retained as a goal, rather than relaxing the error coefficients, to allow for the application to a broad range of missions rather than ASW alone, standardization which results in the use of the most severe requirements, variations in dynamic environments associated with advanced host aircraft, the potential need to improve reaction time below 5 minutes, and uncertainty in the confidence level associated with the simulation program. Potential relaxation in error coefficients will depend upon possible use and the degree of integration of future navigation aids such as the Global Positioning System (GPS) and the Joint Tactical Information Distribution System (JTIDS).

The set of improved error coefficients that was used to provide the satisfactory performance in Table 6 is shown in Table 7. Also shown for direct comparison purposes are the initial coefficients associated with Error Models 1 and 2. The improvement in gyro scale factor contributed to improved velocity and heading accuracies. The improvement in gyro wide-band random noise contributed to improvements in position, velocity, and heading accuracies. The improvement in accelerometer narrow-band random noise contributed to improved position accuracy at reduced reaction time, and also to velocity accuracy. The improvement in accelerometer scale factor contributed to improvement in velocity and position accuracies. If these error coefficient goals are achieved, the analysis indicated that IISA performance goals can be satisfied using a 5 minute reaction time.

Table 6. IISA Errors Over the Anti-Submarine Warfare (AWS) Flight Profile -
5 Minute Reaction Time

IISA ERRORS			ACCURACY GOALS	CAPABILITY WITH IMPROVED ERROR COEFFICIENTS
Position Rate, CEP	NM/HR	(KM/HR)	1.0 (1.85)	0.27 (0.5)
Altitude, 1σ	FT	(M)	150.0 (45.7)	131.0 (39.9)
North Velocity, RMS	FT/SEC	(M/SEC)	3.0 (0.91)	1.24 (0.38)
East Velocity, RMS	FT/SEC	(M/SEC)	3.0 (0.91)	1.31 (0.40)
Vertical Velocity, RMS	FT/SEC	(M/SEC)	3.0 (0.91)	0.365 (0.111)
Roll Angle, (ϕ), 1σ	ARC MIN		2.0	0.13
Pitch Angle, (θ), 1σ	ARC MIN		2.0	0.2
Azimuth Angle (ψ), 1σ	ARC MIN		6.0	1.75
Body Roll Rate (p), 1σ	DEG/SEC		0.01	0.001
Body Pitch Rate (q), 1σ	DEG/SEC		0.01	0.001
Body Yaw Rate (r), 1σ	DEG/SEC		0.01	0.001
Longitudinal Acceleration, 1σ	FT/SEC ²	(M/SEC ²)	0.33 (0.10)	0.00011 (3.35X10 ⁻⁵)
Lateral Acceleration, 1σ	FT/SEC ²	(M/SEC ²)	0.33 (0.10)	0.00011 (3.35X10 ⁻⁵)
Normal Acceleration, 1σ	FT/SEC ²	(M/SEC ²)	0.33 (0.10)	0.00011 (3.35X10 ⁻⁵)

Table 7. Recommended Goals for Error Coefficients

ERROR SOURCES	ERROR COEFFICIENTS (ONE SIGMA VALUES)		
	ERROR MODEL 1	ERROR MODEL 2	RECOMMENDED GOALS
Gyro			
Scale Factor	(PPM)	5.2	1.0
Misalignment	(ARC SEC)	4.85	4.85
Fixed Bias	(DEG/HR)	0.01	0.01
Wide-Band Random Noise	(DEG/ \sqrt{HR})	0.002	0.002
Accelerometer			
Scale Factor	(PPM)	180	50
Misalignment	(ARC SEC)	7.22	3
Fixed Bias	(MICROGEES)	27	27
g^2 Sensitivity	$\frac{\text{MICROGEES}}{(\text{FT/SEC}^2)^2}$	0.001 (0.0108)	0.001 (0.0108)
Narrow-Band Random Noise	(MICROGEES)	42	5
Altimeter			
Narrow-Band Random Noise	(FT)	150	125

C. IISA Configuration Selected for Advanced Development

The selected IISA system is the single IISA design that best satisfies the performance goals with minimum attendant weight and minimum cost. This selection was made after careful evaluation of the fifteen candidate systems, and the refinement to three candidates. Using the evaluation criteria, candidate 2 (the dual skewed triad approach) was determined to be the best. Having arrived at the most desirable configuration for advanced development, preliminary design studies were performed to develop system architecture, physical characteristics, electronics design and system computational functions. A baseline design has been established for ADM development and flight test. The objective

of this design is to develop a system which will interface with an existing digital or analog flight control system for the purpose of demonstrating the IISA concept. The requirements for the ADM IISA are:

- a) the capability of providing fail-safe operation for flight control after the third like failure assuming a 95% confidence in the ability of the system to detect and isolate the failure. This is FO/FO/FS fault tolerance for flight critical data.
- b) fail-operational navigation and weapon delivery data.
- c) a weight limitation of 50 pounds (23 kilograms) per WRA.
- d) use of a flight control coupler to provide the signal conditioning required to interface with the test bed aircraft.
- e) no direct interface with the test bed aircraft cockpit or displays, thus requiring the ADM to have a dedicated Control Display Unit (CDU).
- f) survivability to the extent that flight control functions remain operational after sustaining single-hit battle damage to one WRA from a 23 mm projectile. The flight control system shall be at least fail-safe after the loss of a WRA.
- g) safety of flight reliability for flight control with a probability of loss of 1×10^{-7} catastrophic failures per hour.
- h) reliability of 2500 hours mean-time between failures (MTBF) for each navigation system.
- i) navigation accuracies of 1.0 NM/H CEP (1.85 KMPH CEP) position error and 3 feet per second (0.9 M/SEC) RMS velocity error with a 5 minute reaction time (at sea).
- j) operation of the failure detection, isolation, fault coverage, and redundancy management algorithms using dispersed WRAs in a flexible, vibrating airframe.
- k) maintainability design such that intermediate maintenance is eliminated. The WRAs should be interchangeable without the need for special calibration. Built in test will be required to preclude the need for external test equipment at the organizational level.

Initial mechanical layouts that were prepared for the ADM, using state of the art electronics and microcomputer designs quickly led to the conclusion that packaging all of the electronics, computers, power supplies and inertial sensors (gyros and accelerometers) into one box would lead to a large, bulky and heavy WRA. In order to achieve test bed installation flexibility to the maximum extent possible and not exceed the 50 lb. (23 kg.) weight constraint it was necessary to partition the WRA into two separate assemblies.

The major hardware components to be partitioned between the two WRAs were the gyros, accelerometers, sensor electronics, sensor PROMs, sensor interface electronics, sensor compensation, flight control processing, (including fault detection, isolation, and redundancy management algorithms), navigation processing, timing and control, high voltage power supplies for the gyros, low voltage power supplies, and input and output.

A design trade-off study was made to determine the hardware and software partitioning. The basic system partitioning was determined by evaluating size limitations, thermal isolation, communication between boxes, functional symmetry, timing and control, computer loading, power requirements, fault tolerance and maintainability constraints. Figure 6 represents the selected design for the IISA ADM based on the above evaluation. Note, the system has now been separated into two identical channels, each containing two WRAs. These are the Inertial Sensor Assembly (ISA) and the Dual Computer Assembly (DCA).

Figure 7 presents preliminary dimensional outlines of the WRAs in the ADM using state of the art technology designs.

1) Inertial Sensor Assembly

Figure 8 presents the ISA Functional Block Diagram. Note, each ISA will contain as a minimum three ring laser gyros, three accelerometers, three high voltage power supplies, gyro electronics cards, sensor output electronics, accelerometer digitizers, Built In Test (BIT), and Analog to Digital (A/D) converters. Also included in the ISA is the coning/sculling compensation used to remove spurious signals induced by high frequency motion in the gyro/accelerometer channels respectively. The design concepts involved in the determination of the ISA components were as follows.

The high voltage power supply should be located close to the gyros to minimize Electromagnetic Interference (EMI) and noise susceptibility. This is acceptable since the High Voltage Power Supplies (HVPS) do not generate a significant amount of heat and are small relative to the Low Voltage Power Supplies (LVPS).

It is also desirable to have the sensors Programmable Read Only Memories (PROMs) in the same box with the inertial sensor assembly from a calibration and logistics

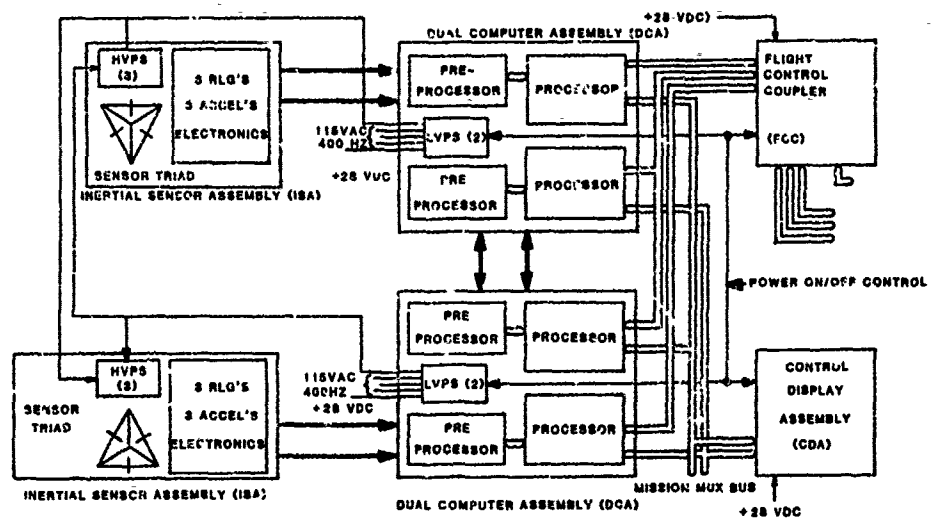


Figure 6. IISA System Functional Diagram

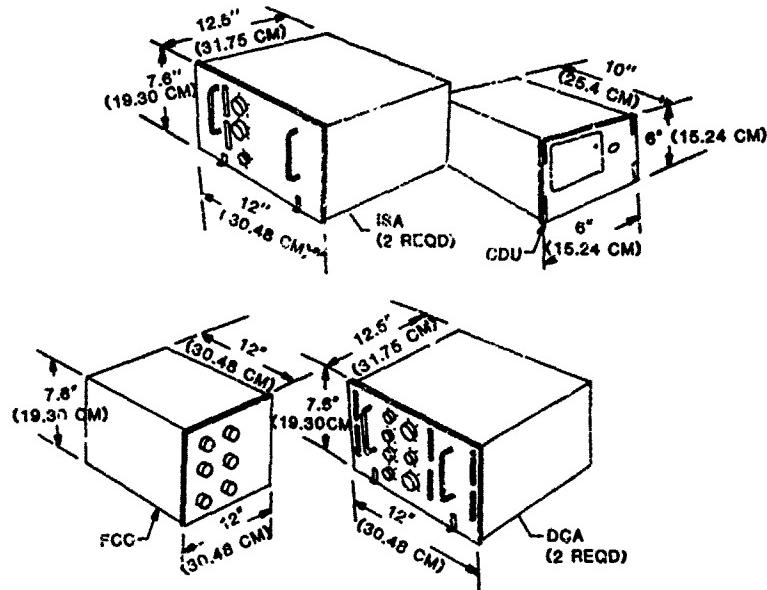


Figure 7. Preliminary IISA Equipment Outlines

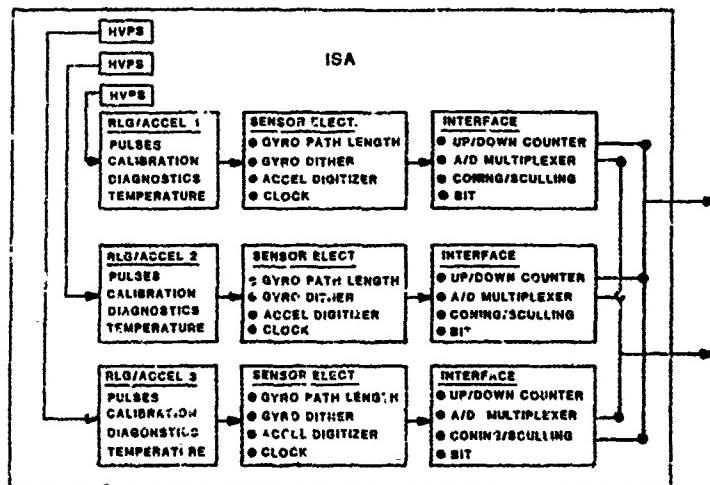


Figure 8. ISA Functional Block Diagram

point of view. These PROMs are designed to compensate for the peculiarities of the associated inertial sensor assembly. Placing these PROMs in a separate assembly would preclude interchangeability of inertial sensor assembly WRAs without altering the associated computer assembly WRA.

Timing/control considerations dictate that the digitization of any sensor analog signals (such as the accelerometer integrator residuals) be done in the WRA containing the sensor. Also to eliminate the transfer of high frequency time critical up/down pulses, the coning, sculling, and up/down counter accumulation will be done within the ISA. Locating these functions in the ISA will keep the number of communication lines into and out of the ISA to a minimum and will also keep the noise susceptibility to a minimum.

2) Dual Computer Assembly

Each of the Dual Computer Assemblies (DCA) will contain two independent channels of digital processing (Figure 9). Also included in the DCA will be low voltage power supplies, timing and control circuitry and the Input/Output (I/O) circuitry required to interface with the mission computer and flight control data busses. The low voltage power supplies are the primary heat source and have purposely been put in the DCA for thermal isolation of the sensors.

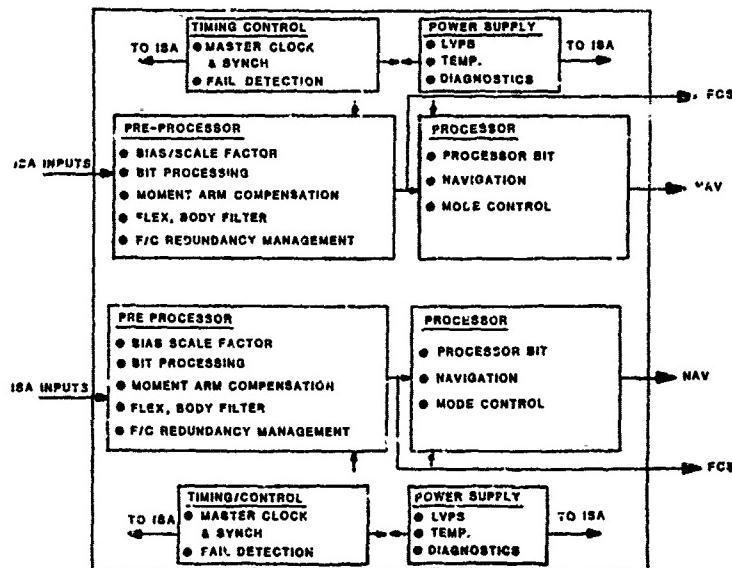


Figure 9. DCA Functional Block Diagram

The software functions to be performed by the digital processors include sensor bias/scale factor compensation, sensor temperature compensation, moment arm compensation, flexible body filtering, sensor BIT, flight control sensor redundancy management, signal select, coordinate transformation functions, navigation processing, navigation mode control, processor BIT and I/O processing.

At present for the ADM application, there is no mil-qualified processor on the market that can handle the throughput required and yet be economical in size and power. It is anticipated that 2 processors per channel (therefore, 4 processors per DCA and 8 processor per IISA) will be necessary for the ADM to handle the computations required. However, for an application in the 1990 time frame, it is reasonable to assume a mil-spec processor will be available which can provide the high throughput required at a low cost. A significant advantage of the single processor approach is that all of the processors would have the same software structure.

3) Control Display Unit (CDU)

A Control Display Unit (CDU) is included in the IISA system for ADM. This unit provides the manual interface for initialization, mode control, fault detection and status. The IISA shall have no interface with cockpit controls or displays other than the IISA control display unit.

For the production system all communication with cockpit controls/displays will be via the flight control system mission computer, or other subsystem that IISA supports.

4) Flight Control Coupler (FCC)

The purpose of the Flight Control Coupler is to provide a "transparent" interface between IISA and the aircraft flight control system. As such, the actual interface definition and performance depends upon the interface configuration and performance requirements of the host aircraft.

Until the specific test bed is identified, the detailed interface with the flight control system cannot be defined. Figure 10 shows the utilization of the FCC for two different interface configurations.

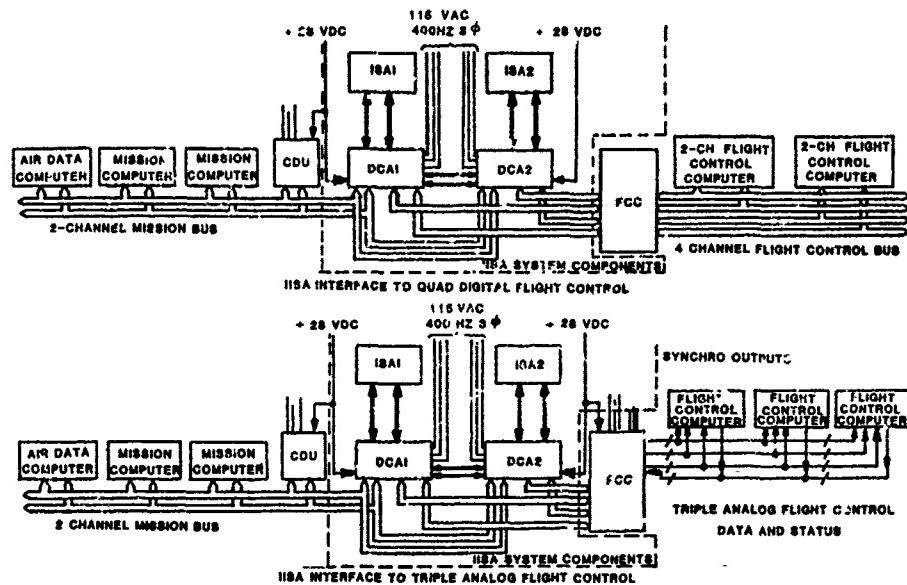


Figure 10. IISA System Interface Configurations

CONCLUSIONS

The potential benefits to be accrued by consolidating inertial sensor functions through sensor redundancy and subsystem integration is being actively pursued by the U.S. Navy. Flight tests conducted under the ASSET exploratory development program have demonstrated that skewed sensors and associated digital data handling technology is compatible with future fly-by-wire control systems. Advancement of this concept through the development of an Integrated Inertial Sensor Assembly is expected to provide inertial data for navigation, weapon delivery, displays and flight control functions on advanced Navy aircraft in the 1985-1990 time period. This will result in minimum weight, fast reaction, high reliability, low maintenance and lower life cycle costs as compared to a conventional implementation.

References

1. Development of an Advanced Skewed Sensory Electronic Triad (ASSET) System for Flight Control, Phases I & II. Analytical and Laboratory Investigations, Report No. NADC-76295-30, Grumman Aerospace Corp., Oct. 1976.
2. Development of an Advanced Skewed Sensory Electronic Triad (ASSET) System for Flight Control, Phases III A & B. Laboratory Verification and Flight Test, Report No. NADC-77043-30, Grumman Aerospace Corp., June 1979.
3. Feasibility and Design Studies of an Integrated Sensory Subsystem (ISS) for Advanced V/STOL Aircraft, Report No. NADC-76259-30, Grumman Aerospace Corp., March 1978.
4. Ring Laser Gyro Integrated Inertial Sensor Assembly Preliminary Design and Analysis, Report No. NADC-77230-60, Honeywell, Inc., April 1979.
5. Integrated Inertial Sensor Assembly Technical Report Studies, Analysis and Approach, McDonnell Aircraft Co., Report No. MDC A5791, June 1980.
6. Integrated Inertial Sensor Assembly (IISA) Final Technical Report, Boeing Military Airplane Co., Report No. N00019-77-C-0506, June 1980.
7. Integrated Inertial Sensor Assembly Preliminary Design Definition and Analysis, Report No. NADC-78161-40 (Preliminary) Honeywell Inc., May 1980.

F-8 DIGITAL FLY-BY-WIRE AIRCRAFT ANALYTIC REDUNDANCY
MANAGEMENT FLIGHT TEST EXPERIENCE

James C. Deckert
The Charles Stark Draper Laboratory, Inc.
Control and Flight Dynamics Division
555 Technology Square
Cambridge, Massachusetts 02139
USA

SUMMARY

In this paper we review the formulation and flight test results of an algorithm to detect and isolate the first failure of any one of twelve duplex control sensors being monitored. The technique uses like-sensor output differences for fault detection while relying upon analytic redundancy relationships among unlike quantities to isolate the faulty sensor. The fault isolation logic utilizes the modified sequential probability ratio test, which explicitly accommodates the inevitable irreducible low frequency errors present in the analytic redundancy residuals. In addition, the algorithm uses sensor output selftest, which takes advantage of the duplex sensor structure by immediately removing a highly erratic sensor from control calculations and analytic redundancy relationships while awaiting a definitive fault isolation decision via analytic redundancy. This study represents a proof of concept demonstration of a methodology that can be applied to duplex or higher flight control sensor configurations and, in addition, can monitor the health of one simplex sensor per analytic redundancy relationship.

INTRODUCTION

The desire for increased maneuvering capability in high performance aircraft is resulting in designs for which the control system is flight critical. Because individual control sensors do not have the reliability required for such control systems, some sensor replication and an accompanying sensor redundancy management technique are necessary. Although redundancy management is simplified for triplex or higher sensor configurations, considerations such as volume, weight, power and life-cycle costs suggest that the required level of sensor redundancy be supplied by keeping sensor replication to a minimum and utilizing the analytic redundancy inherent in the relationships among the variables measured by unlike sensors.

In this paper we review a technique for the detection and isolation of the first failure of any one of twelve duplex control sensors being monitored, and discuss the performance of the technique during flight tests aboard the NASA F-8 digital fly-by-wire (DFBW) aircraft. This study represents a proof of concept demonstration of a methodology that could either be the primary redundancy management scheme for a duplex control sensor design or could enable continued reliable operation following the degradation to duplex of one or more sensor types of an originally triplex or higher configuration following fault isolation using standard voting techniques. The further extension of the methodology to the simplex sensor case is discussed in Ref. 1.

The analytic redundancy management (ARM) technique is dual mode, with fault detection obtained by the comparison of like-sensor outputs, and fault isolation accomplished using modified sequential probability ratio tests (MSPRTs) operating on analytic redundancy residuals. This dual-mode structure results in a low computational load in the normal no-fault situation, and it allows the MSPRTs to be made quite robust since fidelity in the analytic redundancy relationships must be maintained for only the short time between detection and isolation.

Each MSPRT resembles a generalized likelihood ratio test²⁾ in which the failure time is known and the failure mode is assumed to be a bias of predefined magnitude, with the major difference being the inclusion of an effective threshold offset in the MSPRT to accommodate low frequency modeling errors and nominal sensor biases in the analytic redundancy residuals. The bias failure hypothesis is used not only because, in the absence of detailed failure mode information, bias failures are considered likely, but also because the resulting tests are quite effective in isolating other failures, such as ramps and scale factor errors, when observability is sufficiently high.

Sensor output selftest is utilized in the ARM algorithms to minimize the effect of a hard-failed sensor on the aircraft through the control system. Four sensor status levels are defined in decreasing order of reliability: unfailed, provisionally failed, conditionally failed, and unconditionally failed. If both like sensors have equal status, the average of the two sensor outputs is used in the analytic redundancy and control system calculations; otherwise, the output of the sensor having the better status is used. An unfailed sensor is declared provisionally failed when its output differs from its output on the previous sample (and from the output of its companion sensor if unfailed) by a predefined threshold magnitude. If this selftest violation disappears on either of the next two samples, the provisional failure status is removed. Conditional and unconditional failure status declarations are made by analytic redundancy MSPRTs as discussed below.

FAULT DETECTION USING DIRECT REDUNDANCY

For fault detection and isolation (FDI) purposes, it is convenient to define a faulty sensor as one having an output error magnitude larger than a stipulated bias failure magnitude (BFM), and in practice we would like to isolate an instrument having an output error magnitude of the order of BFM. Thus the BFM for each sensor type is chosen to be larger than the observed output errors in good instruments and large enough to be isolated by the available analytic redundancy, and a sensor fault is detected when the moving window average of the output of instrument 1 minus the output of instrument 2 is larger than three-quarters BFM in magnitude. This three-quarter BFM threshold results in equal probabilities of detecting a BFM/2 bias and not detecting a BFM bias. Stipulating these probabilities (10^{-4} for this study) and assuming white Gaussian noise yields the required window size for each sensor type as a function of BFM and noise variance.

FAULT ISOLATION USING ANALYTIC REDUNDANCY

The SPRT⁽³⁾ utilizes sequential observations of a process to decide which of two hypotheses concerning the probability distribution of the process is true. The SPRT is independent of the a priori probabilities of the two hypotheses, and minimizes the average number of observations necessary to reach a decision while meeting prespecified

⁽⁴⁾ misclassification probabilities. Because of these desirable characteristics and the simple form of the test, the SPRT is an ideal candidate for use with analytic redundancy for fault isolation. In particular, assuming that the process being observed is the difference between the output of one suspect sensor and a synthesized output using analytic redundancy, appealing choices for the two hypotheses are that the process has a mean equivalent to a BFM-sized bias (i.e., the sensor has failed) or that the process has zero mean (i.e., the instrument is unfailed).

Unfortunately, such factors as allowable biases on unfailed sensors, errors in the sensor input/output models and parameter uncertainties in analytic redundancy relationships all contribute to low frequency errors in analytic redundancy residual processes for unfailed sensors. Direct application of an SPRT to such a process may result in the acceptance of the failure hypothesis in spite of the fact that the sensor is operating within acceptable tolerances.

The MSPRT is a fault isolation test that systematically accommodates those irreducible factors contributing to low frequency analytic redundancy residual errors that cannot be explicitly removed by modeling. The ARM algorithm utilizes the MSPRT to make conditional and unconditional failure status declarations following fault detection. Underlying the technique is the assumption that one of the following two hypotheses concerning the analytic redundancy residual process γ_j^k for suspect sensor j ($j=1$ or 2) is true:

- 1) At time t_k , γ_j^k is Gaussian with variance σ^2 and mean m_k^j (i.e. sensor j has failed)
- 2) At time t_k , γ_j^k is Gaussian with variance σ^2 and mean 0 (i.e. sensor j has not failed)

Although a straightforward approach would be to design a test for each sensor that could accept either of these two hypotheses, and then declare a failure when either hypothesis for either sensor was accepted, we have chosen a more conservative approach that avoids the tenuous situation of inferring that one sensor has failed merely because its companion sensor appears to be unfailed.

Consistent with the above discussion, following fault detection at time t_1 the MSPRT test statistic, the modified log likelihood ratio (MLLR), is defined at time t_n for suspect sensor j as:

$$u_n^j \equiv \sum_{k=1}^n \left[\frac{m_k^j}{\sigma^2} \left(\frac{m_k^j}{2} - \gamma_k^j \right) + \frac{|m_k^j|}{\sigma^2} t_k \right] \quad (1)$$

and the following decision rule is used:

$$\begin{aligned} u_n^j < \delta & \text{ declare instrument } j \text{ unconditionally failed, terminate the test} \\ \delta < u_n^j < 0 & \text{ declare instrument } j \text{ conditionally failed, take another sample} \\ 0 < u_n^j & \text{ take another sample} \end{aligned} \quad (2)$$

In Eq. (1) the k subscript indicates evaluation at time t_k and the mean m_k^j is computed assuming a BFM-sized bias in sensor j of sign consistent with the direct redundancy window at the detection time. The negative threshold δ in Eq. (2) is the original SPRT threshold calculated using prespecified misclassification probabilities.

The last term in the summation in Eq. (1) differentiates the MLLR from the LLR of the standard SPRT, and represents the contribution of a postulated worst-case residual error magnitude at time t_k , E_k , to the LLR calculation. Equations (1) and (2) indicate that the MSPRT is in essence a one-sided SPRT with a threshold offset arising from the worst-case error term. It follows that so long as the threshold offset is

conservative, the misclassification probabilities for the NSPRT will be no larger than those specified to determine the original SPRT threshold.⁽⁵⁾ The choice of the worst-case error magnitude for each analytic redundancy test requires considerable engineering judgment. An optimistic choice lowers the reliability of the test while an overly pessimistic choice may result in prohibitively long isolation times, although the inclusion of conditional failure declaration using a relaxed test criterion tends to lower the mean isolation times seen by the control system without corresponding increases in the ultimate misisolation probabilities. Specific choices for the worst-case error terms are discussed in subsequent sections on the particular forms of analytic redundancy utilized in this study.

In addition to the decision rules of Eq. (2), the ARM algorithm avoids open-ended isolation tests by utilizing an elapsed time limit (ETL) for each sensor type. When ETL is reached before an unconditional failure has been declared, the detected fault indication is removed, isolation computations cease, and the direct redundancy detection process is reinitiated. Because failure observability and worst-case error magnitude are often maneuver dependent, pilot response to notification that ETL for a sensor type has been reached could result in an enhanced fault isolation environment during the subsequent isolation period. Alternatively, reaching ETL could initiate hardware selfcheck routines.

OUTLINE OF THE ARM ALGORITHM

The ARM algorithm monitors eleven duplex instruments aboard the F-8 DFBW aircraft: longitudinal accelerometer, lateral accelerometer, normal accelerometer, roll rate gyro, pitch rate gyro, yaw rate gyro, vertical gyro (VG), directional gyro (DG), barometric altimeter, Mach meter and alpha vane. (Although the accelerometer and rate gyro complement is triplex, only a duplex subset is utilized by the ARM algorithm.) Additionally, a simplex beta vane is used in some calculation, but not monitored for failure. Each VG gives outputs of Euler roll angle θ and pitch angle ϕ , and these outputs are considered to be two independent sensor types although, in practice, the failure of one channel would probably dictate the failure of the unit. The output of each DG is transformed into Euler azimuth angle ψ as follows:

$$\psi^j = \tan^{-1} \left\{ [\cos \theta \tan (DG^j - B^j) + \sin \theta \sin \psi] / \cos \theta \right\} \quad (3)$$

where B^j is a known constant reflecting the orientation of DG j in the aircraft.

From the large number of analytic redundancy relationships available, practical considerations and aircraft-specific signal-to-noise values reduce the number used in the ARM algorithm to four general types: rotational kinematics, altitude kinematics, translational kinematics and translational dynamics. In the following four sections, the analytic redundancy residual equations and worst-case error terms are discussed for each sensor type, grouped by the type of analytic redundancy employed. The lateral and normal accelerometers employ two types of analytic redundancy each while the remaining sensor types employ one each.

To summarize the ARM FDI process, each sensor type utilizes a threshold test on the moving window average of the difference in the duplex outputs to detect a fault. Following fault detection, one MLLR is computed via Eq. (1) for each suspect sensor for each form of analytic redundancy used, and the NSPRT threshold logic of Eq. (2) is applied to the lowest MLLR. This process is repeated until an unconditional failure is declared or ETL is reached. Additionally, a direct redundancy LLR is computed following fault detection to provide false alarm protection. The process observed is the duplex sensor output difference, and the LLR mean is of BFM magnitude with sign consistent with the detected failure. When this LLR crosses a positive threshold a false alarm is declared, the isolation process ceases, and the detection process is reinitiated. Finally, sensor selftest is continually applied to all sensors having unfailed status.

ROTATIONAL KINEMATICS

Rotational kinematics (RK) is used for fault isolation in the rate gyros and attitude gyros. The roll, pitch and yaw rate gyros provide measurements of the aircraft body rates p , q and r about the aircraft x , y and z axes, respectively; and these body rates are related to the rates of change of the Euler angles measured by the attitude gyros. Thus, following a rate gyro fault detection at time t_1 , the RK residual for instrument j of the suspect type is calculated at general time t_k using the appropriate equation from the following:

$$\gamma_k(p^j) = \sum_{i=1}^k \left\{ p_i^T - [q_i - q_{i-1} - (\psi_i - \psi_{i-1}) \sin \theta_i] \right\} \quad (4)$$

$$\gamma_k(q^j) = \sum_{i=1}^k \left\{ q_i^T - [(\theta_i - \theta_{i-1}) \cos \psi_i + (\psi_i - \psi_{i-1}) \cos \theta_i \sin \psi_i] \right\} \quad (5)$$

$$\gamma_k(r^j) = \sum_{i=1}^k \left\{ r_i^T - [-(\theta_i - \theta_{i-1}) \sin \psi_i + (\psi_i - \psi_{i-1}) \cos \theta_i \cos \psi_i] \right\} \quad (6)$$

In Eq. (4)-(6) and all subsequent equations, T is the ARM sample period and an overbar indicates that the quantity represents the average of its present and previous sample values. This averaging is used to reduce computational errors during high angular rate maneuvers, and the forms of Eqs. (4)-(6) avoid differentiation of the noisy attitude measurements.

At every sample time t_k , following fault detection, the residual for each suspect rate gyro is used to update its MLLR using Eq. (1), where the mean has magnitude equal to the rate gyro BFM times ($t_k - t_0$), the variance reflects attitude gyro noise variance, and the worst-case error is computed as the sum of the magnitudes of terms reflecting initial attitude gyro noise, attitude gyro bias, rate gyro misalignment and rate gyro scale factor error plus a term representing the effect of a small DG spin axis alignment error on Eq. (3).

Treating the roll and pitch attitude signals from a single vertical gyro as independent sensor types, the RK residual for sensor j of an attitude gyro type (θ, ψ, DG) having a detected fault is calculated at time t_k as follows:

$$\gamma_k(\theta^j) = \sum_{i=1}^k \left\{ \theta_i^j - \theta_{i-1}^j - [\bar{p}_i T + (\psi_i - \psi_{i-1}) \overline{\sin \theta_i}] \right\} \quad (7)$$

$$\gamma_k(\psi^j) = \sum_{i=1}^k \left\{ \psi_i^j - \psi_{i-1}^j - T [\bar{q}_i \overline{\cos \theta_i} - \bar{r}_i \overline{\sin \theta_i}] \right\} \quad (8)$$

$$\gamma_k(\text{DG}^j) = \sum_{i=1}^k \left\{ \psi_i^j - \psi_{i-1}^j - [(\theta_i - \theta_{i-1} - \bar{p}_i T) \overline{\sin \theta_i} + T (\bar{q}_i \overline{\sin \theta_i} + \bar{r}_i \overline{\cos \theta_i}) \overline{\cos \theta_i}] \right\} \quad (9)$$

In order to calculate the attitude gyro MLLRs, it is necessary to have stored the instantaneous RK residuals, corresponding to the terms enclosed in braces in Eq. (7)-(9), in a moving window of the same length as the detector window for each sensor type. At the time of fault detection, the instantaneous residual window for each suspect sensor is processed using the appropriate equation from Eq. (7)-(9) to form the MLLR residual for each window time, where t_1 corresponds to the time associated with the oldest window element. The MLLRs are computed at each intermediate window time using Eq. (1), where the mean has BFM magnitude, the variance is of the order of the attitude gyro noise variance, and the worst-case error is the sum of terms reflecting initial attitude gyro error, rate gyro bias, rate gyro misalignment and roll rate gyro scale factor error. After processing the entire window of instantaneous residuals and calculating the MLLRs corresponding to the present time, the threshold logic of Eq. (2) is applied to the lower MLLR. If no unconditional failure declaration is made, the detected failure indication is removed and the detection process proceeds smoothly on the next sample.

We note that the framework used for the attitude gyros of processing a stored window of instantaneous residuals before applying the MSPRT threshold logic is also utilized for the Mach meters and altimeters, and these five sensor types do not require direct redundancy LLR calculations since the isolation process does not extend beyond the time of detection. Additionally, the MLLR for any sensor of these five types is reset to zero whenever it becomes positive. This is done to accommodate the uncertainty in failure time within the window, and requires a slightly higher magnitude threshold for the MSPRTs for these sensor types.⁽⁶⁾ For the 10^{-4} misclassification probabilities used in this study, the threshold δ in Eq. (2) is -11.4 for these five sensor types and -9.2 for the others.

ALTITUDE KINEMATICS

Altitude kinematics (AK) refers to the redundancy between changes in altitude measured by the altimeters and changes in altitude computed as the double integral of vertical acceleration measured by the accelerometers. This redundancy is utilized in isolating failures in the altimeters, normal accelerometers and lateral accelerometers.

The vertical acceleration, as measured by the accelerometers, is computed at time t_i as

$$Av_i = Ax_i \overline{\sin \theta_i} - (Ay_i \overline{\sin \theta_i} + Az_i \overline{\cos \theta_i}) \overline{\cos \theta_i} - g \quad (10)$$

In Eq. (10) and elsewhere, Ax , Ay and Az represent the actual accelerometer readings plus angular rate and angular acceleration correction terms to yield the acceleration at the center of mass. A second-order discrete filter is implemented for each altimeter to estimate altitude and vertical velocity, driven by the vertical acceleration of Eq. (10) and incorporating each altimeter's output as a measurement update on every ARM sample. The nonzero measurement gains are chosen to keep the effects of accelerometer bias and altimeter quantization small. Each altimeter's measurement residual, the difference

between its output and its propagated altitude estimate before measurement incorporation, is stored in a moving window.

At the time of altimeter fault detection, each sensor's window of residuals is processed to convert them to zero-gain residuals in order to enhance the failure signature (1), i.e. the resulting residuals are those that would have ensued if the filters were run open loop (without measurement incorporation) from the time corresponding to the oldest window element to the present time. These instantaneous zero-gain residuals for each altimeter are then summed in a manner analogous to Eq. (7)-(9) in order to form each altimeter's AK residual at the intermediate window times, and these residuals are used via Eq. (1) to form the altimeter MLLRs from the oldest window time to the present time. The threshold logic of Eq. (2) is then applied to the lower MLLR. In the MLLR calculations, the mean has altimeter PFM magnitude, the variance reflects altimeter noise variance, and the worst-case error is the sum of the magnitudes of terms reflecting initial altimeter noise, initial vertical velocity estimation error and accelerometer bias.

Following the detection of a lateral or normal accelerometer fault, two versions of Eq. (10) are double-integrated, each using the output of a different sensor of the suspect type. The difference between these integrals and the measured altitude at each succeeding sample forms the AK residual for each suspect sensor. The AK MLLR mean is obtained by double integrating Eq. (10) with the suspect sensor BFM replacing the acceleration term. The worst-case error is computed as the sum of the magnitudes of terms reflecting initial altimeter noise, initial vertical velocity estimation error and transonic altimeter behavior, plus a term reflecting normal accelerometer scale factor error in the normal accelerometer MLLRs and lateral accelerometer misalignment in the lateral accelerometer MLLRs.

TRANSLATIONAL KINEMATICS

Translational kinematics (TK) refers to the redundancy between changes in aircraft velocity measured by the air data sensors and changes in aircraft velocity obtained by integrating the air-relative acceleration computed using inertial sensor outputs. The ARM algorithm utilizes TK to isolate faults in the longitudinal accelerometers, normal accelerometers and Mach meters.

The TK residual for longitudinal accelerometer j at time t_k , following a detected fault at time t_1 , is given by

$$\gamma_k(Ax^j) = \sum_{i=1}^k T[Ax_i^j - \overline{\sin\theta_i g + Vs_i M_i (r_i \sin\beta_i - q_i \sin\alpha_i)}] \\ - [Vs_k M_k \cos\alpha_k - Vs_o M_o \cos\alpha_o] \quad (11)$$

where Vs is the speed of sound, periodically recomputed as a function of altitude, g is the acceleration of gravity, and α , β and M are the measured angle of attack, sideslip angle and Mach number, respectively.* In the MLLR calculations, the mean at time t_k has magnitude equal to the longitudinal accelerometer BFM times ($t_k - t_1$), the variance reflects air data sensor noise and the worst-case error is the sum of the magnitudes of terms reflecting initial air data noise, a wind shear doublet, misalignment of the suspect accelerometer and transonic Mach meter behavior.

The TK residual for normal accelerometer j at time t_k , following fault detection at time t_1 , is given by

$$\gamma_k(Az^j) = \sum_{i=1}^k T[Az_i^j + \overline{\cos\theta_i \cos\beta_i g + Vs_i M_i (q_i \cos\alpha_i - p_i \sin\beta_i)}] \\ - [Vs_k M_k \sin\alpha_k - Vs_o M_o \sin\alpha_o] \quad (12)$$

The MLLR mean has magnitude equal to the normal accelerometer BFM times ($t_k - t_1$), the variance reflects air data sensor noise, and the worst-case error is the sum of the magnitudes of terms reflecting initial air data noise, a wind shear doublet, suspect accelerometer scale factor error and pitch rate gyro bias. The wind shear doublet magnitude and MLLR variance for the longitudinal and normal accelerometers each assume one of two values depending upon the binary output of a wind turbulence filter operating on lateral channel TK residuals.

* The measured angle of attack and sideslip angle are the vane readings compensated for their distance from the center of mass and supersonic alpha vane bias.

The TK residual for Mach meter j is calculated at time t_k as

$$\gamma_k(M^j) = \sum_{i=1}^k \left\{ v_s M_i^j \cos \alpha_i - v_s M_{i-1}^j \cos \alpha_{i-1} - T [A x_i - \sin \theta_i g + v_s M_i^j (r_i \sin \beta_i - q_i \sin \alpha_i)] \right\} \quad (13)$$

As for the attitude gyros and altimeters discussed earlier, the instantaneous residuals for each Mach meter, the terms in braces in Eq. (13), are stored in a moving window. At the time a Mach meter fault is detected, each sensor's instantaneous residual window is processed using Eq. (13) to compute its TK residual at the intermediate window times, and simultaneously Eq. (1) is used to compute each Mach meter's MLLR, with the threshold logic of Eq. (2) applied to the lower MLLR following complete window processing. The MLLR mean has magnitude equal to the Mach meter BFM times $v_s \cos \alpha$ at the time of detection, the variance reflects the effect of Mach meter noise, and the worst-case error is the sum of terms arising from initial Mach meter error and acceleration uncertainty.

TRANSLATIONAL DYNAMICS

Translational dynamics (TD) refers to the redundancy between the acceleration of the aircraft measured by the accelerometers and the acceleration predicted by stored aerodynamic coefficient functions using air data sensor measurements. TD residuals are used by the ARM algorithm to isolate failures in the lateral accelerometers and alpha vanes.

The TD residual for lateral accelerometer j at time t_k is given by

$$\gamma_k(Ay^j) = Ay_k^j - (CYB_k \beta_k + CYDR_k R_k) Q_k S/m_k \quad (14)$$

where CYB and CYDR are stored lateral coefficient functions of Mach and alpha, R is measured rudder position, Q is computed dynamic pressure, S is the surface area of the wing and m is the estimated aircraft mass. On every sample following fault detection, the residuals given by Eq. (14) are used in Eq. (1) to compute the lateral accelerometer TD MLLRs. The TD MLLR mean has lateral accelerometer BFM magnitude, the variance reflects air data noise and the worst-case error is the sum of the magnitudes of terms reflecting the effects of beta vane bias, lateral accelerometer misalignment, neglected lateral coefficients and scale factor error in the computed aerodynamic sideforce.

The TD residual for alpha vane j at time t_k is given by

$$\gamma_k(\alpha^j) = -(L_k^j \cos \alpha_k^j + D_k^j \sin \alpha_k^j)/m_k - Az_k \quad (15)$$

where the lift L and drag D are computed using each alpha vane output individually in stored functions of Mach, elevator position and angle of attack. The alpha vane TD MLLR mean has magnitude equal to the alpha vane BFM times the magnitude of the computed TD residual gradient, the variance assumes one of two values depending upon indicated turbulence level, and the worst-case error is the sum of the magnitudes of terms reflecting the effects of normal accelerometer scale factor error and aerodynamic coefficient error.

FLIGHT TEST RESULTS

The ARM algorithm has been implemented in the onboard computer software of the F-8 DFBW aircraft in a monitoring mode in which it is able to obtain all required sensor and effector information but its sensor status information does not impact the control law calculations, which are governed by the existing baseline sensor FDI software. The ARM software includes extensive error simulation and fault insertion capability, controlled by the pilot via the computer input panel (CIP), to allow inflight evaluation of ARM algorithm performance. Sensor faults that can be simulated include bias, drift, scale factor error, hardover, transient pulse and loss of signal. All relevant variables are tape recorded for postflight analysis.

Table I shows the BFM and detection window lengths used during the Phase I flight test program. The ARM sample period T is three control law cycles, 60 milliseconds. The simulated bias size is 1.5 BFM, the drift rate magnitude is 1.0 BFM/s and the scale factor error is 0.25 for all sensor types but pitch rate, for which it is 0.5. The simulated transient pulse magnitude is between the bias and hardover values, with a duration of three ARM samples. The Phase I flight test program consisted of six flights which covered the spectrum from trim to edge-of-the-envelope dogfight maneuvers. During these flights a wide variety of sensor faults were simulated. However, before discussing simulated fault isolation results, we mention two instances of actual hardware malfunctions that occurred during flight testing, enabling the ARM algorithm to demonstrate its utility.

Figure 1 depicts the alpha vane outputs, TD residuals and TD MLLRs during the in-

flight isolation of alpha vane 2 as unconditionally failed. The baseline FDI routine, which cannot isolate faults in duplex sensors, detected an alpha vane fault approximately twenty-four seconds after ARM isolation. Postflight examination of alpha vane 2 revealed a broken potentiometer segment.

In Figure 1 and those that follow, the independent variable is ARM samples. Dependent variable scaling is denoted by parentheses enclosing the letter E followed by a signed integer, indicating that the numerical value shown should be multiplied by the given power of ten to obtain the actual variable value. In all figures the sample at which the residuals and MLLRs become nonzero indicates the time of fault detection and initiation of the fault isolation processing.

The second malfunction occurred when one of the triplex computers experienced a memory parity error and was declared failed by the baseline system. Because the failed computer was dedicated to reading the number 1 instrument outputs, the computer loss manifested itself to the ARM algorithm as all number 1 sensors jumping to their negative maximum values. ARM selftest immediately declared all number 1 sensors provisionally failed, and the analytic redundancy tests declared all number 1 instruments unconditionally failed within 1.3 seconds.

Table II summarizes the average times between software fault insertion and fault isolation with the aircraft at trim at an altitude of 6.1 km and a Mach number of 0.6, and these times are in close agreement with predicted values. Although all inserted bias and drift faults were correctly isolated, several other fault types inserted at the trim condition did not produce appreciable output errors and therefore were not isolated. Sensor output selftest provisionally failed all sensors with hardover and pulse faults. The isolation times shown in Table II also reflect ARM algorithm behavior during moderate maneuvers.

Figures 2, 3 and 4 show the sensor outputs, RK residuals and RK MLLRs during the isolation of simulated scale factor errors for the number 1 roll and pitch rate gyros and simulated loss of signal for yaw rate gyro 1, respectively. The figures indicate the effectiveness of the ARM algorithm in isolating nonbias faults when observability is sufficiently high.

The ARM algorithm worst-case error terms and associated parameter values were chosen to reflect the telemetry data available to the design team. This data had been taken early in the baseline test program and included only moderate maneuvers. Therefore it was anticipated that the Phase I ARM flight tests might reveal deficiencies in the algorithm during extreme maneuvers, and this was indeed the case. The major deficiency discovered was the inability of the relatively simple air data sensor models to reflect the effects of extreme maneuvers on the airflow and pressure distributions around these instruments. In lieu of an extensive modeling effort, these model deficiencies can be accommodated by increases in the worst-case error coefficients, and in some cases an additional term, in the TK, TD and AK MLLRs. Although these changes do produce some increase in fault isolation times, they substantially decrease false isolation vulnerability. Another deficiency, consisting of high friction forces and large spin axis misalignment in the DGs, appears to have been corrected through reworking the hardware.

CONCLUSIONS

The Phase I flight test program demonstrated the validity and capability of the ARM concept. Of particular importance was the relative ease with which unforeseen sensor behavior could be accommodated via the worst-case error terms. Although a Phase II flight test program is planned to verify reliability of the modified algorithm, several conclusions can be made at this time:

- 1) Analytic redundancy sensor FDI is much more sensitive to sensor modeling errors than conventional techniques. Those sensor characteristics that cannot be accurately modeled must be accommodated in order to maintain reliability of the analytic redundancy tests.
- 2) The use of a bias failure hypothesis does not significantly restrict the ability to isolate nonbias failures in duplex systems. However, if more than one simplex sensor is involved in an analytic redundancy relationship, elaborate failure mode modeling is required for reliable FDI.
- 3) The potential exists for improving ARM performance by estimating individual sensor biases through continuous monitoring of analytic redundancy residuals. This would allow MLLR worst-case error bias terms to be lowered, and the levels of the estimated biases themselves could be used to make isolation decisions or for trend analysis.
- 4) Reasonability checks in the form of sensor output selftest are a powerful and effective complement to analytic redundancy tests.
- 5) Although the ARM software is more extensive than conventional FDI algorithms, it is similar in complexity to guidance and navigation calculations and poses no unusual implementation problems. Furthermore, its modularized structure lends itself to distributed processing. The F-8 DFBW ARM algorithm occupies approximately 8000 16-bit words of computer memory. Its timing requirements are approximately 5.6 milliseconds per 60 milliseconds with no detected faults and approximately 12 milliseconds per 60 milliseconds with twelve detected faults. These figures could be lowered somewhat by removing research-specific operations.

REFERENCES

1. Desai, M. N., J. C. Deckert and J. J. Deyst, Jr., "Dual Sensor Failure Identification Using Analytic Redundancy", Journal of Guidance and Control, Vol. 2, No. 3, May-June 1979, pp. 213-220.
2. Willsky, A. S., "A Survey of Design Methods for Failure Detection in Dynamic Systems", Automatica, Vol. 12, Nov. 1976, pp. 601-611.
3. Wald, A., Sequential Analysis, Dover, New York, 1973, Chap. 3.
4. Wald, A. and J. Wolfowitz, "Optimum Character of the Sequential Probability Ratio Test", Annals of Math. Stat., Vol. 19, 1948, pp. 326-339.
5. Deckert, J. C., "Definition of the F-8 DFBW Aircraft Control Sensor Analytic Redundancy Management Algorithm", Report R-1178, The Charles Stark Draper Laboratory, Inc., Cambridge, Mass., August 1978, pp. 10-15.
6. Chien, T. T., An Adaptive Technique for a Redundant-Sensor Navigation System, CR-140313, NASA, Washington, D. C., 1972.

ACKNOWLEDGEMENTS

The author wishes to express his sincere appreciation to the following colleagues for their invaluable contributions to the ARM project: R. R. Bairnsfather, M. N. Desai, J. J. Deyst and A. S. Willsky.

This work was supported by the National Aeronautics and Space Administration Dryden Flight Research Center through contract NAS4-2675.

Table I Phase I ARM Parameters

SENSOR TYPE	BFM	DETECTION WINDOW SIZE
Mach	0.045	3
Altimeter	30.5 m	5
Angle of attack	2.0 deg	9
Longitudinal accelerometer	0.15 g	17
Lateral accelerometer	0.15 g	17
Normal accelerometer	0.15 g	17
Roll rate	3.55 deg/s	3
Pitch rate	2.3 deg/s	2
Yaw rate	2.3 deg/s	2
Roll attitude	4.6 deg	6
Pitch attitude	2.1 deg	6
Directional gyro	15 deg	5

Table II Average Times to Fault Isolation at Trim, Seconds

SENSOR	BIAS	DRIFT	SCALE FACTOR	HARDOVER	PULSE	LOSS OF SIGNAL
Mach	0.08	NT	0	0	0.06	0
Altimeter	0.14	NT	NT	0	0.06	0
Angle of attack	0.86	2.04	x	0.18	x	0.24
Long. accel.	8.64	4.44	NT	0.9	x	x
Lat. accel.	0.24	0.84	NT	0.06	x	x
Normal accel.	4.38	4.56	4.32	0.42	x	1.26
Roll rate	0.66	1.56	x	0.12	0.18	x
Pitch rate	0.92	1.74	x	0.18	0.48	x
Yaw rate	0.8	1.68	NT	0.18	0.48	x
Roll attitude	0.16	NT	NT	0	0	x
Pitch attitude	0.18	NT	NT	0	0	0.06
Directional gyro	0.12	NT	NT	0	0.08	0

NT = no test

x = not isolated

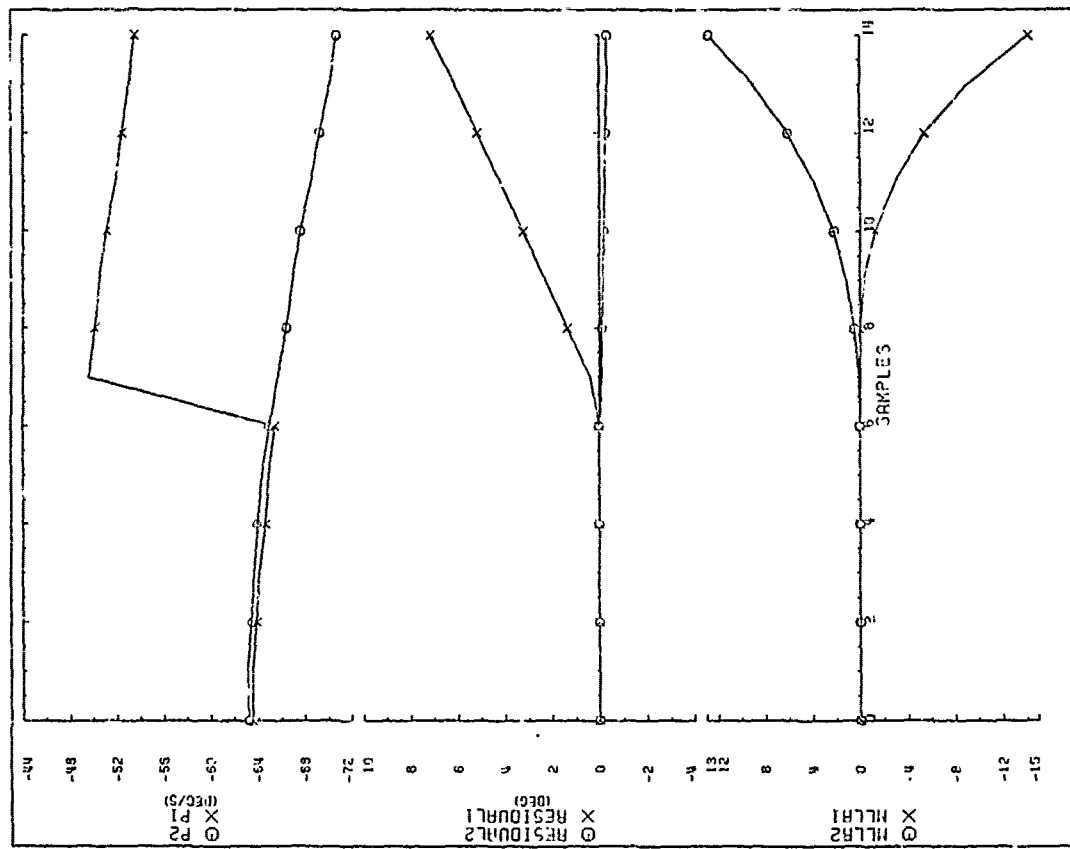


Figure 2 Isolation of simulated scale factor of 0.75
for Roll Rate Gyro 1

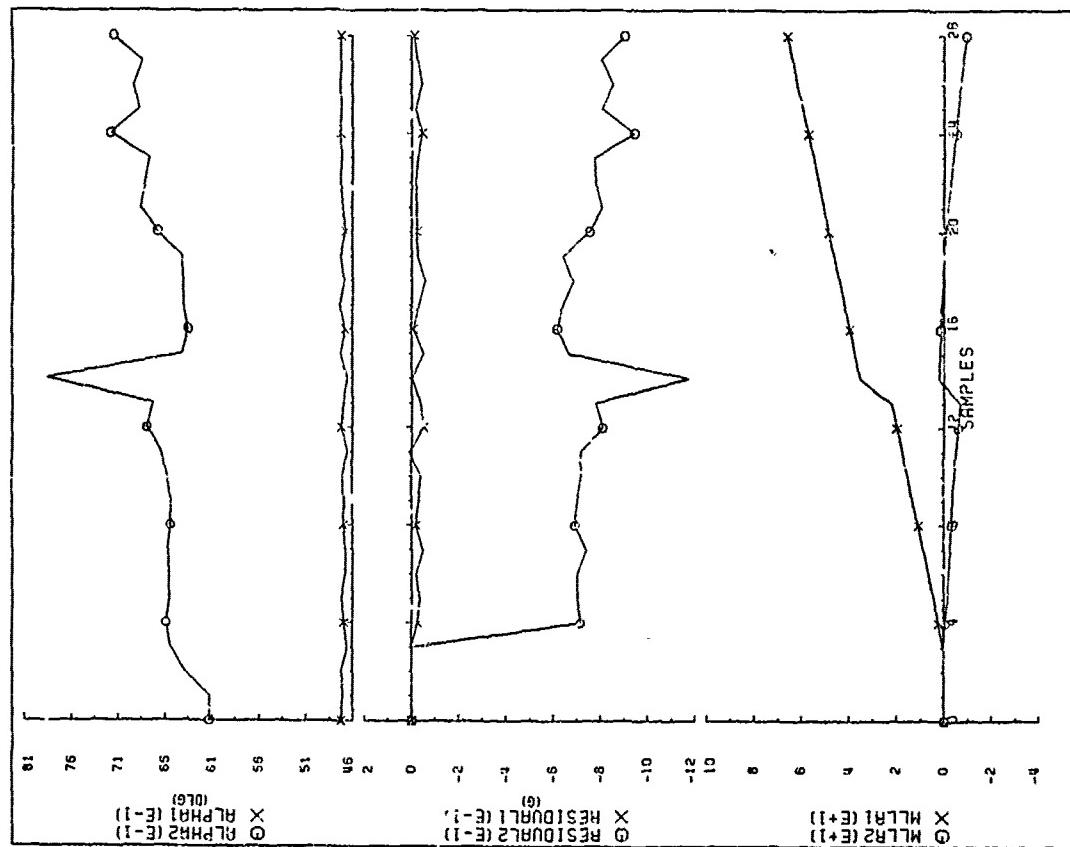


Figure 1 Isolation of actual Alpha Vane 2 Fault

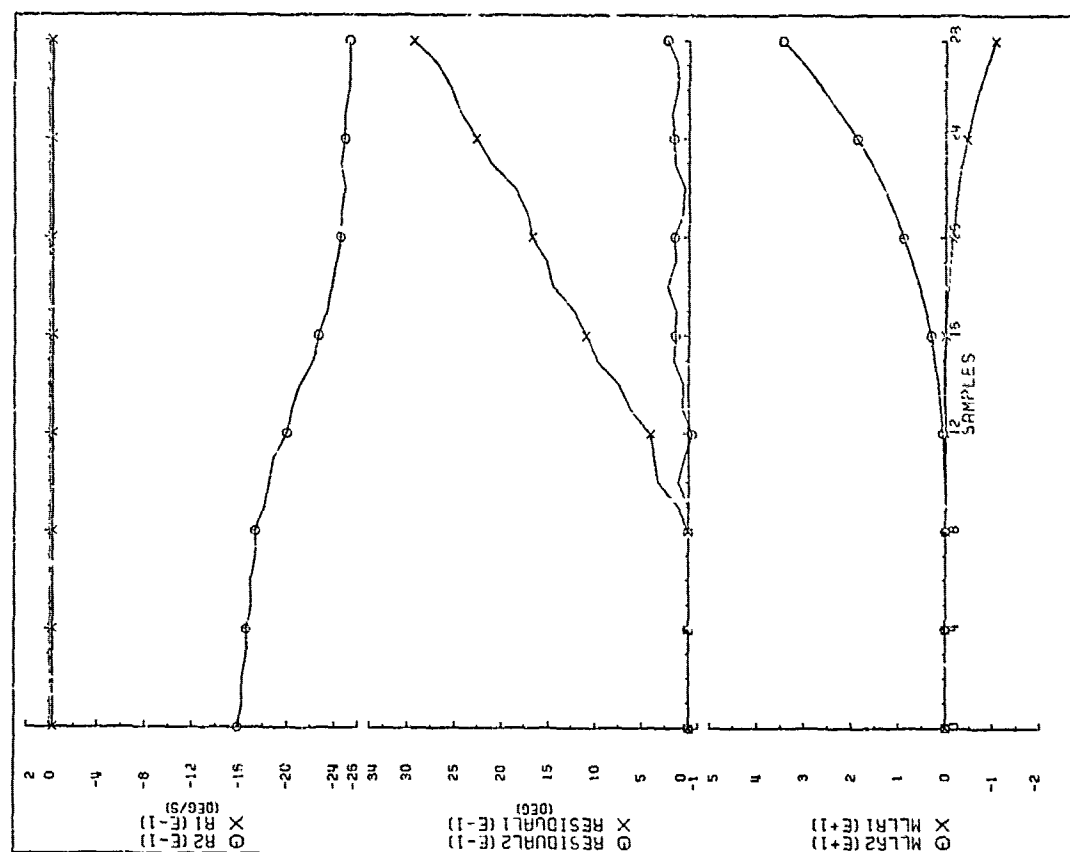


Figure 4 Isolation of Simulated Loss of Signal for Yaw Rate Gyro 1

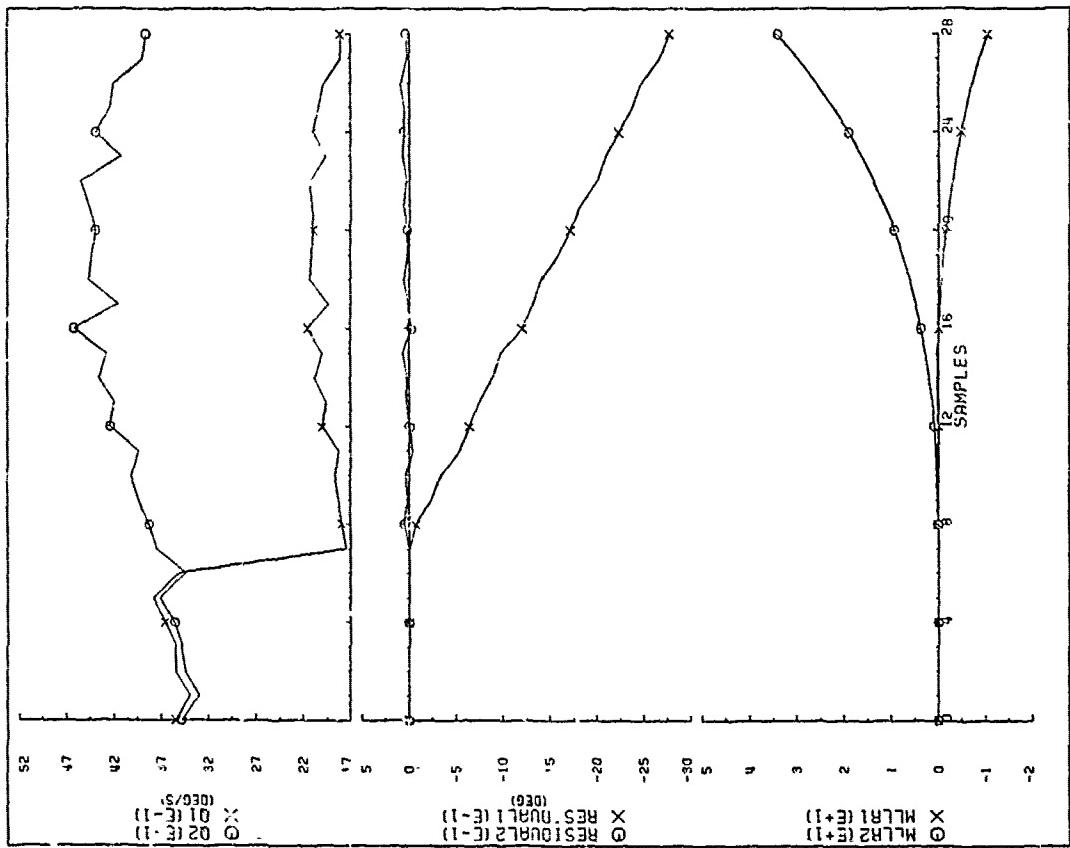


Figure 3 Isolation of Simulated Scale Factor of 0.5 for Pitch Rate Gyro 1

ENHANCING POSITION RELIABILITY BY FULLY INTEGRATING JTIDS AND GPS

By

H. James Rome

University of Lowell, Lowell, Massachusetts

Robert A. Reilly

Charles R. Ward

ITT Avionics Division, Nutley, New Jersey 07110 U.S.A.

ABSTRACT

This paper describes the key functional design features of a fully integrated JTIDS/GPS* receiver. It is shown that by fully integrating the signal processing of both systems, and by appropriate source selection algorithms, the control and slewing of the GPS tracking loops make it possible to dramatically enhance the positional reliability of the two systems. Functional block diagrams of the integrated design approach are described. In addition, the rationale for key elements of the design approach is outlined. A performance estimate is made showing the increase in the tolerable J/S (Jammer to Signal Ratio) made possible through integrating the systems.

1.0 INTRODUCTION

There are several potential advantages to having a GPS receiver and a JTIDS terminal resident on the same platform. Some of these advantages are listed below.

1. GPS can provide the highly accurate geodetic information required to stabilize the JTIDS relative navigation grid to a geoidal reference.
2. Highly accurate geodetic information can be transferred from users having both JTIDS and GPS capability to less capable vehicles having only a JTIDS terminal.
3. The JTIDS link has a potential of transferring satellite ephemeris and other useful GPS data to GPS receivers which must synchronize to satellite signals in a jamming environment.
4. Common hardware and software elements can be shared between GPS and JTIDS functions.
 - a. Both functions normally employ an inertial measurement unit (IMU).
 - b. Both systems require a highly precise time reference.
 - c. Both functions require a high capability navigation computer.
 - d. Both systems operate in L-band, providing the potential for sharing certain front end and signal processing hardware.

The implementation of many of these features to realize synergistic benefits has been investigated in [1].

This paper summarizes the results of a study which investigated further synergistic benefits through full integration of a GPS receiver and a JTIDS terminal. The study was motivated by the development of a MFBARS** system architecture [2]. This architecture is intended to provide a highly integrated multi-band communications, navigation, identification, CNI, radio terminal for a tactical aircraft, where the many functions of the terminal are under direct digital control such that they can be programmed and time shared without processing loss and with considerable savings in size, weight, and cost. The study reported in this paper, however, was not constrained to considering the equipment set on a single platform, nor the related hardware issues. The results of this study consist of purely functional designs concentrating on the navigation functions. Rather than considering the design from the viewpoint of a single platform, the design was conceived under the assumptions that a community of such terminals would exist and that one could aid the other through JTIDS links.

This paper shows that an order of magnitude performance improvement can be achieved by properly integrating the two functions. The great potential improvement is enhanced positional reliability. Accuracy improvement is not the primary objective. When combining two highly precise navigation functions, one can expect that only slightly more precise navigation function will result. Positional reliability implies the ability to navigate precisely in both relative and geodetic frames in virtually any adverse jamming situation. It will be shown that as the number of platforms utilizing the fully integrated functional capability increases, so does the resultant advantage to the system community.

*JTIDS - Joint Tactical Information Distribution System

GPS - Global Positioning System

**MFBARS - Modular multi-Function multi-Band Airborne Radio System

2.0 STRUCTURE OF THE FULLY INTEGRATED JTIDS/GPS TERMINAL

Consider the following analogy (see figure 1). Picture a fly caught in a spider web, the fly representing a given platform and the spider web representing the JTIDS navigation signal links between that terminal and the other community member terminals, as well as the GPS navigation signal links from the satellites to each terminal. The fly may escape only if every link to the spider web is broken (analogous to losing all precise navigation information). While each strand might be easily broken one at a time, for a dense web it is virtually impossible to break all strands simultaneously allowing the fly to escape. This is the situation which could exist within a community of many fully-integrated GPS/JTIDS terminals. It is expected that it will be virtually impossible to simultaneously lose all sources of precise position information and thus lose the capability of precision geoidal navigation required for tactical operations.

2.1 OVERALL DESCRIPTION

There are several key features which are required in a fully integrated terminal such that the desired synergistic benefits will be achieved. They are given below.

1. There should be a single Kalman filter, integrating all measurements in their most fundamental form available from the fully integrated system.

The procedure used to demonstrate these dramatic improvements involved first developing a strawman mechanization of the system. Although no deliberate attempts have been made toward completeness, we believe that the structure generated offers a valid blueprint toward detailed design. Then the generated structure issued a basis of analysis.

In describing the mechanization, first those functions and features of the system which are different from either JTIDS or GPS alone are outlined. This is followed by a functional description of how the various components of the integrated functions interact. Then additional design details of those functions which are critical to operation are given.

The performance projection is based on published data and analysis; some reasonable pencil and paper analysis, and some educated estimation based on the authors' experience.

The analysis shows that improvements in jamming resistance are potentially possible. It is also shown that for some jamming situations position reliability (probability of being able to navigate) can be enhanced by as much as 4 orders of magnitude. Finally some uses of the system in military operations are suggested.

It is anticipated that this filter will model the states associated with three dimensional geodetic position and velocity, as well as primary inertial navigation error states. In addition, it should model two dimensional grid position offset, relative grid velocity error states, and relative grid azimuth error. Furthermore, it should model GPS time and time rate error, JTIDS time and time rate error, and altimeter bias error.[3], [4], [5], [6].

2. Additional information is required on the JTIDS P-message. Currently the JTIDS P-message (Position reporting message) provides optimal estimates of the donor relative and geodetic states and quality data indicating the confidence in these estimates (derived from the Kalman filter). There are two measurements available directly from a JTIDS terminal. One is the time of arrival (TOA) measurement (a measure of range to the donor). The second is the round trip time (RTT) measurement. (These measurements provide a method for synchronizing one terminal to another.) In order to take maximum advantage of the fully integrated terminal it is necessary to allow two additional types of "offset" measurements to be reported as additional data on the JTIDS P-message.

The first type of offset measurement is the difference between JTIDS and GPS time from a fully integrated donor terminal. The usefulness of this data is easily demonstrated. Consider that one's own terminal is in the JTIDS net, is synchronized to JTIDS time, but has ascertained its geodetic position through measurements and reports from other terminals. It now wishes to acquire GPS signals.* In theory, our own terminal could slew its tracking loops to acquire GPS signals immediately if it knew GPS time. Then it could determine the precise PN code phase arriving at the terminal. Since the terminal is synchronized to JTIDS time it need only have a high quality measure of the difference between JTIDS time and GPS time in order to obtain this information. Also note that the quality of the reported time difference should be reported. Alternatively, if high quality GPS time were known on our own platform, this would reduce the requirement for frequent RTT** updates via JTIDS.

*We will assume that the ephemeris data of the specific satellites is known, since this data could also be transmitted within the JTIDS community.

**RTT - Round Trip Timing, used in JTIDS to synchronize the clocks of participating terminals.

The second type of offset information to be added to the JTIDS P-message is reported donor GPS pseudo-ranges. It can be shown that in a community of fully integrated terminals, it is possible to obtain a community geodetic update using reported pseudo-ranges from several terminals, none of whom may be tracking enough satellites to obtain a reasonable geodetic update as a stand-alone terminal.*

As an example, consider figure 2. The positions of three platforms are indicated by the ends of the triangle shown in the figure. The hyperbolic lines in the figure represent the lines of position (LOP's) derived from two GPS navigation satellites (with altitude assumed known). If the relative ranges (the sides of the triangle) between the platforms are known precisely, there is only one orientation of this triangle which satisfies the constraint that each of the platforms must lie on the LOP's indicated. Thus there is the potential for cooperative community geodetic fixing. With the above stated information transmitted among the community members, the computations can be carried out by any given terminal as part of the Kalman filtering process.

3. Apropriately modified source selection logic routines are needed. Critical to the operation of the fully integrated terminal is source selection logic which evaluates the usefulness of all the measurements (both direct and donor reported) available to it. It must properly choose, from among the variety of measurements available, those measurements which will be most effective in maintaining precision of both the geodetic and relative grids. Inputs will include JTIDS P-messages, TOA data, and RMT data, as well as GPS pseudo-ranges and tracking status data. When a complete set of pseudo-ranges is not available from its own GPS receiver, the source selection logic will then select JTIDS-derived geodetic data (according to the quality of data available) to obtain precise geodetic information (in the order of 15 to 30 meters) from donor terminals. Therefore, regardless of whether the GPS receiver is fully operational or not, there is a high potential for accurate geodetic and relative navigation, as well as recovery of both JTIDS and GPS time. This is a key feature of the integrated system and will be discussed in more detail in section 2.4.
4. Feedback from Kalman filter outputs to GPS tracking loops. With properly functioning source selection logic and Kalman filtering, it should be possible to precisely estimate the geodetic position (within 30 meters) and time states associated with the integrated terminal. The precise navigation state data can be provided to the GPS receiver tracking loops to aid tracking of the incoming PN code, even under conditions when the GPS receiver could not operate independently. Thus, with the appropriate tracking loop design (discussed in section 3), it is possible to relock code tracking loops under much more severe signal conditions than would be possible using conventional signal search algorithms. This is another key design feature and is discussed in detail in section 3.

Figure 3 is an overall functional block diagram of the fully integrated GPS/JTIDS terminal. At the heart of the terminal are the source selection logic, the measurement generators, and the Kalman filter which integrates the selected navigation information.

The measurements selected by the source selection logic are fed to the Kalman filter function which integrates the navigation equations pertinent to the IMU (Inertial Measurement Unit) and updates the state variables of the filter. Estimates of JTIDS and GPS time errors are used to correct their respective reference clocks.

A key function of the integrated navigation terminal is the use of optimal estimates of the state of the system to control the GPS receiver tracking loops. Rate aiding computations derived from direct IMU outputs, modified and corrected via the Kalman filter, will create the rate aiding signal, designated as \hat{R}_S .

During normal tracking \hat{R}_S permits a very narrowband tracking loop to be used. For short periods of time during jamming and high G maneuvers, \hat{R}_S can assist the tracking loops to maintain a near code lock position.

A second computation, unique to the fully integrated terminal results in the pseudo-range estimate, \hat{R}_{PS} . The estimated range to the satellite is computed using the optimal estimate of present position and the GPS receiver clock. Note that \hat{R}_{PS} and \hat{R}_S may be computed from information almost completely derived from other platforms. \hat{R}_{PS} could be used to generate precise estimates of the code phase which would be received from the satellite, even in the absence of reliably detectable satellite signals.

The tracking loop control function uses the Kalman filter covariance data and the lock indicator data to determine the type of slewing applied to the code tracking loop. The details of this process are explained in section 3.

*Reporting pseudo-ranges which are properly compensated for staleness is not a trivial matter. However, several suitable solutions exist.

Compare this configuration to that in which the GPS receiver acts as an independent input to a JTIDS source selection and Kalman filter routine. It will still be possible through source selection to maintain high geodetic accuracy even if the GPS receiver becomes inoperable. However, in a high jamming environment, as the GPS receiver loses lock, it also becomes increasingly difficult to relock the GPS tracking loops even when the jamming is reduced below the break lock level. This may happen with all the members of the relative navigation community, in which case, precise geodetic navigation may eventually cease. Rps slewing of the GPS tracking loops should minimize the likelihood of this situation, since \hat{R}_{ps} is the best estimate of the synchronization point and longer signal acquisition time constants can be employed.

2.2 THE KALMAN FILTER MEASUREMENTS

The many types of measurements available for use by the Kalman filter are outlined below. For each type of measurement, the Kalman filter estimate of the parameter is subtracted from the measured value to form a measurement residual which is used in correcting and updating the Kalman filter states. The filter models this residual as a linear combination of error states defined by the computed H, or measurement matrix. The noise (modeled by the noise covariance R) is computed according to quality numbers transmitted on the P-message and other factors related to the measurements.

In addition, the measurement residual magnitudes can be tested against their expected variance to determine whether or not to accept the measurement. Considering the great number of potential measurements, there is the opportunity to perform some highly sophisticated error control based on reasonableness tests. Also, satellite source selection logic can be modified when there are indications of poor received satellite signals.

By suitably configuring the measurement matrix (H) it is possible to formulate many different types of position fixes. They are listed below:

- a. Geodetic Update - derived from GPS terminal pseudo-range measurements, or from JTIDS time of arrival (TOA) measurements together with donor P-message geodetic data.
- b. Relative Position Fix - derived from JTIDS TOA measurements.
- c. Offset Geodetic Error - grid origin information from another platform is used to update the terminal's previous estimate.
- d. Offset Geodetic Fixing - derived from reported Pseudo-Range within the cooperative community.

The proper combination of these various types of position fixes as defined by the source selection logic as well as reported offset times between J1 DS and GPS clocks will tend to result in a virtually invulnerable community of integrated JTIDS/GPS terminals.

2.3 SOURCE SELECTION LOGIC

This section presents a description of a "straw-man" mechanization for the source selection algorithm. In this description, source selection logic pertinent to RTT (JTIDS) time source selection is not discussed, since any modification of the existing techniques employed in current JTIDS terminal designs would not be critical to the overall functioning of the integrated terminal. Such modification might, however, include utilization of internally computed GPS time information such that fewer RTTs would be required in moderate jamming situations.

Inputs to the source selection algorithm are:

- a. JTIDS P-messages received from donor member terminals.
- b. The identification of GPS satellites used for navigation.
- c. Navigation quality of the donor terminal as determined from the Kalman covariance.

The source selection routine has been arbitrarily set up so that screening takes place for geodetic navigation data and for relative navigation data on alternate source selection intervals. Source selection intervals are estimated to be in the order of 10 to 20 seconds. (This is consistent with the 16 second cycle time used in JTIDS [6].)

A flow diagram of the source selection algorithm is illustrated in figure 4. Assume that both JTIDS and GPS functions are operational, and that it is time for a geodetic or satellite update. The three or four pseudo-ranges from the GPS receiver are sampled. If valid signal tracking is indicated, these pseudo-ranges are stored and used for a Kalman update.

If some of the measurements are missed, the algorithm then tests the quality of navigation, Q_p , derived from the Kalman filter covariance. If Q_p exceeds a prescribed threshold, the algorithm simply proceeds as before, ignoring the missing data. If degraded geodetic position quality is indicated, the source selection routine initiates a scan of the P-messages derived from JTIDS. These P-messages and the TOAs measured by the JTIDS terminals may be used to compute a related geodetic position update. The source screening algorithm here may be quite complex. If fewer than four pseudo-ranges are observed, the screening algorithm may choose to use a TOA measurement from a high quality source member which is in a favorable geometric location in order to complete the determination of geodetic position. Alternatively, it may choose to store data for use in an offset geodetic fix. In addition, it may choose one or more offset time fixes. If visibility of satellites is low, and/or Q_p from available sources is low, and if the geometry is favorable, P-message reported pseudo-ranges may be also used as a source of data for offset pseudo-range fix.

If it is time for a relative navigation update, a source selection routine for screening only relative navigation data, as used on existing JTIDS terminals, is implemented.

If the GPS receiver is not operating, then the standard JTIDS source selection routines, which potentially mix geodetic and relative information, are implemented during every source selection cycle.

3.0 THE TIME LOCKED LOOP

One can imagine the pseudo-range estimation function of a GPS receiver as that of an observer viewing a TV picture of a clock on board the satellite. The function of a GPS receiver tracking loop is to adjust its own clock so that its time is synchronized with the observed time from the satellite. The clock time observed at the receiver is delayed proportional to the range from the receiver to the satellite. See figure 5. The receiver servo-controlled clock consists of a local reference oscillator which is rate aided in proportion to the range rate between the receiver and satellite. The output of the on-board clock time at "A" would be $t - R_g/C$, plus a synchronization error.

The code comparison circuits of the GPS receiver tracking loops take the difference between the estimated clock synchronization at point A and the observed clock from the satellite. The error is then fed back through the tracking loop filter so as to drive the clock output to match the observed GPS time. The time difference between the oscillator time output and the servo-control output is a measure of the "pseudo-range" to the satellite. Note that the steady state output of the tracking loop filter is an estimate of the oscillator rate error.

When jamming becomes excessive, no measurable correlation between the received signal and the internally generated reference signal used for time or code comparison will be observed. The result is that a noisy zero average signal enters the delay lock loop filter and the "Lost Signal" detection circuit. The loop will continue to be slewed by the rate aiding signal. If rate aiding were perfect, the loop would continue to be slewed correctly. However, noise from the error detector causes the code to drift from the ideal "zero error" position.

Rate aiding is not perfect, however, even when controlled by the Kalman filter. Thus, there is an additional tendency for the tracking loop to drift from the ideal position. Eventually, the resulting drift could cause a zero output in E_0 because the error in σ_s is greater than one chip (due to the limited tracking range of the error detector). In a conventional GPS receiver, search procedures would eventually have to be instituted when this condition occurred.

In the fully integrated GPS/JTIDS terminal, however, an accurate (30 meters) estimate of pseudorange, \hat{R}_g , is usually available -- if not from internally measured information, then from JTIDS derived information. \hat{R}_g can then be used to drive the tracking loops in the range slewing mode, as is shown in figure 6 (with the switches positioned as shown).

Estimated range rate and clock frequency error (which together make up pseudo-range rate) are input to the integrator in the servo-controlled clock. The output is an estimate of $t - R_g/C$. The time difference generated between the servo-control clock and the local oscillator represents an estimate of the pseudo-range. The pseudo-range estimate from the Kalman filter can then be differenced with this estimate, resulting in an error signal used to slew the loop. This will maintain the loop essentially synchronized with the incoming signal, even though the latter is not observable. Ideally, when the jamming noise is reduced and a valid phase comparison made ($E_s < 1$ chip), the loop would relock almost immediately.

The blocks on this diagram represent high duty cycle logic, for determining if the loop is correctly locked and for mode switching. The lock indicator signals are a direct output of the time comparison circuits of the code tracking loops and can be used to indicate when lock is again achieved (i.e., when the satellite is again observable).

When lock has been reestablished, the tracking loops can be immediately switched to narrowband, or long time constant tracking, by moving the switches from the position shown in figure 6 to the position indicated by the arrows. The estimate of clock frequency would be switched out of the loop in one location and used to initialize the integrator in the tracking loop filter on the right hand side of the figure. This is done to equalize the steady state output of the tracking loop filter to the clock error rate. The loop would only have to cope with small accumulated time and frequency drift errors developed during the signal off time. Conventional tracking with the long tracking loop time constants is immediately implemented.

Now assume that signal lock has been lost again. The expected standard deviation of the pseudo-range estimate from the Kalman filter is then computed and tested against some small threshold value. If the estimated standard deviation is below this threshold, indicating the potential for good range slewing, the switches are changed back again to the position shown in Figure 6. This type of processing can continue, switching back and forth between one mode and the other, for individual tracking loops, in any combination or sequence.

Note that this type of operation in the tracking loops would be impossible without a fully integrated terminal, since the estimate of precise GPS pseudo-range information and the estimated quality of the pseudo-range information would not be developed unless integration was fully designed into the structure of the GPS receiver tracking loops.

With these two operational mode capabilities in addition to the conventional coherent GPS mode, and with a properly functioning, fully integrated terminal, it is then possible to have frequent lock and unlock conditions in the GPS tracking loops without instituting any particular search procedures and experiencing their resulting transients. Also note that violent maneuvers which cause temporary loss of lock should require no specialized initialization. The performance appears to be limited only by the extent of "noise drift" experienced before the "lost signal" detector switches modes.

As currently configured the GPS receiver tracking loop employs coherent COSTAS tracking to demodulate the 50 bit per second bi-phase data superimposed on the GPS coded signal. A six dB S/N loss, which is suffered because of this, could be avoided in high dynamic or high jamming terminals by using data transferred from less highly stressed terminals to strip the data from the signal. It will then be possible to increase the time constants of the correlation averagers. The averaging time would then be limited only by the uncertainty in the received RF doppler frequency. Doppler frequency estimates are naturally generated from the Kalman filter's estimate of pseudo-range rate. Thus it will be possible, by data message stripping, to significantly increase the averaging time of the GPS tracking loops, resulting in greater resistance to noise or jamming.

Furthermore, since temporary loss of GPS lock is of minor importance for a fully integrated GPS/JTIDS terminal, the fact that the 50 bps GPS message can change at unpredictable times (causing a temporary loss of lock) has little impact. Other members of the community (indirectly through source selection, etc.) can provide the appropriate geodetic information by broadcasting the message change, facilitating mode changes to reacquire lock.

4.0 PERFORMANCE IMPROVEMENT ESTIMATES

Given that both the JTIDS and GPS functions are operating close to their full potential, it is doubtful whether there will be significant improvement in geodetic navigation accuracy over that which would be obtained through the GPS receiver and INS alone, or in relative navigation accuracy over that which could be obtained by a JTIDS terminal and INS alone.

The primary improvement from full integration will be the ability to operate under much more severe jamming conditions.

Generally in a real scenario GPS will be severely jammed for only some of the community of vehicles. Others, by virtue of their distance from jammers will be relatively unaffected. Perhaps the best figure of merit would be a comparison of the probability of successful navigation with and without a fully integrated JTIDS/GPS capability, considered over a broad spectrum of missions, force groups and enemy countermeasures. The analysis to develop such a figure of merit is beyond the scope of this paper since detailed simulations would be required to answer such questions. However, through some broad generalizations, some simplification, and some relatively straight forward logic, it is possible to demonstrate the potential for dramatic improvements in system performance.

Below are some of the generalization and simplifications used in the analysis.

1. All vehicles experience the same jamming power (obviously pessimistic).
2. Successful navigation simply implies having a navigation accuracy consistent with having at least 3 code loops in lock (regardless of whether or not a given platform has actually achieved lock).

3. The source selection logic is "smart enough" to do the right thing at the right time.
4. A/J margin improvement is used as a figure of merit.

Consider equation (1) from [3] which describes the RMS error of the GPS code tracking loop:

$$\frac{\sigma_T}{D} = \left[\frac{NB_L}{2C} \left(1 + \frac{2N}{CT_1} \right) \right]^{1/2} \quad \text{EQ (1)}$$

In the above equation, N is the noise spectral density, C is the carrier power, B_L is the bandwidth of the tracking loop, and T₁ is the averaging time of the correlation averagers. σ_T is the RMS code tracking error, and D is the width of a single code chip. In a typical rate-aided receiver, B_L is of the order of 0.01 Hz, and T₁ is of the order of 0.02 seconds, the data bit length.

By implementing data message stripping, it should be possible to increase T₁, conservatively to 0.2 seconds. This will allow a significant increase in jammer-to-signal ratio before lock would be lost. Using an RMS threshold of 0.31 chips for loss of lock [3], it can be shown that the J/S threshold value for GPS code tracking can be as high as 71 dB versus 67 dB if no data stripping were accomplished.

Further improvements are made possible in the fully integrated terminal when members of the community can share navigation information as described in this paper. This is due to two phenomena.

1. The community will only lose highly precise GPS geodetic information when virtually all its members are denied simultaneous access to all the satellites.
2. The more powerful jammers are generally ground based. Therefore directions of arrival of the jammer signals with respect to the satellite signals will be different for each of the fully integrated JTIDS/GPS community members.

First consider point 1. In a conventional, rate-aided GPS receiver, once lock is lost, search algorithms will generally be necessary for relock. Thus, the tolerable J/S threshold level must be reduced by 10 dB or more to relock reliably. Once relocked, the bandwidths (to result in only a 0.1% probability of losing lock, assuming a gaussian distribution) are set to yield a normalized code loop error of σ_{T/D} = 0.31. However, in a community of fully integrated terminals, the tolerable J/S could be increased such that σ_{T/D} = 0.73 chip. Probabilistically, (assuming a gaussian code error) only about 82% of the time will a given code loop be locked. However, in a community of many members, there will be a very low probability that many tracking loops tracking this satellite will be unlocked simultaneously, such that the appropriate sharing of precise information could not take place via JTIDS.

This conclusion is justified by considering two extreme cases where it is shown that the probability of successful navigation of all vehicles is approximately the same for a community of stand alone GPS platforms with σ_{T/D} = 0.31 as it would be with a community of fully integrated platforms with a σ_{T/D} = 0.74. Consider a community of four vehicles, in this example, where it should be apparent that improvements will be greater if there were more terminals, or when some of the terminals are in a less stressed environment. "Truth" should be bracketed by the two extremes considered.

At one extreme, assume that the noise on all tracking loops on a given terminal are perfectly correlated, so that loss of lock on one tracking loop implies loss of lock on all four loops. Also assume that accurate geodetic community navigation will be lost only if all terminals lose lock. Thus, the probability of all integrated vehicles with a σ_{T/D} = 0.74 losing lock is $(1 - 0.82)^4 = 0.001$. This is actually 10 times smaller than the probability (0.004) of at least one of 4 stand-alone platforms with σ_{T/D} = 0.31 losing lock.

At the other extreme, assume the more realistic situation that lock errors on all tracking loops are independent. The same 4 satellites are in view of all platforms. Assume that successful navigation on a stand-alone platform implies that at least three of the four tracking loops are in lock. Thus the probability that a given stand-alone terminal will not have successful navigation is 0.6×10^{-5} . And the probability that at least one of the four is not in lock is 4.4×10^{-5} .

Assume that successful operation with a community of 4 fully integrated terminals will be possible at least if six pseudo-ranges are observed and at least three satellites are observed at least once. (And information can be distributed through pseudo-range reporting.) Through combinatorial analysis (find the probability of 5 or less satellites tracked in 16, add the probability of two or less satellites tracked, subtract the probability of less than 5 loops tracked and less than two satellites observed). It can be shown that the probability of not having successful navigation is 1.7×10^{-5} , which is comparable to 2.4×10^{-5} .

Truth will lie somewhere between the two extremes outlined above. At either extreme it is seen that there can be a J/S advantage approximately 5 dB with the fully integrated system for the same performance (see figure 4 in [3]).

An even more dramatic comparison can be made between the probability of successful navigation for the stand alone platform and $\sigma_{T/D} = 0.74$ for a community of fully integrated platforms when in both cases $\sigma_{T/D} = 0.74$ (assuming the second "extreme situation"). For the stand-alone platform the probability of three or four loops in lock is only 0.85 (vs. 1.7×10^{-5} for the community). Thus, there is a four order-of-magnitude improvement in position reliability for this situation using the fully integrated system.

What is seen here is analogous to performance of coding in a communications channel. A good code will dramatically improve probability of error for a given S/N. However, the S/N advantage in using the code may only be a few dBs. The procedures for the fully integrated receiver is, in effect, an error correcting code for navigation.

Although it has not been quantified, there is a further potential for improvement through the fact that the bandwidths of the tracking loops can be made even narrower since occasional maneuvers on a given platform will not mean permanent loss of lock, requiring a full initial search.

Now consider point two. An appropriate null steering antenna (NSA) can null out a jammer by as much as 50 dB. However, spurious nulls created in the NSA algorithms can potentially null out a satellite signal. There may be several jammers, resulting in a complex null pattern. We expect that the net result of these phenomena will cause the NSA to have an effective resistance against sophisticated jamming of about 8 dB.

We expect that the directional patterns of the antennas will be primarily a function of relative geometry. Since each vehicle in the community of fully integrated systems will be in a different relative geometry, the probability that a given satellite will be unobservable to some member community will go down exponentially with the number of vehicles involved.

Thus, with many vehicles, it is anticipated that the J/S which can be tolerated will approach the null depths of the adaptive array response pattern. In a practical implementation we expect an additional 9 dB resistance to jamming in the community adaptive antenna. (Community because one vehicle can transmit his pseudo-range information to another.) In truth, this number may be grossly conservative since some members of the community will be at significant distances from jammers and thus experience significantly less jammer power.

Table #1 summarizes the results for GPS. These results assume that GPS data message stripping picks up a 4 dB advantage previously lost in the COSTAS loop; that having a community of fully integrated terminals adds a 5 dB advantage; and that having a null steering antenna on a stand-alone GPS receiver has an 8 dB advantage. Having a null steering antenna in a fully integrated GPS/JTIDS terminal community is assumed to provide a 17 dB advantage.

Table 1
Tolerable J/S Estimates (dB) for GPS Tracking Loops
in a Community of Integrated GPS/JTIDS Receivers

	Additional Features			
	None	With Message Stripping	With Null Steering Antenna (NSA)	With Both NSA and Message Stripping
Stand Alone GPS With Inertial Aiding	67	71 Unreliable	75	79
Fully Integrated GPS/JTIDS in a Community of Similar Systems	72	76 Reliable	89	93

A valid comparison between the stand-alone GPS receiver with inertial aiding and a community of fully integrated GPS/JTIDS terminals can be made by referring to the estimates of J/S ratio tolerable by the stand-alone GPS receiver with a null steering antenna (but without data message stripping) and the fully integrated GPS/JTIDS terminal, which incorporates both GPS data message stripping and the null steering antenna. The potential J/S advantage for GPS is a significant 18 dB. Even assuming that only half of this can practically be realized, there would still be a strong incentive for implementing the fully integrated GPS/JTIDS terminal. The potential is so great that the quality of community navigation may not be limited by the GPS signal environment, as assumed herein, but rather by the vulnerability of JTIDS to its signal environment.

Furthermore, less tangible benefits due to integrating GPS and JTIDS terminals exist. For instance, as described above, less than a full complement of available satellite signals can still be extremely useful in maintaining highly accurate geodetic navigation when GPS and JTIDS terminals are integrated. Ease of initial GPS lock, or more importantly, rapid re-acquisition can be a direct result of the full integration.

5.0 ADVANTAGES OF USING FULLY INTEGRATED JTIDS/GPS IN VARIOUS FORCE GROUPS

The information diversity available in the fully integrated terminal allows for flexibility and redundancy which would not otherwise be possible. Below are some obvious and some not so obvious examples of potential interest.

First consider general improvements to the availability of precise navigation capability. Beyond the FEBA there is likely to be a high level of jamming. A remote fully integrated system, far from the FEBA, could transmit GPS-JTIDS time difference so that vehicles in the battle area, without the benefit of suitable JTIDS TOA data, could navigate with precision (in two dimensions) using only two satellites. Of course, the availability of JTIDS TOA's from fully integrated terminals would further improve position reliability. In addition, JTIDS ground terminals at known map locations could provide highly accurate position information to fully integrated terminals so they could maintain their GPS relock capability in a high jamming environment.

Navigation precision can be dramatically enhanced for passive operation at sea. With one or two active, fully integrated airborne terminals, a passive surface ship could synchronize to JTIDS time (via GPS) in order to make maximum use of donor JTIDS TOA's.

Furthermore it is theoretically possible for a passive ship with a fully integrated terminal to obtain all relative and geodetic position and time states with two active GPS/JTIDS donor terminals and only two available GPS satellites (there are enough equations for the unknowns in the static situation, and improvements will result because of vehicle motion).

Note that without the fully integrated terminals it would not be possible (in the static situation) to obtain relative range from the passive ship to the airborne vehicles, to say nothing of azimuth angle.

Now consider potential enhancements to tactical operations. The existence of a community of fully integrated terminals allows near perfect mapping from relative to geodetic coordinates. Thus a forward observer can report map coordinates, JTIDS coordinates or raw GPS measurements and a successful blind bombing is possible with an aircraft using GPS only, JTIDS only (updated by the fully integrated donor terminals), or a fully integrated terminal.

In an analogous scenario, an enemy ship at sea could be tracked from one or two (remotely located) sensors at least one of which has a fully integrated terminal. Then an anti-ship missile, using GPS and/or JTIDS for navigation could be guided to the target with razor sharp precision.

In a cooperative, passive type of emitter location operation, the number of permutations of navigation equipments which could contribute to the location and attack of enemy emitters become huge, because often at least two equivalently accurate sources of time and position exist at one time. Assume there are one or two fully integrated GPS/JTIDS terminals in the area to relate relative and geodetic grids and time frames. Then GPS receivers, JTIDS terminals, and/or fully integrated GPS/JTIDS terminals, on platforms suitably equipped with scanning receivers, could be used to report emitter signal times of arrival and positions at observation, as required for locating the emitter.

6.0 SUMMARY AND CONCLUSIONS

This paper has described the key navigation features of a functional design of a fully integrated JTIDS/GPS terminal. There are two key features of this design. The first feature is the use of a Kalman filter source selection routine which properly weighs and chooses the best measurements available from both the JTIDS community and the GPS satellite constellation for inclusion in navigation updating. The second feature is the use of data derived from a Kalman filter to provide estimated GPS pseudo-range and pseudo-range rate data which can be used to rate aid, control and slew the GPS receiver tracking loops even during periods of high jamming.

The result of these two features is a community navigation system which is nearly invulnerable to electromagnetic interference. The greater the number of community members the greater the potential jam-resistance enhancement.

By providing space in the JTIDS P-message for the measured difference between GPS and JTIDS time, and for observed GPS pseudo-ranges, knowledge of GPS time is possible without direct reception of GPS signals. Also, it is possible for the community to establish a geodetic fix with as few as two GPS satellites.

The full integration of the two systems can provide GPS receivers with as much as an 18 dB improvement in tolerable J/S over that of a stand alone GPS/INS system. Further, the impact of GPS loss-of-lock because of acceleration, rapid changes in antenna patterns, and other short-term maneuver-related effects, can be dramatically reduced.

This paper has merely touched the surface, however, in attempting to define all the advantages of fully integrating the GPS and JTIDS equipments.

Areas which should receive further study include the following:

1. A simulator which will be able to more perfectly estimate the performance enhancement.
2. Development of detailed satellite source selection logic which takes into account the existence of the community of fully integrated terminals where information can be shared readily.
3. Full utilization of more robust error control functions made possible by the "glut" of information available.
4. Optimal control of the GPS tracking loop (time constant) parameters, based on the information available from the fully integrated terminal community.
5. The potential reduction in total platform equipment cost.
6. Quantitative evaluation, through mission analysis and/or simulation studies, of the improved effectiveness possible through the navigational data redundancy and the flexibility in the mixes of terminal configurations which could potentially carry out a mission.

The advantages of fully integrating JTIDS and GPS navigation functions are so overwhelming that it seems clear that there is a need for immediate detailed design studies, equipment development and rapid deployment.

REFERENCES

1. GPS/JTIDS/INS Integration Study, Final Report, Charles Stark, Draper Laboratory, April 1978.
2. Modular Multi-Function Multi-Band Airborne Radio System (MFBARS) Preliminary Report, ITT Avionics, January 1980.
3. Hemesath, "Performance Enhancement of GPS User Equipment", Journal of the Institute of Navigation, Volume 25, No. 2, Summer 1978.
4. Fried, Loeliger, "Principles, System Configuration, and Algorithm Design of the Inertially Aided JTIDS Relative Navigation System Function", Navigation Volume 26, No. 3, Fall 1979.
5. Hughes, JTIDS Rel Nav for Hughes Aircraft Co., Intermetrics Corp. Report 25, August 1978.
6. Navigation Program Spec for JTIDS, Kearfott Division, Singer Corporation.

BIBLIOGRAPHIES

- Milliken, R. J., Zoller, C. J., "Principles of Operation of NAVSTAR and System Characteristics", Journal of the Institute of Navigation, Volume 25, No. 2, Summer 1978.
- Spilker, "GPS Signal Structure and Performance Characteristics", Journal of the Institute of Navigation, Volume 25, No. 2, Summer 1978.
- "GPS High Anti-jam Performance Analysis", McDonald, Analytic Sciences Corp. Report #TR 974-1, January 1979.
- Newman, L., "Navigation Architecture" (of JTIDS) Principles and Operational Aspects of Precision Position Determination Systems. AGARDograph #245, July 1979.
- Rome, H. J., "Evaluation of the Accuracy of Community Relative Navigation Organizational Concepts", ION National Aerospace conference, April 1976.
- Rome, H. J., "Feature of a Fully Integrated JTIDS/GPS Navigation Structure", Report to ITT Avionics, January 1980.
- Kriegsmar, et al, "Navigation Filter for GPS/JTIDS/INS System for Tactical Aircraft". "IEEE Position Location and Navigation Symposium", November 1978.

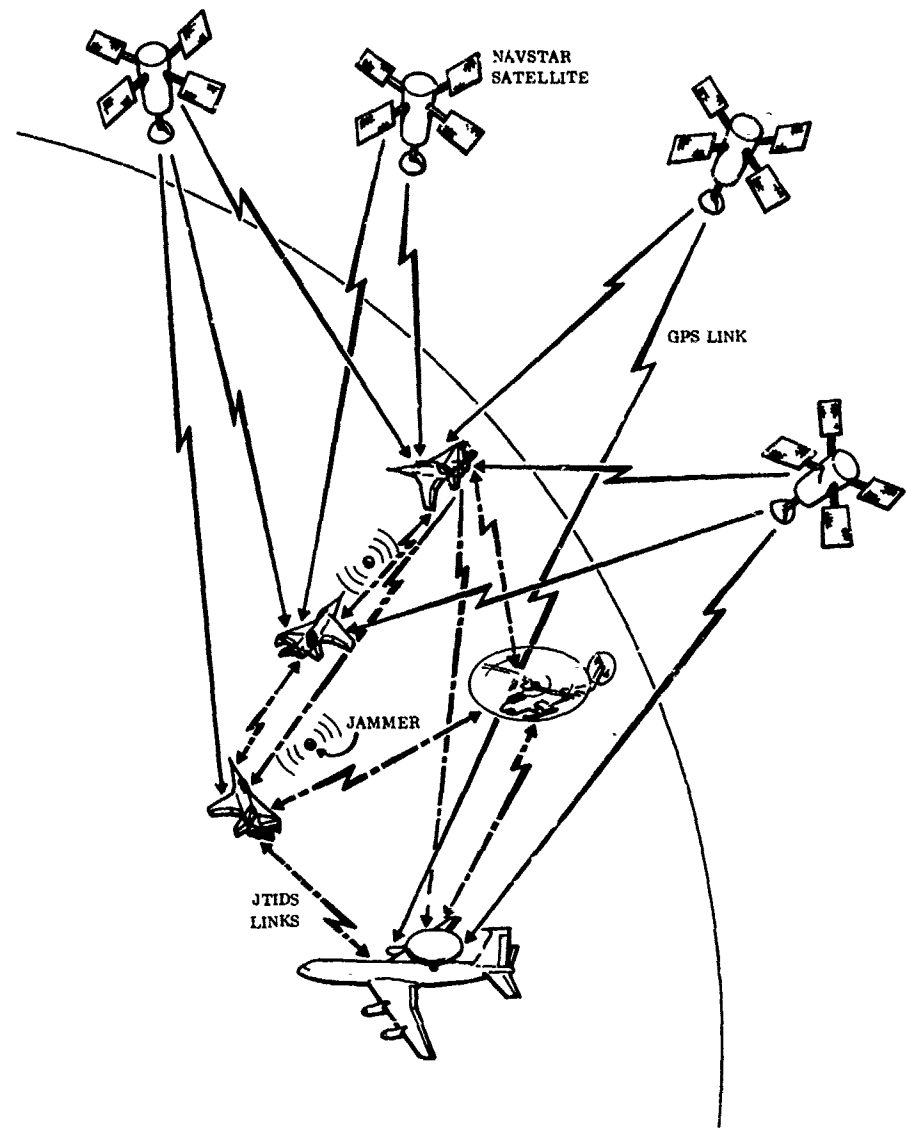


Figure 1. Integrated JTIDS/GPS Operation

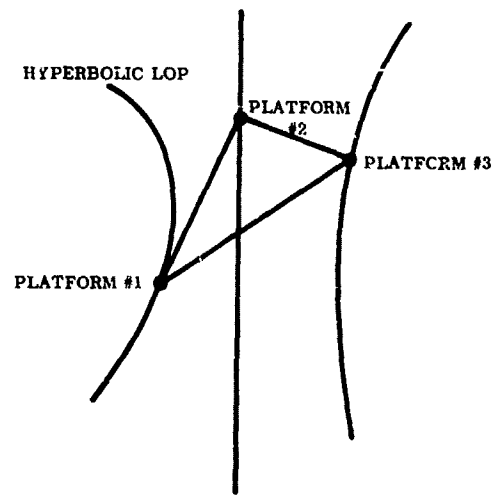


Figure 2. Geometry of Three Platforms in a Field of Hyperbolic Lines of Position (LOP)

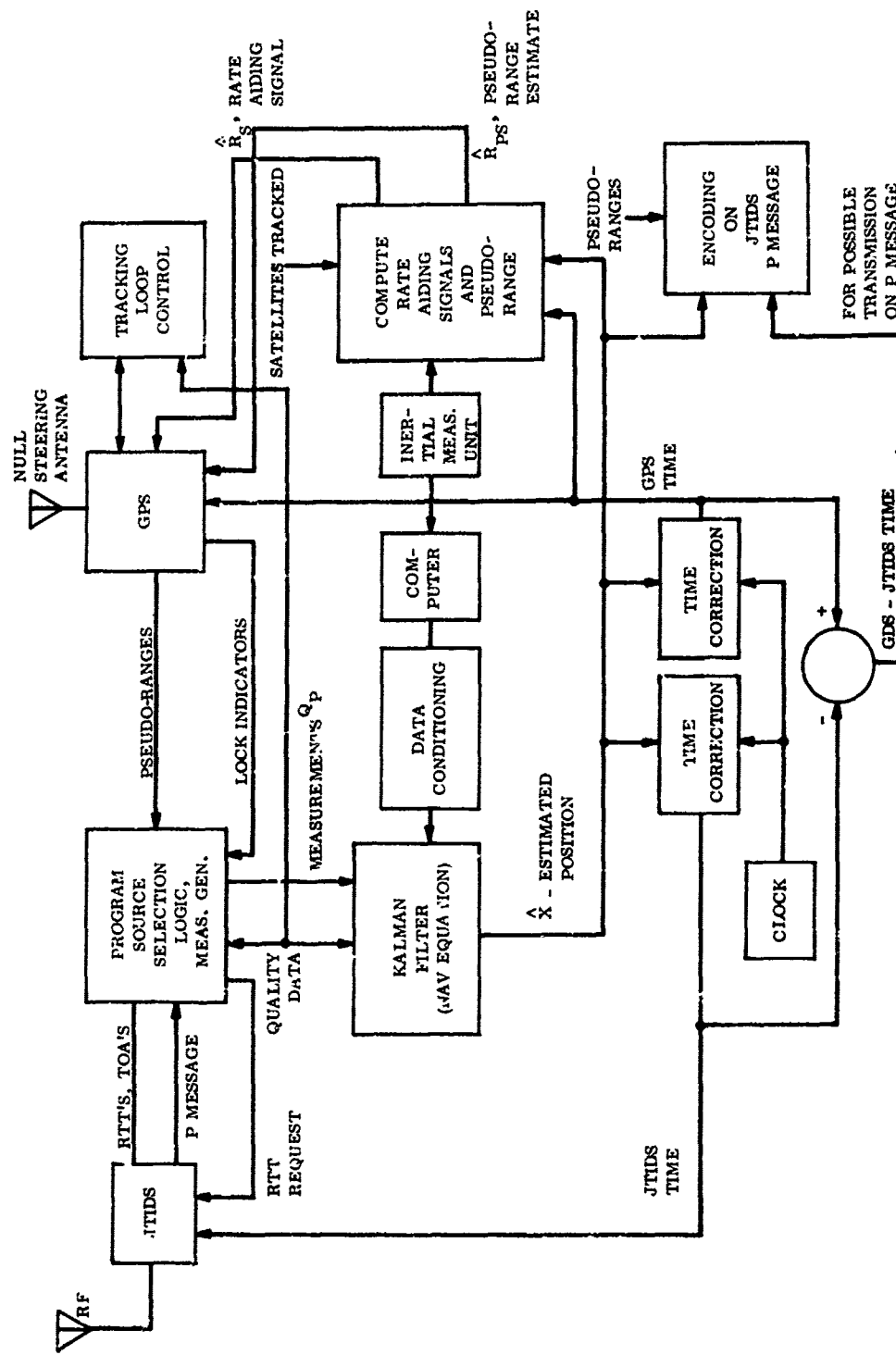


Figure 3. Description of the Hardware and Software Functions for the Integrated JTIDS/GPS System

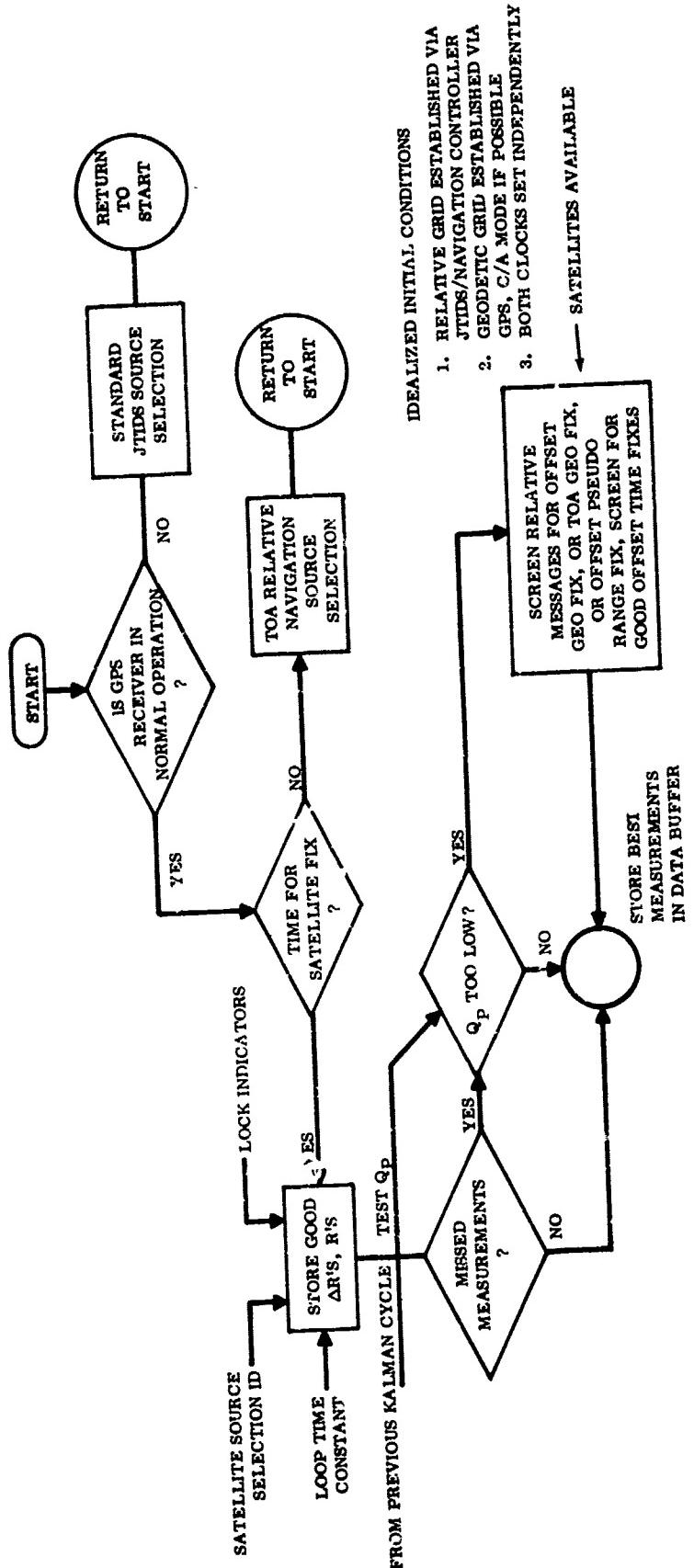


Figure 4. Source Selection Algorithm
for Integrated JTIDS/GPS Operation

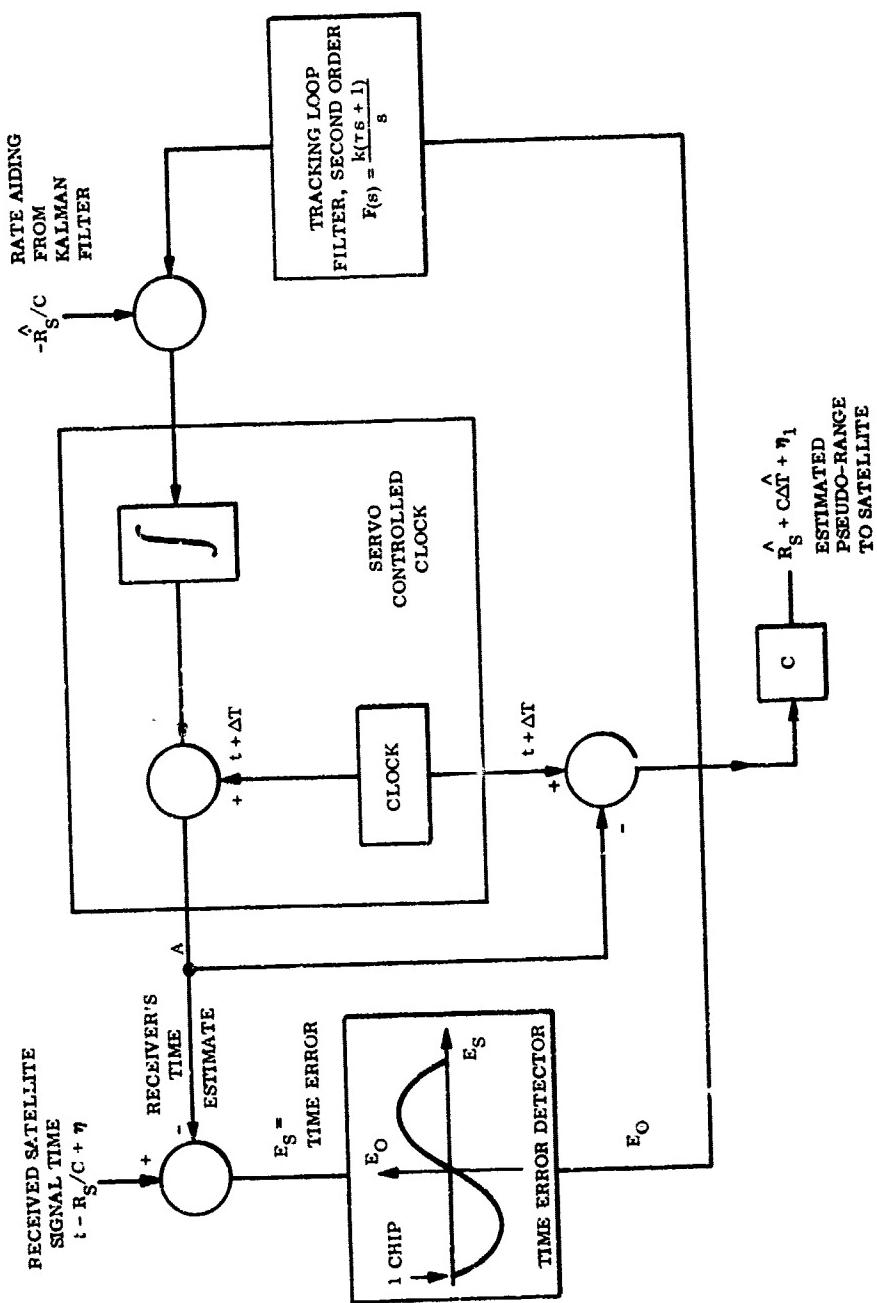


Figure 5. GPS Receive Time Locked Loop - Normal Operation

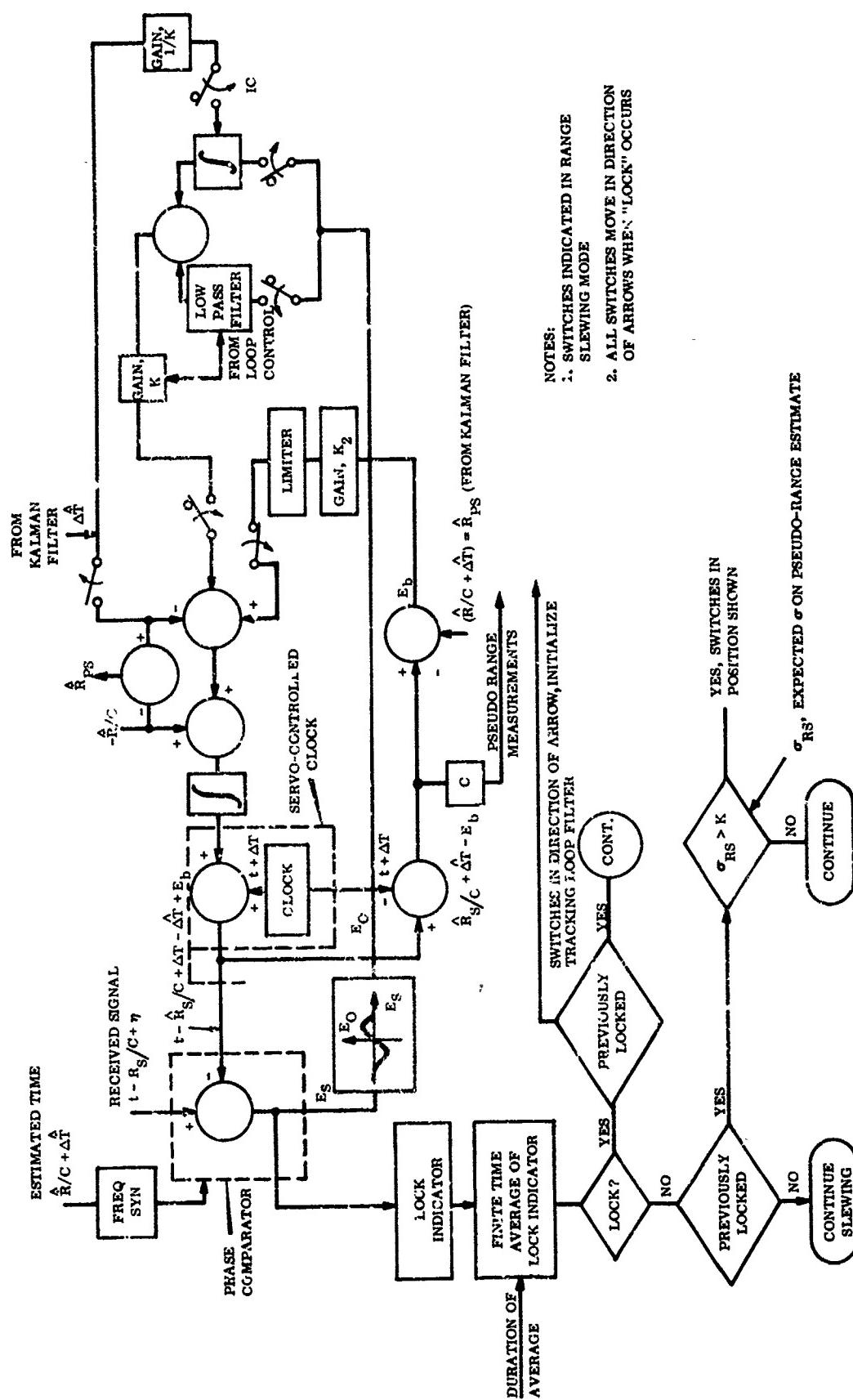


Figure 6. Integrated JTIDS/GPS Terminal Tracking Loop

NAVSTAR GPS RECEIVER FOR SATELLITE APPLICATIONS

R. Thorensen, K. M. Joseph, J. J. Winterhalter, J. R. Champion*
 2829 Maricopa Street
 Torrance, California 90503

SUMMARY

This paper describes a GPS navigation receiver/processor and ancillary units which combined constitute a spaceborne GPS Navigator (GPSPAC). This navigator is intended for use on DOD and NASA low altitude satellite host vehicles, i.e., Landsat D. GPSPAC provides highly accurate three dimensional position and velocity of the host vehicle together with precision time determination using signals from the NAVSTAR/GPS constellation of Navigation Development Satellites (NDS's). GPSPAC system architecture and design are described, functional and operational characteristics discussed as well as principal hardware, software and navigation features. Finally, a description of test support equipment, test methods and test results is presented.

1.0 INTRODUCTION

The Magnavox Company has for the past ten years been a major contributor to the system design, concept validation, and user equipment development for NAVSTAR GPS. Currently Magnavox has contracts with the U.S. Government for continued support of GPS Phase I activities as well as for the full scale engineering development of a broad class of User Equipments on the GPS Phase II program.

These equipments will be suitable for use on military fighter, bomber, and transport aircraft, surface ships and submarines, tanks, trucks and other land vehicles and include as well a special man-portable unit (Manpack) for use by the infantry.

Since 1958 the Applied Physics Laboratory (APL) of the Johns Hopkins University has been engaged in the development and application of systems for determining satellite position and orbital parameters. APL's pioneer work with doppler systems led to the development of doppler beacons on host vehicles and, more recently, "NAVPAC" - the first satellite to satellite navigation system.

Currently APL, with assistance from the Naval Surface Weapons Center, is developing a Global Positioning System Package (GPSPAC) to provide real-time position fixes aboard a host vehicle, using signals from GPS satellites. GPSPAC constitutes the first on-board satellite navigator to use the NAVSTAR system.

Magnavox is under contract with APL to fabricate the spaceborne GPS navigation receiver/processor (R/PA) using a design based on the Magnavox Manpack. The R/PA must interface with a dual oscillator, an antenna and preamplifier, an Interface and Storage Unit (ISU), a Command Switching Unit (CSU), and a DC/DC converter being developed by APL.

This paper describes the GPSPAC system architecture and design, describes its functional and operational characteristics, discusses hardware, software and navigation features and finally, discusses test methods and test results. Before proceeding further, however, a very brief review of the NAVSTAR GPS system will be given.

2.0 THE NAVSTAR GPS SYSTEM

The GPS system consists of three major segments: the space system segment, the control system segment and the user system segment (Figure 1). The operational space system segment deploys a constellation of satellites in three planes separated in longitude by 120° and inclined to the equator at 55° . Each plane will initially have a set of six satellites expandable to eight evenly spaced satellites placed in a nominally 10,900 nautical mile circular orbit with a period of 12 sidereal hours (Figure 2). Thus, each satellite retraces the same ground track twice each day. The expanded deployment provides the satellite coverage necessary for continuous worldwide three dimensional position and velocity determination by assuring a minimum of four satellites in view at all times, anywhere on or near the earth. Reduction of the total number of satellites to 18 gives somewhat less than continuous global three dimensional navigation coverage. For that reason various orbital configurations are currently being evaluated to optimize system availability.

Full 3-D operational capability with 18 satellites is expected by the end of 1987 with 2D operational capability commencing at the end of '85. In the meanwhile a five to six satellite constellation will be maintained for test and evaluation (see Figure 2).

Each satellite transmits a composite signal at the two L-band frequencies of $L_1=1.575$ GHz and $L_2=1.227$ GHz. The composite signal consists of a precision (P) navigation signal and a coarse/acquisition (C/A) navigation signal, quadrature modulated

*R. Thorensen, K.M. Joseph and J.J. Winterhalter are with the Magnavox Advanced Products and Systems Co., Torrance, California. J.R. Champion is with the Applied Physics Laboratory, Laurel, Md.

into the L_1 carrier. The L_2 carrier carries only the P signal. Both the (C/A) and the (P) signals are pseudorandom digital sequences. The (C/A) code is 1023 chips in length of precisely 1 msec period (i.e., 1.023 MHz clock rate), while the (P) sequence is very long (approximately 6×10^{12} chips; 1 week) and clocked at 10 times the rate of the C/A code (i.e., 10.23 MHz rate). The navigation signals contain satellite ephemerides, atmospheric propagation correction data and satellite clock bias information all provided by the control system segment. In addition, the two L-band navigation signals permit the user to perform first order correction for the ionospheric propagation delay and other frequency sensitive propagation anomalies.

A position fix is obtained through measurement of range to several satellites whose orbital positions are known to the user from data broadcast by the satellites themselves.

The range determinations are made through precise measurement of the time it takes the signal to propagate from a given satellite to the user receiver. Only three such measurements are required if the user receiver clock is precisely synchronized with the clocks of the satellite emitters, i.e., with GPS system time. This requirement, however, places an uneconomical restraint on the user clocks. A more practical implementation is to make an additional range measurement to a fourth satellite and use this data to calculate the user clock bias error. The range measurements to the satellites thus include the bias error and for this reason are usually termed "pseudoranges". In an analogous manner the user can determine his three dimensional velocity plus clock frequency bias through measurement of doppler frequency shifts to the same four satellites.

The method of range measurement is based on correlation detection. That is, the user receiver generates replicas of both the (C/A) and (P) pseudorandom sequences and cross-correlates these locally generated signals with the signals received from the satellites. The output signal of the correlator is maximum and proportional to N (where N is the number of sequence chips integrated) when the sequences are precisely in time synchronization and falls off linearly to a signal of zero mean and RMS deviation of \sqrt{N} as soon as the sequences get out of phase by one or more chips.

The phase of the locally generated sequence is under the control of the user receiver; it is easy to see that where large integration times can be used yielding good signal to noise ratio, (i.e., N of the order of 10 to 100 thousand chips), the received and the locally generated sequences can be brought into time synchronization within a small fraction of a chip resulting in time delay measurement to that precision. Since the chip duration of the P sequence is 100 nanosec, time delay measurements can be made to but a few nanoseconds yielding RMS code tracking errors of the order of a meter.

The user receiver can also measure the doppler shifts of the carrier signals from the satellite. By measuring the accumulated phase difference of the received signal over a fixed time interval, the receiver can infer the range change increment. This measurement, called the delta range, includes a bias error which is proportional to relative frequency error between the satellite emitter and the receiver clock. Since the carrier wavelength is short, the delta range is a finely quantized measurement yielding RMS errors of the order of 0.02 meters.

In summary, measurements from four satellites provide the receiver with sufficient information to solve for the three components of user position, the three velocity components plus user clock bias error and clock frequency error. To accomplish the navigation function, pseudorange and delta-range measurements are used to update a running estimate of user positions, with the aid of a Kalman filter.

3.0 APPLICATION - SPACE NAVIGATION

GPSPAC will use signals from the NAVSTAR constellation to make real-time determinations of position and velocity of its host vehicle. When no GPS satellites are in view, the system dead reckons the host vehicle orbit by propagating forward a navigation solution according to a dynamics model. After signal reacquisition, normal navigation continues. The autonomous, onboard operation of GPSPAC will eliminate the post-processing delays, expenses, and the problems associated with the worldwide network of ground stations required by the present doppler beacon system.

When the NAVSTAR system is fully operational, GPSPAC will provide the host vehicle with continuous position fixes having an accuracy on the order of 16 m and velocity determinations with errors on the order of 0.03 m/sec. This information can be used to annotate sensor records aboard the host satellite. An early version of GPSPAC will be included on the NASA spacecraft, Landsat D, where it will perform time coding and geographical identification of sensor data in real-time and at reduced cost.

4. GPSPAC SYSTEM DESCRIPTION

4.1 Overview

GPSPAC is a spaceborne navigation system which provides near real time (3 to 9 second delay) navigation data (position, velocity, and time) to on-board or ground users with an accuracy of a few meters. It can also provide raw pseudorange and delta-pseudorange measurement data to ground users for precision orbit reconstruction. The set can operate in a completely autonomous fashion after initialization; however, ground control of set operations is possible when desired. Data uplinks and pulse commands control the sets' configuration, mode of operation, GPS satellite selection, and telemetry

output. GPSPAC fully exploits all of the capabilities of the GPS system - providing tracking and measurement on C/A and P code on both L₁ and L₂ frequencies. The set provides a capability to mark the time of occurrence of selected events in other HV subsystems. This time mark information allows later correlation by the user of an exact vehicle location with a specific event. GPSPAC is an efficiently packaged, structurally sound, and easily maintained set which is designed to survive the environmental problems of a launch and orbital mission.

4.2 Configuration

The structure of the GPSPAC configuration is shown in Figure 3.

The major component of GPSPAC is the Receiver/Processor Assembly (R/PA) which contains two independent GPS receiver channels, a single processor, an interface subsystem, and a power supply. An external oscillator provides an ultrastable 5.115 MHz reference; an L₁/L₂ antenna and preamp provide the RF input. The R/PA can accept a thrust flag to warn the navigation filter of an impending orbit adjustment. Optional interface and storage units are required for those missions that are either incompatible with the NASA-standard data interfaces or that require non-volatile mass data storage.

GPSPAC has been designed to provide the highest possible accuracy consistent with the limits of a spaceborne set. It is not necessarily the minimum system required for operational use. GPSPAC contains several experimental features to help define the true minimum requirements for future, more compact operational systems. The inclusion of two receiver channels, for example, not only provides a reliability gain, but will also allow in-orbit comparison between simultaneous and sequential measurements on L₁ and L₂. An experimental comparison is necessary because ionospheric rate effect do not lend themselves to convincing analysis. Likewise, the processor is fully reprogrammable from the ground, allowing tuning of the navigation filter, and testing of alternative satellite selection and receiver control algorithms in the real world. Finally, GPSPAC can also output all the raw measurement data that was the basis for the on-board computed position. This allows more powerful post-processing software on the ground to check GPSPAC performance and also to enhance the accuracy by folding in additional tracking data from other sources.

The physical construction of the R/PA is shown in Figure 4. The enclosure is machined with reinforcing vertical and horizontal flanges to assure maximum strength with minimum weight. The set consists of two parallel channels containing easily removable PC cards to facilitate test and maintenance. The major physical parameters of the R/PA are:

SIZE:	16.4 x 12 x 8 inches
WEIGHT:	42.6 lbs.
POWER:	45 watts
RELIABILITY:	20,000 hours (MTBF)

4.3 Major Features

The major features of the set are described below:

- (1) High Navigation Accuracy - Provides the following levels of navigation accuracy for a complete GPS satellite constellation.

POSITION:	3 - 5 Meters
VELOCITY:	0.02 - 0.05 Meters/Second
TIME:	Nanosecond Accuracy

This data is computed in near real-time and available to on-board users with a 3 to 9 second delay.

- (2) Precise Event Marker - Provides 4 independent users with E/V position, velocity, and time, whenever these users send a time strobe to the R/PA.
- (3) Jamming Resistance - Provides the above navigation accuracy at very low signal-to-noise (C/N₀) levels in the presence of considerable jamming-to-signal (J/S) interference.

NOMINAL C/N ₀ AT PREAMP INPUT	
C/A (L ₁):	37.1 db - Hz
P (L ₁):	34.5 db - Hz
C/A or P (L ₂):	32.5 db - Hz

TOLERABLE JAMMING LEVELS (J/S)

C/A:	25 db
P:	36 db

- (4) High Autonomy - After an initial data uplink to provide appropriate initialization data, the set is capable of completely autonomous operation for an extended period of time. The set automatically determines which satellites are visible, selects the optional set of four, acquires and tracks each, and maintains the navigation state.

- (5) Dual Channel Receiver - The R/PA contains two receiver channels which function independently. Either may be used (with the other powered off) to perform sequential L₁ and L₂ measurements, or both may be used to perform simultaneous L₁ and L₂ measurements.
- (6) Ground Mode - In addition to space navigation utilizing the orbital trajectories, the set contains a ground navigation mode for operation on the Earth's surface. This mode facilitates test prior to launch.
- (7) Low Power Standby Mode - The set provides a low power (7 watts) standby mode for power conservation. The processor memory, oscillator, and "time", are maintained to allow rapid resumption of operation when desired.

4.4 Subsystems

GPSPAC contains seven major subsystems. Three (antenna, preamp, and oscillator) are external to the R/PA; four (receiver, processor, interface and power conditioning unit) are internal.

The antenna requirements for GPSPAC differ from those for ground-based sets. The geometry and velocities of an orbiting HV are such that about half the NDG sightings in Phase I will occur at elevations between -10° and +20° relative to local HV horizon. The GPSPAC antenna must therefore have gain preferably down to -10°, as compared to other GPS antennas which intentionally reduce their gain below +10° to reject jammers. The APL-developed antenna consists of L₁ and L₂ quadrifilar helices stacked on a common axis. Its gain exceeds -2 dBic over most of the upper hemisphere, with useful gain down to -10°. The antenna is of extremely rugged design to survive the severe vibration environment present on the HV skin during launch and the extreme temperature variation of its exposed location in orbit.

The preamp must have low noise figure, good rejection of out-of-band signals, and low phase distortion in band. The HV antenna can "see" strong terrestrial interference sources, such as certain radars, that are invisible to most ground users, and the HV itself can also provide interference at nearby frequencies. This places stiff requirements on the preselection filter and tends to make it somewhat larger than would be necessary for ground use. An additional capability is provided for an optional notch filter to reject specific strong EV emitters, such as on-board radars. The APL-developed preamp uses two independent bipolar transistor channels (L₁ and L₂) to provide the required low noise figure with excellent stability. Overall, the preamp provides 35 dB gain at < 4 dB noise figure.

The 5.115 MHz oscillator provides the basic reference frequency for all GPSPAC operations. It must have good stability and low phase noise since it is multiplied all the way to L-band. The APL oscillator is a redundant unit based heavily on TRANSIT and doppler beacon designs. Long-term drift is typically less than 1×10^{-10} /day, yet the oscillator requires only 0.88 watts.

The R/PA contains two identical, independent receiver channels each of which performs the functions of signal search and acquisition, track, data demodulation, pseudo-range and delta-pseudorange measurement. Each receiver channel can track C/A or P code on L₁ or P on L₂.

The R/PA receiver employs a hardware design implementation where detection and tracking functions are accomplished in hardware with the software providing mode and bandwidth selection, initialization data, and rate aiding. This partitioning (shown in Figure 5) provides optimal tracking performance while substantially reducing processor throughput requirements.

The P and C/A coders generate the PRN waveforms required for the correlation detection process. Because the signal received from a satellite emitter is shifted in phase due to propagation delays and shifted in frequency due to relative motion between the user and emitter platforms, the clock driving these coders must be adjustable. It is derived from a voltage controlled oscillator (VCO) which is under the control of the processor through a digital-to-analog converter (DAC). The processor prepositions both the coder phase and clock frequency to a time/frequency window appropriate for the specific satellite selected. Next, the remaining time and frequency errors are searched and when both the locally generated and received signals are precisely aligned in time and frequency a Costas type phase lock loop is closed which tracks the R.F. carrier of the incoming signal. Code tracking is achieved through a t-dither tracking loop where the code phase is alternately advanced and retarded by half a chip. This introduces amplitude modulation into the in-phase component of the loop-output and permits the derivation of an error signal required for code tracking.

The code clock and carrier frequencies of the GPS signals are precisely related, L₁ being exactly 154 times the P coder clock and L₂ being 120 times the clock frequency. Thus, when the phase lock loop is tracking the R.F. carrier the code clock is further inherently phase locked to the received code.

The relative phase of the PRN signal and the doppler frequency shift of the R.F. carrier provide the range and velocity information desired. By time referencing specific epochs of the PRN signal waveforms (i.e., channel time epochs) to the User Time Clock

(UTC) (i.e., the receiver reference clock), precise measurements of both code phase and doppler frequency can be made.

These measurements are performed in three parts. First a coarse range reading, with a resolution of approximately 33 nsecs, is made by strobing the state of the User Time Clock into a buffer, upon the occurrence of a channel time epoch. Next, the range is further refined by a fine range measurement with a resolution of $\lambda/6$ where λ is the carrier wavelength. Finally, delta range is obtained by combining the above two readings with a third measurement taken at the next subsequent channel time epoch providing an indication of change in range to 1/6 of a carrier wavelength. It is therefore obvious that the receiver measurement accuracy is not dominated by the range measurement quantum steps but rather it is principally affected by the noise present in the bandwidths of the signals tracking loops. To operate with the narrowest practical bandwidths and therefore the highest signal to noise ratio the receiver obtains rate aiding information from the processor through the DAC which assists the narrow bandwidth tracking loops to maintain lock. The tracking (measurement) capability of the receiver is

	<u>P Code</u>	<u>C/A Code</u>
Pseudorange	1.5 M	15 M
Delta-Pseudorange	.02 M	.02 M

The Processor selects and controls the receivers, derives pseudorange and delta-pseudorange measurements from the raw receiver data, controls the interface, and performs various self-test diagnostics. The Processor is driven by a DEC LSI 11/03 CPU containing both single and double precision floating point arithmetic. The large instruction set, stack processing, multilevel vectored interrupts, and large throughput provide a powerful computing capability. The Processor contains 56 K of 16 bit memory driven by a memory controller which utilizes power strobing to reduce processor power consumption.

The interface provides a half-duplex command/telemetry to allow uplink of commands and downlink of data. This feature provides efficient system operation and minimizes power consumption. The set provides the HV with 10 analog and 32 discrete signals which monitor the health and status of the GPSPAC.

The power conditioning unit serves two functions - power conversion/regulation and pulse command conditioning. This unit has a power conversion efficiency in excess of 80% at GPSPAC power levels.

5.0 OPERATIONAL REQUIREMENTS

The operation of GPSPAC depends on the system acquiring signals from satellites of the NAVSTAR constellation. In addition, GPSPAC requires interfaces with the telemetry, command, power, thermal, antenna deployment, and structural systems of the host vehicle.

Before automatic operation begins, a coarse host vehicle almanac and at least one NAVSTAR satellite almanac must be uplinked to GPSPAC. This information is needed for the first acquisition of NAVSTAR signals. Initialization data can be in error as much as 200 km and 200 m/sec. Clock error can be up to two seconds. Once a signal from a NAVSTAR satellite is acquired, the R/PA obtains precise ephemeris information for that particular satellite and somewhat less precise almanac information on the total NAVSTAR constellation. GPSPAC continues to accumulate ephemeris information until signals from 4 NAVSTAR satellites are received and processed. Thereafter, the GPSPAC begins on-board navigation. Position and velocity errors depend on the number of NAVSTAR satellites in view, with optimum accuracy occurring when there are 4.

Upon command, GPSPAC can output all the raw data used for the on-board position computation. This allows verification of GPSPAC performance by ground based software and also allows the accuracy to be improved, if desired, by folding in tracking data from other sources. Ten relay commands and a 2 kbps uplink are required for control and loading of the R/PA. Depending on the files requested, GPSPAC can output an average of 35-350 bits/sec.

Since antenna to antenna distance between the Host Vehicle and any NAVSTAR satellite depends, in part, on host vehicle attitude, this latter parameter must be controlled. Further, if the Host vehicle has a thruster used for station keeping, perturbations from this source must be accounted for. During continuous NAVSTAR acquisitions, 10^{-2} g orbit adjust thrusts can induce a peak position error of 135 m. The R/PA, however, can accept a thrust flag input, and, if this is provided, peak error under 10^{-2} g thrust will be reduced to 20 m.

6.0 HARDWARE DESIGN

The GPSPAC R/PA consists of two independent receiver channels which are controlled by a single processor. Associated with the processor is an interface subsystem which handles the information transfer between the R/PA and the Host Vehicle. The interface includes redundant capabilities and can accommodate two different Host Vehicles. The R/PA is powered by the power conditioning unit which also contains some interface logic.

The unit consists of 26 hardware modules which are partitioned as follows:

RECEIVER (Channel 1)	7
RECEIVER (Channel 2)	7
PROCESSOR	6
INTERFACE	5
POWER CONDITIONING UNIT	1

6.1 Receiver Subsystem

The GPSPAC Receiver subunit consists of 2 RF Channels each capable of independent L1 or L2 sequential satellite tracking. Each of the channels consists of an RF module, Synthesizer Module, Baseband module, UTC module, C/A coder module, P coder module and P coder control module and is configured as shown in Figure 6. The RF unit receives a signal from the preamp, via the RF interface module, and amplifies and down-converts the signal for code correlation. After correlation and further amplification, the signal is sent to the baseband module for processing. The baseband module demodulates the incoming signal, derives a noise AGC voltage, and generates carrier lock signals. The baseband also detects code and carrier tracking, and generates a VCXO control voltage to track the signal and close the phaselock loop in the receiver. The UTC (User Time Clock) module receives a 30.69 MHz reference signal from the synthesizer for local time reference for generating all timing signals for the receiver. The C/A coder, P coder, and P coder control modules generate the local C/A or P codes for signal correlation in the RF module.

Each of the receiver channels dissipates 9.33 watts of power during the navigation and tracking mode; this dissipation is reduced to 1.09 W during standby mode which is the power required to keep the critical clocks functioning in the synthesizer and UTC.

RF/IF Module

The RF/IF module receives and linearly amplifies one of two selectable L-Band signals at 240F or 308F where F is the reference frequency used in the receiver. (5.115 MHz.) The band width of the PN signal is 2F for the P code and F/5 for the C/A code. The module down-converts the signal and correlates it with a local C/A or P code with a final output frequency of 1-1/2F. The down conversion is achieved by mixing synthesizer generated signals of 68F and 29-1/2F (see Figure 6).

Gain varies in response to an external AGC signal generated by the baseband module.

Synthesizer Module

The synthesizer module supplies all coherent signals to the receiver modules. It uses a precise, external 5.115 MHz signal (F) as a source to generate 3 coherent CW frequencies (5F, 6F, and 68F). The VCXO output is used to generate two doppler tracking frequencies (2 Fct, 29-1/2 Fct) where the Fct output contains the doppler information scaled to 2F (i.e., 2 F + d' where d' = doppler at L Band/154 or 120.) The divide by 154 or 120 depends on whether it is an L1 or L2 signal being tracked. This 2 Fct frequency is used as the code clock which drives the C/A or P coders.

Baseband Module

The baseband module contains the inphase and quadrature demodulator circuits which translate the 1-1/2F output to baseband, all of the analog detector/signal processing circuits which operate on the baseband signal, and the necessary logic for software signal selection and control.

The baseband signal processing circuits on the module perform the following functions:

- a. Data detection
- b. AGC detection and loop integration
- c. Code sync detection (i.e., Sequential detector)
- d. Carrier lock detection (i.e., Costas Lock detector)
- e. Code tracking error detection circuits
- f. Carrier tracking circuits

User Time Clock (UTC)

The UTC contains a clock for local time reference and provides the basic timing signals required for operation of the sequential receiver. In addition the UTC module contains coarse and fine range buffers which preserve the state of the local time reference when strobed by the coarse and fine range clock epochs. These clock epochs are derived from the code clocks which are divided down from the receiver VCXO preserving the doppler and phase of the incoming signal.

C/A Coder

The C/A Code is produced by modulo two adding two 1023 bit codes, G1 and G2 inside a LSI coder chip. Upon computer command, the C/A Coder can be aligned with the UTC or P Coder, address changed, delayed, or moved ahead.

P Coder

The P Code is the result of modulo two adding four appropriately shifted in time partial codes: X1A, X1B, X2A and X2B. Clocking and inhibit logic is such that each register aligns once in each seven day period. This code is generated by 2 LSI coder chips, each containing a pair of shift registers, surrounded by the logic required to obtain the 1 week long code.

P Coder Control

The P Coder Control is used to generate various P Coder and C/A Coder commands to properly address, slew and maintain the respective C/A and P Codes.

Processor Subsystem

The processor subsystem consists of a central processing unit (CPU), memory control, memory and a dual channel receiver interface. The key features of the processor subsystem are:

- 56K word RAM memory with 16 bits/word
- LSI-11 mini-computer qualified by MAGNAVOX for use in space
- Extended precision floating point arithmetic
- Supportable Digital Equipment Corporation (DEC) software and peripherals
- Low power with approximately 7.5 watts for processor, memory and receiver interface board

The following paragraphs describe the modules that constitute the Processor Subsystem.

Central Processing Unit

The CPU module implements a 16 bit mini-computer with the instruction set of the DEC LSI-11/34-40. It is built around a set of six N-channel metal oxide semi-conductor (MOS) chips which include control and data elements as well as four micro-code ROMS. These ROMS are programmed to emulate the PDP-11/34-40 instruction set along with routines for on-line debugging/operator interfacing and program load capability. The ROMS also implement the extended instruction set including a single precision floating point instruction set and an instruction set which performs one word register save and restore operations. In addition the CPU has the following features:

- 400 plus instruction set
- Eight (8) general purpose registers
- Vectored interrupts
- DMA operation
- Word or byte processing of data
- Power fail/auto-restart
- Stack processing
- Priority structured I/O
- Single and double operand instructions

Receiver I/O

The receiver I/O module functions as the computer bus buffer and as an address decoder to interface the processor to the dual channel receiver. This module also contains certain system status words and additionally accepts eight (8) interrupt lines which are priority encoded and used to generate interrupt vector addresses for the processor.

Memory Controller

The memory control module supplies all control signals necessary to interface 56K of Hybrid RAM to the processor. Memory banking control is provided by the module. The processor stack overflow logic and 8K words of Hybrid RAM are also contained on this module. Memory banking is used to compensate for only 16 bits of memory address availability since this would limit memory size to 48K words.

Memory Module

The hybrid memory module provides low power read-write memory and is designed around a hybrid memory device. This hybrid incorporates a 1024 bit CMOS memory chip and address buffer logic. The buffer logic is power strobed internal to the hybrid to minimize power dissipation. The final module consists of sixteen of these hybrids giving each module a capacity of 16K, 16 bit memory words. A total of three memory modules are used in the R/PA.

Interface Subsystem

The interface subsystem for the R/PA is comprised of three main sections; the RF interface, the command/telemetry interface and the power interface.

The RF interface is accomplished by means of the RF/OSC module whose main function is to interface both the preamp and the dual oscillator to the R/PA.

The telemetry and command interface is shared among different modules. The digital and critical telemetry between R/PA and the host vehicle is accomplished by means of the R/PA I/O module while the command interface is handled by the power units and the R/PA I/O.

The Power Interface is comprised of unregulated +28 VDC which is sent from the Host Vehicle to the R/PA and is received at the PCU.

Besides the interface mentioned above, the R/PA also receives status indicators and delivers required voltages to the preamp and oscillator.

The R/PA for ground testing purposes has DMA capabilities through the bus window connector which interfaces with the processor bus.

RF/OSC Interface Module

The RF/OSC interface module is used to split the antenna/preamp L1/L2 output signal to drive the two receiver channel inputs. It is also used to combine and split the two oscillator (5.115 MHz) outputs for synthesizer operation.

Analog Telemetry Module

The analog telemetry module is used to measure 16 analog telemetry signals generated by the preamplifier, the oscillator, the Host Vehicle (HV) and the R/PA. These 16 telemetry signals are used to determine the general "health" and status of the R/PA.

Time Code Generator Module

The time code generator contains a 45 bit binary counter driven by a 1.023 MHz clock signal derived from the oscillator. Five independent buffers are provided to store the counter reading when an appropriate strobe is received; four are used to record external events when strobes occur on the external host vehicle event lines, and one is used to record time when the receiver measurements occur. The counter provides a resolution of 978 nanoseconds and an unambiguous count to 398 days. The counter is initialized by the Processor in 2.05 second increments; its bias relative to GPS time can be computed and GPS time later derived from counter readings only. In standby mode the counter continues to function, but the buffers, strobe, and read logic are inoperative.

Digital Telemetry Module

The digital telemetry module contains the necessary hardware to transmit or receive signal information to/from the Host Vehicle. This module also contains a boot loader PROM and associated hardware used for R/PA cold starts. The module uses direct memory access (cycle steal) control logic to access memory data 16 bits at a time with a maximum rate of 146.25 kilobits/sec.

R/PA I/O

This module contains most of the R/PA electrical interface circuitry which interconnects the R/PA and the Host Vehicle. It also provides some of the interfaces required between internal R/PA modules. Opto-isolators are used to allow the R/PA and portions of the host vehicle to communicate with one another and yet remain electrically isolated. Capabilities include:

- Digital critical telemetry interface
- Pulse commands interface
- R/PA to Host Vehicle serial interface
- Receiver channel clock select and control
- Time marks interface
- Power on flag and initialization control
- Thrust flag

Power Conditioning Unit

The power conditioning unit (PCU) performs three major functions:

- Provides regulated supply voltages to the preamp, oscillators and R/PA
- Serves as interface for certain pulse commands sent from the host vehicle
- Provides timing and telemetry to R/PA

The following paragraphs describe the major functions of the PCU.

Power Conditioning Circuit

The power conditioning circuit is a dual DC/DC converter which receives unregulated +28 VDC from the host vehicle and supplies regulated voltage to the preamp, oscillators, and the rest of the R/PA in the form of +12, +5, -12 VDC (main power) and +15, +12, +5 VDC (standby power).

Pulse Command Interface

The pulse command interface isolates and conditions pulse commands from the host vehicle which are then output to the rest of the system.

Telemetry/Status Indicator

The telemetry/status indicator monitors the internal states and conditions of the PCU itself and relays this information to the rest of the R/PA.

Mechanical Design

Mechanically the R/PA is divided into three functional areas; the receiver, the processor, and the backplane assembly on which the intermodule connections are made. The receiver area is comprised of two channels of receiver modules arranged in mirror image fashion. On the opposite side of the enclosure is the processor portion of the unit and a power conditioning unit. All of the modules are arranged in the Housing to achieve minimal EMI and to facilitate the lowest possible average length of interconnections. The wire wrap assembly including harness assemblies and RF cables lies on a horizontal plane at the top of the enclosure. This position allows the most direct path for heat conduction from the individual modules to the platform upon which the unit is mounted. The enclosure has two access covers, located at top and bottom; the top cover is for access to the wire wrap plate and the bottom cover for access to the functional modules. Figure 7 shows the mechanical pieces of the R/PA. The wire wrap plate is fastened to a mounting in the enclosure with screws. The functional modules are connected and fastened to the wire wrap plate. The I/O connectors of the unit are located on the long sides of the enclosure and are either harnessed to the wire wrap plate or are mounted directly to modules adjacent to the outside walls.

6.2 Software Design

The GPSPAC R/PA software provides the following capabilities.

- Acceptance of the uplink commands and aiding information containing mode transition requests, time, HV orbital parameters, GPS almanac data, specification of receiver configuration, data file output indices, memory dump request, and command echo request.
- Integration of uplink commands into a software data base for navigation filter and receiver initialization.
- Management of the dual channel receiver hardware to sequentially acquire and track GPS satellite signals based on uplink information and filter estimates of current and predicted GPS satellite and HV positions. One channel of the receiver is selected by command as the primary channel; the other (if selected) is the secondary channel. Demodulated navigation data are obtained from the primary channel. Time-corrected measurements of pseudorange and delta pseudorange are obtained from any selected channel.
- Navigation processing filters of receiver measurement data to form the best estimate of HV position and velocity for GPS satellite acquisition, output telemetry, and use by other systems on the HV.
- Format and initiate downlink transmission of telemetry files that include HV position, velocity and GPS system time, time code generator (TCG) information, pseudorange and delta pseudorange measurements, and status information, all at intervals selectable by command.
- Built-in diagnostics that include processor CPU and memory testing and reporting.
- For ground testing there is provision for test and performance data to an instrumentation device.

6.2.1 Basic Design

The software operates under control of a real-time, multi-tasking executive. In addition, eight vectored interrupts are provided with software with each interrupt separately suppressable. The basic software is comprised of interrupt handling routines for these eight interrupts and of a collection of tasks operating under the executive. Each task has a fixed, unique priority. Tasks are scheduled to run by other tasks (or by themselves) either immediately or in some integer number of .1 seconds in the future. The executive always assures that the highest priority task scheduled to execute at the current time is actually executing. After each task completes, the executive determines which task currently enabled for the current time has the highest priority and starts its execution. If no tasks are currently enabled, the executive relinquishes control of the central processing unit (CPU) to the background loop. When enabled, this loop continuously performs memory and CPU diagnostics.

On each .1 UT interrupt, the executive function updates system time and determines whether any tasks were scheduled to run at this time. If so, execution of the highest priority enabled task is started. If not, control is returned to whatever task was being executed at the time of the interrupt or to the background loop if no task was executing. Interrupt handling subroutines can schedule tasks to execute via the executive function. The priority of each interrupt is determined by its associated line number with 0 having the highest priority down to line 7 with the lowest.

6.2.2 Operational Modes

The R/PA software has different capabilities and requirements depending on the system operational mode. Discussion of the principal modes follows.

Off Mode

No power to the R/PA. Any program or data in the 56K word RAM memory is lost.

Standby Mode

Power is supplied to certain R/PA elements. When entered from the OFF mode, STANDBY is used to warm the oscillator to its stable temperature in preparation for set operation. When entered from the COMMAND mode, STANDBY serves as the mode wherein the program is maintained in memory but not functioning. Since power is supplied to the external oscillator, UT clocks, and TCG, TCG time (if previously established) is maintained. Exit from the STANDBY mode is only performed following the reception of such a command from the Host Vehicle. This exit is to the BOOT mode if the software has not previously been loaded, or if a power loss had occurred; otherwise, this exit is to the COMMAND mode.

Boot Mode

The uplinked software is accepted by the boot loader function of the set. Host Vehicle data commands for memory loading, bit map output, and program start are accepted in this mode. BOOT mode may be entered from any other mode by the issuance of a pulse command by the Host Vehicle and will be entered from the STANDBY mode when conditions defined for exit from that mode into the COMMAND mode are not satisfied. Exit from the BOOT mode is to the COMMAND mode subsequent to receiving a start command or to the STANDBY mode subsequent to receiving a power down command.

Command Mode

Uplink commands are received by the set to provide it with initialization and control data or to request output of data files, command echo, or memory dump. These commands are accepted by the set only in the COMMAND mode. During this mode no telemetry output (except memory dump and command echo) will be provided nor will the receiver channels be powered. Any navigation solution that had been obtained prior to entry into the COMMAND mode will be propagated forward in time. Upon being commanded to enter a navigate mode, the Set will power the receiver channels as requested. The set will return to the COMMAND mode from one of the navigation modes upon software recognition of a pulse command to do so.

Almanac Collect Mode

The primary receiver channel is used to gather almanac data to refresh the data stored in memory. This must be done at least once a week. This mode is entered from one of the navigation modes and exits back to that mode upon successful collection. Telemetry output will be provided during this mode and any navigation solution that had been obtained prior to entry into this mode will be propagated forward in time.

Space Mode

This is the normal mode of operation of the R/PA for navigating in a space environment. Whenever NDS satellites are available, pseudorange and delta pseudorange measurements are provided by receiver processing to the navigation filter. The filter uses these measurements to update the navigation state. Whenever measurements are not available due to lack of NDS satellites or failure of the receiver to track the NDS signal, the navigation state is propagated. The SPACE mode is entered only from the COMMAND and ALMANAC COLLECT modes and exits only back to those modes.

Telemetry output will be provided. Depending upon the commanded receiver configuration, operation in a single channel, sequential four, or dual channel simultaneous four, satellite sequencing pattern will be performed as shown in Figure 8. If both receiver channels are commanded off, the navigation solution is propagated. The sub-modes that use the receiver are described in greater detail as follows:

- a) Single Channel Sequential 4 - The R/PA uses the receiver channel declared as primary by command to sequence over up to four NDS satellites; the secondary channel is off. Six seconds is spent on each satellite. During the first 3 seconds, pseudorange and delta pseudorange measurements are made on L1; during the next 3 seconds the same measurements are made on L2. Ionospheric corrections are computed from the sequential measurements and appropriate compensation introduced.
- b) Dual Channel Simultaneous 4 - The R/PA uses both receiver channels to make simultaneous measurements to the same satellite. The primary channel makes pseudorange and delta pseudorange measurements on the L1 frequency, and the secondary channel makes pseudorange and delta-pseudorange measurements on the L2 frequency for the same satellite being tracked on the primary channel. The measurements made on the two channels are for the same 70 msec epoch detected on each channel to obtain "simultaneous"

L1 and L2 measurements. Ionospheric corrections are computed using the simultaneous L1 and L2 measurements and are used to compensate the primary channel measurement information supplied to the navigation function.

- c) **GROUND Mode** - This is the mode of operation of the R/PA for navigation in a ground environment (i.e., on or near the Earth's surface). Except for differences in the navigation and satellite selection functions inherent in the different host vehicle environment, this mode provides identical capabilities as those described for the SPACE mode. The GROUND mode is entered only from the COMMAND mode and exits only back to that mode.
- d) **CALIBRATE (CAL) Mode** - The software has the capability to calibrate the R/PA oscillator for frequency and phase bias. The calibration method used requires that the set be stationary and that ground navigation be performed. This mode is identical to the GROUND Mode, except that the Kalman filter implementation forces the velocity component of the state to be zero. Telemetry output will be provided during this mode. The CAL mode is entered only from the COMMAND mode and exits only to that mode.

6.2.3 Navigation Processing

Navigation processing consists of the navigation filter software and the receiver processing software, described previously, which provides receiver measurement data for the navigation filter.

Navigation Software

The R/PA navigation filter is a nine state extended Kalman filter estimating Host Vehicle position, velocity, time bias between actual GPS time and the local reference time, frequency bias and a drag factor. The drag factor is important as an aid in obtaining accurate position and velocity propagation over extended periods where no GPS measurements can be made. This is critical during PHASE II GPS where only six GPS satellites are available.

The software uses an Earth-centered-Earth-fixed coordinate system to represent the vehicle's position and velocity. The filter is implemented to be synchronized with the receiver measurement cycles shown in Figure 8. At the end of the delta pseudorange measurement period, the system monitor activates the navigation software which then accomplishes the following tasks:

1. The previous filter state is propagated to the pseudorange measurement time.
2. The previous filter state error covariance matrix is propagated to the pseudorange measurement time.
3. The pseudorange measurement gain is calculated and the measurement is used to determine an estimate of the state error at the pseudorange measurement time.
4. The delta-pseudorange measurement gain is calculated and the measurement is used to update the state error estimate of step 3.
5. The updated state error estimate is used to correct the propagated filter state from step 1 resulting in a new filter state applicable at the pseudorange measurement time.

7.0 STATUS

In June 1980, Magnavox completed a series of tests and simulations to validate the system design concepts. These tests and simulations were divided into the following categories:

- Navigation simulation
- Software stand-alone testing
- Hardware stand-alone testing
- System testing
- Test procedure validation for flight unit acceptance tests.

Prior to discussing the test results it is appropriate to describe, briefly, a key element in the design validation, namely the Ground Support Unit (GSU). This unit was used for part of the software testing and all of the system testing. Furthermore, it will be used for all flight unit acceptance testing and it is an integral part of the Applied Physics Laboratory's integration and test equipments.

7.1 Ground Support Unit

The GSU consists of two major subsystems - a Real Time Controller (RTC) and an Instrumentation Controller (IC). A simplified block diagram of the GSU is presented in Figure 9. These subsystems are physically separable and can be used independently for various purposes.

The RTC generates the NDS satellite signals which are input to the R/PA. The RTC is a sequencing single-channel simulator; that is, it simulates the signal (including both L₁ and L₂) from one satellite at a time but may sequence over any desired subset of the 18 NDS satellites. The transmitted signal is a composite of L₁ and L₂; L₁ is quadrature modulated by both P and C/A codes while L₂ is modulated only by P. An input to the RTC from the R/PA via the IC dictates which NDS satellite signal is to be generated. For stand-alone operation, the RTC generates a single satellite which is input through the RTC control keyboard. The RTC modifies the transmitted signal to account for NDS/GPS/PAC line-of-sight range changes, velocities, accelerations, and jerks. In addition, provision for simulating ionospheric delays is included.

The IC simulates the host vehicle interface to the R/PA and provides a means of generating commands, monitoring R/PA operation, and recording telemetry. Every electrical input to the R/PA can be generated; every output signal can be monitored, displayed, and recorded. The IC and RTC can communicate with each other and provide a means of comparing true GPS/PAC position and velocity (simulated by the RTC) with the computed R/PA navigation solution (as output to the IC). In this fashion, the navigation accuracy for any scenario of interest may be evaluated.

7.2 RTC Capabilities

RTC/ESIM

The RTC reads a 9-track tape every .1 second. The tape is prepared by the Environmental Simulator (ESIM) and User Motion Generator (UMG) data parameters to define R/PA operational scenarios. Precise signal generation, including complex gravity, drag models and thrust flag simulation is used to simulate interaction between a host vehicle and up to 18 NDS satellites.

RTC/CORG

The Circular Orbit Range Generator (CORG) will be used when simple circular orbits for the Host Vehicle and GPS satellites are sufficient. These "perfect orbits" will only allow evaluation of navigational performance under best case orbital conditions.

RTC/Direct Signal Mode

This mode generates a continuous GPS signal with constant range, constant velocity or constant acceleration. Navigation is not possible as this function was designed to support the R/PA Receiver Test Mode (RTM).

IC Capabilities

IC/IDP

The IDP mode is used to simulate real time interaction between the Host Vehicle and up to 18 NDS satellites. This configuration was used for R/PA integration and system development and will be used for final acceptance testing.

IC/PTE

The Post Test Evaluation Mode will be used to maintain historical records of real time R/PA testing. Off-line (non-real time) detailed analysis of R/PA navigation and performance data will be possible through the use of the PTE function.

IC/PDF

User program development is possible in the PDF or Program Development Facility Mode. This mode uses the Hewlett-Packard Real Time Executive (RTE) IV software to create new software programs for user purposes.

7.3 Simulation

Navigation

Prior to integration of the R/PA software and hardware elements an extensive amount of simulation was performed. This simulation was implemented on an IBM 370/145 and included a truth model to simulate Host Vehicle and GPS orbital dynamics, a noise generator to corrupt simulated pseudorange and delta pseudorange measurements and the navigation filter algorithm. The results of this simulation showed that Magnavox could expect steady-state position and velocity errors in the order of 5 meters for position and 0.14 meters/second in velocity based on a four satellite solution in P-code.

Software

After software functions completed design review and coding, they were then tested on a DEC PDP-1134 with test software simulating functions that would interact with the software function being tested. Host Vehicle simulation was accomplished by linking a Hewlett-Packard 2108 computer, with its GSU software, to the PDP-1134. Certain combined software functions were then tested with a subset of R/PA hardware elements and a limited GSU capability. For example, the receiver software was tested with the R/PA receiver sub-units but without the other elements and with only the RTC portion of the GSU. This minimized software design problems prior to final system integration.

Hardware

As normal for any hardware development program test fixtures were designed to prove module design and to support acceptance testing. Some test fixtures were designed and used to test subsystem functions. Thus, a processor test fixture tested the CPU, memory, and interface cards as a set. For this testing, Magnavox used DEC supplied diagnostic software and unique Magnavox diagnostic software such as SERTA, which exercises most receiver functions to verify proper hardware operation.

7.4 System Testing

With the satisfactory completion of sub-element testing, system integration tests were started. The three basic goals for the system testing were:

- Assure that all hardware and software elements operate together.
- Assure navigation performance comparable to simulation results.
- Operational testing sufficient to verify specification compliance.

Successful sub-element integration was verified by systematically incorporating the necessary software elements to exercise the R/PA as detailed below:

- BOOT MODE	Verify program load, power-up procedures, etc.
- COMMAND MODE	Verify transition from boot mode, system monitor operation.
- RTM	Verify simple receiver operation, verify hardware performance for pseudorange and delta pseudorange.
- GROUND/CAL SINGLE CHANNEL & DUAL CHANNEL	Verify basic navigation capability
- SPACE MODE SINGLE CHANNEL & DUAL CHANNEL	Verify space navigation capability

Figures 10 through 15 are plots of the RSS steady-state position and velocity errors as determined by simulation and integration testing. As can be seen, the results compare favorably to expected performance. Other factors were evaluated during navigation testing including:

- GDOP/SATELLITE SELECTION - To minimize the geometric-dilution-of-position (GDOP) a satellites selection algorithm was verified by comparing navigation results for many successive runs.
- TIME-TO-FIRST FIX (TTFF) - The end of the first, four satellite signal dwell in P Code is the point in time defined as first fix. At that time, a first fix bit is set signifying to host vehicle stable R/PA operation and accuracy sufficient for other satellite experiments. The main effort here was to show that the navigation filter convergence agreed with the simulation results.
- PROPAGATE - That the R/PA can operate in a PHASE II satellite scenario was also tested. This showed that the R/PA had the ability to navigate when satellites were in view, go to propagate when satellites disappeared and return to navigate when the satellites reappeared.
- MISCELLANEOUS - Other requirements were tested such as almanac refresh degraded satellite operation, single channel performance, time mark performance and specification signal level and dynamic performance.

8.0 CONCLUSIONS

Extensive tests of the GPSPAC Receiver/Processor Engineering Model have convincingly demonstrated that position and velocity accuracies obtainable for earth or near earth GPS User Equipments can also be met for low orbiting space vehicles. Rugged mechanical design, low power consumption and high reliability coupled with highly flexible operational characteristics under computer control make the GPSPAC Satellite Navigator an ideal candidate for use on low orbiting space vehicles.

9.0 REFERENCES AND BIBLIOGRAPHY

1. NAVSTAR Global Positioning System Spec. No. SS-GPS-101B, 15 April 1974.
2. Specification for GPSPAC Receiver/Processor Assembly - APL Document 7250-9000.
3. Interface Control Document (ICD) for GPSPAC Receiver/Processor Assembly (R/PA).
4. Specification for GPSPAC Receiver/Processor Assembly Ground Support Unit. APL Document 7250-9006.
5. E. M. Lassiter & Col. B. W. Parkinson: "NAVSTAR/GPS Operational Status" Proceedings of the International Navigation Congress, August 1976.
6. B. G. Glazer "GPS Receiver Operation" Navigation, Summer 1978, Vol. 25 No. 2.
7. Hoffman, E. J. and Birmingham, W. P. "GPSPAC a Spaceborne Navigation Set." Proceedings IEEE Position Location and Navigation Symposium, November 1978.
8. Uyeminami, R. T. "Navigation Filter Mechanization for a Spaceborne GPS User." Proceedings IEEE Position Location and Navigation Symposium, November 1978.
9. W. Stein "GPSPAC Space Navigation Simulation Results." ION Proceedings of the National Aerospace Symposium, March 1979.
10. D. W. Henderson, Col. USAF & J. A. Strada, Lt. Cmdr. USN. "NAVSTAR Field Test Results." ION Proceedings of the National Aerospace Symposium, March 1979.

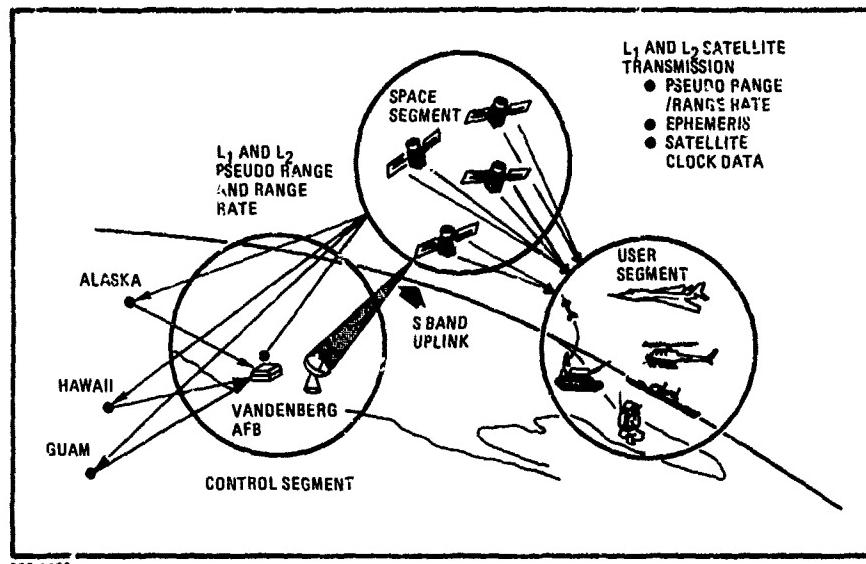
880-4420
UNCLASSIFIED

Figure 1. Navstar GPS Segments

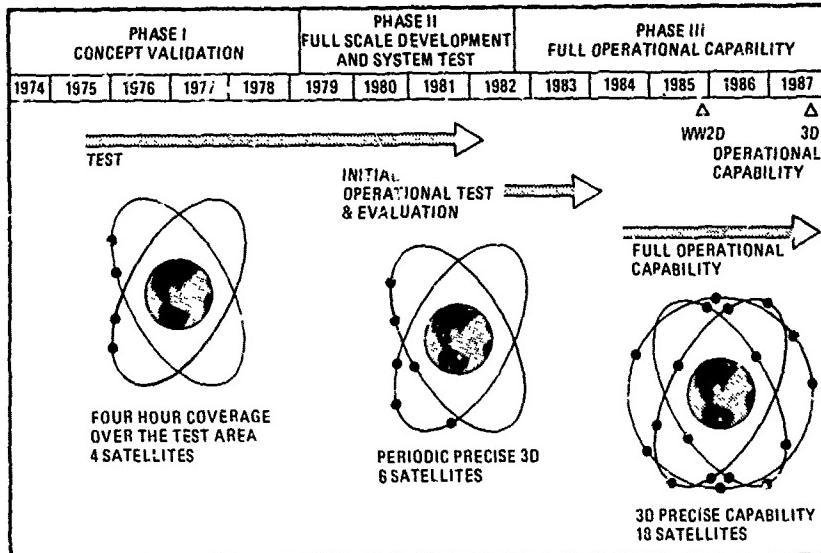
880-4421
UNCLASSIFIED

Figure 2. Schedules and Orbital Configurations

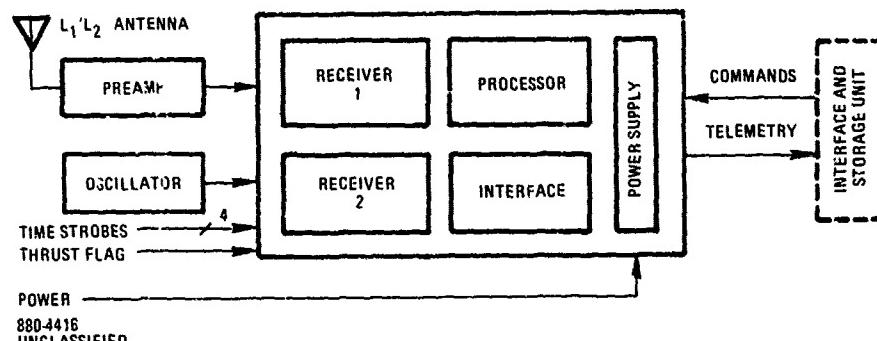
880-4416
UNCLASSIFIED

Figure 3. Receiver/Processor Assembly

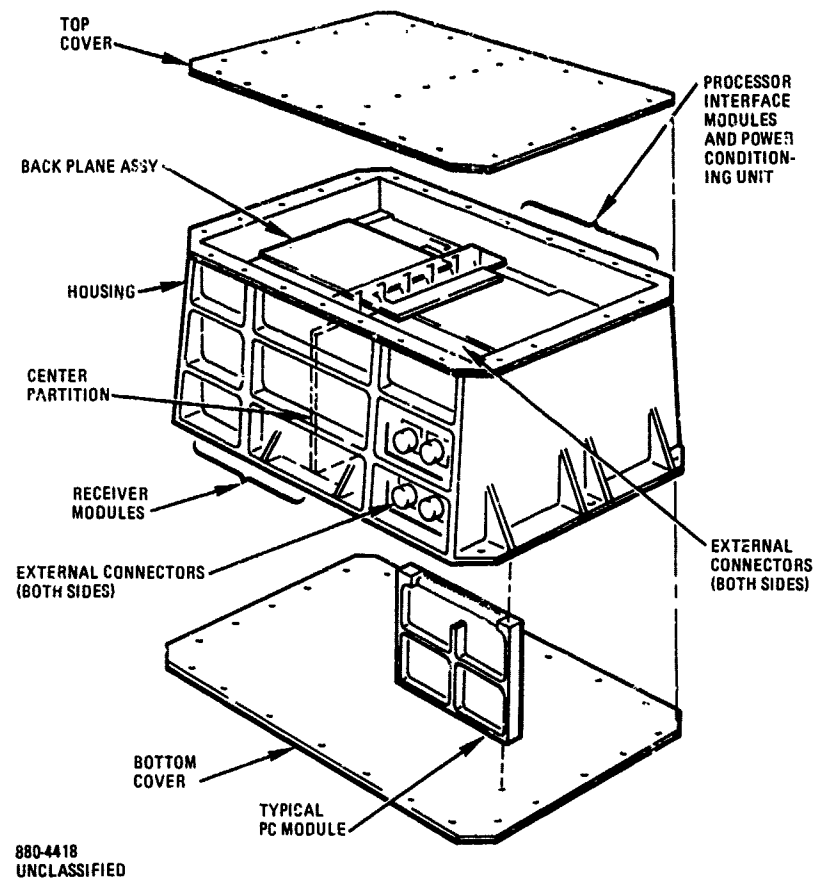


Figure 4. R/PA Construction

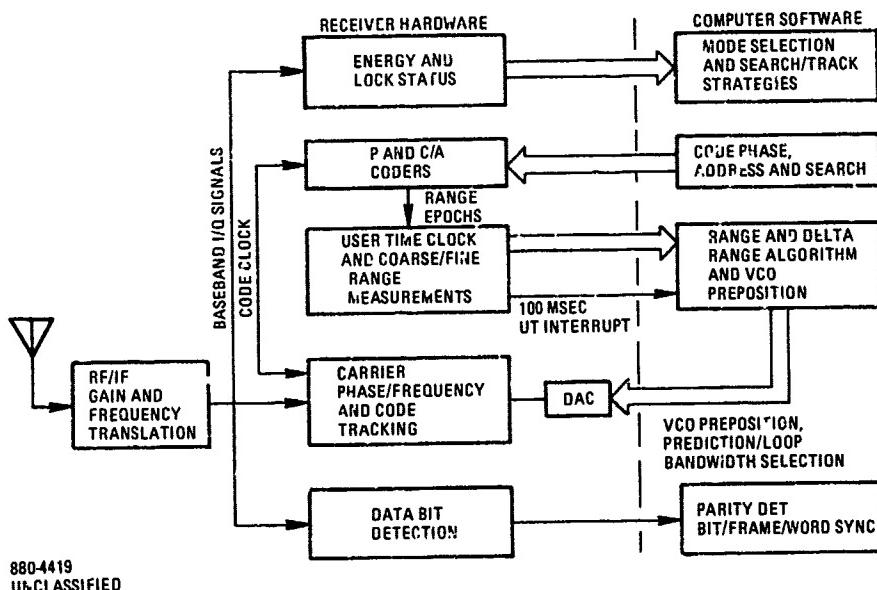


Figure 5. Receiver Hardware/Software Partitioning

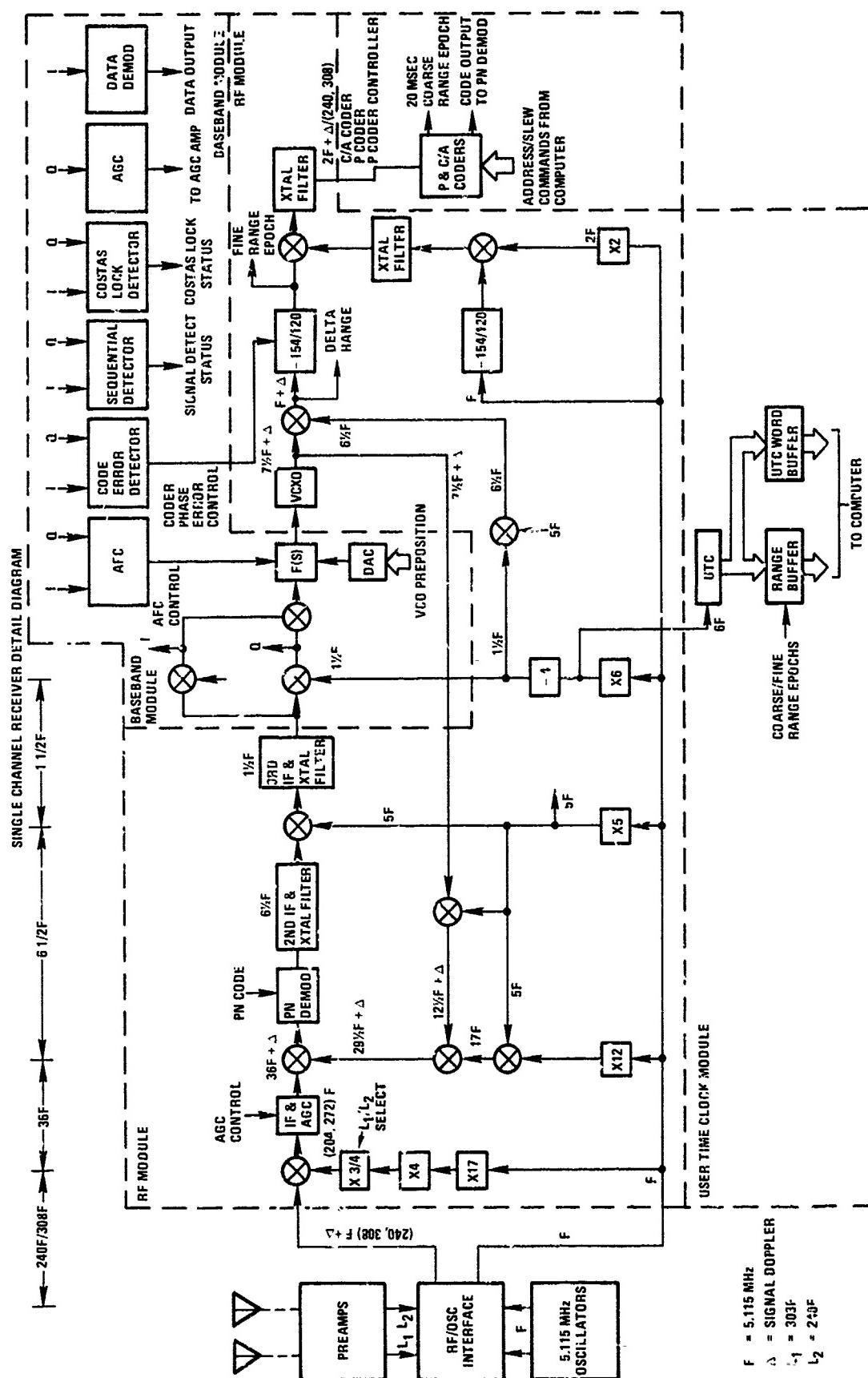


Figure 6. Receiver Configuration

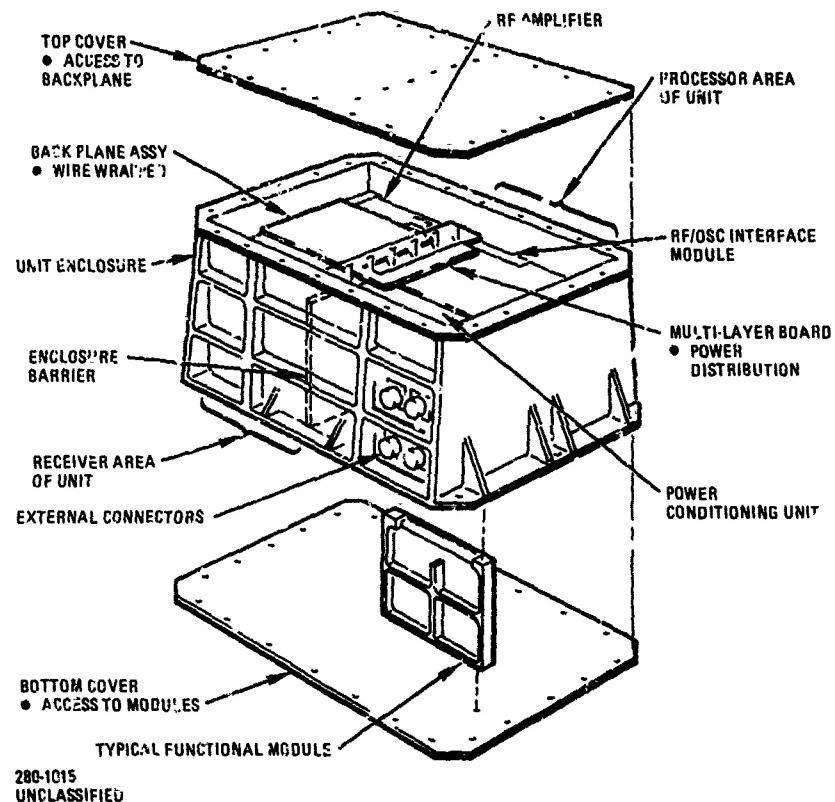
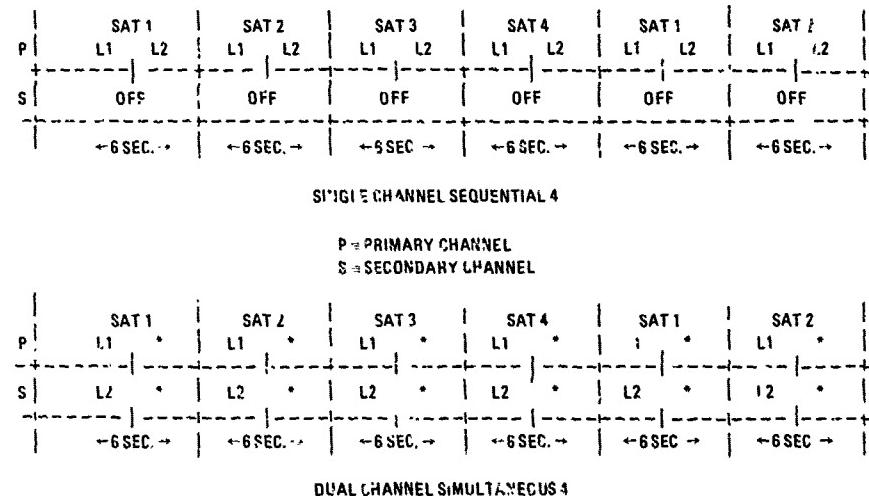


Figure 7. R/PA Unit



*IDLE
880-4417
UNCLASSIFIED

Figure 8. Sequential Track Receiver Sequences

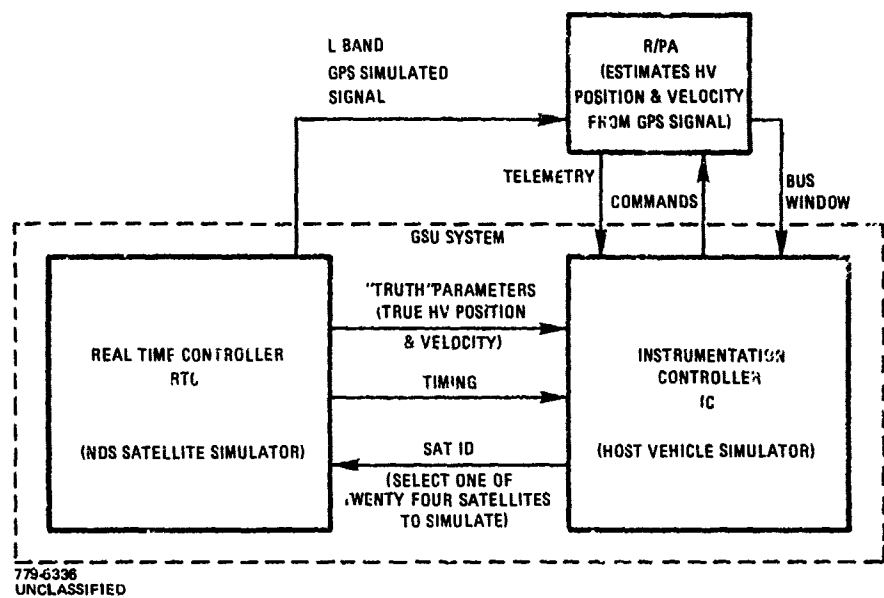


Figure 9. L Band GPS Simulated Signal

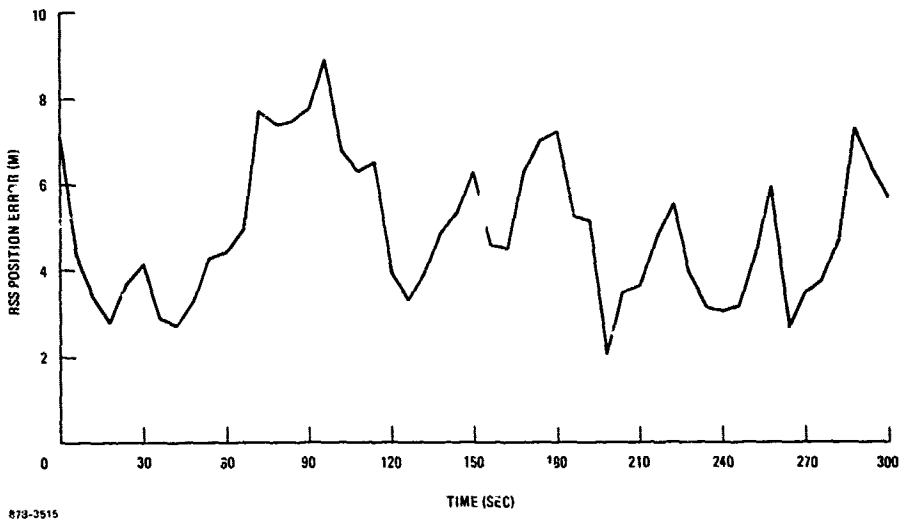


Figure 10. Simulation Results for GPSPAC Filter Position Steady-State Error

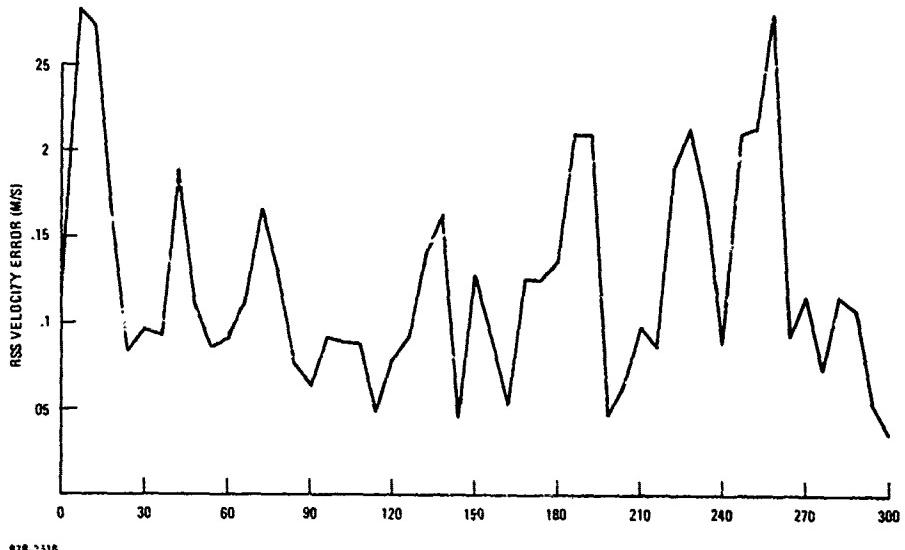


Figure 11. Simulation Results for GPSPAC Filter Velocity Steady-State Error

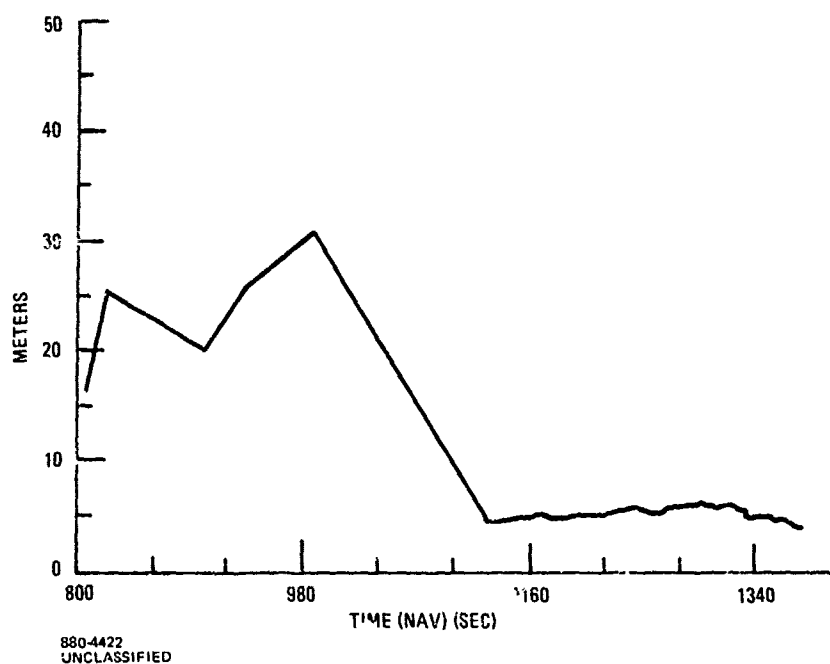


Figure 12. Dual Channel R/PA Position Steady-State Error Using Ground Support Unit Simulation

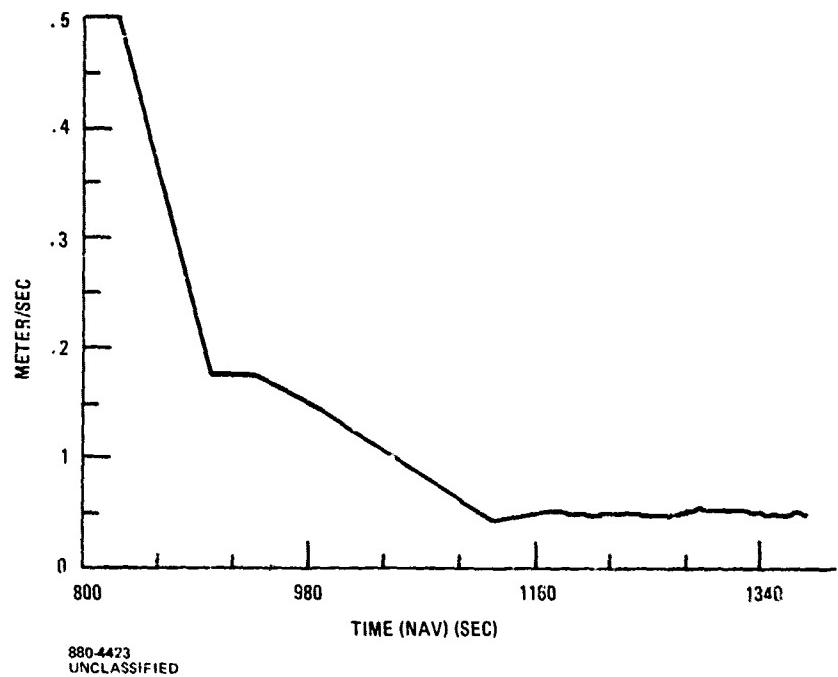
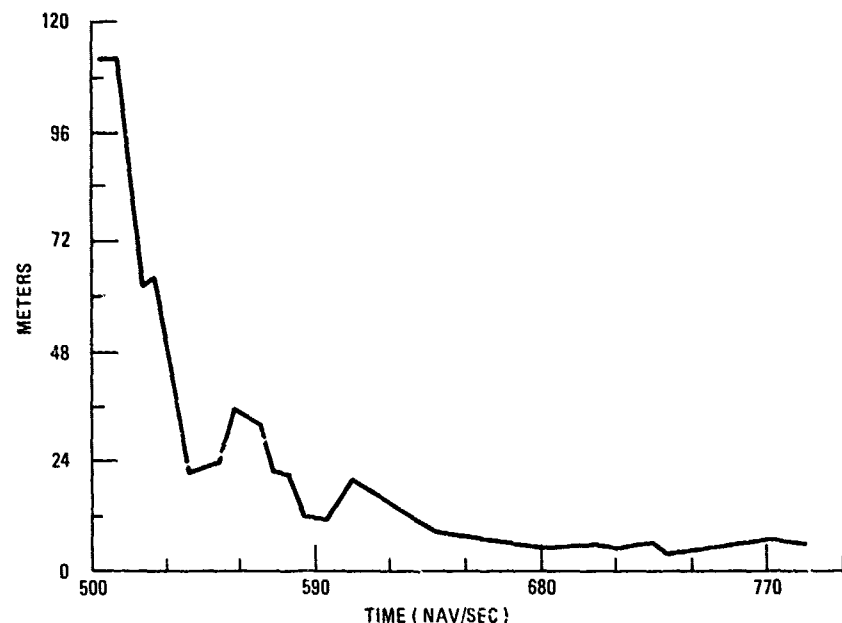
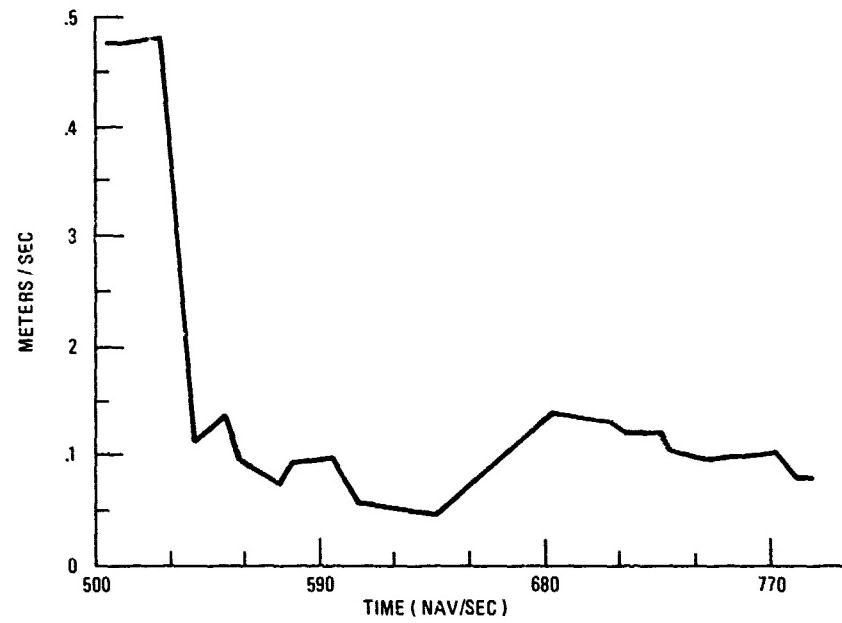


Figure 13. Dual Channel R/PA Velocity Steady-State Error Using Ground Support Unit Simulation



880-4424
UNCLASSIFIED

Figure 14. Dual Channel R/PA Position (Kalman Filter) Convergence Using Ground Support Unit Simulation



880-4425
UNCLASSIFIED

Figure 15. Dual Channel R/PA Velocity Convergence Using Ground Support Unit Simulation

**JTIDS STRAPDOWN INERTIAL
MIDCOURSE GUIDANCE PERFORMANCE ANALYSIS**

by

Dr. Sam C. Bose
Staff to Chief Scientist

LITTON SYSTEMS, Inc.
Guidance & Control Systems Division
5500 Canoga Avenue, Woodland Hills, California 91365, USA

SUMMARY

This paper investigates midcourse guidance performance of ship launched missiles against over-the-horizon airborne targets. The strapdown inertial guidance system of the missile is augmented by JTIDS passive ranging from two Airborne Early Warning aircraft situated between the launching ship and the target. The purpose of midcourse guidance is to place the missile in an acquisition "basket" sufficiently small to permit target sighting by the seeker within the constraints of its field of view and acquisition range. The terminal seeker pointing angle errors of the missile-to-target line-of-sight was selected as the performance index. Seeker pointing angle errors at acquisition time are functions of missile navigation position and attitude errors. Missile navigation errors were obtained as a function of different inertial instrument errors and JTIDS errors. Different shipboard alignment techniques and inertial instrument error budgets were included in the performance analysis. A typical relative range updating scheme in accordance with the timing structure of JTIDS was used in a Kalman filter to augment the strapdown inertial navigation system of the missile. The major error sources affecting midcourse guidance were identified and the results obtained give seeker pointing angle errors as a function of shipboard alignment technique, quality of the inertial instruments, seeker acquisition range and JTIDS relative range updating.

INTRODUCTION

NATO naval task forces are subject to enemy threats such as long range missiles launched from over-the-horizon (OTH) airborne platforms. A viable candidate for wide area defense of naval task forces against such enemy threats is a ship-launched long range rocket boosted ramjet propelled high altitude missile. Tactical missiles launched from surface ships for use against enemy antiship missiles or their surface and airborne launching platforms typically require 200 to 400 nautical mile ranges with over-the-horizon targeting. Such range requirements necessitate that the missile navigate for a period of time before target acquisition occurs. A terminal seeker is employed to aid in the interception of the target. The purpose of the terminal seeker is to acquire, lock-on and track the target until interception. The role of the missile navigator is midcourse guidance to an acquisition "basket" sufficiently small to permit target sighting by the seeker within the constraints of its field of view and acquisition range.

The missile is assumed to be equipped with a strapdown inertial navigator aligned on-board the ship before launching. The missile is also equipped with a Joint Tactical Information Distribution System (JTIDS) terminal which is used to obtain range updates from other members of the JTIDS network as well as receive targeting information. As part of the naval task force two airborne early warning (AEW) aircraft exist between the ship and the target. The two AEW aircraft are equipped with inertial navigation systems to estimate their own position, JTIDS terminals to transmit and receive signals and radars to obtain target location. The ship, which is also a member of the JTIDS network, has a ship inertial navigation system (SINS). For target interception during the terminal phase the missile is equipped with an optical, infrared or radar seeker.

The terminal seeker is subject to a missile-to-target line-of-sight pointing error during the acquisition phase. Seeker pointing angle errors at the end of the midcourse phase at target acquisition time are due to missile navigation (position and attitude) errors and inaccuracies in predicting the target location. The target location process is not within the scope of this paper. The errors in predicting the target location, henceforth, are assumed to be zero in this paper. For any given seeker acquisition range the pointing angle errors, being a function of missile navigation errors, can be parameterized over different alignment accuracies, inertial instrument quality and JTIDS relative range updates.

Seeker pointing angle errors at the end of the midcourse phase (acquisition time) are used as the criterion for midcourse guidance performance. The pointing angle error at acquisition time then establishes the probability of target sighting by the missile. Simulation results obtained give seeker pointing angle errors as a function of shipboard alignment, inertial instrument quality, JTIDS updaung and seeker acquisition range.

This paper is organized in three sections: System Description, Simulation Description and Performance Results. The first section gives an outline of the missile midcourse guidance system which includes a strapdown inertial measurement unit (IMU) for navigation, JTIDS terminals on the missile and on each AEW aircraft and a terminal seeker for target acquisition. The second section gives an overview of the error analysis simulation process including mathematical error models used and the statistical characteristics of the error sources. Performance results along with error values used are presented in the last section. All symbols, unless specified elsewhere, are defined in the List of Symbols.

SYSTEM DESCRIPTION

A functional block diagram of the missile navigation system is shown in Figure 1. As indicated, the strapdown IMU provides missile angular rates and acceleration in body axes. The JTIDS network members provide passive relative ranging between themselves and the missile navigator. Figure 2 defines the coordinate systems used. The coordinate transformation from the body coordinate system (b) to the navigation coordinate system (n) is given in (1) and the coordinate transformation from the navigation coordinate system (n) to the earth fixed coordinate system (e) is given in (2).

LIST OF SYMBOLS

$\mathbf{A}^b = \begin{bmatrix} A_x^b & A_y^b & A_z^b \end{bmatrix}'$	Accelerations in missile body coordinates	$\delta M_{nx}^b, \delta M_{ny}^b, \delta M_{nz}^b$	Missile navigation position errors in body coordinates
$\mathbf{A}^n = \begin{bmatrix} A_x^n & A_y^n & A_z^n \end{bmatrix}'$	Accelerations in navigation coordinates	$\delta M_{nx}^n, \delta M_{ny}^n, \delta M_{nz}^n$	Missile navigation position errors in navigation coordinates
$\mathbf{V}^n = \begin{bmatrix} V_x^n & V_y^n & V_z^n \end{bmatrix}'$	Velocities in navigation coordinates	$\delta T_{nx}^b, \delta T_{ny}^b, \delta T_{nz}^b$	Missile navigation targeting errors in body coordinates
$\mathbf{P}^n = \begin{bmatrix} p_x^n & p_y^n & p_z^n \end{bmatrix}'$	Craft rates in navigation coordinates	$ R_T $	Missile to target range magnitude
$\mathbf{\Omega}^n = \begin{bmatrix} \omega_x^n & \omega_y^n & \omega_z^n \end{bmatrix}'$	Earth rates in navigation coordinates	θ_T, ψ_T	Missile to target aspect angles
$\mathbf{\Omega}^e = [0 \ 0 \ 0]'$	Earth rates in earth fixed coordinates	$\nabla^b = \begin{bmatrix} \nabla_x^b & \nabla_y^b & \nabla_z^b \end{bmatrix}'$	Composite accelerometer errors in body coordinates
$\omega_{b/i}^b$	Inertial angular rate of the body coordinate system in body coordinates	$\nabla^n = \begin{bmatrix} \nabla_x^n & \nabla_y^n & \nabla_z^n \end{bmatrix}'$	Composite accelerometer errors in navigation coordinates
$\omega_{n/i}^n$	Inertial angular rate of the navigation coordinate system in navigation coordinates	$\epsilon^b = \begin{bmatrix} \epsilon_x^b & \epsilon_y^b & \epsilon_z^b \end{bmatrix}'$	Composite gyro errors in body coordinates
$\phi^b = \begin{bmatrix} \phi_x^b & \phi_y^b & \phi_z^b \end{bmatrix}'$	Navigation attitude errors of the body coordinate system in body coordinates	$\epsilon^n = \begin{bmatrix} \epsilon_x^n & \epsilon_y^n & \epsilon_z^n \end{bmatrix}'$	Composite gyro errors in navigation coordinates
$\phi^n = \begin{bmatrix} \phi_x^n & \phi_y^n & \phi_z^n \end{bmatrix}'$	Navigation attitude errors of the body coordinate system in navigation coordinates	$\nabla_{bx}, \nabla_{by}, \nabla_{bz}$	Accelerometer bias
$\psi^n = \begin{bmatrix} \psi_x^n & \psi_y^n & \psi_z^n \end{bmatrix}'$	Inertial attitude errors of the body coordinate system in navigation coordinates	$\nabla_{sx}, \nabla_{sy}, \nabla_{sz}$	Accelerometer scale factor
$\omega\theta^n = \begin{bmatrix} \omega_x^n & \omega_y^n & \omega_z^n \end{bmatrix}'$	Navigation attitude errors of the navigation coordinate system in navigation coordinates	$\nabla_{s2x}, \nabla_{s2y}, \nabla_{s2z}$	Accelerometer quadratic scale factor
$\delta V^n = \begin{bmatrix} \delta V_x^n & \delta V_y^n & \delta V_z^n \end{bmatrix}'$	Velocity errors in navigation coordinates	$\nabla_{s3x}, \nabla_{s3y}, \nabla_{s3z}$	Accelerometer cubic scale factor
$\delta P^n = \begin{bmatrix} \delta p_x^n & \delta p_y^n & \delta p_z^n \end{bmatrix}'$	Craft rate errors in navigation coordinates	$\nabla_{sax}, \nabla_{say}, \nabla_{saz}$	Accelerometer scale factor asymmetry
ϕ, θ, ψ	Missile body roll, pitch, heading in navigation coordinates	$\nabla_{ax}, \nabla_{ay}, \nabla_{az}$	Accelerometer mass unbalance
δg^n	Earth's gravity anomaly in navigation coordinates	$\nabla_{nx}, \nabla_{ny}, \nabla_{nz}$	Accelerometer nonorthogonality
g_0	Gravity constant	$\epsilon_{bx}, \epsilon_{by}, \epsilon_{bz}$	Gyro bias
ϕ, λ	Missile latitude and longitude in earth fixed coordinates after launch	$\epsilon_{sx}, \epsilon_{sy}, \epsilon_{sz}$	Gyro scale factor
Φ_0, λ_0	Missile latitude and longitude in earth fixed coordinates at launch time	$\epsilon_{sax}, \epsilon_{say}, \epsilon_{saz}$	Gyro scale factor asymmetry
h^n	Missile altitude in navigation coordinates	$\epsilon_{mxx}, \epsilon_{myy}, \epsilon_{mzz}$	Gyro mass unbalance
R_m	Earth's meridional radius of curvature	$\epsilon_{mxz}, \epsilon_{myz}, \epsilon_{mzy}$	Gyro quadrature
R_n	Earth's normal radius of curvature	$\epsilon_{axz}, \epsilon_{ayx}, \epsilon_{azz}$	Gyro anisotropy
x, y, z	Missile's position from launch point in navigation coordinates fixed at launch point	$\epsilon_{nxy}, \epsilon_{nyz}, \epsilon_{nzx}, \epsilon_{nyx}, \epsilon_{nzy}, \epsilon_{nxz}$	Gyro nonorthogonality
x_i, y_i, z_i	JTIDS net i th transmitter position from launch point in navigation coordinates fixed at launch point	$\mathbf{Q} = \begin{bmatrix} 0 & 0 & 0 \\ 0 & 0 & 0 \\ 0 & 0 & 0 \end{bmatrix}$	3 x 3 Null matrix
a	Earth's equatorial radius	$\mathbf{Q}(\omega) = \begin{bmatrix} 0 & -\omega_z & \omega_y \\ \omega_z & 0 & -\omega_x \\ -\omega_y & \omega_x & 0 \end{bmatrix}$	3 x 3 skew symmetric matrix of any vector $\omega = [\omega_x \ \omega_y \ \omega_z]'$
$\eta_x^s, \eta_y^s, \eta_z^s$	Missile to target line of-sight pointing angle errors normal to pointing vector	c, s, t	Cosine, sine, tangent
		c^{-1}, s^{-1}, t^{-1}	inverse cosine, sine, tangent

$$C_b^n = \begin{bmatrix} c\theta s\psi & s\phi s\theta s\psi + c\phi c\psi & c\phi s\theta s\psi - s\phi s\psi \\ c\theta c\psi & s\phi s\theta c\psi - c\phi s\psi & c\phi s\theta c\psi + s\phi s\psi \\ s\theta & -s\phi c\theta & -c\phi c\theta \end{bmatrix}$$

$$C_n^e = \begin{bmatrix} c\lambda & -s\phi s\lambda & c\phi s\lambda \\ 0 & c\phi & s\phi \\ -s\lambda & -s\phi c\lambda & c\phi c\lambda \end{bmatrix}$$

The strapdown IMU consists of three accelerometers and two two-degree-of-freedom gyros. The sensitive axes of the accelerometers and gyros coincide with the missile body axes as shown in Figure 2. A functional block diagram of the north-pointing strapdown navigation mechanization equations is given in Figure 3(1).

For target acquisition the missile guidance system is equipped with a terminal seeker. The seeker coordinate system orientation with respect to the missile body coordinate system is shown in Figure 4. The choice of the seeker coordinate system is motivated by the fact that the component of the pointing vector error along the missile-to-target line-of-sight is zero. Hence the component of the pointing vector error along x^s is zero. Additionally the orthogonal components of the pointing vector error along y^s and z^s normal to missile-to-target line-of-sight serve as critical parameters to establish missile seeker requirements(2). The transformation from missile body coordinates (b) to seeker coordinates (s) is defined as

$$C_b^s = \begin{bmatrix} c\theta_T c\psi_T & c\theta_T s\psi_T & -s\theta_T \\ -s\psi_T & c\psi_T & 0 \\ s\theta_T c\psi_T & s\theta_T s\psi_T & c\theta_T \end{bmatrix}$$

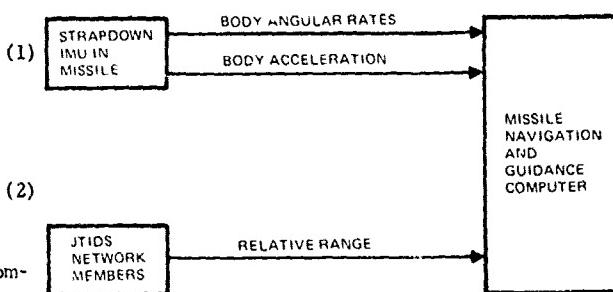


Figure 1 Missile Navigation System Functional Block Diagram

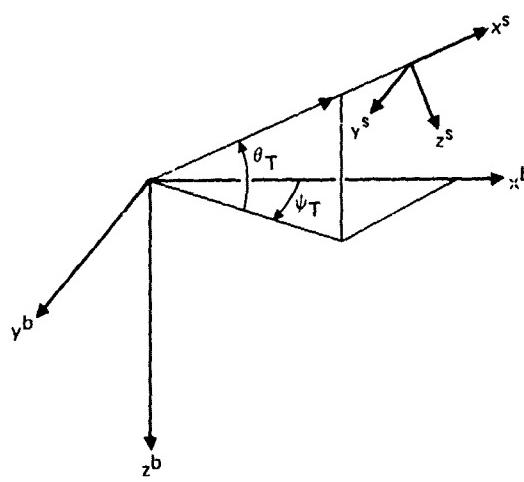


Figure 4 Missile Body and Seeker Coordinate Systems

The missile and two Airborne Early Warning (AEW) aircraft are equipped with JTIDS terminals. The Joint Tactical Information Distribution System (JTIDS) is a high-capacity, time-division multiple-access (TDMA) spread spectrum communication system that has the inherent capability of providing passive, high-accuracy, relative navigation with respect to other terminals within a net of users. The navigation capability of JTIDS stems from the fact that JTIDS terminals perform a very high accuracy time-of-arrival (TOA) measurement on the signals (messages) received from the other terminals in the net. The process involves a form of multilateration where a user passively ranges sequentially to several other terminals in the net and determines its position from the measured ranges. JTIDS is a synchronous system based on a single time reference and hence all terminals attempt to transmit at specified and known times. Since the relative navigation process is a form of pseudoranging such that range measurements are made with respect to the user's own clock, rather than on an absolute or round-trip basis any synchronization error or time bias (as is normally the case) is inherently determined. All active units transmit periodically a position and status message which contains the source terminal's position, speed, course, and altitude as well as its position quality, time quality and relative grid azimuth quality. Using these data the user calculates the predicted range and compares it to the measured range, as obtained from the TOA. On the basis of these sequential TOA measurements and by means of Kalman filtering the user continuously updates its own position, velocity, attitude and time bias (with respect to system time). Between filter updates data from any dead reckoning sensors such as an inertial system can be used to extrapolate the TOA-derived data and to optimally mix the data from the two sensors(3).

Each member of the network can transmit (or relay) messages only at specifically assigned times but can receive (access) from other members at all other times. Members of the network can broadcast information routinely into the net without needing to know who the recipients may be; tactical elements needing the data extract it from the net without needing to know who furnished it. Clock synchronization is a prerequisite of any TDMA net. The synchronous nature of JTIDS means that all user terminals in a net operate on a common time base through the use of stable clock oscillators. These clocks are periodically synchronized to a master time, called the net time reference. The TDMA property of JTIDS results from the use of an epoch of 12.8 minutes which is divided into discrete increments, called time slots. Time slots are renumbered after each epoch and a single time slot number allocated to a particular member must recur at least once per epoch. No member can be given less than one time slot per epoch and as many of the epoch's time slots as necessary can be assigned to any member, depending on the nature of its mission. The 12.8 minute epoch is subdivided into 12 second cycles such that all active units transmit once within this cycle. This cycle is again subdivided into the 7.8125 millisecond time slots. A complete message (e.g., position, status, targeting information etc.) is contained within a single time slot. Time slot assignments for transmission are generally made on the basis of 2^N time slots per 12.8 minute epoch, where N can vary from 0 to 15 (i.e., from 1 to 32768 time slots per epoch). The 7.8125 millisecond time slot is partitioned among a preamble, a synchronization function, the message data and the propagation/guard times. Such a time slot supports both 300 and 500 nautical mile range capabilities. Resistance to jamming is achieved by spread spectrum techniques that result in a much wider transmission bandwidth than required for transmitting the data. Detailed descriptions of the JTIDS design characteristics, such as operating frequency band, modulation waveform, message formats, etc., are presented in (4)-(6) and will not be repeated here.

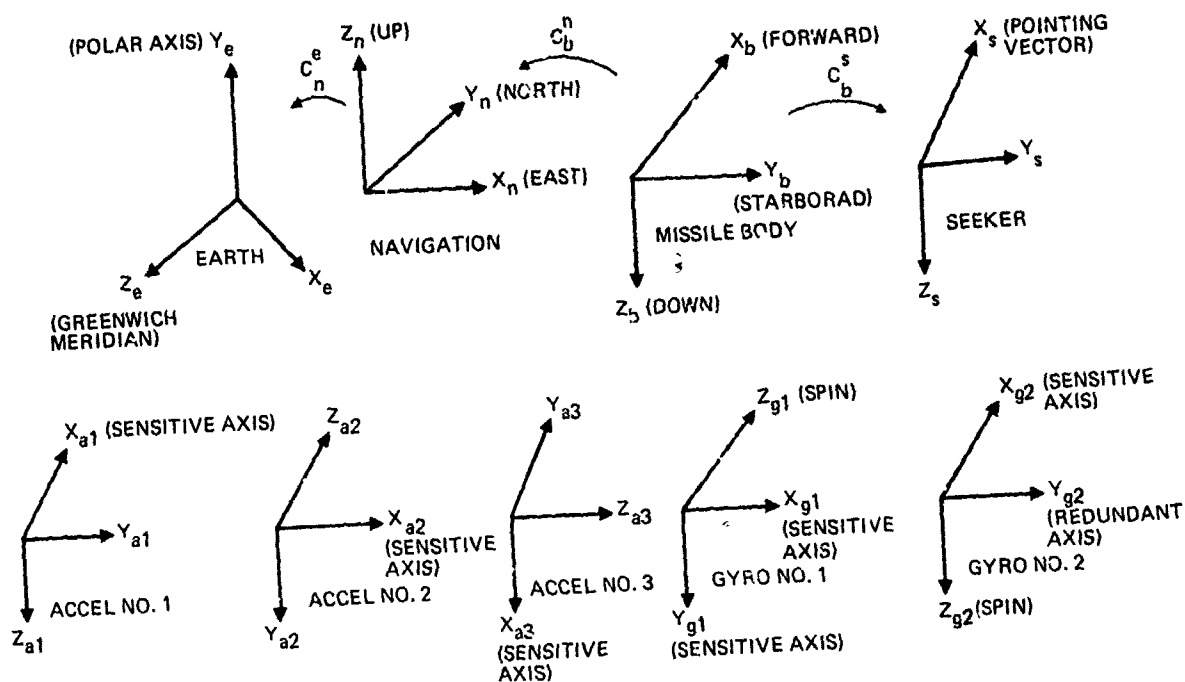


Figure 2. Definition of Coordinate Systems

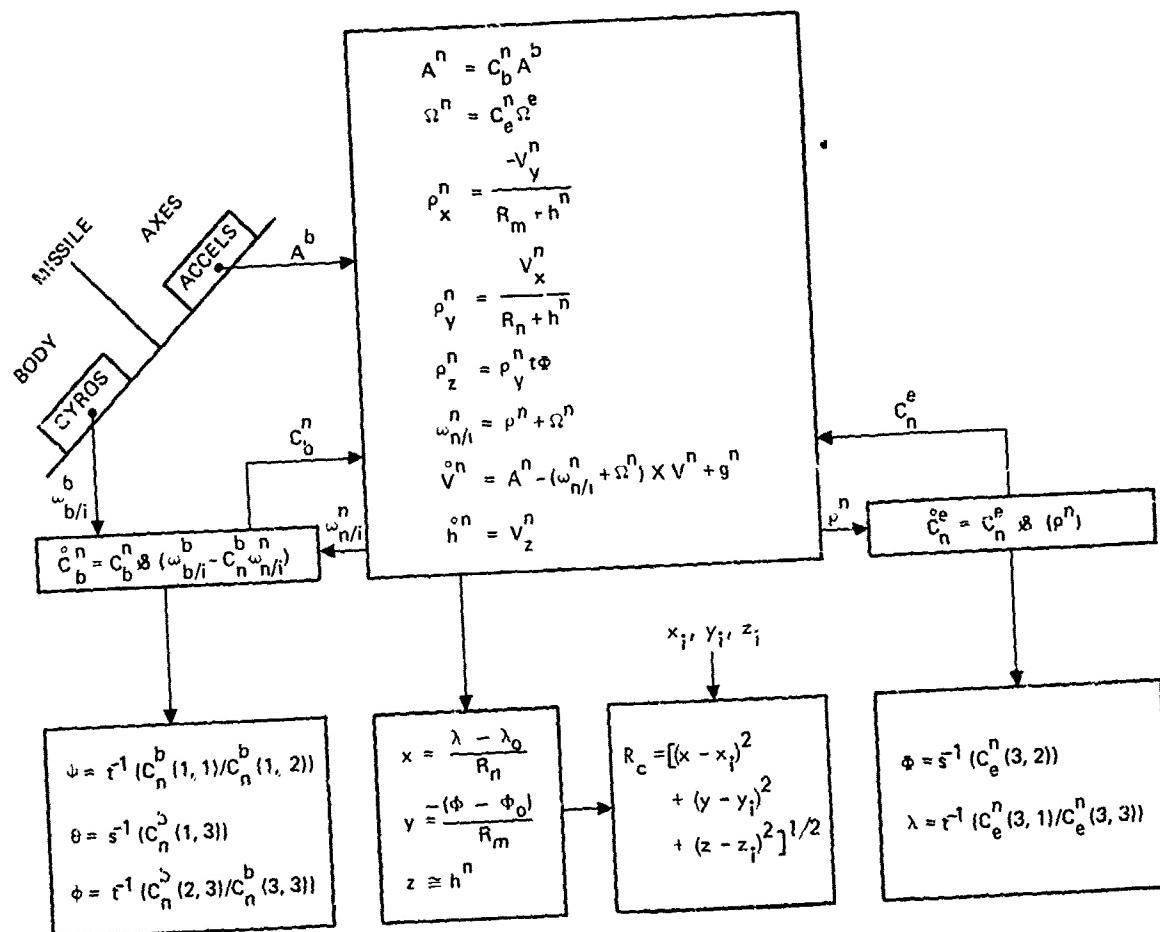


Figure 3. Strapdown Navigation Mechanization Equations

SIMULATION DESCRIPTION

This section gives an overview of the simulation process along with all the mathematical error models used and the statistical characteristics of the error sources. Performance results were obtained from an error simulation as opposed to a mechanization simulation. To this end the JTIDS augmented strapdown navigation system mechanization was used to develop a navigation system error model and a Kalman filter error controller. An error model of the seeker gave the necessary equations for obtaining seeker pointing angle error from the navigation errors⁽²⁾. The error analysis simulation was performed by means of sensitivity simulation and not a covariance simulation. For convenience and cost purpose the entire simulation was done in five separate steps. The five steps in the simulation process were: (I) Generation of a representative missile trajectory (II) Generation of Kalman gains at update times (III) Generation of navigation error sensitivities (IV) Scaling of navigation error sensitivities and snapshot storage of these responses at selected times (V) Processing of scaled responses at snapshot times to obtain pointing angle error.

A functional block diagram of the simulation process is given in Figure 5. In the sequel each box of Figure 5 is discussed in detail. The first step was generation of a representative missile trajectory. The trajectory was generated using a six-degree-of-freedom model and the entire trajectory was stored in the computer for use in the subsequent simulation steps. Since the trajectory generation process, though crucial, is incidental to the performance analysis, and hence details of the trajectory generation process are omitted⁽⁷⁾. The trajectory generation step is shown as Box I in Figure 5.

The second step involved generation of the Kalman filter gains at the different update times. This second step is broken up in several parts in Figure 5. The filter dynamics matrix (F) and the observation matrix (H) are evaluated in Box IIa. The plant equation and the measurement equation of the candidate Kalman filter are given in Figure 6. The plant noise covariance is computed in Box IIb. The plant noise covariance in navigation coordinates (n) is obtained from the plant noise covariance in body coordinates (b) by means of similarity transformations given below:

$$Q_{\epsilon}^n = C_b^n Q_{\epsilon}^b C_n^b \quad (4)$$

where

$$Q_{\epsilon}^b = \begin{bmatrix} Q_{\epsilon_x}^b & & \\ & Q_{\epsilon_y}^b & \\ & & Q_{\epsilon_z}^b \end{bmatrix} \quad \text{and} \quad Q_v^n = \begin{bmatrix} Q_v^b_x & & \\ & Q_v^b_y & \\ & & Q_v^b_z \end{bmatrix} \quad (5)$$

The above similarity transformations given by (4) were necessary only for the gyro and accelerometer errors due to the fact that gyros and accelerometers in strapdown systems are modelled in body coordinates (b) whereas filter equations are in navigation coordinates (n). In (5) the off-diagonal terms are zero since the gyro and accelerometer errors are assumed to be uncorrelated along the three axes of the body coordinates (b) and the on-diagonal terms are given by

$$Q_{\epsilon_i}^b = E\{\epsilon_i^b \epsilon_i^b\} \quad Q_v_i^b = E\{v_i^b v_i^b\} \quad i=x, y, z \quad (6)$$

The gyro errors ϵ_i^b and accelerometer errors v_i^b in body coordinates (b) were modelled as modulated white noise error where the modulation was done by body angular rates and body accelerations as per Figure 7.

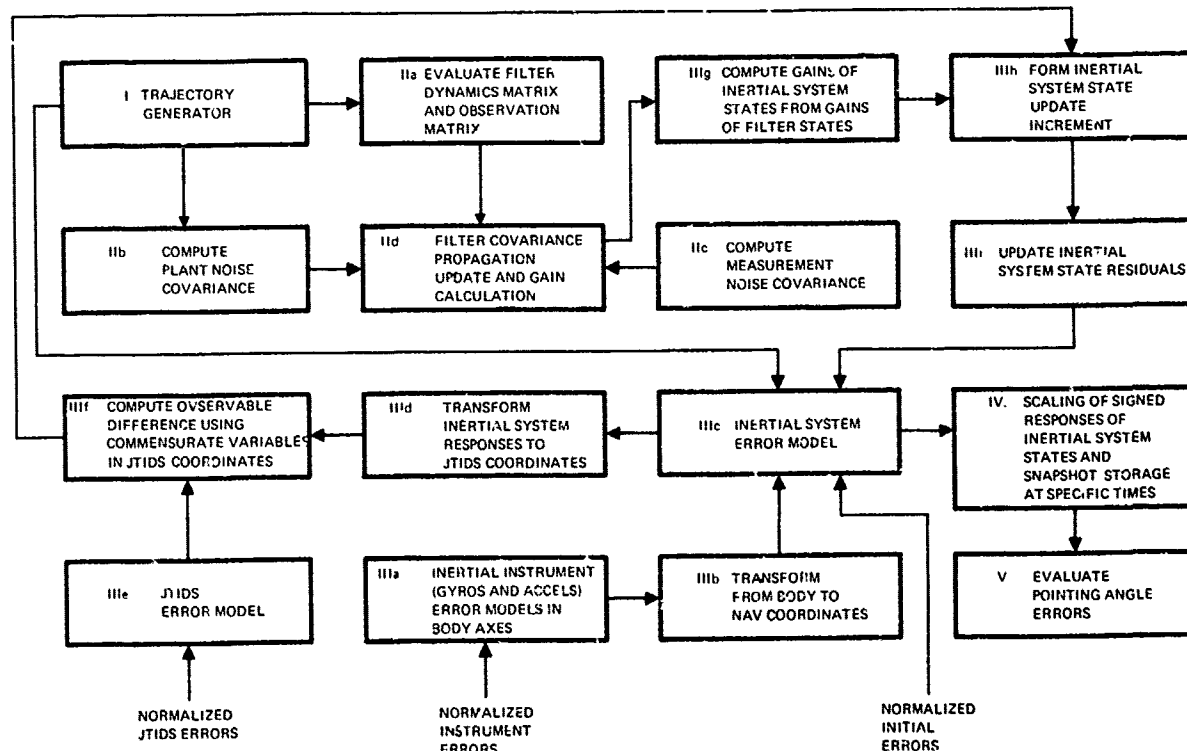


Figure 5. Error Simulation Functional Block Diagram

The measurement noise covariance is computed in Box IIc. The measurement noise covariance is given by

$$R = E[\xi_R \xi_R'] \quad (7)$$

where the measurement noise ξ_R is scalar and is essentially the time-of-arrival (TOA) measurement noise.

The filter covariance propagation, covariance update and Kalman gain calculation of Box 11d are performed using the following equations⁽³⁾

$$\dot{P} = FP^+ + PF^- + Q \quad P^+ = (I - KH) P^- \quad K = P^- H^T (H P^- H^T + R)^{-1} \quad (8)$$

where P is the covariance of the residual error, \bar{P} is the covariance before update, P^+ after the update and K is the Kalman gain for the filter states.

In actual fact the updating is done alternately between the two AEW aircraft equipped with JTIDS terminals and hence two different gains K_1 and K_2 are computed for each terminal as follows:

$$K_i = P_i^- H_i \left(H_i P_i^- H_i + R_i \right)^{-1} \quad P_i^+ = (I - K_i H_i) P_i^- \quad i=1,2 \quad (9)$$

H_i ($i=1, 2$) refers to the H matrix in Figure 6 using x_i, y_i, z_i ($i=1, 2$) when the i th source is transmitting and R_i ($i=1, 2$) refers to the measurement noise covariance R given by (7). Since updating is done from two alternating sources the covariance propagation is such that P_1^+ is propagated to P_2 and P_2^+ is propagated to P_1 .

The objective of the third step of the simulation process is to obtain the navigation errors' sensitivities relative to each error source. The error sources include inertial instrument errors, inertial system initial condition errors, JTIDS errors and JTIDS initial condition errors. All these errors were identified as statistically independent error sources contributing to the missile navigation error responses.

Inspection of Figure 2 shows that the three accelerometers and two gyros that constitute the IMU have their sensitive axes along the three axes of the missile body coordinate system. The composite errors of the accelerometers and gyros along the three axes of the missile body coordinate system (b) are given in Figure 7 (Box IIIa).

The accelerometer and gyro errors as defined in Box IIIa are in missile body coordinates (b). To obtain the accelerometer and gyro errors in missile navigation coordinates (n) the appropriate transformations are performed in Box IIIb as follows.

$$v^n = C_b^n v^b \quad \epsilon^n = C_b^n \epsilon^b \quad (10)$$

where the components of ∇^b, ϵ^b are given in Figure 7 and C_b^n is as defined in (1).

Along each axis of the missile body coordinate system (b) 8 error sources were considered for each accelerometer and each gyro, totaling 48 statistically independent error sources, as given in Table I. The initial condition errors were the initial values for the inertial system states. The 10 states of the inertial system resulted in 10 initial condition errors. In the actual simulation, only 3 initial condition errors for initial attitude errors had non zero values. All other initial errors (position and velocity) were set to zero.

Figure 6. Plant Equation and Measurement Equation in Kalman Filter

Accelerometers

$$\nabla_x^b = \nabla_{bx} + \nabla_{sx} A_x^b + \nabla_{s2x} (A_x^b)^2 + \nabla_{ny} A_y^b - \nabla_{nz} A_z^b + \frac{1}{2} \nabla_{sax} |A_x^b| + \nabla_{ax} A_x^b A_y^b + \nabla_{s3x} (A_x^b)^3$$

$$\nabla_y^b = \nabla_{by} + \nabla_{sy} A_y^b + \nabla_{s2y} (A_y^b)^2 + \nabla_{nz} A_z^b - \nabla_{nx} A_x^b + \frac{1}{2} \nabla_{say} |A_y^b| + \nabla_{ay} A_y^b A_z^b + \nabla_{s3y} (A_y^b)^3$$

$$\nabla_z^b = \nabla_{bz} + \nabla_{sz} A_z^b + \nabla_{s2z} (A_z^b)^2 + \nabla_{nx} A_x^b - \nabla_{ny} A_y^b + \frac{1}{2} \nabla_{saz} |A_z^b| + \nabla_{az} A_z^b A_x^b + \nabla_{s3z} (A_z^b)^3$$

Gyros

$$\epsilon_x^b = \epsilon_{bx} + \epsilon_{sx} \omega_x^b + \epsilon_{nxy} \omega_y^b - \epsilon_{nxz} \omega_z^b - \epsilon_{mxx} A_x^b - \epsilon_{mxy} A_y^b + \epsilon_{axz} A_x^b A_z^b + \frac{1}{2} \epsilon_{sax} |\omega_x^b|$$

$$\epsilon_y^b = \epsilon_{by} + \epsilon_{sy} \omega_y^b + \epsilon_{nyz} \omega_z^b - \epsilon_{nyx} \omega_x^b - \epsilon_{myy} A_y^b - \epsilon_{myz} A_z^b + \epsilon_{ayx} A_y^b A_x^b + \frac{1}{2} \epsilon_{say} |\omega_y^b|$$

$$\epsilon_z^b = \epsilon_{bz} + \epsilon_{sz} \omega_z^b + \epsilon_{nzx} \omega_x^b - \epsilon_{nzy} \omega_y^b - \epsilon_{mzz} A_z^b + \epsilon_{mzy} A_y^b + \epsilon_{azx} A_z^b A_x^b + \frac{1}{2} \epsilon_{saz} |\omega_z^b|$$

Figure 7. Accelerometer and gyro errors in missile body coordinate system

The JTIDS user clock error model used is shown in Figure 8. The error sources in the JTIDS user clock error model include 1) White noise error for User Clock Bias Rate ξ_t^b , 2) White noise error for User Clock Drift Rate ξ_b^b , 3) Initial condition error for User Clock Bias ∇_b^b , 4) Initial condition error for User Clock Drift ∇_b^b . In addition to the above mentioned error sources two other clock errors were included: White noise for TOA flicker noise (ξ_{TOA}) and a Systematic Bias error for transmitter clock (b_t). Six additional transmitter position bias error sources $\delta x_i, \delta y_j, \delta z_i$ ($i=1, 2$) were also included in the sensitivity study. All the above mentioned error sources were considered statistically independent and the navigation error of the missile was obtained for each error source, i.e., a sensitivity analysis was performed.

To obtain the missile navigation error sensitivities to the various error sources an appropriate definition of the strapdown inertial system error model is required. This is outlined in vector form in Figure 9. The inertial system error model given in Figure 9 is considered as the real-world model and used to propagate the updated inertial system state residuals (Box IIIc).

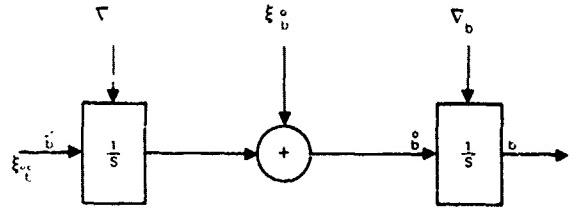


Figure 8. JTIDS Clock Error Model

$$\begin{aligned}\delta \theta^n &= \delta \rho^n + \delta \theta^n \times \rho^n \\ \delta \phi^n &= \delta \rho^n - \delta \theta^n \times \Omega^n + \phi^n \times \omega_{n/i}^n - \epsilon^n \\ \delta V^n &= A^n \times \phi^n - (\rho^n + 2\Omega^n) : \delta V^n - \delta \rho^n \times V^n \\ &\quad + 2(\delta \theta^n \times \Omega^n) \times V^n + \delta g^n + \nabla^n \\ \delta h^n &= \delta V_z^n\end{aligned}$$

where,

$$\delta g^n = [0 \ 0 \ (2g_0/a)\delta h^n]^T$$

$$\delta \rho_x^n = -\delta V_y^n / (R_n + h^n)$$

$$\delta \rho_y^n = \delta V_x^n / (R_n + h^n)$$

$$\delta \rho_z^n = (-\rho_y^n / (C_e^n(2,2))^2) \delta \theta_x^n + (C_e^n(3,2) / C_e^n(2,2)) \delta \rho_y^n$$

Figure 9. Inertial System Error Model

TABLE I

1. ACC#1 BIAS IN MIC-G	25. GYRO IX BIAS IN DEG/HR
2. ACC#1 SCALE FACTOR ERROR IN PRCT	26. GYRO IX SCALE FACTOR ERROR IN PRCT
3. ACC#1 SCALE FACTOR ASYM IN PRCT	27. GYRO IX SCALE FACTOR ASYM IN PRCT
4. ACC#1 G2 SENS. IN MIC-G/G2,(AXAY)	28. GYRO IX MIS'ALNT IN MRAD,(WZ)
5. ACC#1 G2 SENS. IN MIC-G/G2,(AX2)	29. GYRO IX MIS'ALNT IN MRAD,(-WX)
6. ACC#1 G3 SENS. IN MIC-G/G3,(AX3)	30. GYRO IX G DRIFT IN DEG/HR/G,(-AY)
7. ACC#1 MIS'ALNT IN MRAD,(AY)	31. GYRO IX G DRIFT IN DEG/HR/G,(-AZ)
8. ACC#1 MIS'ALNT IN MRAD,(-AZ)	32. GYRO IX G2 DRIFT IN DG/HR/G2,(AXAY)
9. ACC#2 BIAS IN MIC-G.	33. GYRO IY BIAS IN DEG/HR
10. ACC#2 SCALE FACTOR ERROR IN PRCT	34. GYRO IY SCALE FACTOR ERROR IN PRCT
11. ACC#2 SCALE FACTOR ASYM IN PRCT	35. GYRO IY SCALE FACTOR ASYM IN PRCT
12. ACC#2 G2 SENS. IN MIC-G/G2,(AYAZ)	36. GYRO IY MIS'ALNT IN MRAD,(WX)
13. ACC#2 G2 SENS. IN MIC-G/G2,(AY2)	37. GYRO IY MIS'ALNT IN MRAD,(-WY)
14. ACC#2 G3 SENS. IN MIC-G/G3,(AY3)	38. GYRO IY G DRIFT DEG/HR/G,(-AZ)
15. ACC#2 MIS'ALNT IN MRAD,(AZ)	39. GYRO IY G DRIFT DEG/HR/G,(AY)
16. ACC#2 MIS'ALNT IN MRAD,(-AX)	40. GYRO IY G2 DRIFT IN DEG/HR/G2,(AZAX)
17. ACC#3 BIAS IN MIC-G	41. GYRO 2X BIAS IN DEG/HR
18. ACC#3 SCALE FACTOR ERROR IN PRCT	42. GYRO 2X SCALE FACTOR ERROR IN PRCT
19. ACC#3 SCALE FACTOR ASYM IN PRCT	43. GYRO 2X SCALE FACTOR ASYM IN PRCT
20. ACC#3 G2 SENS. IN MIC-G/G2,(AZAX)	44. GYRO 2X MIS'ALNT IN MRAD,(WY)
21. ACC#3 G2 SENS. IN MIC-G/G2,(AZ2)	45. GYRO 2X MIS'ALNT IN MRAD,(-WZ)
22. ACC#3 G3 SENS. IN MIC-G/G3,(AZ3)	46. GYRO 2X G DRIFT IN DEG/HR/G,(-AX).
23. ACC#3 MIS'ALNT IN MRAD,(AX)	47. GYRO 2X G DRIFT IN DEG/HR/G,(-AY).
24. ACC#3 MIS'ALNT IN MRAD,(-AY)	48. GYRO 2X G2 DRIFT IN DEG/HR/G2,(AXAZ)

To update the inertial system states by the Kalman gains requires forming an observable difference. The observable difference requires differencing of commensurate variables between the inertial system and JTIDS. Relative range between the missile and the transmitting AEW aircraft was chosen as the commensurate variable to form the observable difference. From the equation of computed (predicted) Relative Range R_c given in Figure 3 it can be shown that the error in computed relative range is

$$\delta R_c = -\frac{a(y - y_i) \delta \theta_x^n}{R_c} + \frac{a(x - x_i) \delta \theta_y^n}{R_c} + \frac{(z - z_i) \delta h^n}{R_c} - \frac{(x - x_i) \delta x_i}{R_c} - \frac{(y - y_i) \delta y_i}{R_c} - \frac{(z - z_i) \delta z_i}{R_c} \quad (11)$$

where x, y, z are the position coordinates of the user (receiver) and x_i, y_i, z_i are the position coordinates of the i th source (transmitter).

The transformation of inertial system state residuals from navigation coordinates to JTIDS coordinates as given by (10) is done in Box IIId.

The basic relative navigation passive ranging measurement model can be expressed as

$$R_m = c(TOA_m) = c(TOA_t + TOA_e) = cTOA_t + cTOA_e = R_t + \delta R_m \quad (12)$$

where c is the speed of light, TOA_m , TOA_t , TOA_e are respectively the measured, true and errored time of arrival with respect to user's own clock time; R_m , R_t , δR_m are respectively the measured, true and errored relative range. The error in measured relative range is given by

$$\delta R_m = b - b_t - N \quad (13)$$

where b is the time bias of the user (receiver), b_t is time bias of the source with respect to system time, N is the sum of measurement noises. The JTIDS error model in Box IIIe is simply the measurement error in relative range given by (11). In the JTIDS error model b and b_t were modelled as systematic bias errors whereas N was modelled as a white noise error.

The observable difference θ' is formed in Box IIIf by differencing the relative range measurement error δR_m from that of computation error δR_c such that

$$\theta' = \delta R_c - \delta R_m \quad (14)$$

The Kalman gains for the inertial system states $\delta \theta_x^n, \delta \theta_y^n, \delta \theta_z^n, \phi_x^n, \phi_y^n, \phi_z^n, \delta V_x^n, \delta V_y^n, \delta V_z^n, \delta h^n$

are obtained from the filter states $\delta \theta_x^n, \delta \theta_y^n, \delta h^n, \psi_x^n, \psi_y^n, \psi_z^n, \delta V_x^n, \delta V_y^n, \delta V_z^n$ in Box IIIf by using the following equations:

$$\delta \theta_z^n = \delta \theta_y^n \text{ tif } \phi_x^n = \psi_x^n + \delta \theta_x^n \quad \phi_y^n = \psi_y^n + \delta \theta_y^n \quad \phi_z^n = \psi_z^n + \delta \theta_z^n \quad (15)$$

The remaining states are common to both and the gains can be used directly. The update increments from two alternating sources for the inertial system state residuals are formed in Box IIIh as follows

$$\Delta \hat{x}_i = K_i \theta' \quad i=1,2 \quad (16)$$

where K_i are the Kalman filter gains for the inertial system residuals and θ'_i are the observable difference for each alternating update.

The updating of the inertial system state residuals is done in Box IIIi using alternating update increments such that

$$\hat{x}_i^+ = \hat{x}_i^- - \Delta \hat{x}_i \quad i=1,2 \quad (17)$$

Since updating is done from two alternating sources the inertial system state residuals are propagated (Box IIIc) using the inertial system error model given in Figure 8 such that \tilde{X}_1 is propagated to \tilde{X}_2 and \tilde{X}_2 is propagated to \tilde{X}_1 .

Thus far in the simulation process we have achieved in obtaining the missile navigation error responses under Kalman filter error control due to each statistically independent error source. At this point it is instructive to discuss the nature of these statistically independent error sources and their implications in the simulation process. Each error source can be classified as either a random systematic error or a random time series error. A random systematic error is defined to be one that is randomly selected at the initial time and maintained constant throughout the entire propagation period. A random time series error, on the other hand, is random during the entire propagation period with only its probability distribution specified a priori. In what follows we envision that a Monte Carlo technique is employed. Alternately a correlation technique or a mixture of the two could be employed. The comments relative to data handling in the sequel can easily be translated into the two alternate techniques and will hereafter not be belabored further. The efficacy of the various techniques is no concern herein. For the Monte Carlo technique an error source is selected and K independent samples of it are propagated through the inertial system error model, storing all the signed responses for each sample (i.e., K Monte Carlo trials). The process is then repeated for each statistically independent error source. This laborious process can be considerably shortened for those errors classified as random systematic errors by taking advantage of the superposition principle of linear systems. Because these errors are (by definition) constant throughout the entire propagation period and the error model linear, it can be shown that the root mean square (RMS) response of the system is the system's response due to the RMS value of the error source⁽³⁾. Thus the propagation of K independent samples of each of these error sources is replaced by a single propagation of its RMS value. Note that this single propagation will result in a signed RMS response. The same is not true for those errors classified as random time series errors, since in these cases the errors vary randomly as a function of time. In the actual simulation the following errors were treated as random systematic bias errors: a) 3 inertial system initial condition errors, b) 48 inertial instrument errors, c) 2 JTIDS user clock initial condition errors, d) 1 JTIDS transmitter clock bias error, e) 6 transmitter position bias errors. The following errors were modelled as random time series errors: a) JTIDS user clock bias rate, b) JTIDS user clock drift rate, c) JTIDS time of arrival flicker noise.

For both types of error sources the responses stored (i.e., the RMS response for a random systematic error and the K responses of K Monte Carlo trials of a random time series error) are signed responses. This is important since the pointing angle error equations that utilize these responses require that the error responses retain their cross correlations. This is because of the fact that the various terms in the pointing angle error equations are such that they either add constructively or destructively depending on the sign of the missile navigation error responses. Thus maintaining the relative signs and magnitude of the responses is paramount.

Another advantage of sensitivity simulation is that different error budgets can be easily accommodated by simply scaling the RMS error responses. The response is scaled the same amount as the ratio of the new RMS error value to the unit normalized error value used in the simulation. In the case of random systematic errors since the RMS response is a signed response the scaling can be done at the RMS level. However, in the case of random time series errors since K different Monte Carlo trials yielded K different responses and since RMSing these K responses loses the sign of the responses the scaling has to be done to the signed responses of each of the K Monte Carlo trials. For computational purposes it is convenient to treat each of the scaled signed responses (i.e., the scaled signed RMS responses of the random systematic errors and the scaled signed K responses of each of the random time series errors) equally in the ensuing Root-Sum-Square (RSS)ing process. The scaled K responses of the K Monte Carlo trials for the same random time series error source should be further scaled by $1/\sqrt{K}$ so that these responses have the same weighting as the scaled signed RMS error responses of the random systematic errors.

Pursuant to the objective that the pointing angle errors are evaluated at different times of the trajectory a 'snapshot' of all the scaled signed responses are stored for use later by the pointing angle error equations. The process of scaling the missile navigation error responses and snapshot storing them at specific times in the trajectory is the fourth step in the simulation process as shown in Box IV in Figure 5.

The process of obtaining the total pointing angle error at specific times in the trajectory is the next and last step in the simulation process as shown in Box V in Figure 5. This objective is achieved by first obtaining the pointing angle errors' sensitivities to each statistically independent error source and then RSSing to obtain the total pointing angle error. For each statistically independent error source the pointing angle error sensitivities in the missile seeker coordinates are given by⁽²⁾

$$\eta_y^s = \frac{(\delta M_{nx}^b - \delta T_{nx}^b)}{|R_T|} s\theta_T c\psi_T + \frac{(\delta M_{ny}^b - \delta T_{ny}^b)}{|R_T|} s\theta_T s\psi_T + \frac{(\delta T_{nz}^b - \delta T_{nz}^b)}{|R_T|} c\theta_T - \phi_x^b s\psi_T + \phi_y^b c\psi_T \quad (18)$$

$$\eta_z^s = \frac{(\delta T_{ny}^b - \delta M_{ny}^b)}{|R_T|} c\psi_T - \frac{(\delta T_{nx}^b - \delta M_{nx}^b)}{|R_T|} s\psi_T + \phi_x^b s\theta_T c\psi_T + \phi_y^b s\theta_T s\psi_T + \phi_z^b c\theta_T \quad (19)$$

To obtain the missile navigation position and attitude errors the scaled and stored responses (i.e., scaled RMS signed response for each random systematic error and $(1/\sqrt{K})$ scaled signed responses for K Monte Carlo trials of each random time series error) of each statistically independent error source are transformed as follows

$$\delta M_{nx}^n = a\delta\theta_y^n, \delta M_{ny}^n = -a\delta\theta_x^n, \delta M_{nz}^n = \delta h^n, \phi_x^n = \psi_x^n + \delta\theta_x^n, \phi_y^n = \psi_y^n + \delta\theta_y^n, \phi_z^n = \psi_z^n + \delta\theta_z^n \quad (20)$$

As mentioned previously target location errors were assumed to zero and hence

$$\delta T_{rx}^b = \delta T_{ny}^b = \delta T_{nz}^b = 0 \quad (21)$$

The pointing angle errors given by (18) and (19) require missile navigation errors in body coordinates, hence

$$\begin{bmatrix} \delta M_{nx}^b \\ \delta M_{ny}^b \\ \delta M_{nz}^b \end{bmatrix} = C_n^b \begin{bmatrix} \delta M_{nx}^n \\ \delta M_{ny}^n \\ \delta M_{nz}^n \end{bmatrix} \quad \text{and} \quad \begin{bmatrix} \phi_x^b \\ \phi_y^b \\ \phi_z^b \end{bmatrix} = C_n^b \begin{bmatrix} \phi_x^n \\ \phi_y^n \\ \phi_z^n \end{bmatrix} \quad (22)$$

For any particular time and any missile-to-target range ($|R_T|$) and aspect angles (θ_T, ψ_T) (18) and (19) are used to obtain the pointing angle error sensitivities for any statistically independent error source. For the random systematic errors the pointing angle error RMS sensitivities for n_y^s and n_z^s are obtained by simply using the signed RMS response (transformed to the missile body coordinate system) in (18) and (19). For the random time series errors it is necessary to evaluate (18) and (19) for each of the K independent samples and then RMS the results to obtain an RMS value for n_y^s and n_z^s .

To obtain the pointing angle error due to all error sources (i.e., the total error) the previously computed RMS components are RSSed. The final result is two RMS components of the total pointing angle error $n_{y\text{rms}}^s$ and $n_{z\text{rms}}^s$.

These two components can be converted into a single measure of error via

$$n_{\text{cep}} = 0.589 (n_{y\text{rms}}^s + n_{z\text{rms}}^s) \quad (23)$$

n_{cep} (circular error probable, CEP) is interpreted as the radius of a circle centered on the true pointing vector axis in which the target will be found 50 percent of the time^{(8), (9)}. Alternately one could use

$$n_{99} = 1.52 (n_{y\text{rms}}^s + n_{z\text{rms}}^s) \quad (24)$$

which represents the radius of the 99 percentile circle, n_{cep} and n_{99} given by (23) and (24) are simply accepted procedures for specifying the 0.5 and 0.99 probabilities of target acquisition. It should be mentioned that (23) and (24) are strictly correct only if n_y^s and n_z^s are unbiased, uncorrelated Gaussian processes with equal standard deviation⁽⁸⁾.

PERFORMANCE RESULTS

This section gives the error values used in the simulation and the results obtained. The scope of this section includes the following topics: Mission Scenario and Missile Trajectory, Shipboard Alignment of Missile Navigator, Inertial Instrument Errors, JTIDS Updating and Seeker Pointing Angle Errors.

A representative surface-to-air missile trajectory was simulated. A picture of the mission scenario and the missile trajectory is shown in Figure 10. The nominal trajectory simulated considered an airborne target, which could be a jammer aircraft, missile carrying aircraft, bomber or any other airborne target at the selected altitude. A top view of the relative positions of the different elements in the JTIDS network is shown in Figure 11. The two AEW aircraft were assumed to be stationary due to the fact that the average speed of the AEW aircraft were negligible compared to that of the missile.

Alignment of the missile navigator prior to launching greatly influences navigation performance of the missile. Different techniques of alignment give different alignment accuracies. Different initial alignment accuracies yield different position error at acquisition time which result in different seeker pointing angle errors during target acquisition. Navigation system performance of the missile as a function of alignment accuracy and time required in alignment is used to trade off various alignment techniques.

Alignment of the missile navigator prior to launch involves a reference navigator. In addition to other error sources, location of the reference navigator relative to the missile navigator determines whether ship flexure errors will influence the residual alignment error. Reaction time necessary for achieving the required alignment accuracy is another important factor for choosing the shipboard alignment technique.

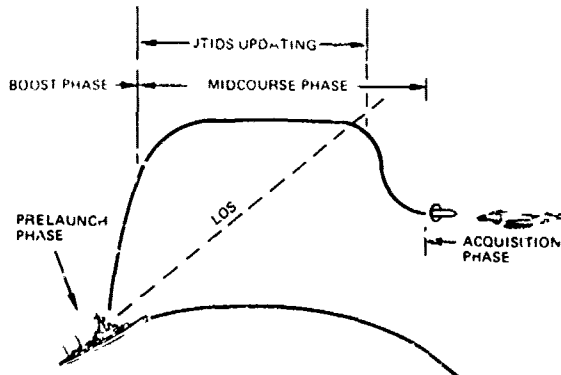


Figure 10. Mission Scenario and Missile Trajectory

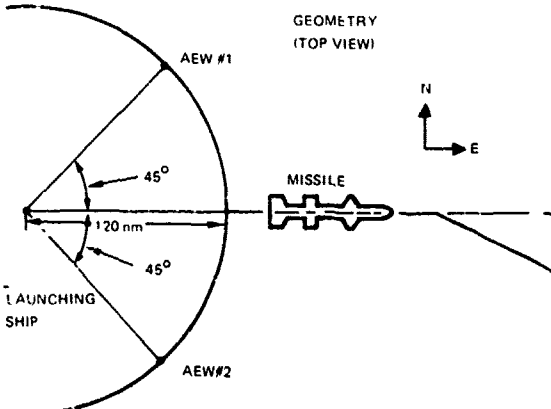


Figure 11. Relative Geometry of JTIDS Net Members

Three different techniques of inertial system shipboard alignment were considered: Remote Source Initialization, Local Source Initialization, and Optimal Calibration/Alignment. Alignment accuracies of these techniques were assumed to be 10, 1 and 0.1 (level), 1.5 (azimuth) in mils respectively.

Inertial instrument errors are the major contributors to the missile's navigation system error. Missile system navigation error (position, velocity, attitude) sensitivity was obtained for each instrument error source. Low to high quality inertial instruments were considered in the study. Gyros with $1^\circ/\text{hr}$ drift and accelerometers with $500 \mu\text{g}$ bias were considered low quality whereas $0.1^\circ/\text{hr}$ drift and $100 \mu\text{g}$ bias referred to high quality gyros and accelerometer respectively.

Missile system navigation error was investigated as a function of JTIDS relative range updating. The updating region with respect to the missile trajectory is shown in Figure 9 with the first update from the AEW aircraft #1 at the beginning of the region. This update is at the end of the boost phase when the missile has completed pitchover maneuver and begins level flight. The last update is from AEW aircraft #2 at the end of the updating region. This update is after the missile goes past the ship line-of-sight but before the missile begins its dive maneuver. The updating scheme is shown in Figure 12 where the update interval from each aircraft is 12 seconds and the update interval between the two aircraft is 6 seconds. This resulted in an update every 6 seconds alternating between the two AEW aircraft, with a total of 58 updates, 29 from each aircraft. The JTIDS error values used in the simulation were as follows:

$$\nabla_b = 10,000.00 \text{ ft (bias)}, \quad \nabla_{\dot{b}} = 10 \text{ ft/sec (bias)}, \quad \xi_{\dot{b}} = 1 \text{ ft/sec } \sqrt{\text{Hz}} \text{ (white noise)}$$

$$\xi_r = 0.1 \text{ ft/sec}^2 \sqrt{\text{Hz}} \text{ (white noise)}, \quad \xi_{\text{TOA}} = 10 \text{ ft (white noise)}, \quad b_t = 70 \text{ ft (bias)}, \quad \delta x_i, \delta y_i, \delta z_i = 70 \text{ ft (bias)}.$$

Missile seeker pointing angle errors for various midcourse guidance configurations were investigated. These errors were obtained for the acquisition time at the beginning of the acquisition phase as shown in Figure 10. Various seeker acquisition ranges were considered for a target head-on ($\theta_T = 0, \psi_T = 0$). The normalized seeker pointing angle error CEP values for the Remote Source Initialization, Local Source Initialization and Optimal Calibration/Alignment are given in Figures 13 through 15 respectively. These figures give normalized seeker pointing angle error CEP with normalized acquisition ranges parameterized over inertial instrument quality. Figures 16 and 17 give the normalized pointing angle error CEP with acquisition range for low and high quality inertial instruments parameterized over alignment technique. Pointing angle error sensitivities were obtained for each error source and the major error sources for the low and high quality inertial instruments are given in Figures 18 and 19. These figures give the total normalized RSS error due to each alignment technique as well as the normalized error due to each major error source. The numbers represent the particular error source as given in Table I. Error source numbers 49 through 50 represent initial tilt errors in x,y,z respectively.

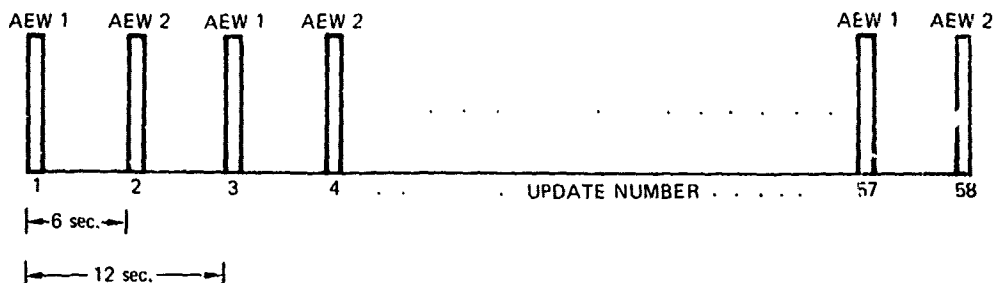


Figure 12. JTIDS Time-of-Arrival Updating Scheme

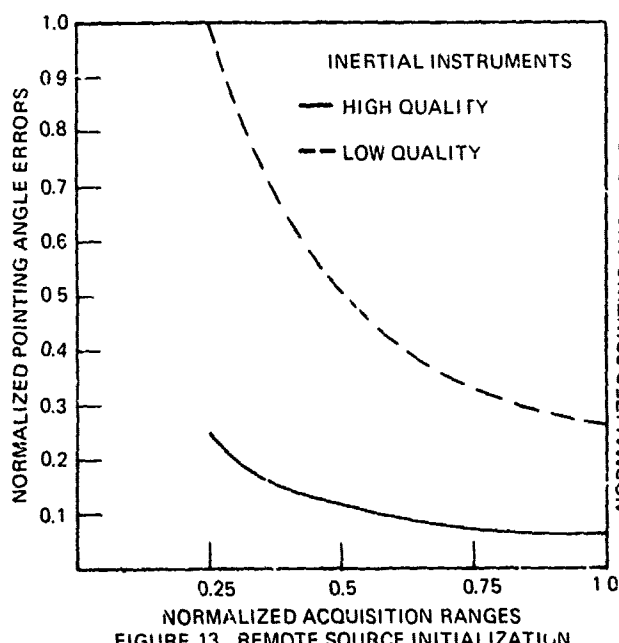


FIGURE 13. REMOTE SOURCE INITIALIZATION

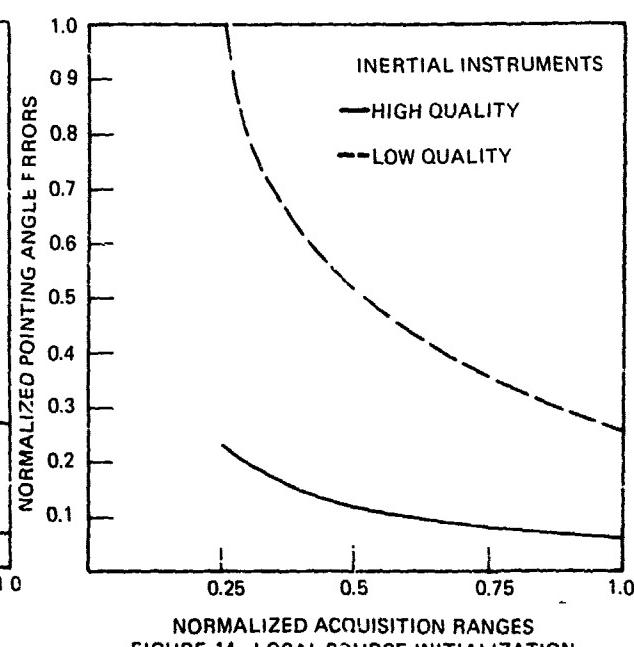


FIGURE 14. LOCAL SOURCE INITIALIZATION

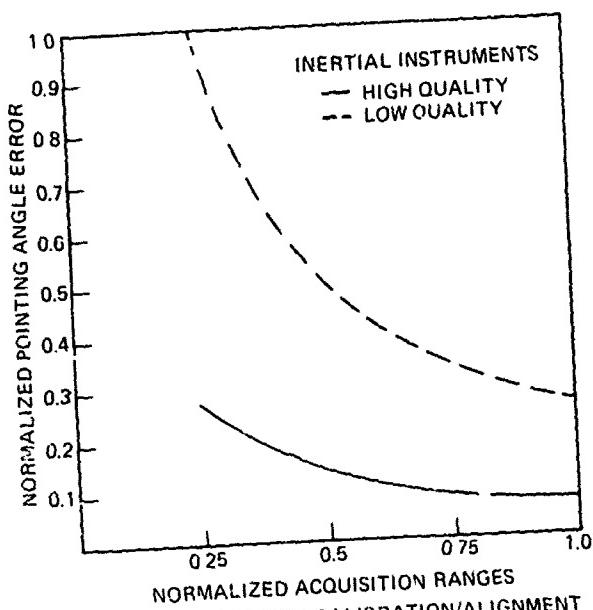


FIGURE 15. OPTIMAL CALIBRATION/ALIGNMENT

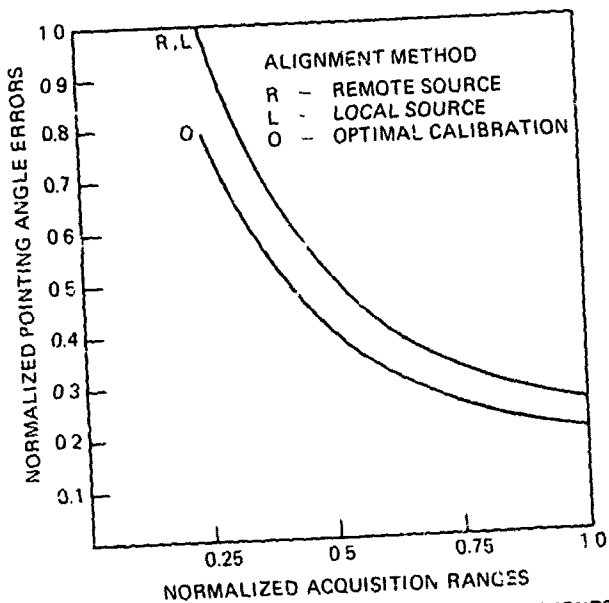


FIGURE 16. LOW QUALITY INERTIAL INSTRUMENTS

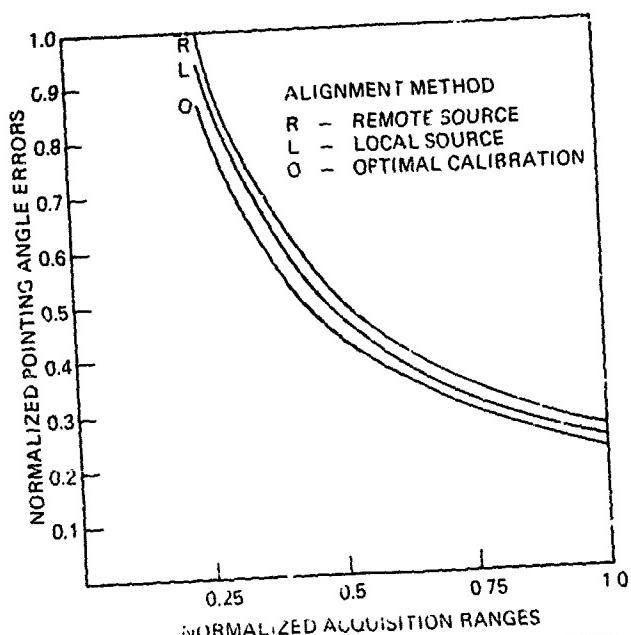


FIGURE 17. HIGH QUALITY INERTIAL INSTRUMENTS

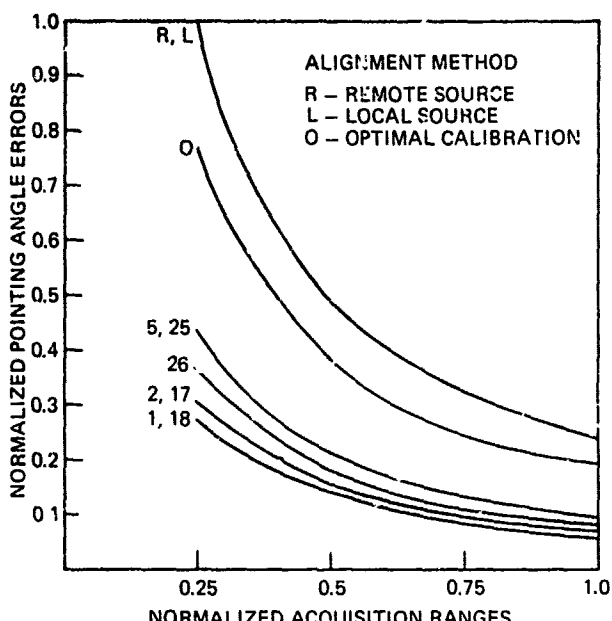


FIGURE 18. LOW QUALITY INERTIAL INSTRUMENTS

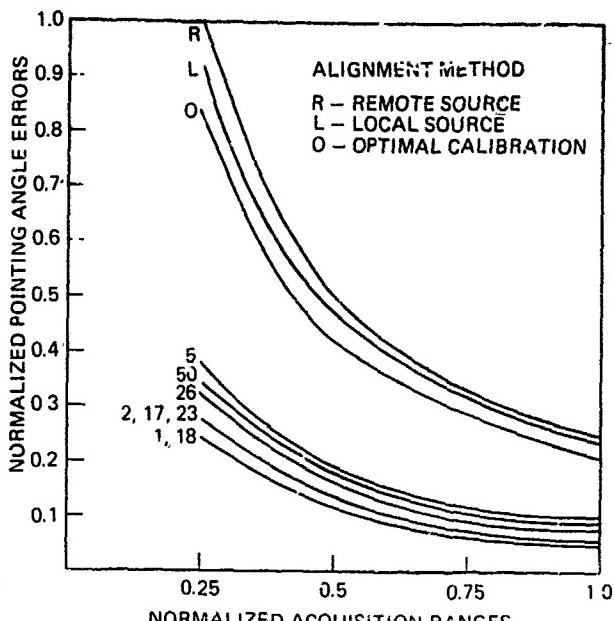


FIGURE 19 HIGH QUALITY INERTIAL INSTRUMENTS

SUMMARY

This paper investigates midcourse guidance performance of ship launched missiles against over-the-horizon airborne targets. The strapdown inertial guidance system of the missile is augmented by JTIDS passive ranging from two Airborne Early Warning aircraft situated between the launching ship and the target. The purpose of midcourse guidance is to place the missile in an acquisition "basket" sufficiently small to permit target sighting by the seeker within the constraints of its field of view and acquisition range. The terminal seeker pointing angle errors of the missile-to-target line-of-sight was selected as the performance index. Seeker pointing angle errors at acquisition time are functions of missile navigation position and attitude errors. Missile navigation errors were obtained as a function of different inertial instrument errors and JTIDS errors. Different shipboard alignment techniques and inertial instrument error budgets were included in the performance analysis. A typical relative range updating scheme in accordance with the timing structure of JTIDS was used in a Kalman filter to augment the strapdown inertial navigation system of the missile. The major error sources affecting midcourse guidance were identified and the results obtained give seeker pointing angle errors as a function of shipboard alignment technique, quality of the inertial instruments, seeker acquisition range and JTIDS relative range updating.

REFERENCES

1. K.R. Britting, *Inertial Navigation Systems Analysis*, Wiley-Interscience, New York, 1971.
2. J.T. Kouba and S.C. Bose, Terminal Seeker Poi.ting-Angle Error at Target Acquisition, *IEEE Transactions on Aerospace and Electronic Systems*, Vol. AES-16, No. 3, May 1980.
3. A. Gelb (ed.), *Applied Optimal Estimation*, MIT Press, Mass, 1974.
4. R.A. Dell-Imagine, JTIDS - An Overview of the System Design and Implementation, *Proceedings of the IEEE Position Location and Navigation Symposium*, San Diego, Calif., Nov. 1976
5. D.E. Neman, Seek Bus - A Time Division Multiple Access System, *Proceedings of the AIAA Digital Avionics Conference*, April 1975.
6. C.E. Ellingson and R.J. Kulpinski, Dissemination of System Time, *IEEE Transactions on Communication*, Vol. COM-21, No. 5, May 1973.
7. S.C. Bose, Real-Time Simulators for Augmented Inertial Navigation Systems, *Proceedings of the IEEE National Aerospace and Electronics Conference*, May 1978.
8. L.L. Rosen and D.L. Harmer, Inertial System Performance Evaluation, *Proceedings of Third Inertial Guidance Test Symposium*, October 1966.
9. G.R. Pitman, Jr., (ed), *Inertial Guidance*, Wiley, New York, 1962.

**INTEGRATION OF POSITIONING AND NAVIGATION
INTO THE C³I STRUCTURE**

by

R. Denaro

F. Karkalik

Systems Control, Inc. (Vt)

1801 Page Mill Road

Palo Alto, California 94304

and

Col. S.W. Gilbert, USAF

Office of the Assistant Secretary of Defense, C³I

Room 3E 1081

Pentagon, Washington, D.C. 20301

SUMMARY

The emergence of new worldwide, highly accurate positioning and navigation (pos/nav) systems has revolutionized some aspects of mission accomplishment, from surveillance to weapon delivery. Concurrently, much emphasis is placed on command, control, and communications (C³I) as the critical element in maintaining the capability to sustain combat operations or to deter such. Analysis of the process and functions of C³I, however, reveals that a great deal of synergism is being missed by not carefully integrating the developments in these two areas from planning through implementation. This paper investigates the role and contributions of pos/nav to the C³I process and mission effectiveness. A general methodology for integrated, objective-based planning is described, and an example mission is described in terms of the potential of deep pos/nav integration for benefiting the C³I process.

INTRODUCTION

Many current plans and developments for Command, Control, Communications and Intelligence (C³I) slight the role and potential of positioning and navigation (pos/nav). Mission planners and system designers quietly assume that pos/nav information is sufficient to meet mission requirements, assuming that the mission or system is mostly insensitive to such aspects of pos/nav information as quality, timeliness, reliability, format, etc. Careful analysis of the C³I process, however, reveals that most of its functions rely on pos/nav information, some extensively. Because of this dependence, many criticisms of C³I plans can be ultimately traced to inadequate consideration of the pos/nav contribution. Even more importantly, improvements in pos/nav capabilities and their exploitation in the C³I structure can reap significant rewards in C³I capability.

Specific examples of the infusion of positioning and navigation information into tactics, doctrine, and technology-based warfare abound. Requirements for all-weather, day/night operations, identification friend or foe, ingress to new geographic locations, forward area operations, precision weapon delivery, reduction of collateral damage, and economy of forces all demand high quality, continuously available pos/nav information and positive control of forces. Unfortunately, this common, underlying role of positioning and navigation is often ignored in the planning stages of C³I. This results in a forced fit of pos/nav systems into the C³I structure after their deployment, with some capabilities lost due to lack of deep integration and other capabilities traded-off due to economic inefficiency of the retrofit.

On a broader scale, there are higher level reasons for early integration and planning of C³I and pos/nav. Clearly one of the primary responses to increasing Soviet buildup in arms has been sophistication of free-world weapons, striving for increased kill power to offset the opposition's increased numbers [1]. But to truly field an effective weapon, one must consider the environment, personnel, procedures, training, response time, etc. In short, these sophisticated weapons demand a well-structured, effective C³I structure supported by pos/nav information to realize their potential effectiveness. The technology is available in communications, computing, ranging, timing, displays, sensors, and the use of ground, sea, air, and space resources. What we lack is applications resulting from proper emphasis in the weapons systems planning stages.

Other less obvious factors motivate even further consideration of the role of positioning and navigation information. Economic constraints require not only that we deploy efficient weapons, but also that we minimize duplication of function and proliferation of systems. Top-down design can meet this objective by ensuring that we follow a logical design process from objectives and requirements through implementation. This will maximize force capability to meet the relevant threats while maintaining efficiency in the numbers and types of systems necessary to do the job. Functional integration of systems also helps maintain economic bounds by increasing commonality and by possible functional synergism resulting from the integration. Functional integration also has payoffs where weight and volume constraints must be traded-off with capability.

Extending these concepts to an international arena, pos/nav integration into the C³I structure increases the potential for worldwide systems of the free-world countries to meet worldwide military aggression and economic pressures. Finally, in meeting these

challenges, effective C³I with quality pos/nav information vitalizes the capability for flexible response appropriate to the conflict, from terrorist activity to organized military maneuvers of a major aggressor force.

This paper defines the role of positioning and navigation information in the C³I structure and presents a candidate methodology to assure its integration in C³I design and mission analysis. The purpose of this paper is not to advocate disproportionate emphasis on navigation system developments, but more to stress the importance of the role of such systems. Pos/nav systems must be planned, programmed, budgeted and developed as integral parts of overall C³I structures in order for pos/nav information to adequately contribute to mission effectiveness.

Scope

The scope of this paper could consider all levels of conflict, from strategic to tactical, since positioning and navigation play an important role at any level. Weapon delivery system effectiveness, for example, is clearly a direct function of the pos/nav information and environment at hand. This is true for strategic cruise missiles or submarine-launched missiles as much as it is for tactical guided missiles or ground artillery. However, to limit the scope of the paper, the C³I environment addressed will be representative of a tactical level conflict. This is broad enough to dramatically show the relationships of interest and, through a composite of tactical groups, represents a theater level of operations which applies directly to the major concern of NATO.

Similarly, we will limit the scope of C³I system discussions to generic system level concepts, independent of any particular existing or developmental C³I system. About pos/nav systems we will be more specific since they are the primary focus of this paper. But for the overall C³I system, we will concentrate on generally applicable functional descriptions.

Let us assume our threat to be a highly developed, sophisticated enemy, since this is not only a worst case, but also a "most probable" case. Tactics, force levels, weapon capability and mix, and electronic offensive and defensive capability, can be assumed to match anticipated Soviet capabilities.

THE ROLE OF POS/NAV IN THE C³I STRUCTURE

The best illustration of the importance of positioning and navigation to C³I is an analysis of the functions and elements of C³I and their individual relationships to pos/nav. In order to arrive at a set of functions, it is necessary to first define C³I and its components in a generic sense.

The C³I Process

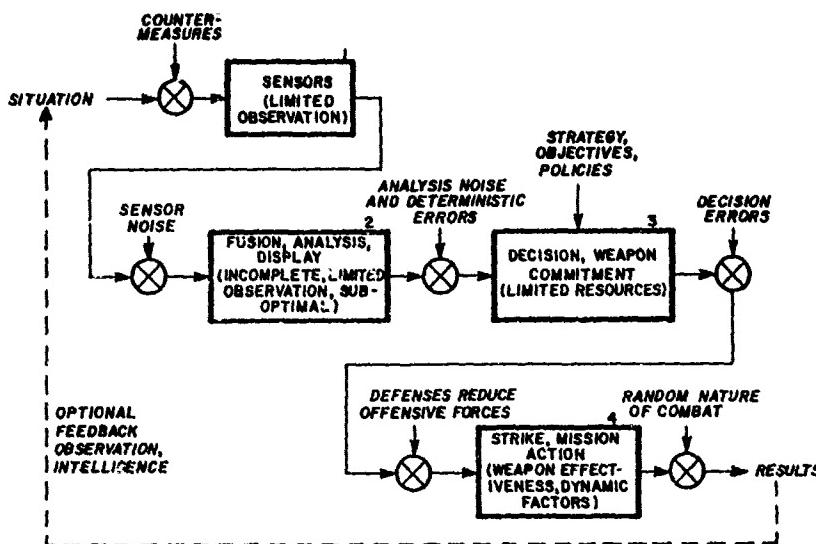
Command, Control, Communications, and Intelligence can be defined from several different perspectives. For example, a communications system designer would probably define C³I in terms of data rates and quantities, error rates, formats, time requirements, and the natural or hostile environment. A military commander would most likely define C³I in terms of command authority, resources, and mission objectives. Our purposes for this paper are best served by defining C³I in terms of the mission-oriented functions which compose it in the tactical environment. To analyze this aspect, let's look at the process of C³I.

Figure 1 describes the C³I process as it exists in the tactical environment [2]. The tactical situation is observed by the sensors shown in block 1, but enemy countermeasures may restrict or corrupt the information sensed. Countermeasures are diverse, from sophisticated electronic emissions to simple visual camouflage. Most sensors will be subject to noise before transmission to the fusion center in block 2.

This function aggregates the sensor information, including pos/nav information, and by necessity includes selective processing, analysis, and condensing. Fusion, analysis, and display are suboptimal, so the condensing process will inevitably discard or lose valuable information. In addition, analysis adds random and deterministic errors, the latter due to errors in the analysis procedures or techniques. Sources of these errors may range from inaccurate computer algorithms to erroneous operator interpretation of an information display.

Block 3 introduces the "commander," who decides on the course of action to be taken based on the presented information, and who commits weapons to meet the threat. The commander has limited resources and must act within the constraints and guidelines of objectives governing previous decisions, battle strategy, and higher-echelon orders including rules of engagement. Even within these constraints, decision errors may result. Before the weapons reach their offensive or defensive target, enemy defenses may attrit a portion of the force.

The strike is shown in block 4. Success is subject to the weapon or system effectiveness and also is subject to the dynamic nature of the situation. Time delays accumulate between sensing of the situation in block 1 and weapon strike in block 4. If the situation has changed sufficiently since it was first observed, the weapon and mission selection may be based on old information and thus the strike may be ineffective or inappro-

Figure 1. The C³I ProcessOperating Definition of C³I

Command and Control is defined in the U.S. Joint Chiefs of Staff Publication Number 1 as: "The exercise of authority and direction by a properly designated commander over assigned forces in the accomplishment of his mission. Command and Control functions are performed through an arrangement of personnel, equipment, communications, facilities, and procedures which are employed by a commander in planning, directing, coordinating and controlling forces and operations in the accomplishment of his mission" [3]. Some describe the "C³ process" as a composite of equipment, skills and techniques which, while not an instrument of combat, is capable of performing the clearly defined function of enabling a commander to exercise continuous control of his forces and weapons by providing him with the information necessary for decisions and the means of disseminating them. Others specifically include exploitation of intelligence data as an integral part of C³ since this information is a critical input to decision making at all levels from the highest commanders to military units in the field [2].

Note the distinction, which is easily and often overlooked, between "system" and "process." The objectives of this paper are best served by thinking in terms of "process" since this is a more generally applicable concept including input information and output mission results. Let us define the "process of C³I" to be:

"The sensing of an operational situation; fusion, analysis, and display of such information to authority; the decision to act and commitment of mission resources by that authority; and the ensuing strike or mission action, with optional feedback of the results of the action."

Dr. Gerald P. Dinneen, Assistant Secretary of Defense for C³I, recently defined the basic elements of the command and control system, whether strategic, theater or tactical, as [4]:

- (1) sensor subsystems which gather information about the location, movement, and activities of enemy forces;
- (2) navigation subsystems which inform our forces of their own location;
- (3) command or fusion centers which assemble, integrate and display enemy and friendly force activities to decision makers who then assess the threat and command the appropriate response; and
- (4) communications links between the sensors and the command centers, between the command centers and the forces, to permit the transmission of information and commands.

Note Dr. Dinneen's references to location of enemy and friendly forces as part of the elements of C³I.

To explore the sensitivity of C³I to pos/nav information, let us assume that the process of C³I can be partitioned into the functions shown in Table 1. These functions follow from various discussions of C³I such as that of Dr. Dinneen. An understanding of the role of positioning and navigation in the C³I structure can be achieved by examining the interdependence of the C³I functions. This examination and definitions of the functions are presented in the next section.

priate. Added to this is the random nature of combat, which can either detract from or add to the success of the mission. Results of the strike may feed back to the beginning of this process through battle damage assessment, intelligence, etc.

The functions of command and control take place primarily within the fusion and decision blocks, but the more encompassing process of C³I is strongly dependent on the input sensors and information as well as the output (strike) weapon resources available and their mission success.

Table 1. Functions of C³I

Surveillance	Positioning and Navigation	Mission Support
Reconnaissance	Electronic Warfare	Identification
Targeting	Data Processing and Analysis	Communications

Contribution of Positioning and Navigation to C³I

One way to illustrate the contribution of pos/nav to C³I is to look at its contribution to each of the C³I functions. Let us look at some definitions of each function and identify specific examples of pos/nav contributions. Most of these definitions are based on combined DOD/NATO official definitions [3].

Surveillance

The systematic observation of aerospace, surface, or subsurface areas, places, persons, or things by visual, aural, electronic, photographic, or other means.

In other terms, surveillance is the viewing or observing, in either real-time or on a post mission basis, of the situation and its dynamics. The area of interest includes the engagement area or potential engagement area as well as any other enemy activities or sites directly or indirectly supporting the engagement. Engagement area surveillance includes observing friendly as well as enemy forces and also includes observing the environment. Generally, surveillance reports contain positioning information on forces, sites, terrain, and obstacles. Also positioning information is needed to determine direction and speed of movement. The positioning information is based on the estimated position of the observer or sensor which may propagate to further errors in position due to systematic or random errors, geometry, or grid transformation.

Reconnaissance

A mission undertaken to obtain, by visual observation or other detection methods, information about the activities and resources of an enemy or potential enemy; or to secure data concerning the meteorological, hydrographic, or geographic characteristics of a particular area.

Reconnaissance focuses on a particular area or activity and is therefore more specific than surveillance. Surveillance information may often prompt a reconnaissance mission in order to more precisely identify and locate targets. The greater precision places a greater demand on the quality of positioning information needed to support the reconnaissance function.

Targeting

The targeting function encompasses several subfunctions that are very dependent on pos/nav information: detection, identification, selection and location.

Target detection involves sensor reaction to a stimulus, regardless of the eventual identity of the object or action against it. For example, a detected target may turn out to be a decoy, non-hostile object, false return, or friendly object as well as a bona fide enemy target to be destroyed. Pos/nav information can aid this task by pre-selecting areas of search or restricting sensor returns to those consistent with the known locations or dynamics of the desired targets.

Target identification is the positive determination that a detected target is in fact an enemy target. This may require refining sensor information, redundant sensing, or pure judgement. Much refined position information or target dynamics sensing, along with a history of these parameters (has the suspected stationary target moved?) can facilitate this subfunction as well.

Target selection is the subjective task of target prioritization and allocation of available resources to the identified target list. In the case of air attack, for example, target velocity and distance from its objective may be a primary factor in the selection process.

Target location permeates the previous three functions as noted, but is further important as a fourth aspect of targeting as the means for getting the weapon on target. This may be gross location, in which case the weapon or weapon system uses an active sensor after arriving at the target area, or it may be a precise location for a preprogrammed coordinate bombing mission or guided weapon.

Identification

The process of determining the friendly or hostile character, and possibly more detailed characteristics, of a contact. Identification, friend, foe, or neutral (IFFN) is a common means for the higher-level identification function. Target identification, defined earlier, may involve the determination of specific characteristics of the contact. The whole subject of theater identification can be aided by application of positive control where there is a continuous record and surveillance of the position and movements of all forces, friendly or hostile, in the area of interest. Such control is one of the most useful inputs to the commander in conducting military operations, and relies heavily on pos/nav and communications.

Communications

The conveying of information of any kind from one person, device, or place to another. The importance of communications in battle has been well known since the origin of warfare, and technology's contributions to warfare communications have been profound over the years. Some of the current techniques for insuring availability and capacity of the communications link in a hostile environment are so sophisticated that pos/nav may even have a contribution here. In essence, accurate position and velocity information allow greater control of the communications function by precisely directing signals to the intended receiver and ensuring that he and only he receives them.

Positioning and Navigation

Positioning is often defined as the process of determining, at a particular time, the physical location of a vehicle, object, person, or site. Navigation involves the directing of vehicle motion from one place to another. It makes use of positioning information at the beginning, continuously along the path, and position of destination. Navigation may be performed under time, path, or dynamics constraints [5].

In this paper we have loosely interpreted the combination of positioning and navigation, or pos/nav, to include velocity and acceleration determination as well. These parameters may be determined for one's own vehicle, for another friendly vehicle, or for an enemy vehicle. Remote positioning may be used to determine the precise location of an enemy location. Finally, note that position information can only be expressed relative to some given location, such as a starting point, another vehicle, or a grid origin.

Electronic Warfare

Military use of electronics involving actions taken to prevent or reduce an enemy's effective use of radiated electromagnetic energy and actions taken to insure effective friendly use of radiated electromagnetic energy. Electronic warfare includes support measures, countermeasures (ECM), and counter-countermeasures (ECCM).

Support measures provide the search, interception, location, and identification of enemy radiations. This information is an input to the process of ECM or ECCM, possibly leading to targeting and tactical strike. As with the targeting and identification functions, pos/nav information is very valuable in locating the source of enemy emissions. The effectiveness of avoidance, ECM, or strike greatly depend on the quality of the pos/nav information.

Countermeasures, jamming and deception, are actions taken to prevent or reduce the enemy's use of radiated electromagnetic energy. Enemy position information allows precise pointing of the transmitter which can then allow lower transmitted power levels.

ECCM are actions taken to insure friendly effective use of radiated electromagnetic energy despite enemy efforts to deny or corrupt such. Pos/nav information is essential in knowing both friendly transmitter/receiver location and enemy transmitter location. In addition, sophisticated communication codes and code tracking schemes can make use of position and velocity to increase jamming or deception immunity.

Data Processing and Analysis

The command support functions which encompass the processing, display, analysis, classification, evaluation, and storing of C³I data and information. The more sophisticated approaches which include advanced algorithms for sensor data correlation and resource allocation are referred to as fusion centers. These functions are performed by analysts and commanders with the aid of interactive computer/display systems. Although pos/nav information does not directly impact this function, data processing and evaluation functions should be considered when designing C³I and pos/nav systems. For example, data processing and display are facilitated if all sensors report pos/nav information in a common reference frame and common units.

Command and Control

This function was discussed and defined in the earlier section on the C³I process. Pos/nav information greatly impacts this function. Indirectly, most of the other functions which serve command and control are dependent on pos/nav information for maximum effectiveness as has been described. Directly, the better position, location, and dynamics information the commander has at his disposal, the more control and feedback he has on the progress of the engagement.

Mission Support

Those subfunctions which are not part of the C³I system, but are required in order to cause the C³I functions to be realized. Included in this category are planning, RDT&E, training, and logistics. Pos/nav information may influence the success of any number of support tasks, particularly in their need for navigation.

Thus a strong case exists for the importance of the role of pos/nav information in the C³I process. A function-by-function analysis shows that pos/nav factors are inseparable from the functions that determine mission success. In fact, what these definitions imply are strong interrelationships within the functions of C³I, not only with the pos/nav function, but between all functions. Figure 2 illustrates these interrelationships within

the C³I structure. All functional elements except communications, data processing and display, and mission support are dependent to some degree on positioning. A case can even be made for a subset of communications. Radio communications using a narrow beam to meet security and anti-jam requirements is clearly dependent upon positioning information. Of course, the dependence of pos/nav on the other functions is not to be overlooked. Loss of communication, for example, may mean loss of pos/nav information carried on those channels.

		INDEPENDENT FUNCTION										
		SURVEILLANCE	RECONNAISSANCE	TARGETING	IDENTIFICATION	COMMUNICATION	POSITIONING AND NAVIGATION	ELECTRONIC WARFARE	DATA PROCESSING AND ANALYSIS	COMMAND	CONTROL	MISSION SUPPORT
DEPENDENT FUNCTION	SURVEILLANCE	O			X	X		X	X	X	X	X
SURVEILLANCE	O				X	X		X	X	X	X	X
RECONNAISSANCE	O			X	X			X	X	X	X	X
TARGETING	X	X	O	X	X	X		X	X	X	X	X
IDENTIFICATION				O	X	X		X				X
COMMUNICATIONS					O			X				X
POSITIONING AND NAVIGATION						O						X
ELECTRONIC WARFARE						X	X	O	X	X	X	X
DATA PROCESSING AND ANALYSIS								O				X
COMMAND	X	X	X	X	X	X	X	X	X	O		X
CONTROL	X	X	X	X	X	X	X	X	X	O	X	
MISSION SUPPORT												O

Figure 2. C³I Functional Interrelationships

information as an input, but greater confidence in highly accurate friendly and enemy locations could speed the decision process in directing offensive or defensive actions and enhance the effectiveness of the commander's resources. The further use of position information about intelligence or mission assessment feedback may remove some of the uncertainty and lack of observability in the control function. Thus enhancement of pos/nav quality directly increases the success of several C³I functions, while greater application of high quality pos/nav information to other functions may similarly enhance their effectiveness.

Although an appreciation for the role of pos/nav information in the C³I process is critical, the important message is how to systematically exploit the benefits of pos/nav information in mission planning or system planning and development. The next section discusses one possibility for accomplishing this.

CONCEPT IMPLEMENTATION AND SYNTHESIS

The methodology chosen in this paper to implement pos/nav integration into the C³I structure is through the use of mission area analysis and functional area analysis. The cost of more effort devoted to planning and analysis is a bargain when compared with the costs of system development, acquisition, and deployment. This process starts by analyzing tactical objectives to derive overall requirements.

Roadmap of Requirements

Clearly if we knew the precise, mission by mission requirements for positioning or navigation information, we could perform the tradeoffs required to guide our developmental programs. But in many cases, we do not have a quantitative feel for how varying qualities of pos/nav information affect mission effectiveness. By pos/nav requirements here, we are referring to more than just accuracy; pos/nav characteristics also include coverage, availability, reliability, timeliness, format, compatibility, precision, etc. Only by analyzing mission objectives, in the threat environment, and in terms of their sensitivities to each of these pos/nav characteristics, can we fully understand our pos/nav requirements.

A first attempt at defining such requirements may be by use of the roadmap methodology simply illustrated in Figure 3. The method starts with general or specific objectives, considers them in the threat environment shown here by the Soviet tactics and capabilities, then progressively derives the resulting conclusions about requirements. For example, the objective of destroying enemy forces, combined with the enemy capability to employ sophisticated defenses and EW implies that one must use standoff weapons (to survive the sophisticated defenses and to perhaps avoid the effects of EW at weapon release, where it may be most critical). Similarly, the enemy numerical superiority, coupled with his probable tactic of using them in an overpowering single wave, when combined with the "destroy" objective, implies that one must destroy the enemy

Although this figure illustrates the broad dependence on pos/nav information, two additional aspects of this dependence underscore its role further. First, the degree of dependence on pos/nav by several functions is significant. Surveillance, reconnaissance, and targeting obviously rely heavily on pos/nav information, and the success of these functions is directly related to the quality of the pos/nav information. Second, mission effectiveness improvements can be dramatic with the application of high quality pos/nav information to all functions, including new applications to those other functions that currently depend only slightly on pos/nav. Positioning information used for communications beam steering and velocity information used for doppler estimation to counter jamming attempts are recent exploitations of pos/nav information for the ECM and communications functions. Command and control use pos/nav in-

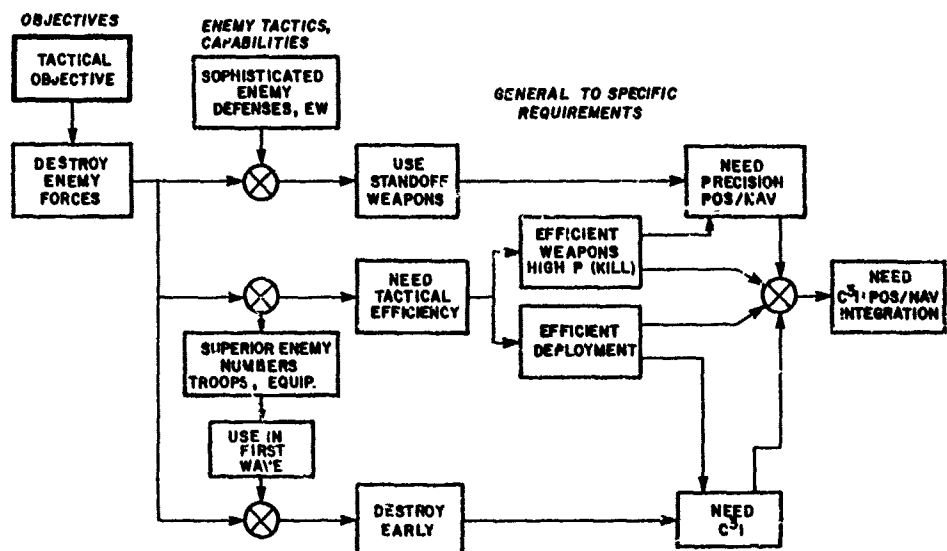


Figure 3. Roadmap of Requirements

And finally, in a technically, fiscally, and time constrained program environment, the only way to economically and efficiently provide all of these capabilities is through a concentrated effort to integrate C³I and pos/nav systems.

This example is not particularly creative in its content, but the real message is in the methodology. The three elements of objectives, environment, and requirements must be combined in an organized roadmap at all levels of force and program planning to best allocate limited resources.

Now let us generalize this methodology. Our "roadmap of requirements" can be broken into a two-phased planning process comprising mission area analysis and functional area analysis [7]. This top-down trade-off optimization process that starts with prioritizing missions and ends with system selection is a way to maximize total mission effectiveness return from each defense dollar spent.

Mission Area Analysis

Mission area analysis provides the "need" and identifies requirements for system development and selection activities. Figure 4 portrays the mission area analysis process with pos/nav planning. The first step is to define a complete set of mission areas, perhaps aggregated under major areas. The objective at this point is a total mission understanding, including objectives, the environment, the threat, and critical mission aspects so that the next step, prioritization, can be accomplished. Prioritization is an unfortunate necessity mandated by economic constraints. Programs funded or resources allocated must contribute to the most essential missions and those with the highest expected payoff. In addition, prioritization provides guidelines for applying new technological breakthroughs or for curtailing developments and deployments when budgets are cut.

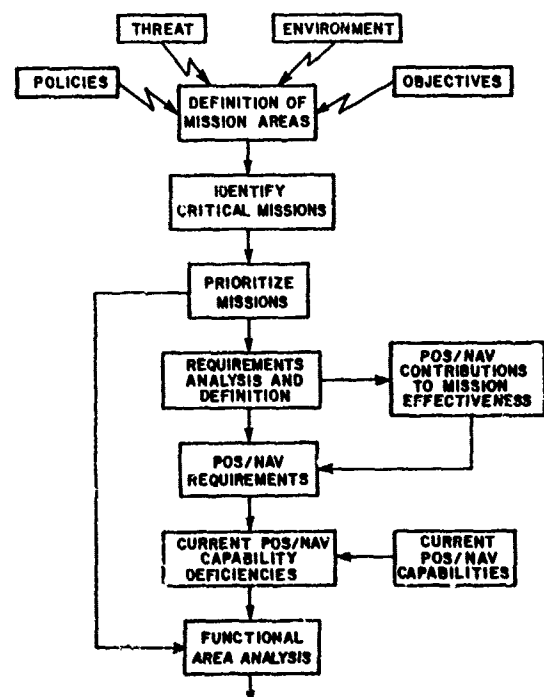


Figure 4. Pos/nav Planning in Mission Area Analysis

forces early (at least on the first wave) [6]. The use of standoff weapons requires precise pos/nav information due to standoff weapon release and guidance constraints. Early response to attack requires reliable sensing, rapid dissemination of information, and quick decisions. An efficient C³I structure is the only way to guarantee this.

At this point in the mission area analysis comes probably one of the most fundamental tasks, and yet one that has been dramatically lacking or incomplete in past analyses: requirements definition. Although mission requirements span all of the C³I functions, for the purposes of this paper we are interested in pos/nav requirements. In this regard, it is absolutely mandatory to quantify pos/nav requirements, possibly down to the mission segment level, to properly allocate developmental or existing pos/nav resources. Evidence that requirements definition may be incomplete is seen in the apparent lack of appreciation for how pos/nav contributes to the other C³I functions as discussed earlier. This implies that pos/nav requirements must not only be specified as discrete, fixed levels, but as continuous functions relating total mission effectiveness to varying quali-

ties of pos/nav information. These relationships exist not only for accuracy, but for other parameters as well, such as coverage, availability, reliability, etc. One cannot trade off mission effectiveness on the basis of pos/nav information alone, because other C³I functions are strongly related, but unless we can understand the contribution of pos/nav information in isolation, we cannot hope to study mission effectiveness as a function of all relevant C³I functions.

When pos/nav requirements have been defined, we can proceed to identify generic capabilities and shortfalls. The earlier mission prioritization points toward those shortfalls for which resolution will yield the greatest margin of return in mission effectiveness. And at this point, we are overlapping with functional area analysis.

Functional Area Analysis

The ultimate goal of functional area analysis is to select development programs to fund or to optimally reallocate existing resources. Figure 5 shows the functional area analysis process with pos/nav resources. For pos/nav systems, this implies correlation of current capabilities and emerging technology with present and predicted shortfalls with respect to pos/nav requirements. Note the future aspect of this process as well as current status review.

The commander needs to know his current capabilities associated with current requirements, so that work-arounds can be implemented to meet the current threat. But, perhaps more importantly, planners must know the future conflict, doctrine, and technological environment so that action is taken now which, after the usual time delays, can result in optimum mission effectiveness for any point in the future, as illustrated in Figure 6. Put another way, today's dollars will field tomorrow's systems, and in tomorrow's environment. One can reasonably question, for example, "will our developmental C³I (and pos/nav) systems be effective in the future Soviet EW and advanced weaponry environment?" More extensive use of pos/nav information for all C³I functions can add to capabilities and provide functional redundancy needed in current and future C³I environments.

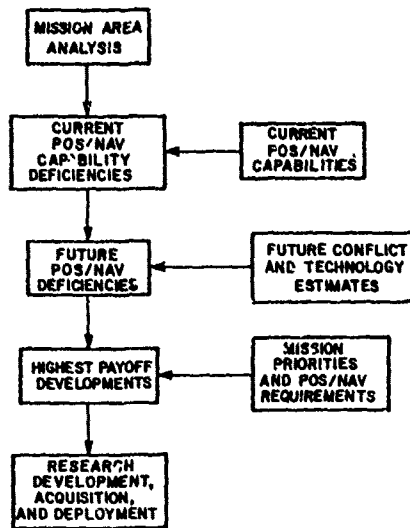


Figure 5. Pos/nav Development Strategies

Specific Pos/nav Benefits to Mission Effectiveness

Even though a thorough determination of pos/nav requirements and functional area correlation has not been accomplished, there are specific areas that have been analyzed. We will select from these few areas and describe some specific benefits, primarily to set up an example coordinate bombing mission discussed later.

The targeting mission can benefit dramatically from precise pos/nav information, whether phototargeting or by other means. In relation to the targeting function of the C³I process described earlier, the targeting mission concerns the target location sub-function.

Current phototargeting missions usually derive target coordinates from photos by measuring the offset from a known position reference point on one of the photos. The reference point is either a previously calculated position landmark or the known position of some natural or cultural feature. However, if the photoreconnaissance aircraft has available precise position and attitude information, target coordinates can be determined from the photos without a ground reference point. In particular, the position information provides the position of the camera at the time of the photograph, and the attitude information provides photo orientation with respect to the local horizontal. Two target photos with accompanying position and attitude data are sufficient to compute target position (the second set of data are used to resolve photo scaling) [8].

Alternatively, reconnaissance aircraft could employ some ranging technique, such as laser ranging, to measure range to the target. Knowledge of aircraft position at three times with three ranges are sufficient to determine target position (assuming singular solutions are avoided). This method could use onboard computation to compute target coordinates immediately, which could then be transmitted on a secure data link to an airborne warning and control aircraft or directly to attack aircraft. This "near real-time" capability has interesting potential for target objectives that can move or be evacuated between the time a photoreconnaissance takes place and the attack aircraft arrives on site. It also has advantages for the Navstar Global Positioning System (GPS) in that slowly varying errors inherent in the solution may be common to both the reconnaissance and at-

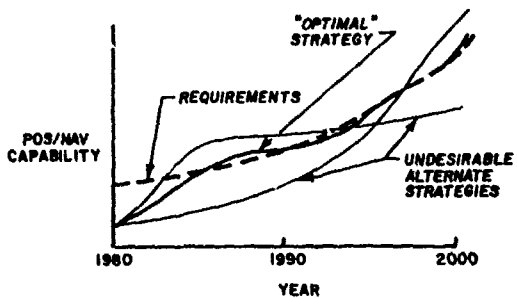


Figure 6.
Pos/nav
Development
Strategies.

tack aircraft, thus their relative errors are smaller yet.

With reasonable geometry of ranges the errors in target position location can be expected to be near the accuracy of the aircraft positioning system. For an aircraft equipped with the GPS, three-dimensional target coordinates should be obtainable to ± 25 meters [8].

Although not a mission in itself, threat avoidance is a critical phase of most missions over enemy-controlled territory toward the mission objective. A fully integrated C³I and pos/nav system provides the precision positioning and means of continuous information dissemination necessary to implement sophisticated onboard threat avoidance capability. Continuous surveillance and reconnaissance information is fed to an airborne warning and control (AWACS) aircraft and to a tactical control center. This information provides accurate position and, where appropriate, velocity of enemy forces. Surveillance radar provides real-time airborne threat tracking. C³I system communication links, along with aircraft self-contained sensors, update on-board battle situation CRT displays, providing the pilot with a reliable, up-to-date "picture" of the threat environment between his origin and destination. On-board computation then provides a path of greatest survivability within time, fuel, and maneuvering constraints. Continuous updating allows the pilot to adapt to changes or apply experience with which the computer is unfamiliar. From a total theater perspective, this capability increases attack force survivability and thus mission effectiveness. Increasing probability of target engagement increases overall probability of kill per sortie, which has a force multiplying effect when compared to the scenario without this threat avoidance capability. Also, threat avoidance is a means of countermeasures to thwart enemy attempts to deny use of radiowaves.

Finally, the third example of benefits from pos/nav is coordinate bombing itself, the final test of mission success in this case. Algorithms are available that very precisely predict the trajectory of unguided ordnance. With accurate target coordinates, and precise knowledge of position and velocity at weapon release, high precision blind weapon delivery is possible. Table 2 lists the typical input data to a complete bomb release computation algorithm.

Table 2. Bomb Release Algorithm Inputs	
Target 3-D position	Bomb position on rack
Aircraft 3-D position	Rack ejection velocity
Aircraft 3-D velocity	Bomb drag characteristics
Aircraft pitch, roll, yaw	Coriolis effect on trajectory
Aircraft pitch, roll, yaw rates	Bomb spin characteristics
Aircraft crab in wind	Ordnance release delays
Temperature and pressure	Ejection rack delays
Standard atmospheric density	Computation delays

Precision blind weapon delivery allows longer stand-off releases for greater crew survivability as well as all weather, day/night operation. The higher impact precision increases the probability of kill on the first

pass which also aids crew survivability. Also evident is the economic advantage of using inexpensive unguided weapons for accurate bombing needs. GPS simulation data published in an Agard Advisory Report earlier this year predicted CEPs of about 32 meters from straight and level delivery at 5000 feet, not including the contribution of target coordinate errors [9]. Statistical combination of this number with the random target coordinate errors should yield total one standard deviation miss distances of less than 50 meters.

Example Mission

It is possible to compile the above benefits into a simple example mission to show a dramatic effect on the C³I process defined earlier. Our example is a coordinate bombing mission, considering the activity from targeting through strike. The scenario illustrates the many roles of pos/nav information as discussed throughout this paper.

An enemy anti-aircraft battery has been identified by pilot reports as causing difficulty in an area of intense low-altitude offensive activities. Due to these activities, site avoidance is not possible, and the local commander decides that an air strike is appropriate. Surveillance information of the general area indicates the approximate location and feasibility of overflying the target for reconnaissance, but this site is sufficiently effective to make surprise an important contributor to survivability and mission effectiveness. In other words, the time delay involved with a photoreconnaissance run may endanger the strike aircraft by tipping off the enemy.

A GPS-equipped reconnaissance aircraft and strike aircraft are dispatched to the area. The local airborne warning and control aircraft provides local threat information to the flight and the status is displayed on cockpit CRTs. Figure 7 shows a typical display. Previously recorded information indicates the jamming frequency to use to defeat enemy radar along the way. This information is factored into the onboard computation of a minimum threat exposure flight path to the objective. The reconnaissance aircraft comes in first at a pre-selected altitude that minimizes threat from the battery itself while still enabling accurate laser ranging. Appropriate jamming prevents detection until just before the overflight. The scene is depicted in Figure 8.

The ranging data are collected. The target coordinates are computed immediately and data-linked to AWACS and the strike aircraft, now already on its bombing run. AWACS detects a diversion of enemy interceptor aircraft to the area, indicating that the battery

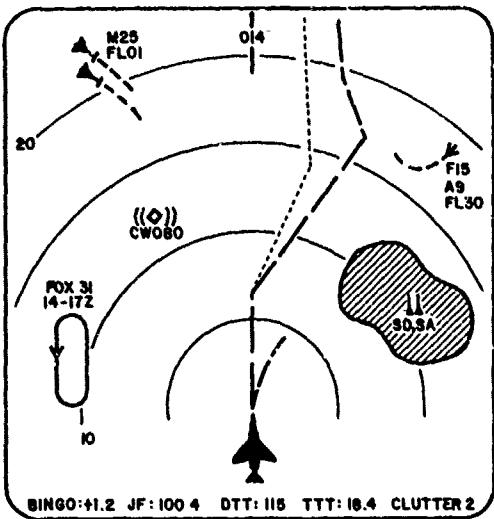


Figure 7. Typical Combat Situation Display

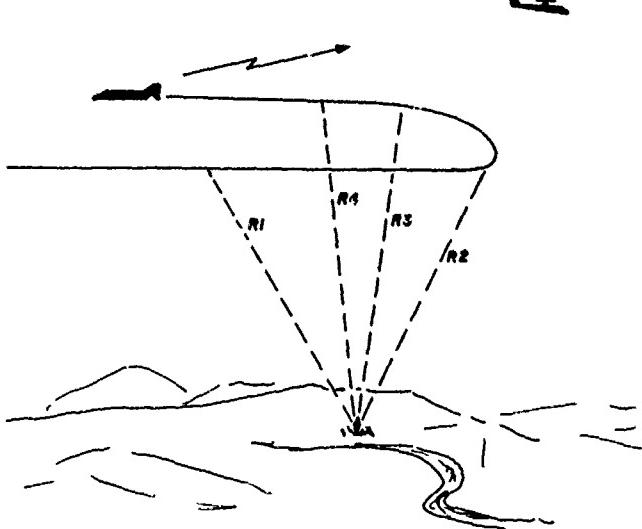


Figure 8. Target Reconnaissance Mission Scenario

personnel are aware of a potential attack. Their speed is such that there is time to complete the attack, and their maneuvers indicate that they are a type of aircraft not typically armed with highly effective, long range missiles. The attack aircraft feeds target coordinates to its weapon release algorithm and directional jammer. The directional jammer forms a narrow beam of increased power to defeat the battery radar at low altitude. Of course, if intelligence indicates that the battery can track jammer emissions, this technique is not used, and a lower altitude approach is made. In any case, low-drag Mark 80 series bombs are released from low altitude a reasonable distance from target as shown in Figure 9. The aircraft executes a hard turn to return to base. Updated threat information from AWACS necessitates a different path home to avoid approaching enemy interceptors.



Figure 9. Weapon Delivery Mission Scenario

Although this example may vary in the tactics and procedures used in a particular combat situation, it does illustrate the extensive use of pos/nav information in performing most of the functions of C³I identified earlier. It also shows a mission enhancement capability by the use of very accurate pos/nav information. The factors improved include kill effectiveness, survivability, EW, target detection, target identification, target location, threat avoidance, and command and control.

Equally important is the C³I process as it exists for this example. Consider again the C³I process presented

earlier, but now with better integration of pos/nav information. Notice how, in this example mission, the process is greatly streamlined, eliminating several sources of delays, errors, and enemy defensive actions. Of course, some elements such as weapon commitment were performed in a separate, earlier process. Obviously weapons were committed before all necessary target information was gathered. But the result is that we have reduced operational risk through real-time pos/nav information dissemination and display, and flexible crew response. We were not compelled to traverse the entire path of the original C³I process and did not suffer the accumulation of errors and time delays. Achievement of this change required, however, a great deal of interaction between the C³I system and the pos/nav system. Only deep integration of these systems will make such interaction feasible.

INITIATIVES

We have taken a high-level look at the process of C³I, its functional constituents, the broad dependence of these functions on pos/nav information, and a means for systematic planning of pos/nav developments through mission area analysis and functional area analysis. Our perspective has been a step back from the forest of black boxes and subsystems in an attempt to consider a total systems approach to C³I implementation. As Dr. Dinneen

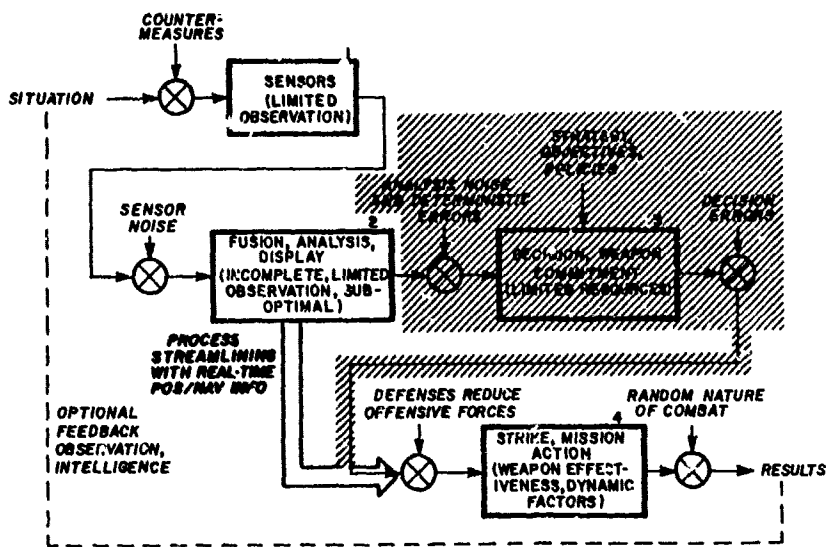


Figure 10. The C³I Process--Example Mission

initiatives. These are:

- (1) Quantify mission pos/nav requirements.
We cannot design or afford pos/nav systems without knowing our precise pos/nav needs.
- (2) Exploit pos/nav information in C³I functions.
The increase in benefits and new capabilities that will accrue justify the effort.
- (3) Maximize real-time dissemination and crew interaction.
Properly sensed pos/nav information must be available in real-time to units conducting combat missions, with appropriate attention to the crew environment through display design and on-board computation.
- (4) Employ new mission tactics now possible with improved pos/nav information.
Not only can we enhance our current mission effectiveness, but we must look for new missions or tactics that may now be possible with the use of the emerging highly accurate, worldwide positioning and navigation systems.

REFERENCES

1. Cameron, Juan, "Bill Perry Keeps the Pentagon's Barrels Loaded," Fortune Magazine, March 1980.
2. Leondes, Dr. Cornelius T., "Command and Control for Air Force, Army, and Naval Systems," Course Notes, July 1979.
3. "Dictionary of Military and Associated Terms," Joint Chiefs of Staff Publication No. 1, June 1979.
4. Dinneen, G. P., "A Systems Approach to C³I," Signal, Vol. 34, No. 5, February 1980.
5. "Joint Chiefs of Staff Master Navigation Plan," July 1980.
6. Donnelly, C. N., "Soviet Tactics for Overcoming NATO Anti-Tank Defense," International Defense Review, July 1979.
7. "Mission Area Analysis," U.S. Air Force Planning Guide, November 1978.
8. Navstar GPS Joint Program Office, "Major Field Test Objective Report on Photomapping/Phototargeting," May 7, 1979, DTIS No. AD-B047387.
9. "The Impact of Global Positioning System on Guidance and Controls System Design of Military Aircraft; Specific Application Study No. 1: Close Air Support," Agard Advisory Report No. 147, February 1980.

ACKNOWLEDGEMENTS

The authors wish to acknowledge the contributions of several members of the U.S. Department of Defense and staff of Systems Control, Inc. In particular, we are grateful for the advice and suggestions of Dr. C. T. Leondes of UCLA, and Messrs. W. Endter, H. Oelmann and Dr. T. Watt of SCI.

said in a recent address, "If we all strengthen our arguments by viewing command and control as a total system... I believe we can continue this trend toward successful acquisition of the modern command and control systems needed to get the most out of our military forces." And, as we point out in this paper, proper attention to the role of pos/nav capabilities and systems in the total C³I structure can reap benefits throughout the many dimensions of tactical mission effectiveness.

Possibly the best summary of the points made in this paper is through some proposed

REPORT DOCUMENTATION PAGE			
1. Recipient's Reference	2. Originator's Reference	3. Further Reference	4. Security Classification of Document
	AGARD-CP-298	ISBN 92-835-0287-6	UNCLASSIFIED
5. Originator	Advisory Group for Aerospace Research and Development North Atlantic Treaty Organization 7 rue Ancelle, 92200 Neuilly sur Seine, France		
6. Title	PRECISION POSITIONING AND INERTIAL GUIDANCE SENSORS. TECHNOLOGY AND OPERATIONAL ASPECTS		
7. Presented at	the Guidance and Control Panel Symposium held at Church House, Westminster, London, UK on 14-17 October 1980.		
8. Author(s)/Editor(s)	Various		9. Date March 1981
10. Author's/Editor's Address	Various		11. Pages 380
12. Distribution Statement	This document is distributed in accordance with AGARD policies and regulations, which are outlined on the Outside Back Covers of all AGARD publications.		
13. Keywords/Descriptors	Inertial components Filtering Fault tolerance Positioning		
14. Abstract	<p>The proceedings include papers presented at a symposium of the Guidance and Control Panel held at Church House, Westminster, London, UK – 14–17 October 1980.</p> <p>Twenty-six papers were presented on the following topics:</p> <ul style="list-style-type: none"> – Inertial sensors and systems technology – Positioning systems. Development and status – Evaluation methods and results – Filtering and estimate – Fault tolerance design and redundancy techniques – Systems requirements and applications. <p>Twenty-two papers are included in this volume, the other four are classified and appear in CP-298 Supplement, classified NATO-CONFIDENTIAL.</p>		

<p>AGARD Conference Proceedings No.298 Advisory Group for Aerospace Research and Development, NATO PRECISION POSITIONING AND INERTIAL GUIDANCE SENSORS. TECHNOLOGY & OPERATIONAL ASPECTS Published March 1981 380 pages</p> <p>The proceedings include papers presented at a symposium of the Guidance and Control Panel held at Church House, Westminster, London, UK on 14-17 October 1980.</p> <p>Twenty-six papers were presented on the following topics:</p> <p>P.T.O.</p>	<p>AGARD-CP-298 Inertial components Filtering Fault tolerance Positioning</p>	<p>AGARD Conference Proceedings No.298 Advisory Group for Aerospace Research and Development, NATC PRECISION POSITIONING AND INERTIAL GUIDANCE SENSORS. TECHNOLOGY & OPERATIONAL ASPECTS Published March 1981 380 pages</p> <p>The proceedings include papers presented at a symposium of the Guidance and Control Panel held at Church House, Westminster, London, UK on 14-17 October 1980.</p> <p>Twenty-six papers were presented on the following topics:</p> <p>P.T.O.</p>	<p>AGARD-CP-298 Inertial components Filtering Fault tolerance Positioning</p>
<p>AGARD Conference Proceedings No.298 Advisory Group for Aerospace Research and Development, NATO PRECISION POSITIONING AND INERTIAL GUIDANCE SENSORS. TECHNOLOGY & OPERATIONAL ASPECTS Published March 1981 380 pages</p> <p>The proceedings include papers presented at a symposium of the Guidance and Control Panel held at Church House, Westminster, London, UK on 14-17 October 1980.</p> <p>Twenty-six papers were presented on the following topics:</p> <p>P.T.O.</p>	<p>AGARD-CP-298 Inertial components Filtering Fault tolerance Positioning</p>	<p>AGARD Conference Proceedings No.298 Advisory Group for Aerospace Research and Development, NATO PRECISION POSITIONING AND INERTIAL GUIDANCE SENSORS. TECHNOLOGY & OPERATIONAL ASPECTS Published March 1981 380 pages</p> <p>The proceedings include papers presented at a symposium of the Guidance and Control Panel held at Church House, Westminster, London, UK on 14-17 October 1980.</p> <p>Twenty-six papers were presented on the following topics:</p> <p>P.T.O.</p>	<p>AGARD-CP-298 Inertial components Filtering Fault tolerance Positioning</p>

<ul style="list-style-type: none"> - Inertial sensors and systems technology - Positioning systems. Development and status - Evaluation methods and results - Filtering and estimate - Fault tolerance design and redundancy techniques - Systems requirements and applications. <p>Twenty-two papers are included in this volume, the other four are classified and appear in CP-298 Supplement, classified NATO-CONFIDENTIAL.</p>	<ul style="list-style-type: none"> - Inertial sensors and systems technology - Positioning systems. Development and status - Evaluation methods and results - Filtering and estimate - Fault tolerance design and redundancy techniques - Systems requirements and applications. <p>Twenty-two papers are included in this volume, the other four are classified and appear in CP-298 Supplement, classified NATO-CONFIDENTIAL.</p>
<p>ISBN 92-835-0287-6</p> <ul style="list-style-type: none"> - Inertial sensors and systems technology - Positioning systems. Development and status - Evaluation methods and results - Filtering and estimate - Fault tolerance design and redundancy techniques - Systems requirements and applications. <p>Twenty-two papers are included in this volume, the other four are classified and appear in CP-298 Supplement, classified NATO-CONFIDENTIAL.</p>	<p>ISBN 92-835-0287-6</p> <ul style="list-style-type: none"> - Inertial sensors and systems technology - Positioning systems. Development and status - Evaluation methods and results - Filtering and estimate - Fault tolerance design and redundancy techniques - Systems requirements and applications. <p>Twenty-two papers are included in this volume, the other four are classified and appear in CP-298 Supplement, classified NATO-CONFIDENTIAL.</p>